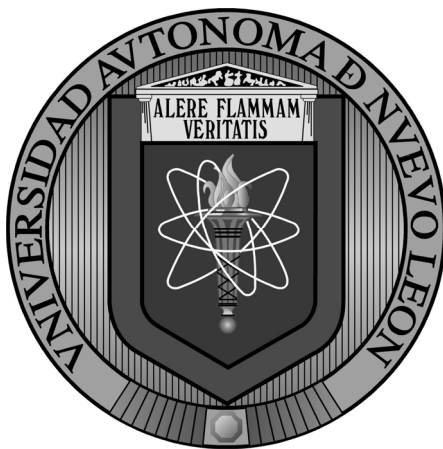


UNIVERSIDAD AUTÓNOMA DE NUEVO LEÓN

FACULTAD DE CIENCIAS DE LA TIERRA



**ANÁLISIS DE PROCEDENCIA DE LAS FORMACIONES
EL ALAMAR, LA BOCA Y LA JOYA, NORESTE DE MÉXICO
(TRIÁSICO SUPERIOR–JURÁSICO MEDIO)**

Tesis

**QUE COMO REQUISITO PARCIAL PARA OPTAR AL GRADO DE
DOCTOR EN CIENCIAS CON ESPECIALIDAD EN GEOCIENCIAS**

PRESENTA

IGOR ISHI RUBIO CISNEROS

LINARES, NUEVO LEÓN A JUNIO DE 2012



UANL

UNIVERSIDAD AUTÓNOMA DE NUEVO LEÓN



FACULTAD DE CIENCIAS DE LA TIERRA

LA TESIS

**ANÁLISIS DE PROCEDENCIA DE LAS FORMACIONES
EL ALAMAR, LA BOCA Y LA JOYA, NORESTE DE MÉXICO
(TRIÁSICO SUPERIOR–JURÁSICO MEDIO)**

ELABORADA POR

IGOR ISHI RUBIO CISNEROS

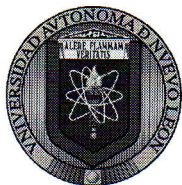
HA SIDO ACEPTADA COMO REQUISITO PARCIAL PARA OPTAR AL
GRADO ACADÉMICO DE
DOCTOR EN CIENCIAS CON ESPECIALIDAD EN GEOCIENCIAS

Vo. Bo.

DIRECTOR DE TITULACIÓN

DIRECTOR DE TITULACIÓN

LINARES, NUEVO LEÓN A JUNIO DE 2012



UANL

UNIVERSIDAD AUTÓNOMA DE NUEVO LEÓN



FACULTAD DE CIENCIAS DE LA TIERRA

LA TESIS

**ANÁLISIS DE PROCEDENCIA DE LAS FORMACIONES
EL ALAMAR, LA BOCA Y LA JOYA, NORESTE DE MÉXICO
(TRIÁSICO SUPERIOR–JURÁSICO MEDIO)**

ELABORADA POR

IGOR ISHI RUBIO CISNEROS

HA SIDO ACEPTADA COMO REQUISITO PARCIAL PARA OPTAR AL
GRADO ACADÉMICO DE

DOCTOR EN CIENCIAS GEOLÓGICAS

Vo. Bo.

COMITÉ DE REVISIÓN DE TITULACIÓN

UWE JENCHEN

TIMOTHY F. LAWTON

CARITA AUGUSTSSON

JUAN ALONSO RAMÍREZ FERNÁNDEZ

JOSÉ RAFAEL BARBOZA GUDIÑO

LINARES, NUEVO LEÓN A JUNIO DE 2012



UANL

UNIVERSIDAD AUTÓNOMA DE NUEVO LEÓN



FACULTAD DE CIENCIAS DE LA TIERRA

LA TESIS

**ANÁLISIS DE PROCEDENCIA DE LAS FORMACIONES
EL ALAMAR, LA BOCA Y LA JOYA, NORESTE DE MÉXICO
(TRIÁSICO SUPERIOR–JURÁSICO MEDIO)**


ELABORADA POR

IGOR ISHI RUBIO CISNEROS

HA SIDO ACEPTADA COMO REQUISITO PARCIAL PARA OPTAR AL
GRADO ACADÉMICO DE
DOCTOR EN CIENCIAS CON ESPECIALIDAD EN GEOCIENCIAS

Vo. Bo.

COMITÉ DE REVISIÓN DE TITULACIÓN



UWE JENCHEN




TIMOTHY F. LAWTON



CARITA AUGUSTSSON

JUAN ALONSO RAMÍREZ FERNÁNDEZ



JOSÉ RAFAEL BARBOZA GUDIÑO

LINARES, NUEVO LEÓN A JUNIO DE 2012

Por este medio declaro bajo protesta, haber realizado esta tesis de manera personal y haber utilizado únicamente los medios, procedimientos y asesorías descritas en la misma.

IGOR ISHI RUBIO CISNEROS

Junio de 2012

Provenance analysis of El Alamar, La Boca and
La Joya formations, northeastern Mexico
(Upper Triassic–Middle Jurassic)

by

IGOR ISHI RUBIO CISNEROS



Disclaimer,

I hereby declare under oath, I have made this thesis in a personal manner and have used only the means, procedures, and advice outlined in it.

*“La mujer reproduce la Tierra,
el hombre la interpreta”.*

“Uno nunca deja de ser doctor en ciencias”.

Dr. Jaime Leal

For Myrna, Nadia, Ignacio, Raúl, and the rest of my family members.

Madre Tierra, Hermana Agua, Abuelo Fuego, Padre Sol.

Acknowledgements

The author thanks the advisors in the committee for the thesis evaluation. Also to, external advisors, tutors, partners, colleagues, friends, fellows, mentors, teachers, neighbors, *working class heroes*, assistants, reviewers, collaborators, supporters, and the technical-administrative workers at the different attended research facilities.

Special thanks to Y.Z.E. Ocampo-Díaz, M. Martínez-Paco, Huna, Ocampo-Díaz Family, R. García-Obregón, H. Medina-Ferrusquía, M. Guerrero-Suastegui, J. Leal, E. Estrada, J. García (Matraca), A. Blanco, L.A. Pérez-Góngora.

My extended appreciation to F. Velasco-Tapia, G. Chávez-Cabello, D. Masuch Oestereich, H. de León-Gómez, F. Medina-Barrera, J.G. López-Oliva, T. Cossio and his thesis students (2009-2011), A. Ramos-Ledezma, V. Dülmer, E. Chacón-Baca, R. Soto-Villalobos, M.A. Maldonado-Leal, Juany Montes, and Laura Villalobos at the Facultad de Ciencias de la Tierra, UANL.

Attentions to R. Molina-Garza, A. Iriundo, U. Martens, ZL. Capra, J. Aranda-Gómez, T. Orozco-Esquivel, A. Izaguirre-Pompa, J.T. Vázquez at the Centro de Geociencias, UNAM (Querétaro); too, M. Martini, D. Keppie at Instituto De Geología, UNAM, and R. López-Doncel at the UASLP.

Kind regards to those who gave me additional discussions and assistance, K. Giles, G. Hunt, D. Lawton, V. Valencia, D. Michalzik, J. Steffan, D. Fastovsky, G. Gray, E. Garzanti, H. von Eynatten, R. Ingersoll, W.R. Dickinson, A. Basu, M. Johnsson, L. Caracciolo, S. Critelli, T. Ohta, J. Pindell, J. Holbrook, K. Mickus, M. Gutierrez, C. Jennings, K. Busby, L. Buatois, G. Mángano, D. Nance, T. Carr, T. Anderson, T. Wawrzyniec, J. Bartholomew, C. Ver Straeten, B. Miller, C. Miller, A. Henkelmann, M. Brooke, L. Rayo, and to ERASMUS and DAAD students.

This work was partially funded by the Posgrado de la Facultad de Ciencias de la Tierra, UANL and CONACyT. The author acknowledges the support for fieldwork and research presentations given by the “Programa de Fortalecimiento Institucional de la Secretaría de Educación Pública (PIFI-SEP)”. Also by the projects “Estratigrafía y geoquímica de sedimentos terrígenos del Mesozoico y Cenozoico en el noreste de México” - PAICyT-UANL CT1377-06, and “Procesos magmáticos relacionados a diferentes etapas de la evolución de la Sierra Madre Oriental, NE de México” - PAICyT-UANL CT1703-07. Some sample analyses were partially funded by the Institute of Tectonic Studies and the Manasse Endowed Chair, College of Arts and Sciences, both at New Mexico State University. National Science Foundation grant EAR- 0443387 supported the Arizona LaserChron Center. International Association of Sedimentologists Series (IASS) – Student Grant; 2008. Society for Sedimentary Geology (SEPM) – Robert J. and Ruth A. Weimer Student Research Grant 2011. GSA-Annual Meeting Travel Grants: 2008, 2010, and 2011.

The author is grateful to the Ejido La Loma (Porfirio Díaz) and Frutería El Azahar, Linares, N.L., México, A. Monroy and family members, D. Gutierrez, P. Platas, S. Gibert, R. Santos, E. Lazcano, G. González, D. Saavedra, O. Muñoz, R. León, M. Roverato, A. Duarte, A. Godínez, G. Cross, F. Flores, E. Sotuyo, E. Gutierrez, E. Dávalos, J. Vargas, A. Ramírez P. Pinzón, S. Chávez, M. Enríquez, D. Pruneda, M. Peña, L. Spinosso, M. Rodríguez, A. Sagahón.

Contents

PREFACE	XIV
ABSTRACT	XV
RESUMEN	XVI
1. INTRODUCTION: RED BEDS AND RELATED TECTONO-SEDIMENTARY ASPECTS	1
1.1. Red Beds	1
1.2. Basin-types for red beds	2
1.3. Provenance analysis	2
1.4. Tectonics coupled to the sedimentary geology of red beds: methodological implications	3
1.5. Northeastern Mexico	4
1.5.1. The basement as basic control on red beds generation in northeastern Mexico	5
1.5.2. Actual state for the tectono-stratigraphic interpretation and subdivision of the Mesozoic red beds succession for the northeastern Mexico	7
1.5.2.1 Red Beds: stratigraphy–sedimentology–paleontology	7
1.5.3. Regional geology	8
1.5.3.1 Related northeastern Mexico basement works: structural and tectonics	8
1.5.4. Stratigraphy of Middle–Upper Triassic to Lower–Middle Jurassic (The Huizachal Group)	11
1.5.4.1 Triassic red beds: El Alamar Formation	11
1.5.4.2 Jurassic red beds: La Boca and La Joya formations	12
2. FACIES, ARQUITECTURAL-ELEMENTS, AND FLUVIAL STYLE ANALYSIS	18
2.1. Introduction	18
2.2. Methodos	19
2.3. Sedimentary (litho-) facies and facies associations of El Alamar, La Boca, and La Joya formations	22
2.3.1. Fluvial facies association (FA-1)	22
2.3.1.1 Conglomerate and fine to medium grained, trough-planar cross-bedded sandstones (FA-1A and FA-1D)	22
2.3.1.1.1. Description	22
2.3.1.1.2. Interpretation	25
2.3.1.2 Fine to medium grained, planar cross-bedded to horizontally laminated sandstones (FA-1B)	27
2.3.1.2.1. Description	27
2.3.1.2.2. Interpretation	28
2.3.1.3 Fine to medium grained, non-bioturbated, sigmoidal bedded sandstones (FA-1C)	29
2.3.1.3.1. Description	29
2.3.1.3.2. Interpretation	30
2.3.2. Overbank facies association (FA-2)	31
2.3.2.1 Bioturbated massive mudstone to siltstone (FA-2A)	31
2.3.2.1.1. Description	31
2.3.2.1.2. Interpretation	31
2.3.2.2 Bioturbated massive to laminated mudstone–siltstone (FA-2B)	34
2.3.2.2.1. Description	34
2.3.2.2.2. Interpretation	34
2.3.2.3 Non-bioturbated massive to laminated mudstone to siltstone interfingered by tuff related deposits (FA-2C)	34
2.3.2.3.1. Description	34
2.3.2.3.2. Interpretation	35
2.3.3. Aeolian facies association (FA-3): very fine to medium grained, well sorted, non-bioturbated, planar cross-bedded sandston (FA-3A)	36
2.3.3.1 Description	36
2.3.3.2 Interpretation	37

2.3.4. <i>Alluvial fan facies association: very coarse grained to granule-pebble grade, matrix to clast supported massive to cross-bedded sandstones and conglomerates (FA-4)</i>	39
2.3.4.1 <i>Description</i>	39
2.3.4.1.1. <i>Interpretation</i>	39
2.4. <i>Litho-stratigraphic sections for the Huizachal Group</i>	42
2.5. <i>Architectural element analysis</i>	46
2.5.1. <i>Architectural concepts</i>	46
2.5.2. <i>Methods: a working bedding diagram</i>	47
2.5.3. <i>Architectural hierarchies and bounding surfaces</i>	47
2.5.4. <i>Classification of architectural elements</i>	48
2.5.4.1 <i>Rationale</i>	48
2.5.4.2 <i>Description</i>	48
2.5.4.3 <i>Interpretation</i>	49
2.5.4.3.1. <i>Architectural elements formed in channels</i>	49
2.5.4.3.2. <i>Architectural elements of the overbank environment</i>	50
2.6. <i>Accommodation and supply: surface architecture</i>	51
2.6.1. <i>Description: A model proposal</i>	53
2.6.2. <i>Interpretation: A case study – La Boca Formation at Valle de Huizachal</i>	54
2.6.3. <i>Closure arguments</i>	56
2.7. <i>Discussion: paleocurrent analysis, evolution of the continental fluvial styles flanking basement blocks, and controllers for processes and products.</i>	60
3. PETROGRAPHY OF ROCK-FORMING MINERALS MINERALS AND SOURCE AREAS	64
3.1. <i>Introduction</i>	64
3.2. <i>Sampling and petrographic methods</i>	65
3.2.1. <i>Grain-types: classification and general composition</i>	66
3.2.2. <i>Sandstones framework grains: nomenclature for a genetic classification</i>	67
3.2.2.1 <i>Petrofacies 1: Quartzolithic (Q1) sands</i>	68
3.2.2.1.1. <i>Subpetrofacies 1A: Quartzolithic (Q1) sands with high content of metamorphic and sedimentary lithic fragments</i>	68
3.2.2.1.2. <i>Subpetrofacies 1B: Quartzolithic (Q1) sands with high content of volcanic and sedimentary lithic fragments</i>	69
3.2.2.2 <i>Petrofacies 2: Lithoquartzose (Lq) sands</i>	70
3.2.3. <i>Source area compositional classification</i>	71
3.2.3.1 <i>Quartz</i>	71
3.2.3.2 <i>Lithic fragments</i>	74
3.2.4. <i>Light mineral synthesis: discussion and conclusion</i>	75
4. ANALYSIS OF HEAVY MINERALS: ASSEMBLAGES AND SOURCE AREAS	78
4.1. <i>Introduction</i>	78
4.2. <i>Methods: theory and practice– analytical procedures, representations, indices</i>	79
4.3. <i>Results of heavy mineral provenance analysis: stratigraphic trends of heavy minerals</i>	82
4.3.1. <i>Heavy mineral: features, concentration and assemblages</i>	82
4.3.1.1 <i>Precambrian–Paleozoic basement units</i>	82
4.3.1.2 <i>El Alamar Formation</i>	84
4.3.1.3 <i>La Boca Formation</i>	85
4.3.1.4 <i>La Joya Formation</i>	88
4.3.2. <i>Detritus: source rocks and sands</i>	88
4.3.2.1 <i>Case study: applying a discriminant function</i>	88
4.4. <i>Discussion: associated heavy minerals indices to sources</i>	89
5. GEOCHEMICAL CLASSIFICATION, COMPOSITIONAL MODIFICATIONS, AND SOURCE AREA COMPOSITION	91
5.1. <i>Introduction</i>	91
5.2. <i>Methodos</i>	92

5.3. Results: data description and visualization	92
5.3.1. Major Elements data	92
5.3.1.1 Cluster analysis: an elemental chain of commands	95
5.3.1.2 Principal Components analysis (PC)	96
5.3.2. Trace Elements and Rare Earth Element (REE) data	99
5.3.2.1 Large ion lithophile elements (LILE): Rb, Cs, Ba, Sr	100
5.3.2.2 High field strength elements (HFSE): Y, Zr, Nb, Hf, Th, U	101
5.3.2.3 Transition Trace Elements (TTE): Co, Ni, V, Sc	103
5.3.2.4 Rare Earth Elements (REE)	103
5.3.2.5 Classification	104
5.3.3. Source area composition	105
5.3.3.1 Major elements systematics	105
5.3.3.2 Trace Elements systematics	107
5.3.4. Weathering: values, indices, representations, and trends	110
5.3.4.1 Chemical Index of Alteration (CIA)	111
5.3.4.2 Mafic–Felsic–Weathering (MFW diagram)	113
5.4. Discussion	114
6. RADIOGENIC ISOTOPES: U-PB DETRITAL ZIRCON DATING	116
6.1. Introduction	116
6.2. Methods	116
6.3. Corollaries: detrital zircons and source terranes	117
6.3.1. Results	117
6.3.2. Discussion	121
7. REGIONAL INTEGRATION AND INTERPRETATION FOR PROCESSES STRATIGRAPHY AND PROVENANCE ANALYSIS	123
7.1. Introduction	123
7.2. Sedimentary petrography	123
7.2.1. Sedimentary petrography: compositional signatures, affinities, indices, and recycling	123
7.2.2. Heavy mineral analysis: mineral content, provenance, and erosion	128
7.3. Geochemistry: compositional mixtures a mineral content signature	130
7.4. Geochronology	131
7.5. Sedimentology	133
7.6. Discussion: preexisting basement massifs and igneous bodies; the fundamental controls/factors for the Mesozoic red-bed genesis	133
7.7. Mesozoic unroofing and exhumation: a coda for a preliminary basin stratigraphy and tectonic evolution of northeastern Mexico	136
7.7.1. Triassic	137
7.7.2. Jurassic	143
7.7.2.1 Early–Middle Jurassic	143
7.7.2.2 Middle Jurassic	147
8. CONCLUSIONS	152
8.1. Suggestions	155
REFERENCES	157
APPENDIX FOR CHAPTER 2: Transition frequency matrix markov chain	190
APPENDIX FOR CHAPTER 3: DETRITAL MODES	193
APPENDIX FOR CHAPTER 4: HEAVY MINERAL INDICES	202
APPENDIX FOR CHAPTER 5: GEOCHEMICAL ANALYSES	208

APPENDIX FOR PATTERN FILLS

217

List of Figures

- Fig. 1.1: Methodological chart for the integration between the discipline of Sedimentary Geology and Tectonics. Big History, *cf.*, Alvarez, 2010 4
- Fig. 1.2: Locality of the studied area. The numbers in circles represent each of the ten studied localities. 5
- Fig. 1.3: Pre-Upper Jurassic localities in central to northeastern Mexico (in Barboza-Gudiño *et al.*, 2010). Shown are Upper Triassic exposures of the marine and continental facies, post-Triassic red beds, exposures of pre-Mesozoic crystalline rocks, in some cases interpreted as areas of no deposition during the Triassic. 9
- Fig. 1.4: Stratigraphic subdivisions proposed by different authors for the early Mesozoic successions exposed in the Sierra Madre Oriental from Nuevo León and Tamaulipas and the Mesa Central province in San Luis Potosí and Zacatecas (after Barboza-Gudiño *et al.*, 2010). References at Barboza-Gudiño *et al.*, 2010 for different stratigraphic relations. The label for “this work” refers to Barboza-Gudiño *et al.*, 2010. 12
- Fig. 1.5: Proposed generalized, schematic stratigraphic relations of the lowermost part of the Mesozoic sequence of the Huizachal Group in the Sierra Madre Oriental. Note the intraformational angular unconformities between the lower and upper member for El Alamar and La Boca formations. Weighted mean ages for this work are at the right side of the column. Units not drawn to scale. Key for symbols are explained in the coming figures. Pgs– Paleozoic Granjeno Schist. P-Tr l– Permian to Lower Triassic. Tr u A l– Upper Triassic El Alamar lower member. Tr u A u– Upper Triassic EL Alamar upper member. J l B l– Lower Jurassic La Boca lower member. J l B u– Lower Jurassic La Boca upper member. J m J– Middle Jurassic La Joya. Sedimentary structures are given at the right of column. The “bone” represents the vertebrate-bearing interval (Early Jurassic; Clark *et al.*, 1994). c: Clay; sl: Siltstone; sa: Sandstone; gr: Gravel. V– volcanic. MBS– Mayor Bounding Surface. C– Carbonate. θ – dip of unconformity. 13
- Fig. 1.6: Stratigraphic correlation for the stratigraphic columns after Michalzik (1988) and Goldhammer and Johnson (2001) for northeastern Mexico (modified by Jenchen, 2007a, b). Colors are from International Stratigraphic Chart 2009. 17
- Fig. 2.1: Lithofacies classification scheme. Modified from Miall (1985, 1996) and Allen (1983a). 20
- Fig. 2.2: Photograph assemblage for some of the low flow regime lithofacies (Sr: ripples, and Sm: trough cross-bedding) contained in facies association FA-1: FA-1A, FA-1B, FA-1C, reported at Valle de Huizachal within the upper and lower members of La Boca Formation. a) overturned foreset bed with trough cross-bedding, notice that scouring produced small, erosional troughs, which were subsequently filled with low-angle cross-laminae at the base (left); b) foreset bed with tabular cross-bedding; c) tabular cross-bedding on a foreset bed of nontangential foreset character overlying a plane (flat) bed; d) ripple cross-lamination in flood deposits; e) small-scale tangential foresets; f) trough cross-bedding. Scale line in black and white represents 30 cm. 23
- Fig. 2.3: Photograph assemblage for selected low flow regime lithofacies (Sh; Sl; Se-Ss: scour fills; Sm: trough cross-bedding) contained in facies association FA-1: FA-1a, FA1-B. a) Lens of coarse grained sandstones with tool mark, possible a scour fill; b) sole marking (erosion of bed) with roll marks; c) lenticular bedding, d) possible flaser or lenticular bedding on lake sediments; e) trough cross-bedding sedimentation unit with some overturned tangential foresets. a, b, c, and d correspond to La Boca upper member at Valle de Huizachal. e– La Boca Formation at the locality of Cañón El Olmo. 24
- Fig. 2.4: Graphic representation from the Markov Chain containing FA-1A for Lomas de San Paulo Tranquitas (LSPT). Data obtained by computing the transition frequency-probability matrix datasets from lithofacies (Appendix for Chapter 2). Key for symbols at Fig. 2.1. 25
- Fig. 2.5: Graphic representation from the Markov Chain containing FA-1D for Cañón Caballeros (CC). Data obtained by computing the transition frequency-probability matrix datasets from lithofacies (Appendix for Chapter 2). Key for symbols at Fig. 2.1. 26
- Fig. 2.6: Graphic representation from the Markov Chain containing FA-1C for the lower member of La Boca Formation at the Valle de Huizachal (VH), by computing the transition frequency-probability matrix datasets from lithofacies (Appendix for Chapter 2). Key for symbols at Fig. 2.1. 30
- Fig. 2.7: a) Photograph assemblage at Valle de Huizachal in La Boca upper member from a bar deposit exhibiting some of the low flow regime lithofacies (Sp, Sh; Sl; Sr) contained in facies FA-1B, FA-1C. Scale bar at the right represents 40 cm 30
- Fig. 2.8: Photograph mosaic for the lithofacies Fm found on facies FA-2B. a) sub-horizontal to linguoidal structures; b) thick simple vertical burrow; c) sub-vertical to linguoidal structures; d) sub-horizontal to linguoidal structures; e–f) “L” form structure of 4 cm with unbranched, partially straight to slightly incline to curved-twisted shafts. a, b, and c were pictured at the lower interval of La Boca Formation at the Valle de Huizachal. e and d are found at the upper member of La Boca Formation at Valle de Huizachal. f– corresponds to the lower most exposure of El Alamar Formation at Lomas de San Paulo Tranquitas. 32

- Fig. 2.9: Graphic representation from the Markov Chain containing FA-2A for the Miquihuana (Mi) locality, by computing the transition frequency-probability matrix datasets for lithofacies (Appendix). Key for symbols at Fig. 2.1. 33
- Fig. 2.10: Photograph mosaic for facies FA-2B and FA-2C. a) Paleosols with organic content; b) fine grained concretions; c) soft ball sediments structures; d) mud cracks developed on a paleosol (plain view); e) interfingered tuff deposits with fine sediments (Fm); f) tuff deposit. a and b are located at El Alamar Formation at Lomas de San Paulo Tranquitas. c and d correspond to strata from La Boca upper member at Valle de Huizachal. e and f are found at La Boca Formation at the west flank of the Aramberri's Uplift. 35
- Fig. 2.11: Graphic representation from the Markov Chain containing FA-2C for the upper member of La Boca Formation at Valle de Huizachal (VH), by computing the transition frequency-probability matrix datasets from lithofacies (Appendix for Chapter 2). Key for symbols at Fig. 2.1. 37
- Fig. 2.12: a–b) Scaled photographs of facies FA-3A found in La Boca upper member at Valle de Huizachal, representing the unidirectional low flow regime of sandy lithofacies Sr with dune generation. Notice the formation of cross-lamination that dips at angles of up to $>30^\circ$. 38
- Fig. 2.13: Photographic assemblage for the facies FA-4. a) Lithofacies Gmm found in La Boca upper member at Valle de Huizachal, b) lithofacies Gci in La Joya Formation at Aramberri, c) lithofacies Gmg in La Boca upper member at Valle de Huizachal, d) lithofacies Gh in La Boca upper member at Valle de Huizachal, e) lithofacies Gcm for the base of La Joya Formation at Cañón Caballeros. 40
- Fig. 2.14: Graphic representation from the Markov Chain analysis containing FA-4 for the study section at Cañón Novillo (CN), by computing the transition frequency-probability matrix datasets from lithofacies (Appendix for Chapter 2). Key for symbols at Fig. 2.1. 41
- Fig. 2.15: Glossary of sedimentary structures found in the measured sections. 42
- Fig. 2.16: Measured sections (Block 1) and stratigraphic levels of collected samples for various analyses. For sedimentary structures description consult Fig. 2.15. Vertical arrows indicate cyclic successions of various types, showing direction of fining and bed thinning. Numbers in circles indicate rank of bounding surfaces. Lithofacies codes are given at left of column. Facies associations are given in white vertical tags at right of column. c: Clay; sl: Siltstone; sa: Sandstone; gr: Gravel. Stratigraphic position of the measured sections (Block 1) with respect to other analyzed areas is plotted on the lower right corner. Correlation by shaded sections: light gray: El Alamar Formation; dark grey: La Joya Formation (LJ). Measured paleocurrents are above measured sections. Underlying the measured sections are reported basement units with calculated age. 43
- Fig. 2.17: Measured sections (Block 2) and stratigraphic levels of collected samples for various analyses. For sedimentary structures description consult Fig. 2.15. Vertical arrows indicate cyclic successions of various types, showing direction of fining and bed thinning. Numbers in circles indicate rank of bounding surfaces. Lithofacies codes are given at left of column. Facies associations are given in white vertical tags at right of column. c: Clay; sl: Siltstone; sa: Sandstone; gr: Gravel. Stratigraphic position of the measured sections (Block 2) with respect to other analyzed areas is plotted on the lower right corner. Correlation by shaded sections: light gray: El Alamar Formation; middle grey tone: La Boca Formation; dark grey: La Joya Formation (LJ). Measured paleocurrents are above measured sections. Underlying the measured sections are reported basement units with calculated age. 44
- Fig. 2.18: Measured sections (Block 3) and stratigraphic levels of collected samples for various analyses. For sedimentary structures description consult Fig. 2.15. Vertical arrows indicate cyclic successions of various types, showing direction of fining and bed thinning. Numbers in circles indicate rank of bounding surfaces. Lithofacies codes are given at left of column. Facies associations are given in white vertical tags at right of column. c: Clay; sl: Siltstone; sa: Sandstone; gr: Gravel. Stratigraphic position of the measured sections (Block 3) with respect to other analyzed areas is plotted on the lower right corner. Correlation by shaded sections: middle grey tone: La Boca Formation; dark grey: La Joya Formation (LJ). Measured paleocurrents are above measured sections. Underlying the measured sections are reported basement units with calculated age. 45
- Fig. 2.19: The eight basic architectural elements in fluvial deposits (Miall, 1985, 1988, 1996). 47
- Fig. 2.20: Bounding surfaces and architectural element unit hierarchies at a road cut exposing the upper member of La Boca formation at the Valle de Huizachal. The analyzed section was divided into 10 smaller control points (numbers in ovals). The sections are approximately equally spaced to analyze the lateral variability of the different lithofacies, facies association, and architectural elements. Bounding surfaces are circled. V– volcanic. FA– facies association with its respective category. Abbreviations like Sh, Sl– correspond to lithofacies at left of column. SG, GB, LS, DA, OF– are assigned architectural elements. For sedimentary structures description consult Fig. 2.15. Vertical arrows indicate cyclic successions of various types, showing direction of fining and bed thinning. Numbers in circles indicate rank of bounding surfaces. c: Clay; sl: Siltstone; sa: Sandstone; gr: Gravel. 52
- Fig. 2.21: Proposed model of the general surface architecture in fluvial environments based on the interpretation for Major Bounding Surfaces (MBS; Miall, 1991; Holbrook, 2001). Description and interpretation of the four different MBS for

surface architecture. AmBS– Amalgamation Bounding Surface; AgBS– Aggradation Bounding Surface ; DeBS– Degradation Bounding Surface ; MFBS– Major Flooding Bounding Surface. 54

Fig. 2.22: Measured sections (Block 1) as in Fig. 2.16. The corresponding fluvial style and accommodation/supply cycle for comparative purposes are given at right of column: amalgamation (AmBS), aggradation (AgBS), degradation (DeBS), and major flooding surfaces (MFBS). 57

Fig. 2.23: Measured sections (Block 2) as in Fig. 2.17. The corresponding fluvial style and accommodation/supply cycle for comparative purposes are given at right of column: amalgamation (AmBS), aggradation (AgBS), degradation (DeBS), and major flooding surfaces (MFBS). 58

Fig. 2.24: Measured sections (Block 3) as in Fig. 2.18. The corresponding fluvial style and accommodation/supply cycle for comparative purposes are given at right of column: amalgamation (AmBS), aggradation (AgBS), degradation (DeBS), and major flooding surfaces (MFBS). 59

Fig. 2.25: Fluvial styles and major bounding surfaces (MBS) for El Alamar Formation with its respective paleocurrent strikes (arrows) for the localities of: 1– Lomas de San Paulo Tranquitas (gravel-sand meandering; DeSB); 2– Cañón El Alamar (deep gravel-bed braided; AgSB); 5– Cañón La Boca (gravel wandering; DeSB). Source areas represent exposed crystalline basement units (consult pattern fill for lithology recognizance). Locality number is based on Figure 1.1. 61

Fig. 2.26: Sketch for the fluvial styles and major bounding surfaces (MBS) for La Boca Formation with its respective paleocurrent strikes (arrows) for the localities of: 3– Aramberri (Shallow perennial braided; DeSB), 4– Cañón El Olmo (Sandy meandering; DeBS), 5– Cañón La Boca (Gravel Wandering; AgBS), 6– Cañón Caballeros (Gravel-bed braided; DeSB and AgBS), 7– Cañón Peregrina (Gravel-bed braided; AgSB), 9– Valle de Huizachal (Gravel-sand meandering; DeSB), and 10– Miquihuana (Sheet food distal braided and Flashy ephemeral sheet flood). Source areas represent exposed crystalline basement units (consult pattern fill for lithology recognizance). Locality number is based on Figure 1.1. 62

Fig. 2.27: Sketch for the fluvial–alluvial styles and major bounding surfaces (MBS) for La Joya Formation with its respective paleocurrent strikes (arrows) for the localities of: 1– Lomas de San Paulo Tranquitas (Gravel-bed braided; DeBS), 4– Cañón El Olmo (Gravel meandering; DeBS), 5– Cañón La Boca (Gravel-bed braided; AgBS), 6– Cañón Caballeros (Gravel-bed braided; AgBS), 7– Cañón Peregrina (Gravel-bed braided; DeBS), 8– Cañón Novillo (Gravel Wandering; AgBS), 9– Valle de Huizachal (Gravel-sand meandering; DeBS). Source areas represent exposed crystalline basement units (consult pattern fill for lithology recognizance). Locality number is based on Figure 1.1. 63

Fig. 3.1: Ternary system of compositional assemblages for metamorphic–Rm, volcanic–Rv, and sedimentary–Rs components. The compositional space is divided in: (1) metamorphoclastics; (2) sedimentoclastic; (3) volcanoclastic; (4) mixed zone. 66

Fig. 3.2: Point-counting for the analyzed samples using the proposed classification of sandstone by Okada (1971). Question mark represents an unidentified stratigraphic position within the stratigraphic succession. *Reinterpreted and recalculated data representing undifferentiated samples from La Boca Formation, provided by Ramos-Ledezma (2007). 67

Fig. 3.3: Diagram for genetic classification of sandstones (Weltje, 2006). Sixfold subdivision of compositional space into Quartzolithic (Ql), Lithoquartzose (Lq), Lithofeldspathic (Lf), Feldspatholithic (F1), Feldspathoquartzose (Fq) and Quartzofeldspathic (Qf) sands. Symbols represent the mean composition for each studied area (Fig. 3.2). 68

Fig. 3.4: Classification scheme of sandstones proposed by McBride (1963), with the entire data collection for this study. Symbols for each studied area (Fig. 3.2). 70

Fig. 3.5: RmRvRs diagram with datasets for the studied areas. (1) metamorphoclastics; (2) sedimentoclastic; (3) volcanoclastic; (center) mixed zone. Symbols represent the mean composition for each studied area (Fig. 3.2). 71

Fig. 3.6: Microphotographs for compositional subpetrofacies 1A. a) Metabasite grain (Lmb₁); b) Metabasite grain (Lmb₂); c) Metapelite grain (Lmp₁); d) Metapsammite/metafelsite grain (Lmf₂); e) Metapsammite/metafelsite grain (Lmf₃); f) Metapelite grain (Lmp₁₋₂); g) Metamorphic lithic fragment, possibly from a quartzite; h) polycrystalline quartz; i) polycrystalline quartz; j) polycrystalline quartz subordinated by monocrystalline quartz grains with undulose and straight extinction; k) polycrystalline with 2-3 and >3 grains, and other volcanic lithics with microlitic textures; l) polycrystalline quartz dominated sandstone; m) coarse-grained sedimentary lithic fragment (Lsp); n) medium-grained sedimentary lithic fragment (Lsp). 72

Fig. 3.7: Microphotographs for subpetrofacies 1B. a) Plagioclase fragment with its typical polysynthetic twinning; b) crystalline fragment of microcline with its double twinning system; c) volcanic detrital fragment with a porfidic texture with phenocrysts of feldspar on a very altered microcrystalline feldspathic matrix and opaque minerals; d) microlitic volcanic grain (Lvmi); e) volcanic felsitic fragment; f) tuffaceous volcanic lithic with fluidal texture; g) lathwork volcanic lithic; h) tuffaceous volcanic lithic fragment; i) volcanic lithic with tuffaceous texture; j) volcanic lithic fragment with phenocrysts of plagioclase, groundmass from laths ; k) porphyry texture (microholocrystalline groundmass with phenocrysts) ; l) granitic texture on a plutonic lithic fragment; m) granophyric texture on a volcanic lithic fragment , n and o) represent plutonic fragments with graphic textures . 73

- Fig. 3.8: Microphotographs for petrofacies 2. a) Volcanic lithic fragment with tuffaceous texture; b) tuffaceous texture lithic fragment; c) volcanic lithic fragment with porphyritic texture; d) sand-size lithic fragments; e) sedimentary lithic fragment; f) tuffaceous texture lithic fragment; g) volcanic lithic fragment with tuffaceous texture; h) volcanic lithic fragment; i) tuffaceous texture lithic fragment; j) plutonic lithic fragment; k) volcanic lithic fragment with felsitic texture (Lv_f), and metapelite grain Lmp rank 1. 74
- Fig. 3.9: Diamond-shape diagram Q_{mo}, Q_{mr}, Q_{p<3}, and Q_{p>3} with the studied samples of this work (after Basu *et al.*, 1975 modified by Tortosa *et al.*, 1991) used to interpret source rocks. Key for symbols at Fig. 3.2. 75
- Fig. 3.10: Q_{mr}–Q_{mo}–Q_p diagram from Arribas *et al.* (1990). The polygons represent the arithmetic mean and their respective standard deviations from the studied samples for each outcrop. Symbols represent the mean composition for each studied area (Fig. 3.2). 76
- Fig. 3.11: Ternary diagram R_gR_sR_m from Critelli and Le Pera (1994) to determine source rocks interoretation. The polygons represent the arithmetic mean and their respective standard deviations from the studied samples for each outcrop. Symbols represent the each studied area (Fig. 3.2). 76
- Fig. 3.12: R_mR_vR_s ternary system proposed on this work for source rock affinity. Polycrystalline quartz and metamorphic lithic fragments constitute R_m. The R_v assemblage contains polycrystalline quartz 2-3, potasic feldspars, plagioclase, and volcanic lithic fragments. The R_s assemblage includes different sedimentary rock fragments. Symbols represent the mean composition for each studied area (Fig. 3.2). 76
- Fig. 3.13: Biplot with the clr- logarithmic transformations for R_m/R_s vs. R_v/R_s. Shaded curves represent the confidence regions for 90, 95 and 99%, and the mean compositional value for Petrofacies 1A and 1B. Petrofacies 1A– Lomas de San Paulo Tranquitas (LSPT); Cañón El Alamar (CA); Cañón El Olmo (COI); Cañón La Boca (CB); Cañón Caballeros (CC); Cañón Peregrina (CHP); Cañón Novillo (CN). Petrofacies 1B– Aramberri (Ab), Valle de Huizachal (VH), Miquihuana (Mi). 76
- Fig. 4.1: Opaque and crystalline mineral percentages generated by point counting for from the basement units and the red beds. 81
- Fig. 4.2: Microphotographs for the heavy mineral assemblage found on the basement units. a) Prehnite, b) Garnet, c) Topaz, d) Olivine, e) Apatite, f) Spinel, g) Andalusite, h) Clinocllore, i) Hypersthene, j) Xenotime, k) Pumpellyte, l) Zoisite, m) Clinopyroxene, n) Amphibole, o) Tremolite, p) Brown hornblende, q) Sillimanite, r) Tourmaline. Microphotographs with no scale bar may be correlated with an scale bar of 0.2 mm from adjacent pictures. 83
- Fig. 4.3: Microphotographs for the heavy mineral assemblage found on El Alamar Formation. a) Hornblende; b) Monazite; c) Prehnite; d) Chlorite; e) Zoisite; f) Chloritoid; g) Zircon (subrounded); h) tetragonal [elongated] zircon; i) Zircon (heudral); j) Chlorite; k) Rutile; l) Augite; m) Talc. Microphotographs with no scale bar may be correlated with a scale bar of 0.2 mm from adjacent pictures. 84
- Fig. 4.4: Microphotographs for the heavy mineral assemblage found on the upper member of La Boca Formation and La Joya Formation. a) Apatite; b) Talc; c) Orthopyroxene; d) Zircon; e) Andalusite; f) Kyanite; g) Enstatite; h) Clinozoisite; i) Zoisite; j) Spinel; k) Tourmaline; l) Sillimanite. Microphotographs with no scale bar may be correlated with an scale bar of 0.2 mm from adjacent pictures. 85
- Fig. 4.5: Bar diagrams depicting heavy mineral frequencies in percentages of the Huizachal Group [El Alamar, La Boca, and La Joya Formations), and some underlying basement units (Precambrian–Paleozoic) from northeastern Mexico. The series are in stratigraphic order. Note the diversification of heavy mineral suits up-section. 86
- Fig. 4.6: Box-plot diagram with values of the studied samples for each of the main heavy mineral indices according to Garzanti and Andò (2007). Huizachal Group (El Alamar, La Boca, and La Joya Formation) and underlying basement units (Precambrian–Paleozoic). 87
- Fig. 4.7: Standardized canonical discriminant functions for provenance analysis of heavy mineral indices. A biplot arranges the discriminant functions at each axis (DF1 [x] vs. DF2 [y]). The simplex contains fields interpreted for provenance source rocks. 89
- Fig. 5.1: Box-plot diagrams with the arithmetic mean and standard deviation values for major elements from a) clastics (n= 82) and b) volcanics (n= 38). 94
- Fig. 5.2: Dendrogram with a typical joining “tree-clustering” coupled to the amalgamation (linkage) rule of a weighted pair-group average with a distance measurement of *IPearson r*. a) Clastics, n=82 (LSPT– Lomas de San Paulo Tranquitas; CA– Cañón El Alamar; COI– Cañón El Olmo; CB– Cañón La Boca; CC– Cañón Caballeros; CHP– Cañón Peregrina; CN– Cañón Novillo). b) Volcanics, n= 38 (VH– Valle de Huizachal; Ab– Aramberri; Mi– Miquihuana). 96
- Fig. 5.3: Compositional biplots for principal component analysis from *ilr*-transformed major element values. Arrows indicate loadings of elements. a) Clastics (n=82); b) volcanics (n= 38); c) crystalline basement units (NG– Novillo Gneiss; GS– Granjeno Schist; n= 7); d) basement boulders (*compiled data; n= 12); e) Paleozoic–Triassic plutons (*compiled data; n= 13); f) volcanic rocks (*compiled data; n= 32). Consult Table 5.4 to see the variability of the variables resulted

from the main principal components and factor axis. Data compiled from: Lopez *et al.*, 2001; Barboza-Gudiño *et al.* 2008, 2010; García-Obregón, 2007 98

Fig. 5.4: Spider diagram with the trace element concentrations normalized to Upper Continental Crust (UCC), after Taylor and McLennan (1981); including mean values and confidence limits at 99.5%. a) Clastics, n=82 (LSPT– Lomas de San Paulo Tranquitas; CA– Cañón El Alamar; COI– Cañón El Olmo; CB– Cañón La Boca; CC– Cañón Caballeros; CHP– Cañón Peregrina; CN– Cañón Novillo). b) Volcanics, n= 38 (VH– Valle de Huizachal; Ab– Aramberri; Mi– Miquihuana). 100

Fig. 5.5: Trace element concentrations normalized to the Bulk Earth composition after Hickey *et al.* (1986), including mean values and confidence limits at 99.5%. a) Clastics, n=82 (LSPT– Lomas de San Paulo Tranquitas; CA– Cañón El Alamar; COI– Cañón El Olmo; CB– Cañón La Boca; CC– Cañón Caballeros; CHP– Cañón Peregrina; CN– Cañón Novillo). b) Volcanics, n= 38 (VH– Valle de Huizachal; Ab– Aramberri; Mi– Miquihuana). 103

Fig. 5.6: Chondrite-normalized REE patterns. Upper pattern and calculations corresponds to Volcanics, n= 38 (VH– Valle de Huizachal; Ab– Aramberri; Mi– Miquihuana). Lower pattern and mean composition is for Clastics, n=82 (LSPT– Lomas de San Paulo Tranquitas; CA– Cañón El Alamar; COI– Cañón El Olmo; CB– Cañón La Boca; CC– Cañón Caballeros; CHP– Cañón Peregrina; CN– Cañón Novillo). HREE– La_N/Sm_N; LREE– Gd_N/Yb_N. 104

Fig. 5.7: SiO₂/Al₂O₃ vs. Na₂O/K₂O ratios of sandstones from clastics and volcanic datasets corresponding to the red bed in northeastern Mexico (after Pettjohn *et al.*, 1972). 105

Fig. 5.8: (Left) Geochemical classification for red beds in northeastern Mexico, classification after Nathan (1976) and Jenchen & Rosenfeld (2007). Significant negative correlation of Al₂O₃ and SiO₂. (Right) Recalculated values normalized to CaO_{tot} (wt %), notice a slight slipping of samples toward the increase of CaO_{tot}. Key for symbols is found at Fig. 5.7. 106

Fig. 5.9: K₂O/Na₂O ratios (after Pettjohn, 1963) for Clastics, n=82 (LSPT– Lomas de San Paulo Tranquitas; CA– Cañón El Alamar; COI– Cañón El Olmo; CB– Cañón La Boca; CC– Cañón Caballeros; CHP– Cañón Peregrina; CN– Cañón Novillo); and Volcanics, n= 38 (VH– Valle de Huizachal; Ab– Aramberri; Mi– Miquihuana). Key for symbols can be found at Fig. 5.7. 106

Fig. 5.10: (left) SiO₂ vs. K₂O/Na₂O ratio (Roser and Korsch, 1986) of Clastics, n=82 (LSPT– Lomas de San Paulo Tranquitas; CA– Cañón El Alamar; COI– Cañón El Olmo; CB– Cañón La Boca; CC– Cañón Caballeros; CHP– Cañón Peregrina; CN– Cañón Novillo); and Volcanics, n= 38 (VH– Valle de Huizachal; Ab– Aramberri; Mi– Miquihuana). (right) Recalculated values normalized to CaO_{tot} (wt %). Key for symbols can be found at Fig. 5.7. 107

Fig. 5.11: (log)SiO₂/K₂O vs. (linear)Ti/Nb ratios for the mean values of datasets: a) Clastics, n=82 (LSPT– Lomas de San Paulo Tranquitas; CA– Cañón El Alamar; COI– Cañón El Olmo; CB– Cañón La Boca; CC– Cañón Caballeros; CHP– Cañón Peregrina; CN– Cañón Novillo), and b) Volcanics, n= 38 (VH– Valle de Huizachal; Ab– Aramberri; Mi– Miquihuana). Confidence range plots are at 99.5%. Plot after Ocampo-Díaz and Jenchen (*submitted*). 108

Fig. 5.12: Ti/Nb ratio of investigated sections and formations and comparison with potential metamorphic and magmatic source rocks after Jenchen (1998). a) Clastics, n=82 (LSPT– Lomas de San Paulo Tranquitas; CA– Cañón El Alamar; COI– Cañón El Olmo; CB– Cañón La Boca; CC– Cañón Caballeros; CHP– Cañón Peregrina; CN– Cañón Novillo). b) Volcanics, n= 38 (VH– Valle de Huizachal; Ab– Aramberri; Mi– Miquihuana). Additional explanations for symbols of each locality see Fig. 5.7. Confidence range plots are at 99.5% 109

Fig. 5.13: Zr/Sc–Th/Sc ratios (McLennan *et al.*, 1993) of: a) Clastics, n=82 (LSPT– Lomas de San Paulo Tranquitas; CA– Cañón El Alamar; COI– Cañón El Olmo; CB– Cañón La Boca; CC– Cañón Caballeros; CHP– Cañón Peregrina; CN– Cañón Novillo). b) Volcanics, n= 38 (VH– Valle de Huizachal; Ab– Aramberri; Mi– Miquihuana). Additional explanations for symbols see Fig. 5.7. 109

Fig. 5.14: A comparison of the composition for the sediment in this study at different constructed fields for the La–Th–Sc ternary system. a) Original compositional diagram after Bhatia and Crook (1986). b) Modified version with fields for metamorphic sources after Cullers (1994). c) Volcanics, n= 38 (VH– Valle de Huizachal; Ab– Aramberri; Mi– Miquihuana). d) Clastics, n=82 (LSPT– Lomas de San Paulo Tranquitas; CA– Cañón El Alamar; COI– Cañón El Olmo; CB– Cañón La Boca; CC– Cañón Caballeros; CHP– Cañón Peregrina; CN– Cañón Novillo). Additional explanations for symbols of each locality see Fig. 5.7. Confidence range plots are at 99.5%. 110

Fig. 5.15: Al₂O₃–(Na₂O+CaO*)–K₂O diagram with the Chemical Index of Alteration (CIA) scale shown on the left (from McLennan and Murray, 1999). Note that weathering trends for the a) Clastics, n=82 (LSPT– Lomas de San Paulo Tranquitas; CA– Cañón El Alamar; COI– Cañón El Olmo; CB– Cañón La Boca; CC– Cañón Caballeros; CHP– Cañón Peregrina; CN– Cañón Novillo). b) Volcanics, n= 38 (VH– Valle de Huizachal; Ab– Aramberri; Mi– Miquihuana). Additional explanations for symbols of each locality see Fig. 5.7. Confidence range plots are at 99.5%. 113

Fig. 5.16: Weathering trends depicted on the MFW diagram (Ohta and Arai, 2007) for a) Clastics, n=82 (LSPT– Lomas de San Paulo Tranquitas; CA– Cañón El Alamar; COI– Cañón El Olmo; CB– Cañón La Boca; CC– Cañón Caballeros; CHP– Cañón Peregrina; CN– Cañón Novillo). b) Volcanics, n= 38 (VH– Valle de Huizachal; Ab– Aramberri; Mi– Miquihuana). Weathering trends of the Volcanics intersect with the igneous rock trend in the plot domain of rhyolite, granites, and dacite. Additional explanations for symbols of each locality see Fig. 5.7. 114

- Fig. 6.1: U-Pb concordia plots for detrital zircons from lower member of La Boca Formation (VH31-03 and VH31-02), upper member of La Boca Formation (VH31-06, VH31-08, and VH31-09), and La Joya Formation (VH31-10). Errors are shown at the one-sigma level for laser ablation–multicollector–inductively coupled plasma–mass spectrometry analyses (Rubio-Cisneros and Lawton, 2011). 117
- Fig. 6.2: Bedrock zircon sources in North America (modified from Dickinson and Gehrels, 2008). Shaded (yellow) section corresponds to the denominated Zone II: eastern Mexico (accreted Precambrian–Paleozoic) after the Terrane tectonostratigraphic zonation proposed by Campa and Coney, 1983. Red-shaded area denotes the Oaxaquia (ca. 1.0–1.2 Ga) basement at northeastern Mexico. Black dots are Oaxaquia /Chortis block exposures. Black triangles represent Early–Middle Jurassic sedimentary/igneous rocks. Filled black squares are Late Triassic sedimentary rocks. 118
- Fig. 6.3: Simplified lithostratigraphic column of La Boca and La Joya formations in Valle de Huizachal (modified by García-Obregón, 2007). Letters correspond to the stratigraphic levels documented in measured sections of Figures 2 and 6. Mu—mudstone; Sil—siltstone; SS—sandstone; P.Clg—polimitic conglomerate; V—volcanic rock (tuff); θ —dip of unconformity (Rubio-Cisneros and Lawton, 2011). 119
- Fig. 6.4: Age probability plots and histograms of detrital zircon ages from the lower member and upper member of La Boca Formation, and La Joya Formation. Each curve sums probability distributions from all of the grains analyzed for that sample. Histogram bin width equals 50 Ma. Vertical axis for each histogram is equal at 60-grain analyses. Some probability peaks that are unlabeled result from a single-grain analysis with low analytical error (Rubio-Cisneros and Lawton, 2011). 120
- Fig. 6.5: Pie charts for detrital zircons content from the four main group provenance in analyzed samples (Rubio-Cisneros and Lawton, 2010). 121
- Fig. 6.6: Binary diagram for U/Th and the age 206/238 (Ma). a) The two lower La Boca samples (empty circles– VH31-03, filled circles– VH31-02). b) The three upper La Boca samples (empty squares– VH31-06, empty rhomb– -08, and filled rhomb– -09). c) Sample from the base of La Joya Formation (filled triangles– VH31-10). 122
- Fig. 7.1: Ternary diagram QmFLt for tectonic environment (Dickinson *et al.*, 1983). Hexagonal fields of variation *versus* air-based regions (after Weltje 2002). Solid lines: predictive regions of population mean. Confidence limits are 90%, 95% and 99%. a) Hexagonal region constructed from intersections of univariate normal approximations; b) air-based regions transformed to ternary compositional space. Key for symbols for each studied area at Fig. 3.2. 124
- Fig. 7.2: QFL ternary diagram to discriminate tectonic environments of rift-type (after Garzanti *et al.*, 2001 and modified by Marsaglia *et al.* 2007). Polygons represent the arithmetic mean and standard deviation. Symbols represent the mean composition for each studied area (Fig. 3.2). 125
- Fig. 7.3: Binary diagrams confronting parameters; a) F/Qt vs. Qp/Qt [from Arribas *et al.*, 1990]; b) Ls/Qm vs. Lm/Lv; c) Ls/Qm vs. Qp/Qt (Rubio-Cisneros and Ocampo-Díaz, 2010). Huizachal Formation is referred to El Alamar Formation 126
- Fig. 7.4: Outline of possible source areas for Upper Triassic–Early to Middle Jurassic red beds on northeastern Mexico, including SeReIn values in relation to the unconformities and changes in sediment supply (after Rubio-Cisneros and Ocampo-Díaz, 2010). SeReIn– Sedimentary Recycling Index. 127
- Fig. 7.5: Ternary diagram that graphs the discriminant functions with the fields from the different obtained basin-types. Figure includes the petro-tectonic evolution of the clastic sequences (Late Triassic–Early Cretaceous) from northeastern Mexico (after Rubio-Cisneros and Ocampo-Díaz, *in review*). DF– Discriminant function. Huizachal Formation is referred to El Alamar Formation. 128
- Fig. 7.6: Based ZTR ternary systems and other heavy mineral content. a) after Garzanti *et al.*, 2008. b) after Dinis and Soares 2007. c) wo– wollastonite, sch– scheelite (after Augustsson, 2003). Other abbreviations are at Table 4.1. Key for symbols for each studied area at Fig. 3.2. 129
- Fig. 7.7: MF– (mafic magmatic rocks): ol, iddingsite, px, green-blue hb. MT– (mafic-metamorphic complexes): green-blue hb, ep, gr. GM– (granitoids and quartz-rich metamorphic complexes): zr, to, st, mo, ky, sil, and (after Zimmermann 1999). Key for symbols for each studied area at Fig. 3.2. 130
- Fig. 7.8: Tectonostratigraphic terranes from México (after Campa and Coney, 1983). 132
- Fig. 7.9: Middle America – periGondwana Terranes. Modified after Campa and Coney, 1983; Nance *et al.*, 2008; Keppie and Ortega, 2010. 132
- Fig. 7.10: Tectonomagmatic events plotted against age (modified after Ocampo-Díaz and Rubio-Cisneros, *in preparation*). Data represents a collection from various authors*. 133
- Fig. 7.11: Normalized relative age probability plots of U–Pb detrital zircon analyses from the Granjeno Schist of the Sierra Madre terrane (compiled data from Nance *et al.* 2007 and Barboza-Gudiño *et al.* 2011). VA–various authors. 133

- Fig. 7.12: Paleogeographic reconstruction for Mexico during the Late Triassic. Arrows indicate the possible sedimentary pathways and source areas with major detrital input from the Texas Uplift into the NL–Nuevo León vicinities. (after Dickinson and Gehrels, 2008; 2010). 138
- Fig. 7.13: Correlation table of key litho-stratigraphic columns with special emphasis on reported red beds in México (red frames), and the underlying Precambrian–Paleozoic crystalline basement with calculated ages. Data based on Centeno-García (2005), Lawton *et al.* (2010), and other various authors cited on this work. c.GM– circum Gulf of Mexico. Pattern fills are located at the Appendix for Pattern Fills. Colors are from International Stratigraphic Chart 2009. 139
- Fig. 7.14: Sedimentary framework yields as inferred from detrital modes and heavy mineral assemblages of the entire analyzed samples. The corresponding locality is in circled numbers. Bulk petrography explanation can be consulted on Chapter 4. Rank of metamorphic grains is explained on Chapter 4 (MI index; Garzanti and Vezzoli, 2003). Heavy Minerals indices abbreviations can be verified on Chapter 5. Pr– Precambrian; Pz– Paleozoic; TrsAl– Late Triassic El Alamar; TrsAlI– lower member of the Late Triassic El Alamar Formation; TrsAlS– upper member of the upper Triassic El Alamar Formation; JiLB– Early Jurassic La Boca Formation; JiLBi– lower member of the Early Jurassic La Boca Formation; JiLBS– upper member of the Early Jurassic La Boca Formation; JmLJ– Middle Jurassic La Joya Formation. 140
- Fig. 7.15: Pie charts for detrital zircons from Late Triassic sandstones data at Barboza- Gudiño *et al.*, 2010. RC– Real de Catorce. SM– San Marcos. CH– Charcas. LB– La Boca. 141
- Fig. 7.16: Ternary system QFL to discriminate tectonic environments within rift-type basins. After Garzanti *et al.* (2001) modified by Marsaglia *et al.* (2007). Polygons represent the standard deviation for each formation: Hz– Huizachal (referred to El Alamar Formation); LB– La Boca; LJ– La Joya; LC– La Casita; Ts– Taraises. Data representation after Rubio-Cisneros and Ocampo-Díaz (2010) and Ocampo-Díaz and Rubio-Cisneros (*submitted*) 141
- Fig. 7.17: Sketch for El Alamar Formation depositional environment, with its probable source rocks. Fluvial styles are oriented according the measured paleocurrents. Subsurface interpretations include the interpreted fluvial-architectural design, and the underlying units from the Precambrian– Paleozoic crystalline basement. Rock-type pattern fills are in Appendix. 142
- Fig. 7.18: (A) Tectonic reconstruction by Early Jurassic time. Rocks of Triassic submarine fan and Triassic ocean basin were accreted toward continental margin. (B) After collision of Arteaga basin, arc magmatism was widespread in Zihuatanejo, Central, and Sierra Madre terranes. Abbreviations of names for terranes after Centeno-García *et al.*, 2005. 143
- Fig. 7.19: Compiled geological elements interpreted for the Early–Middle Jurassic depositional environments, adapted from Campa and Coney (1983), Centeno-García (2005), Anderson *et al.* (2005), García-Díaz (2004), and Mickus *et al.* (2009). Notice the black polygons that represent Jurassic outcrops. Borderline RIFT system is now considered Border Rift System to avoid confusion with Cenozoic California Borderland province related to strike-slip faulting. Border Rift System is defined by siliciclastic. 144
- Fig. 7.20: U-Pb age probability plots and pie charts for the main group of detrital zircons in the Todos Santos Formation (Godínez-Urban, 2009; Godínez-Urban *et al.* 2011a and Lawton *et al.*, 2010). Pattern fills can be consulted at Fig. 7.15. 145
- Fig. 7.21: Sketch for La Boca Formation depositional environment, with its probable source rocks. Fluvial styles are oriented according the measured paleocurrents. Subsurface interpretations include the interpreted fluvial-architectural design, and the subsequent underlying depositional sequences form El Alamar Formation, and the Paleozoic–Precambrian crystalline basement. Rock-type pattern fills are in caption for Fig. 7.17. 146
- Fig. 7.22: Early Mesozoic tectonic map of southwest Laurentia (after Mickus *et al.*, 2009). Borderlands rift system is now considered Border Rift System to avoid confusion with Cenozoic California Borderland province related to strike-slip faulting. Border Rift System is defined by siliciclastic. Buried and partially exposed uplifts of interest: WU– Wiggins Uplift, LU– Llano Uplift. COB– Continent-ocean boundary. 146
- Fig. 7.23: Youngest U-Pb detrital zircon ages and tectonomagmatic events from for correlated red beds at different localities in México. Notice the volcanic age variability. Sketch adapted from Lawton *et al.*, 2010. Plotted data form: a– Barboza-Gudiño *et al.* (2010), b– Rubio-Cisneros and Lawton (2011); Lawton *et al.* (2010), and c– Godínez-Urban *et al.* (2011a); Lawton *et al.* (2010). SLP– San Luis Potosí; c.GM–circum Gulf of Mexico 148
- Fig. 7.24: Sketch for La Joya Formation alluvial fan with its fluvial style depositional environments and its most probable source rocks. Fluvial styles are oriented according the measured paleocurrents. Subsurface interpretations include the interpreted fluvial-architectural design, and the subsequent underlying depositional sequences form La Boca and El Alamar formations, and the Paleozoic–Precambrian crystalline basement. Rock-type pattern fills are in Fig. 7.17. 149
- Fig. 7.25: Geotectonic reconstruction of Mexico from Middle Jurassic time (164 Ma, base of the Callovian) to the Jurassic–Cretaceous time boundary (144 Ma). Euler pole for Yucatán (Yuc) rotation (anticlockwise) with respect to North America (NA) after Marton and Buffler (1994). South of migratory triple junction, solid barbs are on overriding plate of Guerrero intraoceanic island-arc complex, and open barbs are on dormant continental-margin subduction zone (subducted slab rolling back to induce intra-arc rifting within continental margin). Abbreviations: B–Bisbee basin, C–Chihuahua trough, Cab–Caborca block, Coa–Coahuila block, DS–Del Sur block, G–Guajira Peninsula, J/C–Juarez/ Cuicateco terrane, M–

McCoy basin, MC–Mesa Central subduction complex, P–Península de Paria, RGE–Rio Grande embayment, Tam–Tampico block, Yuc–Chi–Yucatán–Chiapas block. From Dickinson and Lawton, 2001). 151

List of Tables

Table 2.1: Table summarizing the main facies, lithofacies and facies associations identified in the Huizachal Group for northeastern Mexico, with their corresponding interpretations.	22
Table 2.2: Fluvial facies summary for applied interpretations in bedding diagram built-up (Holbrook, personal communication).	48
Table 2.3: Bounding surfaces hierarchy and descriptions used in this study.	48
Table 3.1: Compositional variables and ternary systems referred to in this study.	65
Table 3.2: Mean values and numerical relations for the compositional parameters in each used ternary diagram for source area and tectonic environment interpretations. n– number of samples used to calculate the corresponding [sub]petrofacies. Std. Dev– Standard Deviation.	69
Table 4.1: Key indices used for a synthetic representation of heavy mineral assemblages (after Garzanti and Andò, 2007).	80
Table 5.1: Chemical composition: a) Clastics: LSPT– Lomas de San Paulo Tranquitas; CA– Cañón El Alamar; COI– Cañón El Olmo; CB– Cañón La Boca; CC– Cañón Caballeros; CHP– Cañón Peregrina; CN– Cañón Novillo). b) Volcanics: VH– Valle de Huizachal; Ab– Aramberri; Mi– Miquihuana. n– number of analyzed samples. For the complete dataset, visit the Appendix for Chapter 5.	93
Table 5.2: Correlation matrix of major elements at 95% of confidence (highlighted) for two calculated datasets. a) Clastics, n=82 (LSPT– Lomas de San Paulo Tranquitas; CA– Cañón El Alamar; COI– Cañón El Olmo; CB– Cañón La Boca; CC– Cañón Caballeros; CHP– Cañón Peregrina; CN– Cañón Novillo). b) Volcanics, n= 38 (VH– Valle de Huizachal; Ab– Aramberri; Mi– Miquihuana).	95
Table 5.3: Geochemical cluster correlation matrices between major elements with the 99.5% of confidence (highlighted). a) Clastics, n=82 (LSPT– Lomas de San Paulo Tranquitas; CA– Cañón El Alamar; COI– Cañón El Olmo; CB– Cañón La Boca; CC– Cañón Caballeros; CHP– Cañón Peregrina; CN– Cañón Novillo). b) Volcanics, n= 38 (VH– Valle de Huizachal; Ab– Aramberri; Mi– Miquihuana).	97
Table 5.4: Four main factors analysis results for the principal components analysis required for constructing the projection of the variables on a factor-plane (Fig. 5.3; Table 5.3; Appendix for Chapter 5). Tables a, b, and c, contain representative datasets for this work (LSPT– Lomas de San Paulo Tranquitas; CA– Cañón El Alamar; COI– Cañón El Olmo; CB– Cañón La Boca; CC– Cañón Caballeros; CHP– Cañón Peregrina; CN– Cañón Novillo); VH– Valle de Huizachal; Ab– Aramberri; Mi– Miquihuana; NG– Novillo Gneiss; GS– Granjeno Schist. Data on tables d)– (Lopez <i>et al.</i> , 2001), e)– (Lopez <i>et al.</i> , 2001), and f)– (Barboza-Gudiño <i>et al.</i> 2008, 2010; García-Obregón, 2007), represent compiled geochemical sets.	99
Table 5.5: Correlation matrices for major elements vs. trace elements and REE. Values are with the 99.5% of confidence (highlighted). a) Clastics, n=82 (LSPT– Lomas de San Paulo Tranquitas; CA– Cañón El Alamar; COI– Cañón El Olmo; CB– Cañón La Boca; CC– Cañón Caballeros; CHP– Cañón Peregrina; CN– Cañón Novillo). b) Volcanics, n= 38 (VH– Valle de Huizachal; Ab– Aramberri; Mi– Miquihuana).	102
Table 5.6: Weathering indices mean values with their standard deviation (Std. Dev) for samples from a) Clastics, n=82 (LSPT– Lomas de San Paulo Tranquitas; CA– Cañón El Alamar; COI– Cañón El Olmo; CB– Cañón La Boca; CC– Cañón Caballeros; CHP– Cañón Peregrina; CN– Cañón Novillo). b) Volcanics, n= 38 (VH– Valle de Huizachal; Ab– Aramberri; Mi– Miquihuana). CIA–Chemical Index of Alteration; M– Mafic; F– Felsic; W– Weathering.	112
Table 5.7: Correlation matrices for CIA, and key major and trace element ratios. All values are at 99.5% of confidence (highlighted). a) Clastics, n=82 (LSPT– Lomas de San Paulo Tranquitas; CA– Cañón El Alamar; COI– Cañón El Olmo; CB– Cañón La Boca; CC– Cañón Caballeros; CHP– Cañón Peregrina; CN– Cañón Novillo). b) Volcanics, n= 38 (VH– Valle de Huizachal; Ab– Aramberri; Mi– Miquihuana).	112
Table 6.1: Young grain ages of Huizachal Group detrital samples (datasets at Rubio-Cisneros and Lawton, 2011: http://geosphere.gsapubs.org/content/7/1/159/suppl/DC1).	118
Table 6.2: U/Th ratios, percentages, and grain participation of Huizachal Group detrital samples	121

PREFACE

From the *praxis* to the reconstruction. This thesis involves a series of methodological steps that encounter a common starting point structured by a sedimentological-stratigraphical perspective, which concerns rock sampling and petrography analysis, among other more elaborated measurements for a better understanding of a geological system. This work contributes not only to solve issues over a specific geologic time, but enables to project knowledge into the future.

Energy transfer from within the earth to its surface and from the sun to the Earth drives the process of magmatism, tectonism, and the interactions between the lithosphere, atmosphere, hydrosphere, and biosphere, which collectively control the composition of sands and sandstones.

The outline of ideas about sandstone provenance studies has varied through out time, related to the emergence and development of the human working forces with the arrival of constant new technologies, to clarify a synergic living Earth. The concept of this genetic and dialectic objective relies within this thesis to partially uncap some infinite complex interrelated events>factors>controllers.

The logical sequence achieved by rock sampling and microscopic analysis contributes to the Big History of sandstones, constitute fundamental elements for a heuristic reasoning that breed into more interpretations about geodynamic phenomena, crustal processes at different scales, to solve provenance and geogenetic intentions, and to restore stage by stage the history of tectonic reorganizations.

As we further integrate basin analysis with detailed sedimentary petrography from both light and heavy minerals, geochemical, radiogenic isotope studies, and the distribution of key elements and factors controlling sediment genesis, no doubt our understanding of Earth and our requirements to live will increase our human capabilities. Developments that are still more fruitful will emerge to speak about in the years to come.

ABSTRACT

In the northeastern Sierra Madre Oriental of Mexico, red beds of the Mesozoic form the Huizachal Group overlie the Precambrian–Paleozoic crystalline basement. The group includes El Alamar, La Boca, and La Joya Formations and records the beginning of a major tectono-sedimentary cycle that extended from Upper Triassic to Middle–Late Jurassic.

Progress is hindered by a provenance scope of the genetic problems, by the spatial-temporal scale and complexities of the controlling factors for the red bed evolution close to the convergence of petrotectonic sets near the Western Equatorial Margin of Pangea.

Facies of the continental depositional environments are restricted to gravel- and sand-dominated rivers of high and low sinuosity characteristics. Fluvial styles oscillate from mix-energy to low- and high-energy systems that transport fluvial products from basement highs on the east, with the formation of sedimentary gravity flows and gravel bed bars. Sediments were shed to the depositional sites from the southernmost termination escarpment of the Texas Uplift and the west footwall of what are now the Huizachal-Peregrina Anticlinorium and the interpreted position of the Tamaulipas Arc.

Fluvial effects like amalgamation, aggradation, degradation, and flooding were interpreted by surface architecture using bounding surfaces. Low accommodation/supply processes stack fluvial elements one another into high subsidence rates. High accommodation/supply processes controlled flooding environments and conditioned sediment dispersion for low suspended load fluvial styles.

Petrofacies defined from detrital modes suggest compositions defined from (1) metapelite metapsammite/metafelsite, and metabasite sources, and (2) volcanic successions with felsic, basic, and plutonic/granitic signatures. Heavy mineral indices include (i) low- to high-grade metamorphic source rocks (LgM, Gt, HgM), (ii) a subsequent input from amphiboles (Hb, &A), pyroxenes (CPX, OPX), olivine, and spinel (OS) by the rejuvenation of intermediate and mafic source rocks; and (iii) sedimentary and felsic igneous source rocks shed ultra stable heavy minerals (ZTR).

Petrography discriminates the onset for different extensional processes in the basin starting with (1) an undissected rift (suture/orogen) with an amagmatic paradox lithospheric thinning and break up of basement massifs, (2) a subsequent extensional back arc, and (3) a final stage of tectonic reactivation with exhumation and unroofing of the underlying strata.

Whole-rock geochemistry depends on the sediment classification from the mixture of detritus of high- to low-grade metamorphic, dominant intermediate–felsitic volcanic, and minor constituents form a plutonic provenance, albeit in different proportions for sedimentary recycling, mineral fractionation, and weathering. Material from magmatic sources dominates the sediments of La Boca. Outcrops with volcanic affinity present REE concentrations controlled by mineral reemplacements. Some measured sections show an upsection source area transition as volcanic < metamorphic.

U-Pb detrital-zircon ages for La Boca and La Joya formations include four age groups: (1) Grenville grains (~1.3–1.0 Ga) derived from Oaxaquia (Novillo Gneiss); (2) early–middle Paleozoic grains (430–300 Ma) derived from peri-Gondwanan accreted rocks (Granjeno Schist, tonalite, and Asseradero Rhyolite); (3) Permian–Triassic grains (296–222 Ma) derived from volcanic and plutonic rocks (West Pangaeon arc); and (4) Early–Middle Jurassic grains (199–164 Ma), locally derived from the Nazas arc. Groups 1–3 increase in abundance upsection by the unroofing of Jurassic volcanic and sedimentary carapace from uplifted basement. Age measurements constrain the maximum depositional age for La Boca Formation at 184–183 Ma of its lower part and for its upper part 167–163 Ma. The position for La Joya Formation between Bathonian–Callovian red beds and overlying Oxfordian strata is consistent with a Callovian age indicated by young grain ages of 164 ± 3 Ma. Other isolated basement massifs related to tectonomagmatic events in the interior part of Oaxaquia were probably also important sources for the Huizachal Group.

The complex physical-chemical sedimentary system of the Huizachal Group depended on source-area distribution that relates to the litho-tectonic evolution of basement, extensional loci, transfer zones, juxtaposition of volcanic successions, and the geology of fluvial styles

RESUMEN

En la Sierra Madre Oriental en el noreste de México, lechos rojos del Mesozoico del Grupo Huizachal sobreyacen el basamento cristalino del Precámbrico–Paleozoico. El grupo incluye las formaciones El Alamar, La Boca y La Joya y registra el inicio de un gran ciclo tectono-sedimentario desde el Triásico superior al Jurásico medio–tardío.

El progreso se ve obstaculizado por el ámbito de procedencia de los problemas genéticos, por la escala espacio-temporal y la complejidad de los factores que controlan la evolución de los lechos rojos próximos a la convergencia de conjuntos petrotectónicos cerca del margen ecuatorial occidental de Pangea.

El análisis de facies de los sistemas deposicionales continentales está restringido a ríos de alta y baja sinuosidad dominados por gravas y arenas. Los estilos fluviales oscilan entre sistemas de mezcla, de baja y alta energía que transportan productos fluviales desde los altos de basamentos situados en el este, con la formación de flujos de masas por gravedad y barras de gravas. Los sedimentos fueron distribuidos a los sitios de depósito desde la terminación sur del escarpe de Texas y al oeste del límite base de lo que ahora es el Antilinario Huizachal-Peregrina y la interpretación de la posición del Arco de Tamaulipas.

Los efectos fluviales como amalgamación, agradación, degradación e inundación fueron interpretados por la arquitectura de superficies utilizando superficies delimitadoras. Los procesos de bajo aporte/acomodación apilan elementos fluviales para dar altas tasas de subsidencia. Los procesos de alto aporte/acomodación controlan a los ambientes de inundación y condicionan la dispersión de sedimentos en estilos fluviales de baja carga en suspensión.

Las petrofacies definidas por los modos detríticos sugieren composiciones relacionadas a fuentes (1) metapelíticas, metapsamíticas/metafelsíticas y metabásicas, y (2) sucesiones volcánicas con firmas félsicas, básicas, plutónicas y graníticas. Los índices de minerales pesados incluyen (i) rocas fuentes metamórficas de bajo-alto grado (LgM, Gt, HgM); (ii) un subsecuente aporte de anfíboles (Hb, &A), piroxenos (CPX, OPX), olivino y epinela (OS) por el rejuvenecimiento de rocas fuente intermedias y máficas; y (iii) rocas fuentes sedimentarias e ígneas félsicas que contribuyen con minerales pesados ultra estables (ZTR).

La petrografía discrimina el comienzo de diferentes procesos extensionales en la cuenca iniciando con (a) un rift no disectado (sutura/orógeno) con un adelgazamiento cortical a-magmático y el rompimiento de los macizos del basamento; (2) una subsecuente cuenca del tipo tras arco extensional; y (3) una etapa final de reactivación tectónica con la exhumación y exposición de la secuencia subyacente.

La geoquímica de roca total depende de la clasificación del sedimento, la mezcla de detritus de alto a bajo grado metamórfico, la dominancia de rocas volcánicas intermedias-felscas, y de los pocos constituyentes de procedencia plutónica; aunque en diferentes proporciones de reciclamiento sedimentario, fraccionación mineral e intemperismo. El material de las fuentes magmáticas domina a los sedimentos de la Formación La Boca. Los afloramientos con afinidades volcánicas presentan concentraciones de REE controladas por el reemplazamiento de minerales. Algunas secciones medidas muestran áreas fuentes características de transición como volcánica < metamórfica.

Las edades U-Pb en circones detríticos para las Formaciones La Boca y La Joya proceden de cuatro grupos de edades: granos Grenvillianos (~1.3–1.0) derivados de Gondwana (Gneiss Novillo); granos del Paleozoico temprano-medio (430–300 Ma) derivados de rocas acresionadas peri-Gondwanicas (Esquisto Granjeno; tonalita y Riolita Aseradero); (3) granos Permico-Triásicos (296–222 Ma) procedentes de rocas volcánicas y plutónicas (Arco del oeste de Pangea); y (4) granos del Jurásico Temprano-Medio (199–164 Ma), derivados localmente del arco Nazas. Los grupos 1–3 incrementan en abundancia hacia la cima de la sección por la exposición de la cubierta de rocas volcánicas y sedimentarias del Jurásico de bloques levantados. Las mediciones de la edad constriñen la edad máxima de depósito para la Formación La Boca de 184–183 Ma en parte inferior y 167–163 Ma en su parte superior. La posición de la Formación La Joya entre los lechos rojos del Bathonian-Caloviano y estratos subyacentes del Oxfordiano es consistente con una edad del Calloviano indicado por las edades más jóvenes en granos de 164 ± 3 Ma. Otros macizos aislados del basamento relacionados con eventos tectonomagmáticos en el interior de Oaxaquia también pudieron ser fuentes importantes para el Grupo Huizachal.

El complejo sistema físico-químico y sedimentario del Grupo Huizachal depende de la distribución de las áreas fuentes que está relacionada con la evolución litotectónica del basamento, extensión local, zonas de transferencia, yuxtaposición de las sucesiones volcánicas y de la geología de los estilos fluviales.

1. INTRODUCTION: RED BEDS AND RELATED TECTONO-SEDIMENTARY ASPECTS

1.1. Red Beds

A red bed can informally be denominated to every red colored cataloged deposit, with physical and/or diagenetic characteristics, which favored a red pigmentation by the content of hematite (Clark, 1962; Turner, 1980). This definition is similar to the one made by Pettijohn *et al.* (1972) and Stow (2006), for red sandstones or siltstones.

Red beds (*Rotschichten; Variegated-interbedded red and non-red layers and lenses: cf., van Houten, 1973; Bates and Jackson, 1987*) are sedimentary continental facies from alluvial, fluvial (including paleosols), deltaic, and desertic environments, which poses a diagenetic suite with magnetic properties. Their optical characteristics have intrigued scientists for almost a century (Henning, 1913; Krynine, 1949). The pigment hosted in grains, pores and matrix varies according to the iron hydroxides enrichment on claystones and siltstones and/or the content of hematite (van Houten, 1973; Morton and Hallsworth, 1999). There exists a relationship between the depositional environment, weathering, and diagenesis (Henning, 1914; Dorsey, 1926; Krynine, 1949; Robb, 1947; Walker *et al.*, 1978; Berner, 1969; Schmidt and Embleton, 1976; Folk, 1976; Walker, 1967, 1978; Turner, 1980).

Other meanings have described red beds genetic relationship to highly oxygenated deep-sea environments. Nevertheless, this work does not sympathize with definitions in correspondence to red beds in continental environments.

Red beds record the embryonic evolution of a sedimentary cycle on a basin in response to specific tectonic activity. The evolving tectonic stages are characterized by two initial lapses from the Wilson Cycle, the 1) rifting– with lithospheric attenuation→extension→cortical breakup, and basin fill of the rift, and the 2) drifting– with reactivation of the structural elements, ocean floor generation and dispersion (Krabbendam, 2001).

The most important variables that control red beds deposit are the nature and geotectonic position of the basin determined by the mechanisms of sedimentary basin (van Millot, 1970; van Houten 1973; Prosser, 1993; Fulford and Busby, 1999; Karner *et al.*, 2004; Allen and Allen, 2005). Red beds are restricted to the tectonic setting category of extensional basins (Drake, 1972; Ingersoll and Busby, 1995). They occur in tectonic environments of intracontinental rift systems (including aulacogens, Dickinson, 1974; Frostick and Reid, 1987; Shepard, 1986; Robert, 2008; Christian, 2008), transform systems (strike-slip basins), and transtensional settings or pull-apart basins (Zuffa *et al.*, 1980; Ballance, 1980; Frostick, 1986; Mastalerz and Wojedowa, 1993; Wilson *et al.*, 2001; Willan and Hunter, 2005).

1.2. Basin-types for red beds

Sedimentary deposits at extensional systems are characterized by the initial mechanism of multiphase reactivation of faults that allow different stages, types, and styles of erosion, redistribution, and dispersion of sediments into the basin. These processes start by the erosion of the carapace from preexisting sediments, the underlying basement, and finally an internal recycling of the deposit (Contreras and Scholz, 2001; Trudgill and Underhill, 2002; McLeod *et al.*, 2002). A sedimentary provenance analysis on red beds discloses the evolution of the operating systems, but also determines the composition of the sandstones, and respective source areas.

Tectonic activity in extensional basins is considered as the main controlling factor of sedimentation (Prosser, 1993). The basin fill for these basin systems is generally contributed by eroded material from flanking highs bordering the depocenter. The sediment generation is the result of the continuously lithospheric extension and crustal block rising associated with fault reanudation.

Particularly, the first stage of the rift and pull-apart basins starts with the erosion of the preexistent sedimentary cover and in lesser extent the rocks that constitute the basement (volcanic rifted-margin provenance to rift-shoulder provenance; Garzanti *et al.*, 2003). The subsequent stages involve deep erosion of the basement units and the internal recycling of formations during the deposit.

1.3. Provenance analysis

The conjunction between sedimentary geological subdisciplines like stratigraphic-sedimentological and provenance analysis is helpful for paleogeographic and tectonic reconstructions. The evolution of extensional basins may be precluded by sedimentary provenance analysis for sediment genesis, including the related compositional print from the underlying basement blocks (Johnson, 1993; Caracciolo and Critelli, 2010; Zuffa and Critelli, 2010). The identification of source areas arises as a sensitive result upon the classification for sandstones composition by using petrofacies, which serves to define depositional sequences (Blatt *et al.*, 1972; Dickinson, 1970; Pettijohn *et al.*, 1972; Dickinson *et al.*, 1983; Ingersoll, 1983; Zaghoul *et al.*, 2010).

Zuffa and Critelli (2010) suggest that source area controls and dispersal pathways are reflected in siliciclastic sediments/rock compositions. They are influenced by many factors: →source area composition, →relief, →basin morphology, →climate, and →diagenesis (Blatt, 1967a; Suttner *et al.*, 1981; Ricci-Lucchi, 1985; Johnson, 1993; Cox and Low, 1995). In addition, the tectonic environment may be constrained by the compositional signatures in sandstones (Dickinson and Suczek, 1979; Dickinson *et al.*, 1983; Mack, 1984; Valloni, 1985).

Many publications have contributed to characterize sandstones composition (Hiscott, 1978, DeCelles and Hertel, 1989; Critelli and Le Pera, 1994; Critelli, 1999), by the use of tectonic settings on compositional ternary diagrams according to Dickinson *et al.* (1983). Others have intended to categorize sandstones by relating their principal components with basin-types on distinctive tectonic settings (Ingersoll and Suczek, 1979; Marsaglia and Ingersoll, 1992; Garzanti *et al.*, 2003). While others have documented provenance analysis for extensional

systems, including rift and pull-apart basins (Dickinson, 1985; Zuffa *et al.*, 1980; Ingersoll, 1990; Marsaglia, 1991; Garzanti *et al.*, 2001; Jenchen, 2001, Jenchen and Rosenfeld, 2002; Critelli *et al.*, 2002; Arribas *et al.*, 2003; González-Acebrón *et al.*, 2007; Caja *et al.*, 2007; Marsaglia *et al.*, 2007).

Despite the structural importance of margins, many of the systematic for sedimentary geology of red beds, including the processes (factors and effects) for sediment genesis (sedimentary pathways or sediment routing systems) that shape them, are poorly understood.

1.4. Tectonics coupled to the sedimentary geology of red beds: methodological implications

Tectonics as a sedimentary control involves the structural characteristics of the basin and the connection between stratigraphic and structural events (Fig. 1.1). The geotectonic environment determines the structural, stratigraphic, and sedimentological style. The description of depositional systems according to facies, architectural elements, structural geology, petrology, and tectonic environments led to a series of basin models. The purpose of these models is to interpret any sedimentary basin by implementing prototectonic assemblages or sets (Coney *et al.*, 1980; Miall, 2005; Dickinson, 1980, 1981).

The methods carried in terrane stratigraphy, tectonostratigraphy or stratotectonics aims for a stratigraphic analysis by a practical use of prototectonic units, which remain attached to the concept of tectonostratigraphic units (Longoria, 1993; Coombs, 1997; Vaughan *et al.*, 2005). The conceptual units diversify a terrane into: prototectonic sets (basal or overlying; Campa, 1981), lithic characteristics (e.g., Restrepo-Pace, 1992; Dickinson, 1971a,b), paleogeographic domains, the relationship between the sets (e.g., suspect, accretion: by contact or juxtaposition; Schermer *et al.*, 1984; Scholl *et al.*, 1986), drift affinity nomenclature (accretion or transpressive), and finally by stratigraphic characteristics (tectonostratigraphic or lithotectonic).

Plate-tectonics on Earth is governed by slab-pull and ridge-push that function from the generation, conduction/convection of the lithosphere by the loss of radiogenic heat on the planet (von Huene and Scholl, 1991; Stock and Lee, 1994; Rogers 1996; Condie 2007; Dewey, 2007; Hatcher *et al.*, 2007; Scholl and von Huene, 2007). Another heat loss mechanism is by the formation of igneous provinces, which are the crustal expressions of mantle plumes.

Regarding the evolution of the planet, there is little uncertainty that a style of secular tectonic evolution took place in the history of the Earth (Dewey and Spall, 1975). These secular tendencies were interrupted by episodic, and possibly periodic events. The assemblage, fragmentation, and dispersion of at least three supercontinents during the Proterozoic–Phanerozoic left planetary tectonics conducted by cyclicity of structural, sedimentary, igneous, metamorphic and climatic events/periods (Dewey 1988). This cyclicity is summarized on the Wilson cycle with the opening and closure of an ocean (Dewey, 2007). This is fundamental to comprehend the time line division for the Earth's history according to eons and other important tectonomagmatic events that serve as identifiable stages on the continental crust (breakup, introversion, extroversion, combination; Murphy and Nance, 2005; Santosh *et al.*, 2009).

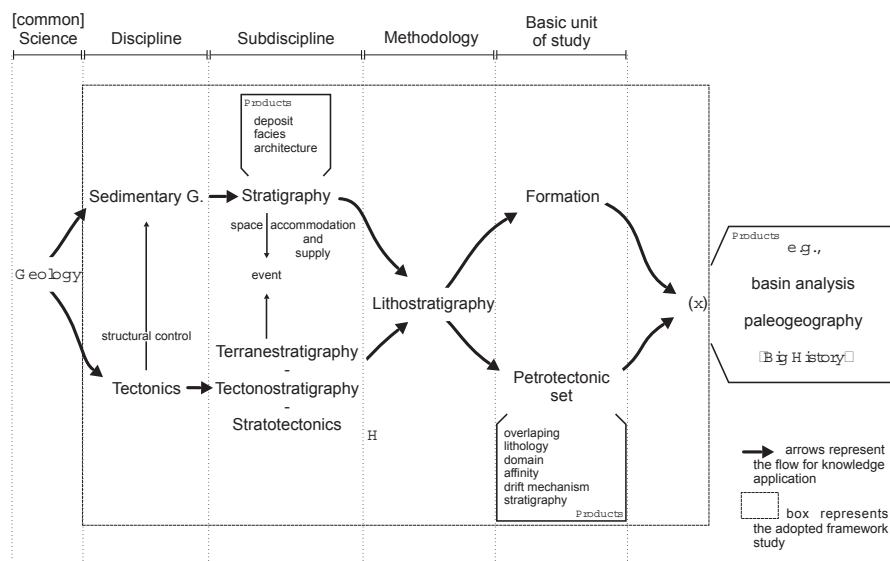


Fig. 1.1: Methodological chart for the integration between the discipline of Sedimentary Geology and Tectonics. Big History, *cf.*, Alvarez, 2010

1.5. Northeastern Mexico

Northeastern Mexico is characterized by a poorly exposed heterogeneous Precambrian–Paleozoic basement configuration. The underlying basement units are assumed to have controlled the subsequent Mesozoic sedimentary environments, and the development of their equivalent depositional sequences. The direct overlying sedimentary rocks on top of the crystalline basement represent the main basin fill record for Upper Triassic to Middle Jurassic. This sequence sustains a fundamental basin fill pattern derived from basement units, underlying and contemporaneous strata that includes volcanic successions, which extends from Monterrey–Galeana in Nuevo León to Miquihuana in Tamaulipas (Fig. 1.2). Red beds are considered as part of a rift–drift evolution associated with the *modus* of break up of Pangea and related paleo–Pacific volcanic activity (Michalzik, 1988; Freydier *et al.*, 1997). Within these localities, the Huizachal Group, composed El Alamar (Late Triassic), La Boca (Early Jurassic), and La Joya (Middle Jurassic) formations, crops out.

This study documents the sedimentary environment, composition, and source area localization that gave ride to the clastic sequences that crop out on the eastern border of the Oaxaquia basement exposures (Huizachal-Peregrina Anticlinorium) and/or the flanking depocenters at the western part of the Tamaulipas Arc. The work integrates a detailed analysis consisting of stratigraphic–sedimentological, petrographic aspects (light and heavy minerals), whole-rock geochemistry, and radiogenic isotopes of detrital zircons.

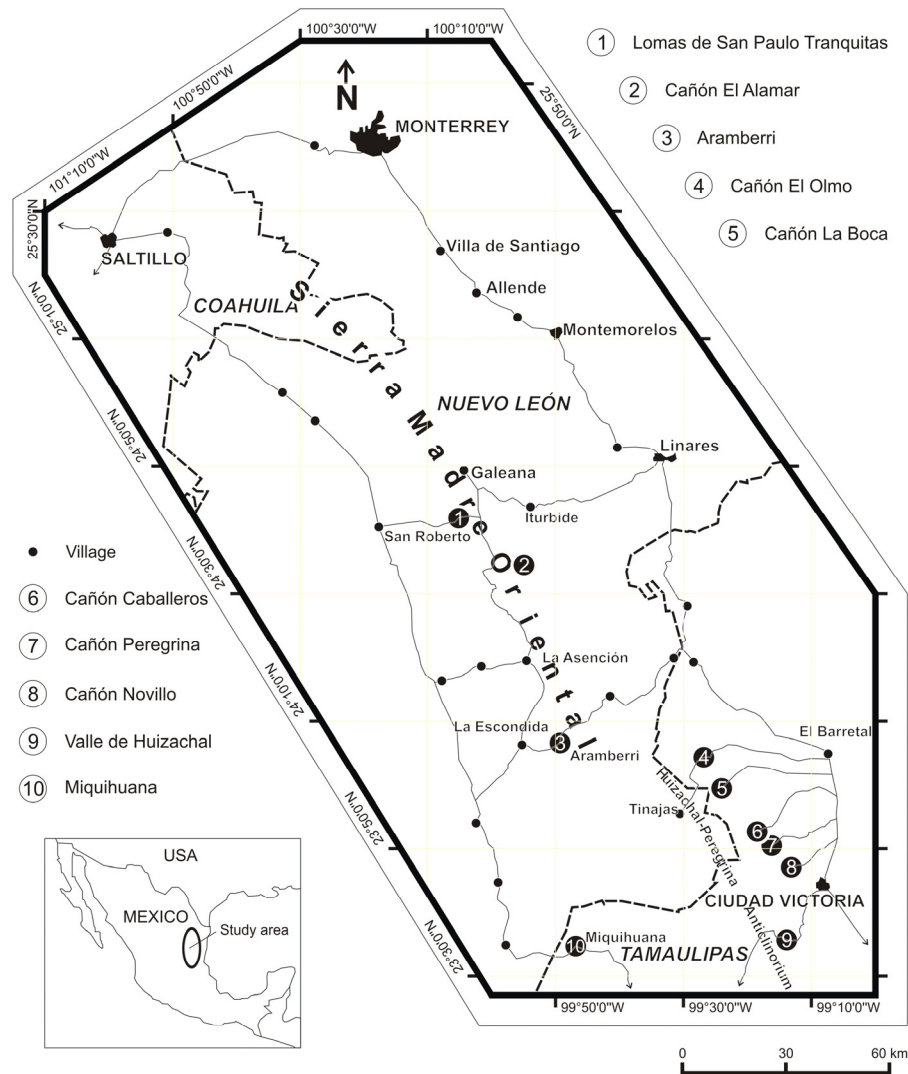


Fig. 1.2: Locality of the studied area. The numbers in circles represent each of the ten studied localities.

1.5.1. The basement as basic control on red beds generation in northeastern Mexico

The underlying basement in northeastern Mexico records a peculiar history that has been only partially defined. Its position at Middle–Late Triassic was a result of a complex systematic tectonic interaction of processes identified by discrete orogenic events: starting during Precambrian time with the Grenville Orogeny (~1.4 Ga), and followed by Rodinia assembly (~800 Ma), Pan-African-Brazilian orogeny (~650), a Silurian–Devonian arc (~470), related tectonomagmatic Rheic events (~370), and a Permian–Triassic arc (~240). This discrete series of events leads to a key idea for the possible mechanism for the development of accommodation (Allen and Allen, 1990) needed for the availability of space for sediment accumulation during the Mesozoic. It also serves to identify other controlling factors affecting sediment genesis.

The Mesozoic successions and their “process stratigraphy” (*cf.*, Allen and Allen, 1990), were undertaken by the subsequent historical event scenario related to Pangea’s breakup, which denotes the production of

extensional basin(s) and continental basin fills. By the Late Triassic, the rift stage marks an extensional regime in the proto-Gulf of Mexico, and possibly a strike-slip kinematic style in northeastern Mexico (Ocampo-Díaz, 2008). The Lower Jurassic records other processes, products, and successions attributed to volcanism that contributed to other basin panorama with stratigraphy unlike to Upper Triassic. The Middle Jurassic stands for drift to passive margin environments related to lateral displacements resulted from oblique subduction at the Pacific margin (Salvador, 1987; Marton and Buffler, 1994; Haenggi and Muehlberger, 2005).

Until now, some contributions have precluded a better interpretation of the Mesozoic red beds at the northeastern Mexico. Moreover, the most recent findings lack of a detailed distiller analysis of the controlling-factors for the red-beds genesis. The main available factors to be assert are controlled by provenance i.e. the location and nature of source area, the pathways by which sediment is transferred from source to basin of deposition, and other pre-depositional and pre-burial factors that influence the composition of sedimentary siliciclastic rocks (e.g., relief and tectonic setting).

If red beds were considered only as a sandstones with dun or red color for the strata in northeastern of Mexico this would include all the Mesozoic clastic strata deposited between 251–65.5 Ma; including for example the La Casita Formation (Imlay, 1936, Michalzik, 1988; Michalzik and Schumann, 1994), and the Galeana Sandstone Member of the Taraises Formation (Michalzik, 1988, Ocampo-Díaz, 2008; Ocampo-Díaz, 2011). By including those units the purpose for the actual research will be inadequate to satisfy the official term. Therefore red beds must be adapted to our time and necessities to perform as a solution for the occurrence of continental red beds linked to continental (Pangea) rupture and the tectonic mechanisms involved during their genesis.

The interpretative approximations encounter a general hypothesis by describing sedimentological characteristics (fluvial–alluvial), depositional environments, tectonic setting, and source area. Some previous geotectonic models have been proposed for continental arc and continental rift (grabens and half grabens), by Michalzik (1991), Jones *et al.* (1995), Bartolini *et al.* (2003), García-Díaz (2004), Molina-Garza and Iriondo (2005), and Barboza-Gudiño *et al.* (2008). This work goes straightforward to identify (1) exogene crustal evolution and nature of regional uplift; (2) quantitative contributions from different source bedrock-types; (3) analysis of depositional systems; (4) sediment recycling; (5) petrofacies characterization.

The methodologies contained in this work examine the results for a detailed contemporary resolution about the main controlling factors from each geotectonic environment that conditioned genetic designations for the red beds.

This work integrates various types of studies used in research (Dankhe, 1986). The study is divided as: exploratory, descriptive, correlational, and explicative or experimental. The uncertainties between the relationships in variables are supported by the use of organized and systematized knowledge that may be considered throughout the work as a correlative, differential, or causal hypothesis. Therefore, this work follows a correspondence between study-types, hypothesis and the design of research (Hernández-Sampieri *et al.*, 1998).

The sense of the objective of this work is the sediment genesis interpretation for most Upper Triassic to Middle Jurassic red beds that are cropping out from Galeana in Nuevo León to Miquihuana in Tamaulipas; by the use of fieldwork and lab techniques in relationship with the previous studies.

The goals to approach the objectives are: 1) document the stratigraphy of the continental red beds; 2) reinterpret the sedimentary environments of Upper Triassic to Middle Jurassic strata; 3) interpret the tectonic environment by determining the provenance and controlling factors by means of petrography of light and heavy minerals, whole-rock geochemistry, and radiogenic isotope geology.

1.5.2. Actual state for the tectono-stratigraphic interpretation and subdivision of the Mesozoic red beds succession for the northeastern Mexico

In summary, the first red bed scientific contributions in the early 1900s, were attributed at the basis of lithostratigraphic characterizations. These logical results trespassed into a more suitable lithostratigraphic conception for the following years (1950s) by the addition of sedimentary environments with facies interpretations for a more consistent position of the red beds in the regional stratigraphic chart. For the next decades (1960s–1970s), research facilitated a better correlation between the already designated units and discarded information from previous years. A modern study grid (1990s) enhanced a more complete justification by assembling biostratigraphic, whole-rock geochemistry, and isotope analysis into more regional implications. The latter studies revised previous interpretations into a more robust paleotectonic characterization of the sedimentary environment and tectonic setting. Hence, structural and tectonic analyses were not absent at all.

Until the present, results have enabled us to discard about the kinematics that controlled the red beds, starting at the early 1900s with the eugeosinclinal geologic model, and further one reassert during the 70s and 80s with the development of the “terrane theory” by the Plate-Tectonic theory. The theoretical conceptions about Earth amplified progressively the descriptions and interpretations from the previously described contributions. Different works have stood as pioneer regional reports that have clarified a better regional kinematic scenario. The works include the classification of regional structural elements, paleomagnetism, ages and tectonic settings, basement rocks age, petrogenetic differentiation, deformation styles, basement morphologies with respect to sedimentation patterns, basin subdivision, and the main tectonic organization framework to the Gulf of Mexico, the Caribbean, and the Pacific by coupling tectono-sedimentary approaches.

1.5.2.1 Red Beds: stratigraphy–sedimentology–paleontology

Mesozoic Red Beds *sensu stricto* in Mexico have been reported from the north of the country in the state of Sonora (e.g., Lucas and Estep, 1999) to the south in the state of Chiapas (e.g., Godínez-Urban, 2009). Outcrops are widely scattered in different physiographic provinces of Mexico (Humphrey, 1956b), and are located within established terranes (e.g., Campa and Coney, 1983). Strata reported as red beds were recognized in

northeastern Mexico first by Buckhardt and Scalia, 1905, as a result of interest by the petroleum industry (Salvador, 1991; Humphrey and Díaz, 2003).

Typical localities of red beds in northeastern Mexico comprise Triassic and Jurassic ages. The outcrops of Triassic red beds are isolated in the morphotectonic provinces of the La Mesa Central and the Sierra Madre Oriental (Nieto-Samaniego *et al.*, 2005; Barboza-Gudiño *et al.*, 2010; Fig. 1.3). The provinces include the states of Zacatecas, Durango, San Luis Potosí, Nuevo León and Tamaulipas (Díaz and Humphrey, 1953; Chandler, 1957; Watson, 1958; Carrillo-Bravo, 1961; Mixon, 1959, 1963; Padilla y Sánchez, 1982; Clark and Hopson, 1985; Michalzik, 1986; Rueda-Gaxiola 1993; Rueda-Gaxiola *et al.*, 1993; Fastovsky *et al.*, 2005).

The first paleontologic, paleobotanic, and palinologic studies were made by Burckhardt and Scalia (1905), who determined a Triassic age for the marine red-red strata (turbidites) in Zacatecas, Durango, San Luis Potosí. Latter, the studies were complimented by Mixon *et al.* (1959), Cantú-Chapa (1969), and other more recent publications by Weber (1997), Gómez-Luna *et al.* (1998); Silva-Pineda and Buitrón-Sánchez (1999).

In the Sierra Madre Oriental, the continental red beds have been assigned to the Huizachal Formation (*cf.*, Carrillo-Bravo, 1961) or to La Boca Formation (*cf.*, Mixon *et al.*, 1959). Rueda-Gaxiola *et al.* (1999) proposed for the latter succession the name of Allogrupo Los San Pedros, however this unit includes both Upper Triassic and Lower Jurassic beds. Recently, an older Triassic unit has been proposed by Barboza-Gudiño *et al.* (2010), with the name of El Alamar Formation. In addition recent work has revised age interpretations for La Boca and La Joya Formations (Rubio-Cisneros and Lawton, 2011¹).

1.5.3. Regional geology

1.5.3.1 Related northeastern Mexico basement works: structural and tectonics

The current status of interpretation and subdivision of the Precambrian–Paleozoic basement in northeastern Mexico and its tectonomagmatic affinity are found at Keppie and Ortega-Gutierrez (2010) and Sánchez-Zavala *et al.*, (1999; Geological Society of America-Data Repository Item #200021 [DR#200021]), plus citation therein.

Proterozoic metamorphic and igneous rocks and Paleozoic strata of the mid-continent Oaxaquia (Ortega-Gutierrez *et al.*, 1995; Keppie *et al.*, 2004) are widely exposed at northeastern Mexico in the Huizachal-Peregrina Anticlinorium. The recognized Mesoproterozoic crystalline basement on northeastern of Mexico includes the ~1 Ga. Novillo rocks, which is correlated in age with similar rock-types from Huiznopala, Oaxaca; Guichicovi (Herrmann *et al.*, 1994; Murillo-Muñeton, 1994; Murillo-Muñeton and Anderson, 1994; Lawlor *et al.*, 1999; Weber and Köhler, 1999; Keppie *et al.*, 2001; Weber *et al.*, 2002; Keppie *et al.*, 2003; Ortega-Obregón *et al.*, 2003; Solari *et al.*, 2003; Weber and Hecht, 2003; Keppie, *et al.*, 2004; Keppie and Dostal, 2007.

¹ This publication was generated by the implementation of one of the methodologies used within this work for the fulfillment of the requirements of the degree, and is explained at Chapter 6: Geochronology of Detrital Zircons.



Fig. 1.3: Pre-Upper Jurassic localities in central to northeastern Mexico (in Barboza-Gudiño *et al.*, 2010). Shown are Upper Triassic exposures of the marine and continental facies, post-Triassic red beds, exposures of pre-Mesozoic crystalline rocks, in some cases interpreted as areas of no deposition during the Triassic.

Outcrops of the Novillo Gneiss, a granulite facies metamorphic and igneous complex (Orozco, 1991), represent the northernmost exposures of ~1 Ga. basement of Oaxaquia in northeastern Mexico. The gneiss consists of metasedimentary rocks intruded by two gabbro-anorthosite suites (~1010–1035 Ma and ~1115–1235 Ma; Cameron *et al.*, 2004) that experienced polyphase deformation and granulite facies metamorphism at 990 ± 5 Ma (Cameron *et al.*, 2004), and post-tectonic anorthositic pegmatite emplacement at 978 ± 13 Ma (U-Pb zircon, Cameron *et al.*, 2004). Two sets of mafic dikes intruded the complex (550 Ma, Keppie *et al.*, 2006).

In structural juxtaposition with the gneiss is the Carboniferous Granjeno Schist, which consists of polydeformed, low-grade pelitic metasedimentary and metavolcaniclastic rocks that enclose lenses of serpentinized metabasites (~430–300 Ma; Garrison, 1978; Dowe *et al.*, 2005; Nance *et al.*, 2007).

An unmetamorphosed succession of Paleozoic marine clastic strata nonconformably overlies the Novillo Gneiss (Carrillo-Bravo, 1961; Robinson and Pantoja-Alor, 1968; Pantoja-Alor, 1970; Ramírez-Ramírez, 1978; Boucot *et al.*, 1997; Stewart *et al.*, 1993; Centeno-García *et al.*, 1997). The base of the Paleozoic succession

consists of Middle Silurian clastic shallow-marine strata containing Gondwanan fauna (Stewart *et al.*, 1999). The formations that comprehend this succession are the Cañón Caballeros and La Yerba (Carrillo-Bravo, 1959, 1961; Gursky and Ramírez-Ramírez, 1986; Stewart *et al.*, 1993; Boucot *et al.*, 1997; Stewart *et al.*, 1999). This succession is correlated at some point with other outcrops located on the Chihuahua, Caborca, and Cortéz terranes, but also for some states at the west of the USA (Cooper and Arellano, 1946; Mulchay and Velasco, 1954; Brunner, 1975; Mullan, 1978; Ortega-Gutierrez, 1978, 1993; Speed 1979; Gastil and Miller, 1983; Campa and Coney, 1983; Ross and Ross, 1985; Poole and Madrid, 1988; Stewart, 1988; Almazán-Vázquez, 1989; Stewart *et al.*, 1990; Campbell and Crocker, 1993; Leier-Engelhardt, 1993; Lothinger, 1993; Sedlock *et al.*, 1993; Poole *et al.*, 1995; Gehrels and Stewart, 1998; Stewart *et al.*, 1999; Stewart and Poole, 2002; Barth *et al.*, 2000; Vachard *et al.*, 2004; Keppie and Dostal, 2007; Miller *et al.*, 2007).

This succession is unconformably overlain by Lower Mississippian sandstone and shale containing a shallow-marine fauna of Laurentian affinity (Stewart *et al.*, 1999). The carboniferous sandstone and shale are represented by the following formations Vicente Guerrero, Del Monte, and Guacamaya (Stewart *et al.*, 1999; Sour-Tovar *et al.*, 2005). The Mississippian unit is correlated with others in age located with other several Mexican terranes and the west of Texas, but few are overlapping big tectonic contacts (Boese, 1923a, 1923b; King, 1934, 1944; Cooper and Arellano, 1946; Mulchay and Velasco, 1954; Richards, 1963; Bridges, 1964; Diaz and Navarro, 1964; Viveros, 1965; Silva-Pineda, 1970; Pantoja-Alor, 1970; Carrillo-Martínez, 1971; Hills, 1972; Aponte-Barrera, 1974; Wardlaw *et al.*, 1979; Patterson, 1978; Corona-Esquivel, 1981; Ortega-Gutierrez, 1981; Jones *et al.*, 1984; Shurbet and Cebull, 1987; Villaseñor-Martínez *et al.*, 1987; McKee and Jones, 1988; Poole and Madrid, 1988; Stewart *et al.*, 1990; Campbell and Crocker, 1993; Torres-Vargas *et al.*, 1993; Weber and Ceballos, 1994; Molina-Garza and Geissman, 1996; Carpenter, 1997; Stewart *et al.*, 1997; Stewart *et al.*, 1999; Gehrels and Stewart, 1998; Grajales-Nishimura, 1998; Grajales-Nishimura *et al.*, 1999; González-León *et al.*, 2005; Buitrón-Sánchez *et al.*, 2007; Weber *et al.*, 2005; Weber, 2006; Weber *et al.*, 2009; Solari, *et al.*, 2010).

These Lower Mississippian clastic rocks are positionally overlain by a flow-banded Aserradero Rhyolite dated at 334 ± 34 Ma (lower intercept U-Pb zircon age; Stewart *et al.*, 1999), which is in turn unconformably overlain by Permo-Carboniferous turbidites and volcanoclastic flysch deposits (Gursky and Michalzik, 1989).

All Proterozoic and Paleozoic rocks contain N-NW trending folds and associated northeast-vergent thrusts and dextral transcurrent faults (Carrillo-Bravo, 1961; Gursky, 1996; Stewart *et al.*, 1999; Dowe *et al.*, 2005).

A belt of Permo-Triassic dioritic and granodioritic intrusive rocks cuts all older units along a northwest-southeast trend extending from the Sierra Madre Oriental, through the Coahuila block, and into the North American craton in the Northwest of Mexico. Geochemical and isotopic analyses indicate a continental arc origin, which range in age from 287 to 232 Ma (Bartolini *et al.*, 1999; Torres *et al.*, 1999; Dowe *et al.*, 2005). This arc has been termed the East Mexican arc (Dickinson and Lawton, 2001); herein it referred as the West Pangaeian arc after its inferred paleogeographic position on the western edge of Pangaea and possible extent into Laurentia in current northwestern Mexico (e.g., Arvizu *et al.*, 2009).

The following resumed overview about the pre-Mesozoic landmasses in northeastern Mexico their distribution and connections with Laurentia, Gondwana, and among themselves, is crucial for the understanding of the late Paleozoic assembly of Pangea (Rowley and Pindell 1989; Ortega-Gutiérrez *et al.*, 1995 Vachard *et al.*, 1997; Barth *et al.*, 2000). Their connectivity is important to the understanding of the tectonomagmatic affinity histories (Handschy and Dyer 1987) that enable characteristic structures, displacements, and crustal extensions (Flawn and Diaz, 1959). This distribution of potential source areas for sediment will serve to improve understanding of the history behind the sediment genesis of Upper Triassic–Middle Jurassic red beds northeastern Mexico.

1.5.4. Stratigraphy of Middle–Upper Triassic to Lower–Middle Jurassic (The Huizachal Group)

1.5.4.1 Triassic red beds: El Alamar Formation

In the localities of the Sierra Madre Oriental like Galeana in Nuevo León and the Huizachal-Peregrina Anticlinorium in Tamaulipas, the Triassic red beds consist of conglomerates, sandstones, siltstones and claystones. Facies correspond to proximal alluvial fan, braided rivers, and distal meandering deposits (Michalzik, 1988, 1991; Laubach and Ward, 2006; Rubio Cisneros, 2008a; Rubio-Cisneros and Ocampo-Díaz, 2010; Barboza-Gudiño *et al.*, 2010). The base of the sequence is not exposed (Barboza-Gudiño *et al.*, 2010).

At the vicinities of Galeana Triassic fluvial–alluvial sequences are present (Davis, 2005; Rubio-Cisneros, 2008b; Alejandro-Torres, 2010). Barboza-Gudiño *et al.* (2010), proved a Triassic maximum depositional age by finding Grenville, Pan–African–Brazilian, and Permian–Triassic grain age populations by measuring U–Pb in detrital zircons for rock samples from the El Alamar canyon, San Marcos (southern Galeana), and at the western part of the Huizachal-Peregrina Anticlinorium.

Considering the confusion where the Triassic age for the Late Triassic–Early Jurassic unit (La Boca Formation; *cf.*, Mixon *et al.*, 1959) Barboza-Gudiño *et al.* (2010) proposed a new lithostratigraphic unit called El Alamar Formation to represent the Triassic succession (Fig. 1.4; Fig. 1.5; Fig. 1.6)². The typical locality is at the El Alamar Canyon in the Sierra de Pablillo at Nuevo León, where the base of the sequence is not exposed.

At the Huizachal Peregrina Anticlinorium the incomplete section of El Alamar Formation overlies Precambrian–Paleozoic basement rocks, and is overlain by Jurassic red beds and volcanogenic rocks from La Boca Formation (*cf.*, Mixon *et al.*, 1959), and/or Middle Jurassic rocks from La Joya Formation (upper part of the Huizachal Group; *cf.*, Mixon *et al.*, 1959).

² Within this work some figure references remain as Huizachal Formation that is now reinterpreted as El Alamar Formation.

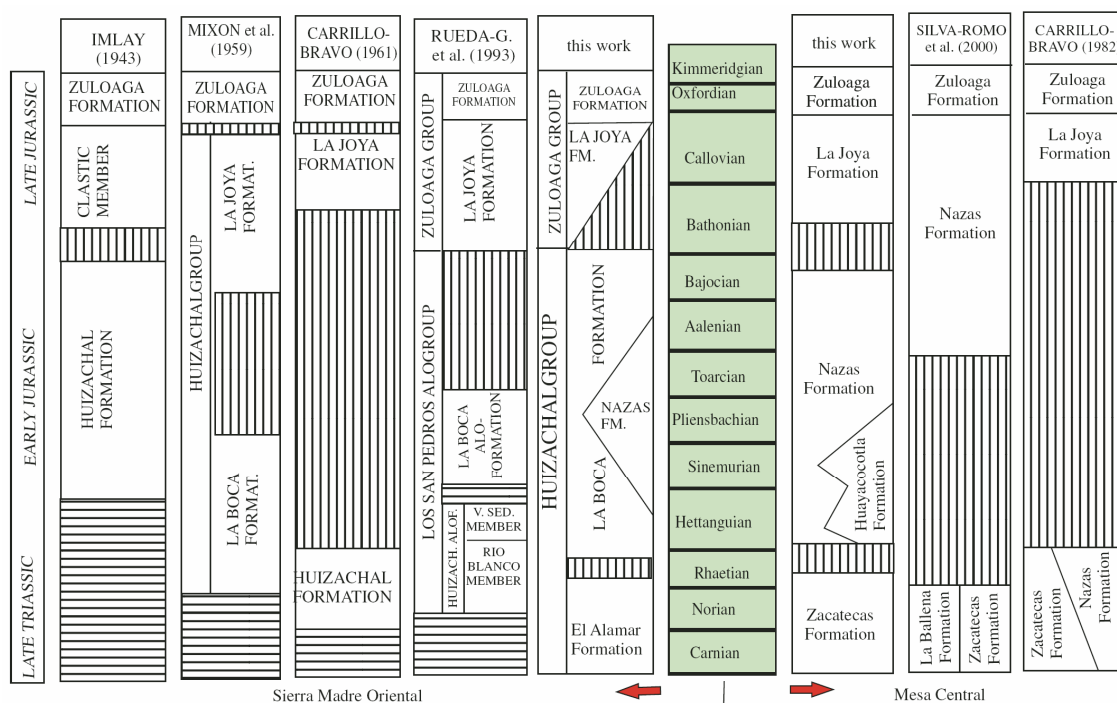


Fig. 1.4: Stratigraphic subdivisions proposed by different authors for the early Mesozoic successions exposed in the Sierra Madre Oriental from Nuevo León and Tamaulipas and the Mesa Central province in San Luis Potosí and Zacatecas (after Barboza-Gudiño *et al.*, 2010). References at Barboza-Gudiño *et al.*, 2010 for different stratigraphic relations. The label for “this work” refers to Barboza-Gudiño *et al.*, 2010.

El Alamar Formation is correlated in age with the Zacatecas Formation, which is the marine counterpart facies system (Barboza-Gudiño *et al.*, 2010). Based on the lithologies and facies of El Alamar Formation, similar characteristics can be found at San Marcos–Lomas de San Paulo Tranquitas in Galeana, and with those seen at the core or the western flank of the Huizachal-Peregrina Anticlinorium. Using this field relationship El Alamar Formation is not exposed nor deposited at the Valle de Huizachal in Ciudad Victoria (Rubio-Cisneros and Lawton, 2011; Rubio-Cisneros and Lawton, 2010; Rubio-Cisneros *et al.*, 2011³), Miquihuana, and Aramberri at the south of the state of Nuevo León next to the border limits with Tamaulipas.

1.5.4.2 Jurassic red beds: La Boca and La Joya formations

In the states of Nuevo León and Tamaulipas the Jurassic formations of La Boca and La Joya (*cf.*, Grupo Huizachal, Mixon *et al.*, 1959; Mixon, 1963) are overlain by carbonate strata of the Sierra Madre Oriental. Initially, Fehr and Bonnard (1930) consider them with a post-Liassic and pre-Oxfordian in age, correlating them with red beds of the saline sequence from the Tehuantepec Isthmus, and with similar upper Jurassic deposits at the Tampico-Tuxpan.

³ This publication was generated by the implementation of one of the methodologies used within this work for the fulfillment of the requirements of the degree, and is explained at Chapter 4: Petrography of Light Minerals and Source Areas.

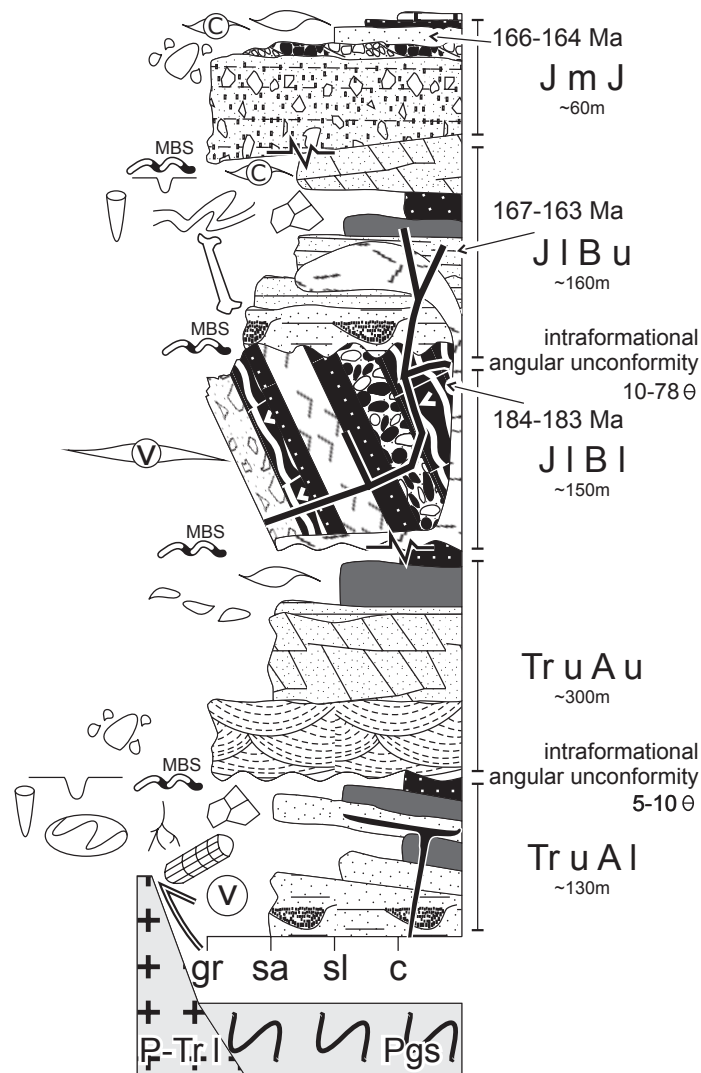


Fig. 1.5: Proposed generalized, schematic stratigraphic relations of the lowermost part of the Mesozoic sequence of the Huizachal Group in the Sierra Madre Oriental. Note the intraformational angular unconformities between the lower and upper member for El Alamar and La Boca formations. Weighted mean ages for this work are at the right side of the column. Units not drawn to scale. Key for symbols are explained in the coming figures. Pgs– Paleozoic Granjeno Schist. P-Tr l– Permian to Lower Triassic. Tr u A l– Upper Triassic El Alamar lower member. Tr u A u– Upper Triassic EL Alamar upper member. J I B l– Lower Jurassic La Boca lower member. J I B u– Lower Jurassic La Boca upper member. J m J– Middle Jurassic La Joya. Sedimentary structures are given at the right of column. The “bone” represents the vertebrate-bearing interval (Early Jurassic; Clark *et al.*, 1994). c: Clay; sl: Siltstone; sa: Sandstone; gr: Gravel. V– volcanic. MBS– Mayor Bounding Surface. C– Carbonate. θ – dip of unconformity.

Heim (1940), Burckhardt (1930), and Muir (1936) assigned them a pre-Late Jurassic age. Imlay (1943a,b,c) and Imlay *et al.* (1948), considered a late Jurassic age (Early Oxfordian), correlated with the Eagle Mills Formation at the south of Arkansas and Louisiana.

La Boca Formation present an important fossiliferous content (Clark and Hopson, 1985; Clark *et al.*, 1991, 1994; Fastovsky *et al.*, 1995, 2005; Weber, 1997). The Valle de Huizachal is the *locus typicus* where the age and nomenclature were defined (Carrillo-Bravo, 1961; Robertson, 1925 in Imlay *et al.*, 1948; Burckhardt, 1930; Muir, 1936; Humphrey, 1956a,b; McKee *et al.*, 1997). A debate remained concerning the stratigraphical

position and age for the two formations due to the paucity of biostratigraphic information. However, the stratigraphical gap was indicated by geochronology (Gray *et al.*, 2008; Rubio-Cisneros and Lawton, 2011).

The stratigraphic section that includes red strata exposed in the core of the dome at Valle de Huizachal are divided into three stratigraphic successions or intervals: (1) a lower and (2) an upper member for La Boca Formation, and (3) an upper interval for La Joya Formation (Fig. 1.4; Fig. 1.5; Fig. 1.6; Rubio-Cisneros and Lawton 2011; Rubio-Cisneros *et al.*, 2011).

The lower interval was previously interpreted as part of an unnamed Permian-Triassic volcanic succession (Burckhardt, 1930; Muir, 1936; Bartolini *et al.*, 1999). The nomenclature of the pre-Upper Jurassic strata in Valle de Huizachal has varied significantly since their initial description, and age interpretations are likewise debated due to a paucity of biostratigraphic and geochronologic data. The lower interval has been interpreted as part of an unnamed Permian-Triassic volcanic succession (Bartolini *et al.*, 1999), as a Late Triassic (Mixon *et al.*, 1959; García-Obregón, 2007) and/or Early Jurassic volcanic succession included in La Boca Formation (Mixon *et al.*, 1959), or termed it as the Volcanic and Epiclastic Suite of pre-Early Jurassic age (VES, Fastovsky *et al.*, 2005), which consists of feldspathic to lithic arenites (Rubio-Cisneros and Ocampo-Díaz, 2010; Rubio-Cisneros *et al.*, 2011). The lower interval contains a succession of volcanic and volcanoclastic strata that include lapilli tuffs, crystal tuffs, lava flows, volcanoclastic breccias, ignimbrites, shale, siltstone, sandstone, and conglomerate (Fastovsky *et al.*, 1995, 2005; García-Obregón, 2007; Barboza-Gudiño *et al.*, 2008; Rubio-Cisneros *et al.*, 2011). Siliciclastic strata (shale) are well indurated and contain a pronounced steep cleavage. Interbedded basaltic flows are massive or locally have flow breccias and brecciated vesicular flow tops. Peperites consisting of red clastic dikes and mixtures of red siltstone and brecciated basalt are common in the basalt flows (García-Obregón, 2007). Most of the rocks have undergone extensive late-stage or post-depositional silicification.

The upper member of La Boca Formation is dominantly red siliciclastic strata. The middle interval unconformably overlies the lower volcanic interval and consists of conglomerate and overlying siliciclastic and subordinate volcanoclastic strata (Fastovsky *et al.*, 1995, 2005; García-Obregón, 2007). Vertebrate fossils near the base of La Boca Formation suggested a Middle Jurassic age (Clark and Hopson, 1985; Fastovsky *et al.*, 1995). An inferred tuff at the base of the upper member of La Boca Formation, unconformably overlying the lower La Boca member or VES, yielded a U-Pb zircon age of 189.0 ± 0.2 Ma (early Pleinsbachian; time scale of Walker and Geissman, 2009) on the basis of a concordia intercept age calculated from eleven age groups, each consisting of 8–20 zircon grains, which range from 194 to 186 Ma (Fastovsky *et al.*, 2005). Red, vertebrate-bearing silty mudstone and pebbly mudstone in the lower part of the interval are interpreted as debris-flow deposits, possibly of syneruptive origin (Fastovsky *et al.*, 1995; Rubio-Cisneros *et al.*, 2011). The matrix-supported rocks grade upsection to interbedded clast-supported conglomerate, sandstone, and siltstone lacking fossil material (Fastovsky *et al.*, 2005). The sandstones consist of compositional lithic arenites (Rubio-Cisneros *et al.*, 2011). The middle interval displays gentle radial dips near the Valle de Huizachal, where it forms an open domal structure (García-Obregón, 2007). Angular unconformity between the lower and middle

intervals ranges from slight, only a few degrees, to as much as 70° where strata in the lower interval are steep (Fastovsky *et al.*, 2005; García-Obregón, 2007; Rubio-Cisneros *et al.*, 2011). This interval was termed the superjacent red bed suite (SS) by Fastovsky *et al.* (2005). The unit dips generally moderately to steeply (20° – 40°) with local subvertical dips near rhyolite intrusions. Rhyolite bodies that have been interpreted as domes intrude the lower and middle intervals (García-Obregón, 2007; Barboza-Gudiño *et al.*, 2008; Rubio-Cisneros *et al.*, 2011). These rhyolites have steep to vertical flow banding, commonly with spherulites of devitrified glass aligned with the banding (Barboza-Gudiño *et al.*, 2008). The rhyolite domes were included in unit A of the VES, and the aligned spherulites were interpreted as layers of accretionary lapilli, which led to the interpretation of a widespread, strongly angular unconformity between the lower and middle intervals (Fastovsky *et al.*, 2005), which is only locally the case. Elsewhere, the typical angularity between the lower and middle intervals is 10° – 20° (Fastovsky *et al.*, 2005; García-Obregón, 2007). The locally steep dips of volcanic flows in the lower interval resulted from folding during rhyolite intrusion; therefore, the strongly angular unconformity developed locally because of dome emplacement and does not indicate the representative degree of regional tectonic tilting between deposition of the lower and middle intervals.

Both members of La Boca Formation represent rejuvenation of source areas accordingly to their petrographical compositional characteristics (Rubio-Cisneros and Ocampo-Díaz 2010; Ocampo-Díaz and Rubio-Cisneros, *submitted*).

The interpreted maximum depositional ages determined by Rubio-Cisneros and Lawton (2011), systematically decrease upsection through La Boca Formation. Lower La Boca samples have Early Jurassic (ca. 184–183 Ma) maximum depositional ages, and upper La Boca samples have Middle Jurassic (ca. 167–163 Ma) ages. The progressive decrease in maximum depositional age, common interbedded volcanic and pyroclastic rocks, and stratigraphic position beneath Middle-Upper Jurassic evaporitic strata suggest that the Early-Middle Jurassic maximum depositional ages of La Boca Formation approximate the true depositional age of these red beds.

An apparent conflict in the geochronology of La Boca Formation required discussion. The 184–183 Ma and 167–163 Ma weighted mean ages in the lower and upper La Boca samples, respectively, are significantly younger than the 189 Ma U-Pb age (Fastovsky *et al.*, 2005) for the tuff at the base of the upper La Boca member. A plausible explanation is that the intercept age obtained by Fastovsky *et al.* (2005) was calculated based on reworked grains from older strata of the volcanic-rich lower member (Rubio-Cisneros and Lawton, 2011). Detrital zircon ages in the lower member of La Boca Formation in Valle de Huizachal corroborate previous inferences of an Early to Middle Jurassic age for La Boca Formation (Clark *et al.*, 1994; Fastovsky *et al.*, 1995, 2005; Stewart *et al.*, 1999; Barboza-Gudiño *et al.*, 2008).

The third and uppermost interval is of red sandstone, shale, and subordinate conglomerate that overlies a basal conglomerate and is itself overlain by Upper Jurassic carbonate strata. The middle interval is overlain in an erosive unconformity by an upper red siliciclastic section with a basal conglomerate of crudely bedded, clast-supported conglomerate with angular clasts (Rubio-Cisneros *et al.*, 2011). The conglomerate grades

upsection into brick-red sandstone and shale significantly less indurated and blocky than those of the lower and middle intervals. Previous workers have generally referred to this upper interval as the basal strata of La Joya Formation (Mixon *et al.*, 1959; Fastovsky *et al.*, 1995, 2005).

The La Joya Formation consists of continental to marginal-marine siliciclastic strata with subordinate thin strata of freshwater limestones (Fig. 1.4; Fig. 1.5; Fig. 1.6; Michalzik, 1988, 1991). The coarse rock constituents in the conglomeratic horizons are sedimentary fragments from preexisting units, including volcanic or metamorphic sources. The petrographical principal components validated the detrital provenance, which represents the recycling from underlying crystalline basement, El Alamar, and La Boca formations (Rubio-Cisneros and Ocampo-Díaz, 2010; Ocampo-Díaz and Rubio-Cisneros, *submitted*). The age of La Joya was constrained by a single late Middle Jurassic grain (164 Ma), which is not statistically different from the young grain ages in the upper member of La Boca Formation. Detrital zircon ages are inconclusive as to the depositional age of La Joya Formation, but its position between Bathonian–Callovian red beds and overlying Oxfordian strata is consistent with a Callovian age (Rubio-Cisneros and Lawton, 2011).

La Joya records infilling of areally restricted rift basins (Salvador, 1987; Rubio-Cisneros *et al.*, 2011). The La Joya pinches out onto basement highs and is overlain by Oxfordian evaporate strata (Salvador, 1987). The uppermost La Joya Formation marks the onset of prolonged Late Jurassic marine transgression (Rueda-Gaxiola *et al.*, 1991; Goldhammer, 1999).

In the locality of Aramberri, red beds been interpreted as Triassic in age (Lazzeri, 1979; Meiburg *et al.*, 1987; de León-Gómez, 1988). Nevertheless, the deposits contain similar facies as La Boca and La Joya formations. Rueda-Gaxiola *et al.* (1993, 1999) proposed the Los San Pedros allogroup, which includes a basal volcanogenic unit in the Rio Blanco allomember, which is overlain by a volcano-sedimentary allomember, forming both the Rhaetian–Hettangian Huizachal alloformation. The overlying Sinemurian–Pliensbachian red bed succession was defined by Rueda-Gaxiola *et al.* (1993) as La Boca alloformation. However, the type locality of the Rio Blanco allomember was defined north of Aramberri Nuevo León. At this locality, 65 km away from the type locality of La Boca alloformation, the volcanic rocks yielded a U-Pb zircon age of 193 ± 0.2 Ma (Barboza-Gudiño *et al.*, 2008) directly overlying Paleozoic schist (Meiburg *et al.*, 1987; Torres-Sánchez *et al.*, 2010; Barboza-Gudiño *et al.*, 2011), and the Triassic succession was not deposited.

Other red beds have been identified on the localities of Bustamante and Miquihuana (Fig. 1.3), overlying the Granjeno schist. These deposits contain by volcanic rock of intermediate composition and were considered Triassic in age (Hill, 1893; Burckhardt, 1930; Imlay, 1937), but now are correlated with lower–middle Jurassic outcrops (Barboza-Gudiño *et al.*, 2010).

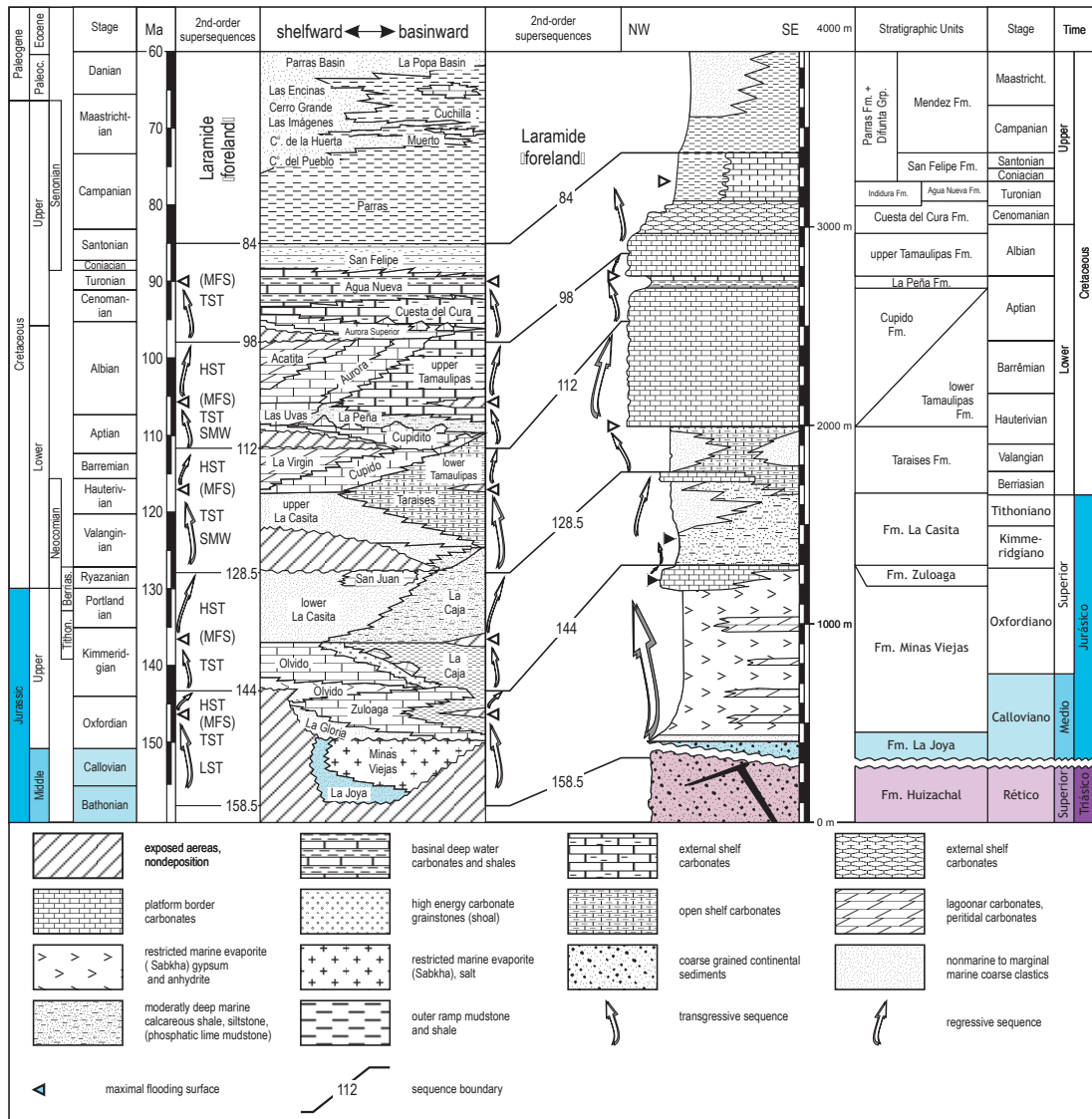


Fig. 1.6: Stratigraphic correlation for the stratigraphic columns after Michalzik (1988) and Goldhammer and Johnson (2001) for northeastern Mexico (modified by Jenchen, 2007a, b). Colors are from International Stratigraphic Chart 2009.

2. FACIES, ARQUITECTURAL-ELEMENTS, AND FLUVIAL STYLE ANALYSIS

2.1. Introduction

This chapter provides an integrated view for the characteristics and aspects of operation from the fluvial system of Upper Triassic-Middle Jurassic red beds.

Bedrock morphology at continental sedimentary environments marks sites of primary erosion in the landscape, fixing accommodation and supply for all points upstream. Fluvial deposits represent the preserved record of one of the major nonmarine environments. The following sections provide an integrated view for the characteristics and aspects of operation of the fluvial system of Upper Triassic-Middle Jurassic red beds.

Thick accumulations of fluvial sediments occur in a variety of all basin-types (e.g., extensional, and strike-slip basins), which alluvial architecture varies with tectonic setting (Miall, 1996), and are conditioned to the abrupt fault-defined margins that the basin poses (Steel, 1974). The deposition of sedimentary sequences and distribution of the depositional environments in active extensional basins are controlled by the interplay of many processes of short- to long-term effects like uplift and subsidence (Leeder and Gowthorpe, 1987; Frostick and Steel, 1993).

The construction of a stratigraphic framework of fluvial deposits, lithofacies, architectural elements (geometry), and facies associations permits to understand the differences in behavior from the sedimentary environment and the recognition of the controls that determine the channel style into a closer insight for sediment provenance. This construction forms the basis for a discussion of causes and processes of autogenic and allogenic nature that control the development of accommodation and supply of clastic material in nonmarine sequences.

Previous work on Upper Triassic–Middle Jurassic continental red beds in northeastern Mexico have contributed with the categorization and correlation to define a well-structured stratigraphy (Chapter 1: section 1.5.4). Only a limited number of publications focus in detail on the sedimentology of El Alamar, La Boca, and La Joya Formations. There have been a number of contradictory interpretations of the geology of the fluvial deposits. None of these publications investigate the vertical and lateral variations in facies distribution and architectural style, for a revisited regional analysis.

Using an integrated dataset of 17 field sedimentary profiles this chapter provides a detailed description and interpretation of the 20 facies, 4 facies associations, architectural style analysis of the sand bodies, and an overview of the controlling factors for accommodation and supply that contributed for the existence of the resulting sedimentary depositional system.

2.2. Methodos

This work is based on the present-day concepts out of earlier studies for fluvial environments discussed in Miall (1996) and Bridge (2003), which include descriptive fluvial geomorphology, quantitative fluvial geomorphology, sediment transport studies, bedforms, paleocurrents, facies, and hydraulics.

Well-exposed outcrops up to ~360 m high extend laterally in variable proportions depending on the locality. A total of seventeen stratigraphic sections were structured in 10 different localities. However, objective field measurements commonly are difficult to make, particularly in areas of poor exposure and access. The data collected at the field was grain size, sedimentary structures, palaeocurrent information, and special constituents (e.g., root tracks). This data ensures lithofacies interpretations. Representative samples were collected. Correlations were made using both photomosaics in combination with the field mapping of major correlateable surfaces recognizable on the outcrops. Terminology for describing the thickness of beds and laminae are from McKee and Weir (1953).

Walther's Law, states that only those facies that can be found forming side by side in nature can occur in contact with one another in vertical succession, unless the succession contains internal erosion surfaces (Middleton, 1973; Cant and Walker, 1976; Collinson, 1978). This enables to interpret lateral facies relationships to apply a methodological recognizance and classification for strata. The word facies has various meanings and can be used interchangeably in the plural or singular (Prothero, 1990). It is here that facies are features of a unit portraying the processes of origin and source, and environments of deposition (Fischer and Smith, 1991). The ichnology found on the studied nonmarine environments was assisted by the observations of Buatois and Mángano (1995, 1998), Genise *et al.* (2000), among others considerations (Seilacher 1954, 1963, 1964, 1967; Frey *et al.*, 1980; Byers, 1982; Bromley and Ekdale, 1986; Bromley, 1990; Pemberton, 1992; Goldring, 1993; Buatois and Mángano, 1993a,b; Buatois *et al.*, 1998; Bertling *et al.*, 2006).

Sedimentation in fluvial systems produces erosive-based sequences of planar, tabular cross-bedded sands with subordinate trough cross-bedding, and ripple-cross-lamination. In view of the constant shifting of bars and low-stage sub-channels, these sequences are unlikely to show a high degree of order and it is also improbable that their facies patterns can be summarized in a single vertical sequence. Instead a family of sequence (Facies and Facies Associations) is required (*cf.*, Cant and Walker, 1978).

Allen and Visher (1965) and Miall (1978) systematized some fluvial sedimentology aspects by detailing the sedimentary structures and vertical sequences in deposits. Miall (1996) described bedforms and fluvial elements as indicators of changes in flow regime (lower vs. upper). A fluvial style is a complex response to a number of autogenic and allogenic controls (Miall, 1996).

The analysis for the sedimentology of El Alamar, La Boca, and La Joya formations have been undertaken by grouping sediments into four facies associations (FA), which define a particular depositional environment. To shorten explanation, each FA is defined by a combination of lithofacies modified from Miall (1985, 1996) and Allen (1983a; Fig. 2.1), and sedimentary structures that define its particular process (Fig. 2.15).

Lithofacies classification for this work, from Miall, 1996

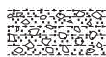





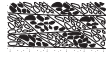


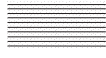



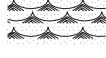
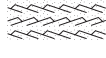





Code	Lithofacies	Description	Interpretation
Gravels			
Gmm		Poorly sorted clasts floating in a silt matrix. Massive beds and no clast imbrication. Sharp contacts.	High-stream debris flow in a pre-existing alluvial flow (e.g., channel).
Gmg		Poorly sorted clasts floating in a silt matrix showing some in grading in clasts and/or matrix. Sharp contacts.	High-stream debris flow in a pre-existing alluvial flow (e.g., channel).
Gci		Clast-supported, Inverse-Graded Gravel.	Clast-rich, high strength debris flow, or a low-strength flow with an inertial bed load transported by laminar turbulent flow.
Gcm		Clast-supported massive gravel.	Low-energy pseudo-plastic debris flow with viscous to laminar turbulent flows.
Gh		Clast-supported, Horizontally Stratified Gravel.	Low regime debris flow, with clast-supported pebble and covel gravel, with crude horizontal stratification. Imbricated clast fabric.
Gt		Clast-supported gravel showing trough cross-bedding. Maximum foresets dip 30°.	Minor channel fills. Fluvial reworked alluvial fans.
Gp		Planar-Cross-Bedded Gravel.	Minor channel fills, linked to shifts in hydraulic conditions, and controlled by overpassing process.
Sands			
Se-Ss		Coarse to very coarse grained, very poorly sorted sand with cross-bedding and abundant clasts and lag materials.	Rapid depositional of poorly sorted bedloads in scours.
Sp		Planar cross-bedded, moderate to well sorted sandstones (angle 15°-35°). Sharp base and top.	Migration of 2D dunes under lower flow regime.
Sh		Horizontal laminated, moderate to well sorted sandstones. Parting lineation can occur on the bedding planes.	Planar bed flow under lower and upper (flash floods) flow regime.
Sl		Similar to Sh, but low angle cross-bedding dipping <15°.	Washed-out dunes and antidunes that occur between subcritical and supercritical flows.
St		Massive sandstones, no structures. Moderate to well sorted.	Rapid deposition, sedimentary gravity flow and postdepositional modification.
Sm		Trough cross-bedded, moderate sorting. Lag of poorly sorted sand might be present at the base of trough.	Migration of 3D dunes under lower regime.
Sw		Symmetric bidirectional ripples.	Depositional under oscillatory motion of top surface of a water body (e.g., waves).
Sr		Asymmetric-unidirectional ripples. Type A ripples: mutually erosive ripples. Type B ripples: climbing ripples.	Type A: migration of ripples with low rate of sedimentation. Type B: addition of sediment from suspension during ripple migration.
Fine grained			
Fm		Massive (no structures) mudstone-siltstone. Occasional presence of calcareous bands, rootlets and desiccation cracks.	Deposits from standing pools of water during low-stage channel abandonment. Floodplain facies.
Fl		Interlamination of mud, silt or very fine sand. Formation of small-scale ripples in sandy beds. Similar structures than Fm.	Deposition from suspension in overbank areas.
Nonclastic Facies			
P		Pedogenic Carbonates, and general Paleosol facies classification.	Floodplains exposed to weathering processes for extended periods. Development of carbonate cements, nodules, carbonate substrates with a block fracturing.
Af		Ash fall. Beds generally less than one meter in thickness. Beds are almost always eroded by coarser overlying strata.	Deposition from eruption episodes. Possible size grading, bed thickness are generally the result of fluctuations in eruption intensity.
Cb		Limestones.	Limestones from unidentified carbonate related facies (including fresh water and marine environments).

Fig. 2.1: Lithofacies classification scheme. Modified from Miall (1985, 1996) and Allen (1983a).

In order to reinforce interpretations for sedimentation models and quantitative stratigraphy this work used one from various stochastic processes (Chapter 5 and citations therein from Schwarzacher, 1975). Markov process is a stochastic process in which a random variable depends on its past history. Markov chain analysis is a comparatively simple statistical technique for the detection of repetitive processes in space or time (Miall, 1973). The Markov chain model was first introduced by Vistelius (1949).

A simple, or first-order, Markov chain depends only on single steps, that is, the relationship between a given bed and the next bed immediately succeeding it. The probabilities offered by this method are two definite probabilities, which are in no way affected by how often the experiment is repeated nor by what happens during earlier or latter trials.

Each of the measured sections in this work has been assigned with lithofacies. Any lithofacies is considered to be a variable. The values of the random variable are discrete and they are, therefore, referred to as “the states of the system”. The Markov chain is well illustrated by considering the successive positions of a lithofacies going a random transition from one state to another. Each lithological unit, regardless of its thickness, forms a step in the Markov chain.

The starting point in Markov chain analysis is the transition count matrix. This is a two-dimensional array, which tabulates the number of times that all possible vertical lithologic transitions occur in a given stratigraphic succession (see Appendix for Chapter 2). The lower bed of each transition couplet is given by the row number of the matrix, and the upper bed by the column number, each lithofacies present being assigned a code number for the purpose of the analysis. At a Markov matrix the rows add up to unity and which consists of non-negative elements. This matrix may also be called the transition-probability matrix of the process.

The Huizachal Group was analyzed through the principles of architectural element analysis proposed by Miall (1985, 1988, 1996), which then served to assess fluvial bounding-surface relationships. The hierarchy of bounding surfaces (Table 2.3) recognized in the field were used for correlation between sections based on Bridge (1993a,b), Miall (1988, 1995), Gibling (2006). Tracing of surfaces from photographs was guided by a set of assumptions considered by Holbrook (2001), to apply to primary/depositional bedding that are derived ultimately from principles of superposition and cross-cutting relationships. Origin of surfaces was then interpreted with reference given by the order of interpretations after Miall (1988, 1996).

Four FAs were identified in the study areas are: (i) Fluvial Facies Association (FA-1), (ii) Overbank Facies Association (FA-2), (iii) Aeolian Facies Association (FA-3), (iv) Alluvial fan Facies Association (FA-4; Table 2.1). Indicators for paleocurrent data are (1) cross-bedding, (2) ripple cross-lamination, (3) flaser and lenticular bedding, by following the methodologies proposed by Potter and Pettijohn (1977) and Collinson and Thompson (1989). The obtained paleocurrents were restored applying a modified criterion by Briggs and Cline (1967), Shukla *et al.* (1999), and Filguera–Flores (2010). The fabricated datasets allowed understanding the effects of relative accommodation and supply as a dual control on the measured stratigraphic sequences (e.g., Schlager, 1991).

Table 2.1: Table summarizing the main facies, lithofacies and facies associations identified in the Huizachal Group for northeastern Mexico, with their corresponding interpretations.

Facies Association	Facies (FA)	Lithofacies	Interpretation
Fluvial (FA-1)	Facies-1A	Sh, Sp, Sm, Se-Ss, Sl, Sr	Elements associated with erosion, infill and abandonment of a channel. (epiclastic processes: erosion and sediment transport-deposition of volcanic rocks)
	(subfacies-1Aa)	(+Af)	
	Facies-1B	Sp, Sh, Sl, Sr	Downstream accretion braided bars
	Facies-1C	Sp, Sr	Lateral accretion bars deposited on sides of braided bars or edges of the channel
Overbank (FA-2)	Facies-1D	Gt, Gp	Channel fills from reworked alluvial deposits
	Facies-2A	Fm	Overbank deposits
	Facies-2B	Fm, Fl, P, Cb	Overbank deposits with developed paleosols, or carbonate precipitation
	Facies-2C	Fl, Af, Sl	Volcanic related deposits
Aeolian (FA-3)	Facies-3A	Sp, Sl	Aeolian dunes, reworking the bars deposited in overbank areas due to aridity of climate conditions
Alluvial fan (FA-4)	Facies-4A	Gmm, Gmg, Gci, Gem, Gh	Sedimentary gravity Flow deposited as alluvial fans sourced from erosion of scarp.

A theoretical display based on a bounded-cycle stratigraphy was built up by assigning each of the following definitions: (a) amalgamation, (b) aggradation, (c) accommodation, (d) degradation, and (e) major flooding; each of the latter corresponding as bounding surfaces ([a] Dalrymple *et al.*, 1994; Aitken and Flint, 1995; Flint *et al.*, 1995; Hampson *et al.*, 1997; Davies *et al.*, 1999; Hampson *et al.*, 1999; [b] Schumm 1977; Womack and Schumm 1977; Allen, 1982, 1983; Bridge, 1985; Miall, 1996; Bridge, 2003; Heller, *et al.*, 2001; Bridge, 2003; [c] Wheeler, 1964; Smith, 1973; Van Wagonor *et al.*, 1988; 1990; Todd, 1996; Cross and Lessenger, 1998; Ethridge *et al.*, 1998; Knighton, 1998, 1999; Homewood *et al.*, 2002; Rhee, 2006; [d] Shanley and McCabe, 1993; Wright and Marriott, 1993; Retallack, 2001; [e] Straub *et al.* (2009). Each assigned surface spike represents a susceptible response to the different known processes, controllers and factors, to formulate a better interpretation of the fluvial styles and their cyclic-succession.

2.3. Sedimentary (litho-) facies and facies associations of El Alamar, La Boca, and La Joya formations

2.3.1. Fluvial facies association (FA-1)

FA-1 comprises four major sedimentary facies (see Table 2.1).

2.3.1.1 Conglomerate and fine to medium grained, trough-planar cross-bedded sandstones (FA-1A and FA-1D)

2.3.1.1.1. Description

Facies FA-1 consist of 1 to 5 m thick units than can be traced for 10 m perpendicular to the depositional dip. They have erosive concave up bases, overlain by coarse-grained sandstones, which normally erode into mudstones. The top of each unit is normally horizontal. A multi-storey fill forms each unit, with each storey showing an average thickness ranging from a few cm to ~5 m, and bound by a 4th to 5th order erosion surface. Individual units show a fining upwards trend from conglomerate at the base (Gt, Gp) to medium-fine grained sandstone at the top (Sr, Sm).

The conglomerates at the base (FA-1D) are matrix-supported granule to cobbles graded with coarse grain sized intraformational (mud clasts), and extraformational (lithic fragments and quartz) subangular to

subrounded clasts. Bed dimensions are from thin to very thick and bedding type oscillates from planar to dipping laminae (planar cross-laminar). Conglomerates present normal graded bedding, planar or tabular to trough cross-bedding, exhibiting big amounts of lithic fragments derived from underlying units. These facies is overlain by FA-2 with a denotable disconformity contact, or with a paraconformity relationship with the rest of the FA-1 facies. FA-1D conformably underlies massive sandstones from FA-1 – FA-3. Examples of these successions are in outcrops located in the canyons of El Olmo, La Boca, and Caballeros (Fig. 2.4; Fig. 2.5).

The overlying red beds, medium-fine grained sandstone, show subrounded to subangular grains with fair to poor to well sorting. The individual sequences contain internally low to high angle planar and trough cross-bedding (Sl, Sh, Sp, St; Fig. 2.2; Fig. 2.3), commonly showing ripple lamination at the top (Sr). Stratification generally varies from thick to thin beds. Stratigraphic relationships prevail as uneven erosional surfaces (unconformity), and internally behave as informal amalgamated bed units. Mud-cracks, mud drapes, clay chips, mud lenses, and ripple clasts occur at the top of some units especially at medium-fine grained sandstones with parallel laminae and ripples configuration.

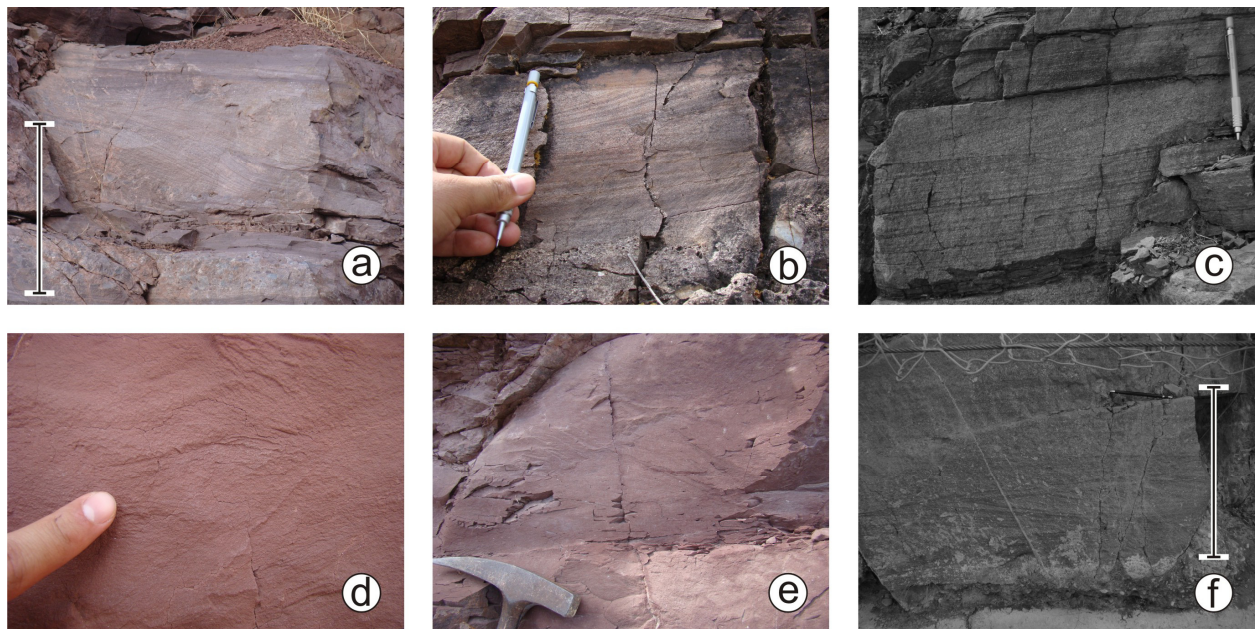


Fig. 2.2: Photograph assemblage for some of the low flow regime lithofacies (Sr: ripples, and Sm: trough cross-bedding) contained in facies association FA-1: FA-1A, FA-1B, FA-1C, reported at Valle de Huizachal within the upper and lower members of La Boca Formation. a) overturned foreset bed with trough cross-bedding, notice that scouring produced small, erosional troughs, which were subsequently filled with low-angle cross-laminae at the base (left); b) foreset bed with tabular cross-bedding; c) tabular cross-bedding on a foreset bed of nontangential foreset character overlying a plane (flat) bed; d) ripple cross-lamination in flood deposits; e) small-scale tangential foresets; f) trough cross-bedding. Scale line in black and white represents 30 cm.

Cross-bedding varies from small-scale (~15 cm) to large-scale sets (~30 cm). Sedimentation units contain tabular or trough cross-bedding beds. Tabular cross-bedding consists mainly by fine to coarse grained sandstones with trapped pebbles and cobbles within its foresets. Trough cross-bedding presents several foreset sedimentation units of micro to meso-scale. Numerous load structures (simple load casts and flame structures; *cf.*, Owen, 2003), flute marks, and tool marks are also present at the base of the units that compose FA-1, providing valuable palaeocurrent information. Other lenticular units have an erosive concave-up base of 10 cm

to 2 m thick comprising clast-supported imbricated conglomerate and sandstones. Uncommon imbrication is represented by clasts with the a–b plane dipping upstream and the α axis perpendicular to paleoflow. Internally the units show trough cross-bedding, which can be picked out by the clast imbrication within the lithofacies (Gt in FA-1D).

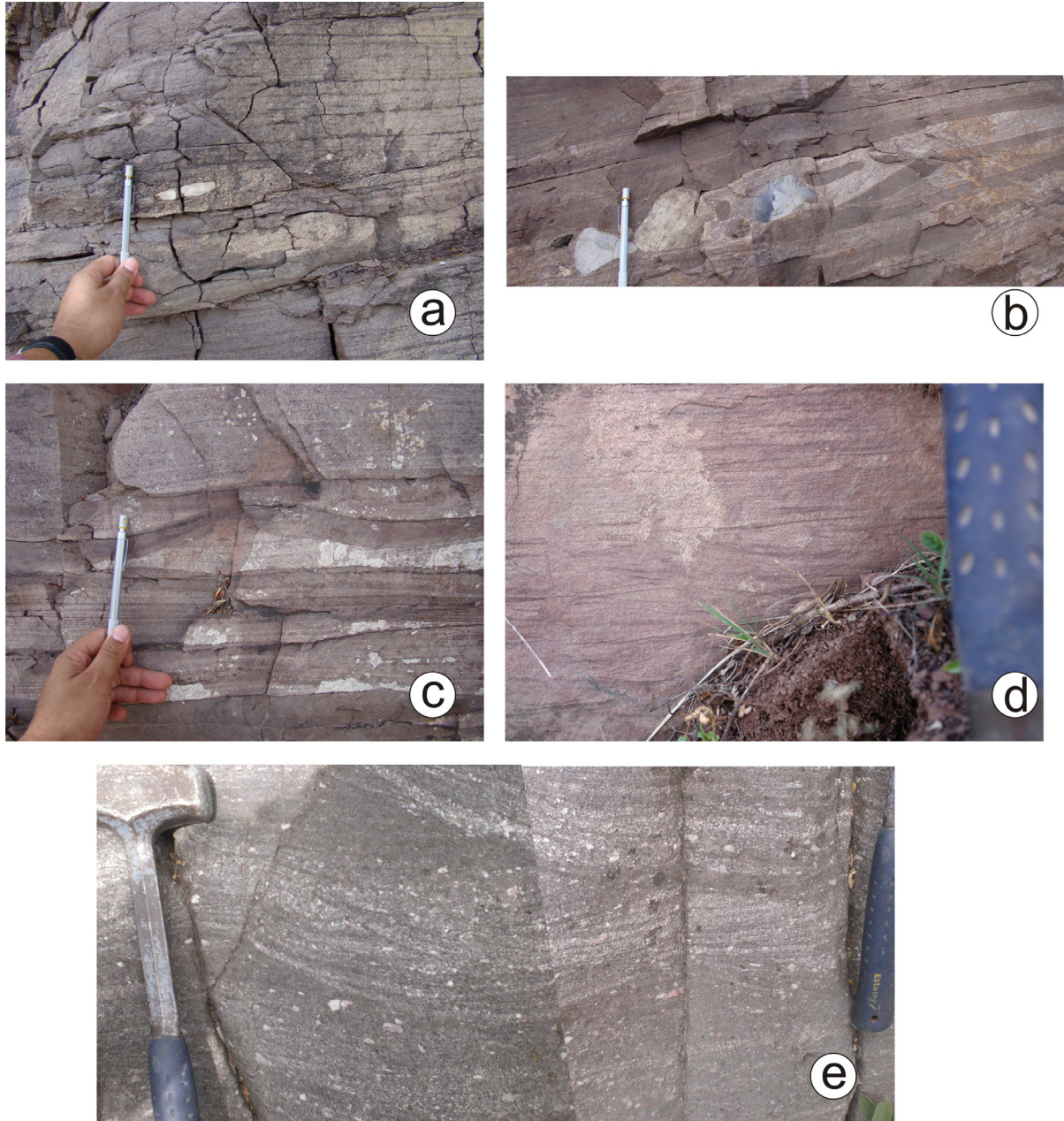


Fig. 2.3: Photograph assemblage for selected low flow regime lithofacies (Sh; Sl; Se-Ss: scour fills; Sm: trough cross-bedding) contained in facies association FA-1: FA-1a, FA1-B. a) Lens of coarse grained sandstones with tool mark, possible a scour fill; b) sole marking (erosion of bed) with roll marks; c) lenticular bedding, d) possible flaser or lenticular bedding on lake sediments; e) trough cross-bedding sedimentation unit with some overturned tangential foresets. a, b, c, and d correspond to La Boca upper member at Valle de Huizachal. e– La Boca Formation at the locality of Cañón El Olmo.

Facies association 1A has not been divided into further sub-facies subdivisions based on the degree of bioturbation. The lack of consistency of beds that exhibit bioturbation makes unnecessarily their characterization. Nevertheless, the uncommonly observed burrows are present at the medium-fine grained

conjunction with lateral migration of the fluvial systems, it creates laterally extensive channel-base lag deposits.

This facies association of sandstones and conglomerates grades upward into a finer-grained sandstone sequence in the upper parts of the sequence, reflecting the erosional destruction of source area relief through time. Some sedimentary structures are indicative of fluctuating discharge or discontinuous recession of floodwaters. Water levels include alternate layers of clast-supported and matrix-supported gravels inferred from outcrops that show the stepped [channel] margin of a conglomerate.

Facies subdivision FA-1Aa fits for the necessity to interpret the origin of epiclastic rocks generated from complex underlying volcanic and pyroclastic deposits (lahars, ignimbrites, and other types of tuffs).

The preserved internal voids, which would have collapsed under subaqueous conditions, plus the striations observed on the wall of the burrows are typically produced by digging activity of organisms into a firm substrate that suggest burrowing when sediment was sub-aerially exposed (Bromley and Asgaard, 1979). This bioturbation are interpreted in combination with the occurrence of desiccation mud-cracks on FA-2B to be indicative of a short period of sub-aerial exposure of the sediments before consolidation (Bridge, 2003). The lack of bioturbation observed in FA-1A is interpreted to be a consequence of a reduced falling flow stage cycle and therefore a lack of time for organisms to colonize.

2.3.1.2 Fine to medium grained, planar cross-bedded to horizontally laminated sandstones (FA-1B)

2.3.1.2.1. Description

Facies 1B consists of ~60 cm up to ~2 m thick units that can be traced for up to 40 m perpendicular to paleoflow, and up to 100 m parallel to paleoflow depending on the localities. Each unit exhibits a sharp to concave-up base and concave-down top, resulting in an overall wing shape geometry (e.g., Fabuel-Perez *et al.*, 2009). They comprise fine to medium grained sandstones with subangular grains and fair sorting. Each unit can be internally subdivided into several sets or bedforms (0.1 to 0.9 m thick) showing lithofacies Sp, Sh, Sl, and Sr. Each set is bounded by 2nd to 3rd order surfaces (Fig. 2.2; Fig. 2.3). The direction to which these units prograde is subparallel to the local paleoflow. Grain-size grading is not as evident as in facies 1A, although an occasional fining-upwards trend is observed in individual sets. Ripple-cross lamination (Sr) occurs at the top of some units. Mud rip-up clasts and clay chips are common at the base, although they are also present in reduced proportions throughout the unit. Concretions are occasionally observed at the middle and top units of these successions. FA-1B shows a lack in bioturbation and therefore no subdivision has been made into other subfacies. Beds with ripple bedding occasionally appear within the cross-stratification structures of FA-1B with thin streaks of mud, they occur between sets of cross-laminated or ripple-laminated sandy sediment.

2.3.1.2.2. Interpretation

Channel-fill deposits (FA-1A and FA-1D) grade laterally into channel-bar deposits. Facies 1B is interpreted as deposits of fluvial bars that are characteristic of a braided system. (Allen, 1983; Bridge 1993a,b; Miall, 1996). Braided channels have zones where the flow divides and rejoins around compound braid bars. Characteristic features are complex patterns and ephemeral bars of numerous types. Deposition on both point bars and braid bars is commonly in the form of unit-bar that accreted onto the compound bars during floods. Unit bars and supposedly related sets of planar cross strata have been specifically associated with braided rivers.

Parallel laminae are the product of grain separation by the differentiation of upper flow regime (Cheel, 1984; Cheel and Middleton, 1985; Paola *et al.*, 1989). The association between normal grading and parallel laminae evidences transport and deposition of unidirectional flows highly concentrated in gravels under upper and lower flow regime, which favors an environment for grain-to-grain segregation. Beds with parallel laminae and cross-ripples represent episodic low energy flows. Local hydrodynamic shifts mark the increase of turbulence, which in turn enables the transition from parallel laminae to ripples (Leeder, 1983; Middleton, 1966 a,b; Allen, 1971, 1983b, 1984; Stow, 1979; McCaffrey *et al.*, 2001). Cross-stratification is the result by the migration of ripples or dunes of any scale. Since dunes occur at various sedimentary environments, the interpretation of the sedimentary structures depends on the facies with which they are associated.

The flaser or lenticular bedding found occasionally on the few analyzed sections evidence fine sedimentary deposits found in suspension within the depositional zone of ripples, where fluctuation in sediment supply and current velocity are common (e.g., lakes, fan deltas, and other deposits related to marginal-marine; Reineck and Singh, 1980).

The presence of bars is usually inferred by the visibility of smaller-scale sedimentary structures such as avalanche slipfaces and horizontally bedded upstream slopes (Hubert and Forlenza, 1988; Steel and Tompson, 1983). The geometry, spatial distribution, and migration of elements (bars) within channels control the plan geometry (channel pattern) of the channel belt; expressed as the sinuosity of channels and the degree of channel splitting (braiding). The prograding geometries observed for these facies suggest downstream accretion bars (or mid-channel bars; Miall, 1996). Accretion of unit bars is indicated by accretion topography in the form of bar-head lobes and bar-tail scrolls. The plane geometry or bed configuration represents the conduit pattern. Shifts between conduit patterns generate alternate bars or simple epsilon sets with banks or beaches. Hydraulic shifts are generated at flow separation eddies or tight bends (point bars) dissected by chutes. The changes in stage, direction or flow regime were bedforms randomly interact may produce architectural reactivation surfaces (Collinson, 1970; McCabe and Jones, 1977). Well-known end members channel deposits may be included in the mobile-channel belt (active and abandoned channels and bars) deposit concept (*cf.*, Miall, 1996).

Downstream accretion is the principal product of accretion within bar complexes of major sand-bed channels (Allen, 1983a,b; Bridge 1993a; Miall, 1996). Bars are a direct indicator for the size of the host channel and their height can be related to the minimum channel depth (Miall, 1996). This allows reconstructing the dimensions of the rivers. Downstream accretion bars can be related to i) a simple 2D dune cross-channel bar acting as the nuclei for new sediment added as fields of dunes and ripples migrate downstream (Cant and Walker, 1978; Allen, 1983b); or ii) to stacked groups of 3D linguoid dunes (Crowley, 1983). Mid-channel bars may accrete both downstream and laterally at the flanks (Allen, 1983b, Miall 1993, 1994), but they also can be formed by upstream accretion (Bristow 1987, 1993). Dunes and unit bars current ripples are an evidence of falling flow stage. Therefore, variations in composition and geometry are related to fluctuation in flow and sediment supply (Collison, 1970; Germanoski and Schumm, 1993) or changes in deposition and erosion during fluctuations in flow stage (Bridge, 1993a).

Specifically for longitudinal bars, migration takes place only during flood. If the prevailing internal structure is a poorly defined horizontal bedding it suggest that that gravel deposition took place on the upper bar surfaces (deposition from suspension and traction), rather than on foreset slopes (suspension) at the down stream margins. At lower stage, sand accumulates with internal high-angle cross-stratification and ripples cross-lamination (“burst-sweep cycle”; *cf.*, Allen, 1984). During rising flow stage, erosion occurs in the deepest parts of bends, confluence scours, and at the upstream ends of bars, whereas these areas receive deposits during falling stages.

Discontinuities in inclination may be associated with the occurrence of unit bars, their bar-type accretion, and channel filling. Discordances in large-scale inclined strata form by discharge fluctuations and shifts in channel position, and are related to the formation of cross-bar channels. Different types of vertical sequence of lithofacies depend mainly on the position of the bar and on the mode of channel migration rather than on channel pattern (Bridge, 2006).

2.3.1.3 Fine to medium grained, non-bioturbated, sigmoidal bedded sandstones (FA-1C)

2.3.1.3.1. Description

Sedimentary units with facies 1C show similar lithologies and sizes as facies 1B. However, FA-1C shows a distinctive geometry with bedforms exhibit sigmoidal shapes, and accretes perpendicularly to local palaeoflow. Bedform stratification is composed of two sedimentation units, an upper foreset bed dominated by plane-bedded sandstone, and lower cross-bedded sandy sandstone. Form sets have been termed humpback dunes (Allen, 1983c). Bedforms downlap onto erosive bases and have offlapping upper terminations (Fig. 2.7).

The foreset commonly show a maximum angle of 25° and have erosive bases. It is predominantly to observe unidirectional asymmetric ripples (Sr) at the top of units, with crests perpendicular to the accretion direction of the sigmoids. Frequently, facies 1C are deposited in contact with facies 1A and 4A. FA-1C is commonly observed at the successions in Valle de Huizachal (Fig. 2.6; Fig. 2.7; Fig. 2.18).

2.3.1.3.2. Interpretation

Facies 1C is interpreted to be lateral accretion bars (Miall, 1996). FA-1C represents the migration of a bar with similar hydraulic characteristics as in FA-1B, but with a lateral development. Internally, the bars are formed by sand dunes, which accumulate by both vertical aggradation and lateral accretion (Miall, 1993). When Sr is present in bedforms, it exhibits sigmoidal shapes developed in segregated gravel-sand mixtures. The latter is the result by the mixture of flat-bed and dune-like fluid dynamic conditions (Sauderson and Lockett, 1983; Miall, 1996).

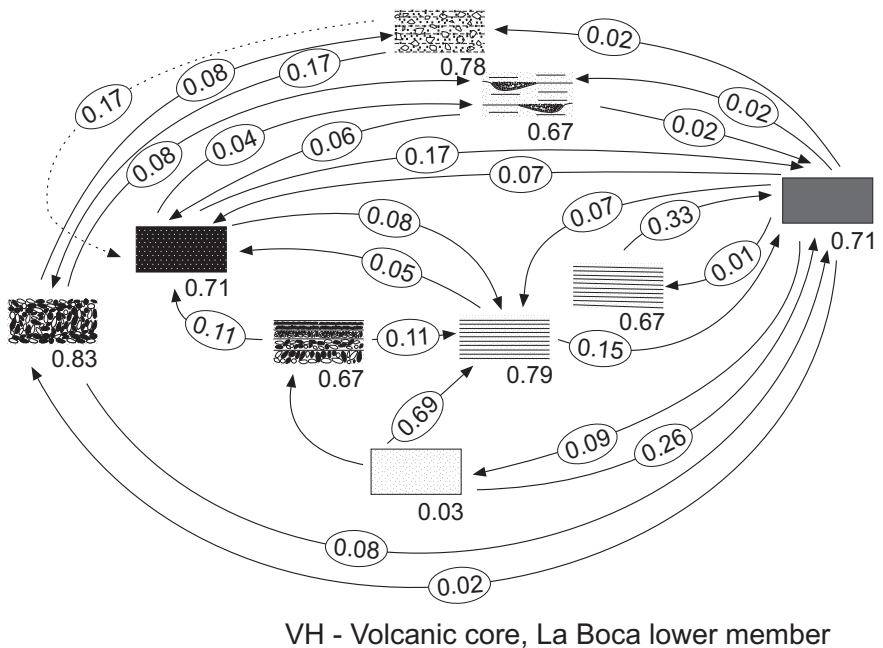


Fig. 2.6: Graphic representation from the Markov Chain containing FA-1C for the lower member of La Boca Formation at the Valle de Huizachal (VH), by computing the transition frequency-probability matrix datasets from lithofacies (Appendix for Chapter 2). Key for symbols at Fig. 2.1.



Fig. 2.7: a) Photograph assemblage at Valle de Huizachal in La Boca upper member from a bar deposit exhibiting some of the low flow regime lithofacies (Sp, Sh; Sl; Sr) contained in facies FA-1B, FA-1C. Scale bar at the right represents 40 cm

FA-1C are commonly juxtaposed to downstream accretion bars (facies 1B) or to sedimentary gravity flows (FA-4A). They are produced when downstream accretion bars change orientation and begin to migrate laterally (Allen, 1983a,b; Miall 1994), or when alluvial fans sourced from erosion invade channelized regimes to become a gravel bar and displace its morphology laterally to develop into a lateral bar, compound bar (Miall, 1977), sand flats (Cant and Walker, 1978), or sand shoals (Allen 1983a). When geometries of FA-1B and FA-

1C are similar, discrimination between downstream and lateral accretion bars on a 2D outcrop is difficult, although it can be done by using a cut-off angle of 60° between the accretion surface and cross-bedding within the element. Angles less than 60° indicate downstream accretion bars, whereas angles greater than 60° are classified as lateral accretion bars (Miall, 1996; Fabuel-Perez, 2009). Channel-bar deposits that present large-scale stratasets thicken laterally as the large-scale strata increase in inclination (Bridge, 2006). Although different types of bars are recognized in modern sedimentation flume study analogues (Allen 1983a; Best *et al.*, 2003; Lunt and Bridge 2004; Lunt *et al.*, 2004) the bars identified in this study can be classified as composite-compound bars (Allen, 1983a), as they all show a combination of lithofacies Sr, Sp, Sl, arranged in two or more erosively related sets.

2.3.2. Overbank facies association (FA-2)

2.3.2.1 Bioturbated massive mudstone to siltstone (FA-2A)

2.3.2.1.1. Description

Facies 2A consists of clay to siltstone thin lamina to very thick beds, which are laterally extensive in both dip and strike depending on the locality. This facies are commonly poorly exposed and covered by modern vegetation, but when outcropping they show a structureless aspect (lithofacies Fm) and isolated ichnofossils. The morphology of organo-sedimentary structures varies in five-type morphological cases, from: (1) simple vertical burrows in FA-1A, (2) sub-horizontal to linguoidal structures, (3) unbranched, partially straight, bulb-morphology, straight tubular form in vertical position, from 2 to 3 cm in diameter and 700 mm long, (4) an “L” form of 4 cm with unbranched, partially straight to slightly incline to curved-twisted shafts, and (5) a plane disc-morphology, with scarce recognizable surface with a diameter of ~ 20 cm (Fig. 2.8). Incipient pedogenic structures are at times present. Red bed outcrops near Galeana may present concretions, logs, and root traces. Within FA-2A carbonate lenses appear randomly on the top of the massive sequences, like they occur in at the successions of Cañón de Caballeros and Miquihuana (Fig. 2.9).

2.3.2.1.2. Interpretation

Facies 2A corresponds to overbank sediments deposited in a river channel-floodplain environment. A floodplain is a strip of land that borders a stream channel and that is normally inundated during seasonal floods. Floodplains develop in all alluvial valleys, alluvial fans, and fandeltas, irrespective of the channel pattern (Bridge, 2006). Most sedimentation occurs over floods, when sediment is transported over the floodplain as bed load and suspended load during flood-flow conditions (Schumm, 1981). Water completely covers the floodplain and flows more or less down valley during peak flood.

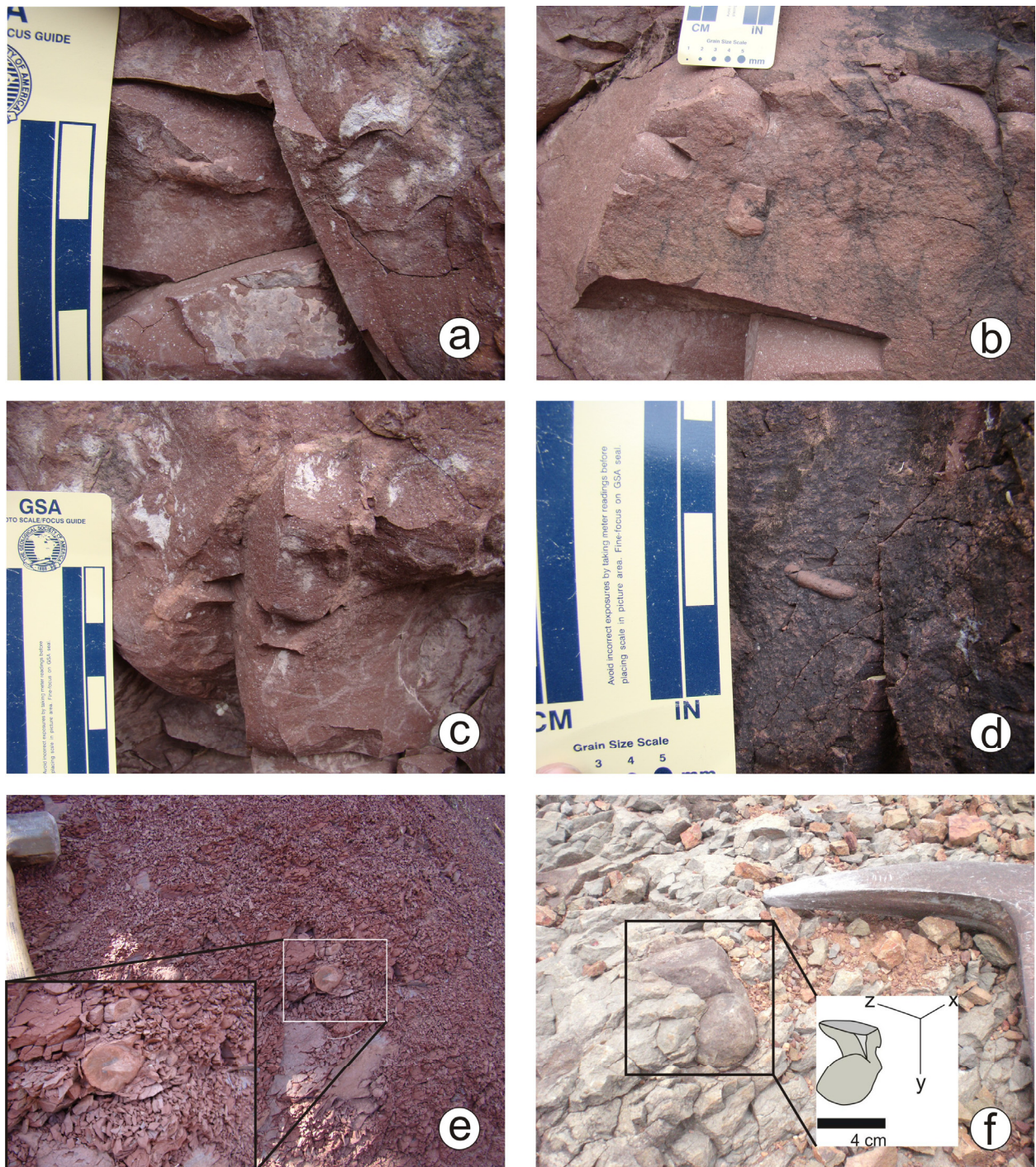


Fig. 2.8: Photograph mosaic for the lithofacies Fm found on facies FA-2B. a) sub-horizontal to linguoidal structures; b) thick simple vertical burrow; c) sub-vertical to linguoidal structures; d) sub-horizontal to linguoidal structures; e–f) “L” form structure of 4 cm with unbranched, partially straight to slightly incline to curved-twisted shafts. a, b, and c were pictured at the lower interval of La Boca Formation at the Valle de Huizachal. e and d are found at the upper member of La Boca Formation at Valle de Huizachal. f– corresponds to the lower most exposure of El Alamar Formation at Lomas de San Paulo Tranquitas.

FA-2A is interpreted as sheet flood deposits, strictly speaking, unchanneled by definition. None of the individual-burrow manifests as a recurrent ichnofacies through out the red bed sequences, despite of the facies specificity for burrow distributions [or assemblage] and morphologies. Therefore, the use of the classification for overbank deposits according to the presence of tracefossils, structures, and previous and subsequent

environments remains as unnecessary (Smoot and Olsen, 1985). However, by applying tracefossils descriptions preliminary interpretations can be built about the ichnologic record of the continental red beds (Buatois *et al.*, 1998; and Buatois and Mángano 1993b; Buatois *et al.*, 1996). Some considerations were taken for the environmental significance of individual ichnofacies, which has become a point of debate between researchers.

Sandstone beds in localities near Galeana apparently contain well to partially preserved logs and trace-fossil individuals: *Scoyenia* ichnofacies, *Planolites*, and *Scoyenia* ichnoguild (Buatois and Mángano, 1993a). These interpretations are based on the reported Triassic conditions for tracefossils on floodplain and paleosol environments (Buatois *et al.*, 1998). The occurrence of these tracks is in close association with the sandstone interval of a major second fining-upward cycle that presents subaerial surfaces. Morphological cases 1, 4, and 5 are appreciated within these sequences (Fig. 2.22).

Floodplain deposits at Valle de Huizachal contain well to partially preserved logs and trace-fossil individual: *Scoyenia?* or *Mermia?* ichnofacies. That interpretation is based on the global climatic conditions reported for the Jurassic to generate *Roselia* trace fossils (Pemberton, 2001). Individuals from the morphological cases 1, 2, and 3 occur in silt to fine grained sandstone in floodplain facies at La Boca Formation (Fig. 2.18).

The implications for the low trace fossil diversity of individuals are the following: (a) tier establishment of suspension-feeding infaunal organisms with progressive ecospace utilization (spatial/functional); (b) burrows are scarce and restricted to shallow penetrating traces on some mud-silt bedding planes; (c) tracks are associated with subaerial environments of fluvial, alluvial of low-middle energy with long-term period of exposure (variable water table); (d) low monologic stage ponds developed in a floodplain basin, filled by overbank processes or desiccation in some areas; (e) tracks represent *Scoyenia* and *Mermia* ichnofacies or ichnofamily affinities (Buatois and Mángano, 2002); (f) structures were made by an infaunal arthropod, perhaps an insect or other invertebrate organism (e.g.: beetle, annelids); and (g) the number of individual and morphology of the traces is too simple in to be diagnostic of specify an environment.

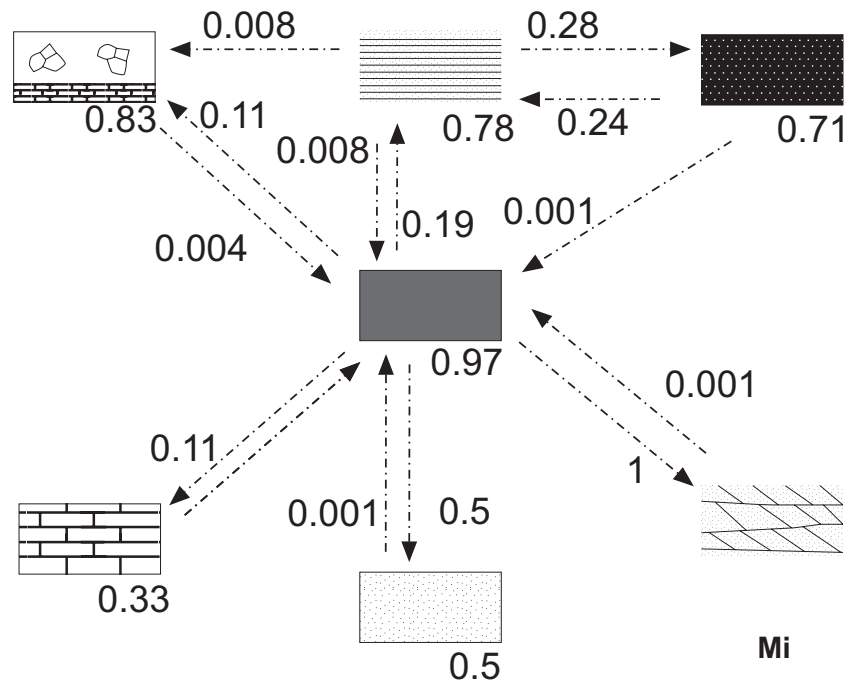


Fig. 2.9: Graphic representation from the Markov Chain containing FA-2A for the Miquihuana (Mi) locality, by computing the transition frequency-probability matrix datasets for lithofacies (Appendix). Key for symbols at Fig. 2.1.

2.3.2.2 Bioturbated massive to laminated mudstone–siltstone (FA-2B)

2.3.2.2.1. Description

Facies 2B consists of a 2 m up to 25 m thick sequence. This facies is characterized by alternation of mudstone and siltstone laminae showing horizontal lamination (lithofacies Fl; Fig. 2.10). The sandy laminae are thin lamina with a moderately erosive base. Clay and siltstones dominate a >90% of the total stone mass contained in the beds, while sandstones a <10%. Bioturbation is rare or completely absent. Root traces are also found at FA-2B. Deposits may present postdepositional modification, “slumps”. Occurrence of floodplain slumps coincides with local cross-bedding vectors (Fig. 2.10; Fig. 2.17).

2.3.2.2.2. Interpretation

Facies 2B is interpreted similar to FA-2A, but with more subaerial exposures that permitted a well development for paleosols and carbonate precipitation. Floodplain deposits are planar-stratified fine to very fine sands interbedded with silt and clay. In general, an overbank deposit closest to the roots. The stratasets may be sheet-like, wedge-shaped, or lenticular depending on the local environment of deposition. These deposits are associated with the channelized flow and sheet floods from overbank areas. The absence of bioturbation and the presence of mud cracks indicate a relative ease deposition, while graded strata evidences soft material emplacement by flood recurrence. Overbank deposits with postdepositional modifications and related to the flow regime orientation served as an indicative of a “westward” paleoslope (e.g., Cañón de Caballeros).

Caliche profiles are the most common soil types found in most of rift basins (Lorenz, 1988). Caliche-type, carbonates often form as isolated nodules or kankar within muddy floodplain soils. When fluvial processes erode the muddy floodplains, the muddy sediments wash away the larger and more resistant kankar nodules that subsequently are incorporated into the fluvial deposits as intraclasts (e.g., clay chips, or ripple clasts). As a result, carbonate nodules may be found at other channel-fill facies, even if no evidence remains from the contemporaneous overbank mudstone and soils.

2.3.2.3 Non-bioturbated massive to laminated mudstone to siltstone interfingered by tuff related deposits (FA-2C)

2.3.2.3.1. Description

Facies 2C has beds that oscillate from 8 cm to 2 m thick. FA-2C presents alternations of laminar units from lithofacies Fm, Fl, Af, Sl (i.e., Fig. 2.11). The FA-2C can extend horizontally up to 5 km, serving as a surface boundary for correlation. The fine-grained thin laminae posses an erosive base and culminated its sequence with erosive tops. Bioturbation is absent (Fig. 2.10).

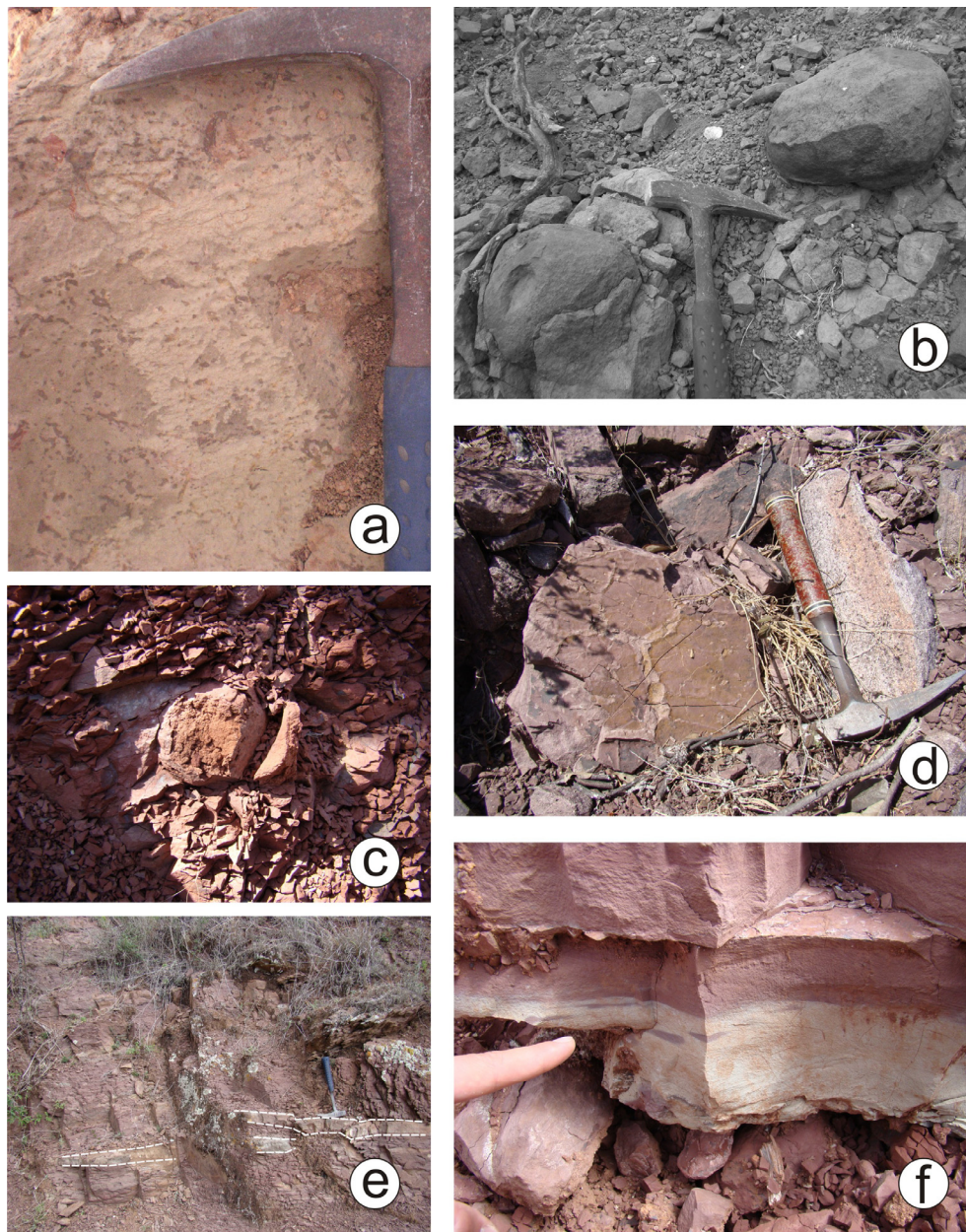


Fig. 2.10: Photograph mosaic for facies FA-2B and FA-2C. a) Paleosols with organic content; b) fine grained concretions; c) soft ball sediments structures; d) mud cracks developed on a paleosol (plain view); e) interfingered tuff deposits with fine sediments (Fm); f) tuff deposit. a and b are located at El Alamar Formation at Lomas de San Paulo Tranquitas. c and d correspond to strata from La Boca upper member at Valle de Huizachal. e and f are found at La Boca Formation at the west flank of the Aramberri's Uplift.

2.3.2.3.2. Interpretation

Since the objective is to associate and relate lithofacies for a common and simplified classification scheme, this work has been omitted further explanation and interpretation about any of the possible types of pyroclastic deposits and their eruptions. The author encourages revising the methods about the studying of ancient and modern volcanic succession (Cas and Wright, 1987) for a complete understanding of the following statements in this section.

FA-2C is interpreted as an independent facies related to epiclastic deposits (*cf.*, Cas and Wright, 1987) with flow transformations (*cf.*, Fisher, 1983) linked to proximal volcanic source areas. The terms epiclastic, pyroclastic, and hydroclastic however refer to processes by which particles are formed and they cannot change from one particle type to another merely by changing the agent of transportation. This concept is a critical nontrivial distinction for problems relating penecontemporaneous volcanism and deposition to understand volcanoclastic facies. This distinction is also critical to find differences in sedimentation in volcanic and nonvolcanic areas. Most nonvolcanic siliciclastic sediments are epiclastic, subjected to various degrees of supply depending weathering and erosion rates at the source area.

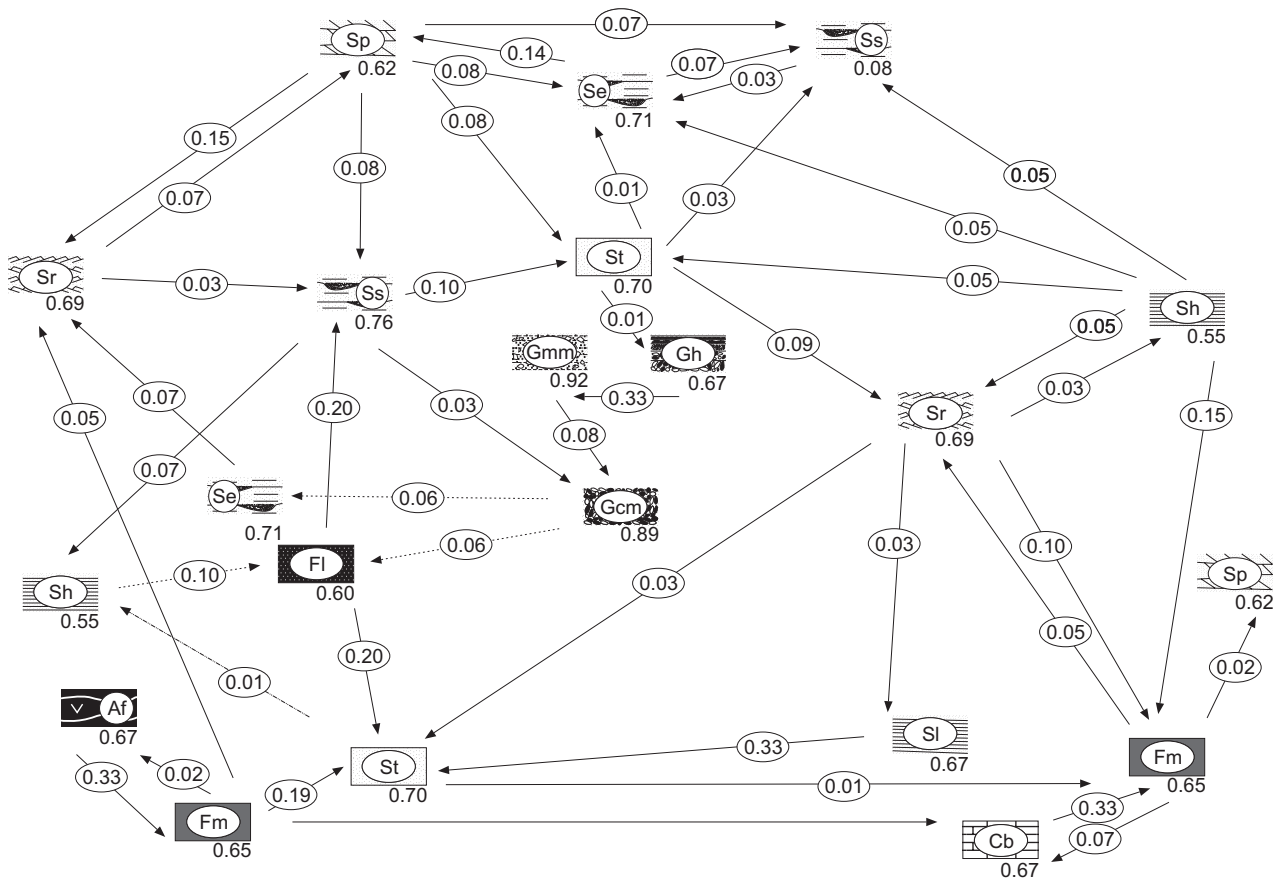
The fine lithic content on FA-2C is considered as volcanoclastic fragments. This volcanic material was generated instantaneously and in large volumes producing unique facies distributions and geometries not encountered in nonvolcanic epiclastic sediments. The lateral distribution of rock-types from the source volcano into adjacent nonmarine depocenters is determined by the rate at which materials are extruded from a volcanic source, their total volume, and the processes of transportation linked to flow transformations. Volcanoclastic accumulations are reflected almost instantly in the sedimentary record on surrounding regions that directly receive supply from pyroclastic flows, surges, eruption related debris, avalanches, lahars, and fluvial materials, or by the remobilization of loose material between volcanic events.

The transport pathways from the volcano to adjacent basins during active or inactive eruptive events involve flow transformations that change in behavior from laminar to turbulent or viceversa within a sediment gravity flow. These changes in Reynolds number are caused by: (1) density separations within a moving sediment gravity flow caused by gravity segregation of particles (gravity transformations); (2) velocity variations related to slope changes (body transformation); and (3) separations of particles caused by turbulent mixing in between the ambient fluid and the flow (surface transformation). Laminar turbulent or turbulent laminar transformations commonly result in changes by transport agents. Prevailing agents in FA-2C might be subaerial pyroclastic type-flow deposits (and surges?) that turn into normal fluvial transport systems. Therefore, a facies lineage tends from FA-2C—pyroclastic surge, flow debris flows, or hyperconcentrated flood flows, to FA-1B—normal fluvial erosion-transport processes (Fig. 2.11).

2.3.3. *Aeolian facies association (FA-3): very fine to medium grained, well sorted, non-bioturbated, planar cross-bedded sandston (FA-3A)*

2.3.3.1 Description

Facies 3A consist of 2 m up to 12 m thick units, traceable for up to 25 m laterally. The red coloured sandstones are well sorted and made up of rounded grains (Fig. 2.12). They show sharp bases and tops. Each bedset is composed by the superposition of several sedimentation units bound by sharp surfaces (3rd order). Internally all the bed sets exhibit tabular-planar cross-beds (Sp) and wedge planar cross-beds.



VH - Quarry east from volcanic core, la Boca upper member

Fig. 2.11: Graphic representation from the Markov Chain containing FA-2C for the upper member of La Boca Formation at Valle de Huizachal (VH), by computing the transition frequency-probability matrix datasets from lithofacies (Appendix for Chapter 2). Key for symbols at Fig. 2.1.

Each cross-bed set shows stable, unidirectional, and tangential to base morphologies with dips of about 25°, although they show higher angles in some cases. The internal sets increase progressively in thickness from bottom to top, they are formed by alternation of homogeneous sand bed laminae and inversely graded very fine-grained sand at the base.

2.3.3.2 Interpretation

Sandstones in facies association 3 are interpreted as deposits of aeolian dunes based on the presence of well sorted and well rounded very fine to medium-grained sand. Deposits show large sets of planar cross-bedding (Hunter, 1977; Kocurek and Dott, 1981). The aeolian stratification (McKee, 1979) and their deposits can exhibit various characteristics depending on the proximity of the water table to the surface, the degree of aridity of the climate, and the chemistry of the groundwater. These interpretations are complimented by the presence of sedimentary structures based on previous studies in modern aeolian environments. The high angle cross-bed sets are similar to those found in modern aeolian dunes with a well-developed slip face (Inman *et al.*, 1966; McKee, 1966). The wedge-shaped cross-bedding is related to the presence of several types of dunes

giving as a result a complex dune association (Rubin and Hunter, 1983). The absence of rip-up clasts is also a diagnostic for aeolian facies. Aeolian environments are the most dependant on climatic conditions for their formation. Aeolian environments have hydrodynamic conditions of low flow regime (Simons *et al.*, 1965; Middleton, 1965). Moreover, aqueous dunes are related to high velocity ranges of subcritical flow (Froude number; *cf.*, Middleton, 1977). Their formation is correlated to height and wavelength of deep water conditions (Allen 1968), and controlled by the outer turbulent layer.

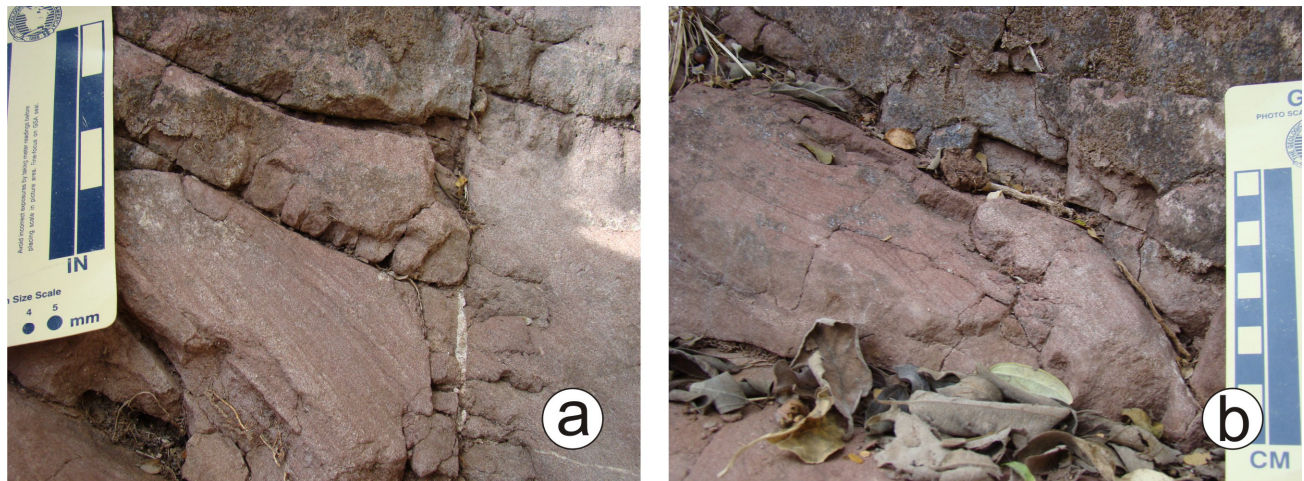


Fig. 2.12: a–b) Scaled photographs of facies FA-3A found in La Boca upper member at Valle de Huizachal, representing the unidirectional low flow regime of sandy lithofacies Sr with dune generation. Notice the formation of cross-lamination that dips at angles of up to $>30^\circ$.

Wind blow deposits, although not strictly representative in the red beds sequence of northeastern Mexico, are defined based on aeolian transportation and deposition. These ancient environments at the Valle de Huizachal were subjected to rivers with fine beds. Wind-formed dunes represent sand deposits with a higher suitable angle than those from aqueous sedimentation, and most of the wind-blown silt forms scattered fine-grained deposits in the foresets (Allen; 1982; “burst-sweep cycle”; Allen, 1984).

Bedforms that superimpose on gravel bars or debris flows during floods are the most common dunes, irrespective of grain size or channel pattern (e.g., at the Valle de Huizachal). The latter allows us to discard interdune deposits or related aeolian deposits that occur in vadose zones or lake environments, which present adhesion ripples (structures hard to define and document in the ancient). This feature is produced as damp sand or mud traps wind-blow sediment by surface tension. Interdune deposits are recognized by two main characteristics: (i) adhesion ripples, (ii) interbedded red to brown siltstones and shales and bearing desiccation cracks. The few aeolian deposits found on extensional or rift basins exemplify only a small part of the total possible variability of aeolian sedimentary deposits.

2.3.4. *Alluvial fan facies association: very coarse grained to granule-pebble grade, matrix to clast supported massive to cross-bedded sandstones and conglomerates (FA-4)*

2.3.4.1 Description

Facies FA-4 is exposed in sharp-based tabular bedding that ranges from 25 cm up to 15 m thick of matrix- and clast-supported, non-imbricated conglomerate and sandstone. It can be traced laterally over hundred of meters. Beds are formed by massive sedimentation sets with thicknesses ranging from 10 cm to 65 cm (Fig. 2.13). Grading is observed on small fining upwards grading lithofacies (Gmm, Gmg, Gcm), or at inverse-graded gravels within the facies successions (Gci; Fig. 2.14). Occasionally, unidirectional current cross-ripples can be observed within graded sandstones at the top of some units. A wide variety of grain sizes characterize this facies from very coarse sandstones up to granule, and pebble conglomerates interbedded at the same outcrop. Clasts are mainly extraformational, leaving lithic fragments as the main components. Rock fragment are subrounded to subangular shape. The medium to coarse-grained sandstone forms the matrix in matrix-supported units.

2.3.4.1.1. Interpretation

Debris flows [including mudflows] and grain flows are particularly common in pre-existing alluvial flows or channelized apex areas, where slopes are steep like in adjacent areas to fault scarps. The high potential energy created by relief brought sediments rapidly from the source terrane to the depositional basin, usually leaving them texturally and compositionally immature. Deposition will be rapid and the sedimentary deposit will contain many discontinuities with a high sand-body ratio (Allen, 1978). The coarsening-upward cycles resulted from rapid progradation following pulses of relative uplift on the source areas of alluvial fans. Therefore, coarsening-upward cycles are of tectonic origin (allocyclic). Breccias consisting of fragments of a single lithology are the product of avalanches. These sedimentary bodies extend down into the heads of alluvial fans.

A hyperconcentrated grain flow of sand-size and larger particles commonly produces inverse grading, a gradational decrease in grain size from top to bottom of the layer deposited by the flow. Inversely graded grain-flow deposits are characterized by a hydraulic equivalence that differs from that based on settling velocities or entrainment. It is dispersive pressure that controls the development of the inverse grading. Dispersive equivalence, derived from the dispersive pressure agrees reasonably well with observed relationships between grain sizes and densities in grain-flow deposits (e.g., avalanche deposits).

Inverse grading involves an upward increase in either or both of clast size and percentage (avalanche deposits, hyperconcentrated grain flows). Nevertheless, debris flows with their high viscosity and yield strength; may remain also as satisfactory mechanisms for inverse grading.

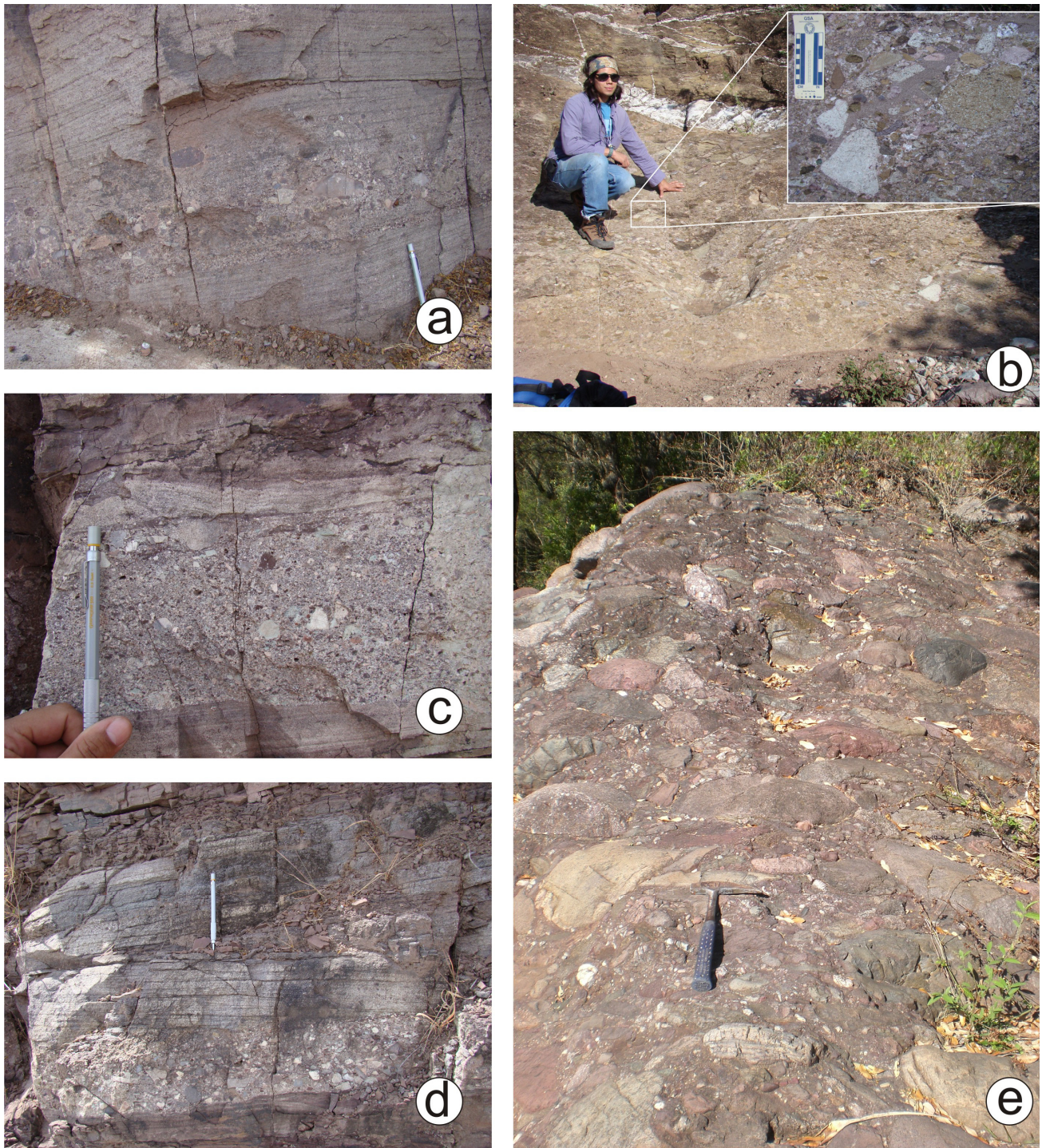


Fig. 2.13: Photographic assemblage for the facies FA-4. a) Lithofacies Gmm found in La Boca upper member at Valle de Huizachal, b) lithofacies Gci in La Joya Formation at Aramberri, c) lithofacies Gmg in La Boca upper member at Valle de Huizachal, d) lithofacies Gh in La Boca upper member at Valle de Huizachal, e) lithofacies Gcm for the base of La Joya Formation at Cañón Caballeros.

The strength loss (sensitivity) that clay suffers on deformation can explain inverse grading; the lowest, most strongly sheared layers of debris are weakest and support relatively small clasts. Other processes that may contribute are reduced buoyancy due to dilation, strength/fabric anisotropy, variable clast fall-out rate, inherited stratification (e.g., mud decollement in slumps) and sediment assimilation during flow. The sensitivity mechanism may also apply to density-modified muddy grain-flow.

2.4. Litho-stratigraphic sections for the Huizachal Group

The data from field observations, the description and interpretation for each of the facies were put into together on the following measured sections Fig. 2.16; Fig. 2.17; Fig. 2.18; Fig. 2.15. The order of the sections is built by considering the northern most outcrop to the southernmost studied locality.

Sedimentary structures (Rubio-Cisneros)

Description

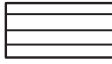

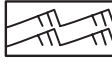


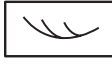







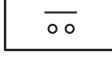
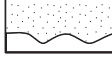
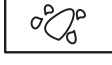


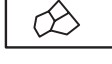


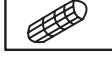
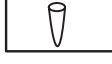


	Parallel lamination		Planar cross-stratification
	Current ripple lamination		Current ripple tops
	Climbing ripple lamination		Trough cross-stratification
	Sigma cross-bedding		Tangent (epsilon) cross-bedding ripples
	Clay chips		Sand lenses
	Charge moulds		Soft-sediment deformational structures
	Normal grading		Inverse grading
	Load casts.		Ripple clasts
	Volcanic intrusions		Interbedded carbonate lenses
	Desiccation Cracks		Erosional base Paleosols
	Mayor surface boundary		Plan fragments
	Trace fossils		Root structures
	Concretions		

Fig. 2.15: Glossary of sedimentary structures found in the measured sections.

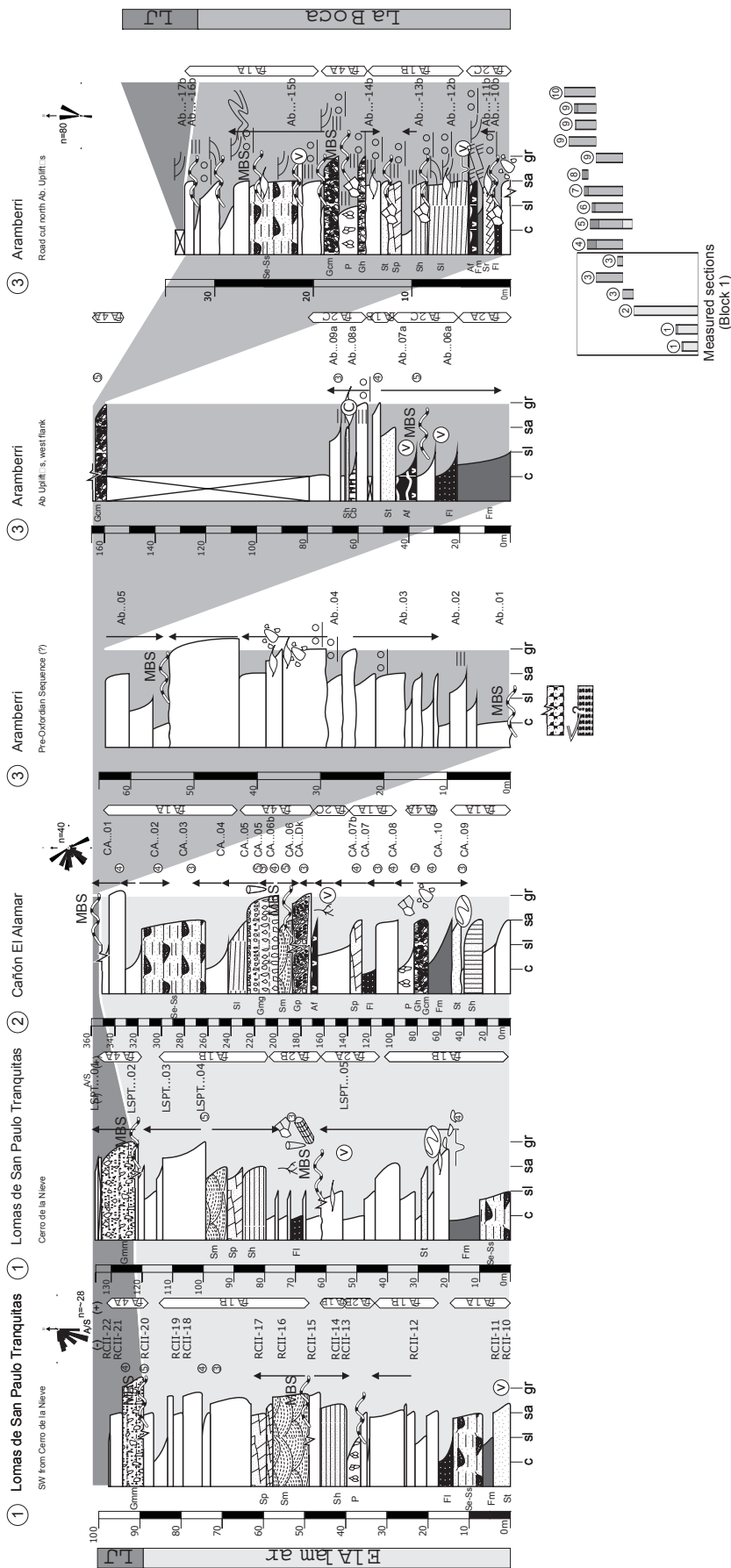


Fig. 2.16: Measured sections (Block 1) and stratigraphic levels of collected samples for various analyses. For sedimentary structures description consult Fig. 2.15. Vertical arrows indicate cyclic successions of various types, showing direction of fining and bed thinning. Numbers in circles indicate rank of bounding surfaces. Lithofacies codes are given at left of column. Facies associations are given in white vertical tags at right of column. c: Clay; sl: Siltstone; sa: Sandstone; gr: Gravel. Stratigraphic position of the measured sections (Block 1) with respect to other analyzed areas is plotted on the lower right corner. Correlation by shaded sections: light gray: El Alamar Formation; dark gray: La Joya Formation (LJ). Measured paleocurrents are above measured sections. Underlying the measured sections are reported basement units with calculated age.

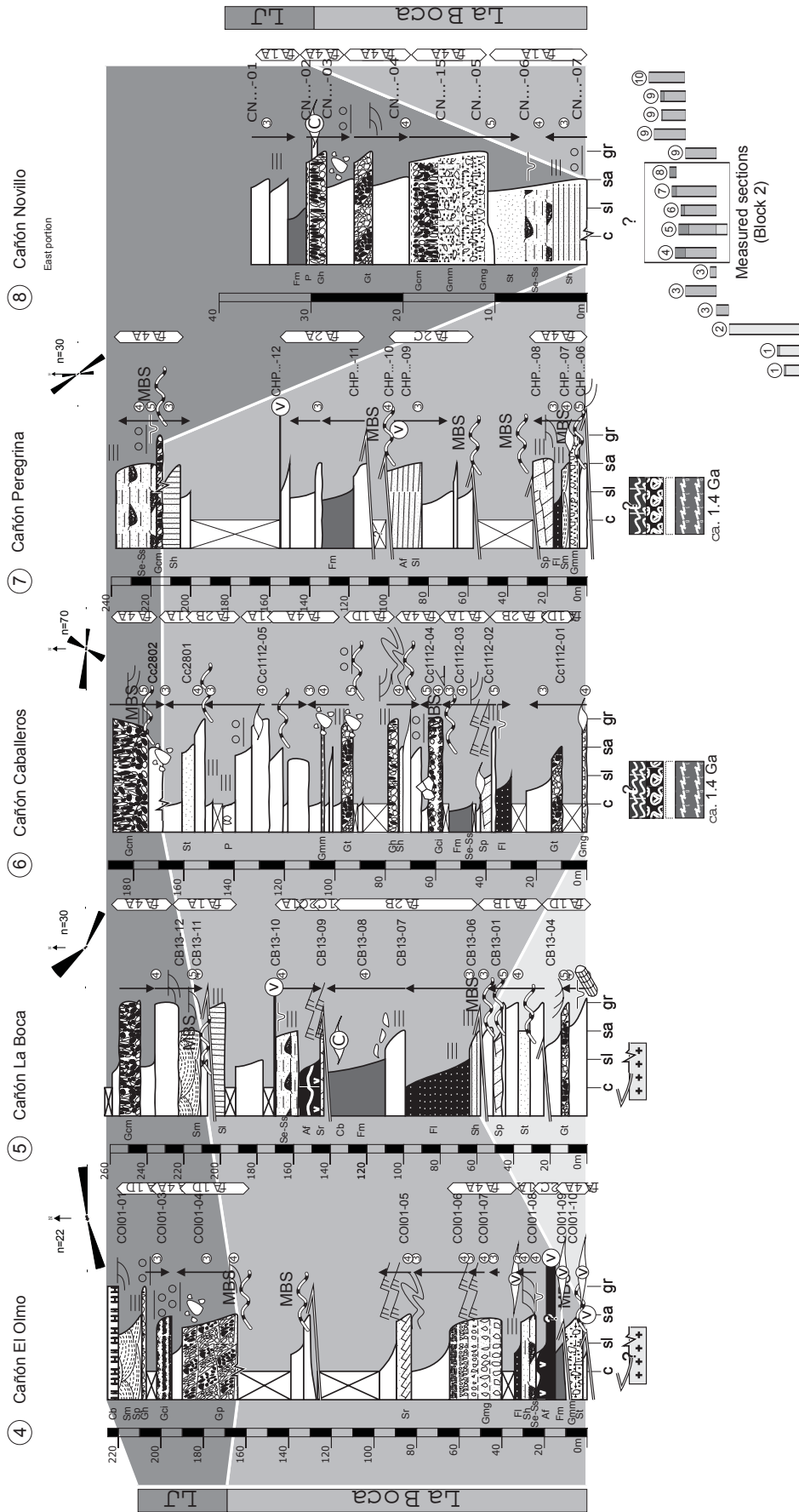


Fig. 2.17: Measured sections (Block 2) and stratigraphic levels of collected samples for various analyses. For sedimentary structures description consult Fig. 2.15. Vertical arrows indicate cyclic successions of various types, showing direction of fining and bed thinning. Numbers in circles indicate rank of bounding surfaces. Lithofacies codes are given at left of column. Facies associations are given in white vertical tags at right of column. c: Clay; sl: Siltstone; sa: Sandstone; gr: Gravel. Stratigraphic position of the measured sections (Block 2) with respect to other analyzed areas is plotted on the lower right corner. Correlation by shaded sections: light gray: El Alamar Formation; middle grey tone: La Boca Formation; dark grey: La Joya Formation (LJ). Measured paleocurrents are above measured sections. Underlying the measured sections are reported basement units with calculated age.

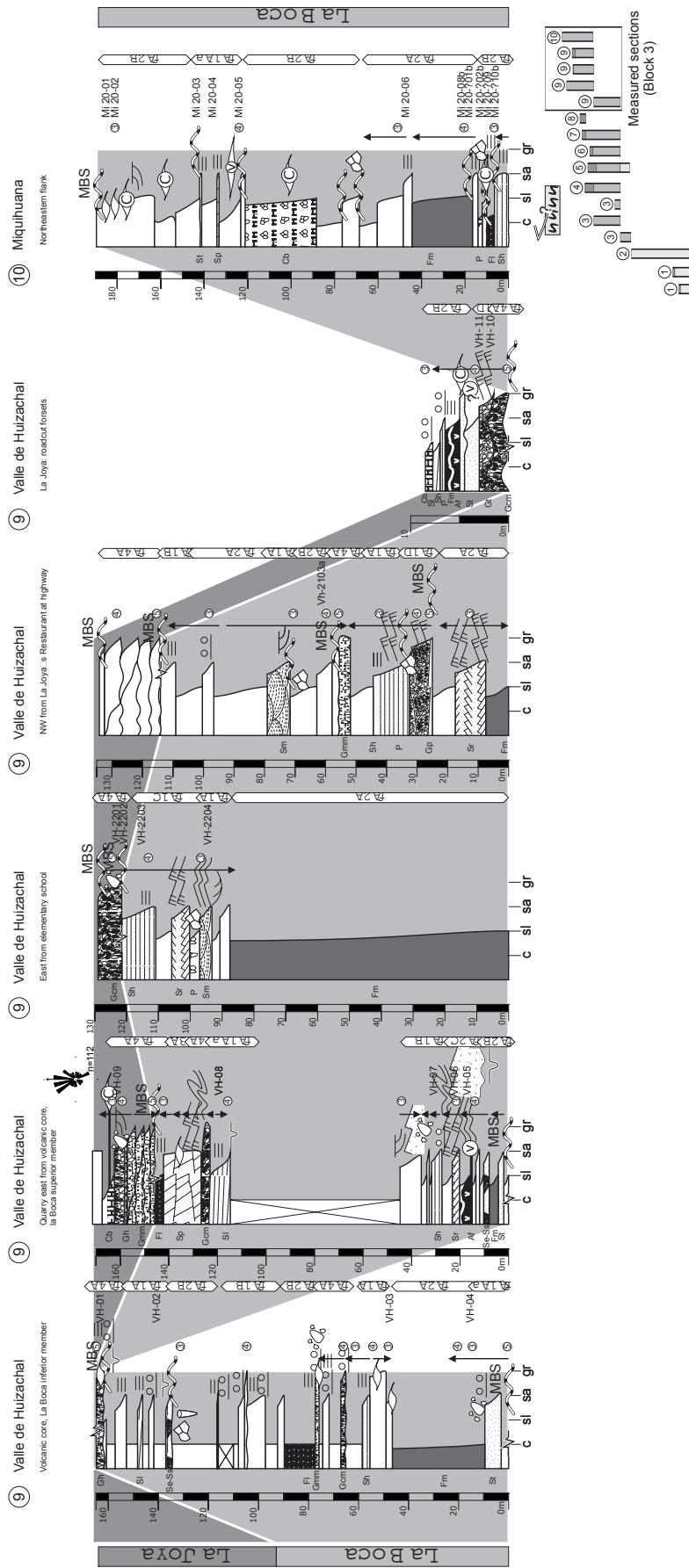


Fig. 2.18: Measured sections (Block 3) and stratigraphic levels of collected samples for various analyses. For sedimentary structures description consult Fig. 2.15. Vertical arrows indicate cyclic successions of various types, showing direction of fining and bed thinning. Numbers in circles indicate rank of bounding surfaces. Lithofacies codes are given at left of column. Facies associations are given in white vertical tags at right of column. c: Clay; sl: Siltstone; sa: Sandstone; gr: Gravel. Stratigraphic position of the measured sections (Block 3) with respect to other analyzed areas is plotted on the lower right corner. Correlation by shaded sections: middle grey tone: La Boca Formation; dark grey: La Joya Formation (LJ). Measured paleocurrents are above measured sections. Underlying the measured sections are reported basement units with calculated age.

2.5. Architectural element analysis

2.5.1. Architectural concepts

The research of how rivers operated under a wide range of controls to deposit a large body of sediment is referred as “[fluvial-] architecture”. Architectural elements are the unique details and component parts that together form recognized surfaces and structures in a hierarchic manner to define sedimentary environments and styles. The application of architectural element analysis as an interpretive tool is an extended function of allostratigraphy from a stratigraphic context (for citation of definition see, Miall, 1985, 1986, 1996; Holbrook, 2001; Fielding and Gibling, 2005; Strong and Paola, 2006). This term has been coined to describe extensive accumulations of fluvial deposits in sedimentary basins formed over millions of years. These deposits normally show distinctive spatial variations in the mean grain size, geometry, proportion, and spatial distribution of channel-belts and floodplain deposits (referred to as alluvial architecture by Allen, 1978).

The study of architecture has well defined controls operating over element genesis. Controls on alluvial architecture are for example extrinsic (extrabasinal) which includes factors such as tectonism by decreasing the rate of sediment transport down valley (by flow expansion associated with tectonic subsidence or base-level rise), and controlling aggradation rates from channel belts. Fluvial architecture helps to understand models based on processes for long-term or large-scale erosion in rivers and floodplains. Deposition in alluvial valleys is commonly a long period of widespread erosion to form incised valleys and river terraces. Long-term and large-scale erosion in alluvial valleys results by increasing sediment transport rate in the down-flow direction. These erosion conditions are caused by basin uplift or baselevel fall, or by climate influences that decrease the upstream sediment supply. Previous studies have modeled the interpretations for terrain (river terraces) conditions (channel incision) up and down valley (Bridge and Tye, 2000, Bridge, 2003; 2006; Gibling, 2006). These results optimize the understanding about different episodic processes (degradation and aggradation) that build distinctive elements with differentiated and complex internal features.

Alluvial architecture is conditioned to tectonic activity that controls the rate, amount and location of uplift and subsidence gradients, but also the position of rivers (Schumm *et al.*, 2000). Thick accumulations of fluvial sediments [sedimentary basins] occur in a variety of different tectonic settings, hence alluvial architecture varies with tectonic setting (Miall, 1996). Tectonic uplift and subsidence can be gradual or episodic expressed as the sum of motions along all of the different active structures (Schumm *et al.*, 2000). Such movements could be responsible for diversion of major rivers and growth or dissipation of alluvial fans (Gawthorpe and Leeder, 2000).

Alluvial architecture in extensional basins is configured by tectonic stretching and thermal subsidence (*cf.*, Allen and Allen, 1990; Leeder, 1999). Lateral propagation and joining of fault segments leads to enlargement and coalescence of rift basins, and further on the development of drainage systems. The active tectonism for these basin-types ensures frequent avulsions and episodes with high rates of erosion and deposition that are recorded in architectural elements (Fabuel-Perez *et al.*, 2009).

2.5.2. Methods: a working bedding diagram

Architectural element analysis is a methods of stepwise interactions between the observer and the outcrop with its elements. Holbrook (2001) exemplifies in four steps the way and rules that govern for constructing bedding diagrams. (1) Surfaces: Each surface is considered unique and laterally continuous until truncated or deemed indiscernible. A surface may truncate another but surfaces may not cross. Though surfaces may be diachronous, any location on a surface must be younger than the material/surfaces it cuts and older than material/surfaces it binds. (2) Assign Orders: Bedding surfaces bounding lamina sets are considered as 1st order. Lower-order surfaces will be bound by higher-order surfaces. The order of a surface will be one order higher than the highest-order surface it binds, and maybe of higher order where guideline 4 should be satisfied. Surfaces truncate against surfaces of equal or higher rank. Similar, but nested, surfaces maybe treated as a set of boundaries of equal order, but the set should be ultimately bounded by a surface of higher rank. (3) Incorporate facies architecture. (4) Apply Interpretations: The Original “Elements” of Miall - Fluvial “Legos” (Table 2.2; Fig. 2.19).

2.5.3. Architectural hierarchies and bounding surfaces

The principles of the hierarchical classification of depositional units are detailed in Miall (1996), in comparison to other nomenclature schemes (Smith, 1990; Soegaard, 1990, 1992; Bridge, 1993c). The hierarchies of bounding surfaces (Table 2.3) used to correlate sections are based on Miall (1988) and Gibling (2006).

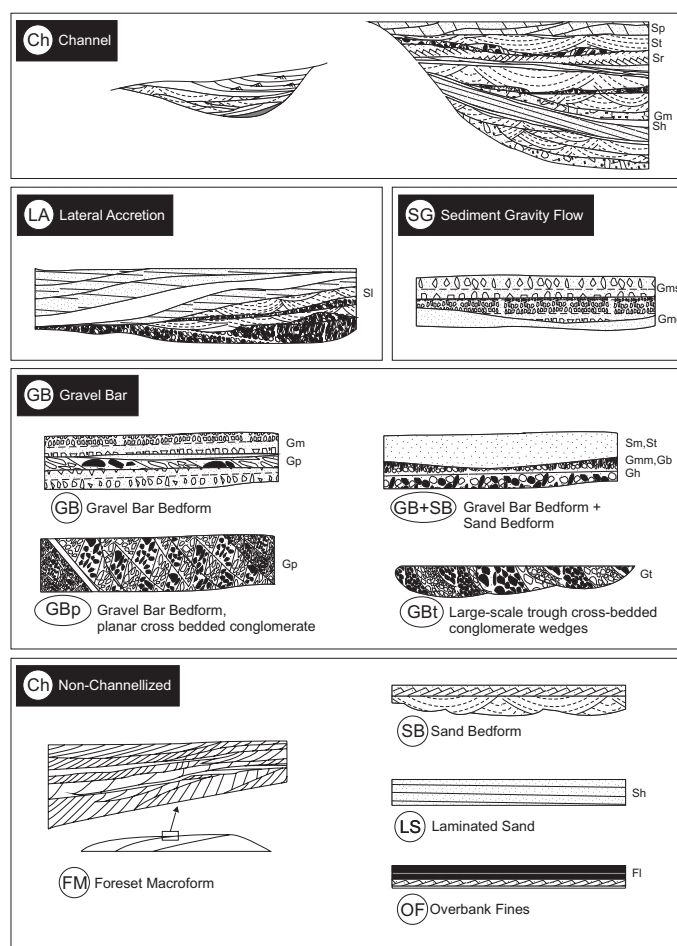


Fig. 2.19: The eight basic architectural elements in fluvial deposits (Miall, 1985, 1988, 1996).

Table 2.2: Fluvial facies summary for applied interpretations in bedding diagram built-up (Holbrook, personal communication).

Interpretation	Description	Sedimentary structure rock-state	Deposits in architectural elements
Still waters	clay, silty clay, peat long-term settling	Non-Bioturbated Bioturbated	floodplain, mud flat, overbank fine, levee lake
Lazy river	loams and heterogeneous generally weak erratic flow	Non- Bioturbated Bioturbated	levee/splay active channel
Swift current	sand and loamy sand sustained strong flow	Non-Bioturbated Bioturbated	thin splay, channel and lobe bar, thick channel thalweg fill

Table 2.3: Bounding surfaces hierarchy and descriptions used in this study.

Bounding surface order unit	Depositional unit	Surface Description	Sequence Characteristics
1	Bedform set-ripple (microform, microscale set)	Flat and non-erosional (except for scour associated to separation of eddies).	Train of bedforms of similar type.
2	Bedform coset-dune (mesoform, mesoscale set)	Flat and non-erosional.	Staking of same facies type.
3	Macroforms, marking "large-scale" reactivation. Indicate stage changes or changes in bedform (stratum) orientation.	Cross-cutting erosion surfaces dipping up to 15° and truncate underlying bedding surfaces (1st and 2nd order) at low angle.	Similar facies assemblages and geometries above and below.
4	Bounding surfaces of macroforms and inclined strata (minor channel and bars).	Flat to convex upwards. Underlies 1st to 3rd order surfaces and is truncated by next erosional event.	Mud drapes below the surface and intraclasts resting on the surface. Different facies assemblages above and below.
5	Bounding small channels belts (group macroscale sets).	Flat to concave upwards marked by local cut-and-fill relief.	Channel infill exhibiting rip-up clasts or lag breccias.
6	Bounding main channel belts, palaeovalleys	Regional erosional surface.	Channel belts.

Modified from Miall (1985) and Gibling (2006).

2.5.4. Classification of architectural elements

2.5.4.1 Rationale

Architectural element analysis is dependant on the exposure dimensions of the studied outcrops, when ever the larger the exposure the more available variables to interpret. Only few of the red beds sections are satisfied under the latter statement. The Valle de Huizachal offers road cuts at different strata levels that any other studied area has, this to construct better bedding diagrams to achieve reasonable interpretations. The exposed sections throughout the Valle de Huizachal correspond to the upper member of La Boca Formation and to La Joya Formation. This analysis has been focused on the upper member of La Boca Formation at the Valle de Huizachal by the lack of diversity in facies associations at La Joya.

2.5.4.2 Description

Architectural element analysis of fluvial strata reveals five orders of bounding surfaces in the upper member of La Boca Formation. Each order is bundled by surfaces of the succeedingly higher orders, thus the surface can be fit in a hierarchical progression. Nevertheless, regressions might be present, when succeedingly into lower surface orders. Two levels of surfaces bind channel-fills at the scale of architecture elements. The surfaces record in an ascending order rank: overbank fines (FF), down stream accretion (DA), laminated sand

sheet (LS), sand bedform (SB), sediment gravity flows (SG), gravel bars (GB), and gravel bar with sand bedforms (GB+SB). The characteristics, strata fill, and genesis for each surface and element are discussed below. Sand bodies extend up to 100 m, with a variety of thickness, depending on the facies content in the element (Fig. 2.20).

2.5.4.3 Interpretation

2.5.4.3.1. Architectural elements formed in channels

Although the nature and geometry of architectural elements are mostly determined by autogenic factors their large-scale arrangement seems to be a function of the interplay between different allogenic controls. Short-term changes occur during stage changes with macroform increment. Macroforms are governed by the bounding surface characteristics from flash floods and seasonal fluctuations. Longer-term changes reflect aggradational and reduction in water depth as seen on the levee and splay macroforms by controlling processes of channel and bar migration. Other long-term effect in depositional units is avulsion under a 5th order bounding surface regime. Since either of the both long-term interpretations have similar lithofacies assemblages and successions it is one major problem while developing a profile analysis.

GB– gravel and bedforms: lithofacies Gt and Gp define the main mesoforms. The formation of these mesoforms is discussed on previous sections in the description and interpretation for facies FA-4A. The nature of gravel transport makes the mesoforms and lithofacies commonly interbedded produced by water table variability and sediment discharge. “Slugs” or sediment pulses supply gravel at irregular rates from conduits into the system. The thin and simplest deposits are the thin diffuse gravel sheets at lithofacies Gh with lobate margins and migrate only during peak flow. These gravel beds are amalgamated to produce macroforms (bars). Element GB forms multistory sheets of 30 cm to 60 cm. Surfaces between mesoforms are flat or irregularly eroded. GB may be occasionally interbedded with minor to predominant sheets or lenses from element SG (sediment gravity flows). Whenever SB occurs it comprises 5-10% of the coarsest gravel succession. GB+SG represent slack-water non-bioturbated deposits such as abandoned channel fills (minor CH element), bar-edge sand wedges, fandeltas, or the deposition of topographically elevated parts of a deep gravel-bed river style (*cf.*, Miall, 1996).

SG– sediment-gravity-flow element occurs as narrow, elongated lobes in multistory sheets, and is typically interbedded with elements GB or SB. Predominant lithofacies are Gmm, Gmg, Gci, and Gcm. SG is correlated in facies with FA-4A (Fig. 2.14). The element forms by debris flows and related mechanisms, as described in previous sections. Individual beds average 0.5-3 m in thickness. Flow units typically have irregular, nonerosive bases. Flow events occupy passively the existing erosional channels or the irregular topography made by earlier sediment-gravity-flow and sheet-flood events. Grading and inverse grading are common. This element is part of a sand and loamy sand sustained strong flow. SG lacks of non-bioturbated characteristics constraining the element into a lobe deposit.

SB– sandy bedforms includes lithofacies associated with upper flow regime bedforms that form in sand-dominated river systems. Lithofacies Sm and Sh occur in a variety of fluvial settings and show a range of assemblages and vertical sequences within channel fill deposits. SB has similar facies as those on FA-1A. Whenever convex-up bedding contacts are found below a major fourth order surface, they represent bedforms resting on dipping bounding surfaces interbedded with each other formed at a simultaneous event. Otherwise, deposits will represent fields or trains of individual bedforms that accumulated in geometries of vertical aggradation. Related deposits contain first-, second, and third-order contacts. Vertical stacking of the different bedform types indicates long- short-term changes in flow regime.

DA and LA– Downstream-accretion and lateral-accretion deposits are the principal products of accretion within the bars complexes at major sand-bed channels. DA and LA elements are very common in braided sheet sandstones. Sh is the predominated lithofacies for DA and LA. Lithofacies approximations can correlate DA and LA with facies FA-1B. This outcrop lacks of three-dimensional geometrical complexities making almost impossible to interpret with confidence any of the occurring elements. It was also difficult to find oriented accretionary surfaces and cross-bedding with high perpendicular angles ($> 60^\circ$ difference) to prove an LA element. DA and LA elements represent bar macroforms that contain second- and third-order surfaces gently dipping downstream or to the outer bank. The changes in sediment load and channel geometry (discharge variability) are reflected on variations of composition and geometry of the macroforms. These sandbody represents a thin splay, channel, and lobe under strong flow conditions. Deposits are non-bioturbated sand and have loamy sand characteristics (Fig. 2.2).

LS– laminated sands sheets includes lithofacies 1) Sh, Sl, Fl, Fm with minor 2) Sp, Sm or Sr. Facies FA-1B and FA-2B are correlated by the two lithofacies intervals, respectively. Element LS is a sand deposit with upper flow-regime plane bed conditions or by flash floods (Miall, 1977, 1984; Tunbridge 1981; Sneh, 1983; Stear, 1985). Individual sand sheets are <2.5 m thick and rest on flat to slightly scoured erosion surfaces (Se-Ss lithofacies). Sp and Sm gradationally capped the sand sheets indicating waning flow conditions at the end of the flood event. Individual sheets may be traced for more than 100 m. Sheets thin and split into thinner units dominated by finer-grained sands and silts of waning lithofacies. These non-bioturbated beds represent the margins of individual food sheets conditioned by weak erratic flows at levee/splay deposits.

2.5.4.3.2. Architectural elements of the overbank environment

FF– overbank fines element consists of sheet-like sedimentary units some tens of meters extent. Fines present lithological variability in the vertical, reflecting the fact that the depositional surface is flat and readily susceptible to small changes in depositional processes (Miall, 1996). Sedimentation takes place by separate increments during flood events, or a continual slow settling of fine-grained sediment from suspension in clay, silt, clay, and peat (e.g., floodplain, mudflat, overbank, and levee). Desiccation, pedogenic processes, and bioturbation mark major bounding surface, which is important to explain seasonal or longer-term drying-out of

the sedimentary environment and the availability of niches. This element is topped with paleosols and lithofacies Fl. Overbank fines correlated with facies FA-2B.

The architectural element analysis for the upper member of La Boca Formation at the Valle de Huizachal supports the generation of river terraces. The terraces are parts of floodplains that have become elevated above the bankfull level of the active channel because of widespread channel incision. Terrace risers would also experience erosional retreat associated with mass wasting (creep, debris flows; e.g., FA-4A), overland flow (e.g., FA-2), and gullying. Terraces differ in height and valley fills have a complicated internal structure. The processes of degradation and aggradation turns from swift current downstream, to the outer bank of lazy rivers, and into still waters.

2.6. Accommodation and supply: surface architecture

Changes in sediment supply have a large effect on sequence geometry, as well as by changes in accommodation space (Cloetingh *et al.*, 1993; Puigde-Fabregas 1993; Schlager, 1993; Shanley and McCabe, 1994). The construction and use of bounding surfaces leaves open criteria for other hierarchical usage of mappable stratigraphical limits for nonmarine stratigraphy. Bounding surfaces designated as Major Bounding Surfaces (MBS) are traces on a section that represent both processes and products from geomorphic (autogenic) or tectonic–eustatic (allogenic) origin. MBS are independent to the rank and characteristics of bounding surfaces based on the hierarchy for depositional units in alluvial deposits (Miall 1991). MBS remains as a traceable surface guided as Holbrook (2001). Surface architecture is an approximate interpretation made by Major Bounding Surfaces (MBS) on how must a fluvial system had operated. Surface architecture is driven by the information contained in architectural elements and adjacent units of analysis (lithofacies and facies association).

This work intends to preserve a genetic coherence in its interpretations. It is hoped that this erected reconfiguration of a variant for bounding surfaces helps to clarify geological controls registered on the stratigraphic architecture of fluvial depositional systems. The main idea for surface architecture works on the basis of genetic significant surfaces such as unconformities and disconformities (e.g., flooding surfaces). Any further interpretation must consider the development of paleosols within interfluvial deposits.

The nonmarine realm of accommodation is somewhat hard to define and can be a function of (1) climate and tectonism in the source area, (2) the climate and tectonism at the site of deposition (3) the climate and tectonism downstream of the depositional site, and (4) relative sea level changes (e.g., Sequence Stratigraphy,). Surface architecture is not attached to relative sea level history. It aims for mayor sedimentary responses to basin-forming mechanisms* for subsidence and uplift (e.g., overburden).

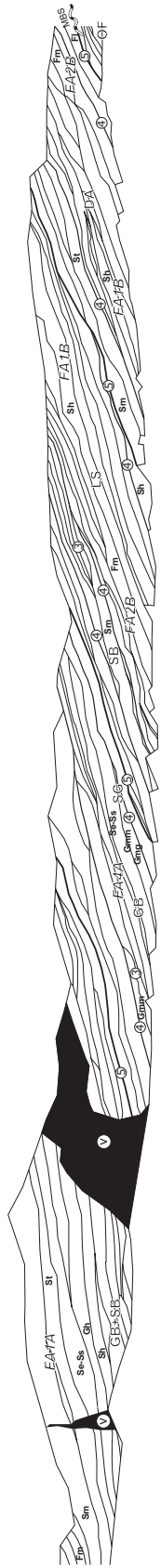
* Further details can be found at Dickinson, 1974, 1976, 1993; Allen and Allen, 1990; Ingersoll and Busby, 1995; Leeder, 1999; Einsele, 2000; Miall, 2000.



SE

~3.5m

NW



~500m
La Boca Formation upper member

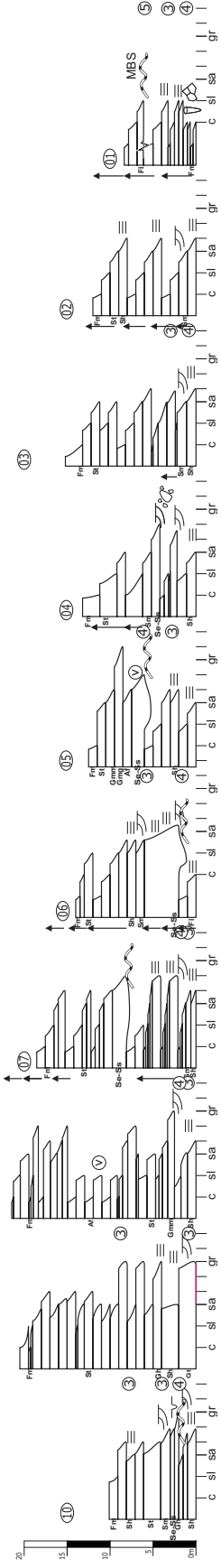


Fig. 2.20: Bounding surfaces and architectural element unit hierarchies at a road cut exposing the upper member of La Boca formation at the Valle de Huizachal. The analyzed section was divided into 10 smaller control points (numbers in ovals). The sections are approximately equally spaced to analyze the lateral variability of the different lithofacies, facies association, and architectural elements. Bounding surfaces are circled. V- volcanic. FA- facies association with its respective category. Abbreviations like Sh, Sl- correspond to lithofacies at left of column. SG, GB, LS, DA, OF- are assigned architectural elements. For sedimentary structures description consult Fig. 2.15. Vertical arrows indicate cyclic successions of various types, showing direction of fining and bed thinning. Numbers in circles indicate rank of bounding surfaces. c: Clay; sl: Siltstone; sa: Sandstone; gr: Gravel.

2.6.1. Description: A model proposal

The development of fluvial stratigraphy in sedimentary basins in a continental setting is controlled at first order by three factors accommodation space, sediment supply, and the hydraulic characteristics of the fluvial system. Accommodation and supply operate as dual controls on stratigraphic sequences (Schlager, 1993; Ryer, 1994). The differences among depositional systems can strongly influence sequence patterns (Schlager, 1991). Controls overlap in scale and time to manipulate the meso-architecture of sedimentary deposits (Van Wagoner *et al* 1990; Leeder 1993).

Accommodation is the space available for sediment accumulation. The magnitude and rates of change of accommodation are critical in determining the packaging of strata (Shanley and McCabe, 1998). Sediment supply reflects the way in which surface processes have interacted with the tectonic input of material to the regolith (Hovius, 1998).

Major bounding surfaces (MBS) are subdivided into four main types of surfaces according to sedimentary processes. The four surfaces aim to identify low to high accommodation/supply successions. MBS may also contribute to correlate the variations in flow stages with sediment supply from potential source rocks or source areas rejuvenation.

Amalgamation bounding surfaces (AmBS) stand for the lowest rank of accommodation/supply from all four MBS (Fig. 2.21). AmBS indicates processes operating under low accommodation, fast subsidence rate (channel fill<overbank), and low deposition. Alluvial sequences may lay over this unconformity. Amalgamation bounding surfaces are related with facies FA-4A (Fig. 2.22; Fig. 2.23; Fig. 2.24).

A higher rank surface for accommodation/supply after AmBS is the aggradation bounding surfaces (AgBS; Fig. 2.21). AgBS details avulsion and entrenchment (less lateral migration), slow subsidence rate (channel fill>overbank), incision of channels, floodplains associated with terrace formation, fan propagation, low sinuosity, coarsening upward sequences, reduction of valley width, up-valley migration of "knickpoints" (*cf.*, Bridge, 2003), and development for unconformities (Schumm *et al.*, 1987; Sloss, 1988, 1991; Dalrymple *et al.*, 1994; Aitken and Flint, 1995; Flint *et al.*, 1995; Hampson *et al.*, 1997; Hampson *et al.*, 1999; Davies *et al.*, 1999). AgBS coincides with bounding surfaces of 4th and 5th order. However, lowering accommodation/supply does not always result in incision and rejuvenation of a fluvial system (Ethridge *et al.*, 1998). These surfaces may appear as a simple bedding plane, or as a nondeposition or erosive feature. Aggradation bounding surfaces seem to be occurring with a wider spectrum of facies associations than the other major bounding surfaces. AgBS is shared among lithofacies FA-1A, FA-1B, FA-2A, FA-4A (Fig. 2.22; Fig. 2.23; Fig. 2.24).

Degradation bounding surfaces (DeBS) is the third rank for accommodation/supply (Fig. 2.21). It describes water table or base level regression, high sinuosity, and fining upward sequences. DeBS occurs as a MBS with characteristics of an unconformity or a disconformity. Degradation bounding surfaces are accompanied by lithofacies associated in FA-1A and FA-1B (Fig. 2.22; Fig. 2.23; Fig. 2.24).

A major flooding bounding surface (MFBS) is a non-marine bounding surface that represents a significant stratigraphic flood boundary within the sequence (Fig. 2.21). The MFBS is marked by fine-grained siliciclastic with mature paleosols. It represents the onset of a period where accommodation space is greater than the rate of sediment supply. Burrowing occasionally penetrates surfaces. Its occurrence appears to be related to disconformities or 5th order surfaces. Major flooding surfaces are associated with the lithofacies from FA-2B (Fig. 2.22; Fig. 2.23; Fig. 2.24).

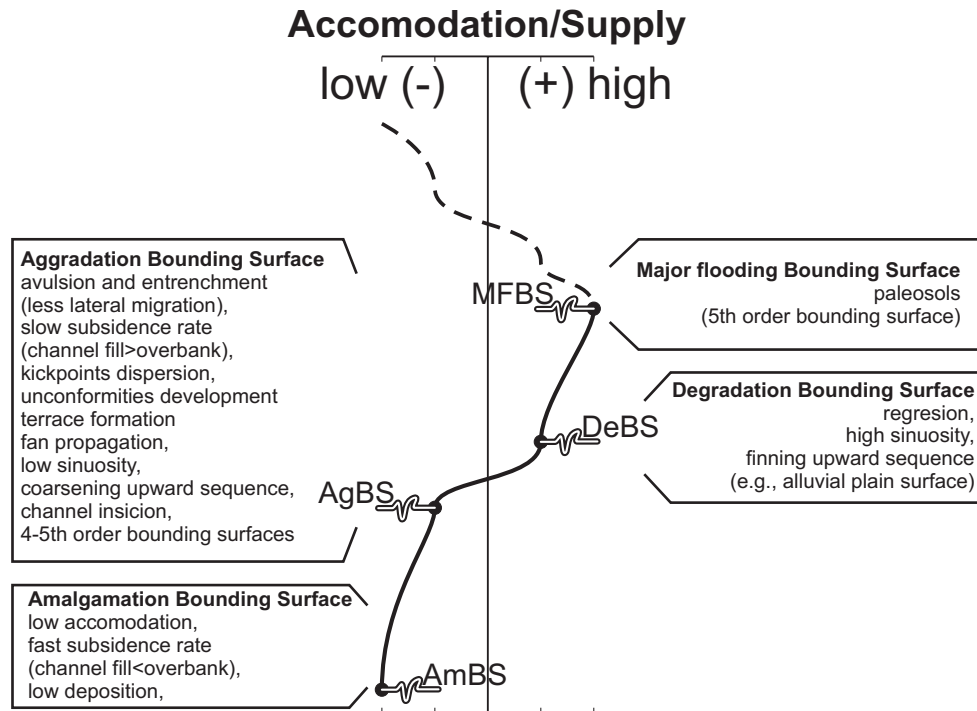


Fig. 2.21: Proposed model of the general surface architecture in fluvial environments based on the interpretation for Major Bounding Surfaces (MBS; Miall, 1991; Holbrook, 2001). Description and interpretation of the four different MBS for surface architecture. AmBS– Amalgamation Bounding Surface; AgBS– Aggradation Bounding Surface ; DeBS– Degradation Bounding Surface ; MFBS– Major Flooding Bounding Surface.

2.6.2. Interpretation: A case study – La Boca Formation at Valle de Huizachal

The results for these case study contributes for a theoretical model or representation at a belt scale for episodic behaviors (cycles; *cf.*, Schumm, 1981), which are the products of processes that occur in the geology of fluvial deposits. Changes in sediment supply have a large effect on fluvial environments, styles, and sequence geometry, but also by changes in accommodation space (Cloetingh *et al.*, 1993; Puigde-Fabregas 1993; Schlager, 1993; Shanley and McCabe, 1994).

AmBS– represents superimposed channel-belt deposits with extensive lateral amalgamation of channels during environmental conditions related to low accommodation space/supply. This non-bioturbated deposits overlie angular unconformities. The supposed accumulations are associated with low rates of deposition and to restricted floodplain width by valley incision. Facies help to interpret swift currents with sand and loamy sand

sustained under strong flow conditions. The amalgamated beds are related to sediment gravity flows deposited as a channelized debris flow. Sediment is fed by erosion at a fan dominated by the source on a scarp.

It is clear that the nature of fluvial sequences differ considerably from marine sequences, except that accommodation is a primary control for the compensation of sequences. If compared to dip-oriented marine stratigraphic sequences, the most peculiar feature of strike-oriented fluvial facies is that accommodation in inland settings cannot be easily defined (Ethridge *et al.*, 1998; Cross and Lessenger, 1998). An abstract base level makes it difficult to figure out how the accommodation works in alluvial settings.

AgBS— A surface above the AmBS rank denotes sediment accumulations under conditions of relatively high depositional rates at a broad alluvial plain. Ags responds to a relative increase of accommodation/supply. A slight rejuvenation of a channel will cause incision that is followed by deposition. Incision of channels and floodplains is associated with terrace formation, reduction of valley width, and up-valley migration of knickpoints. A “knickpoint” is a point in the river profile where the increase of slope and erosion start. As river erosion proceeds the “knickpoint” moves progressively up valley (Bridge, 2003). River terraces are parts of floodplains that have become elevated above the bankfull level of the active channel because of widespread channel incision. Terrace risers would also experience erosional retreat associated with mass wasting (creep, debris flows), overland flow, and gullying. Incision of fan channels and local growth of fans are associated with more or less random increases in sediment supply and river avulsions. Episodes of fan progradation into the basin result in upward-coarsening sequences of variable thickness.

The initiation of an avulsion is recorded in floodplain deposits by an erosion surface overlain by relatively coarse-grained deposits (associated with a major overbank flood). Sedimentary deposits over avulsion surfaces present different facies associations in comparison to prior sediment accumulations. An increase in avulsion frequency produces a major channel-deposit proportion and connectedness, but increases in deposition rate and width of floodplains decrease these characteristics of fluvial systems. Avulsion frequency is expected to be low in areas of erosion (Bridge, 2006). Channel diversions or avulsions are common on alluvial fans during floods, and occur following a period of aggradation near the fan apex. It is possible that fan-head aggradation, avulsion, and entrenchment are associated with pulses of sediment supply from the hinterland, perhaps associated with episodic tectonism. Whenever avulsions build topography to the point that regional avulsions occur, the river channel moves to a lower part of the basin, and produces local clusters. Avulsion clusters are autocyclic events that occur less frequently and over larger areas than the local avulsions that compose the cluster. As such, these events are not necessarily tied to sea level (Heller, *et al.*, 2001).

Arguments in favor of tectonism includes the i) coarse grained nature of the deposits, ii) thick coarsening upward and fining upward sequences adjacent to actual or inferred uplifted terrane, iii) evidences for unroofing with relatively high sedimentation rates, and iv) occasional syntectonic intraformational unconformities. In general, the zone of incision caused by lowering accommodation/supply propagates further upstream than the zone of deposition caused by the rise of accommodation/supply. Major aggradational events occur only when large amounts of bed load sediment manifest. The elements generated under these hydraulic conditions are

related to lithofacies found on FA-1A, FA-1B. AgBS also occurs when the susceptibility (*cf.*, Schumm, 1991) of landforms (e.g., overbank) becomes high in response to external changes (facies FA-2A). Aggradation is impossible without readily available sediment sources.

DeBS– Erosion of channels and floodplains is a long-term process (e.g., AgBS), but the short-term response may be to increase sinuosity of rivers. Avulsion frequency is expected to be low in areas of erosion. The proportion for channel deposits and connectedness may decrease by the reduction of avulsion frequency. Episodes of fan recession into the basin result in fining-upward sequences. The eroded material will be deposited but the remainder is transported through the river system as a sediment load depending on the distribution and the magnitude of accommodation space in the sediment routing system. Erosion in the upstream part of a catchment has two components. Material is removed from hillslopes by a range of denudational processes, but also by the erosive power and transport capacity of the fluvial system. Denudation is generally considered a product of the interaction between erosivity and the erodibility. Erosivity is the potential of denudational systems to remove material from a certain locality. Erodibility is the interaction of physical and chemical properties of the particles in a medium. FA-1 and its lithofacies constrain sediment transport systems that infill topographic lows (eroded sites, e.g., alluvial plain surfaces) through lazy rivers and swift currents conditions (Straub, 2009).

MFBS– In areas of high sediment supply, i.e., depocenters flanked by basement highs, the rate of sediment supply may keep pace with the rate of relative accommodation. During this process, major flooding bounding surfaces mark a change in stacking from a progradational to an aggradational sequence. The formation of MFBS is done in still waters, with grain size lithologies that vary from clay to silt, and occasionally are bioturbated. MFBS are created under depositional conditions for floodplains, mud flats, overbank fines, levees, and lakes. The presence of major flooding surfaces is correlated with the hydraulic interpretations for facies FA-2B.

2.6.3. *Closure arguments*

The bounded-cycle stratigraphy conditioned by MBS illustrates the lowering or increasing of accommodation/supply. This dual control enhances diversion in processes of the drainage system with reciprocity to sedimentary environments. They buffer sediment production and the characteristics of sedimentary patterns in fluvial styles.

Active tectonism ensures frequent avulsions (AmBS) and episodes of high erosion and depositional rates (DeBS). For this reason, a basal conglomerate in a sequence can be genetically related to both AmBS and DeBS. Nevertheless, to identify a coherent interpretation one must establish a genetic relationship with the underlying and subsequent lithostratigraphic components.

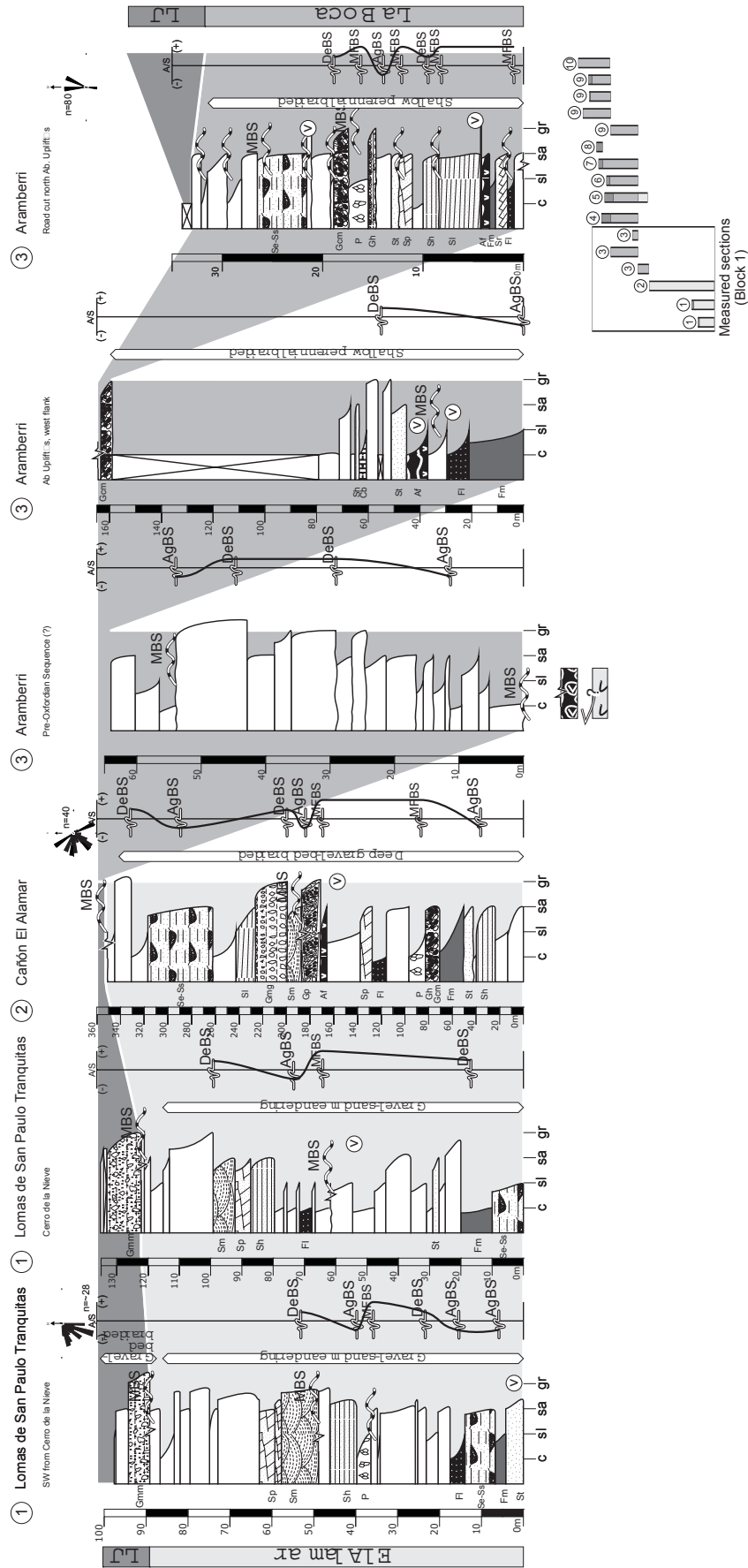


Fig. 2.22: Measured sections (Block 1) as in Fig. 2.16. The corresponding fluvial style and accommodation/supply cycle for comparative purposes are given at right of column: amalgamation (AmBS), aggradation (AgBS), degradation (DeBS), and major flooding surfaces (MfBS).

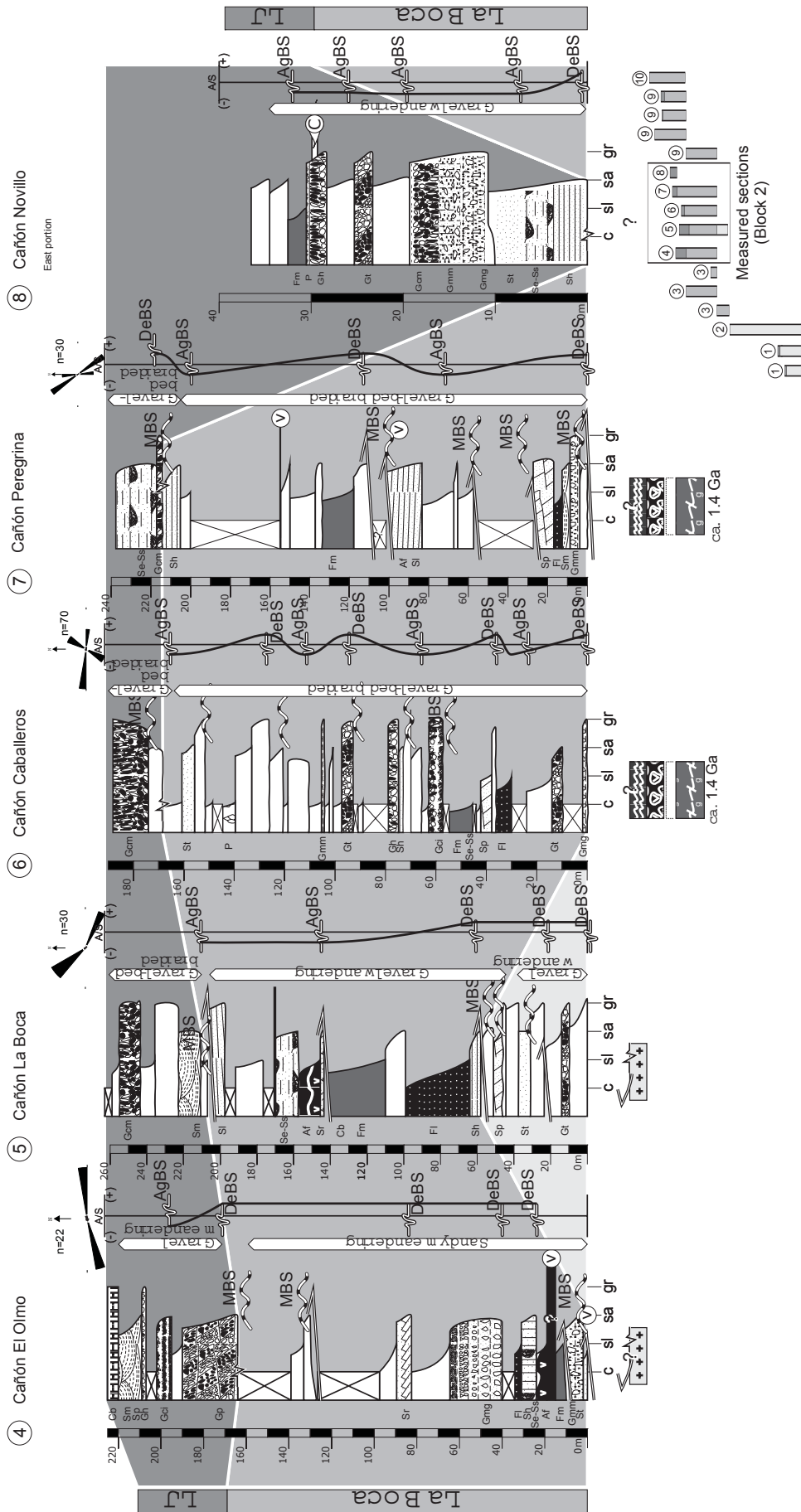


Fig. 2.23: Measured sections (Block 2) as in Fig. 2.17. The corresponding fluvial style and accommodation/supply cycle for comparative purposes are given at right of column: amalgamation (AmBS), aggradation (AgBS), degradation (DeBS), and major flooding surfaces (MFS).

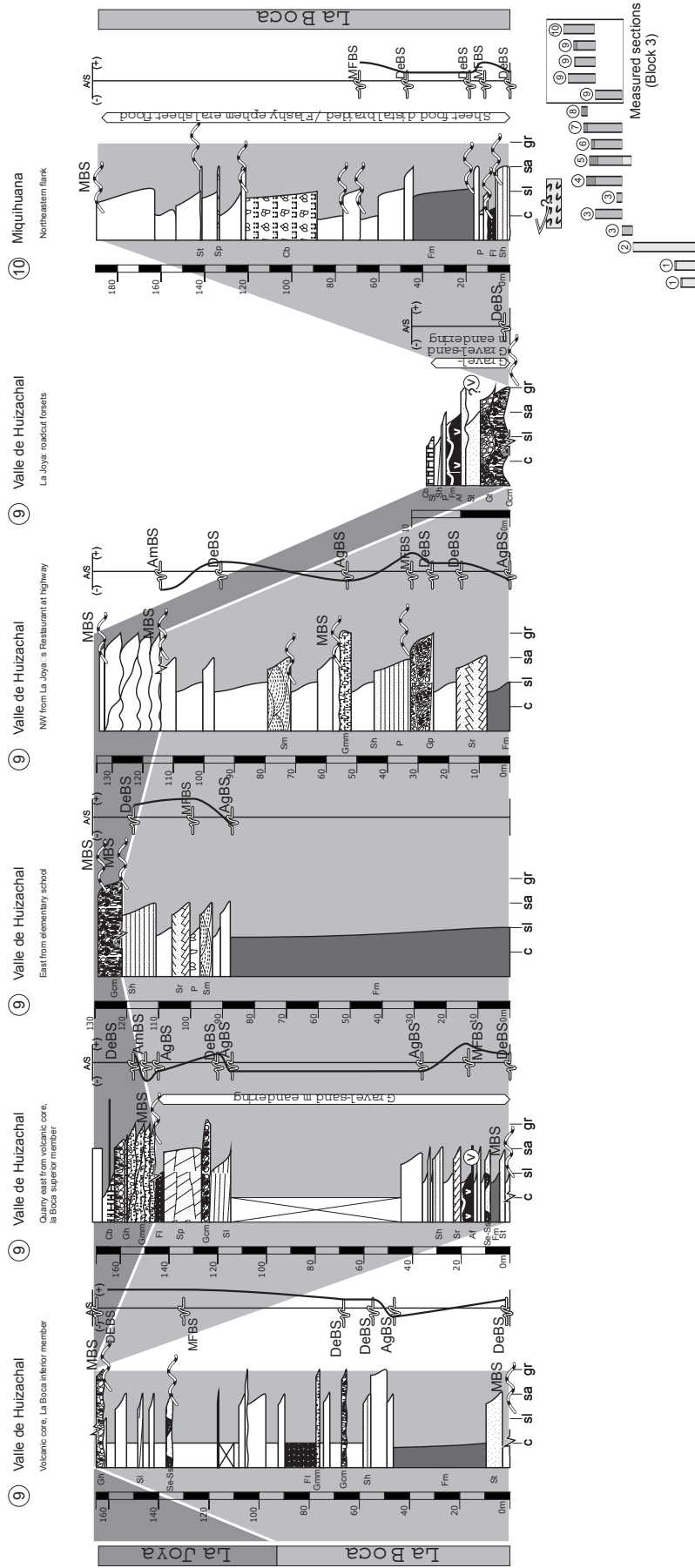


Fig. 2.24: Measured sections (Block 3) as in Fig. 2.18. The corresponding fluvial style and accommodation/supply cycle for comparative purposes are given at right of column: amalgamation (AmBS), aggradation (AgBS), degradation (DeBS), and major flooding surfaces (MFBS).

The major bounding surface concept concludes that a rise in accommodation/supply will generally cause alleviation, but a fall in accommodation/supply develops incision. Slower raising rates in accommodation will result in a more extensive reworking of fluvial strata. It will favor a higher potential of preservation and connectivity of channel deposits no matter what the fluvial system. However, almost any scenario with “convergence” is possible given the competing geological factors, tectonics, and climate conditions (*cf.* Schumm, 1991). Therefore, considerations must be made while distinguishing various controls in fluvial systems, because: (1) similar erosional and depositional features and sequences can be produced by different processes and vice versa; and (2) different levels of sensitivity may result in a minor, a major, or no response of a system to an extrinsic perturbation (Rhee, 2006).

2.7. Discussion: paleocurrent analysis, evolution of the continental fluvial styles flanking basement blocks, and controllers for processes and products.

The systematic results from the sedimentological and stratigraphical methodologies enable an informative legacy of interpretations and contributions. The conjunction of variables as lithofacies, facies association, hydraulic conditions, architectural analysis, and major bounding surfaces enhance fluvial style acquisition (*cf.*, Miall, 1996).

At some point during the Triassic, northeastern Mexico suffered the consequences from lithospheric stretching, causing brittle fracture and normal faulting in relatively shallow parts of the lithosphere. Upwelling of hot asthenosphere beneath the thinned lithosphere increases the thermal gradient and causes decreasing density and thermal expansion of the lithosphere at the now Gulf of Mexico. This results in both isostatic and expansional uplift at the margins of the thinned lithosphere near the actual northeastern Mexico.

By the Late Triassic, sediments were eroded from peripheral uplifts (and local flanking blocks) and deposited in an extensional basin. During the fault-initiation stage, the extensional basin was isolated. Antecedent river courses start to become influenced by the emerging fault-related topography, and some rivers diverted in and along the developing extensional [rift] basin (Michalzik, 1988). Sediment production and intervening factors defined the establishment of facies FA-1 and FA-4. Sandstones deposited in non-marine environments that consistently dominated stratigraphic sequences. As lateral propagation and joining of fault segments advance, it lead to enlargement and coalescence of the extensional basin and the further development for drainage systems (accommodation/supply reconfiguration). The fluvial styles for El Alamar Formation (Fig. 2.25) oscillate transitionally between localities from sandy meandering, gravel-bed braided (1 Lomas de San Paulo Tranquitas), to deep gravel-bed braided, gravel-sand meandering (2 Cañón El Alamar), and gravel wandering (5 Cañón La Boca). The hydraulic interpretations needed for facies constructions are correlated with the processes triggered by accommodation/supply, which are record on degradational bounding surfaces overlain by aggradational bounding surfaces. Consequently, river avulsion is diminished by river sinuosity and the deposition of fining-upward sequences (Michalzik, 1992, Barboza-Gudiño *et al.*, 2010). Previous interpretations support the hypothesis about the development of a depositional zone flanked by basement highs

and the uncapping of their units. Bias paleocurrent analysis on unidirectional structures the fluvial systems conduit was a transverse drainage pattern on the north (SW), and an axial drainage lineation on the southern outcrops (NW-SE).

As the lithosphere cools, density increases and subsidence occurs because of isostasy and thermal contraction. Nevertheless, during the Early Jurassic Nazas volcanic arc took influence on the ongoing sedimentary environments. Basement was not extensively exposed during the Early Jurassic, when Jurassic volcanic rocks eventually buried it. The volcanic succession for La Boca Formation is distinguished by the building lithofacies for facies FA-1Aa, FA-2C, and FA-4A. The volcanic sequences might present some

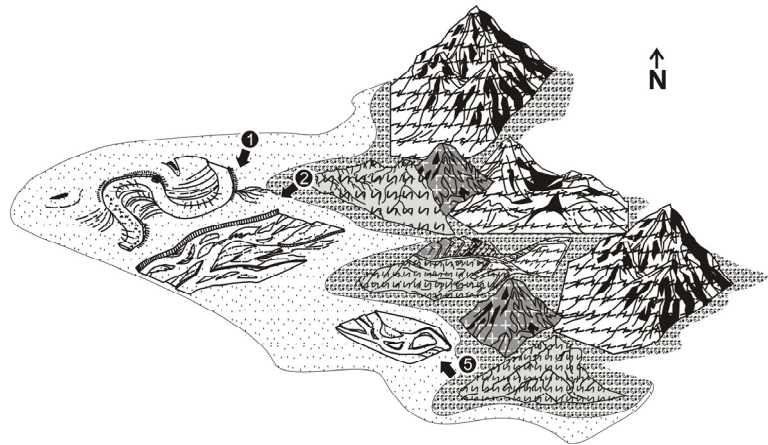


Fig. 2.25: Fluvial styles and major bounding surfaces (MBS) for El Alamar Formation with its respective paleocurrent strikes (arrows) for the localities of: 1– Lomas de San Paulo Tranquitas (gravel-sand meandering; DeSB); 2– Cañón El Alamar (deep gravel-bed braided; AgSB); 5– Cañón La Boca (gravel wandering; DeSB). Source areas represent exposed crystalline basement units (consult pattern fill for lithology recognizance). Locality number is based on Figure 1.1.

reactivation surfaces that condition the internal characteristics of the deposits, by controlling their hydraulic behavior, the subsequent facies [associations] generation, and architectural elements (Fig. 2.26).

At the north, the locality of (3) Aramberri evolves the genetic conditions of a shallow perennial braided to an ephemeral sandy meandering, with paleocurrent orientations almost N-S. The conduit orientations were affected by the ongoing local volcanic activity. The volcanic loading affect the accommodation/supply regime with aggradational processes to alternated into degradational and major flooding processes.

To the south, the locality of (4) Cañón El Olmo prevails as a sandy meandering with well-developed degradational surfaces and minor crevassing conditions with paleocurrent orientations W-E.

In contrast, the southern locality of the (5) Cañón La Boca presents a gravel wandering fluvial style dominated by facies associated with degradational processes by interacting between a low sinuosity, multiple channel river – braided river, – and high sinuosity, single channel river – to meandering river. Channel-fill deposits form the upper part of bar deposits. The initial fluvial style shifts to ephemeral sandy meandering, by trespassing from coarse sandstones to middle grained sandstones, and finer laminae. The change on style raises aggradational bounding surfaces under flashy discharge and still water conditions.

Even southern, the localities of (6) Cañón Caballeros and (7) Cañón Huizachal-Peregrina are composed of gravel-bed braided styles. This distributary fluvial system relates to deposits of high-energy stream flow with alluvial fans, in which sediment-gravity-flows denotes. The areas vicinity was mainly controlled not by the volcanic setting but by the proximity to emerged basement units, which contribute to modify the sediment supply levels.

The entire depositional style situation on either locality integrates degradational and aggradational processes for accommodation. The style and processes are interpreted by the frequency of debris flows, and other sediment-gravity-flows dependant on the source area. Flows dominantly range in orientation from W-E to NW-SE.

Apart from the Huizachal-Peregrina Anticlinorium canyons is the (9) Valle de Huizachal with an entire volcanic succession. At its base, few erosive facies sustain the uncapping from underlying strata (DeBS) that continually become less sinuous in their depositional style (Ags). The frequency of debris flows and other sediment-gravity flows at the base outlined this lower interval

(La Boca Formation lower member) as a gravel-bed braided fluvial style. The upper member of La Boca Formation converts into a gravel-sand meandering. This second interval combines oscillations of aggradational and degradational processes by the incisions and terrace formation (facies FA-2, FA-4A), and the subsequent sediment infill from intraformational recycling (facies FA-1, FA-2C). Paleocurrent analysis suggests a NW trend.

Farther S-SW, the (10) Miquihuana locality represents for La Boca Formation a sheet food distal braided system and a flashy ephemeral sheet flood fluvial style. Both styles are conceived by the lithofacies FA-2A and FA-2B. Degradational processes (FA-1Aa) and major flooding events mark this succession. The increase in deposition rate and width of floodplains decrease channel-deposit proportion and connectedness for this area.

Paleocurrents for La Boca predominantly project a trend with a longitudinal (axial) character, with flow being parallel to strike, along the basin axis. Axial drainages are particularly sensitive to the large scale of plate-tectonic changes in the region. The influence of the volcanic activity printed on the massive succession and the partially gone thermal contraction from the previous setting favored sedimentary loading in the basin. The flexural mechanism caused a dipping of the lithosphere to the east and an onlap of sediment at the basin margins in some localities (e.g., Valle de Huizachal).

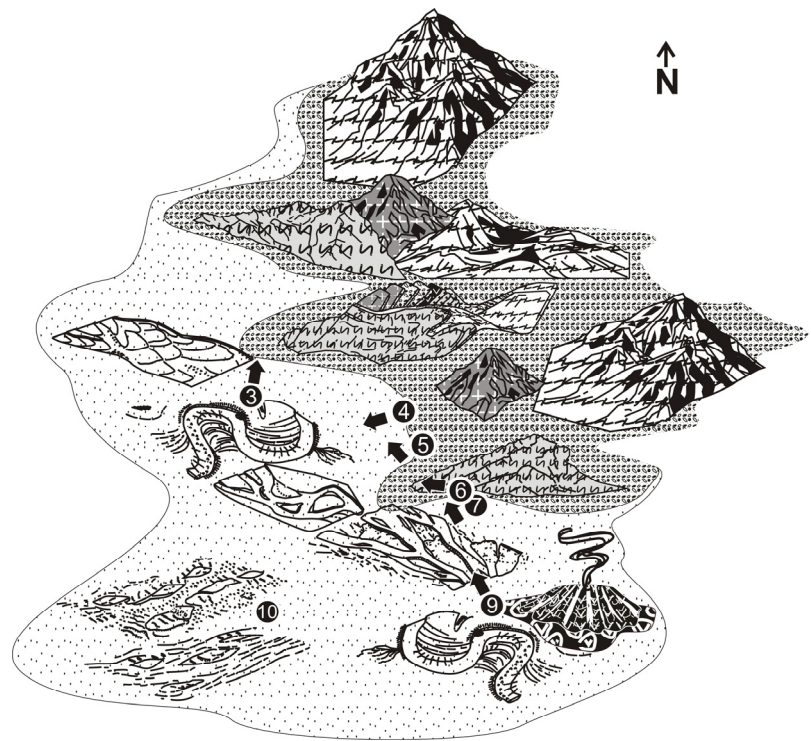


Fig. 2.26: Sketch for the fluvial styles and major bounding surfaces (MBS) for La Boca Formation with its respective paleocurrent strikes (arrows) for the localities of: 3– Aramberri (Shallow perennial braided; DeSB), 4– Cañón El Olmo (Sandy meandering; DeBS), 5– Cañón La Boca (Gravel Wandering; AgBS), 6– Cañón Caballeros (Gravel-bed braided; DeSB and AgBS), 7– Cañón Peregrina (Gravel-bed braided; AgSB), 9– Valle de Huizachal (Gravel-sand meandering; DeSB), and 10– Miquihuana (Sheet food distal braided and Flashy ephemeral sheet flood). Source areas represent exposed crystalline basement units (consult pattern fill for lithology recognizance). Locality number is based on Figure 1.1.

The incision of new drainage systems in the uplifted footwalls lead to the development of small regularly spaced alluvial fans. The size of the drainage basins and fans decreases toward the fault tips. The center of the extensional basin [rift but possibly back arc] was occupied by eolian sands, ephemeral or perennial lakes, or axial rivers with floodplains.

Finally, La Joya Formation accumulated during a concluding extensional episode, which is evidenced by the recycling from the underlying red beds, volcanic strata, and nearby basement rocks. The tectonic episode is marked by basal angular unconformity of La Joya Formation. The transition between La Boca and La Joya formations

represents a setting configuration where crustal extension juxtaposed thin arc volcanics and uplifted basement blocks. The La Joya sequence predominates as a gravel-influenced fluvial style (Gravel-bed braided, Gravel meandering, Gravel Wandering, Gravel-sand meandering). Degradation and occasional amalgamation bounding surfaces stand for the angular unconformity beneath La Joya Formation. Facies FA-1D and FA-4A occur similarly within the styles. Facies constrain a strong flow development necessary for thick multistory conglomerates, and sediment-gravity-flow deposits formed in alluvial-fan distributaries. Incision of fan channels and local growth of alluvial fans can also be associated with random increases in sediment supply and river avulsions (AgBS). The La Joya fluvial-alluvial styles carried coarse sediments loads and represent a typical transverse system. The subsequent “fault death” stage is associated with relatively low deposition rates, with increasing basin areas for the incoming marine transgression system track.

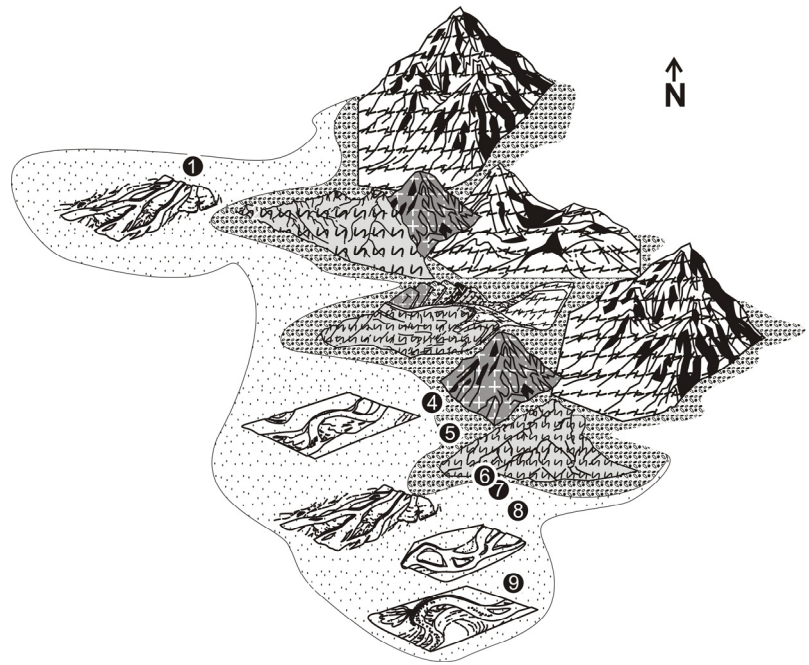


Fig. 2.27: Sketch for the fluvial-alluvial styles and major bounding surfaces (MBS) for La Joya Formation with its respective paleocurrent strikes (arrows) for the localities of: 1– Lomas de San Paulo Tranquitas (Gravel-bed braided; DeBS), 4– Cañón El Olmo (Gravel meandering; DeBS), 5– Cañón La Boca (Gravel-bed braided; AgBS), 6– Cañón Caballeros (Gravel-bed braided; AgBS), 7– Cañón Peregrina (Gravel-bed braided; DeBS), 8– Cañón Novillo (Gravel Wandering; AgBS), 9– Valle de Huizachal (Gravel-sand meandering; DeBS). Source areas represent exposed crystalline basement units (consult pattern fill for lithology recognizance). Locality number is based on Figure 1.1.

3. PETROGRAPHY OF ROCK-FORMING MINERALS MINERALS AND SOURCE AREAS⁴

3.1. Introduction

The evolution of sedimentary petrography has been improved by the developments on sedimentary geology under a methodological spectrum that includes sample classification, tectonic setting recognizance, and depocenter determination.

The establishment for qualitative and quantitative data classification dates the late 1800s with pioneer works, to the beginnings for the twenty-century that extended up to the 1950s (Cross, 1902; Wright, 1910; Pettijohn, 1931; Chayes, 1949; Bokman, 1952; Friedman, 1962). Nonetheless, the most relevant works that described sandstones in a numbered manner appeared until the 1960s (McBride, 1963; Okada, 1966), which serve as a future guideline to picture the genetic print in sandstones (Ingersoll, 1983; Weltje, 2006).

The second advance for the evolution of sedimentary petrography involves defining the petrogenesis for source-areas and composition that gave rise to clastic sediments. This upgrade in petrography can be seen by the classification and interpretation of: (1) quartz grain-types (Basu *et al.*, 1985; Ingersoll, 1974; Tortosa *et al.*, 1991), (2) feldspar characterization (Marsaglia and Tazaki (1992), and (3) lithic fragment associations (Dickinson, 1970; Marsaglia, 1991; Garzanti and Vezzoli, 2003b; Arriba and Arribas, 2007).

Once achieved a consolidation between sediment and source-areas compositions, the last important academic stage for sedimentary petrography was to solve sandstones deposition at a specific tectonic environment (Dickinson and Suczek, 1979; Ingersoll and Suczek, 1979; Zuffa *et al.*, 1980; Garzanti *et al.*, 2001). The final integration of the data from Quantitative Provenance Analysis (QPA) into sediment generation paths aims for the closure of a big spatial and temporal cycle known as Source-to-Sink analysis.

Previous works for northeastern Mexico have contributed through light mineral provenance analysis. However, few studies have documented the main petrographic characteristics for El Alamar, La Boca, and La Joya formations, whose accommodation/supply processes and products rely in a transitional setting configuration where extensional tectonics (rift) juxtaposed thin arc volcanics and uplifted basement blocks. Therefore, this chapter documents the petrographic characteristics for El Alamar, La Boca, and La Joya formations deposited as fluvial and volcanic successions that crop out on the eastern border of the Oaxaquia and Granjeno-Acatlán Belt basement exposures (Huizachal-Peregrina Anticlinorium) and/or on the flanking depocenters at the western part of the Tamaulipas Arc.

⁴ This chapter has been partially documented in:

–Rubio-Cisneros, I.I., *et al.* (2011). Análisis preliminar de procedencia de rocas clásticas jurásicas del Valle de Huizachal, Sierra Madre Oriental: Influencia del vulcanismo sinsedimentario y el basamento cristalino. Avances y paradigmas de la tectónica y la historia geológica del Noreste de México. J.C. Montalvo-Arrieta, G. Chávez-Cabello, and F. Velasco-Tápia, Boletín de la Sociedad Geológica de México. 63: 137-156.

–Rubio-Cisneros, I.I., and Ocampo-Díaz, Y.Z.E. (2010). Compositional analysis and sedimentary recycling evidences associated to unconformities in northeastern Mexico, a Late Triassic-Early Cretaceous example. Abstracts with Programs - Geological Society of America 42(2): 70.

–Rubio-Cisneros, I.I. and Ocampo-Díaz, Y.Z.E. (2011a). Source-to-sink: a retrospection of the sedimentary petrography evolution. Abstracts with Programs - Geological Society of America 43: 431.

–Rubio-Cisneros, I.I. and Ocampo-Díaz, Y.Z.E. (2011b). Using a discriminant function for determining a relationship between detrital modes and tectonic settings: an approach toward unveiling some source-to-sink factors. Abstracts with Programs - Geological Society of America 43(5): 547.

3.2. Sampling and petrographic methods

In order to determine the compositional variations for the red beds, 150 sandstone samples were collected by intervals of 30 to 50 m within 17 sections described in Chapter 2 that correspond to the lithostratigraphic divisions proposed by Barboza-Gudiño *et al.* (2010), and Rubio-Cisneros and Lawton (2011; see sections in Chapter 2: Fig. 2.16; Fig. 2.17; Fig. 2.18).

Both specific source areas as well as average source-area composition can be determined depending on the compositional maturity and grain size from the sedimentary rock in used. Immature sandstones are best used when specific source areas are to be ascertained, and fine-grained clastics are better for determining the average composition of large regions. Therefore, sample collection was built by unweathered middle to coarse-grained sandstones, with the purpose to minimize the compositional dependency as a function on grain size. Some problems related with the compositional dependency are hydraulic

segregation and the linked effects of sedimentary recycling by autogenic factors in continental environments (the first and second order *sensu stricto* proposed by Ingersoll *et al.*, 1993). The used methodological criteria were those of Gazzi-Dickinson and Gazzi-Zuffa (Gazzi, 1966; Dickinson, 1970; Ingersoll *et al.*, 1984; Zuffa, 1985; Garzanti, 1991; Weltje, 2002). The classification of metamorphic lithic fragments was done using Garzanti and Vezzoli (2003) proposal, which consists of four main groups with various metamorphic ranks that represent the stages of increasing recrystallization and progressive deformation of cleavage and schistosity.

Both petrographical methods were used in conjunction for a better interpretation. The Gazzi–Zuffa method is a classification scheme encompassing all grain types occurring in sand and sandstone. This extended classification scheme also includes detailed subdivisions for other categories of framework elements: carbonate extrabasinal (CE), non-carbonate intrabasinal (NCI), and carbonate intrabasinal (CI) grains. Compatibility between the Indiana and Gazzi–Dickinson methods is achieved by subdividing each category of phanerites into a category comprising monocrystalline grains and several categories of sand-size crystals within larger rock

Table 3.1: Compositional variables and ternary systems referred to in this study.

<i>Grain categories</i>	
Total quartzose grains: $Q = Q_m + Q_p$	
Q_m = monocrystalline quartz	
Q_{mr} = monocrystalline non-undulose quartz	
Q_{mo} = monocrystalline undulose quartz	
Q_p = polycrystalline quartz	
Q_{p2-3} = polycrystalline quartz (2-3 crystals)	
$Q_{p>3}$ = polycrystalline quartz (>3 crystals)	
Total feldspar grains: $F = P + K$	
P = plagioclase grains	
K = alkali feldspar grains	
Total unstable lithic fragments: $L = L_v + L_s$	
L_{vp} = (meta)volcanic lithic fragments	
L_s = (meta)sedimentary lithic fragments	
Total lithic fragments: $L_t = L + Q_p$	
Total metamorphic lithic fragments $L_m = L_{mp} + L_{mf} + L_{mb} + L_{mi}$	
L_{vf} = volcanic lithic fragment with felsitic texture	
L_{vmi} = volcanic lithic fragment with microlithic texture	
L_{vl} = volcanic lithic fragment with lathwork texture	
Ch = chert	
R_g = [plutonic] phaneritic rock fragments (coarse-crystalline quartz-feldspar grains)	
R_s = sedimentary rock fragments	
R_m = metamorphic rock fragments	
R_v = volcanic rock fragments	
<i>Ternary systems</i>	<i>Parameter</i>
QFL+Ch	$Q = Q_{mr} + Q_{mo} + Q_{p2-3} + Q_{p>3}$ $F = Plg + K$ $L = L_m + L_v + L_p + L_s + Ch$
QFL (Framework (emphasis on maturity))	$Q = Q_{mr} + Q_{mo} + Q_{p2-3} + Q_{p>3}$ $F = Plg + K$ $L = L_m + L_v + L_p + L_s$
QFR	$Q = Q_{mr} + Q_{mo} + Q_{p2-3} + Q_{p>3}$ $F = Plg + K$ $R = L_m + L_v + L_p + L_s$
QmFLt (Framework emphasis on parent rock)	$Q_m = Q_{mr} + Q_{mo}$ $F = Plg + K$ $L = L_m + L_v + L_p + L_s + Ch$
QmrQmoQp	$Q_{mr} = Q_{mr}$ $Q_{mo} = Q_{mo}$ $Q_p = Q_{p2-3} + Q_{p>3}$
RgRsRm	$R_g = Q_{p2-3} + Plg + K + L_{mb} + L_v + L_p$ $R_s = L_s$ $R_m = Q_{p>3} + L_{mf} + L_{mp} + Mi$
RmRvRs	$R_m = Q_{p>3} + L_{mf}$ $R_v = Q_{p2-3} + F + L_v$ $R_s = L_s$
LmLvpLs	
LvflLvmiLvl	

fragments, as originally proposed by Gazzi (1966). For instance, Qm may be defined as a monocrystalline quartz grain, Qrp as a quartz crystal within a plutonic rock fragment, and Qrm as quartz crystal within a meta-sedimentary rock fragment, etc (Weltje, 2002).

Point-counting rock-forming mineral data were collected upon a grid of 500 to 1000 points. Minerals were recognized by their optical properties. The compositional variables for the ternary systems, QFL, QmFL, LmLvLs, were recalculated according to Dickinson (1970, 1985), and Ingersoll and Suczek (1979).

This chapter begins by proposing petrofacies (Pf) designed upon the nomenclature for genetic classification of sandstones designed by Weltje (2006). The description of the main components and the compositional classification of the source areas are dependent to the petrofacies. This structure validates the sediment genesis according to interpretations of minerals and source areas.

In addition, this work extends the use of a ternary diagram made by three compositional assemblages RmRvRs (Fig. 3.1; Table 3.1), intended to evaluate the possible combination of lithic fragments from metamorphic and volcanic source components. This diagram was erected to determine the provenance for sandstones with affinities that derived from crystalline basement rocks and related-continental arc rocks.

3.2.1. Grain-types: classification and general composition

The non-carbonate extrabasinal grains (NCE) cover a wide range, from monomineralic grains (quartz, feldspars, mica, heavy minerals) to silica–silicate lithoclasts (e.g., polycrystalline quartz, chert, serpentinite, quartz–chlorite–mica aggregates), and lithic fragments of volcanic, plutonic, sedimentary (rip-up clasts) or metamorphic sources (metamorphic rank). Feldspars are commonly replaced by illite and smectite and/or occasionally by cements (micritic calcite, sparitic calcite).

The pelite lithic fragments have a varietal metamorphic rank, which includes slate lithic fragments with rough cleavage (Lmp₁), phyllite lithic fragments with strong cleavage (Lmp₂), and micaceous schist lithic fragments Lmp₃₋₄). Others like metapsammite/metafelsite grains evolve from a sandy siltstone lithic fragment with detrital micas (Lsp) into a metasilstone lithic fragment with rough cleavage (Lmf₁), progressively into a

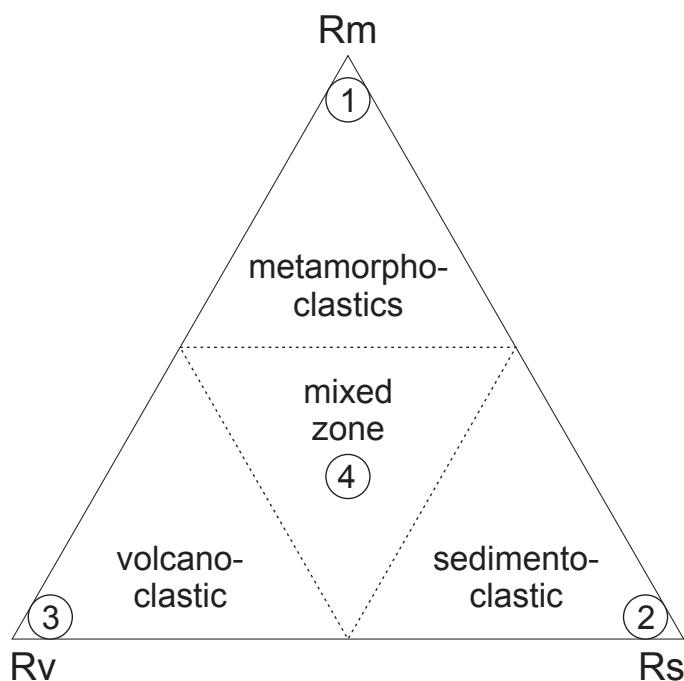


Fig. 3.1: Ternary system of compositional assemblages for metamorphic–Rm, volcanic–Rv, and sedimentary–Rs components. The compositional space is divided in: (1) metamorphoclastics; (2) sedimentoclastic; (3) volcanoclastic; (4) mixed zone.

quartz-sericite lithic fragment with strong cleavage (Lmf₂), and a (quartz-) mica lithic fragment with schistosity (Lmf₃₋₄).

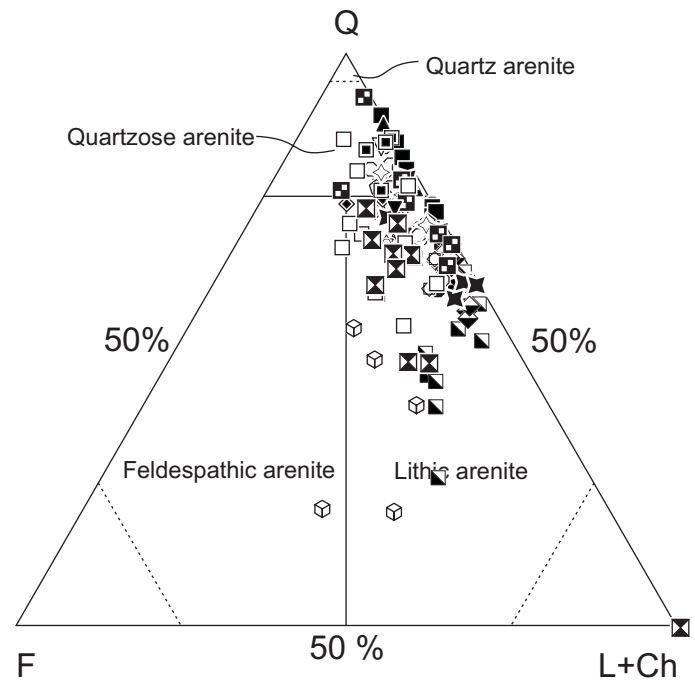
Metacarbonate grains are nearly absent (Lmc₁). Metabasite grains are also present and include metabasalt lithic fragments (Lmb₁), and chloritoschist lithic fragments (Lmb₂). Meanwhile, volcanic lithic fragments show textures like felsitic, tuffaceous, lathwork, and microlitic. The occasional occurrences of plutonic rock fragments display myrmekite or symplectite rock microstructures. Chert grains are sporadically detected and show isotropic tectonic microtextures.

Some samples show small amounts (<10%) of non-carbonate intrabasinal grains (NCI), e.g., rip-up clasts). These grains represent deformed claystone and siltstone fragments by compaction, commonly associated with quartzofeldspathic.

Carbonate extrabasinal grains (CE) and carbonate intrabasinal grains (CI) are not present in the analyzed samples.

3.2.2. Sandstones framework grains: nomenclature for a genetic classification

The samples have been subdivided in two petrofacies (Pf), classified according the observed and calculated occurrence of principal components (Fig. 3.2; Table 3.2; Appendix for Chapter 2). The data distribution and their nomenclature are dependant to the classification scheme. Then, petrofacies assignment (Petrofacies 1 and 2) is conditioned to the position of the mean value of each compositional assemblage within a constructed compositional space (i.e., Quartzolithic, Q1; Lithoquartzose, Lq; Fig. 3.3). Compositional quantification gave presence for two rock fragment groups (Lm and Lv), and the



Lomas de San Paulo Tranquitas– SW de Cerro de la Nieve: Alamar lower member ●; Alamar Fm upper member ◐; La Joya Fm ◑. Cerro de la Nieve: Alamar Fm upper member ◐; La Joya Fm ◑. Mina la Huiche: El Alamar Fm lower member ⊗. **Cañón El Alamar**– El Alamar ? Fm ◑. **Aramberri**– La Boca ? Fm ◑. **Cañón El Olmo**– La Boca ? Fm ◑; La Joya Fm ◑. **Cañón La Boca**– El Alamar Fm lower member ◑; El Alamar Fm upper member ◑; La Boca ? Fm ◑; La Joya Fm ◑. **Cañón Caballeros**– La Boca ? Fm ◑; La Joya Fm ◑. **Cañón Huizachal-Peregrina**– La Boca ? Fm ◑; La Joya Fm ◑. **Cañón Novillo**– La Joya Fm ◑. **Valle de Huizachal**– La Boca Fm lower member ◑; La Boca Fm upper member ◑; * Ramos-Ledezma ? ◑; La Joya Fm ◑. **Miquihuana**– La Boca ? Fm ◑; La Joya Fm ◑.

Fig. 3.2: Point-counting for the analyzed samples using the proposed classification of sandstone by Okada (1971). Question mark represents an unidentified stratigraphic position within the stratigraphic succession. *Reinterpreted and recalculated data representing undifferentiated samples from La Boca Formation, provided by Ramos-Ledezma (2007).

opportunity to generate subdivisions for petrofacies 1 (subpetrofacies 1A and 1B). Under particular cases, compositional polygons share various compositional fields, which may serve for provenance interpretations.

3.2.2.1 Petrofacies 1: Quartzolithic (Q1) sands

3.2.2.1.1. Subpetrofacies 1A: Quartzolithic (Q1) sands with high content of metamorphic and sedimentary lithic fragments

Quartzolithic sandstone petrofacies 1 has a subdivision “A” within its composition ($\sim Q_{72}F_3L_{25}$). This subpetrofacies corresponds to the upper member of El Alamar Formation (cf., Rubio-Cisneros, 2008a), the upper member of La Boca Formation, and to La Joya Formation. It contains abundant quartz and metamorphic lithic fragments, with minor proportions of plagioclase and potassic feldspars. Polycrystalline quartz is greater in abundance ($Q_p/Q_m \sim 54$), than monocrystalline non-undulose quartz from volcanic/plutonic sources ($Q_{mr}/Q_{mo} \sim 72$). Low-grade metamorphic polycrystalline quartz presents rounded to subrounded grain morphologies, with undulose extinction and occasional suture contacts (Fig. 3.6). Some other polycrystalline quartz grains remains stretched or deformed grains with tectonic fabric textures.

Some evidence on contact-types between grains precludes a plutonic origin (e.g., “Y” contacts). Feldspars of subpetrofacies A remain as plagioclase with its typical polysynthetic twinning, commonly replaced by sericite/illite. This petrofacies subdivision contains different metamorphic rock fragments that consists in order of predominance on metapelite ($L_{mp_{2,3-4}}$), metapsammite/metafelsite ($L_{mf_{2,3-4}}$), and metabasite grains ($L_{mb_{1-2}}$; Fig. 3.6). Rarely but seen are metacarbonate grains (L_{mc_1}), obscured by its texture similar to cleavage from L_{mp} lithic fragments. Fine-grained sandstone and siltstone lithics are grouped within the sedimentary rock assemblage. Volcanic rock fragments occur but not in a remarkable manner, remaining a consideration those with microlitic textures. Sandstones with major metamorphic content remain as metamorphoclastic rocks (Fig. 3.5).

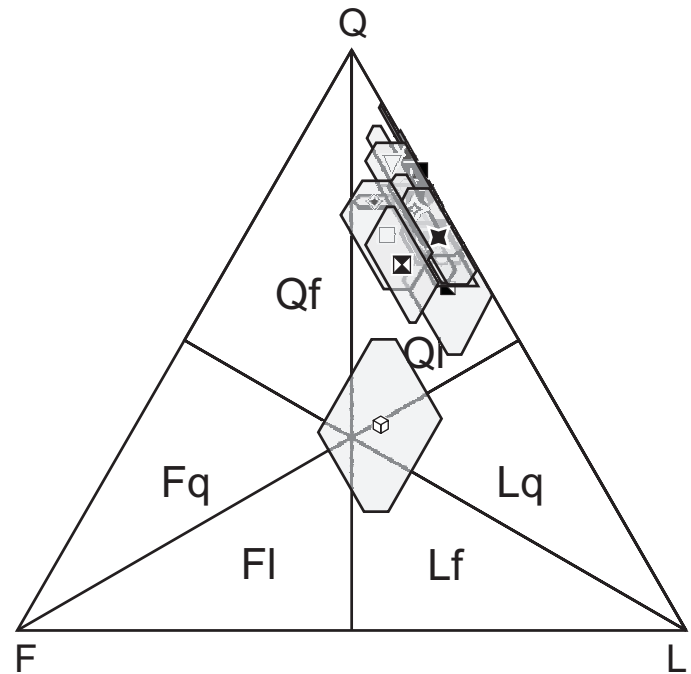


Fig. 3.3: Diagram for genetic classification of sandstones (Weltje, 2006). Sixfold subdivision of compositional space into Quartzolithic (Ql), Lithoquartzose (Lq), Lithofeldspathic (Lf), Feldspatholithic (Fl), Feldspathoquartzose (Fq) and Quartzofeldspathic (Qf) sands. Symbols represent the mean composition for each studied area (Fig. 3.2).

Subpetrofacies 1A presents a matrix content of <15%, and it is constitute by mica minerals that integrate the protomatrix and epimatrix. Accesory minerals like tourmaline, monazite, zircon, and epidote flote within the matrix (for heavy mineral content visit Chapter 4).

3.2.2.1.2. Subpetrofacies 1B: Quartzolithic (Q1) sands with high content of volcanic and sedimentary lithic fragments

Quartzolithic sandstones under the category of subpetrofacies 2 ($\sim Q_{66}F_8L_{26}$), partly corresponds to the lower member of El Alamar Formation and the lower volcanic member of La Boca Formation. This petrofacies is characterized by higher proportions of volcanic assemblages (Lv and Rv; Table 3.2). The volcanic lithics that were distinguished in order of abundance are those with microlitic and felsitic textures, lathwork lithic fragments (laths; Dickinson, 1970), and tuffaceous textures (glomeroporfidic, holohyaline, fiamme, fluidal, spherulitic texture, porfidic, vitrophyric texture, devitrified-, and shards).

The volcanic lithic fragments with microlitic textures (Lv_mi) represent grains that contain microliths of plagioclase floating on a devitrified black matrix. Volcanic lithic fragments with felsitic textures (Lv_f) are characterized by anhedral quartz and feldspars, arranged on a granular or seriated microcrystalline mosaic. In most of the cases, Lv_f contains fractions of feldspathic material of fine proportions. Lathwork (Lv_l) grains are defined by plagioclase crystals and other phenocryst sand-sized particles within an interstitial or devitrified intergranular mass (e.g., clinopyroxene).

Lithic fragments form the plutonic

Table 3.2: Mean values and numerical relations for the compositional parameters in each used ternary diagram for source area and tectonic environment interpretations. n– number of samples used to calculate the corresponding [sub]petrofacies. Std. Dev– Standard Deviation.

Ternary system	Parameter	Petrofacies 1 (n= 118)		Subpetrofacies 1A (n= 56)		Subpetrofacies 1B (n= 57)		Petrofacies 2 (n= 11)	
		Mean	Std. Dev.	Mean	Std. Dev.	Mean	Std. Dev.	Mean	Std. Dev.
QFL+Ch	Q %	69	9.9	72	9.2	66	9.7	35	17.4
	F %	5	4.4	3	2.1	8	4.9	24	10.8
	L+Ch %	25	9.0	25	8.7	26	9.2	41	11.9
QFL	Q %	70	9.7	72	9.1	66	9.6	35	17.4
	F %	5	4.4	3	2.1	8	5.0	24	10.9
	L %	25	8.8	25	8.6	26	9.0	41	11.9
Q+ChFLt	Q+Ch %	70	9.6	72	9.1	67	9.5	35	17.4
	F %	5	4.4	3	2.1	8	4.9	24	10.8
	Lt %	25	8.7	25	8.6	26	8.9	41	11.9
QmFL	Qm %	63	10.7	64	10.8	62	10.5	33	16.7
	F %	6	4.7	4	2.5	9	5.3	25	12.4
	L %	31	10.7	32	10.5	30	10.6	42	9.7
QmPK	Qm %	91	6.7	94	3.8	88	7.7	59	26.5
	P %	8	6.2	5	3.5	11	7.1	35	24.8
	K %	1	1.4	1	1.4	1	1.4	5	6.2
Qp2-3QmrQmo	Qp2-3 %	11	4.4	11	4.1	11	4.3	20	12.5
	Qmr %	38	12.0	35	11.5	40	11.8	40	8.1
	Qmo %	51	12.5	54	11.4	49	13.1	40	8.8
Qp>3QmoQmr	Qp>3 %	19	12.5	27	10.8	11	8.6	27	10.2
	Qmo %	47	12.3	44	10.1	49	13.8	37	8.4
	Qmr %	35	13.1	29	11.5	40	12.3	36	5.4
QmrQmoQp	Qmr %	31	11.8	27	10.7	36	10.8	31	6.6
	Qmo %	42	11.5	40	9.4	44	13.0	32	8.2
	Qp %	26	11.7	33	10.2	20	8.7	37	12.3
RmRgRs	Rm %	39	15.1	50	8.4	28	11.4	17	10.6
	Rg %	52	16.4	39	8.3	63	12.9	74	16.3
	Rs %	10	6.1	10	6.7	9	5.1	9	7.2
RmRvRs	Rm %	38	15.6	50	8.0	27	11.6	17	11.6
	Rv %	48	16.6	35	7.4	59	12.7	69	16.0
	Rs %	14	8.1	15	8.5	14	7.2	14	7.1
LmLvLs	Lm %	29	13.5	33	12.8	24	13.2	11	12.0
	Lv %	42	15.9	35	13.4	48	13.8	64	17.4
	Ls %	29	15.4	31	16.0	27	13.4	25	10.6
Lv/Lv _m i/Lv _l	Lv _f %	25	22.8	19	17.2	31	26.3	28	18.7
	Lv _m i %	70	24.5	76	19.4	65	27.7	58	25.3
	Lv _l %	4	5.8	5	5.7	4	6.0	14	28.8
QpLvLs	Qp %	38	14.3	45	13.6	30	11.8	24	15.3
	Lv _m %	29	13.1	21	8.6	36	12.1	47	19.8
	Ls _m %	33	11.6	34	12.4	33	9.5	29	12.0
<i>Numerical relations</i>									
	Qmr/Qmo	86	62.4	72	42.5	99	76.6	105	34.5
	Qp/Qm	39	28.3	54	32.2	26	14.4	69	36.4
	Lm/Lt	29	13.2	34	12.6	24	11.8	11	11.0
	Rm/Rs	10	50.8	7	15.5	3	2.5	1	1.3
	Rv/Rs	18	80.7	5	10.6	6	6.5	7	4.4

assemblage with a matrix on mosaic, quartz, equigranular feldspars, and minor proportion of mica. Though the presence of plutonic detrital fragments is scarce, the main plutonic textures are graphic textures, myrmekite or symplectite rock microstructures.

Feldspars possess euhedral to subhedral habit. It is possible to distinguish two types of feldspars: (a) potassic feldspars with or without Carlsbad and two-direction twinning; and (b) plagioclase with its characteristic polysynthetic twinning remains as the most frequent type. Predominantly plagioclase is truncated and/or altered. Grain size fragments make the sedimentary assemblage for subpetrofacies 1B from siltstone and claystone.

Quartzolithic sandstones with high content of volcanic and sedimentary lithic fragments present accessory minerals related to volcanism, like orthopyroxene, clinopyroxene, and olivine. Nevertheless biotite and muscovite prevail from the rest.

Particles less than 0.03 mm were considered as matrix (cf., Dickinson 1970), and include epimatrix and pseudomatrix. Matrix represents <25% of the rocks components.

3.2.2.2 Petrofacies 2: Lithoquartzose (Lq) sands

Petrofacies 2 comprehends lithoquartzose compositions and a mixed interaction between the adjacent lithofeldspathic (Lf) and feldspatholithic (F1) sand fields ($\sim Q_{33}F_{25}L_{42}$). The main characteristic for petrofacies 2 includes the presence of volcanic and sedimentary assemblages. Monocrystalline quartz prevails as the standing quartz-type. The volcanic lithic group is conformed by detrital grains with microlitic and felsitic textures (Table 3.2). Tuffaceous textures are aligned to the group for volcanic lithics. Another important but less frequent assemblage is the plutonic. Plutonic lithic fragments have phaneritic–equigranular textures.

The sedimentary assemblage remains similar in optical characteristics as for the latter [sub-] petrofacies, by presenting fine-grained sandstone and siltstone lithics with volcanic detritus. Metamorphic grains prevail as aggregates, occurring as metapelite (Lmp_1) and metapsammite/metafelsite varieties.

The lithoquartzose petrofacies has a matrix built by argillaceous minerals and undifferentiated diagenetic phases. Matrix represents sized-particles below 0.03, and less than 15% of the total rock components.

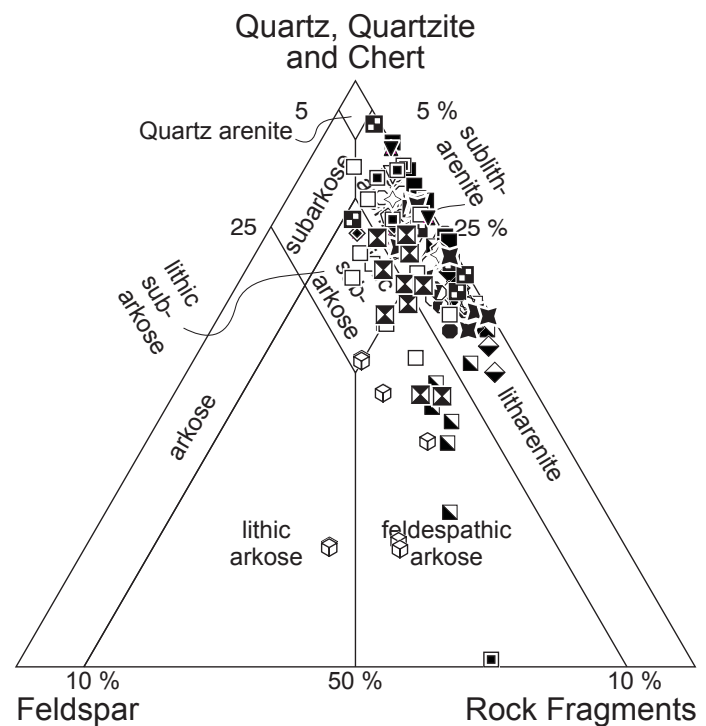


Fig. 3.4: Classification scheme of sandstones proposed by McBride (1963), with the entire data collection for this study. Symbols for each studied area (Fig. 3.2).

Epimatrix and pseudomatrix affect the original composition of the samples. Some diagenetic processes like mechanical and chemical compaction have consumed the prime porosity of the sediments and replaced some unstable minerals such as feldspars and plagioclase. The most representative accessory minerals are zircon, tourmaline and rutile (see Chapter 4).

3.2.3. Source area compositional classification

The source area composition was evaluated on the basis on quantitative and qualitative measurements from the selected principal components quartz and lithic fragments on sedimentary rocks.

3.2.3.1 Quartz

The study of quartz grains links the grain diversity according to its type (monocrystalline, polycrystalline) and extinction (straight, and undulatory), with source area composition (Basu *et al.*, 1975; Tortosa *et al.*, 1991). The analyzed samples were subjected through these parameters on the diagram Q_{mo} , Q_{mr} , $Q_{p<3}$, and $Q_{p>3}$. Samples present abundant monocrystalline quartz.

The morphology of quartz that prevails is subangular to subrounded. Monocrystalline quartz grains display undulose or straight extinction. Volcanic quartz appears sometimes with erosive embayments. Polycrystalline quartz

is presented with an undulatory (blotchy) extinction, stretched or deformed grains, subrounded grain morphologies, and tectonic fabric textures that sometimes are mistaken as chert (Ch). According to quartz content, the reported petrofacies reflect a provenance from low- to middle-grade metamorphic rocks (e.g., schists, serpentinites, and gneisses) and felsitic igneous rocks (e.g., rhyolites; Fig. 3.9).

By using the Q_{mr} – Q_{mo} – Q_p diagram from Arribas *et al.* (1990) the studied samples for the subpetrofacies 1A and 1B display a similar compositional consistency of undulose and straight quartz, and polycrystalline variety. Petrofacies 2 preserves compositional values for volcanic rocks and low- to middle-grade metamorphic rocks.

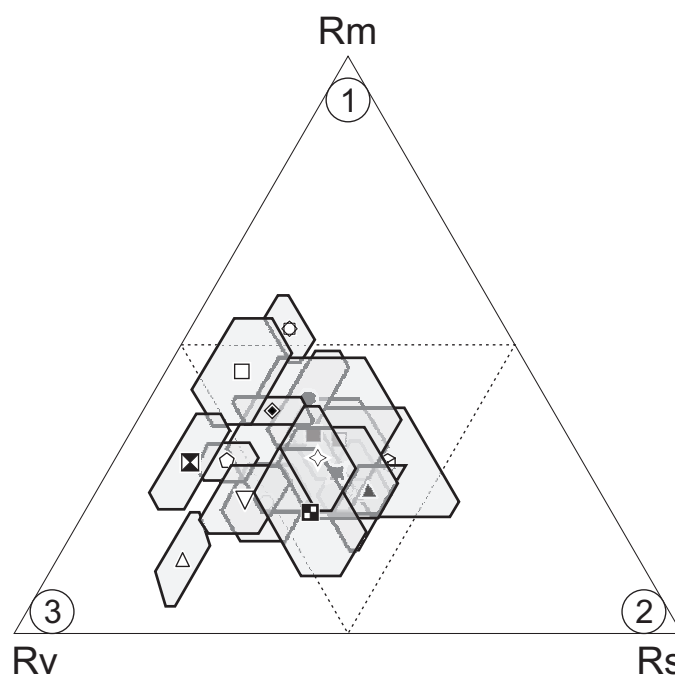


Fig. 3.5: RmRvRs diagram with datasets for the studied areas. (1) metamorphoclastics; (2) sedimentoclastic; (3) volcanoclastic; (center) mixed zone. Symbols represent the mean composition for each studied area (Fig. 3.2).

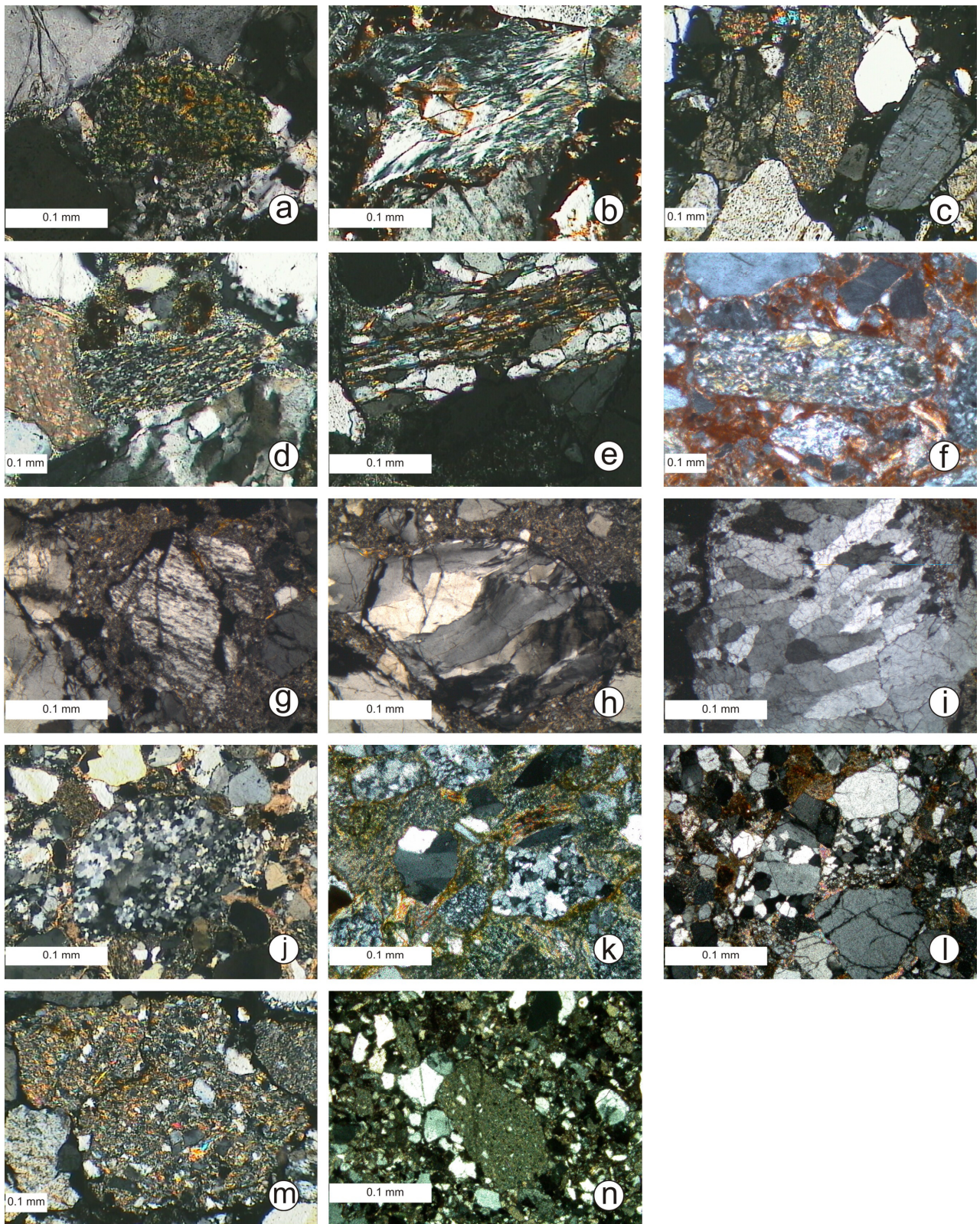


Fig. 3.6: Microphotographs for compositional subpetrofacies 1A. a) Metabasite grain (Lmb_1); b) Metabasite grain (Lmb_2); c) Metapelite grain (Lmp_1); d) Metapsammite/metafelsite grain (Lmf_2); e) Metapsammite/metafelsite grain (Lmf_3); f) Metapelite grain (Lmp_{1-2}); g) Metamorphic lithic fragment, possibly from a quartzite; h) polycrystalline quartz; i) polycrystalline quartz with undulose and straight extinction; j) polycrystalline quartz subordinated by monocrystalline quartz grains with undulose and straight extinction; k) polycrystalline with 2-3 and >3 grains, and other volcanic lithics with microlitic textures; l) polycrystalline quartz dominated sandstone; m) coarse-grained sedimentary lithic fragment (Lsp); n) medium-grained sedimentary lithic fragment (Lsp).

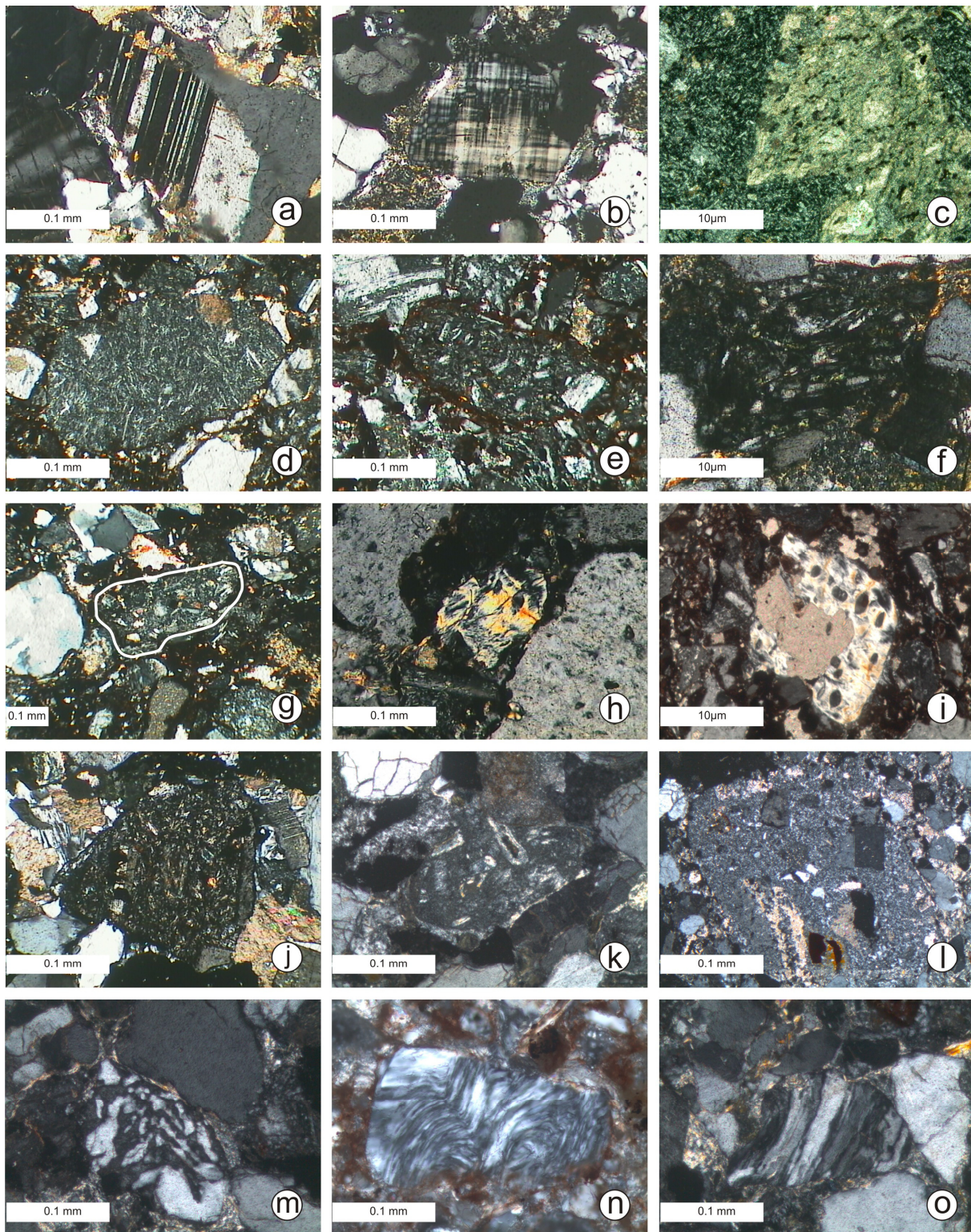


Fig. 3.7: Microphotographs for subpetrofacies 1B. a) Plagioclase fragment with its typical polysynthetic twinning; b) crystalline fragment of microcline with its double twinning system; c) volcanic detrital fragment with a porphyritic texture with phenocrysts of feldspar on a very altered microcrystalline feldspathic matrix and opaque minerals; d) microlitic volcanic grain (Lvmi); e) volcanic felsitic fragment; f) tuffaceous volcanic lithic with fluidal texture; g) lathwork volcanic lithic; h) tuffaceous volcanic lithic fragment; i) volcanic lithic with tuffaceous texture; j) volcanic lithic fragment with phenocrysts of plagioclase, groundmass from laths; k) porphyry texture (microholocrystalline groundmass with phenocrysts); l) granitic texture on a plutonic lithic fragment; m) granophyric texture on a volcanic lithic fragment, n and o) represent plutonic fragments with graphic textures.

3.2.3.2 Lithic fragments

Volcanic lithic fragments occur with microlitic and felsitic textures, lathwork and tuffaceous textures, Pf1A (Rv/Rs ~5), Pf1B (Rv/Rs ~6), Pf2 (Rv/Rs ~7), which sustain a provenance from andesitic, rhyolitic, and basaltic compositional rock-types. Rock fragments from plutonic sources are also considered by the presence of myrmekite or symplectite rock microstructures in both petrofacies.

Besides the volcanic lithic fragment interpretation, the metamorphic grain characterization permits to exclude different metamorphic grade source rocks. Pf1A and Pf2 have metapelite (Lmp₁₋₂), metafelsite /metapsammite (Lmf₁₋₂) grains, unveiling low- to middle-grade metamorphic sources (e.g., varietal schist rocks). Mean while, middle- to high-grade metamorphic sources (e.g., gneiss) may be assessed by higher metamorphic rank grains on Pf1 than on any other petrofacies: metapelite (Lmp₃₋₄), metapsammite/ metafelsite (Lmf₃₋₄) grains.

By using the RgRsRm diagram it was possible to differentiate inputs of compositional varieties according to the assemblages on each petrofacies (Critelli and Le Pera, 1994; Fig. 3.11). Pf1A contains metamorphic detritus (RM: e.g., phyllites, schists) and sedimentary rock fragments (Rs: e.g., siltstones, shales sandstones). Pf1B corresponds to the granitic detritus axis (Rg: e.g., granitoids, gneiss). Moreover, Pf2 involves a mixture of Rm, Rg, and Rs assemblages.

To complete the function of the RgRsRm diagram the RmRvRs diagram helps to maximize the relationship between metamorphic, volcanic, and sedimentary assemblages. RmRvRs was adequate for the purpose of this

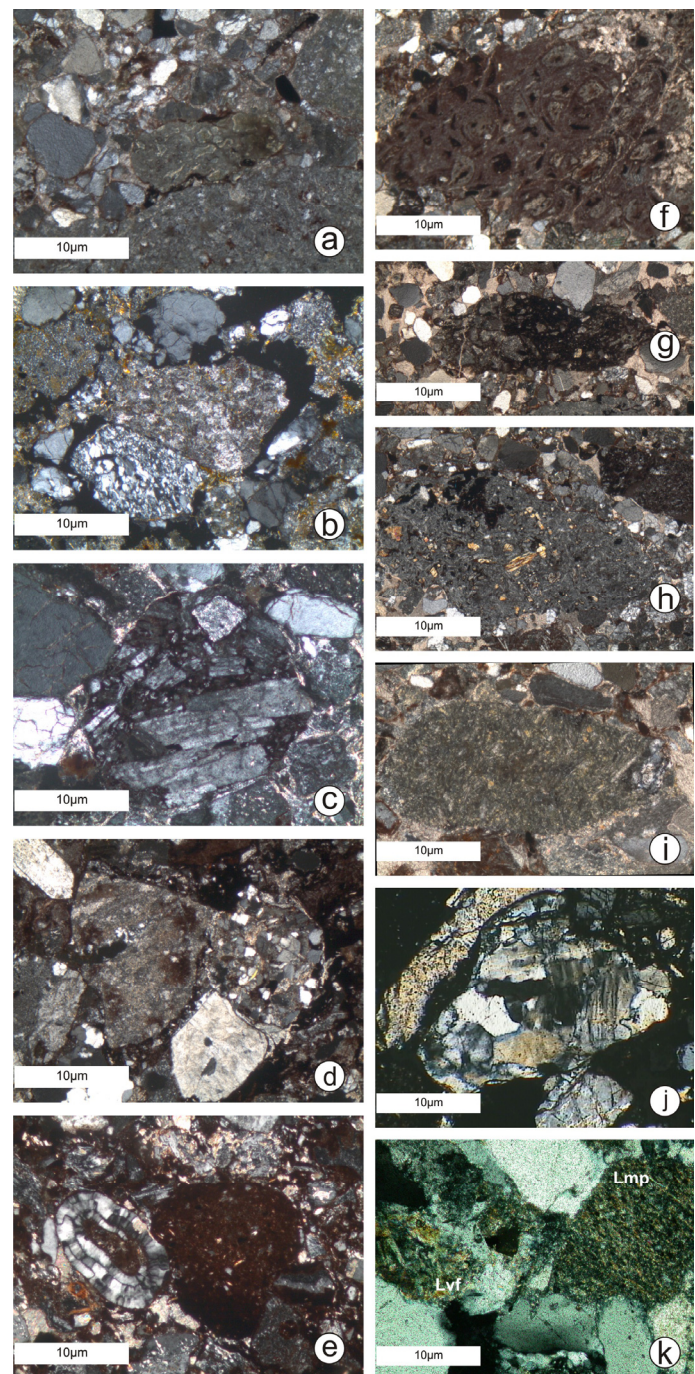


Fig. 3.8: Microphotographs for petrofacies 2. a) Volcanic lithic fragment with tuffaceous texture; b) tuffaceous texture lithic fragment; c) volcanic lithic fragment with porphyritic texture; d) sand-size lithic fragments; e) sedimentary lithic fragment; f) tuffaceous texture lithic fragment; g) volcanic lithic fragment with tuffaceous texture; h) volcanic lithic fragment; i) tuffaceous texture lithic fragment; j) plutonic lithic fragment; k) volcanic lithic fragment with felsitic texture (Lvf), and metapelite grain Lmp rank 1.

work to identify the most relevant lithic fragments that exist (Fig. 3.12). The assemblage Rm is constituted by polycrystalline quartz and metamorphic lithic fragments. The Rv assemblage contains polycrystalline quartz 2-3, potassic feldspars, plagioclase, and volcanic lithic fragments with various textures. The Rs assemblage includes different sedimentary rock fragments (e.g., siltstone, sandstone).

Samples at the RmRvRs diagram display an unrelated compositional swarm to any of the three parameters. To enhance a better interpretation a biplot diagram was created using the *clr*-logarithmic transformations of Rm/Rs vs. Rv/Rs (Fig. 3.13). The biplot separates in the simplex two main groups according to the dominance of Rm or Rs. One group represents the localities with mayor volcanic content or Pf1B plus Pf2. Another group stands for metamorphic dominated sandstones or Pf1A (Fig. 3.13).

3.2.4. Light mineral synthesis: discussion and conclusion

The petrographic parameters indicate that the analyzed samples range from dominant feldspathic arkoses less abundant to sublitharenites. Sandstones are genetically sorted as (a) metamorpho- and volcano-clastic, (b) quartzolithic (Ql), and (3) lithoquartzose (Lq).

Sandstones had various source contributors that promote the construction of several petrofacies. Subpetrofacies 1A represents source rock compositions from (1) low- to high-grade metamorphic rocks, (2) recycled sedimentary detritus from preexisting units, and (3) volcanic rocks, derived from felsitic sources. This interpretations are substantiated by the presence of metapelite (Lmp_{2,3-4}), metapsammite/metafelsite (Lmf_{2,3-4}), metabasite grains (Lmb₁₋₂), fine-grained sandstone and siltstone lithic fragments, and volcanic detritus with microlitic textures.

Subpetrofacies 1B states a more volcanic print from (1) felsic volcanic rocks, (2) basic composition volcanic rocks, and (3) plutonic/granitic sources. The results supported by volcanic lithics with microlitic and felsitic textures, lathwork lithic fragments, and tuffaceous textures (e.g., glomeroporfidic, holohyaline, fiamme, fluidal, spherulitic texture, porfidic, vitrophyric texture, devitrified-, and shards).

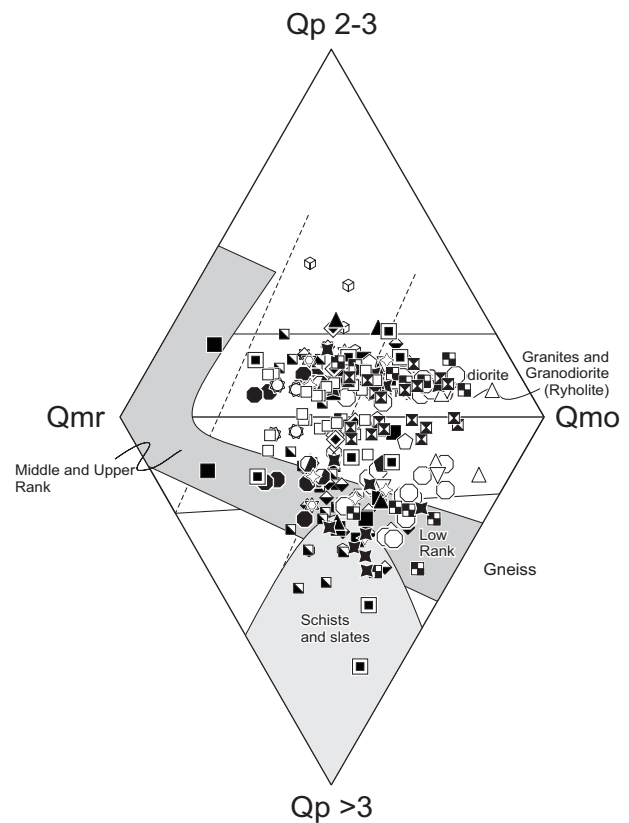


Fig. 3.9: Diamond-shape diagram Qm₀, Qm_r, Qp<3, and Qp>3 with the studied samples of this work (after Basu *et al.*, 1975 modified by Tortosa *et al.*, 1991) used to interpret source rocks. Key for symbols at Fig. 3.2.

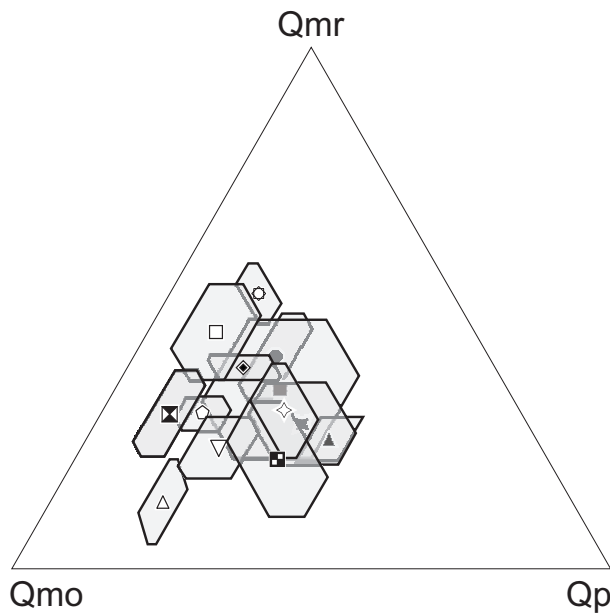


Fig. 3.10: Qmr–Qmo–Qp diagram from Arribas *et al.* (1990). The polygons represent the arithmetic mean and their respective standard deviations form the studied samples for each outcrop. Symbols represent the mean composition for each studied area (Fig. 3.2).

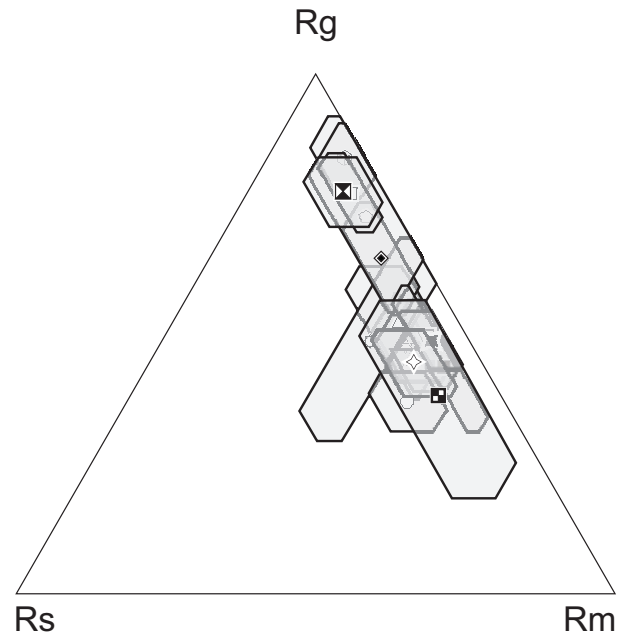


Fig. 3.11: Ternary diagram RgRsRm from Critelli and Le Pera (1994) to determine source rocks interretation. The polygons represent the arithmetic mean and their respective standard deviations form the studied samples for each outcrop. Symbols represent the each studied area (Fig. 3.2).

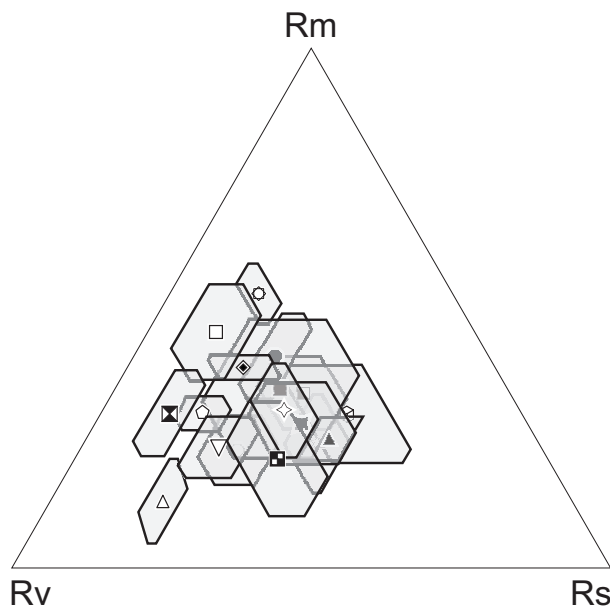


Fig. 3.12: RmRvRs ternary system proposed on this work for source rock affinity. Polycrystalline quartz and metamorphic lithic fragments constitute Rm. The Rv assemblage contains polycrystalline quartz 2-3, potasic feldspars, plagioclase, and volcanic lithic fragments. The Rs assemblage includes different sedimentary rock fragments. Symbols represent the mean composition for each studied area (Fig. 3.2).

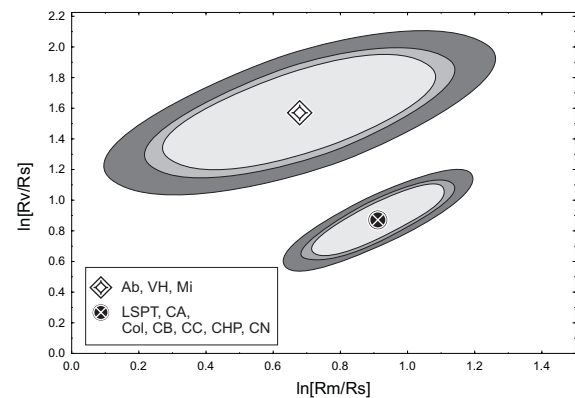


Fig. 3.13: Biplot with the clr- logarithmic transformations for Rm/Rs vs. Rv/Rs. Shaded curves represent the confidence regions for 90, 95 and 99%, and the mean compositional value for Petrofacies 1A and 1B. Petrofacies 1A– Lomas de San Paulo Tranquitas (LSPT); Cañón El Alamar (CA); Cañón El Olmo (COI); Cañón La Boca (CB); Cañón Caballeros (CC); Cañón Peregrina (CHP); Cañón Novillo (CN). Petrofacies 1B– Aramberri (Ab), Valle de Huizachal (VH), Miquihuana (Mi).

Petrofacies 2 reflects a compositional mixture by a minor contribution from metamorphic sources and a constant from volcanic and epiclastic rocks. Pf2 contains monocrystalline quartz, volcanic detrital grains with microlitic, felsitic, and tuffaceous textures, plutonic rock fragments with phaneritic–equigranular textures, and low- middle-grade metamorphic source rock compositions (Lmp₁ and Lmf₁; e.g., schist and slates).

The usage of *clr*- logarithmic transformations (Rm/Rs vs. Rv/Rs) ease for the discrimination of two main source rock-types. In other words, this statistical representation strengthens the petrographic solutions to distinguish between metamorphic (Pf1A) and volcanic (Pf1B+Pf2) sources.

The information from light-mineral petrography will be seen to tie up with further interpretations explained on the next chapters. These first insights about the source rock of the red beds will fit in together with the reported regional/local geology, by the influence of the underlying crystalline basement (Precambrian–Paleozoic) and the volcanic successions (Early Jurassic). This information may be outlined in agreement or disagreement from previous scientific facts about the sediment genesis for the red beds (provenance: source areas, paleocurrent analysis, and tectonic evolution).

4. ANALYSIS OF HEAVY MINERALS: ASSEMBLAGES AND SOURCE AREAS⁵

4.1. Introduction

Heavy mineral concentrations are sensitive indicators for sediment genesis, by examining their prime dependence on the chemistry and tectonostratigraphic level of rock eroded within source terranes (Stattegger, 1987). The concentration of heavy mineral grains in sand-sized terrigenous clastic sediments may fluctuate considerably because of several exogenic factors (Mange and Maurer, 1992; Morton and Hallsworth, 1999). Heavy minerals are useful indicators of alimentary areas for sedimentary basins (Felicka, 2000).

Provenance quantification intrudes several problems for interpreting mineral compositions from sediments. The study of sedimentary petrography by heavy minerals analysis considers the controls exerted by source lands and dispersal pathways; with particular attention of the last sedimentary cycles of weathering, pre-deposition (abrasion, hydrodynamic fractionation, transport, recycling/cannibalism; Garzanti *et al.*, 2003) and pre-diagenetic factors (e.g., eodiagenesis) influencing siliciclastic rocks (e.g., relief, climate, tectonic setting). This knowledge serves as guidance for plate-tectonic evolution.

Heavy mineral concentration is primarily determined by the density hosted on the rock forming minerals from the exposed [source] rocks (Heinrich, 1956; Tröger and Bambauer, 1967; Van An del, 1959; Garzanti *et al.*, 2006; Garzanti and Andò, 2007). Heavy mineral assemblages or heavy mineral associations result from the differentiation (density–sorting) of physical characteristics in a flow environment (erosion, transport, or deposition). Hydraulic conditions can very effectively segregate minerals with even small differences in density into distinct grain-size fractions and sedimentary environments (e.g., fluvial channel *versus* overbank; Dickinson, 1970). However, depleted heavy mineral assemblages may result from severe diagenetic dissolution in ancient sandstones (Gazzi, 1966; Morton, 1985). Thus, the information given by the optical characterization of heavy minerals gives crucial lithological information, including the chemical and mechanical durability. Data calculation can serve for numerical ratios indices, suites, or assemblages (Morton *et al.*, 1994; Morton and Hallsworth 1994; Hounslow and Morton, 2004; Morton *et al.*, 2007).

Provenance analyses need to demonstrate systematically the relationship between qualitative and quantitative characteristics from optical properties of minerals to bear out source lithologies (Vavra, 1990; Hoskin and Schaltergger, 2002).

The main goal is to join in place qualitative/quantitative results from heavy mineral analysis in sandstones and underlying basement units, for a provenance determination purpose. Although previous provenance contributions have been made to clarify the provenance of the red beds, none of them applies a same case study methodology for an integrated result from both basement units and overlaying strata to determine a compatible provenance connection. The results will not only contribute for a catalog of heavy mineral varieties, but will

⁵ This chapter was partially funded by a Postgraduate Grant from the International Association of Sedimentologists (2008): Continental red bed deposits (Late Triassic–Lower Jurassic) in the NE of México: provenance analysis from framework petrography and heavy mineral assemblages.

also provide a better recognition and a functional discrimination between the sources that influence the composition of the Huizachal Group.

4.2. Methods: theory and practice— analytical procedures, representations, indices

The development of heavy mineral studies is parallel to the evolution of sedimentary petrography, with the rising of mineral textures (e.g., Rahmani, 1973; Friis, 1978; Moral-Cardona *et al.*, 2005). Whenever the variable HM concentration is established, the results can be related to differences in sediment composition or source rock lithology (Imbrie and Van Andel 1964; Garzanti *et al.*, 2008). Interpretations of bigger scale raise the possibility for other sedimentary geology insights as sedimentary environmental analysis (Flores and Shideler 1982; Anfuso *et al.*, 1999). This research enables complementary fundamentals about the hydrodynamic factors that control the distribution of heavy minerals (e.g., Vaughn Barrie, 1981; Best and Brayshaw, 1985). Evenmore, heavy minerals assemblages can serve as framework for tectonic applications (Loring, 1991).

Samples of middle to coars grained sandstones were submitted to high-resolution heavy mineral (HM) recognizance to build a classification of mineral assemblages. Heavy mineral data will be acquired by a petrographic study of mineral residues as described by Mange and Maurer (1992), Nelson Eby (inedit internet fileⁱ), and Hounslow and Morton (2004). Samples will be gently disaggregated by the use of a pestle and mortar, avoiding grinding action. Chemical pretreatment is avoided, precluding any modification of the assemblages. Later, samples are immersed in water and cleaned by ultrasonic probe to remove and disperse any fraction. Samples are then washed through a 63 mm sieve and resubjected to ultrasonic treatment. Analysis is confined to a 63–125 mm fraction in order to minimize the effects of hydrodynamic fractionation. An afterwards fraction, which is acquired by sieving through 125 and 63 mm sieves, is put into magnetic separation. The Frantz Isodynamic Magnetic Separator must be controlled meticulously on its magnetic intensity to avoid the leakage of susceptible minerals of interest (e.g., hornblende). Then, the obtained fraction is placed in LST fast float heavy liquid (concentrated solution of lithium hetropolytungstate) with a measured specific gravity of 2.83 g/cm³. Heavy minerals are allowed to separate under gravity. The HM residues are mounted under Beuer resin for optical study using a binocular microscope with transmitted and reflected light features (polarizing microscope). HM proportions are estimated by counting 100–150 non-opaque detrital grains (Galehouse 1971). The optical identification aims for physical properties (colour, morphology, and roundness), as described for grain mounts by Mange and Maurer (1992).

The microscopic properties that were found for each mineral helped to distinguish typology of detrital grains, color, grade of transparency or opacity, external morphologies, and the development of the geometry, textures, inclusions, fractures, zonations, and alterations (Carroll 1953, Pupin, 1980, Rahmani, 1973; Viswanathan, 1986; Corfu *et al.*, 2003; Hay and Dempster, 2009). Mineral varieties act as petrogenetic indicators (Force, 1980; Henry and Dutrow, 1992; Abzalov, 1998; Withers *et al.*, 2003). It is important to keep

ⁱ http://faculty.uml.edu/nelson_eby/Forensic%20Geology/Exercises/Heavy%20Minerals%20and%20Magnetic%20Separation.pdf

in mind that the interpretation of some features such as growth zoning or resorption phenomena can be somewhat ambiguous and controversial. Thus, some caution must be considered whenever textural interpretations are expressed.

Determination of sandstone provenance directly from HM data is not straightforward. While HM assemblages are sensitive indicators of sediment provenance, other processes that operate during the sedimentary cycle may obscure the original provenance signal. To counteract the effects of these overprinting processes, this work aimed for the identification of provenance-sensitive parameters made from HM assemblages. Ten Key Indices–Heavy Mineral Suites (HM%) were defined from mineral counting. Indices represent relatively homogeneous standard groups of transparent heavy minerals with similar provenance implications (Garzanti and Andò, 2007; Table 4.1). In addition, this method has the ability to construct or combined mineral groups into further supergroups (e.g., triangular plots), or split the parameters into subgroups, as required by the specific case under scrutiny.

This work proceeded by using the 10 conventional tabulated indices and one mineral-accessory group to represent petrogenetic suites: (i) ultrastable to relatively stable minerals, mainly derived from sedimentary, felsic igneous, and metamorphic source rocks (ZTR, T&); (ii) minerals chiefly provided by low- to high-grade metamorphic source rocks (LgM, Gt, HgM); (iii) and amphiboles (Hb, and A), pyroxenes (CPX, OPX), olivine, and spinel (OS) largely supplied by intermediate, mafic, and ultramafic igneous or meta-igneous source rocks.

Other useful indices are found on the literature, but did not apply for this case study. They remain to determine ratios of minerals with similar hydrodynamic and diagenetic behavior, and quantify the varietal characteristics shown by a single stable mineral group (e.g., Garzanti and Andò, 2007). These other provenance-sensitive ratios are apatite:tourmaline, garnet:zircon, rutile:zircon, monazite:zircon, and chrome spinel:zircon. These ratios are expressed as index values (ATi, GZi, RuZi, MZi, and CZi; Hounslow and Morton, 2004).

Table 4.1: Key indices used for a synthetic representation of heavy mineral assemblages (after Garzanti and Andò, 2007).

Non-Opaque key indices	Description	Mineral Group	Mineral
ZTR	Ultrastable minerals		Zircon (Z) Rutile (R) Tourmaline (T)
T& (also & HM)	Titanium minerals		Sphene (Titanite; Sp) Anatase (An) Brookite (Br) Apatite (Ap) Monazite (Mo) Baryte (By)
		Epidote Group	Epidote (Ep) Zoisite (Zo) Clinzoisite (Czo) Axinite (Ax)
LgM	Low grade metamorphic minerals	Chloritoid Group Chlorite Group	Chloritoid (Cl) Chlorite (Ch) Chlorite-Mg-rich Serpentine (Se) Prehnite (Pr) Pumellyite (Pu) Talc (Ta)
Gt			Garnet (Gt)
HgM	High-grade metamorphic minerals		Staurolite (St) Andalusite (ad) Kyanite (Ky) Sillimanite (Sil)
Hb			Green Hb (Hb) Green-Brown Hb Brown Hb
& A			Amphibol (Am) Actinolite (Ac) Tremolite (Tr)
tPx			Pyroxene (Px) Clinopyroxene (Cpx) Orthopyroxene (Opx) Hypersthene (Hy) Diopside (Di) Enstatite (En) Diallage (Dl) Augite-Aegirine (Au)
OS			Olivine (Ol) Spinel (Chromite; Cr)
Other HM		Phosphate Silicate	Xenotime (Xe) Topaz (To)
Mica			Muscovite (Ms) Biotite (Bi)

The collected compositional data was transformed to a center logratio transformation (*clr-*), and to an isometric logratio transformation (*ilr-*). The operations are intended to observe the compositional information in a real scale within the *simplex* to fit into a Euclidean real sample space (Aitchison, 1986; 1992; Barceló *et al.*, 1996; Weltje, 2002; Egozcue *et al.*, 2003; Pawlowsky-Glahn and Olea, 2004; Ohta and Arai, 2007). Prior to *clr-* and *ilr-* logarithmic transformations, all values of zero in the raw data spreadsheet were replaced by the lowest mean detectable limit of 0.5 (e.g., Weltje, 2002; Martín-Fernández and Thio-Henestrosa, 2006; Ingersoll and Eastmond, 2007).

After data was transformed, some other methodologies were used for determining and predicting the appropriate predictor variables to perform a canonical discriminant analysis (Agrawal 1999; Agrawal *et al.*, 2004). The analysis produces a set of linear functions from the variables. The values from the linear functions separate into groups of samples (Molinarolli *et al.*, 1991; Swan and Sandilands, 1995; Reyment and Savazzii, 1999).

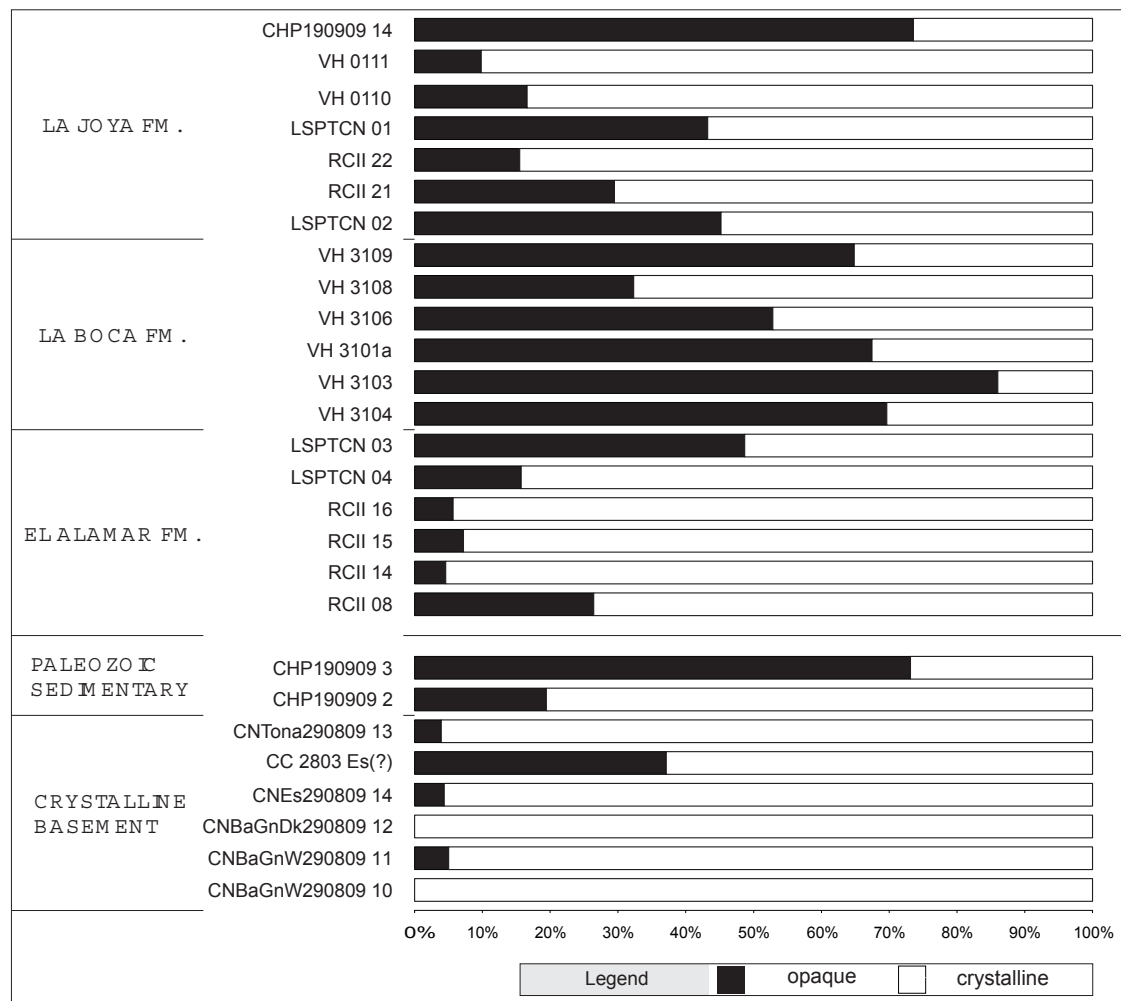


Fig. 4.1: Opaque and crystalline mineral percentages generated by point counting for from the basement units and the red beds.

4.3. Results of heavy mineral provenance analysis: stratigraphic trends of heavy minerals

4.3.1. Heavy mineral: features, concentration and assemblages

Twenty-seven (n= 27) samples were collected from distinct stratigraphic levels of the Huizachal Group, and from some of the underlying Precambrian–Paleozoic basement units (Fig. 1.2; Fig. 4.1). Samples collection may be identified in the measured sections (Fig. 2.16; Fig. 2.17; Fig. 2.18). In total the twenty-seven samples yield 44 varietal grains. The ten distinct heavy mineral assemblages were recognized in the whole sample set (Fig. 4.5). The characteristics of each group of samples referred to their respective formation or basement unit are listed in Appendix for Chapter 4.

Two samples were collected from the underlying Novillo Gneiss complex. One sample belongs to the white-banded unit (CNBaGnW290809-10), and the other to the black-banded unit (CN BaGnB290809-11). One sample was collected from the set of mafic dikes that intrude the Novillo Gneiss (CNBaGnDk290809-12). Two other samples were collected from the structural juxtaposed Carboniferous Granjeno Schist, (CNEs290809-14 and CC2803Es). One sample was taken from the tonalite that cut the Granjeno Schist (CNTona290809-13). Two other samples were collected at base and top from the unmetamorphosed succession of Paleozoic marine clastic strata that nonconformably overlies the Novillo Gneiss (CHP190909-02 and CHP190909-03).

The rest 19 samples correspond to the Huizachal Group. Six samples were collected from El Alamar Formation at the measured section of Lomas de San Paulo Tranquitas (Fig. 2.16). Another six samples were collected for La Boca Formation at the measured sections at Valle de Huizachal (Fig. 2.17). And, the representative samples for La Joya Formation were taken from several localities of interest (Lomas de San Paulo Tranquitas; Valle de Huizachal, and Cañón Peregrina).

4.3.1.1 Precambrian–Paleozoic basement units

The assemblages for the Precambrian crystalline basement units are dominated by non-opaque minerals (Fig. 4.1). The non-opaque minerals identified in the Precambrian–Paleozoic basement units are: a) prehnite, b) garnet, c) topaz, d) olivine, e) apatite, f) spinel, g) andalusite, h) clinochlore, i) hypersthene, j) xenotime, k) pumpellyite, l) zoisite, m) clinopyroxene, n) amphibole, o) tremolite, p) brown hornblende, q) sillimanite, r) tourmaline (Fig. 4.2).

The ZTR index (zircon-tourmaline-rutile; Hubert, 1962) decreases from the Novillo Gneiss to the Granjeno Schist (Fig. 4.5). Rutile is much more abundant than the other ultra-stable heavy minerals in younger units. Zircon and tourmalines are more abundant in older units. The gneiss has a greater garnet and high-grade metamorphic grain (HgM) content than the schist, which has light-grade metamorphic grains (LgM: e.g., chloritoid, chlorite, serpentinite, prehnite). Dikes impress a high content on hornblende and pyroxene assemblages, similar results are found on the tonalite.

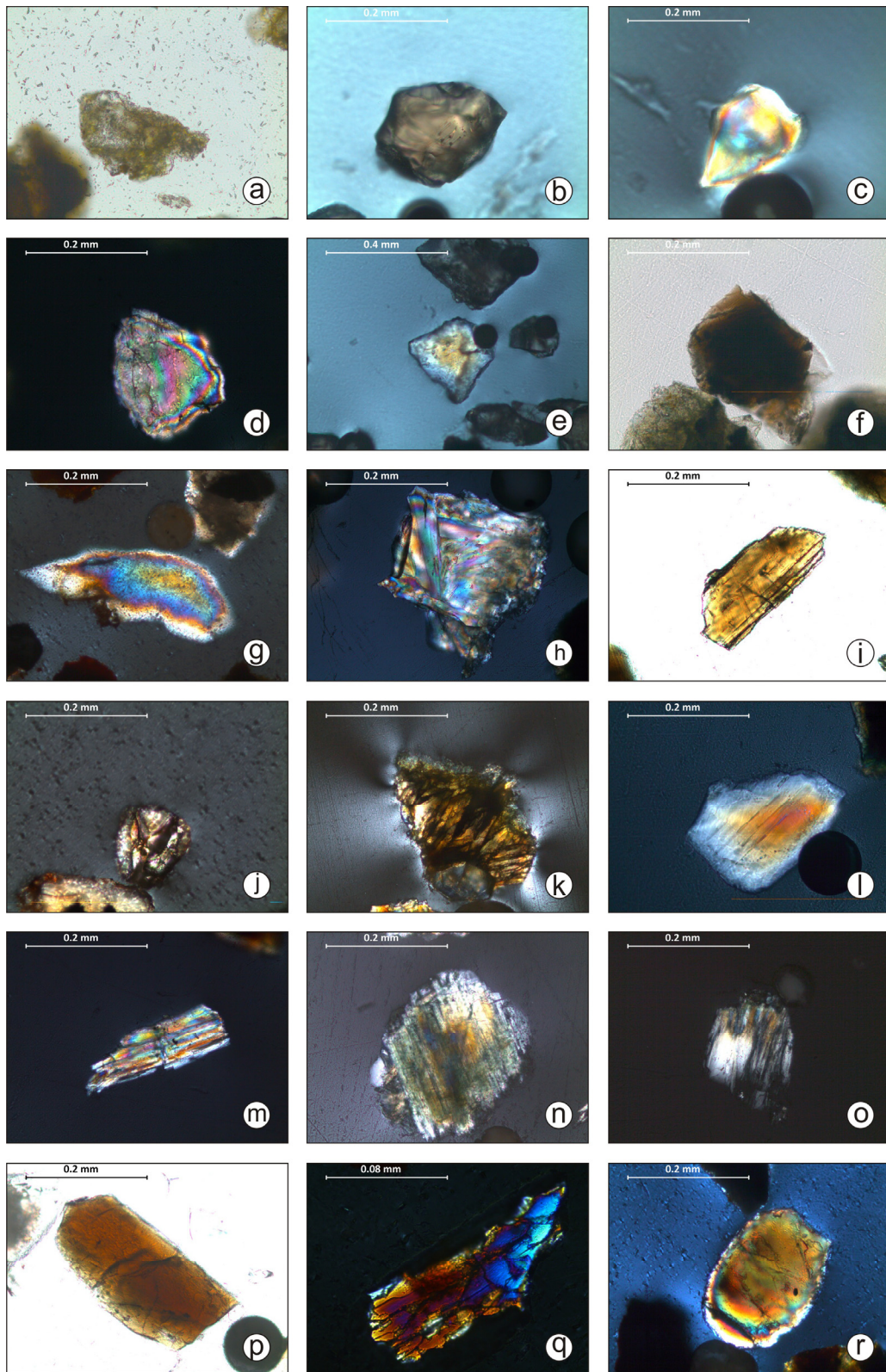


Fig. 4.2: Microphotographs for the heavy mineral assemblage found on the basement units. a) Prehnite, b) Garnet, c) Topaz, d) Olivine, e) Apatite, f) Spinel, g) Andalusite, h) Clinocllore, i) Hypersthene, j) Xenotime, k) Pumpellyte, l) Zoisite, m) Clinopyroxene, n) Amphibole, o) Tremolite, p) Brown hornblende, q) Sillimanite, r) Tourmaline. Microphotographs with no scale bar may be correlated with a scale bar of 0.2 mm from adjacent pictures.

The crystalline basement units have mean values for heavy mineral indices in relationship to the mineral content from other measured samples: (1) *Ilr-ZTR*: 0.214; (2) *Ilr-T&*: 0.537; (3) *Ilr-LgM*: 2.078; (4) *Ilr-Gt*: -0.272; (5) *Ilr-HgM*: -0.109; (6) *Ilr-Hb*: -0.042; (7) *Ilr-&A*: -0.267; (8) *Ilr-tPx*: 1.113; (9) *Ilr-OS*: 0.346; (10) *Ilr-otherHM*: 1.438 (Fig. 4.6: Appendix for Chapter 4).

A sedimentary Paleozoic source area is represented by only two samples. The succession presents at its base a major rock forming mineral variegation than uppermost sample. Therefore, the statistical representations for this succession might be considered unrepresentable and lack in acceptable confidence regions (Fig. 4.6). The base contains titanium minerals (T&) and light grade-metamorphic grains (LgM). While at the topmost sample, there is an increase in ultra-stable heavy minerals (ZTR), plus the occurrence of garnet and high-grade metamorphic grains (HgM; Fig. 4.5). The mean compositional indices are: (1) *Ilr-ZTR*: -30.17; (2) *Ilr-T&*: -2.92; (3) *Ilr-LgM*: -1.28; (4) *Ilr-Gt*: -18.21; (5) *Ilr-HgM*: -18.21; (6) *Ilr-tPx*: -13.34; (7) *Ilr-OS*: -6.06; (8) *Ilr-otherHM*: -2.45 (Fig. 4.6).

4.3.1.2 El Alamar Formation

Some of the main non-opaque minerals identified in El Alamar Formation are: a) hornblende; b) monazite; c) prehnite; d) chlorite; e) zoisite; f) chloritoid; g) zircon (subrounded); h) zircon (elongated); i) zircon (eudral); j) chlorite; k) rutile; l) augite; m) talc (Fig. 4.3).

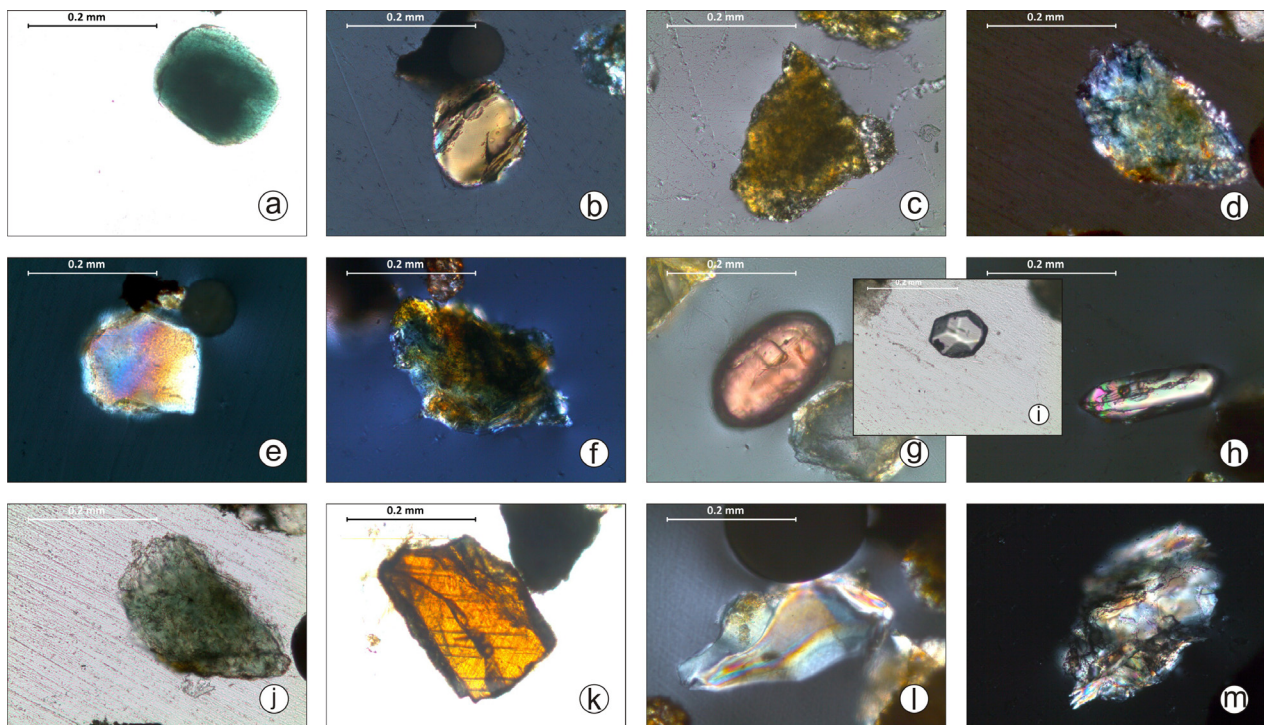


Fig. 4.3: Microphotographs for the heavy mineral assemblage found on El Alamar Formation. a) Hornblende; b) Monazite; c) Prehnite; d) Chlorite; e) Zoisite; f) Chloritoid; g) Zircon (subrounded); h) tetragonal [elongated] zircon; i) Zircon (euhedral); j) Chlorite; k) Rutile; l) Augite; m) Talc. Microphotographs with no scale bar may be correlated with a scale bar of 0.2 mm from adjacent pictures.

In general, the base of Upper Triassic sequence increases its content on ultra-stable heavy minerals (ZTR), decrease in relatively stable titanium minerals (T&), light grade-metamorphic grains remain constant (LgM), and Gt, HgM, and tPx appear occasionally. Meanwhile the top of the analyzed El Alamar sequence increases its content on ZTR, LgM, and high-grade metamorphic grains (Fig. 4.5). The mean compositional indices are: (1) *Ilr*-ZTR: 4.298; (2) *Ilr*-T&: 2.733; (3) *Ilr*-LgM: 9.987; (4) *Ilr*-Gt: -0.652; (5) *Ilr*-HgM: -0.878; (6) *Ilr*-Hb: -0.893; (7) *Ilr*-&A: -0.831; (8) *Ilr*-tPx: -0.760; (9) *Ilr*-OS: -1.821; (10) *Ilr*-other HM: 3.271 (Fig. 4.6).

4.3.1.3 La Boca Formation

La Boca Formation is generally dominated by opaque minerals that obscure the confidence values from the few erected assemblages of the entire analyzed suite (Fig. 4.1). It was unsuccessful to obtain 100 or 150 detrital non-opaque grains from the lowermost part of the exposed [volcanic] lower member of La Boca Formation, but the remainder of the volcanic succession of the red beds is represented by productive samples. Samples at the base of the succession show an inconsistent occurrence of ultrastable to relatively stable minerals (ZTR, T&), yet there is a low presence of light-grade metamorphic grains (LgM), but an increase in hornblends (Hb), amphiboles (&A), and pyroxenes (tPx; Fig. 4.4).

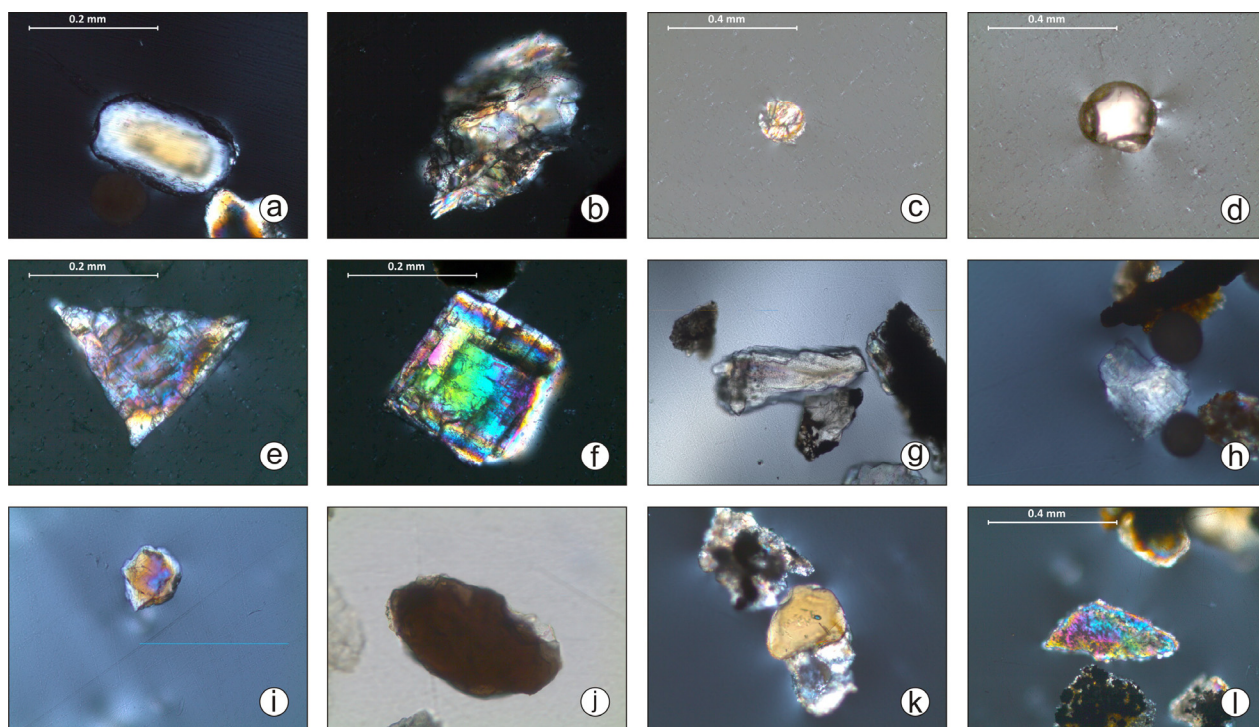


Fig. 4.4: Microphotographs for the heavy mineral assemblage found on the upper member of La Boca Formation and La Joya Formation. a) Apatite; b) Talc; c) Orthopyroxene; d) Zircon; e) Andalusite; f) Kyanite; g) Enstatite; h) Clinozoisite; i) Zoisite; j) Spinel; k) Tourmaline; l) Sillimanite. Microphotographs with no scale bar may be correlated with a scale bar of 0.2 mm from adjacent pictures.

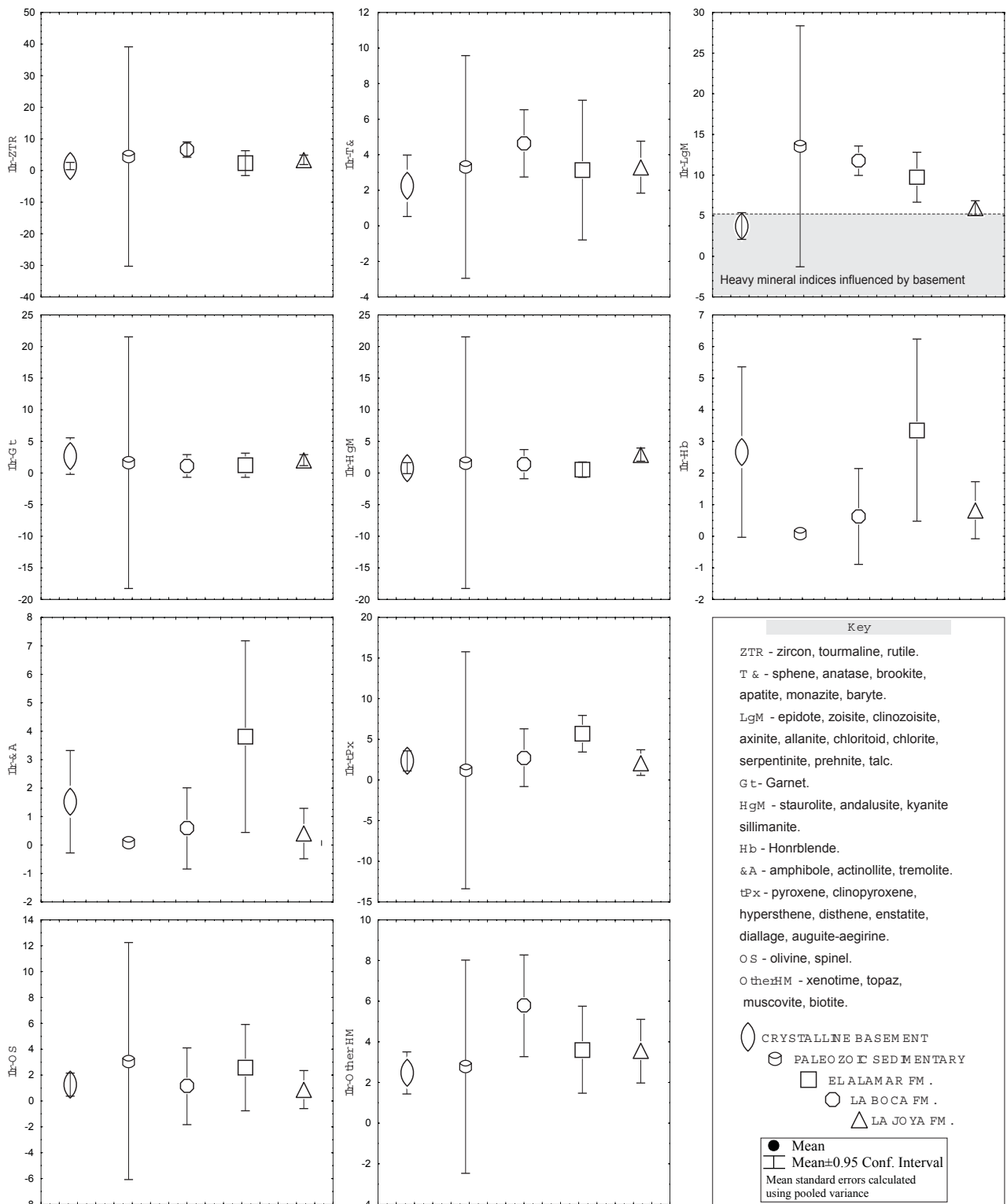


Fig. 4.6: Box-plot diagram with values of the studied samples for each of the main heavy mineral indices according to Garzanti and Andò (2007). Huizachal Group (El Alamar, La Boca, and La Joya Formation) and underlying basement units (Precambrian–Paleozoic).

The uppermost samples increase in concentration of ZTR, T&, LgM, Gt, HgM, with a notorious decrement on amphiboles (Hb, &A), pyroxenes (CPX, OPX), olivine, and spinel (OS). Transformed *Ilr*- mean compositional indices suggest the following values: (1) *Ilr*-ZTR: -1.550; (2) *Ilr*-T&: -0.779; (3) *Ilr*-LgM:

6.648; (4) *Ilr*-Gt: -0.6740; (5) *Ilr*-HgM: -0.065; (6) *Ilr*-Hb: 0.466; (7) *Ilr*-&A: 0.433; (8) *Ilr*-tPx: 3.405; (9) *Ilr*-OS: -0.756; (10) *Ilr*-otherHM: 1.467 (Fig. 4.6).

4.3.1.4 La Joya Formation

Previous sections have interpreted La Joya Formation as the recycling from the underlying units (Chapter 3), consequently heavy mineral assemblages represent it too (Fig. 4.4). The most resistant mineral indices prevail as the main HM print. There is a constant occurrence of ultra-stable heavy minerals (ZTR). In addition, there is a prevalence of garnet (Gt) and high-grade metamorphic grains (HgM), but an upsection decrease of titanium minerals (T&).

However, one of the samples differs from the other three (CHP190909-14), it has pyroxenes (tPx), olivine (Ol), amphiboles (&A), and aggregates of Gt, HgM, and LgM. The *Ilr*- transformed indices are expressed as follows: (1) *Ilr*-ZTR: 1.993; (2) *Ilr*-T&: 1.832; (3) *Ilr*-LgM: 5.031; (4) *Ilr*-Gt: 1.184; (5) *Ilr*-HgM: 1.843; (6) *Ilr*-Hb: -0.0860; (7) *Ilr*-&A: -0.478; (8) *Ilr*-tPx: 0.584; (9) *Ilr*-OS: -0.586; (10) *Ilr*-otherHM: 1.990 (Fig. 4.6).

4.3.2. *Detritus: source rocks and sands*

4.3.2.1 Case study: applying a discriminant function

Variations in the detrital mineral spectra of sediments is best studied using comparative analysis of average values from both the source rocks (provincial mineral assemblages) and those in the individual areas of a particular sink [deposit] (Derkachev and Likolaeva, 2007). Several [ternary] diagrams have been proposed for the discrimination of heavy mineral assemblages to identify source rock and tectonic setting (Garzanti *et al* 2006, 2007). Nevertheless, the diagrams were built upon distinctive geological settings some based on ancient or actual sedimentary environments, thus or datasets remain as unsatisfactory to set in those prefabricated interpretations. Therefore, heavy mineral concentration data was subjected through statistical operations to aim for a discriminant function (DF; Fig. 4.7; Appendix for Chapter 4). It is for consideration that the DF serves only for the used analyzed samples, and the interpretations will only compliment this diagram projection.

Discriminant analysis has revealed an intimate relationship between heavy mineral assemblages and the available source rocks for the red-bed genesis. The heavy mineral trends from Upper Triassic to Early–Middle Jurassic allude to progressive enrichment of heavy mineral assemblages. The rock forming minerals are derived from five main sources: (1) high- to middle-grade metamorphic rocks, (2) hydrothermal alteration source rocks, (3) low-grade metasedimentary rocks, (4) volcanic sources, and a (5) mixed provenance (Fig. 4.7). According to the samples distribution in the *simplex* and the five main sources of HM the results of assemblages may be correlated to a lithostratigraphic unit: (1) crystalline basement units, (2) tonalite, (3) related-Paleozoic units, (4) La Boca Formation and (5) El Alamar and La Joya formations. Samples located in major bounding surfaces (MBS) at the measured sections and interpreted as intraformational (member)

boundaries; served in the DF diagram as indicators for heavy mineral compositional interpretations (e.g., lower and upper member of La Boca Formation).

4.4. Discussion: associated heavy minerals indices to sources

Multivariate and comparative analyses of the spatial distribution for heavy mineral assemblages show that detrital mineral compositions are primarily determined by the availability of basement source rocks and from subsequent volcanic sources. It is therefore possible to identify that the provenance of the heavy mineral assemblages are defined by the litho-tectonic evolution of the basement and the geology of fluvial styles of Upper Triassic to Middle Jurassic sedimentary cover.

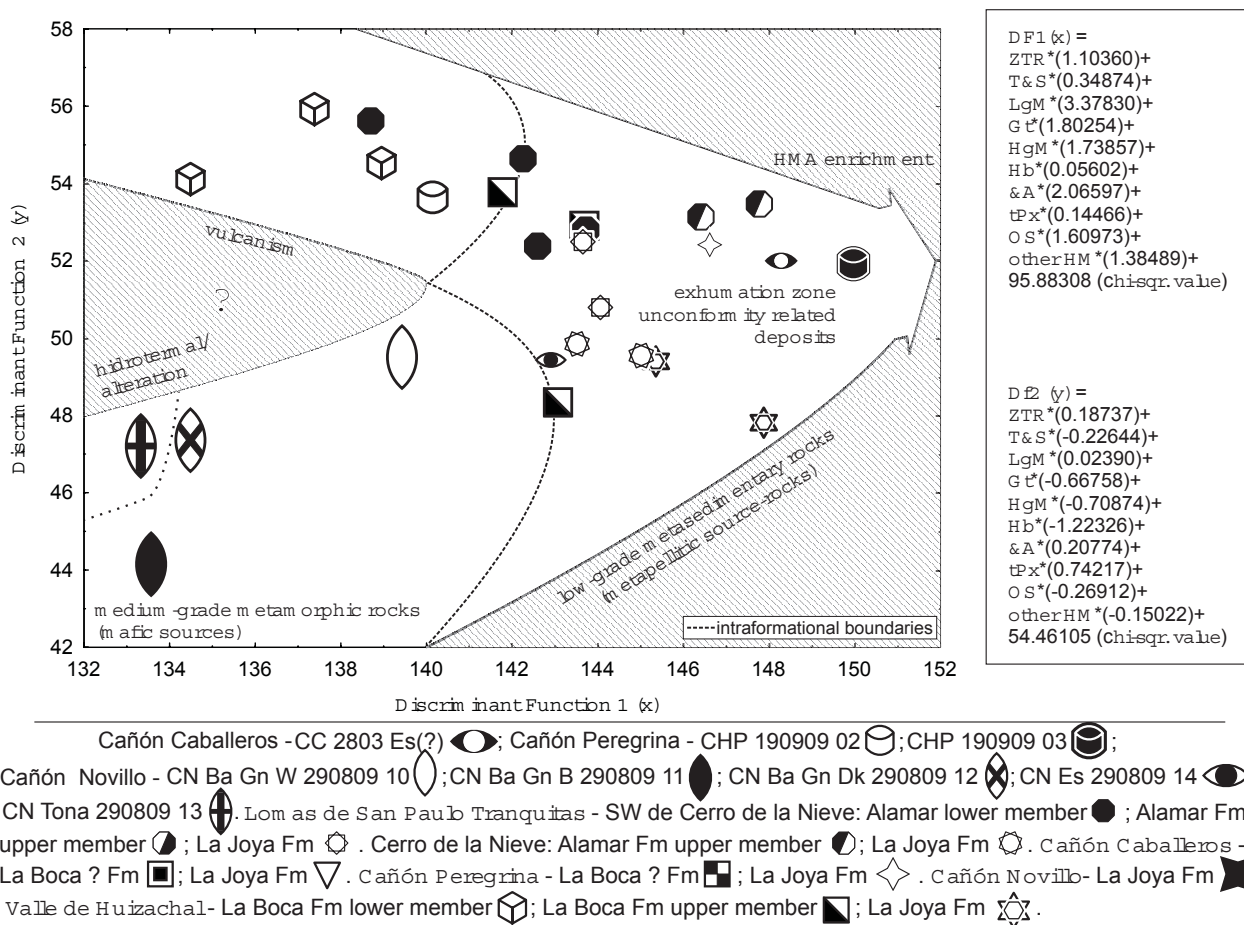


Fig. 4.7: Standardized canonical discriminant functions for provenance analysis of heavy mineral indices. A biplot arranges the discriminant functions at each axis (DF1 [x] vs. DF2 [y]). The simplex contains fields interpreted for provenance source rocks.

Zircon types at the lower volcanic interval of the Valle de Huizachal present elongated and skeletal morphologies, which must have been controlled by the variability of velocity of crystallization from the mafic and undersaturated alkaline rocks. The needle morphologies and acicular form in crystals are common in fast crystallization, like in porphyry, sub-volcanic intrusions, high-level granites and gabbros. Meanwhile, the stubby and equate forms are more common in emplaced intrusions with low cooling velocities. The presence of surface textures may be attributed to weathering differentiation between the source area and the depocenter.

The mineral suites of Gt and HgM are significant important because they demonstrate that the presence of garnet and kyanite assemblages indicate derivation from high-grade metamorphic sources, which were not reported earlier for the basement units in northeastern Mexico.

The evolutionary trends of sedimentary deposits, connected with an increase in heavy mineral enrichment of the available source rocks at the earth's crust, are clearly expressed. The increase in (i) minerals were chiefly provided by low- to high-grade metamorphic source rocks (LgM, Gt, HgM), (ii) the subsequent input from amphiboles (Hb, &A), pyroxenes (CPX, OPX), olivine, and spinel (OS) were largely supplied by the rejuvenation of intermediate, mafic source rocks, and (iii) an enrichment in heavy mineral assemblages was derived from sedimentary and felsic igneous source rocks (ZTR). This results support an interpretation for a genesis of an extensional basin by the uplifting of basement massifs, subsequent continental volcanic arc, and a final stage of tectonic reactivation with exhumation and unroofing of the underlying strata.

Only a general heavy mineral concentration analysis is outline in this chapter but it can be further refine by the availability of new data, or serve as a complement for an integral provenance study (e.g., light+heavy mineral assemblages; or U-Pb detrital zircon ages+zircon typology). By the hand of this last statement, it will be seen at Chapter 7 how this integral provenance approaches will considerably support and potentiate the resolution for the sediment generation of the red beds.

5. GEOCHEMICAL CLASSIFICATION, COMPOSITIONAL MODIFICATIONS, AND SOURCE AREA COMPOSITION

5.1. Introduction

Whole-rock geochemistry from siliciclastic sedimentary rocks reflects the course of the sediment genesis. Interpretations define an eroded compositional source [area/rock], weathering effects, and sink variables including transport, diagenesis and metamorphism (Nesbitt, 1979; Dinelli *et al.*, 1999; Nesbitt, 2003; Caja, 2004; von Eynatten, 2004; Parsons *et al.*, 2005; Pe-Piper *et al.*, 2005; Reynaud *et al.*, 2006; Blinski, 2008; Krenn *et al.*, 2008; Tribovillard *et al.*, 2008). The study of provenance and geological processes in sedimentary rocks encounter common multiple components to interpret sediment history in favor of a common analytical pathway (Pettijohn *et al.*, 1972; Nesbitt and Young, 1982; Bhatia, 1983; Roser and Korsch, 1986; 1988; Herron, 1988; McCann, 1991; McLennan *et al.*, 1993; Bailey *et al.*, 1998; Toulkerides *et al.*, 1999). The integration of methodologies produces information to constrain models for tectonic association, climate and paleoclimate, crust-mantle evolution, diagenesis, and so forth.

This chapter aims for geochemical approaches in provenance and sedimentary processes, among other intrinsic advantages for unsolved problems from latter chapters. The issues to be attended include the influence from source area composition, modifications during chemical weathering, and the influence gestated between alkali and alkaline earth elements. Goals will be assisted by quantifying the chemical composition from selected elements (major elements, trace elements, and REE) and mixing systems. In many cases geochemistry can “see through” the physical and mineralogical changes associated with the formation of terrigenous clastic sedimentary rocks (obscuring the ability to discern rock fragments), mineral sorting, and mineral reactions that took place during weathering and diagenesis (Dapples 1972; McLennan *et al.*, 1993).

The mixing systems that transfer mass and energy are found at different Earth spheres. The chemical composition of the upper continental crust was constrained by sandstones composition from basement shielded zones. The studies reflect the source [area/rock] composition and proportions of sedimentary rocks through time (Ronov and Yaroshevskiy, 1969; Shan, *et al.*, 1998; Lentz, 2003). The relative proportions of fine-grained and coarse-grained sedimentary rocks are critical because the proportion of coarse sediment will undoubtedly affect the amounts of the most abundant components and thus determine the crust average composition (granodioritic, tonalitic, or dioritic; Condie, 1993). The endogenic processes at the continental crust preferentially separate incompatible elements from the mantle and accumulate them especially in the upper crust. The heat and dynamic energy from the mantle provides the majority of the needs for crustal activities. Other factors driven by the mantle are processes for material fractionation, hydrothermal alteration, and metamorphism (Heier, 1973; Storey and Meneilly, 1985; Wedepohl 1991; Emmett, 1996; Turner and Rushmer 2009). Weathering products, hydraulic classification, sedimentation, and diagenesis are another exogenic-cycle of fractionation (Middleton, 1960; Weber and Middleton, 1961a 1961b; McLennan, 1989; Hiscott, 1984; Cox *et al.*, 1995;

Fedo *et al.*, 1995; Bock *et al.*, 1998; Fralick and Kronberg, 1997; Nesbitt *et al.*, 1997; Fralick, 2003; Nesbitt, 2003; Ochoa *et al.*, 2007; Peterson, 2009).

Chemical concentrations of sediments reflect distinctive environments by their differences in element concentrations added or depleted along the operating systems. These validate when using insoluble elements to aqueous solutions, or low element mobility during weathering, transport, diagenesis and metamorphism (Cullers, 1994; Condie *et al.*, 1995; Bauluz *et al.*, 2000; Amorosi *et al.*, 2007). Rare Earth Elements (REE) and immobile elements as Zr, Th, Sc, Hf, Ti and Nb, are the most recommended for geochemical approaches to determine provenance (Bhatia, 1985a,b; Taylor and McLennan 1985; Bhatia and Crook, 1986; McLennan *et al.* 1990; McLennan and Taylor 1991; Hole *et al.* 1992; Girty *et al.* 1994; Jenchen 2001; Wandres *et al.*, 2004; Joo *et al.*, 2005). The intricate controlling-factors on chemical composition for terrigenous clastic rocks make of vital importance the quantification for the chemical attributes/variables related to geological processes on sediment genesis.

5.2. Methodos

Sampling collection consider fresh representative examples with the widest possible variety of sources or provenance as far as possible to avoid weathering effects and other factors over sediment genesis. A total of 124 samples were collected of middle to coarse-grained sandstones. Samples were crushed and pulverized using standard procedures for whole-rock geochemical analyses at ACME Labs in Vancouver, Canada. In addition, 16 different samples were collected from the underlying units, like those considered in the literature as “pre-Oxfordian” (*cf.*, Meiburg *et al.*, 1987), Paleozoic unmetamorphosed and metamorphose sediments, and Precambrian crystalline basement rocks. The major and trace elements were analyzed by Inductively Coupled Plasma atomic emission spectroscopy (ICP-ES) and high-resolution inductively coupled plasma mass spectrometry (ICP-MS). Trace elements include 46 different elements, meanwhile Rare Earth Elements (REE) include 14 types. The CO₂ values were calculated according to the algorithm proposed by Ocampo-Díaz (2011) to evaluate the content of calcium carbonate in all the analyzed samples.

The structure for the results section was designed upon the statistical analysis of compositional data. Sandstone classification was used according to previous works and their interpretations are dependent to the numerical analysis. Results of the geochemical analysis can be consulted at Appendix for Chapter 5.

5.3. Results: data description and visualization

5.3.1. Major Elements data

The major element concentrations include the Loss on Ignition– LOI values, (Appendix for Chapter 5), and the calculated results at Table 5.1 are in units of weight %.

The SiO₂ concentration dominates all the samples (Table 5.1), with ~75.4% for clastics (C) localities or those representative samples within the subpetrofacies 1A (Chapter 3), and ~64.6% for volcanic (V) related-outcrops or its homologous classifications belonging to subpetrofacies 1B and petrofacies 2. High values of silica may be petrographically justified by the well-developed quartz crystals, and their characteristic syntaxial overgrowths. Other variations on element concentrations are seen with Al₂O₃ values (C– ~9.8% and V– 10.5%), which increase whenever Na₂O (C– 0.9% and V– 1.9%) and K₂O (C–1.7% and V– 3.3) rise (Fig. 5.1; Table 5.1; Appendix for Chapter 5). The alumina, potassic, and sodic concentrations increase by the occurrence of matrix, feldspars and plagioclase that alter into argillaceous minerals. Moreover, MgO content (C– 1.3% and V– 1.5%) represents similar increasing values with the incidence of epimatrix, opaque minerals, and volcanic rocks. Furthermore, TiO₂ preserves stabilized records and is particularly controlled by grained size particle variations (medium to coarse). Herein CaO values have been calculated as done by Ocampo-Díaz (2011) to diversify the content into several representative operations with genetic(?) interpretation: CaO_{tot} (CaO total), CaO* (CaO in Silicates), and CaO_{carb} (CaO in Carbonates). Concerning CaO*, it presents low concentrations for C– 1.0% and remains relatively low for V– 3.8% with respect to CO₂ percentages (C– 1.1% and V– 4.9%). These results are intimately related to the burial status of the samples determined by the lack of occurrence from porosity, but also to LOI (C– 3.5% and V– 7.1%).

In addition to the calculated perceptual values with their respective standard deviations of major elements, other analyses were taken into consideration, including a)

Table 5.1: Chemical composition: a) Clastics: LSPT– Lomas de San Paulo Tranquitas; CA– Cañón El Alamar; COL– Cañón El Olmo; CB– Cañón La Boca; CC– Cañón Caballeros; CHP– Cañón Peregrina; CN– Cañón Novillo). b) Volcanics: VH– Valle de Huizachal; Ab– Aramberri; Mi– Miquihuana. n– number of analyzed samples. For the complete dataset, visit the Appendix for Chapter 5.

	a) Clastics; n= 82		b) Volcanics; n= 38	
	Mean	Std.Dev.	Mean	Std.Dev.
SiO ₂	75.483	7.5283	64.6737	7.8885
Al ₂ O ₃	9.8734	2.9897	10.5455	2.2312
Fe ₂ O ₃	4.281	2.3248	3.2097	1.2624
MgO	1.3745	0.8238	1.5295	0.8568
CaO _{total}	1.7267	2.5487	6.7632	5.6358
CaO*	1.0388	1.4593	3.8242	3.2242
CO ₂	1.106	1.8758	4.9366	4.5322
Na ₂ O	0.9944	0.7666	1.9161	1.4395
K ₂ O	1.7613	1.1304	3.3005	1.3534
MnO	0.0545	0.0428	0.0911	0.0523
TiO ₂	0.6755	0.4308	0.5418	0.2289
P ₂ O ₅	0.0873	0.0498	0.1018	0.034
Cr ₂ O ₃	0.0069	0.0042	0.0081	0.0039
Lol	3.5878	1.757	7.1658	4.2307
Sc	9.0976	4.6071	8.4737	3.1856
V	88.439	86.7598	73	44.16
Cr	9.3878	19.3662	0.0028	0.0013
Co	10.6878	8.3407	8.3316	6.6444
Ni	18.9927	10.1288	17.7842	8.1701
Zn	50.9512	41.3715	42.5526	32.4684
Ga	11.0671	3.6752	10.1211	2.8279
Rb	51.878	31.9503	69.5474	26.4691
Sr	55.4683	68.3919	93.1447	77.0438
Y	18.5512	9.1293	20.3158	7.7281
Zr	237.8537	238.2256	217.7684	132.6561
Nb	8.4671	5.0985	7.5395	3.5943
Ba	454.5732	439.1598	671.1316	650.0553
Hf	6.6976	6.4086	5.9105	3.3614
Ta	0.603	0.3762	0.5658	0.2694
Pb	10.6121	61.4866	7.1921	6.5413
Th	6.9037	4.1261	7.2211	2.3766
U	1.8305	1.2022	1.9211	0.775
Cs	3.389	1.9322	3.4737	2.3801
La	52.8643	27.0356	53.7875	31.3157
Ce	44.2283	22.9207	43.1296	23.6573
Pr	36.1938	17.6023	36.8467	19.2202
Nd	27.2957	12.6933	28.3122	14.4237
Sm	16.5472	7.391	16.8831	8.0389
Eu	10.2714	4.577	9.5201	4.2981
Gd	11.2454	5.1705	11.634	5.5325
Tb	9.7486	4.5609	10.1293	4.755
Dy	8.3955	4.0889	8.5492	3.9809
Ho	7.5107	3.6739	7.7438	3.5944
Er	7.6804	3.8775	7.7319	3.5771
Tm	0.8146	0.3898	0.8146	0.3715
Yb	7.4777	3.6752	7.6069	3.5162
Lu	7.6021	3.8074	7.4803	3.4714

joining “tree-clustering” coupled to the amalgamation (linkage) rule of weighted pair-group average under the command of distance measurement of *IPearson r*, and b) principal components or classification analysis using

a 2D projection with factor variable coordinates. These multivariate exploratory techniques were used to identify any linear tendency and correlation between major element concentrations within the pair of datasets (calstics *versus* volcanics). Samples from different authors were compiled to strengthen interpretations for the calculations of this work.

Math operations start with a correlation matrix made by considering the 95% of confidence, for both sample sets clastics (C) and volcanics (V; Table 5.2). Clastics reveal an inconsistent positive correlation of SiO_2 with the rest of the major elements, probably because of the profound heterogeneity of the sources, and the subsequent uneven sandstone maturity expressed as a sublitharenite (see Chapter 3). Meanwhile Al_2O_3 presents moderate positive correlations with K_2O ($r=0.45$), P_2O_5 ($r=0.59$), and slightly positive values of Na_2O ($r=0.29$) and TiO_2 ($r=0.29$), with a plausible explanation from progressive alteration of feldspars, clay minerals, and an input of the mica group. There is a negative predominance of correspondence between Fe_2O_3 ($r=0.58$) and MgO ($r=0.53$) with respect to CaO_{tot} , CaO^* and CO_2 ($r= <-0.03$), indicating an oxide concentration that derivates mainly from rich-oxide minerals or mineral alteration, but not from matrix nor cement.

The volcanic datasets reveal a different perspective of element correlations (Table 5.2), headed by SiO_2 with positive associations with Al_2O_3 ($r=0.19$), K_2O ($r=0.18$), and slightly positive values of Na_2O ($r=0.01$), evidencing the

arkosic nature of the samples (see Chapter 3). Al_2O_3 has also positive values with Na_2O ($r=0.42$), K_2O ($r=0.22$), P_2O_5 ($r=0.58$), and TiO_2 ($r=0.41$), representing the compositional modifications of feldspars, argillaceous minerals, mica group, and volcanic aggregates (e.g., apatite; Jenchen, 2001; Jenchen and Rosenfeld, 2007). The negative correlations of Fe_2O_3 and MgO with CaO_{tot} , CaO^* and CO_2 refer to an input from mafic minerals from epiclastic rocks (Fe+Mg) rather than oxides within the matrix or epimatrix.

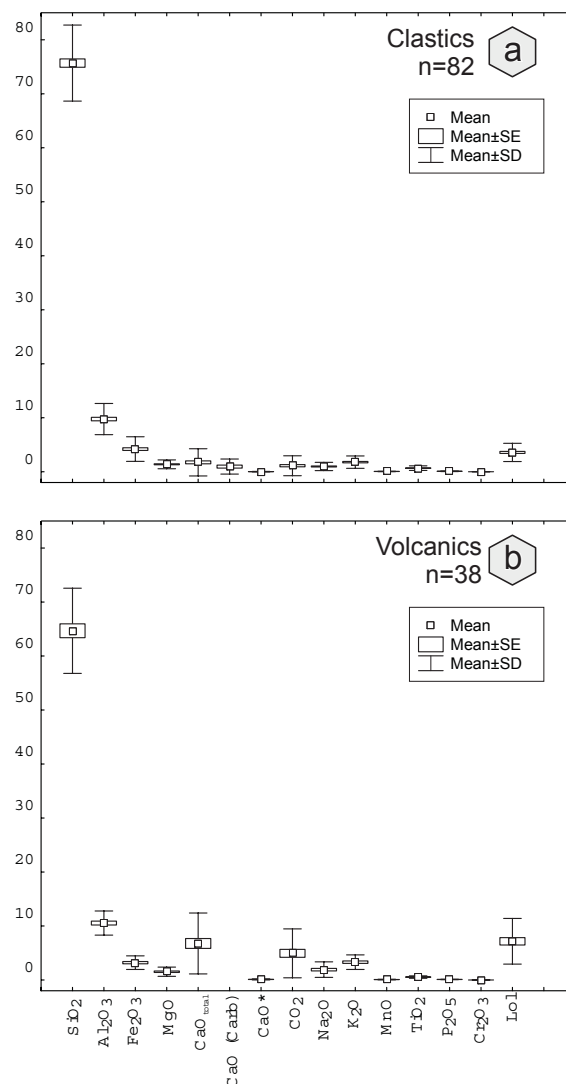


Fig. 5.1: Box-plot diagrams with the arithmetic mean and standard deviation values for major elements from a) clastics ($n= 82$) and b) volcanics ($n= 38$).

5.3.1.1 Cluster analysis: an elemental chain of commands

The cluster analysis is an exploratory data analysis that encompasses a number of different [geochemical] classification algorithms used to develop sediment groups (Fischer, 1989; Smosna *et al.*, 1999; Baaske, 2005). The purpose of this algorithm is to join objects (e.g., elements concentrations) into successively larger clusters using a measurement of similarity or [Euclidean] distance. A hierarchical tree is a typical result for this type of clustering. The horizontal axis on the plots denotes the linkage distance where we can read off the criterion distance, to which elements are linked on to generate new single clusters.

Table 5.2: Correlation matrix of major elements at 95% of confidence (highlighted) for two calculated datasets. a) Clastics, n=82 (LSPT– Lomas de San Paulo Tranquitas; CA– Cañón El Alamar; COI– Cañón El Olmo; CB– Cañón La Boca; CC– Cañón Caballeros; CHP– Cañón Peregrina; CN– Cañón Novillo). b) Volcanics, n= 38 (VH– Valle de Huizachal; Ab– Aramberri; Mi– Miquihuana).

a) Clastics (LSPT, CA, COI, CB, CC, CHP, CN); n= 82													
	SiO ₂	Al ₂ O ₃	Fe ₂ O ₃	MgO	CaO _{tot}	CaO*	CO ₂	Na ₂ O	K ₂ O	MnO	TiO ₂	P ₂ O ₅	Lol
SiO ₂	1.00	-0.78	-0.62	-0.61	-0.50	-0.50	-0.43	-0.23	-0.37	-0.50	-0.24	-0.63	-0.68
Al ₂ O ₃		1.00	0.58	0.53	-0.06	-0.06	-0.05	0.29	0.45	0.20	0.29	0.59	0.18
Fe ₂ O ₃			1.00	0.56	-0.11	-0.11	-0.13	-0.01	-0.05	0.27	0.37	0.42	0.17
MgO				1.00	0.09	0.09	-0.03	0.11	0.12	0.40	0.24	0.46	0.15
CaO _{tot}					1.00	1.00	0.88	0.09	0.05	0.46	-0.20	0.08	0.86
CaO*						1.00	0.86	0.09	0.05	0.45	-0.20	0.08	0.85
CO ₂							1.00	0.10	0.10	0.56	-0.20	0.09	0.80
Na ₂ O								1.00	-0.10	0.16	0.05	0.36	-0.06
K ₂ O									1.00	-0.02	-0.07	0.40	0.15
MnO										1.00	0.01	0.34	0.49
TiO ₂											1.00	0.52	-0.05
P ₂ O ₅												1.00	0.20
Lol													1.00

b) Volcanics (VH, Ab, Mi); n= 38													
	SiO ₂	Al ₂ O ₃	Fe ₂ O ₃	MgO	CaO _{tot}	CaO*	CO ₂	Na ₂ O	K ₂ O	MnO	TiO ₂	P ₂ O ₅	Lol
SiO ₂	1.00	0.19	0.07	0.05	-0.87	-0.87	-0.86	0.01	0.18	-0.71	0.02	-0.01	-0.89
Al ₂ O ₃		1.00	0.66	0.56	-0.63	-0.63	-0.63	0.42	0.22	-0.50	0.41	0.58	-0.58
Fe ₂ O ₃			1.00	0.78	-0.46	-0.46	-0.47	0.19	-0.04	-0.38	0.73	0.67	-0.43
MgO				1.00	-0.40	-0.40	-0.41	-0.04	-0.01	-0.29	0.65	0.62	-0.31
CaO _{tot}					1.00	1.00	1.00	-0.14	-0.28	0.81	-0.28	-0.33	0.98
CaO*						1.00	1.00	-0.14	-0.28	0.81	-0.28	-0.33	0.98
CO ₂							1.00	-0.15	-0.27	0.81	-0.30	-0.33	0.98
Na ₂ O								1.00	-0.56	0.06	0.04	0.04	-0.26
K ₂ O									1.00	-0.33	-0.12	0.00	-0.19
MnO										1.00	-0.30	-0.36	0.77
TiO ₂											1.00	0.85	-0.25
P ₂ O ₅												1.00	-0.25
Lol													1.00

To conceal the statistical step-maneuver an informatical matrix was made using the number of samples and the major elements concentrations. In addition, a principal component analysis developed to validate the significance of each element used in the cluster method (Fig. 5.2; Fig. 5.3).

Cluster analyses interpretations remain parallel to latter results. SiO₂ represents the quartz concentration, while Al₂O₃, Na₂O, and K₂O are for argillaceous minerals, phyllosilicates, and feldspars. The ferric fraction (Fe₂O₃, MgO, and MnO) is related to epimatrix and indicator minerals of volcanic rocks (see Chapter 3). Nevertheless, the compositional signature may also be granted to heavy minerals (see Chapter 4). Other elements like TiO₂ and P₂O₅ are consistent with the occurrence of some heavy mineral assemblages (e.g., ZTR and T&; see Chapter 4). Finally, yet importantly, CaO_{tot} and MgO shall be consider deriving from argillaceous minerals, feldspars, and heavy minerals, iron oxides and volcanic lithics, respectively. In addition, CO₂ is consider being part of LOI and serves as an artifact of correlation for working interpretations.

The results for the clustering analysis from the clastic samples developed four groups out of two main branches (Fig. 5.2). The main hierarchical arranged cluster comprehends an interpretative petrographical domain built by the abundance of primary and secondary minerals. Quartz content (SiO₂) marks the litharenite classification, while argillaceous minerals, feldspars, and their subsequent alteration into clay minerals are responsible for the Al₂O₃–P₂O₅–K₂O grouping. The two assembles made by Fe₂O₃, MgO, TiO₂, and Cr₂O₃ may represent volcanic rock fragments, [opaque] heavy minerals, and epimatrix. The secondary arranged cluster of CaO_{tot}, CO₂, LOI, MnO, and Na₂O has a common origin on the linkage distance and denotes the volatile effect

form either carbonate cement(?), titanium minerals (e.g., apatite), and epimatrix (Jenchen (2001; Jenchen and Rosenfeld, 2007).

The volcanic samples manifest a different clustering pattern with six groups compared to the clastics samples (Fig. 5.2). The main hierarchical arranged cluster is led by SiO_2 and K_2O , proofing the arkose sandstone classification derived from a mineral domain of quartz and feldspars. Al_2O_3 prevails as a lonely group concerning argillaceous minerals and phyllosilicates. The groupings of Fe_2O_3 with MgO can fundament the presence of minerals of acid rocks, opaque heavy minerals, and epimatrix from epiclastic rocks. Meanwhile TiO_2 – P_2O_5 – Cr_2O_3 may have a similar heavy mineral association to Fe_2O_3 with MgO . Na_2O remains as another single element group representing compositional modifications from clay minerals and feldspars including epimatrix. The secondary hierarchical arranged cluster is almost similar to the found on the clastics samples, but is constituted by grouping CaO_{tot} , CO_2 , LOI , and MnO . It may represent the volatile effect form either insignificant carbonate cement(?) and titanium heavy minerals.

5.3.1.2 Principal Components analysis (PC)

Principal components analysis is another exploratory tool with two-dimensional graphs (biplot) for compositional data arrays (Aitchison and Greenacre, 2002). Sample sets were transformed into centered logcocientes (*Clr*-) before the construction of graphics. The *Clr*- transformations were performed by calculating the logcociente for each sample over the geometric mean of the respectively sampleset. PC analysis involves the rotation of the eigene vectors (Swan and Sandilands, 1995). Principal components consider the total variation of a dataset within a small number (*q*-say) of [geological] statistical factors. Each of them represents a degree of correlation (elongation) in a *n*-dimensional database. The vector analysis only looks for *q*-vectors, which examine the variance of the data to maximize their representation by rotating the axes.

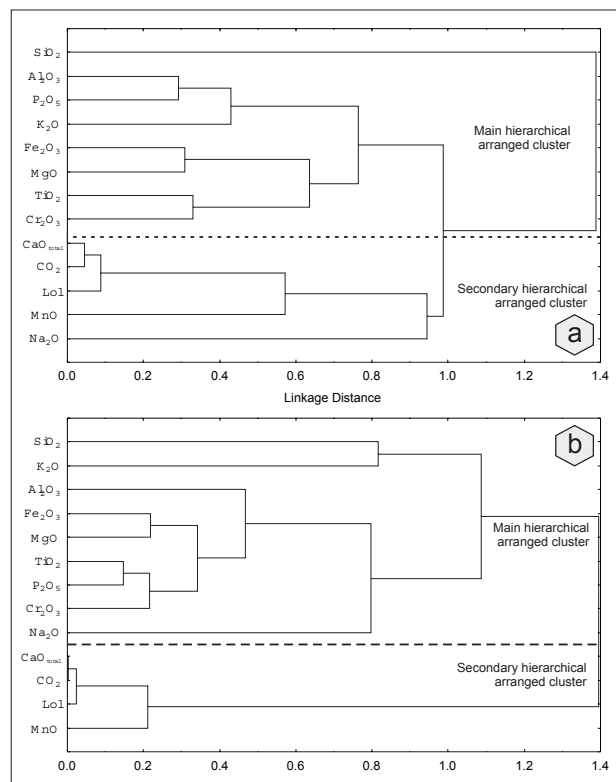


Fig. 5.2: Dendrogram with a typical joining “tree-clustering” coupled to the amalgamation (linkage) rule of a weighted pair-group average with a distance measurement of $1/Pearson\ r$. a) Clastics, $n=82$ (LSPT– Lomas de San Paulo Tranquitas; CA– Cañón El Alamar; COL– Cañón El Olmo; CB– Cañón La Boca; CC– Cañón Caballeros; CHP– Cañón Peregrina; CN– Cañón Novillo). b) Volcanics, $n= 38$ (VH– Valle de Huizachal; Ab– Aramberri; Mi– Miquihuana).

Table 5.3: Geochemical cluster correlation matrices between major elements with the 99.5% of confidence (highlighted). a) Clastics, n=82 (LSPT– Lomas de San Paulo Tranquitas; CA– Cañón El Alamar; COL– Cañón El Olmo; CB– Cañón La Boca; CC– Cañón Caballeros; CHP– Cañón Peregrina; CN– Cañón Novillo). b) Volcanics, n= 38 (VH– Valle de Huizachal; Ab– Aramberri; Mi– Miquihuana).

Clastics													
Mayor element (%)	SiO ₂	Al ₂ O ₃	Fe ₂ O ₃	MgO	CaO _{total}	CO ₂	Na ₂ O	K ₂ O	MnO	TiO ₂	P ₂ O ₅	Cr ₂ O ₃	Lol
SiO ₂	0.00	1.73	1.52	1.59	1.56	1.45	1.13	1.50	1.38	1.16	1.61	1.19	1.63
Al ₂ O ₃		0.00	0.41	0.46	1.07	1.19	0.81	0.47	0.96	0.70	0.29	0.78	0.99
Fe ₂ O ₃			0.00	0.31	1.17	1.28	1.09	0.93	0.81	0.47	0.52	0.68	1.04
MgO				0.00	0.96	1.12	0.90	0.90	0.65	0.69	0.54	0.70	0.93
CaO _{total}					0.00	0.05	0.95	0.93	0.57	1.31	1.09	1.16	0.09
CO ₂						0.00	1.02	0.91	0.56	1.34	1.10	1.15	0.08
Na ₂ O							0.00	1.11	0.83	0.98	0.77	1.09	1.13
K ₂ O								0.00	1.11	1.08	0.38	0.86	0.81
MnO									0.00	1.06	0.83	1.04	0.58
TiO ₂										0.00	0.61	0.33	1.18
P ₂ O ₅											0.00	0.64	0.93
Cr ₂ O ₃												0.00	1.02
Lol													0.00

Volcanics													
Mayor element (%)	SiO ₂	Al ₂ O ₃	Fe ₂ O ₃	MgO	CaO _{total}	CO ₂	Na ₂ O	K ₂ O	MnO	TiO ₂	P ₂ O ₅	Cr ₂ O ₃	Lol
SiO ₂	0.00	0.81	0.93	0.95	1.87	1.86	0.99	0.82	1.71	0.98	1.01	1.08	1.89
Al ₂ O ₃		0.00	0.34	0.44	1.63	1.63	0.58	0.78	1.50	0.59	0.42	0.58	1.58
Fe ₂ O ₃			0.00	0.22	1.46	1.47	0.81	1.04	1.38	0.27	0.33	0.36	1.43
MgO				0.00	1.40	1.41	1.04	1.01	1.29	0.35	0.38	0.34	1.31
CaO _{total}					0.00	0.00	1.14	1.28	0.19	1.28	1.33	1.21	0.02
CO ₂						0.00	1.15	1.27	0.19	1.30	1.33	1.22	0.02
Na ₂ O							0.00	1.56	0.94	0.96	0.96	1.26	1.26
K ₂ O								0.00	1.33	1.12	1.00	0.89	1.19
MnO									0.00	1.30	1.36	1.34	0.23
TiO ₂										0.00	0.15	0.23	1.25
P ₂ O ₅											0.00	0.20	1.25
Cr ₂ O ₃												0.00	1.10
Lol													0.00

The graphic planes formed by PC1 (Factor 1) and PC2 (Factor 2) are well defined by the 82 and 38 samples from the clastics and volcanic major element concentrations, respectively (Table 5.3; Table 5.4; Fig. 5.3). Principal component analysis allows seeing other levels of representativeness compared to other exploratory tool, given by the [re]construction of the biplot. Oxides with major weight (load) on either factor axes are represented by the projection of the rays (lines that unite the common center of the 2D graph to each component; Table 5.3). The variability of each component or element is determined by the longitude of the rays, therefore, the longer the ray the greater the compositional variability. The results from the cluster analysis are similar to the grouping of highly correlated components on the PC analysis. The latter is interpreted from the small angle that separates the rays from one another (cosines of angles between rays near 1). Thus, the grouping systems in PCs from clastic and volcanic datasets can be associated with the number of groups from the clustering pattern of each datasets. This suggests that whenever a major element (components) group is far or with distinct ray length from another group, there must be a poor correlation between them. The distance between groups is a function of the differences in logcociente of an element or the entire group of elements. Other ray positions may be use for interpretation, i.e., an alignment between components suggest a linear relationship in the subcomposition (e.g., Fig. 5.3b).

Compositional arrays from this work may be assisted for interpretations when compared to the possible source rocks from the: (i) underlying crystalline basement units (Fig. 5.3c), (ii) basement boulders from regional vicinities (Fig. 5.3d), (iii) Paleozoic–Triassic plutons (Fig. 5.3e), and (iv) Jurassic volcanic rocks (Fig. 5.3f).

Table 5.4: Four main factors analysis results for the principal components analysis required for constructing the projection of the variables on a factor-plane (Fig. 5.3; Table 5.3; Appendix for Chapter 5). Tables a, b, and c, contain representative datasets for this work (LSPT– Lomas de San Paulo Tranquitas; CA– Cañón El Alamar; COI– Cañón El Olmo; CB– Cañón La Boca; CC– Cañón Caballeros; CHP– Cañón Peregrina; CN– Cañón Novillo); VH– Valle de Huizachal; Ab– Aramberri; Mi– Miquihuana; NG– Novillo Gneiss; GS– Granjeno Schist. Data on tables d)– (Lopez *et al.*, 2001), e)– (Lopez *et al.*, 2001), and f)– (Barboza-Gudiño *et al.* 2008, 2010; García-Obregón, 2007), represent compiled geochemical sets.

a) Clastics (LSPT,CA,COI,CB,CC,CHP,CN);n= 82

Mayor Element	Factor 1	Factor 2	Factor 3	Factor 4
SiO ₂	0.039824	-0.494968	0.124163	0.615498
Al ₂ O ₃	-0.652548	-0.563877	0.157577	-0.023728
Fe ₂ O ₃	-0.502109	-0.556078	-0.403554	-0.417387
MgO	-0.726915	-0.409880	-0.069063	-0.117727
CaO _{total}	-0.614302	0.758323	0.010969	0.047175
CaO*	-0.611117	0.753372	-0.006215	0.063485
CO ₂	-0.591449	0.736050	0.014466	0.103876
Na ₂ O	-0.204413	-0.017555	0.822949	-0.310389
K ₂ O	-0.464004	-0.207077	0.384358	0.431278
MnO	-0.740625	0.219654	-0.023591	-0.061031
TiO ₂	-0.395532	-0.657620	-0.166401	-0.119763
P ₂ O ₅	-0.727827	-0.372205	0.293823	-0.182465
Cr ₂ O ₃	-0.422842	-0.604289	-0.182911	0.423954
Lol	-0.758392	0.378897	-0.337994	0.152129

b) Volcanics (VH,Ab,M i);n= 38

Mayor Element	Factor 1	Factor 2	Factor 3	Factor 4
SiO ₂	0.235602	0.928029	0.017455	0.098068
Al ₂ O ₃	-0.142397	0.831511	0.213031	-0.154139
Fe ₂ O ₃	-0.584261	0.300459	0.504646	-0.460707
MgO	-0.633359	0.014024	0.628645	-0.293228
CaO _{total}	0.898632	-0.330633	0.213212	-0.179956
CaO*	0.878503	-0.389990	0.206742	-0.165245
CO ₂	0.878934	-0.386456	0.201458	-0.155416
Na ₂ O	-0.117949	0.018109	-0.660154	-0.575209
K ₂ O	0.032041	0.340843	0.352465	0.731244
MnO	-0.038065	-0.926615	-0.076107	0.065749
TiO ₂	-0.651516	-0.568933	0.362661	-0.146382
P ₂ O ₅	-0.533306	-0.807358	0.051307	0.147565
Cr ₂ O ₃	-0.458502	-0.846518	-0.019423	0.191900
Lol	0.883272	-0.192289	0.375442	-0.083691

c) Crystalline Basement units (NG,GS);n= 7

Mayor Element	Factor 1	Factor 2	Factor 3	Factor 4
SiO ₂	-0.915225	-0.291628	0.219229	0.159552
Al ₂ O ₃	0.302239	0.581460	-0.653514	-0.347410
Fe ₂ O ₃	0.933944	0.242475	-0.167589	-0.011127
MgO	0.829897	0.038500	0.434576	-0.345030
CaO _{total}	0.940098	0.032686	0.029208	0.057268
CaO*	0.942444	0.015324	0.029025	0.047970
CO ₂	-0.199368	0.860803	0.069773	0.400345
Na ₂ O	0.632161	-0.260450	-0.086141	0.698557
K ₂ O	-0.694318	-0.150288	-0.516728	-0.365309
MnO	0.836880	0.344510	0.151390	0.168769
TiO ₂	0.701356	-0.402056	-0.504150	0.076918
P ₂ O ₅	0.799333	-0.533634	-0.270510	0.004119
Cr ₂ O ₃	0.638236	-0.202560	0.457411	-0.566698
Lol	0.035949	0.979020	-0.000281	-0.097527

d) Basement Boulders (*compiled data);n= 12

Mayor Element	Factor 1	Factor 2	Factor 3	Factor 4
SiO ₂	0.930627	-0.142826	0.077315	0.215270
Al ₂ O ₃	-0.706879	-0.361420	-0.305942	-0.485829
MgO	0.049172	0.901855	-0.086507	-0.347466
CaO _{total}	-0.800164	-0.171027	0.547824	0.111312
CaO*	-0.801405	-0.165752	0.547569	0.116803
Na ₂ O	-0.243549	-0.896358	0.188455	-0.121312
K ₂ O	-0.595183	-0.616534	-0.336484	-0.000651
MnO	-0.716852	0.464521	-0.437588	0.224601
TiO ₂	-0.734245	0.642285	-0.093155	0.175012
P ₂ O ₅	-0.927639	0.094006	-0.221481	0.142986
Lol	-0.217631	0.597616	0.683263	-0.221550

e) Paleozoic Triassic Plutons (*compiled data);n= 13

Mayor Element	Factor 1	Factor 2	Factor 3	Factor 4
SiO ₂	0.925563	-0.035377	0.129643	-0.030461
Al ₂ O ₃	-0.972432	-0.099739	0.075907	0.087071
MgO	-0.937603	0.126421	0.095906	-0.072911
CaO _{total}	-0.942153	0.303528	-0.042792	0.025271
CaO*	-0.941561	0.306688	-0.052302	0.020910
Na ₂ O	0.369421	0.021801	0.893697	0.237080
K ₂ O	0.642577	-0.588601	-0.410349	0.239417
MnO	-0.953127	-0.149278	0.058902	-0.105466
TiO ₂	-0.894033	-0.336748	-0.099789	0.227336
P ₂ O ₅	-0.897766	-0.295136	0.049555	0.172596
Lol	-0.348109	-0.835609	0.289776	-0.299476

f) Volcanics (*compiled data);n= 32

Mayor Element	Factor 1	Factor 2	Factor 3	Factor 4
SiO ₂	0.923988	0.282374	-0.182224	0.061729
Al ₂ O ₃	-0.274924	-0.711688	0.460797	-0.360562
Fe ₂ O ₃	-0.420584	-0.679424	-0.150495	0.241273
MgO	-0.895326	0.160476	0.072242	-0.163954
CaO _{total}	-0.961216	0.221696	0.104129	-0.008377
CaO*	-0.961264	0.219936	0.105146	-0.011158
CO ₂	-0.951817	0.268320	0.087900	0.043169
Na ₂ O	-0.259555	-0.046371	-0.429794	-0.851562
K ₂ O	0.497028	-0.441575	0.663106	-0.109027
MnO	-0.920411	0.266230	0.036448	0.115518
TiO ₂	-0.610317	-0.643473	-0.351199	0.015845
P ₂ O ₅	-0.408724	-0.714292	-0.287888	0.304463
Lol	-0.935354	0.161364	0.169274	0.112869

5.3.2. Trace Elements and Rare Earth Element (REE) data

Some effects of several geological agents at sedimentary processes (e.g., weathering, transport) have been partially understood by interpreting the compositional data from resistant elements contained in terrigenous clastic samples (Lentz, 2003). The subatomic design of each element conditions its geochemical resistance or immobile characteristic. Rock erosion tends to enrich in elements the sediment generation throughout the sedimentary cycle, which can be translated into quantification and interpretations (Bhatia and Crook, 1986;

Roser and Nathan, 1997; Toulkerides *et al.*, 1999). This work uses ppm units for the analyzed trace element concentrations (Table 5.1: Appendix for Chapter 5).

5.3.2.1 Large ion lithophile elements (LILE): Rb, Cs, Ba, Sr

The clastics dataset (C) has a Rb concentration of $\sim 51.8 \pm 31.9$ ppm compared to samples from the volcanic set (V) with $\sim 69.5 \pm 26.4$ ppm (Table 5.1). The Cs concentrations oscillate slightly between both sample sets, with C: $\sim 3.3 \pm 1.9$ ppm and V: $\sim 3.4 \pm 2.3$ ppm. Barium (Ba) has a geochemical value of $\sim 454 \pm 439$ for the clastics set, and $\sim 671 \pm 650$ for volcanic data. Meanwhile the quantified residence of Sr is of $\sim 55.4 \pm 68$ for the clastics dataset, but is higher in concentration for volcanic samples ($\sim 93 \pm 77$).

Samples for the clastics dataset are more enriched by LILE than the volcanic set of samples (Table 5.5). The K_2O concentrations in the clastics set have high positive correlations with Rb ($r=0.76$), Cs ($r=0.60$), a low positive correlation with Ba ($r=0.13$), and a negative value for Sr ($r=-0.08$). The volcanic sampleset show similar element correlations for K_2O with high positive values on Rb ($r=0.78$), Cs ($r=0.57$), low positive correlation with Ba ($r=0.05$), and a negative cipher for Sr ($r=-0.44$). Positive correlations for K_2O can be associated with trace elements controlled by argillaceous minerals rich in potassium (e.g., illite), and feldspars

(McLennan *et al.*, 1983; Feng and Kerrich, 1990; Marfil *et al.*, 1998; Price and Velbel, 2000; Roddaz *et al.*, 2006; Kasanzu *et al.*, 2008; Li and Yang, 2010; Verdecchia and Baldo, 2010; Zaghloul *et al.*, 2010).

However, the negative Sr correlations must not be discarded from a genetic explanation related to carbonate cement. To valid the latter, further information shall be used to interpret the compositional participation of Sr. On either datasets Sr presents positive correlations with CaO_{tot} ($r=0.29$; 0.48), CaO^* ($r=0.29$; 0.48), CO_2 ($r=0.20$; 0.48), and LOI ($r=0.19$, 0.44), evidencing that its incorporation or depletion is possibly controlled by the presence of carbonate cement. Nevertheless, on Chapter 3 no considerable carbonate

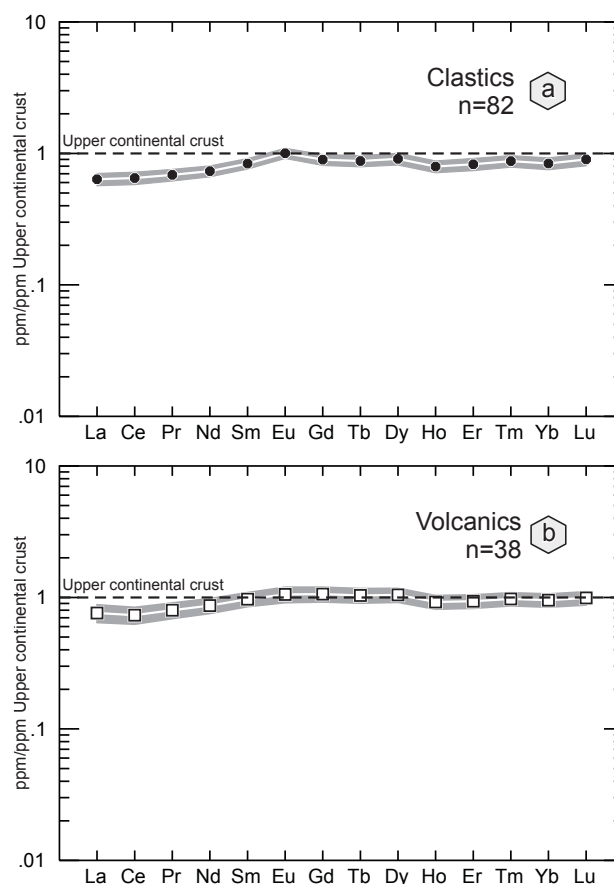


Fig. 5.4: Spider diagram with the trace element concentrations normalized to Upper Continental Crust (UCC), after Taylor and McLennan (1981); including mean values and confidence limits at 99.5%. a) Clastics, n=82 (LSPT– Lomas de San Paulo Tranquitas; CA– Cañón El Alamar; COI– Cañón El Olmo; CB– Cañón La Boca; CC– Cañón Caballeros; CHP– Cañón Peregrina; CN– Cañón Novillo). b) Volcanics, n= 38 (VH– Valle de Huizachal; Ab– Aramberri; Mi– Miquihuana).

cement was petrographical characterized from the grained-size analyzed samples. In addition, some coarse grained samples excluded petrographically from La Boca and La Joya formations present carbonate cement, this might serve as indicators for the latter interpretation. Unless Sr is derived from the silicate fraction (CaO*) the latter may be valid.

5.3.2.2 High field strength elements (HFSE): Y, Zr, Nb, Hf, Th, U

High field strength elements (Y, Zr, Nb, Hf, Th, U) are conditioned by 1) source rock, 2) grade of partial melting, and 3) magma evolution. The evolution of HFSE is overprinted by the petrogenesis of felsic rocks (Feng and Kerrich, 1990; Wilson, 2007). Their design conditions the chemical immobility and serves to identify source rocks composition while studying the sedimentary geology of siliciclastic rocks (Basu *et al.*, 1982; Taylor and McLennan, 1985; Floyd *et al.*, 1989; Rollinson, 1993; Gill *et al.*, 1994; Bock *et al.*, 1998, 2004; Ochoa *et al.*, 2007).

The HFSE concentrations on clastics or volcanic sample sets present faintly variations (Table 5.5). The mean element concentration of HFSE remains under the reported values for Upper Continental Crust (UCC; *cf.*, Taylor and McLennan, 1981), except for the volcanic samples (Fig. 5.4). These ambiguities of the values can be seen on the two datasets by the SiO₂ correlations, with negative values on the clastics set ($r \leq -0.1$) and positive integers for the volcanic data ($r \geq 0.1$). Al₂O₃ presents another noticeable positive correlation is with the entire HFSE, Y ($r=0.55$; 0.48), Zr ($r=0.13$; 0.18), Nb ($r=0.48$; 0.55), Hf ($r=0.15$; 0.2), Th ($r=0.60$; 0.63), U ($r=0.37$; 0.55). The major positive correlations on Al₂O₃ are consistent to the presence of argillaceous minerals in the matrix, or even derived from albitization. Elements that remain unrelated to mica or argillaceous minerals, and albitization are in correspondence to changes in source rock or autigenic minerals considered as accessory.

Other correlations of interest are those found on TiO₂ and Y ($r=0.60$; 0.78), Zr ($r=0.83$; 0.79), Nb ($r=0.80$; 0.9), Hf ($r=0.84$; 0.8), Th ($r=0.71$; 0.62), U ($r=0.48$; 0.73). The correlations suggest that elements are mainly controlled by the abundance of heavy mineral assemblages (zircon, rutile, clinopyroxene, monazite, and xenotime; see Chapter 4).

The multi-element concentrations from the analyzed clastic and volcanic datasets were normalized to the Bulk Earth composition proposed by Hickey *et al.* (1986; Fig. 5.5). Both sets show similar patterns with enrichment from large ion lithophile elements (Rb, Cs, Ba, Sr), and depletion of high field strength elements (Y, Zr, Nb, Hf, Th, U) and REE (La, Ce, Sm Yb). The two sample sets have negative anomalies on K, Nb, Sr, and Ti.

Table 5.5: Correlation matrices for major elements vs. trace elements and REE. Values are with the 99.5% of confidence (highlighted). a) Clastics, n=82 (LSPT– Lomas de San Paulo Tranquitas; CA– Cañón El Alamar; COI– Cañón El Olmo; CB– Cañón La Boca; CC– Cañón Caballeros; CHP– Cañón Peregrina; CN– Cañón Novillo). b) Volcanics, n= 38 (VH– Valle de Huizachal; Ab– Aramberri; Mi– Miquihuana).

a) Clastics (LSPT, CA, COI, CB, CC, CHP, CN); n= 82

	SiO ₂	Al ₂ O ₃	Fe ₂ O ₃	MgO	CaO _{total}	CaO*	CO ₂	Na ₂ O	K ₂ O	MnO	TiO ₂	P ₂ O ₅	Lol
Sc	-0.70	0.80	0.62	0.70	0.01	0.02	-0.08	0.14	0.15	0.23	0.51	0.51	0.16
V	-0.14	0.19	0.15	0.26	-0.09	-0.09	-0.10	0.17	-0.10	0.21	0.28	0.21	-0.04
Cr	-0.20	0.20	0.45	-0.06	-0.11	-0.11	-0.15	0.01	-0.16	-0.09	0.52	0.23	0.07
Co	-0.25	0.16	0.46	0.37	-0.03	-0.03	-0.05	0.00	-0.14	0.40	0.24	0.24	0.05
Ni	-0.18	0.16	0.50	0.27	-0.24	-0.24	-0.18	-0.30	0.06	0.06	0.29	0.19	0.04
Zn	-0.27	0.28	0.68	0.40	-0.26	-0.25	-0.26	-0.14	-0.06	0.15	0.17	0.13	-0.01
Ga	-0.73	0.95	0.60	0.53	-0.12	-0.12	-0.09	0.24	0.41	0.22	0.32	0.60	0.14
Rb	-0.42	0.65	0.07	0.16	-0.06	-0.06	0.00	-0.04	0.76	0.06	0.03	0.46	0.10
Sr	-0.35	0.24	0.13	0.20	0.29	0.29	0.20	0.52	-0.08	0.24	-0.04	0.22	0.19
Y	-0.45	0.55	0.37	0.24	-0.09	-0.09	-0.03	0.21	0.15	0.25	0.61	0.60	0.12
Zr	-0.11	0.13	0.17	0.11	-0.15	-0.15	-0.14	0.10	-0.03	0.02	0.83	0.50	-0.09
Nb	-0.29	0.48	0.35	0.23	-0.28	-0.29	-0.25	0.03	0.16	-0.01	0.80	0.55	-0.09
Ba	-0.14	0.10	0.06	-0.07	0.10	0.10	0.14	-0.07	0.13	0.09	-0.06	0.15	0.14
Hf	-0.11	0.15	0.18	0.11	-0.16	-0.16	-0.15	0.11	-0.03	0.01	0.84	0.51	-0.09
Ta	-0.35	0.55	0.34	0.23	-0.25	-0.25	-0.20	0.07	0.27	0.00	0.72	0.56	-0.05
Pb	0.05	-0.07	0.07	0.07	-0.08	-0.08	-0.07	-0.03	-0.10	0.00	0.18	-0.03	-0.06
Th	-0.41	0.60	0.39	0.27	-0.21	-0.21	-0.17	0.15	0.25	0.09	0.71	0.66	-0.02
U	-0.26	0.37	0.25	0.20	-0.17	-0.18	-0.14	0.18	0.12	0.22	0.48	0.45	-0.03
Cs	-0.44	0.59	0.11	0.13	0.03	0.03	0.11	-0.05	0.60	0.06	0.03	0.34	0.24
La	-0.36	0.58	0.40	0.19	-0.24	-0.25	-0.17	0.14	0.19	0.17	0.45	0.49	-0.02
Ce	-0.34	0.56	0.40	0.19	-0.26	-0.26	-0.18	0.13	0.14	0.19	0.50	0.49	-0.05
Pr	-0.37	0.57	0.40	0.20	-0.22	-0.22	-0.13	0.14	0.18	0.23	0.50	0.53	0.00
Nd	-0.39	0.58	0.37	0.22	-0.20	-0.21	-0.11	0.18	0.21	0.25	0.50	0.58	0.00
Sm	-0.45	0.57	0.40	0.22	-0.11	-0.12	-0.03	0.21	0.20	0.33	0.58	0.68	0.09
Eu	-0.53	0.58	0.42	0.22	0.01	0.00	0.08	0.30	0.17	0.39	0.57	0.72	0.20
Gd	-0.44	0.54	0.37	0.24	-0.10	-0.10	-0.02	0.19	0.18	0.33	0.64	0.68	0.10
Tb	-0.45	0.56	0.38	0.24	-0.09	-0.10	-0.02	0.20	0.18	0.31	0.61	0.63	0.12
Dy	-0.45	0.56	0.39	0.26	-0.11	-0.11	-0.05	0.20	0.17	0.26	0.65	0.64	0.11
Ho	-0.45	0.56	0.39	0.26	-0.11	-0.11	-0.06	0.18	0.16	0.24	0.66	0.61	0.10
Er	-0.46	0.57	0.42	0.26	-0.12	-0.12	-0.08	0.19	0.15	0.21	0.68	0.62	0.10
Tm	-0.47	0.59	0.41	0.26	-0.12	-0.13	-0.08	0.19	0.18	0.2	0.69	0.64	0.09
Yb	-0.46	0.58	0.41	0.28	-0.12	-0.12	-0.08	0.16	0.19	0.19	0.71	0.63	0.08
Lu	-0.45	0.57	0.39	0.26	-0.12	-0.12	-0.07	0.18	0.17	0.18	0.72	0.63	0.07

b) Volcanics (VH, Ab, M); n= 38

	SiO ₂	Al ₂ O ₃	Fe ₂ O ₃	MgO	CaO _{total}	CaO*	CO ₂	Na ₂ O	K ₂ O	MnO	TiO ₂	P ₂ O ₅	Lol
Sc	0.06	0.58	0.86	0.83	-0.41	-0.41	-0.42	0.11	-0.11	-0.33	0.88	0.8	-0.36
V	0.02	0.43	0.56	0.73	-0.28	-0.28	-0.29	0	-0.13	-0.26	0.74	0.77	-0.21
Cr	-0.08	0.42	0.64	0.66	-0.21	-0.21	-0.22	-0.26	0.11	-0.34	0.77	0.8	-0.1
Co	-0.1	0.03	0.33	0.44	0.01	0.01	0	-0.02	-0.27	0.04	0.27	0.28	0.04
Ni	0	0.44	0.65	0.77	-0.3	-0.3	-0.3	-0.16	0.09	-0.33	0.6	0.62	-0.2
Zn	0.22	0.26	0.44	0.74	-0.37	-0.37	-0.37	-0.09	-0.11	-0.22	0.24	0.25	-0.29
Ga	0.17	0.8	0.81	0.84	-0.58	-0.58	-0.59	0.02	0.23	-0.53	0.62	0.68	-0.49
Rb	0.14	0.37	0.12	0.19	-0.32	-0.32	-0.31	-0.34	0.78	-0.32	-0.17	-0.08	-0.22
Sr	-0.48	-0.19	-0.13	-0.19	0.48	0.48	0.48	0.3	-0.44	0.42	-0.12	-0.08	0.44
Y	-0.12	0.48	0.74	0.62	-0.19	-0.19	-0.2	0.31	-0.26	-0.03	0.78	0.61	-0.21
Zr	0.16	0.18	0.43	0.24	-0.25	-0.25	-0.27	0.07	-0.07	-0.3	0.79	0.6	-0.29
Nb	0.02	0.55	0.75	0.64	-0.33	-0.33	-0.34	0.19	-0.12	-0.34	0.9	0.78	-0.32
Ba	-0.14	-0.21	-0.18	-0.11	0.19	0.19	0.2	-0.18	0.05	0.16	-0.22	-0.12	0.23
Hf	0.17	0.2	0.44	0.26	-0.26	-0.26	-0.28	0.04	-0.05	-0.32	0.8	0.61	-0.3
Ta	-0.03	0.58	0.74	0.6	-0.3	-0.3	-0.32	0.19	-0.05	-0.32	0.83	0.72	-0.29
Pb	-0.21	-0.14	0.13	0.12	0.23	0.23	0.22	0.12	-0.5	0.14	0.08	0.05	0.2
Th	0.13	0.63	0.54	0.35	-0.42	-0.42	-0.43	0.39	0.09	-0.37	0.62	0.51	-0.45
U	0.14	0.55	0.67	0.6	-0.42	-0.42	-0.43	0.24	-0.07	-0.41	0.73	0.62	-0.43
Cs	-0.02	0.45	0.39	0.52	-0.25	-0.26	-0.25	-0.34	0.57	-0.32	0.11	0.19	-0.14
La	0	0.5	0.52	0.5	-0.26	-0.26	-0.27	0.23	-0.11	-0.15	0.68	0.62	-0.26
Ce	-0.04	0.46	0.48	0.46	-0.21	-0.21	-0.23	0.17	-0.05	-0.14	0.69	0.61	-0.21
Pr	-0.07	0.49	0.59	0.53	-0.22	-0.22	-0.23	0.22	-0.12	-0.13	0.75	0.65	-0.22
Nd	-0.07	0.5	0.65	0.56	-0.22	-0.22	-0.23	0.23	-0.14	-0.12	0.77	0.66	-0.22
Sm	-0.1	0.46	0.71	0.57	-0.19	-0.19	-0.2	0.24	-0.17	-0.08	0.79	0.63	-0.2
Eu	-0.18	0.32	0.69	0.55	-0.08	-0.08	-0.09	0.12	-0.16	0.01	0.77	0.58	-0.09
Gd	-0.11	0.42	0.72	0.58	-0.17	-0.17	-0.19	0.26	-0.23	-0.03	0.78	0.6	-0.19
Tb	-0.11	0.42	0.74	0.6	-0.17	-0.17	-0.19	0.25	-0.24	-0.04	0.77	0.57	-0.19
Dy	-0.09	0.44	0.76	0.62	-0.2	-0.2	-0.21	0.25	-0.24	-0.06	0.78	0.59	-0.22
Ho	-0.09	0.49	0.77	0.65	-0.22	-0.22	-0.24	0.26	-0.23	-0.1	0.8	0.63	-0.23
Er	-0.06	0.51	0.75	0.61	-0.24	-0.24	-0.26	0.33	-0.25	-0.13	0.82	0.64	-0.26
Tm	-0.06	0.52	0.75	0.62	-0.25	-0.24	-0.26	0.3	-0.22	-0.15	0.83	0.66	-0.26
Yb	-0.01	0.53	0.72	0.58	-0.28	-0.28	-0.3	0.34	-0.23	-0.18	0.82	0.67	-0.31
Lu	-0.01	0.54	0.72	0.57	-0.29	-0.29	-0.31	0.34	-0.22	-0.21	0.84	0.69	-0.31

5.3.2.3 Transition Trace Elements (TTE): Co, Ni, V, Sc

This section briefly describes the TTE concentrations from the analyzed clastics and volcanics datasets. Both sets tend to portrait similar values to the UCC. This similarity is consistent with positive correlations on Al_2O_3 , Fe_2O_3 , MgO , TiO_2 , and P_2O_5 , suggesting that Co, Ni, V, and Sc are derived mainly from phyllosilicates and other related minerals to volcanic and igneous processes (see Chapter 3, Chapter 4, and Appendix for Chapter 5).

5.3.2.4 Rare Earth Elements (REE)

The main geochemical effects are related to the elements capacity for solubility. Elements with short residence are virtually transferred quantitatively to the clastic sequences. The limited value of insoluble elements to estimate the composition of Upper Continental Crust resides on their capacity to disperse easily within sedimentary environments (e.g., zircon). This is why trace and REE elements in post-Archean sedimentary rocks are strongly different from igneous source rocks, which testifies the efficiency of compositional mixing or homogenization during transport, sedimentation, and diagenesis (Taylor and McLennan, 1985, 1995; 2009; McLennan *et al.*, 1993; Bock *et al.*, 1998, 2004; González-Álvarez *et al.*, 2006).

The mean compositional pattern of REE is express as Upper Continental Crust (UCC). The crucial group of rare-earth elements is strongly enriched by heavy mineral assemblages (e.g., zircon, garnet, monazite). McLennan (1989) McLennan *et al.* (1990), Totten *et al.* (2000), Jenchen (2001), and Lambeck *et al.* (2008) have considered the influence of heavy mineral over whole-rock composition of sedimentary rocks (e.g., HREE). In contrast, quartz-rich sediments tend to show low REE ratios, due to their dilute concentration of REE with respect to other minerals.

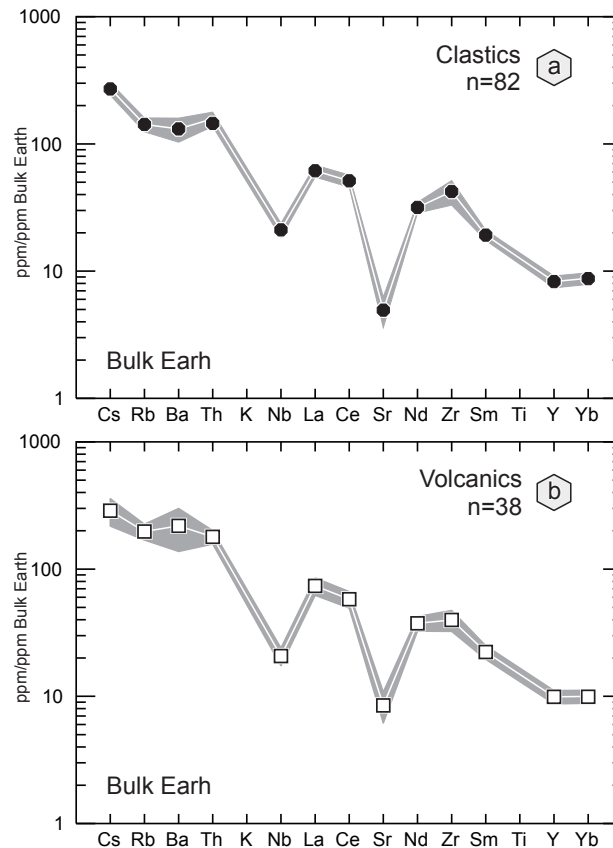


Fig. 5.5: Trace element concentrations normalized to the Bulk Earth composition after Hickey *et al.* (1986), including mean values and confidence limits at 99.5%. a) Clastics, n=82 (LSPT–Lomas de San Paulo Tranquitas; CA– Cañón El Alamar; CO– Cañón El Olmo; CB– Cañón La Boca; CC– Cañón Caballeros; CHP– Cañón Peregrina; CN– Cañón Novillo). b) Volcanics, n= 38 (VH– Valle de Huizachal; Ab– Aramberri; Mi– Miquihuana).

Rare Earth Elements are subdivided into Light Rare Earth Elements (LREE: La–Sm), and Heavy Rare Earth Elements (HREE: Gd–Lu). The REE groups are separated one another by Europium and its logical calculation of Eu/Eu^* , is founded the by ionic substitution of elements (Ca^{2+} to Eu^{+2}) when replacing plagioclase (McLennan, 1989). During this reaction, Eu^{+2} substitutes Ca^{2+} in the site where Sr^{2+} existed. This processes is the reason for the positive anomaly of Eu ($\text{Eu}/\text{Eu}^* > 1$) in plagioclase.

The mean compositional signature of REE for the clastics and volcanics datasets is shown in Fig. 5.6. Numerical calculations

were undertaken by normalizing to chondrite (McLennan, 1989). Both datasets present similar compositional patterns to the UCC, with a medium impoverishment on HREE, MREE and LREE. The REE impoverishment is related to a general mineral dilution caused by the predominance of quartz and possibly by the occurrence of clay minerals. However, the volcanic set highlights a less depleted pattern than the clastics sample sets. Both datasets also present slightly negative anomalies of Eu (Eu/Eu^*), $r=6.07$ for clastics and $r=7.5$ for volcanics. Eu anomalies may be used to step forward into provenance analysis by combining the element concentrations into element relations like Th/Sc and Cr/Ni (Condie, 1967; Condie *et al.*, 1970; 1986; Hiscott, 1984; Critelli *et al.*, 2008). Nevertheless, this work excluded the element relations for provenance interpretations.

5.3.2.5 Classification

Sedimentary rocks classification can be assisted not only by petrographical means (McBride, 1963; see Chapter 3), but also by geochemical analysis. This work adopted the whole-rock categorization for sandstones after Pettijohn *et al.* (1972), where chemical composition is a function of mineral constituents with SiO_2 (quartz) and Al_2O_3 (matrix) versus Na_2O (plagioclase) and K_2O (feldspars). According to this schema, sample sets from the clastics fall within the lithic arenites field with variations to arkose, subarkose, and greywacke; while the volcanics set of samples fall over the greywacke and arkose area (Fig. 5.7).

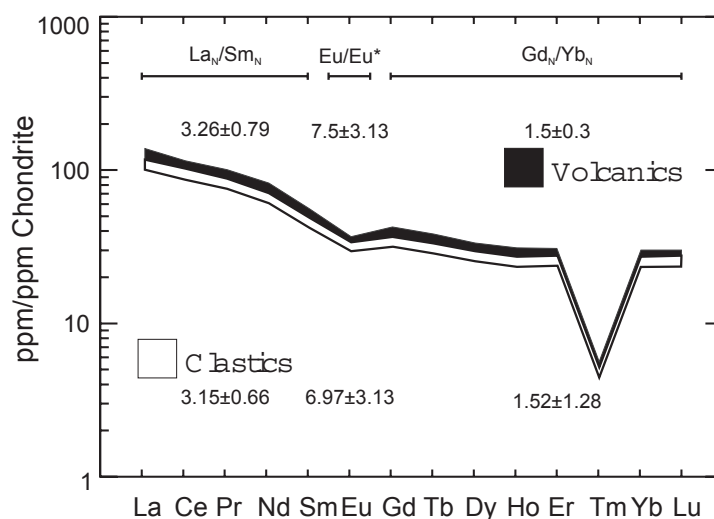


Fig. 5.6: Chondrite-normalized REE patterns. Upper pattern and calculations corresponds to Volcanics, $n=38$ (VH– Valle de Huizachal; Ab– Aramberri; Mi– Miquihuana). Lower pattern and mean composition is for Clastics, $n=82$ (LSPT– Lomas de San Paulo Tranquitas; CA– Cañón El Alamar; COL– Cañón El Olmo; CB– Cañón La Boca; CC– Cañón Caballeros; CHP– Cañón Peregrina; CN– Cañón Novillo). HREE– La_N/Sm_N ; LREE– Gd_N/Yb_N .

5.3.3. Source area composition

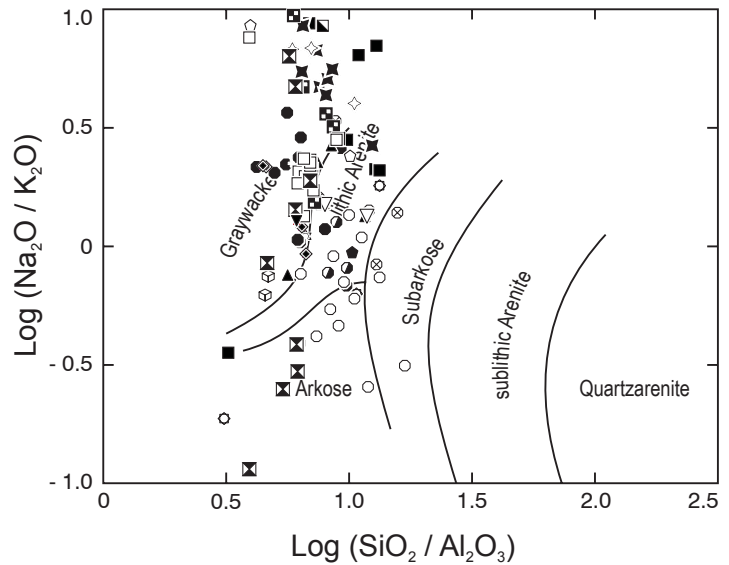
5.3.3.1 Major elements systematics

The geochemical classification for rock-types by using major element concentrations was carried out according to Nathan (1976) and Jenchen (2001). The analyzed samples from the clastics and volcanics datasets share common ratios of SiO_2 and Al_2O_3 (Table 5.1), lying on the classification fields for psammite, pelite, and rest (Fig. 5.8). Accordingly, psammites are sediments with a high SiO_2 and a low Al_2O_3 content ($\text{SiO}_2 > 68\%$ and $\text{Al}_2\text{O}_3 < 14\%$) and similar in content to the arenites of Pettijohn *et al.* (1987). Pelites are fine-grained sediments with high clay mineral content and low quartz concentrations ($\text{SiO}_2 < 68\%$ and $\text{Al}_2\text{O}_3 > 14\%$). The aluminum fraction is mostly bound to phyllosilicates.

Rocks with a CaO_{tot} content significantly greater than in the total random sample ($\text{CaO} > 5\%$) are classified as “Ca-enriched rocks” (e.g., carbonate mudstones and marls). The “rest” are sediments that cannot be classified according to the latter three categories ($\text{SiO}_2 > 68\%$ and $\text{Al}_2\text{O}_3 > 14\%$ or: $\text{SiO}_2 < 68\%$ and $\text{Al}_2\text{O}_3 < 14\%$). They include poorly sorted sandstones (“greywacke”) and iron-rich sediments.

During sediment transport minerals begin to separate according to size, density, and shape. For the major mineralogical components [major elements] the processes of weathering and sorting may be difficult to differentiate, because weathering clastics processes continue during all the sediment transport processes (Johnson, 1993). With the increase of textural maturity in sandstones the concentrations of quartz and feldspar typically increase independently to clay-sized material [argillaceous minerals], resulting in higher ratios of $\text{SiO}_2/\text{Al}_2\text{O}_3$ and lower content of trace elements.

During weathering and transport plagioclase is less stable than K-feldspar leading to an increase in $\text{K}_2\text{O}/\text{Na}_2\text{O}$ ratios (Pettijohn, 1963). In the biplot for the geochemical systems of $\text{K}_2\text{O}/\text{Na}_2\text{O}$ the samples from the clastics and volcanic sets can be readily seen as divergence from weathering trends into distinct sand populations of arkose and greywacke (Fig. 5.9; Table 5.1).



Lomas de San Paulo Tranquitas- SW de Cerro de la Nieve: Alamar lower member ●; Alamar Fm upper member ◐; La Joya Fm ○.
 Cerro de la Nieve: Alamar Fm upper member ◑; La Joya Fm. ◒
 Mina la Huiche: El Alamar Fm lower member ⊗. Cañón El Alamar - El Alamar ? Fm ○. Aramberri - La Boca ? Fm ◑ Cañón El Olmo - La Boca ? Fm ◒; La Joya Fm ◓. Cañón La Boca- El Alamar Fm lower member ◔; El Alamar Fm upper member ◕; La Boca ? Fm ◖; La Joya Fm ◗. Cañón Caballeros- La Boca ? Fm ◘; La Joya Fm ◙. Cañón Peregrina- La Boca ? Fm ◚; La Joya Fm ◛.
 Cañón Novillo- La Joya Fm ◜ Valle de Huizachal- La Boca Fm lower member ◝; La Boca upper member ◞; La Joya Fm ◟.
 Miquihuana- La Boca ? Fm ◠; La Joya Fm ◡.

Fig. 5.7: $\text{SiO}_2/\text{Al}_2\text{O}_3$ vs. $\text{Na}_2\text{O}/\text{K}_2\text{O}$ ratios of sandstones from clastics and volcanic datasets corresponding to the red bed in northeastern Mexico (after Pettijohn *et al.*, 1972).

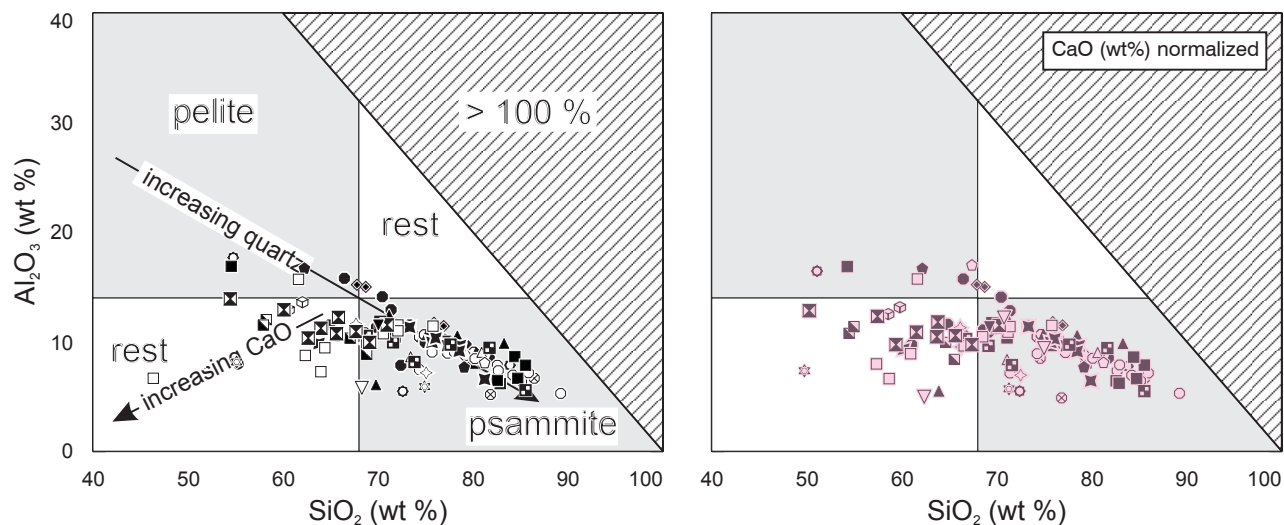


Fig. 5.8: (Left) Geochemical classification for red beds in northeastern Mexico, classification after Nathan (1976) and Jenchen & Rosenfeld (2007). Significant negative correlation of Al_2O_3 and SiO_2 . (Right) Recalculated values normalized to CaO_{tot} (wt %), notice a slight slipping of samples toward the increase of CaO_{tot} . Key for symbols is found at Fig. 5.7.

To avoid potential statistical problems associated with natural sedimentary processes, data requires a statistically relevant total random sample and partial random samples with identical features, to reflect a reliable representation for compositional maturity and grain size of the sandstones. Most changes that bring about geochemical partitioning also result in removal of unstable grains in the clastic sediments by various geological effects. Hence, with the increase of compositional maturity there is a greater chance that the whole-rock geochemistry becomes a statistically complex classification criterion with less representativeness of source-area composition, but a more reflective scope for weathering transport, and burial histories.

Geochemical methods use major element concentrations usually based on the alkali ratio and the Al concentration to determine the plate tectonic setting for a sedimentary provenance purpose (Roser and Korsch, 1986). The biplot using SiO_2 vs. the $\text{K}_2\text{O}/\text{Na}_2\text{O}$ ratio produce a reliable and reproducible results especially when samples are normalized to CaO_{tot} . Most of the analyzed samples can be assigned to passive continental margins, i.e. to stable provenance areas (Fig. 5.10a). Nevertheless, to avoid any sample miss positioning by the carbonate concentrations, samples were normalized to CaO_{tot} (Fig. 5.10b; Table 5.1). This calculation enables to redistribute the datasets within the *simplex* for more

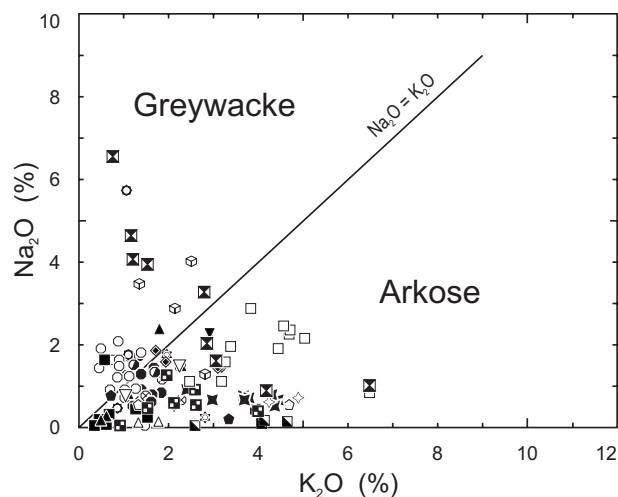


Fig. 5.9: $\text{K}_2\text{O}/\text{Na}_2\text{O}$ ratios (after Pettijohn, 1963) for Clastics, $n=82$ (LSPT– Lomas de San Paulo Tranquitas; CA– Cañón El Alamar; COL– Cañón El Olmo; CB– Cañón La Boca; CC– Cañón Caballeros; CHP– Cañón Peregrina; CN– Cañón Novillo); and Volcanics, $n=38$ (VH– Valle de Huizachal; Ab– Aramberri; Mi– Miquihuana). Key for symbols can be found at Fig. 5.7.

reliable explanations. Samples tend to diminish their SiO_2 after normalizing to CaO_{tot} , leaving more samples within the active continental margin and arc fields. This agrees with the results of the modal analysis and provenance interpretations (see Chapter 3).

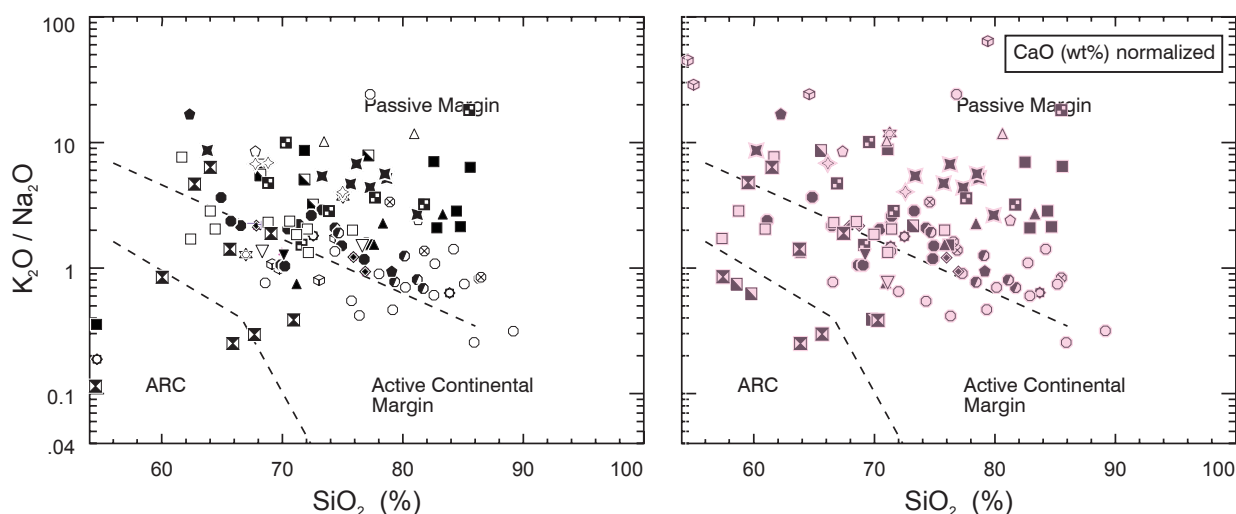


Fig. 5.10: (left) SiO_2 vs. $\text{K}_2\text{O}/\text{Na}_2\text{O}$ ratio (Roser and Korsch, 1986) of Clastics, $n=82$ (LSPT– Lomas de San Paulo Tranquitas; CA– Cañón El Alamar; COL– Cañón El Olmo; CB– Cañón La Boca; CC– Cañón Caballeros; CHP– Cañón Peregrina; CN– Cañón Novillo); and Volcanics, $n= 38$ (VH– Valle de Huizachal; Ab– Aramberri; Mi– Miquihuana). (right) Recalculated values normalized to CaO_{tot} (wt %). Key for symbols can be found at Fig. 5.7.

5.3.3.2 Trace Elements systematics

Besides other sedimentary factors, sedimentary sorting also results in an enrichment of heavy minerals (e.g., zircon, tourmaline, monazite) in sands and siltstones (Pettijohn *et al.*, 1972). Trace element ratios or heavy mineral assemblages (HMA) tend to be less affected by sedimentary transport processes than major mineral concentrations (Morton and Johnson, 1993). Repeated reworking (recycling) of sediments enriches sands in heavy minerals and their associated trace elements signature (McLennan *et al.*, 1993; McLennan, 2001).

The geochemical interpretations for sorting, maturity, and grain size in the sandstones may be complemented by the early calculations on Chapter 4, to explain how with minor changes in heavy-mineral content in immature sandstones significant effect on the entire element abundance.

The distribution of trace elements involves competing processes by leaching cations from the original parental minerals, clay mineral alterations, and the interactions between exchange/adsorption of clay minerals at depth. The lithological characteristics for source rocks (acidic vs. basic) were obtained by using a hybrid biplot formed by major and trace element ratios ($\text{SiO}_2/\text{K}_2\text{O}$ vs. Ti/Nb ; Ocampo-Díaz and Jenchen, *submitted*), the Ti/Nb quotient (Jenchen and Rosenfeld, 1998), and other compositional quotients (McLennan *et al.*, 1993).

The clastics sample sets present a mean composition from $\text{SiO}_2/\text{K}_2\text{O}$ of ~ 43 and ~ 520 for Ti/Nb , while the volcanic dataset has $\text{SiO}_2/\text{K}_2\text{O} \sim 19$ and $\text{Ti}/\text{Nb} \sim 446$ (Fig. 5.11).

The volcanic sample sets remain closer to the mixed zone or (Ti/Nb: 300–400), consistent with petrographic parameters for a differentiated sources. The clastics dataset is richer in SiO₂ and Ti, representing more mature sandstones richer in matrix and rutile content (see Chapter 3 and Chapter 4).

The Ti/Nb quotient was used as an indicator for sediment provenance (Zeibig 1991; Jenchen 2001). In ultrastable titanium minerals (ZTR; especially rutile), Nb substitutes Ti. Rutile can survive longer transport distances whereby the original Ti/Nb ratio is preserved. Hence, the Ti/Nb ratio is a direct indicator of the source rock. A low Ti/Nb ratio indicates an acidic provenance area (<300), while a high quotient points to a basic source (>400). Reliable indications of the source of a sediment result from comparison of the Ti/Nb ratio with reference quotients (Jenchen, 2001).

The present calculations revealed intermediate as well as metamorphic lithologies for source rocks (Fig. 5.12). The samples from the clastics datasets show good agreement with intermediate to basic sources, but also indicate phyllite as a source rock (Ti/Nb ~301; Jenchen and Rosenfeld, 2002). Some samples may present a variable [confidence region] Ti /Nb ratio that reflects the main components from the available rock sources or principal components (see Chapter 3). This differences in composition correspond to the strongly tectonized state of the related source-massifs and the great transport variability conditioned by the sedimentary environment. The volcanic localities show more differentiated Ti/Nb ratios indicating either different provenance areas (igneous and metamorphic) or compositional trends toward UCC composition. This includes a more complicated tectonic history of the region with possibly juxtaposed tectonic environments.

Reworking and transport of debris is considered as an additional effect over geochemical composition to determine the source areas for sediments. If physical weathering and transport degrade a source rock into a clay-sized deposit, it should essentially preserve the geochemical composition of the original rock (Nesbitt and Young, 1982; 1996).

The Th/Sc and Zr/Sc quotients provide information on the composition and tectonic state of source terranes and the reworking of the debris (McLennan *et al.*, 1993). All the sedimentary rocks considered in this work have Zr/Sc and Th/Sc ratios similar to or higher than UCC (Fig. 5.13; McLennan, 2001; Taylor and McLennan, 1985).

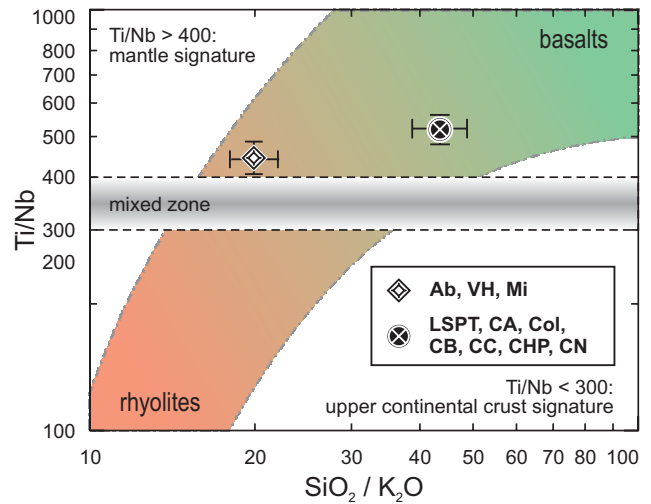


Fig. 5.11: (log)SiO₂/K₂O vs. (linear)Ti/Nb ratios for the mean values of datasets: a) Clastics, n=82 (LSPT– Lomas de San Paulo Tranquitas; CA– Cañón El Alamar; COI– Cañón El Olmo; CB– Cañón La Boca; CC– Cañón Caballeros; CHP– Cañón Peregrina; CN– Cañón Novillo), and b) Volcanics, n= 38 (VH– Valle de Huizachal; Ab– Aramberri; Mi– Miquihuana). Confidence range plots are at 99.5%. Plot after Ocampo-Díaz and Jenchen (*submitted*).

Within the diagrams the pair of datasets present different compositional clouds that tend from instable to stable (Fig. 5.13). The clastics set shows a more heterogeneous and disperse group, which signifies that the sedimentary cycle involved several rock-type contributions from magmatic or metamorphic terranes (Fig. 5.13a). The volcanic set of samples prevail with a more homogenous composition, representing a linear rise from instable mantle to a stable upper continental crust source rock composition meddling with rhyolitic volcanism (basic to acid; Fig. 5.13b).

Geochemical compositional ternary diagrams have also contributed for source rock characterization (e.g., Plank and Langmuir, 1998; V–Ni–Th*10), nevertheless, they are restricted to petrogenetic similarities (i.e., volcanism).

The La–Th–Sc diagram for determining tectonic environments and related sources was constructed by Bhatia and Crook (1986) and has served for this thesis outline (Fig. 5.14a). This diagram has an additional value as a provenance indicator by the modifications after Cullers (1994). He associated the preexisting La–Th–Sc composition to relate metamorphic source rocks (Fig. 5.14b). Samples from the volcanic localities fit with better genetic implications on the original ternary fields.

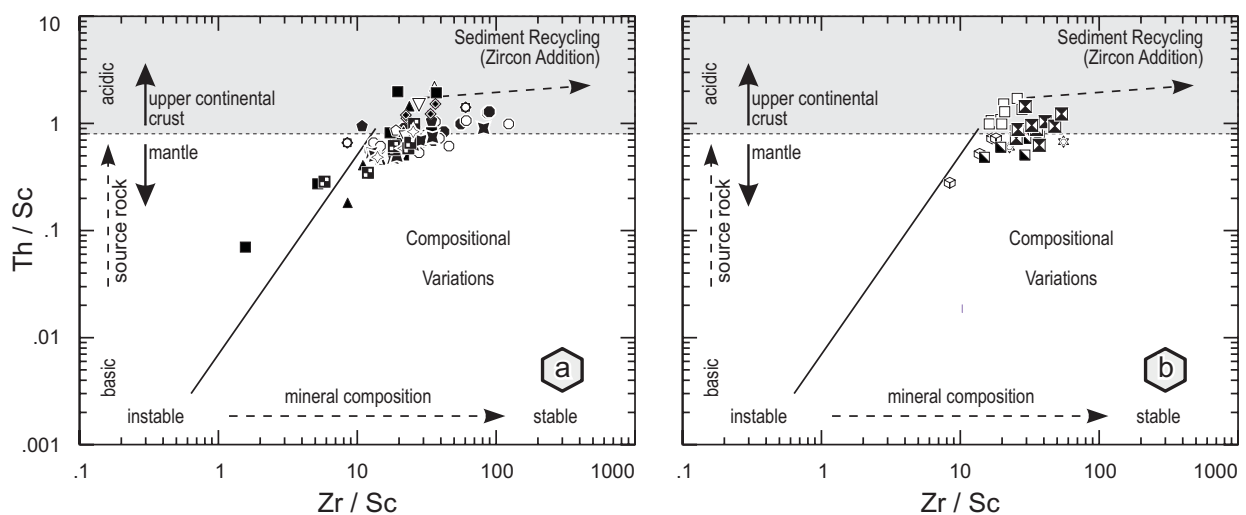


Fig. 5.13: Zr/Sc–Th/Sc ratios (McLennan *et al.*, 1993) of: a) Clastics, n=82 (LSPT– Lomas de San Paulo Tranquitas; CA– Cañón El Alamar; COL– Cañón El Olmo; CB– Cañón La Boca; CC– Cañón Caballeros; CHP– Cañón Peregrina; CN– Cañón Novillo). b) Volcanics, n= 38 (VH– Valle de Huizachal; Ab– Aramberri; Mi– Miquihuana). Additional explanations for symbols see Fig. 5.7.

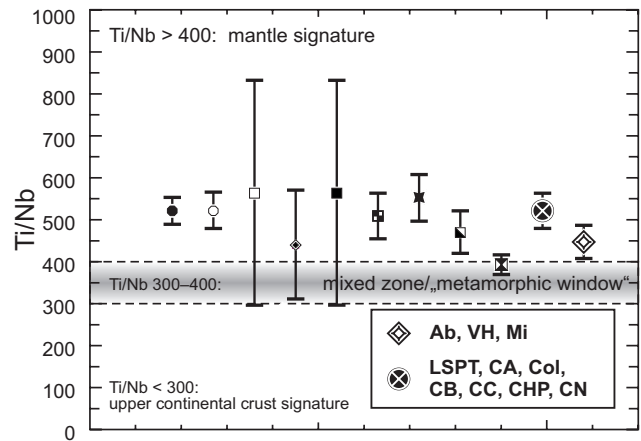


Fig. 5.12: Ti/Nb ratio of investigated sections and formations and comparison with potential metamorphic and magmatic source rocks after Jenchen (1998). a) Clastics, n=82 (LSPT– Lomas de San Paulo Tranquitas; CA– Cañón El Alamar; COL– Cañón El Olmo; CB– Cañón La Boca; CC– Cañón Caballeros; CHP– Cañón Peregrina; CN– Cañón Novillo). b) Volcanics, n= 38 (VH– Valle de Huizachal; Ab– Aramberri; Mi– Miquihuana). Additional explanations for symbols of each locality see Fig. 5.7. Confidence range plots are at 99.5%

The mean compositional value for the clastics set falls within the fields for clays, silts, sands, and gravels from mixed sources of typical granitic gneiss and metabasic rock-types (Fig. 5.14d).

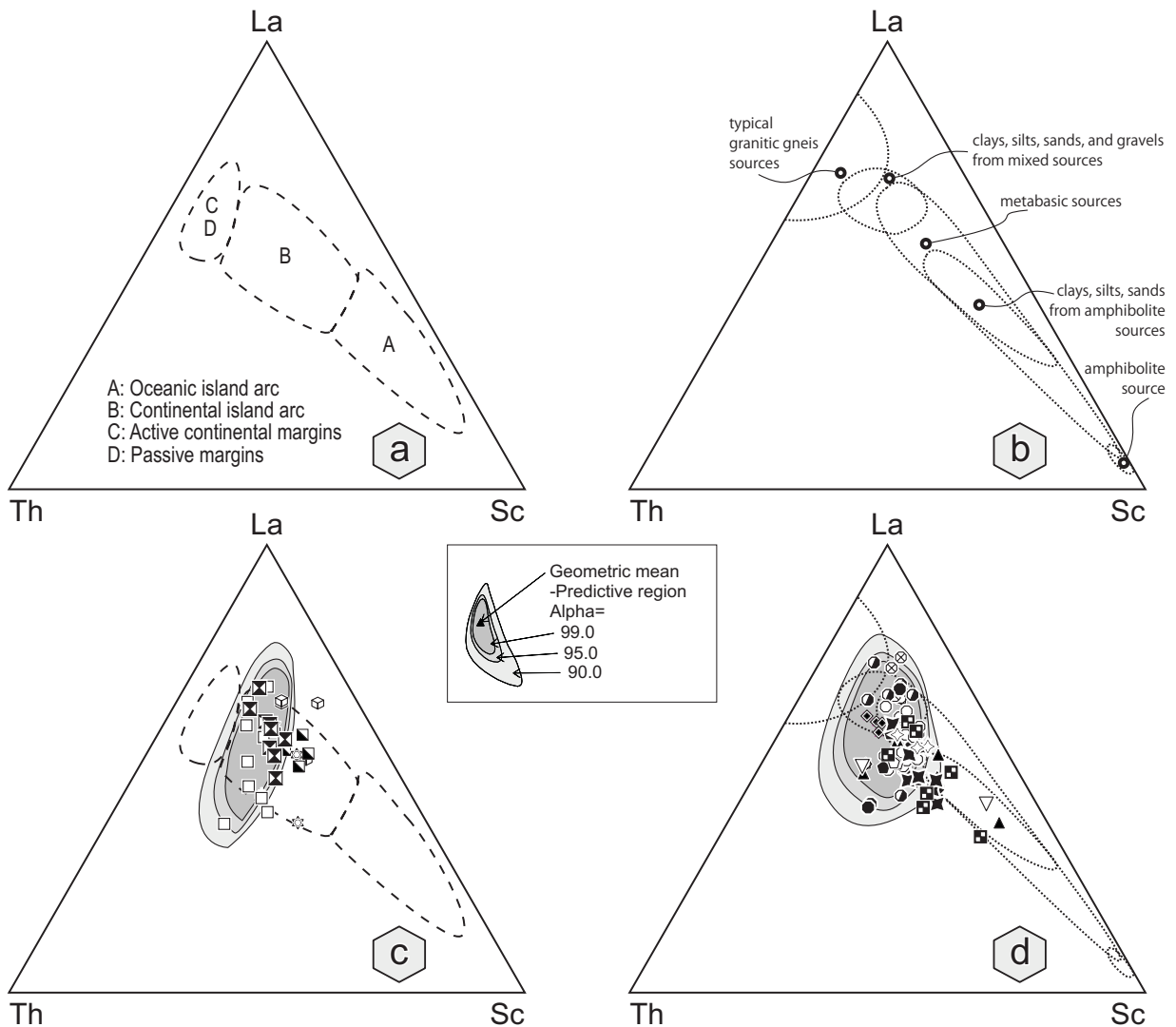


Fig. 5.14: A comparison of the composition for the sediment in this study at different constructed fields for the La–Th–Sc ternary system. a) Original compositional diagram after Bhatia and Crook (1986). b) Modified version with fields for metamorphic sources after Cullers (1994). c) Volcanics, $n=38$ (VH– Valle de Huizachal; Ab– Aramberri; Mi– Miquihuana). d) Clastics, $n=82$ (LSPT– Lomas de San Paulo Tranquitas; CA– Cañón El Alamar; COL– Cañón El Olmo; CB– Cañón La Boca; CC– Cañón Caballeros; CHP– Cañón Peregrina; CN– Cañón Novillo). Additional explanations for symbols of each locality see Fig. 5.7. Confidence range plots are at 99.5%.

5.3.4. Weathering: values, indices, representations, and trends

Weathering is perhaps the process that most significantly influences the geochemistry of terrigenous clastic sedimentary rocks. The mineralogy and geochemistry of sediments commonly reflect the compositions of weathering profiles of the source rock, rather than that of the source rock itself (e.g., Nesbitt *et al.*, 1996). This work includes the use of explicit quantitative weathering indices capable of explaining the dissolution of a single mineral (e.g., the CIA index) and the bulk geochemical response during weathering (e.g., the W index). The A-CN-K and the MFW diagrams have a potential application for provenance analyses. Fedo *et al.* (1995),

Nesbitt and Young (1982, 1996), Nesbitt *et al.* (1996) and Otha and Arai (2007) described an innovative approach that implicitly considers geochemical modifications associated with intrinsic and extrinsic weathering factors (e.g., White and Brantley, 2003). However, a consideration must be taken into account, while two important variables are not evaluated in the MFW scheme, which are the role of volatile components and the redox behavior of iron.

5.3.4.1 Chemical Index of Alteration (CIA)

The Chemical Index of Alteration (CIA; Nesbitt and Young, 1982) is the most accepted provenance tool to reflect the available weathering indices (Price *et al.*, 1991; Fedo *et al.*, 1995; Bahlburg and Dobrzinski, 2011). Exposed rocks are affected by a combination of chemical and physical weathering to variable degrees (Johnson, 1993; Duzgoren-Aydin *et al.*, 2002). The environmental conditions can be reliably inferred if is applied in combination of a comprehensive facies and petrographical analyses.

The CIA diagram represents the typical weathering of the upper continental crust using a ratio of predominantly immobile Al_2O_3 with a progressive chemical weathering (i.e. hydrolytic weathering; Kramer (1968) of labile minerals like feldspar and volcanic glass. These weathering trend leads to the loss of mobile cations Ca^{2+} , K^+ and Na^+ , and the transformation to [illite and kaolinite, and Fe-oxyhydrates like goethite] more stable minerals under surface conditions (Nesbitt and Young, 1984; Fedo *et al.*, 1995; Taylor and McLennan, 1985). Mg^{2+} is derived from glasses, sheet silicates, and mafic minerals and resides in chloritic and smectitic clays (Nesbitt and Young, 1984; Pettijohn *et al.*, 1987).

Major element oxides given in molecular proportions define CIA. CaO^* represents the CaO content only of silicate minerals (Fedo *et al.*, 1995). In such a formulation, CaO^* refers only to the calcium associated with silicate minerals and thus corrections to bulk chemical compositions are required to account for calcium associated with carbonates (e.g., calcite, dolomite) and phosphates (e.g., apatite). The easiest method for using this correction is to assume CO_2 and P_2O_5 are entirely associated with calcite (and/or dolomite) and apatite respectively, or to use point count data (Ocampo-Díaz, 2011).

CIA values typically range from about 50 or less for most unweathered igneous and metamorphic rock, to 100 for pure aluminosilicate residues. In the ternary A-CN-K diagram on Fig. 5.15 the provenance compositions and weathering trends can be depicted and predicted. Kaolinite has a CIA value of 100 and represents the highest stage or degree of weathering. Illite is between 75 (early weathering stage) and c. 90 (intermediate and late weathering state: smectite), muscovite at 75, and the feldspars at 50. Fresh basalts have values between 30 and 45, fresh granites and granodiorites of 45 to 55 (Nesbitt and Young, 1982; Fedo *et al.*, 1995).

The CIA mean compositional values for the clastics set fall within a CIA value of ~60 (Table 5.6; Fig. 5.15). Clastics data presents contracting Na^+ and Ca^{2+} modifications and change rock composition toward the A apex with even higher CIA values than the volcanic samples. The framework heterogeneity and a possibly

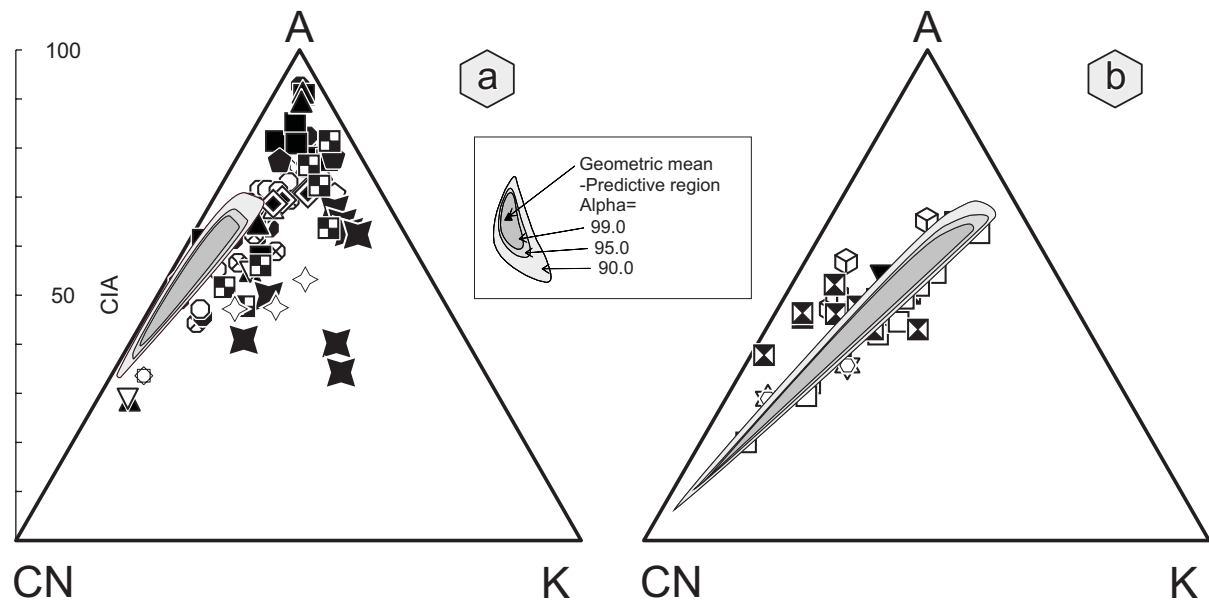


Fig. 5.15: Al_2O_3 - $(\text{Na}_2\text{O}+\text{CaO}^*)$ - K_2O diagram with the Chemical Index of Alteration (CIA) scale shown on the left (from McLennan and Murray, 1999). Note that weathering trends for the a) Clastics, $n=82$ (LSPT– Lomas de San Paulo Tranquitas; CA– Cañón El Alamar; COI– Cañón El Olmo; CB– Cañón La Boca; CC– Cañón Caballeros; CHP– Cañón Peregrina; CN– Cañón Novillo. b) Volcanics, $n=38$ (VH– Valle de Huizachal; Ab– Aramberri; Mi– Miquihuana). Additional explanations for symbols of each locality see Fig. 5.7. Confidence range plots are at 99.5%.

5.3.4.2 Mafic–Felsic–Weathering (MFW diagram)

Ohta and Arai (2007) presented a statistical approach whose degree of weathering (W) index and parent rocks is based on principal component analysis of eight major oxides using *ilr*-transformations. Yet, it has been applied only to igneous rocks. Geochemical estimations of weathering effects need to be considered carefully for provenance analysis because the major cations Na^+ , K^+ and Ca_2^+ may be mobile also under diagenetic conditions. The ternary system is governed chiefly by the three latent variable vertices, representing fresh mafic source, fresh felsic source and weathered rocks, M, F and W, respectively (Fig. 5.16). The equations used to calculate the M, F and W vertices are listed at Fig. 5.16. The capabilities of the diagram are concordant with the desired attributes for a useful weathering index from (Price and Velbel, 2003).

Accordingly, to the petrographic bearings for the clastics datasets, the geochemical weathering trends depicted on the MFW diagram show a pattern that suggests that biotite-, fayalite-, ferrosilite-, and chlorite rich rocks would yield for the high W values (Table 5.7; Fig. 5.16). High weathered values for phyllosilicates in samples extend toward the W vertex and highly weathered samples plot close to the W vertex.

The volcanic sample set records a more felsitic–intermediate signature near the variance of igneous minerals with high F compositions (Table 5.7). They distributed along the defined compositional linear trend that extends between the M and F vertices, near the reference rocks samples of (1) rhyolite, (2) granite and (2) dacite (Fig. 5.15). Thus, the effect of these minerals upon the net W value is limited except in the rare case where these minerals are the predominant constituent of the rock (e.g., serpentinite). Weathering interpretations

rely on evidence for processes affecting REE distributions during weathering of granitic rocks by the replacement of primary trace phosphatic minerals (e.g., monazite, allanite, apatite) by secondary LREE-enriched phosphates (e.g., Banfield and Eggleton, 1989; McDaniel *et al.*, 1994; Aubert *et al.*, 2001; McLennan *et al.*, 2003).

The rich igneous mineral samples with F–W trending join toward the W vertex, and represent a mineralogical weathering translation for the decomposition of plagioclases to kaolinite (see above: CIA). Clastics share a similar weathering degree trending, but include a transformation of muscovite to illite during weathering. This transformation is expressed with an increase in the W value, and a mineralogical translation along the M–W, probably attributed to the mineralogy from the underlying basement units (chlorite to biotite; see Chapter 3 and 4).

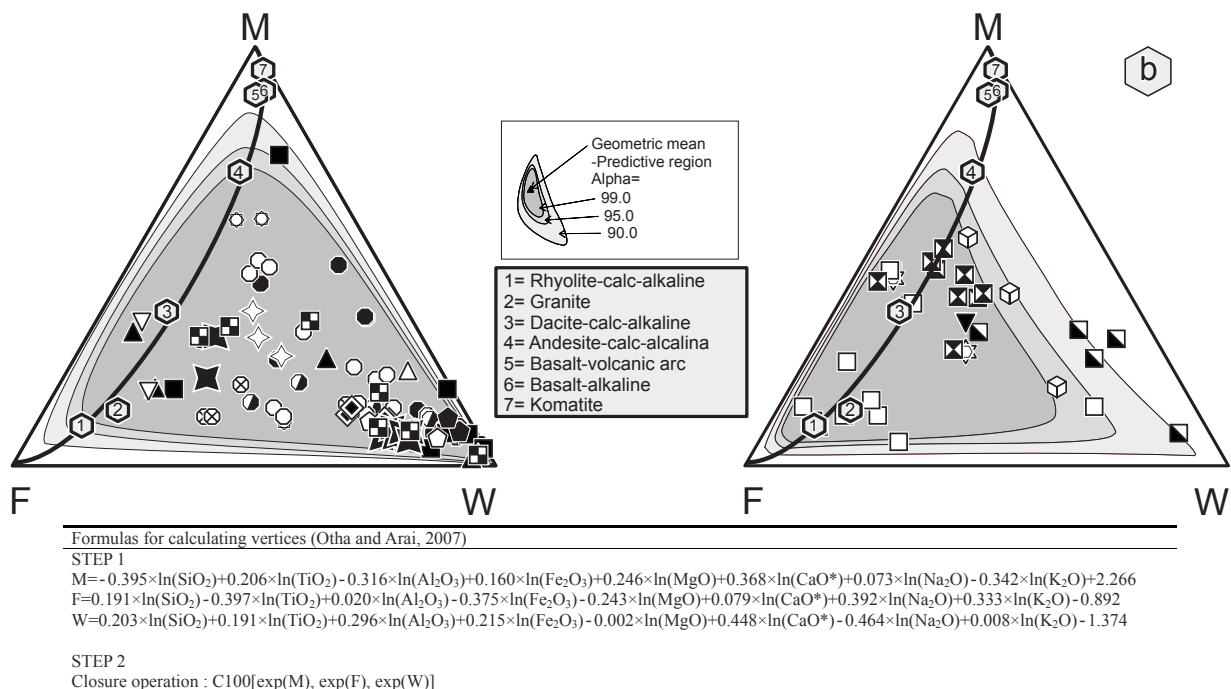


Fig. 5.16: Weathering trends depicted on the MFW diagram (Ohta and Arai, 2007) for a) Clastics, n=82 (LSPT– Lomas de San Paulo Tranquitas; CA– Cañón El Alamar; COI– Cañón El Olmo; CB– Cañón La Boca; CC– Cañón Caballeros; CHP– Cañón Peregrina; CN– Cañón Novillo. b) Volcanics, n= 38 (VH– Valle de Huizachal; Ab– Aramberri; Mi– Miquihuana). Weathering trends of the Volcanics intersect with the igneous rock trend in the plot domain of rhyolite, granites, and dacite. Additional explanations for symbols of each locality see Fig. 5.7.

5.4. Discussion

The chemical composition of Upper Triassic–Early to Middle Jurassic red beds in northeastern Mexico was used to deduce (i) sediment classification, (ii) source area composition, (iii) sedimentary recycling, (iv) mineral fractionation, and (v) weathering.

The compositional information was evaluated upon basic descriptive statistics, correlation matrices, and multivariate exploratory techniques (i.e., cluster analysis and principal components and classification analysis).

Despite the differences in petrogenesis and optical characteristics of the two main sample sets, the chemical values from both seem to demonstrate a relatively dependant classification of mixture of detritus from metamorphic, volcanic and minor constituents from plutonic provenance; albeit in different proportions for sedimentary recycling, mineral fractionation, and weathering.

So far, the information shared between latter chapters complements interpretations to disclose processes and factors of autogenic (Chapter 3), allogenic (Chapter 4), and petrogenetic nature (Chapter 5). The integral approach followed through this work tends toward a true provenance concept by an interdisciplinary understanding. The next chapters (Chapters 6 and 7) will continue to contribute a clear outlook for the intervening tectonic system(s) that gave breed to the red beds. Detrital configurations encapsulate a varietal of tectonomagmatic events that demonstrate the validity for the provenance-print to disclose.

6. RADIOGENIC ISOTOPES: U-PB DETRITAL ZIRCON DATING⁶

6.1. Introduction

The U-Pb detrital zircon analysis contributes critical information for pre-Late Jurassic strata of the Huizachal Group. This chapter explains the detrital zircon age populations of continental Mesozoic strata in the Valle de Huizachal (VH), located ~15 km southwest of Ciudad Victoria in northeastern Mexican state of Tamaulipas (Fig. 1.2), in order to determine sandstone provenance and place age constraints to the red bed stratigraphic succession (Section 1.7).

Isotopic approaches to provenance analysis in sedimentary rocks using U-Th-Pb isotope systems permits a precise single-grain radiometric dating (e.g., Gehrels *et al.*, 2008). The analysis of single grains permits synthesis interpretative relations between space and time, by covering large times scales and physical scales of geological controls–events–processes (e.g., tectonomagmatic events; Hemming and McLennan, 2001; Heller and Frost, 1988). Isotopic studies of clastic deposits can be used to delineate source areas or maximum depositional ages of a stratigraphic unit, to a degree not always possible using other basin-analysis techniques (Dickinson and Gehrels, 2008, 2009a,b; Lawton *et al.*, 2009). The ages may be related to the crystallization age or metamorphic event of the source rock. The population of grains includes detritus from different source areas, and the resulting age groups indicate the source rock ages.

Detrital zircon (DZ) favors provenance studies by its ultrastable characteristic derived from high-grade metamorphic rocks and felsic igneous source rocks (Hoskin and Schaltegger, 2003). Its high temperature of formation reduces its susceptibility to subsequent thermal resetting by burial in sedimentary and low-grade metamorphic conditions.

6.2. Methods

The concepts used herein about geochronology and chronostratigraphic units were according to Walsh (2001). Zircons were extracted and mounted from field samples using standard procedures for mineral separation (Gehrels, 2000). Age determinations of ~100 individual grains per sample were conducted by laser ablation–multicollector–inductively coupled plasma mass spectrometry (LA-MC-ICP–MS) at the Arizona LaserChron Center. The maximum and minimum depositional ages and the estimate of maximum depositional age from the youngest single concordant grain in the sample were estimated and graphed in Isoplot after Ludwig (2005) and Dickinson and Gehrels (2009b), respectively (Table 6.1). Source area interpretations were

⁶ This chapter has been partially documented in:

–Rubio-Cisneros, I.I., and Lawton, T.F., 2011, Detrital zircon U-Pb ages of sandstones in continental red beds at Valle de Huizachal, Tamaulipas, NE Mexico: Record of Early-Middle Jurassic arc volcanism and transition to crustal extension: *Geosphere*, v. 7, p. 1-12.

–Rubio-Cisneros, I.I., and Lawton, T.F., 2010, Provenance interpretations combining petrography and Zircon U-Pb ages of sandstones in continental red beds at Valle de Huizachal, Tamaulipas, NE Mexico: Record of Early-Middle Jurassic Arc volcanism and transition to crustal extension: Abstracts with Programs - Geological Society of America.

–Lawton, T.F., Barboza-Gudiño, J.R., González-León, C.M., Gary, G., Iriondo, A., Leggett, W.J., Peryam, T.C., and Rubio-Cisneros, I.I., 2010, Latest Triassic-Middle Jurassic age of Cordilleran-Nazas Arc in Mexico, indicated by U-PB Detrital Zircon and volcanic rock ages: Abstracts with Programs - Geological Society of America.

employed using the source rock composition (igneous and metamorphic) upon the ratio Age vs. U/Th (Rubatto and Gebauer, 2000; Rubatto, 2002; Belousova *et al.*, 2002; Hoskin and Schaltegger, 2003; de Barros *et al.*, 2010).

6.3. Corollaries: detrital zircons and source terranes

6.3.1. Results

U-Pb detrital-zircon ages ($n = 576$) from six Huizachal Group sandstones (five from La Boca and one from La Joya) consist of four groups indicating a mixed provenance: (1) Precambrian grains (~ 1.3 – 1.0 Ga) derived from Oaxaquia (Novillo Gneiss); (2) early–middle Paleozoic grains (430–300 Ma) derived from peri-Gondwanan accreted rocks (Granjeno Schist, tonalite, and Asseradero Rhyolite); (3) Permian-Triassic grains (296–222 Ma) derived from volcanic and plutonic rocks (East Mexican arc); and (4) Early-Middle Jurassic grains (199–164 Ma), locally derived from the Nazas arc (Fig. 6.2). Groups 1–3 increase in abundance upsection as a result of unroofing of Jurassic volcanic and sedimentary carapace from uplifted basement.

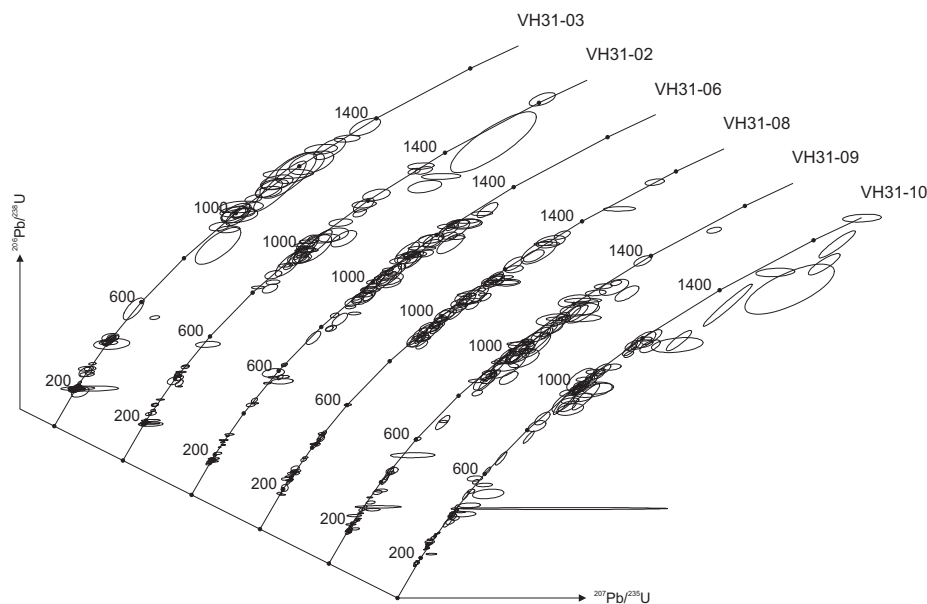


Fig. 6.1: U-Pb concordia plots for detrital zircons from lower member of La Boca Formation (VH31-03 and VH31-02), upper member of La Boca Formation (VH31-06, VH31-08, and VH31-09), and La Joya Formation (VH31-10). Errors are shown at the one-sigma level for laser ablation–multicollector–inductively coupled plasma–mass spectrometry analyses (Rubio-Cisneros and Lawton, 2011).

Table 6.1: Young grain ages of Huizachal Group detrital samples (datasets at Rubio-Cisneros and Lawton, 2011: <http://geosphere.gsapubs.org/content/7/1/159/suppl/DC1>).

Young grain ages of Huizachal Group detrital samples.

Formation/Member	Sample Number	Stratigraphic Level, meters	Weighted Mean Age, Ma	MSWD	n	Youngest Grain Age, Ma
La Joya	VH31-10	315	168±17	3.7	3	164±3
Upper La Boca Member	VH31-09	301.5	163.3±2.6	1.3	4	158±3
Upper La Boca Member	VH31-08	260	184±14	3.7	3	166±2
Upper La Boca Member	VH31-06	164	167.0±1.5	1.4	3	162±5
Lower La Boca Member	VH31-02	117	184.2±1.2	1.1	12	179±1
Lower La Boca Member	VH31-03	22	183.4±0.9	1.0	20	179±2

Stratigraphic level indicates cumulative meters above base of measured section A. Weighted mean age error is 2 -sigma. n is number of grains used to calculate weighted mean age. Youngest grain age error is 1 -sigma. MSWD for the weighted mean age is Mean Square of Weighted Deviates, a measure of ratio between observed deviation or scatter of points (from best-fit line) to expected scatter. MSWD near unity indicates assigned errors are the only cause of scatter (Ludwig, 2005).

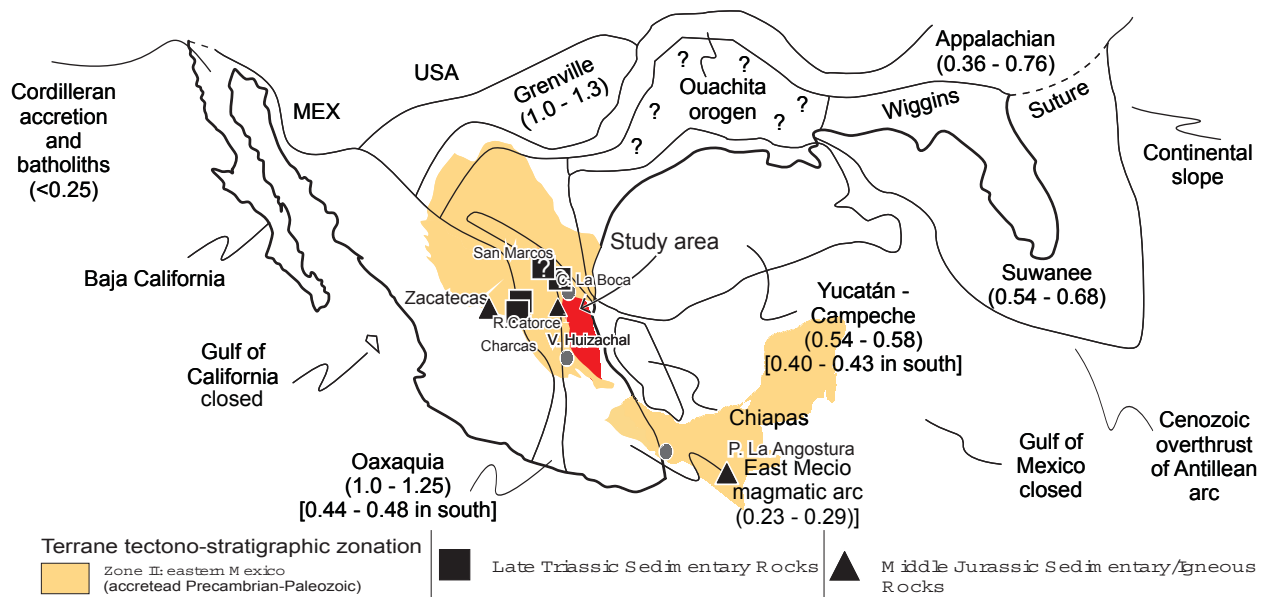


Fig. 6.2: Bedrock zircon sources in North America (modified from Dickinson and Gehrels, 2008). Shaded (yellow) section corresponds to the denominated Zone II: eastern Mexico (accreted Precambrian-Paleozoic) after the Terrane tectono-stratigraphic zonation proposed by Campa and Coney, 1983. Red-shaded area denotes the Oaxaquia (ca. 1.0–1.2 Ga) basement at northeastern Mexico. Black dots are Oaxaquia /Chortis block exposures. Black triangles represent Early–Middle Jurassic sedimentary/igneous rocks. Filled black squares are Late Triassic sedimentary rocks.

Two samples (VH31-03 and -02) were collected from steeply dipping beds of the lower member of La Boca Formation along measured section A (Fig. 6.3). Three samples (VH31-06, -08, and -09) were collected from the upper member along measured section B. The uppermost sample (VH31-10) was collected from the base of La Joya Formation within a coarse-grained pebbly sandstone bed on measured section C (Table 6.1; Fig. 2.18). Most of the zircon grain ages lie along and near the concordia (Fig. 6.1).

The two lower La Boca samples (VH31-03 and -02) have similar age spectra (Fig. 6.4). The maximum depositional age is indistinguishable from that of VH31-03 and indicates a likely Early Jurassic (Pliensbachian) age for the lower member. The two lower La Boca samples are dominated by Jurassic grains (201–164 Ma; 53%), fewer Precambrian grains (1.3–1.1 Ga; 21%), and subordinate Early Paleozoic (Cambrian–Devonian; 10%) and Permian-Triassic grains (292–243 Ma; 7%). Neoproterozoic grains (900–550 Ma) are uncommon (2%; Fig. 6.5). The lower La Boca samples have a source area compositional signature by U/Th, of 96.22% igneous and 3.78% metamorphic (Table 6.2; Fig. 6.6).

The three upper La Boca samples (VH31-06, -08, and -09) have similar age spectra among them, but with older grains than the lower La Boca samples. The maximum depositional age for the upper member is thus Middle Jurassic (Bathonian–early Callovian). The upper La Boca samples are dominated by Precambrian grains (44%), followed in decreasing abundance by Permian-Triassic grains (296–234 Ma; 13%), Jurassic grains (196–166 Ma; 11%), and subordinate Early Paleozoic grains (7%). Neoproterozoic grains are more abundant (8%) than in the lower La Boca interval (Fig. 6.5). The upper La Boca samples present a contribution from a source with a higher metamorphic composition ($[U/Th]_m = 90.78\%$) than the lower La Boca samples (Table 6.2; Fig. 6.6).

Sample VH31-10 from the base of La Joya Formation contains an age spectrum similar to that of the upper La Boca samples. It lacks a coherent group of young grains from which to calculate a maximum depositional age, but its youngest grain is concordant at 163.6 ± 2.6 Ma, statistically indistinguishable from the maximum

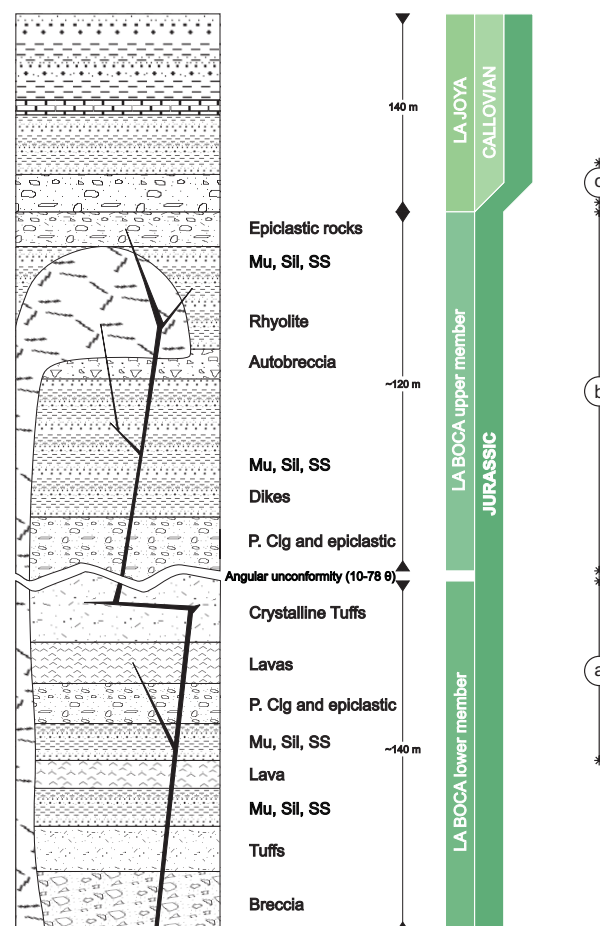


Fig. 6.3: Simplified lithostratigraphic column of La Boca and La Joya formations in Valle de Huizachal (modified by García-Obregón, 2007). Letters correspond to the stratigraphic levels documented in measured sections of Figures 2 and 6. Mu—mudstone; Sil—siltstone; SS—sandstone; P.Clg—polimitic conglomerate; V—volcanic rock (tuff); θ —dip of unconformity (Rubio-Cisneros and Lawton, 2011).

depositional ages of the upper La Boca samples. The La Joya sample is dominated by Precambrian grains (36%), followed in abundance by early Paleozoic grains (17%), Permian-Triassic grains (292–222 Ma; 16%), and uncommon Jurassic grains (188–164 Ma; 4%). Neoproterozoic grains (8%) are similar in abundance to the upper La Boca samples (Fig. 6.5). The sample of La Joya Formation increases a source signature with a more igneous composition ($[U/Th]_i = 94.74\%$) than the underlying stratigraphic interval.

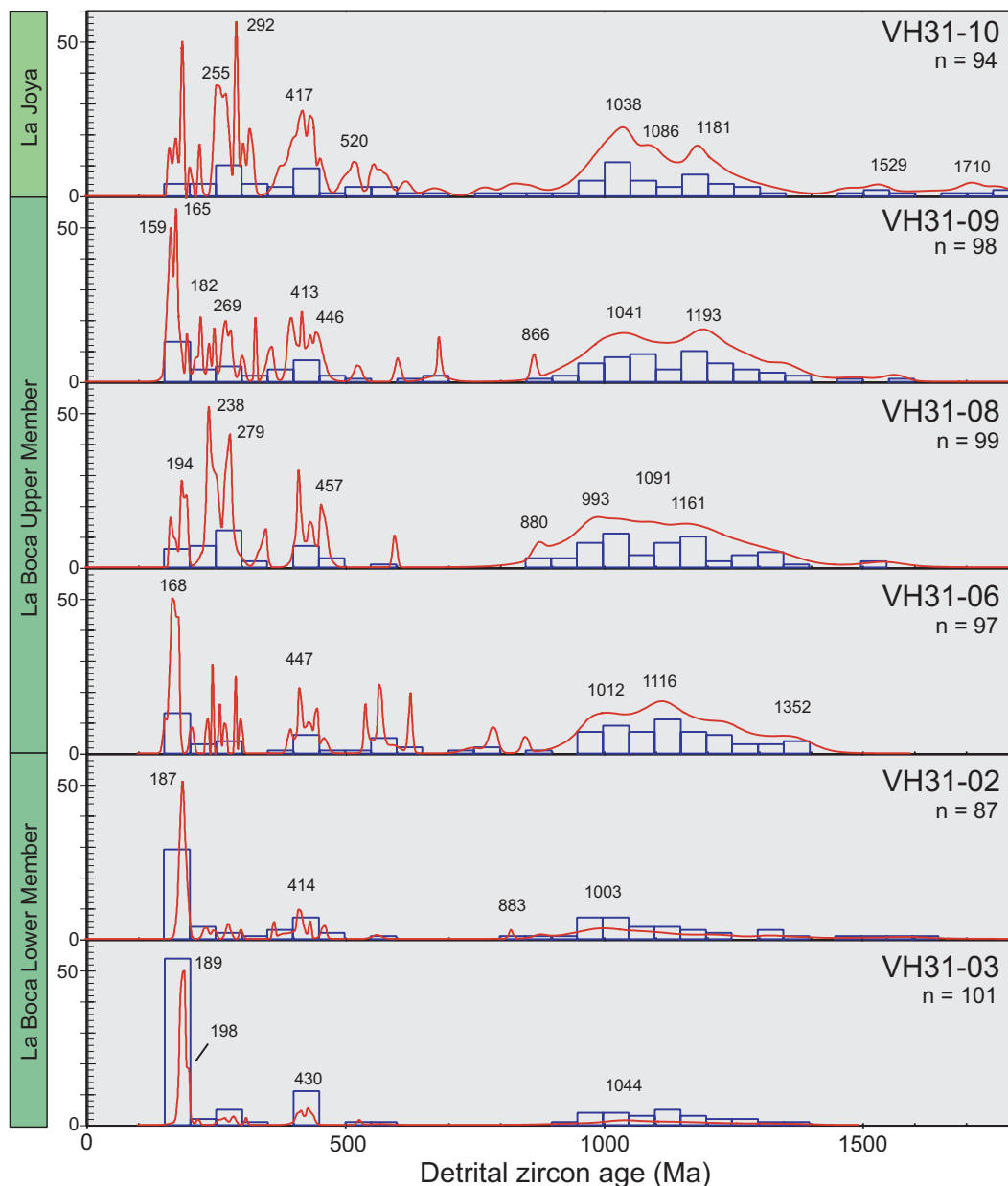


Fig. 6.4: Age probability plots and histograms of detrital zircon ages from the lower member and upper member of La Boca Formation, and La Joya Formation. Each curve sums probability distributions from all of the grains analyzed for that sample. Histogram bin width equals 50 Ma. Vertical axis for each histogram is equal to 60-grain analyses. Some probability peaks that are unlabeled result from a single-grain analysis with low analytical error (Rubio-Cisneros and Lawton, 2011).

6.3.2. Discussion

Abundances of the different zircon grain age groups change markedly upsection. Jurassic grains decrease from the base to the top, whereas Precambrian, Neoproterozoic, early Paleozoic and Permian-Triassic age groups increase. This suggests a progressive erosional unroofing of uplifted blocks, consistent with depositional in an extensional (rift) basin formed during the breakup of Pangaea (Rubio-Cisneros and Ocampo-Díaz, 2010).

DZ data provides evidence for the depositional ages of the strata. On the basis of the systematic stratigraphic decrease in maximum depositional ages upsection, it is inferred that magmatism was active in the age range of ~184-163 Ma and shut down immediately before the onset of sea-floor spreading in the Gulf of Mexico.

An apparent conflict in younger weighted

mean ages in the lower and upper La Boca with the 189 Ma U-Pb age (Fastovsky *et al.*, 2005) for the tuff at the base of the upper La Boca member requires discussion with the 189 Ma U-Pb age (Fastovsky *et al.*, 2005) for the tuff at the base of the upper La Boca member. A plausible explanation is that the intercept age obtained by Fastovsky *et al.*, (2005) was calculated based on reworked grains from older strata of the volcanic-rich lower member. Then the tuff age is a pseudo-Concordia intercept age based on a sampling of detrital zircon grains.

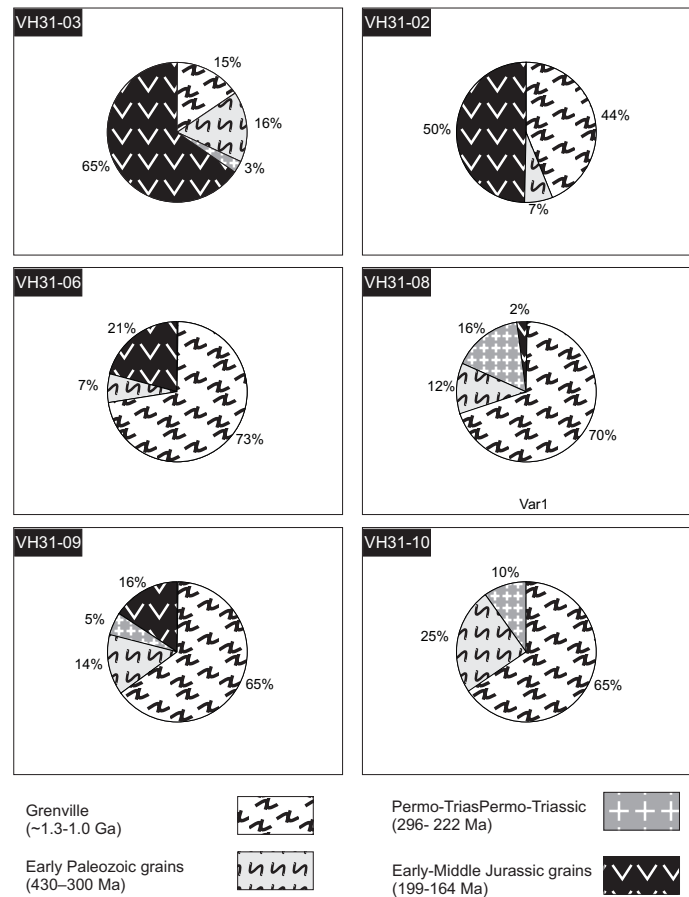


Fig. 6.5: Pie charts for detrital zircons content from the four main group provenance in analyzed samples (Rubio-Cisneros and Lawton, 2010).

Table 6.2: U/Th ratios, percentages, and grain participation of Huizachal Group detrital samples

Formation	Sample	Grains	U/Th (source area prediction)	
			Igneous (0.1-6)	Metamorphic (>7)
			La Boca lower member	VH31-03
	VH31-02	98	93	5
	total	185	178	7
La Boca upper member	VH31-06	94	87	7
	VH31-08	94	85	9
	VH31-09	94	84	10
	total	282	256	26
La Joya	VH31-10	95	90	5

Detrital zircon ages in the lower member of La Boca Formation corroborate previous inferences of an Early to Middle Jurassic age for La Boca Formation (Clark *et al.*, 1994; Stewart *et al.*, 1999; Fastovsky *et al.*, 1995, 2005; Barboza-Gudiño *et al.*, 2008).

The new age of La Boca Formation indicates equivalence with Lower-Middle Jurassic volcanic successions elsewhere in northeastern Mexico (Barboza-Gudiño *et al.*, 2008). Volcanism recorded by volcanic and volcanoclastic rocks of the Huizachal Anticlinorium was likely related to arc magmatism of the correlative Nazas Formation near Torreón, Coahuila (Imlay *et al.*, 1948; Belcher, 1979; Salvador, 1987; Bartolini *et al.*, 2003; Barboza-Gudiño *et al.*, 2008; Rubio-Cisneros *et al.*, 2011).

Compilation of U-Pb detrital zircon ages that indicate Jurassic Cordilleran-Nazas volcanic arc magmatism was separated in time from earlier Permian-Triassic (Torres *et al.*, 1999; Dowe *et al.*, 2005) and later Cretaceous igneous activity. The Nazas magmatic belt which followed a general southeastward trend from the Mojave Desert region to the northern extent of the Sierra Madre Oriental, and then turned southward to pass through what is now eastern Mexico (Lawton *et al.*, 2010).

Valle de Huizachal lies on the eastern edge of a band of Jurassic volcanic exposures with an east-west extent and may represent the east flank of the Nazas arc, where crustal extension juxtaposed thin arc volcanics and uplifted basement blocks. Arc rocks of the same age in the southwestern United States and northwestern Mexico have been interpreted as the record of a generally extensional arc system (Busby-Spera, 1988) that continued into what is now eastern and southern Mexico (Grajales-Nishimura *et al.*, 1992; Dickinson and Lawton, 2001).

Depositional ages and the age range of detrital zircons suggest that magmatism in the Nazas volcanic arc of northeastern Mexico ceased prior to the opening of the Gulf of Mexico. In addition, no zircon-yielding volcanic rocks younger than Callovian age provided detritus to the Huizachal Group.

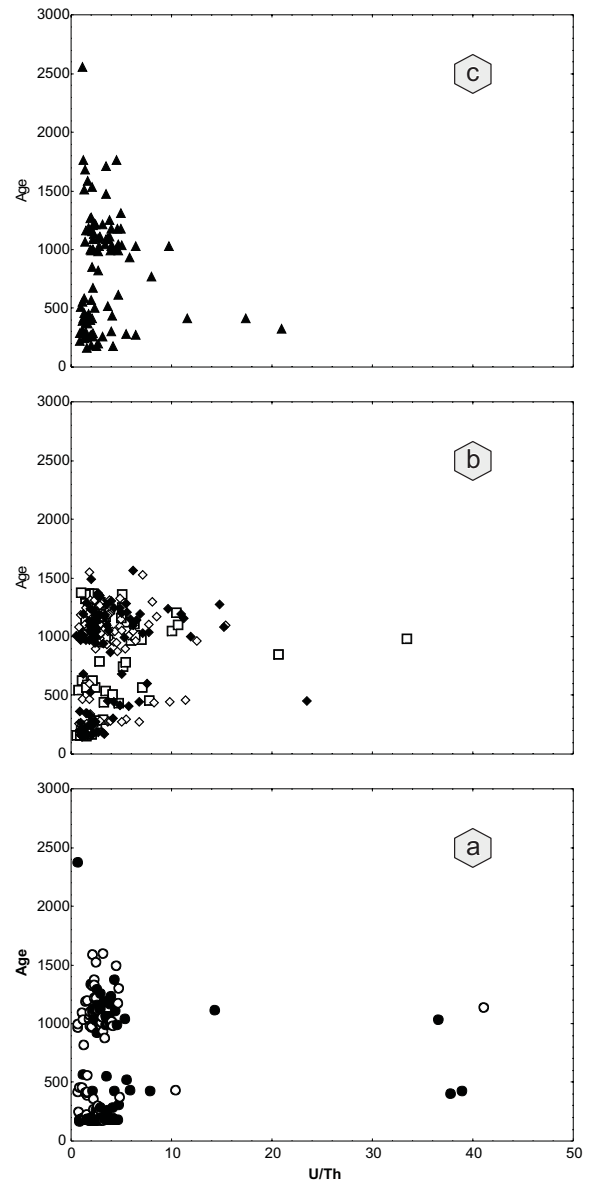


Fig. 6.6: Binary diagram for U/Th and the age $^{206}\text{Pb}/^{238}\text{U}$ (Ma). a) The two lower La Boca samples (empty circles– VH31-03, filled circles– VH31-02). b) The three upper La Boca samples (empty squares– VH31-06, empty rhomb– -08, and filled rhomb– -09). c) Sample from the base of La Joya Formation (filled triangles– VH31-10).

7. REGIONAL INTEGRATION AND INTERPRETATION FOR PROCESSES STRATIGRAPHY AND PROVENANCE ANALYSIS⁷

7.1. Introduction

This chapter integrates previous interpretations to establish an interdisciplinary provenance analysis and to characterize, locate, document, and reconstruct the provenance pathways and the distribution of lithologies from source regions for the basinal Mesozoic sequence. Red beds record the local crustal lithology in the source area composition, basin-types, and tectonic setting that operate for the sediment genesis.

7.2. Sedimentary petrography

7.2.1. *Sedimentary petrography: compositional signatures, affinities, indices, and recycling*

The petrographical composition of red beds reflects two main detrital assemblages, metamorphic and volcanic, both including sedimentary lithic fragments. Assemblages are a statistical representation made upon petrofacies characterization by optical means. The mainland petrofacies characterization of sandston is complimented by adding a description of framework modes using the QmFLt plot from Dickinson *et al.*, (1983) to support the light mineral synthesis: discussion and conclusion in section 3.3.4.

Detrital modes serve to identify quantitative contributions from different tectonic scenarios. Typically, a provenance type is made up from samples with a genetic relationship including their locality, sedimentary basin, sedimentary province, and tectonic setting (Dickinson *et al.*, 1983). Dickinson and Suczek (1979) showed that mean compositions in sandstone suites derived from different kinds of provenance terranes controlled by plate tectonic tend to lie within discrete and separate fields on the QmFLt diagram.

Detrital modes on Fig. 7.1 show Subpetrofacies 1A (~Qm₆₄;F₄;Lt₃₂) related to Recycled Orogen Provenance–quartzose recycled. Subpetrofacies 1B (~Qm₆₂;F₉;Lt₃₀) evidences a shared provenance between Mixed and Recycled Orogen Provenance–transitional and quartzose recycled. Meanwhile, Petrofacies 2 (~Qm₃₃;F₂₅;Lt₄₂) indicates a more disperse compositional group from various provenance contributors of Magmatic arc provenance to Recycled Orogen Provenance (Table 3.1; Table 3.2). The compositions are derived from the volcanic succession at la Boca Formation.

⁷ This chapter has been partially documented in:

–Rubio-Cisneros, I.I., and Ocampo-Díaz, Y.Z.E., 2010, Compositional analysis and sedimentary recycling evidences associated to unconformities in northeastern Mexico, a Late Triassic-Early Cretaceous example: Abstracts with Programs - Geological Society of America, v. 42, p. 70.

–Ocampo-Díaz, Y.Z.E., and Rubio-Cisneros, I.I., *submitted*, Análisis composicional y evidencias de reciclamiento sedimentario asociado a las discordancias del Noreste de México, un ejemplo del Triásico Tardío–Cretácico Temprano: Boletín de la Sociedad Geológica Mexicana, v. X, p. X-X.

–Rubio-Cisneros, I.I., and Ocampo-Díaz, Y.Z.E., *in review*, Using a discriminant function for determining a relationship between detrital modes and tectonic settings: an approach towards unveiling some source-to-sink factors: Special Issue: Actualistic Models - Sedimentary Geology.

–Ocampo-Díaz, Y.Z.E., and Rubio-Cisneros, I.I., *in preparation*; Relating detrital zircon U-Pb ages to tectonomagmatic events using a discriminant.

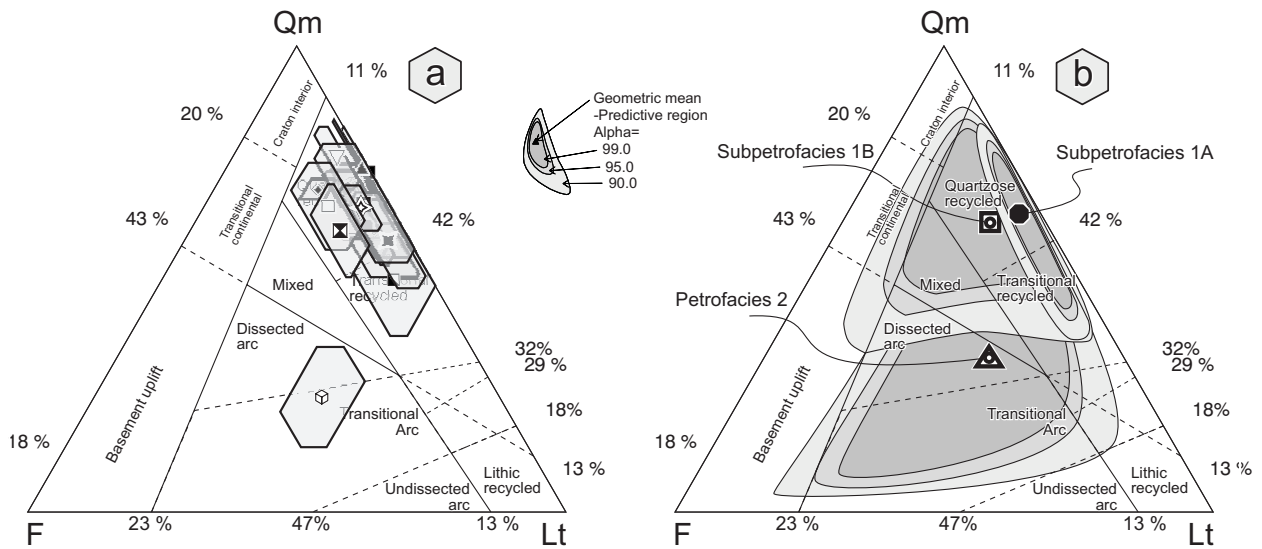


Fig. 7.1: Ternary diagram QmFLt for tectonic environment (Dickinson *et al.*, 1983). Hexagonal fields of variation *versus* air-based regions (after Weltje 2002). Solid lines: predictive regions of population mean. Confidence limits are 90%, 95% and 99%. a) Hexagonal region constructed from intersections of univariate normal approximations; b) air-based regions transformed to ternary compositional space. Key for symbols for each studied area at Fig. 3.2.

The modal analysis demonstrates a significant varietal composition mainly denoted on the lithic and feldspar content. Changes in lithic content are related to the concentration of low- to mid-grade metamorphic and volcanic fragments. The scatter arrays of samples mark the petrologic evolution of the basin, but also rock input periods. Upper Triassic sandstones from El Alamar Formation present a high textural maturity and plot in the upper part of the recycled orogen field. The upsection formations from the Early–Middle Jurassic from La Boca and La Joya formations have a contrasting behavior upon their Qt content. The most immature samples are those from the Early–Middle Jurassic La Boca Formation, while they are enriched in lithic fragments. Both, La Boca and La Joya formations represent an evolution from dissected arc to continental transition (Rubio-Cisneros *et al.*, 2011).

Interpretations for detrital modes can be assisted by using the QFL diagram proposed by Garzanti *et al.* (2001) and modified by Marsaglia *et al.* (2007) to explain the affinity of compositional signatures to extensional tectonics related like rift basin-types. The ternary system indicates that samples from subpetrofacies 1A ($\sim Q_{72}F_3L_{25}$) and petrofacies 2 ($\sim Q_{35}F_{24}L_{41}$; Fig. 7.2) are related to the undissected rift field, influenced by suture/orogen rock-types; while few samples from the subpetrofacies 1B ($\sim Q_{66}F_8L_{26}$) remain near the undissected rift with contribution from volcanic principal components (Table 3.1; Table 3.2).

Framework petrography (QFL) coupled to the systematic of compositional indices (e.g., SeReIn), and subject through a discriminant analysis, enables to validate not only controlling factors in the genesis of clastic sequences (e.g., recycling process), but enhances a detailed way to connect source rocks, tectonic setting, and basin-types.

The selected parameters have their own justified discriminative potential as describes by means of the Sedimentary Recycling Index (SeReIn), according to Rubio-Cisneros and Ocampo-Díaz (2010).

The parameters for compositional indices (F/Q_t , Q_p/Q_t from Arribas *et al.*, 1990; and P/K , L_m/Q_m , L_s/Q_m , L_m/L_v) are those principal components that control transport processes, source area composition (L_m , L_s , L_v , F , P), and textural maturity (Q_t , Q_m , Q_p); while others correspond to variables that control source area composition and recycling/cannibalism (*cf.*, Rubio-Cisneros and Ocampo-Díaz, 2010; Ocampo-Díaz and Rubio-Cisneros *in press*).

The compositional indices of F/Q_t vs. Q_p/Q_t suggest an immature La Boca Formation from the rest of the other two formations (Fig. 7.3). Based on the F/Q_t ratio the samples from La Boca Formation have high compositional values representing erosion and influence of volcanic and crystalline rocks. The increase in compositional variation might be related to the angular unconformity at the base of La Boca succession. The wide levels of confidence within these samples are interpreted as a function of an intraformational unconformity that rests within the volcanic succession.

The enrichment for Q_p/Q_t index on the analyzed formations is attributed to i) differences in grain size with more polycrystalline quartz on coarse-grained sandstones, and ii) an influence from metamorphic rocks.

The L_m/L_v ratio is used to discriminate the influence from volcanic or metamorphic source areas. This index suggests that samples from El Alamar Formation are more enriched from underlying basement units, while volcanic rocks influence La Boca Formation.

The degree of sedimentary recycling was assessed by using L_s/Q_m , which suggests a compositional contribution from El Alamar Formation to La Boca Formation. Meanwhile, La Joya denotes an input of metamorphic fragments comprising the underlying crystalline basement.

SeReIn is sensible and enables to interpret source area compositional variations, cannibalism, changes in facies, as well as compositional shifts linked to tectono-sedimentary or intraformational unconformities*. The tectonic significance of unconformities in the geologic record and sediment composition are translated into low SeReIn values, meanwhile autogenic factors gain higher SeReIn values. El Alamar Formation exhibits high SeReIn values ($\sim 0.81-0.67$), representing a tectono-sedimentary unconformity constraining the recycling of underlying basement units (Fig. 7.4).

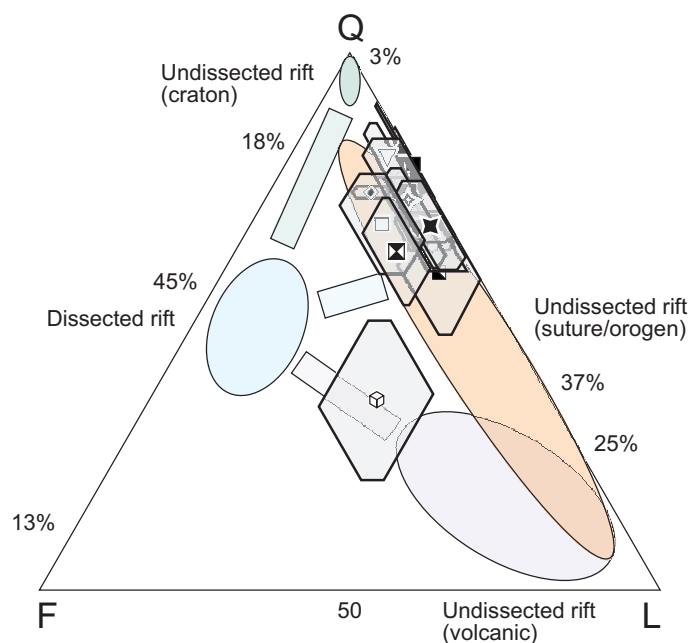


Fig. 7.2: QFL ternary diagram to discriminate tectonic environments of rift-type (after Garzanti *et al.*, 2001 and modified by Marsaglia *et al.*, 2007). Polygons represent the arithmetic mean and standard deviation. Symbols represent the mean composition for each studied area (Fig. 3.2).

* Considering that tectono-sedimentary unconformities imply source area changes related to tectonics, as well as a hiatus representation within the sedimentary record, printed on the sandstones' composition (Shanmugam, 1988; Zuffa *et al.*, 1995; Aubry, 1995; Widdowson, 1997; Alessandro Amorosi and Zuffa, 2011) Rely within the principles of practical tectonic analysis of cratonic regions (*cf.*, Lyatsky *et al.*, 1999).

An important unconformity separates El Alamar Formation and the overlying La Boca Formation. The SeReIn values (~ 0.37) record a shift in composition indicating increased derivation of detritus from volcanic successions and demonstrating source area rejuvenation. Rejuvenation is simply the development of an arc, or a renewed basement or thrust uplift. Within La Boca Formation intraformational unconformity (SeReIn= 0.37 to 0.66) serves as a boundary between the lower member (VES, Fastovsky *et al.*, 2005) and the upper member. The SeReIn values indicate increasing upsection the erosion of detritus from underlying succession (Fig. 7.4).

The angular unconformity between La Boca and La Joya formations presents the highest shift in SeReIn values (~ 0.90), attributed to important sedimentary recycling (Fig. 7.4). La Joya Formation is considered as the final deposit from a major sedimentary cycle beginning in the Late Triassic to Middle Jurassic.

Compositional signatures have not been previously assigned to sedimentary basins, so no such affinity can be made between basin** -types and detrital modes (e.g., Ingersoll and Suczek, 1979; Marsaglia and Ingersoll, 1992; Garzanti *et al.*, 2003; Marsaglia *et al.*, 2010). Therefore, this work refers to compositional signatures exclusively when interpreting detrital modes for provenance analysis. The three main categories of provenance type terranes plus a fourth mixing zone, distinguish the settings of continental blocks, magmatic arcs, recycled orogens, and hybrid/transitional sources on the QmFLt diagram. Variants for each provenance type can be related to specific plate tectonic settings (Dickinson and Suczek, 1979; Garzanti *et al.*, 2004; Garzanti *et al.*, 2007).

Light fraction petrography and mineralogical statistical discriminant parameters are apt to exclude detrital

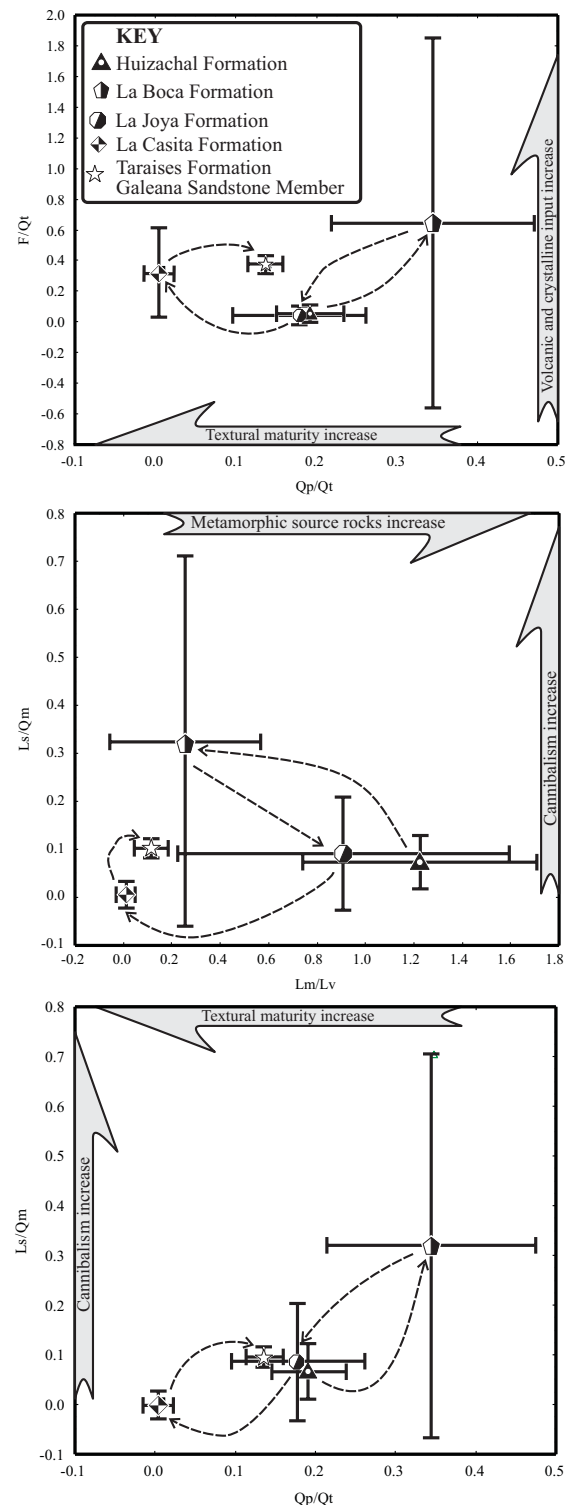


Fig. 7.3: Binary diagrams confronting parameters; a) F/Qt vs. Qp/Qt [from Arribas *et al.*, 1990]; b) Ls/Qm vs. Lm/Lv; c) Ls/Qm vs. Qp/Qt (Rubio-Cisneros and Ocampo-Díaz, 2010). Huizachal Formation is referred to El Alamar Formation

** It is important to remember that "basin" as used herein, refers to any sedimentary (and/or volcanic) stratigraphic succession (*cf.*, Ingersoll and Busby, 1995).

populations to quantify and characterize basin-types provenance and evolution (Rubio-Cisneros and Ocampo-Díaz, *in review*). This partially allows evaluating source rock rejuvenation and unroofing history as deeper structural levels are brought to the surface.

The reported compositional trends from Upper Triassic to Middle Jurassic formations allude for a tectonic evolution on northeastern Mexico to distinct basins-types from rift, back-arc, and hybrid extensional basin (Fig. 7.5). This interpretations are built considering the descriptions of basin-types according to their tectonic occurrence, compositional features, and their association to the plots from Dickinson *et al.* (1983) in relationship to the framework modes for provenance types.

(1) During the Late Triassic there is an evident sediment contribution related to detrital addition and recycling processes from crystalline basement rocks and the sedimentary Paleozoic carapace, associated with framework content with high indices for metamorphic lithics, polycrystalline and monocrystalline quartz.

(2) The Early–Middle Jurassic witnessed an abrupt compositional change from source rocks, implying rejuvenation of source areas recorded by the input of lithic fragments from volcanic and metamorphic compositions and feldspars.

(3) The Middle–Late Jurassic is characterized by a period in which the unstable components disappear progressively with a subsequent low-rate recycling from the underlying formations, suggesting a moderate input from sedimentary sources.

These inferences are supported by the interpretation from the scatter data on Fig. 7.5, and the overlapping ranges from samples.

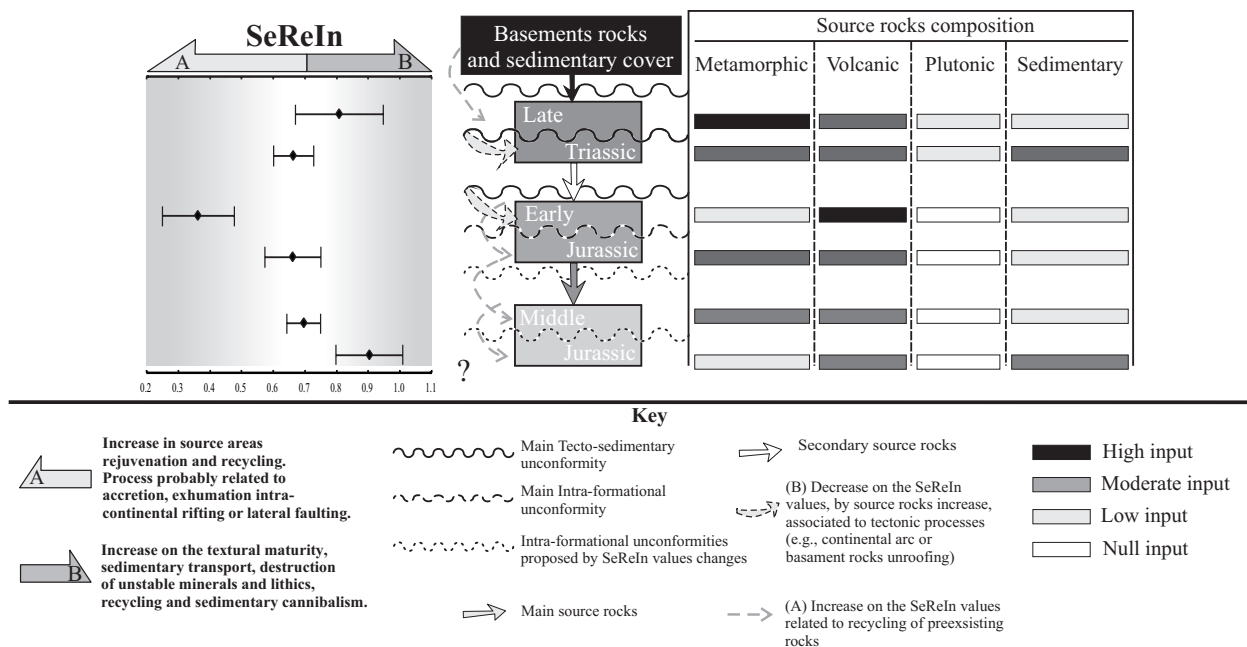


Fig. 7.4: Outline of possible source areas for Upper Triassic–Early to Middle Jurassic red beds on northeastern Mexico, including SeReIn values in relation to the unconformities and changes in sediment supply (after Rubio-Cisneros and Ocampo-Díaz, 2010). SeReIn– Sedimentary Recycling Index.

7.2.2. Heavy mineral analysis: mineral content, provenance, and erosion

Compositions of the red beds change as the sedimentary systems cut gradually the preexistent crystalline basement and sedimentary cover (Fig. 7.6a). The rich high-grade mineral samples join toward the Grt+Ky+Sil vertex, and represent the mineralogical high- to medium-grade metamorphic rock samples derived from mafic sources or protoliths. Samples with a more feldspar-rich signature are near the variance of igneous minerals with high Px compositions. They distributed along the defined compositional linear trend that extends between the ZTR+Amp+Ep and Px vertices; the mineralogical variations define a hydrothermal/alteration or volcanism. Samples near the ZTR+Amp+Ep vertex represent the transformation of sediments into more quartzose deposits and less rich in unstable heavy minerals. Samples with a translation along ZTR+Amp+Ep – Grt+Ky+Sil are attributed to mineralogy of metamorphic rank from the underlying basement units (see Chapter 3 and 4).

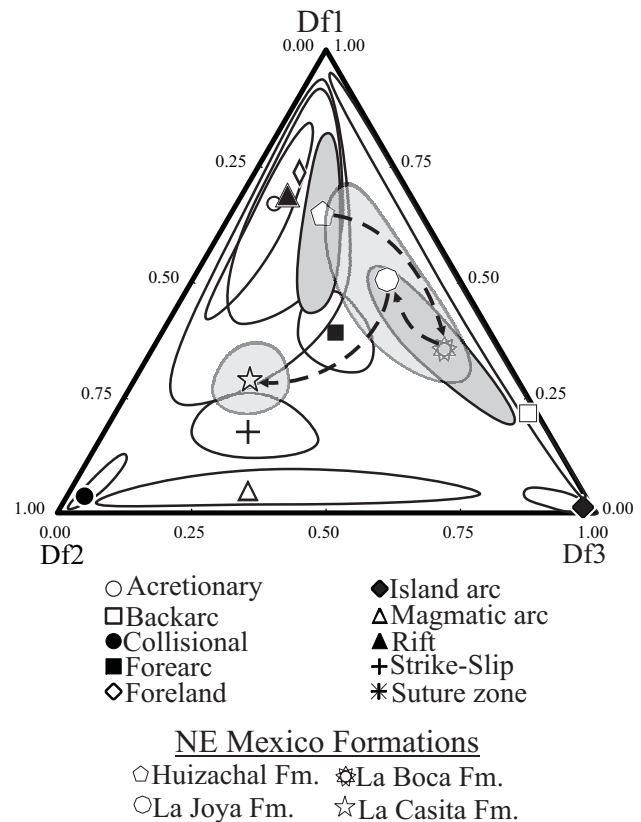


Fig. 7.5: Ternary diagram that graphs the discriminant functions with the fields from the different obtained basin-types. Figure includes the petro-tectonic evolution of the clastic sequences (Late Triassic–Early Cretaceous) from northeastern Mexico (after Rubio-Cisneros and Ocampo-Díaz, *in review*). DF– Discriminant function. Huizachal Formation is referred to El Alamar Formation.

The distribution of samples with a trending along the compositional vertices ZTR–Sil+Ky+Gr+Mic suggests the formation of two mineralogical variations to assess source rock influence and source area proximity (Fig. 7.6b). One variant is characterized by a decrease in the percentage of ultrastable elements with an influence from high-grade mineral source rocks. The other mineralogical variant is characterized by an increase in ultrastable species and represents a more differentiated composition by sedimentary processes or source area proximity.

The sorting index of sandstones, the ZTR-index, and the use of magmatic and metamorphic minerals in a ternary plot suggests that the analyzed samples present high content of metamorphic heavy minerals dominating over magmatically formed heavy minerals, in concordance to the regional geology (Fig. 7.6c). The ultra-stable mineral concentration remains with values below 50.

Some samples present wide detrital variability between mineral indices or group minerals (e.g., T&) indicating a major contribution from metamorphic sources over magmatically formed heavy minerals. However, in some other samples these index minerals are absent. Mineralogical variability during sediment generation is produced by sedimentary systems which change through time, fed by oscillating fluvial systems, and differences in the sedimentary recycling processes (e.g., >ZTR). Heavy-mineral modes might also mirror tectonomagmatic activity in the source regions. Heavy mineral content must be considered as partly an artifact conditioned by the breakdown of unstable minerals during post-depositional diagenesis and metamorphism for those heavy mineral assemblages rich in ZTR. The sediments with relative high ZTR values can be expected to have different main heavy mineral sources from those with low ZTR values and high contents of metamorphic heavy minerals.

Heavy mineral compositional modes may also serve to identify genetic interpretations for tectonic environments by using Zimmermann's proposal (Zimmermann, 1999). The analyzed samples with more metamorphic mineral content remain at the passive plate margin field or the low section from the ternary diagram. Metamorphic content might be dominated by compositions from mafic protoliths or granitoids and quartz-rich metamorphic complexes. The samples at the middle section of the plot at the active plate margin field present a mixed mineralogical assemblage that evidences volcanic (magmatic) sources and metamorphically formed heavy minerals. Possibly representing a sedimentary process under a tectonic regime, this conditioned a mineralogical content by the adjacent arc activity and pre-established [metamorphic] rocks. The upper field of the ternary system is ocean basin that is governed by mineralogy from mafic magmatic source rocks. This field is occupied by samples at the base of the red beds volcanic succession (La

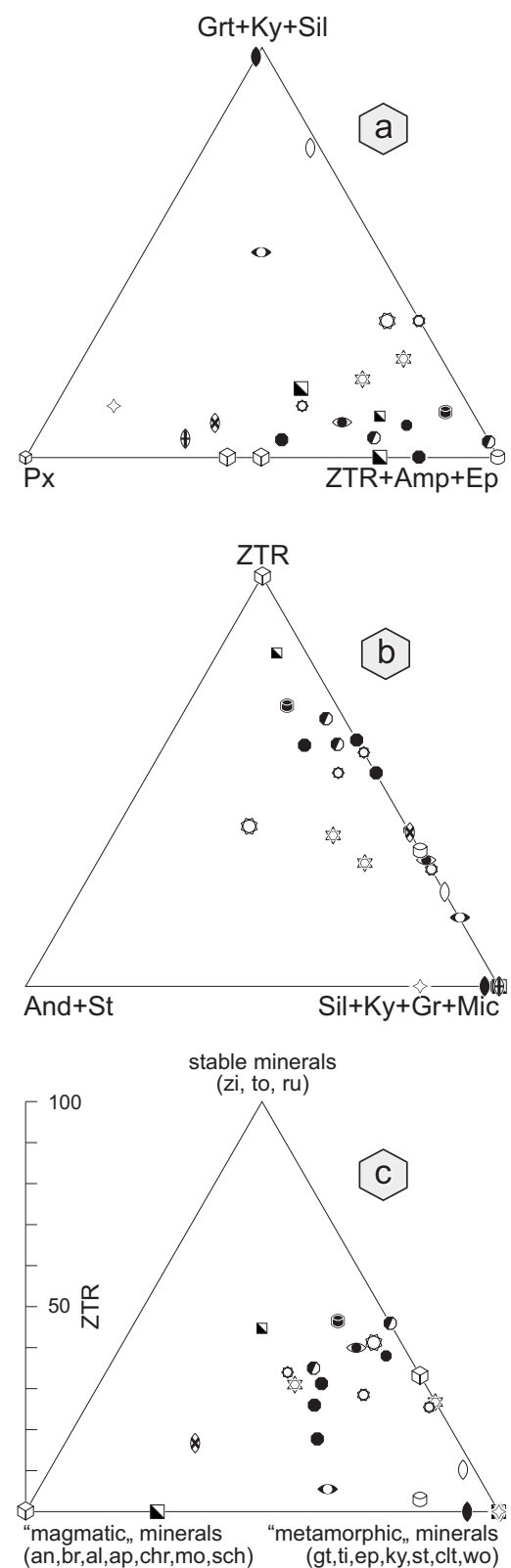


Fig. 7.6: Based ZTR ternary systems and other heavy mineral content. a) after Garzanti *et al.*, 2008. b) after Dinis and Soares 2007. c) wo– wollastonite, sch–scheelite (after Augustsson, 2003). Other abbreviations are at Table 4.1. Key for symbols for each studied area at Fig. 3.2.

Boca Formation).

The presence of mica minerals (e.g., muscovite) and LgM mineral indices (see Chapter 4) support the recognition for low-grade metamorphic pelite schists. Evenmore, chlorite permits to identify the contribution from the reported Granjeno Schist formed at green schist facies. (Ramirez-Ramirez, 1992). However, the occurrence of a strong identifiable HgM mineral assemblage evidences high-grade metamorphic petrogenesis (e.g., kyanite), in correspondence with the granulitic facies of the Novillo Gneis. This high metamorphic rank mineralogy complements previous optical descriptions made on basement units at northeastern Mexico (e.g., Ramirez-Ramirez, 1992).

7.3. Geochemistry: compositional mixtures a mineral content signature

Without a proper statistics, classification scheme, and nomenclature the analyzed samples can remain absent in geochemical distinctions. Two mayor geochemical groups were differentiated and classified as clastics and volcanics. Sample sets are related to passive and active margins with sources of mafic and felsitic or mixed zone geochemical print, respectively.

The analyzed red beds remain close to two main compositions, i) one with stable compositions from mixed sources of basic to intermediate character, rich in quartz and metamorphic minerals, and ii) another with intermediate to felsic chemical signatures with volcanic mineral content.

One example for geochemical effects can be seen by plotting the ratios Th/Sc against Zr/Sc (Fig. 5.13). During most igneous differentiation processes both Th and Zr are incompatible and typically become more enriched than the more compatible element Sc. Samples with Th and Zr are enriched in heavy minerals were monazite is typically far less abundant than zircon, respectively. During sedimentary recycling Zr/Sc tends to become increasingly higher nearly independent to changes in Th/Sc. Other elements that may be affected similarly are Hf (zircon), Sn (cassiterite), Ti (ilmenite, titanite, rutile), Cr (chromite), and Th (monazite). These chemical manifestations are controlled by heavy mineral content as seen by the distribution in the datasets. Both ratios typically increase with increasing igneous differentiation; such chemical pattern can be correlated with samples at the base of the volcanic succession (i.e. at Valle de Huizachal).

Volcanic dataset has a more relative simple provenance and maintains a minimal heterogeneity on the sedimentary recycling tendency. Clastics sample set is conditioned to sedimentary environments near basement

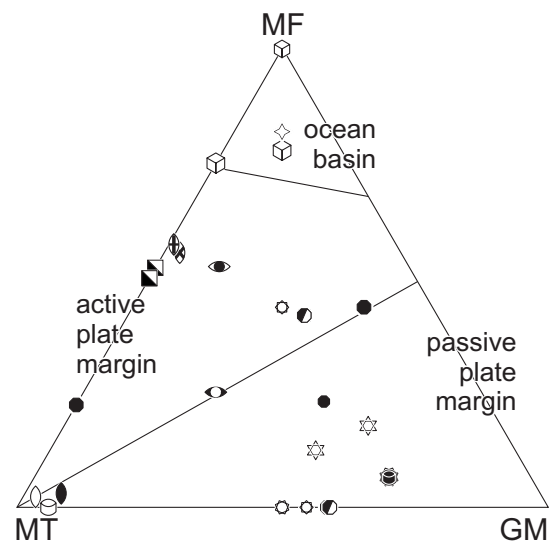


Fig. 7.7: MF– (mafic magmatic rocks): ol, iddingsite, px, green-blue hb. MT– (mafic-metamorphic complexes): green-blue hb, ep, gr. GM– (granitoids and quartz-rich metamorphic complexes): zr, to, st, mo, ky, sil, and (after Zimmermann 1999). Key for symbols for each studied area at Fig. 3.2.

and extensional faulted edge margins were sedimentary recycling is much more influenced over composition ($Zr/Sc > Th/Sc$). Samples tend to diminish their Ti/Nb ratio from north to south, or from unrelated volcanic to incomparable metamorphic outcrops. The clastics sample set maintains a stable ratio, while the volcanics dataset mark a decrease in Ti/Nb (e.g., Miquihuana; Fig. 5.12).

Despite the differences in petrogenesis and optical characteristics of the two main sample sets, the chemical values from both seem to demonstrate a relatively dependant classification upon the mixture of detritus from metamorphic, volcanic and minor constituents from plutonic provenance; albeit in different proportions for sedimentary recycling, mineral fractionation, and weathering.

The sources that supply the sediment routing system for Upper Triassic to Middle Jurassic have profound heterogeneities in composition. Eventhough two main groups were disclose, the complete data set remains as a heterogenous and disperse group, which signifies a sedimentary cycle influenced by several rock-type contributors and components that operate under a metamorphic and magmatic character.

7.4. Geochronology

Early analysis showed the different age groups in detrital zircons for the red beds, shed by the progressive erosional unroofing of the Oaxaquia units and Upper Triassic to Early–Middle Jurassic sedimentary carapace. An important feature for age group generation in continental deposits resides in the hydrodynamic fractionation of ultrastable mineral age populations during sedimentary pathways (Lawrence *et al.*, 2011; see Chapters 4 and 6). In addition, the U/Th–Age ratio is found useful for source rocks identification with magmatic or metamorphic compositions.

Magmatic or metamorphic detrital zircons are genetically related to tectonomagmatic events. Planetary events are driven by plate tectonics including the dynamics of [super-] plumes through geological time (Maruyama *et al.*, 2007; Yuen *et al.*, 2007).

Mexico has been shaped by the inception of supercontinents (e.g., Rodinia and Pangea), throughout the capture, accretion, collision, and amalgamation of magmatic arc-types (Fig. 7.8, Fig. 7.9; Campa and Coney, 1983; Sedlock *et al.*, 1993; Dickinson and Lawton, 2001; Keppie, 2004; Centeno-García, 2005). Along these orogenic events between terrane margins or continents remains an evident U/Pb–Age relation. This new breed of information contributes for a better understanding of the Sierra Madre Terrane with its new available ages for a better differentiation of tectonomagmatic affinities (Ocampo-Díaz and Rubio-Cisneros, *in preparation*).

The tectonomagmatic event affinity for the DZ from the analyzed red beds corresponds for example to crustal crystallization ages from the Mesoproterozoic (~1.3–1.0 Ga) derived from the Oaxaquia block, early–middle Paleozoic (430–300 Ma) Rheic-related, Permian-Triassic arcs (296–222 Ma), and the Cordilleran Nazas arc. Nevertheless, some insignificant single-grain ages remark some Pan-Africana-Brazilian tectonomagmatic affinity (580 ± 4 Ma; Fig. 7.10). The presence of unrepresentative single-grain ages within a sample or the overlapping of age ranges between tectonomagmatic events have a plausible explanation by the diachronism of geological events. This interpretations match with previous works that relate tectonomagmatic events for the

Gondwana margin terrane characterization in Mexico, or the pre-Permian metasedimentary rocks found in the Sierra Madre terrane (Fig. 7.11).

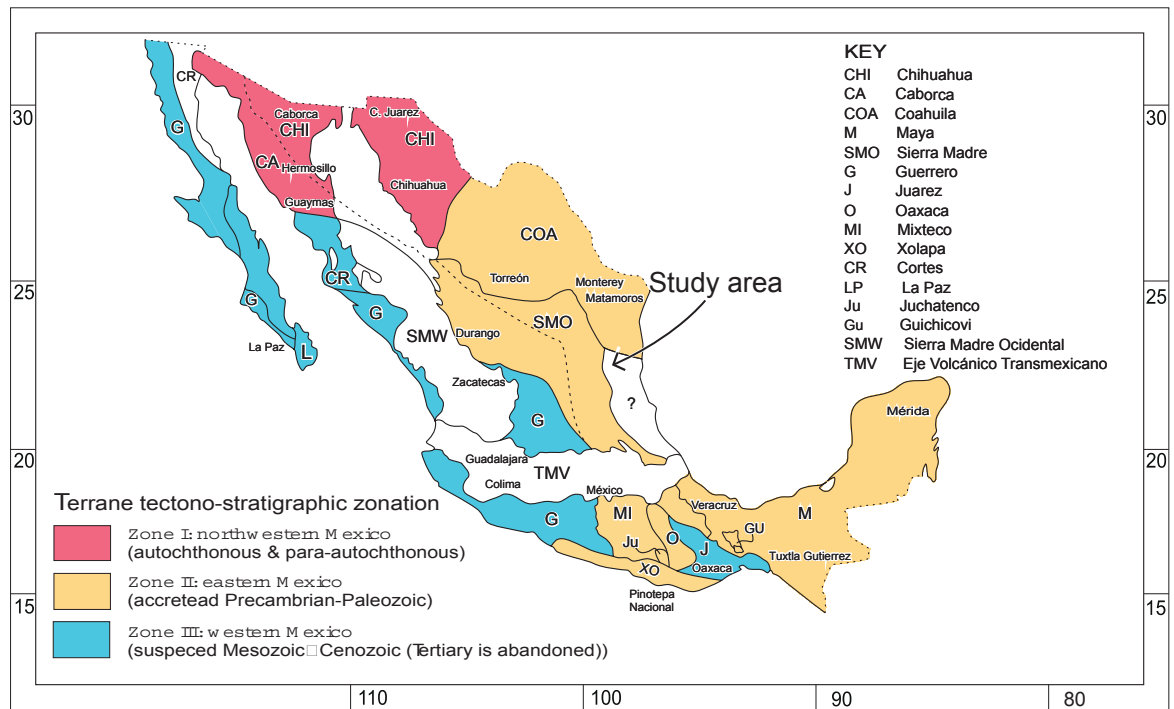


Fig. 7.8: Tectonostratigraphic terranes from México (after Campa and Coney, 1983).

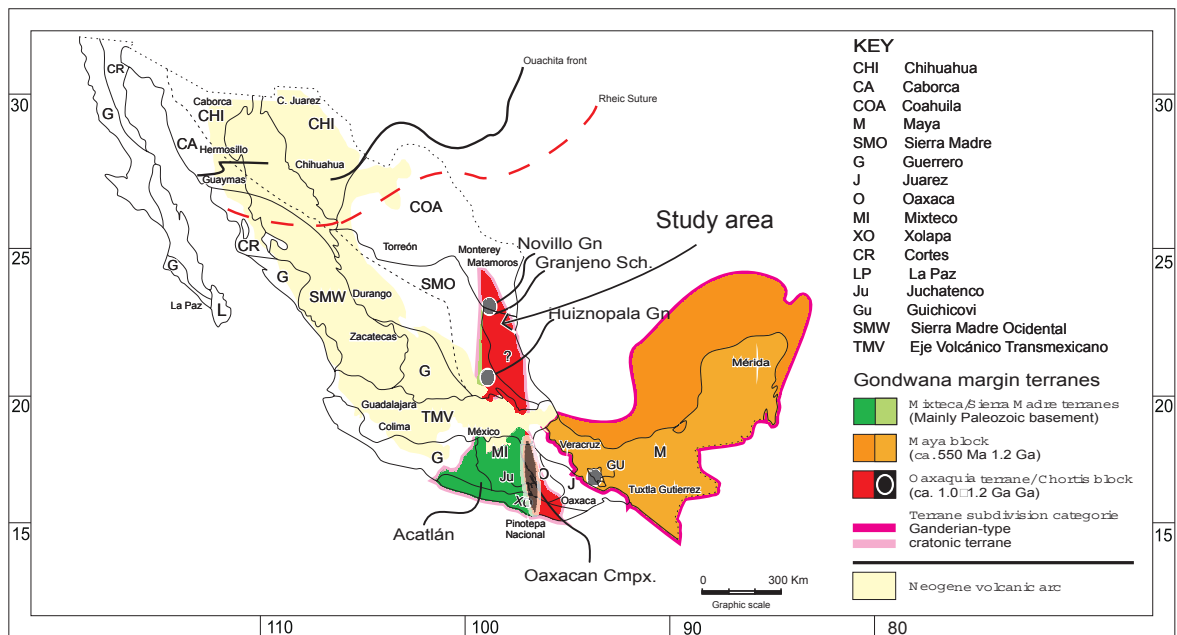


Fig. 7.9: Middle America – periGondwana Terranes. Modified after Campa and Coney, 1983; Nance *et al.*, 2008; Keppie and Ortega, 2010.

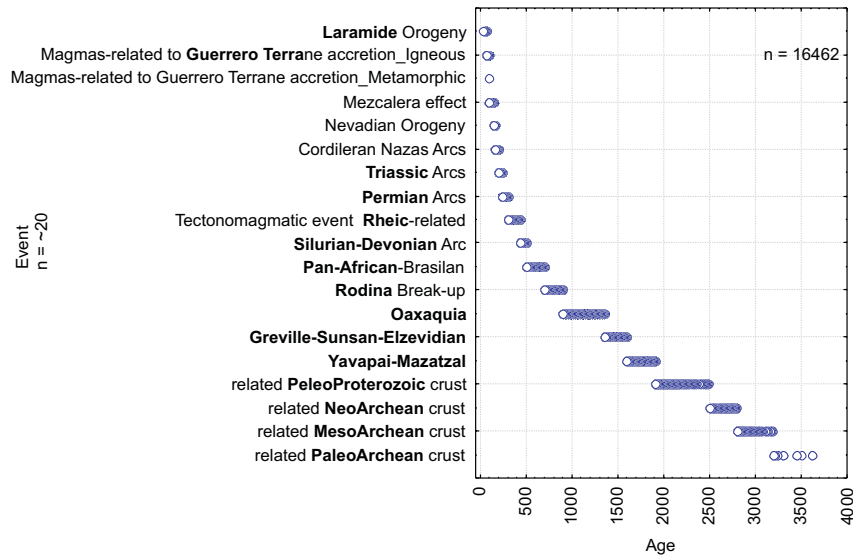


Fig. 7.10: Tectonomagmatic events plotted against age (modified after Ocampo-Díaz and Rubio-Cisneros, *in preparation*. Data represents a collection from various authors*.

7.5. Sedimentology

In addition to the latter observations the analysis for depositional systems and restoration of paleocurrents indicate the sediment sources are at a eastern position, and interpreted to be the underlying Oaxaquia with relative proximity to the juxtaposed peri-Gondwanan accreted rocks, and the West Pangaea arc rocks. The Lower-Middle Jurassic volcanic succession present particular sediment pathways originated or controlled by near volcanic sources related to the East Mexican magmatic arc (Fig. 2.25; Fig. 2.26; Fig. 2.27).

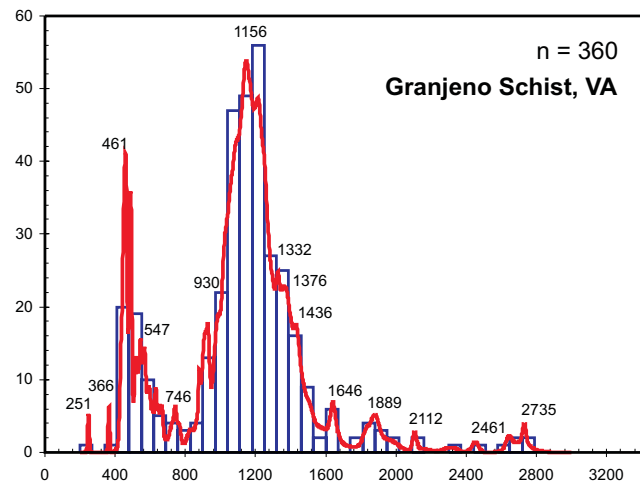


Fig. 7.11: Normalized relative age probability plots of U-Pb detrital zircon analyses from the Granjeno Schist of the Sierra Madre terrane (compiled data from Nance *et al.* 2007 and Barboza-Gudiño *et al.* 2011). VA-various authors.

7.6. Discussion: preexisting basement massifs and igneous bodies; the fundamental controls/factors for the Mesozoic red-bed genesis

It has been proposed that Upper Triassic to Lower-Middle Jurassic continental red beds have sedimentary genetic attributes carried by pathways that seemingly belong to foreign terrain dominions. Previous works have contributed to identifying the underlying basement at northeastern Mexico as having Pan-African affinities, but interpretations lack detrital zircon data. Sandstone composition and sedimentological analysis, especially for El Alamar Formation, constrain a nearby provenance by taking into account light- and heavy-mineral

petrography, and DZ age analysis (Chapters 3, 4 and 6). The next paragraphs describe disclose how within the basement units some massifs of yet unconsiderable composition and age may occur and how basement composite massifs may have played a role in the genesis of red beds.

The Meso-Proterozoic history addresses aspects of the ~1.3–1.0 Ga Grenville Orogeny (Bennett and DePaolo, 1987; Sadowski and Bettencourt, 1996; Dalziel, 1997). Mayor rock comparisons have been erected between grenvillian age rocks (Keller and Shurbet, 1975; Shurbet and Cebull 1987; Culotta *et al.*, 1992; Walker, 1992; Samson *et al.*, 1995; Mosher 1998; Bickford *et al.*, 2000; Dalziel *et al.*, 2000; Reese *et al.*, 2000; Morris, 2006). The Grenvillian interaction of Laurasia–Amazonia served to reveal Oaxaquia’s tectonic role (Tohver *et al.*, 2006; Bartholomew and Hatcher, 2010).

Separation of Laurentia from Rodinia at 725 Ma marks the reorganization of lithospheric plate motions that resulted in the Pan–African–Brazilian Orogeny (~0.6 Ga and 0.8 Ga) and the assembly of Gondwanaland that lasted from 725 to 500 Ma (Karlstrom *et al.*, 2001; Rino *et al.*, 2008). This breakup created the opening of the Iapetus Ocean during Early Cambrian and modulated the coming breed of supercontinents (Rogers, 1996; Unrug 1997; Pisarevsky *et al* 2003).

By Early Ordovician (540 Ma) the Iapetus Ocean had formed between Laurentia and Gondwana by the interaction between micro-plate boundaries (Katz, 1985; Young 1986; Unrug, 1992; Stern, 1994; Rogers *et al.*, 1995; Meert and Van de Voo, 1997; Nance *et al.*, 2010). Volcanic arc emplacements occurred on the southernmost margin of Laurentian during the existence of the Iapetus (Tull *et al.*, 2007). Arcs and continental collisions assembled Gondwana at ca. 540 Ma. (Karlstrom *et al.*, 2001).

By 460 Ma Avalonia-Carolina had separated from Gondwana creating the Rheic Ocean. By 370 Ma Laurentia, Baltica, and Avalonia–Carolina had collided to form Laurussia, and the Rheic Ocean began to contract. From the Late Ordovician to Late Silurian–Early Devonian a series of peri–Gondwanan magmatic arcs prevail between the Iapetus Ocean and the Rheic Sea Way in a south–southwestern position from North America (Vega-Granillo *et al.*, 2008).

The Rheic closed by Mississippian (280 Ma) to form Pangea and developed the Alleghanian structural front of the Appalachian fold-thrust belt in junction with the structural front of the Ouachita fold-thrust belt (Nicholas and Rozendal, 1975; Handschy *et al.*, 1987; der Voo, 1988; Hale-Erlich and Coleman, 1993; Dalziel *et al.*, 1994). The most eastward-southeastward Rheic-related suture remains in the south Appalachians. The Suwannee-Wiggins suture represents the joint between Laurentia and the African craton that extends to Ganderia (Heatherington and Mueller, 1991; McBride and Nelson, 1991; Horton *et al.*, 1994; Smith, 1982; Bartholomew *et al.*, 2009).

Some comparative analysis of the Suwannee-Wiggins suture terranes show differences between basement isotopic compositions that constrain their relative palaeogeography in the late Neoproterozoic and allow the geometry of the margin to be reconstructed for this time interval. These differences permit the terranes to be subdivided into four main ‘palaeogeographical’ categories (Nance *et al.*, 2008; Nance *et al.*, 2009).

This work has a particular interest on the Paleozoic basement of Mexico with affinity to terranes identified as exotic: (i) Ganderian-type terranes (e.g., Florida, Maya) that recycled Avalonian and older crust along the Amazonian margin of Gondwana and presumably lay inboard of the Avalonian-type terranes in the late Neoproterozoic; and (ii) cratonic terranes (e.g. Oaxaquia) that represent displaced Amazonian portions of cratonic Gondwana. In addition, the kinematics of some terranes are consistent with interpretations for a transform margin (Murphy and Nance, 1991; Murphy *et al.*, 1999; Hibbard *et al.*, 2007; Murphy *et al.*, 2010). These data supports the idea that Yucatán remained in a position between North and South America (Pindell, 1985, Pindell and Barrett, 1990). The circum-Atlantic terranes (Horton *et al.*, 1989) including those at the circum-gulf of Mexico represent peri-Gondwanan terranes (Dallmeyer *et al.*, 1987). Peri-Gondwanan terranes at Mexico are known as Middle America–peri–Gondwana Terranes (Keppie *et al.*, 2006; Nance *et al.*, 2007; Nance *et al.*, 2008; Keppie and Ortega, 2010).

The accretionary complexes formed during the diachronous Suwannee-Wiggins suture constitute Permian–Carboniferous peripheral foreland basins with metamorphosed and unmetamorphosed trench sediments, and orogenic flysch thrusting platform sequences of the North America (Pindell and Dewey, 1982; Sinclair, 1997). Relicts for this progressive suturing crop out in northeastern Mexico (e.g., Las Delicias and Ciudad Victoria). The position for the accretionary and thrust-loaded basins suggest a southeastern subduction for the North American plate (Pindell, 1985). It is speculated for the suture zone in Mexico exists nearby the Marathon belt and the Permian–Triassic intrusions, which underly the Coahuila Block at the south of the Coahuila Basin. Volcanic and plutonic rocks dominated the West Pangaeon, also known as the East Mexican arc (Pindell and Dewey, 1982; Pindell, 1985; Walker, 1988; Wilson, 1990; Dickinson and Lawton, 2001; Scherer *et al.*, 2010).

Pangaea's breakup started by rifting in the circum-Atlantic (~250 Ma; Smith and Livermore, 1991; Veevers 2005) and prograde to the west into the pre-Gulf of Mexico. Extensional tectonics followed pre-existing belt margins or shear boundary zones (Bird, 2001), but also might have cross them leaving remnants of juxtaposed terranes, and intervening sutures attached on both continents after separation (e.g., Woods and Addington, 1973; Feldman 1987; Hatcher *et al.*, 2007).

On section 7.4 U-Pb ages for this work were correlated to various ages of the main global tectonomagmatic events. These geological occurrences may contribute for a better understanding about the tectonic development at the southern margin of North America (Stewart, 1988). Oaxaquia must have suffered various effects of a moving terrain (e.g., Schedl and Wiltschko, 1984) like for other peri–Gondwana terranes.

Basement constitutes rocks that belong to a previous orogenic cycle, which have been reactivated and incorporated into a younger cycle. Basement massifs may be classified according to their relative position in an orogen, and tend to be part of several kinds of structures (*cf.*, Hatcher, 1984). Massifs are simple or complicated structures, with similar characteristics in their history. Massifs can get intimately involved with the Paleozoic folding sequence like the rocks that have been super-imposed on both the basement and the enclosing cover rocks that surround them; or may represent transported composite tectonic masses.

Therefore, the suspicious basement massifs at the Sierra Madre Oriental are considered composite in composition but not in mechanics (Torres-Sánchez, 2010). This work sustains that Oaxaquia must have had remained at the east, close to Ganderian-type terranes, near to West Africa and northeastern border of Amazonia. This position favored a Pan-African tectonomagmatic print or basement massif generation found by detrital composition and age-similarities (Weber *et al.*, 2006; Nance *et al.*, 2009). The Sierra Madre Oriental Pan-African massifs that fed the upper Triassic red beds must exist immediately to the gravity gradient of the Huizachal-Peregrina Anticlinorium along the southern Grenville-Sunsan-Elzevidian tectonomagmatic trend.

Other previous works have provided evidence for Pan-African/Brasiliano-age basement (580 Ma) in Mexico from cobbles and boulders in a Paleozoic conglomerate (Lopez *et al.*, 2001), and from shocked zircon (~545 Ma) in an impact breccia of the Chicxulub crater in eastern Yucatan (Krogh *et al.*, 1993). Nance *et al.* (2007) reported detrital zircon ages of ca. 650 to 525 Ma from the Sierra Madre terrane in Mexico and suggested provenance from the Maya terrane beneath the Yucatan Peninsula or the Brazilian orogens of South America. Similar ages are found at Upper Santa Rosa Formation (Weber *et al.*, 2006). Detrital Pan-African ages have also been reported from sandstone samples in Florida (515 – 637 Ma; Mueller *et al.*, 1994).

7.7. Mesozoic unroofing and exhumation: a *coda* for a preliminary basin stratigraphy and tectonic evolution of northeastern Mexico

The study in the genetic structure of stratigraphy aims for “process stratigraphy” to understand the driving mechanisms for the range of depositional systems, stratigraphic architectures, and cycles formed in sedimentary depocenters or basins.

The cratons, continents, and boundaries generated during the Precambrian then assembled and dispersed during the Paleozoic served as founding elements and transfer zones for the record of the Mesozoic rock cycle system (e.g., Bonda *et al.*, 1984; Mancini and Markham, 2005; Anderson and Mahoney, 2006; Ernst, 2007). Basement relief conditioned the Mesozoic sedimentary cover on the northeaster of Mexico (Fig. 7.13). Basement relief bears the marks of the pre-cover erosional physiography as well as subsequent vertical tectonic movements (*cf.*, Lyatsky *et al.*, 1999).

Pangaea’s break up started at the Atlantic. The extensional boundary at the east of the southern Laurentia margin changes to a volcanic rifted margin to the west in Texas, and continues its extensional percussion into the south. The northeastern Mexico stands for a transitional setting with tectonics for an amagmatic rift, back arc basin, and a transform fault boundary.

The continental depositional systems of the Huizachal Group include depocenters of rivers, alluvial fans, fan deltas, and lakes. El Alamar Formation developed within a depocenter with predominant transverse drainage with well-established river systems conditioned by extensional tectonics. La Boca Formation remains restricted to volcanism on a basin with volcanic successions characterized by internal axial through drainage from ephemeral river systems, sediment gravity flows, and short-lived lakes. The La Joya Formation constrains alluvial depocenters fed by transverse drainage directly from the source areas.

The stratigraphic succession for the three different formations develops under contrasting scenarios, – by sediment supply, erosion, and underfilling of the available accommodation. The loci conditions of each basin-forming mechanism gave breed to peculiar sediment routing systems that contribute to the sediment basin-fill. Run-off transported sediment from source region to sinks. Routing systems liberate, transport, and deposit sediment throughout the fluvial styles.

Each of the formations from the Huizachal Group presents a relation of depositional style to basin setting. Sediment accumulations and cycles are related to sediment accommodation/supply or surface architecture (Chapter 2). Each unconformity between sedimentary intervals (formation or member) suggests a shift in basin-forming mechanisms.

7.7.1. Triassic

During the Triassic Pangaea's break up extended westward from its origin point at the Atlantic along an extensional reactivation of a major Appalachian crust fault (Pindell, *et al.*, 2002). The structural lineament is consistent with grabens at the north of the Yucatan block and restores on line with the Rio Grande Embayment, Georgia Rift, and Apalachicola Embayment (Longoria, 1988; Bartok, 1993; Tardy *et al.*, 1989). At the same time, other subducting tectonic controllers operated at the paleo-Pacific margin. During the Late Triassic the continuing fragmentation gave pace for North and South America migration and other various crustal zones (Yucatán–Florida–Gulf of México and Caribbean; White, 1980; Salvador, 1987; James, 2009a,b). The Tamaulipas Arch, Balcones trend, and the southern flanks of the Sabine and Wiggins 'arches' are probable asymmetric rift footwalls that were tectonically unroofed by extension along a low-angle detachment (Pindell *et al.*, 2002).

The mechanism of crustal attenuation led to massive nonmarine clastic sequences at the Atlantic margin (Newark Supergrup, e.g., Lorenz, 1988; Witte and Kent, 1991; Olsen, 1997) and inland from Laurasia (Kayenta Formation, e.g., Bazard and Butler, 1991), with subsequently circum-gulf continental red beds (El Alamar, Huayacocotla, and Eagle Mills Formations; Michalzik, 1988, 1991; Schmidt-Effing, 1980; Marzoli *et al.*, 1999).

A tectonic mechanical percussion triggered by the loci of rifting at the Atlantic affected the rigid continental crust from the northeast of Mexico during the Late Triassic. The percussion developed a non-magmatic rift (Rubio-Cisneros and Ocampo-Diaz, 2011a). At the west the subduction zone remained far away in the paleo-Pacific margin (Dickinson and Lawton, 2001; Centeno-Garcia, 2005). The crustal thinning such as caused primarily by stretching or surface erosion was a consequence of basement relief. The isostatic basement relief from basement massifs and the controls of position of thrusts conditioned erosion and accommodation, respectively.

During Upper Triassic the depocenter of El Alamar Formation developed by lithospheric stretching from continental rifting. The nature of the sedimentary fill depends on the uplift pattern, with the shoulders and arches acting as sediment sources or barriers. Sediments were shed from to main areas the southernmost

termination escarpment of the Texas Uplift (e.g., Dickinson *et al.*, 2010; Fig. 7.12), and the west footwall from the future Huizachal-Peregrina Anticlinorium. The distribution of El Alamar red beds is restricted to the valleys of the peri-Gondwanic paleo-margin, or the Huasteca-Paleozoica tectonic belt (*cf.*, de Cserna, 1969).

Depositional environments rely on a major tectonic tough shared by minor depocenters (grabens and half-grabens). Batholiths and metamorphic massifs delimited the basin (e.g., Huizachal-Peregrina Tough). Depocenters developed within a embryonic continental abortive breakup zone explained by the absence of outcrops at the surrounding terranes of the Sierra Madre Oriental.

El Alamar Formation progrades from east to west into the Zacatecas Formation on the Arteaga Basin (Centeno-García and Silva-Romo, 1997; Barboza-Gudiño *et al.*, 1999; Silva-Romo *et al.*, 2000; Hoppe *et al.*, 2002; Centeno-García, 2005; Barboza-Gudiño, 2009; Barboza-Gudiño *et al.*, 2010). The sedimentation of the stratigraphic cycle was related to a scenario of high sediment supply rates (Dickinson *et al.*, 2010). Sediment routing systems conditioned fluvial styling. Sediment accumulation depends on the tectonic subsidence from the available accommodation. The detrital products from source areas were transported away by channelized flows.

The compositional signature and sediment contribution for basin infill are related to detrital addition by recycling/cannibalism from crystalline basement blocks, and [preexistent] sedimentary carapace (*cf.*, Rubio-Cisneros and Ocampo-Díaz, 2010).

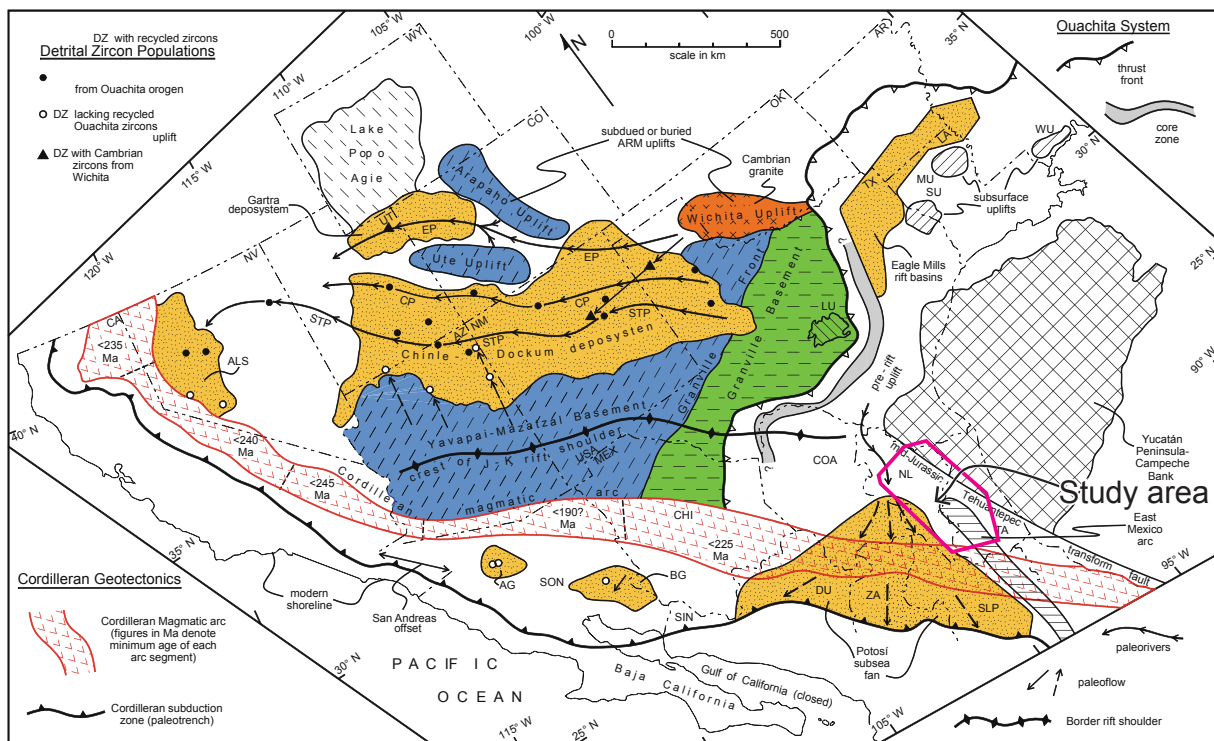


Fig. 7.12: Paleogeographic reconstruction for Mexico during the Late Triassic. Arrows indicate the possible sedimentary pathways and source areas with major detrital input from the Texas Uplift into the NL–Nuevo León vicinities. (after Dickinson and Gehrels, 2008; 2010).

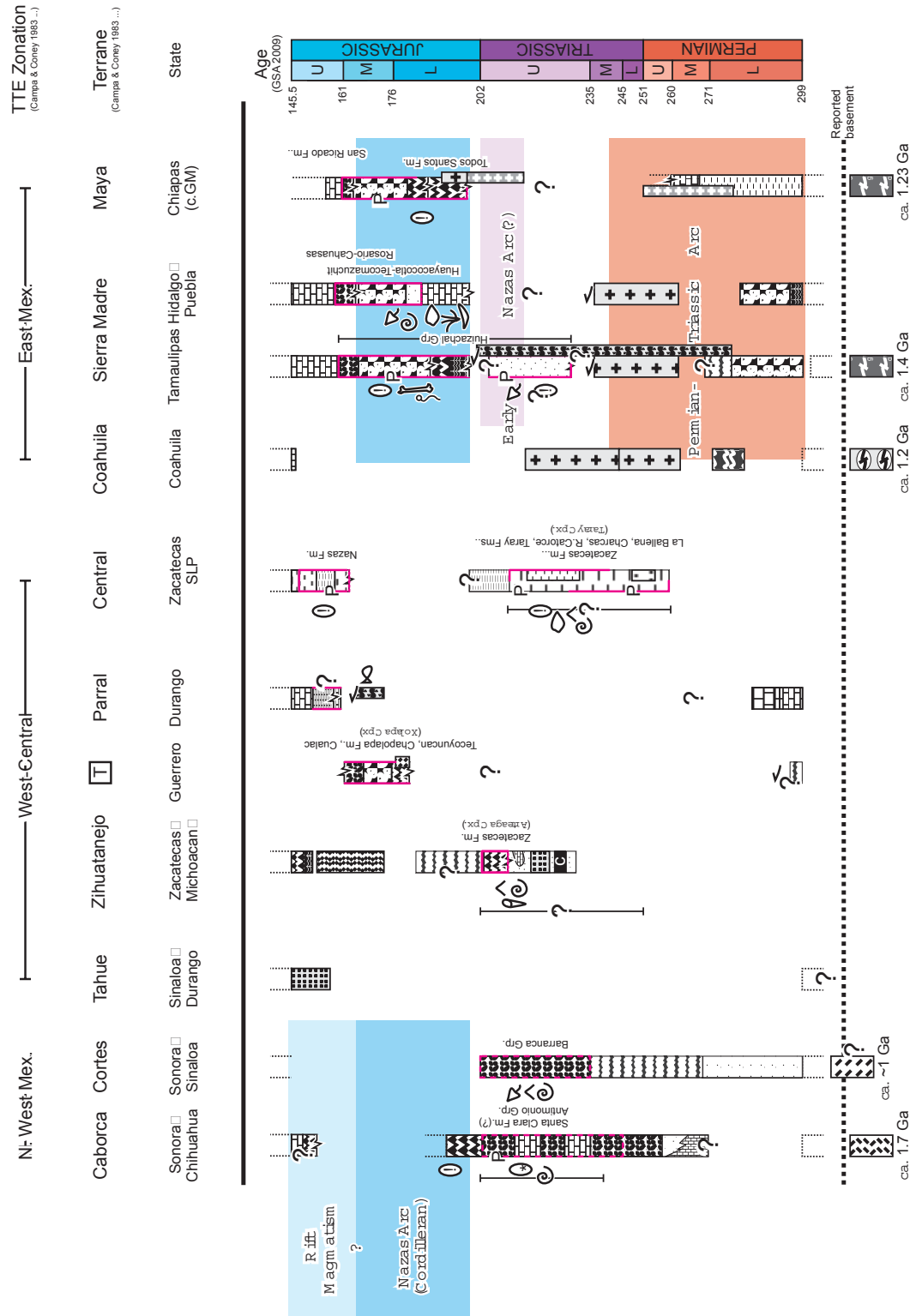
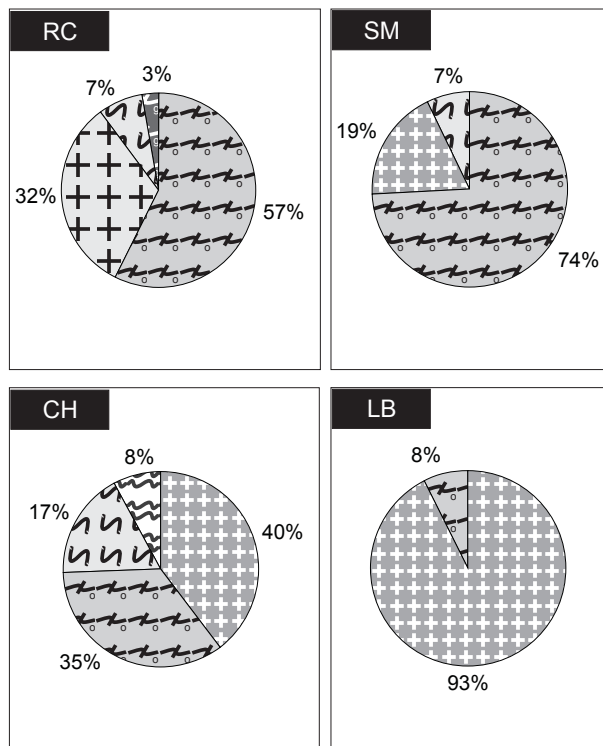


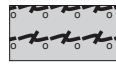
Fig. 7.13: Correlation table of key litho-stratigraphic columns with special emphasis on reported red beds in México (red frames), and the underlying Precambrian–Paleozoic crystalline basement with calculated ages. Data based on Centeno-García (2005), Lawton *et al.* (2010), and other various authors cited on this work. c.GM– circum Gulf of Mexico. Pattern fills are located at the Appendix for Pattern Fills. Colors are from International Stratigraphic Chart 2009.



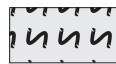
Grenvillite grains (~1.6–1.3 Ga)



Oaxaquia grains (~1.3–1.0 Ga)



Early Paleozoic grains (430–300 Ma)



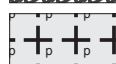
Silurian-Devonian Arc grains (199–164 Ma)



Rheic Tect-Mag grains (~440–300 Ma)



Permian Arc grains (~302–339 Ma)



Permo-Triassic (296–222 Ma)



Triassic Arc grains (339–199 Ma)



Early-Middle Jurassic grains (199–164 Ma)



Fig. 7.15: Pie charts for detrital zircons from Late Triassic sandstones data at Barboza-Gudiño *et al.*, 2010. RC– Real de Catorce. SM– San Marcos. CH– Charcas. LB– La Boca.

Along the basin genesis and before the sedimentary cover buries the deposit into a continuum stage of subsidence, there is a prevalence in the course of the El Alamar paleoriver delivering sediment to the Potosí fan from the Texas uplift with high compositional indices from the framework content of metamorphic lithics, polycrystalline, and monocrystalline quartz (Fig. 7.14). The dominant sources are Precambrian and Paleozoic rocks from nearby basement composite massifs (Fig. 7.15). Detrital modes fundament an increasing depth of erosion level (undissected stages) to establish a recycled orogen provenance (Fig. 7.16). The reported compositional trend for the Late Triassic alludes to a tectonic evolution of a rift basin-type.

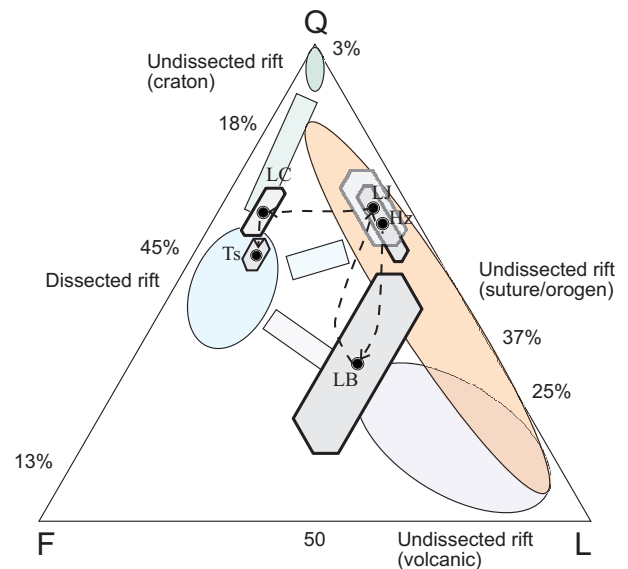


Fig. 7.16: Ternary system QFL to discriminate tectonic environments within rift-type basins. After Garzanti *et al.* (2001) modified by Marsaglia *et al.* (2007). Polygons represent the standard deviation for each formation: Hz– Huizachal (referred to El Alamar Formation); LB– La Boca; LJ– La Joya; LC– La Casita; Ts– Taraises. Data representation after Rubio-Cisneros and Ocampo-Díaz (2010) and Ocampo-Díaz and Rubio-Cisneros (*submitted*)

Rubio-Cisneros and Ocampo-Díaz (2011a) suggested that by using compositional discriminant function values the reported rift recorded on the formations or sedimentary sequence for northeastern Mexico has no strict sense of genetic relationship to a rift system as described by Buck (1991, 2004). He states there must exist a tectonic force operated by magmatic accommodation commonly during the modes of continental extension in a rift, which is commonly known as an extra subsidence or the *underplate paradoxen*.

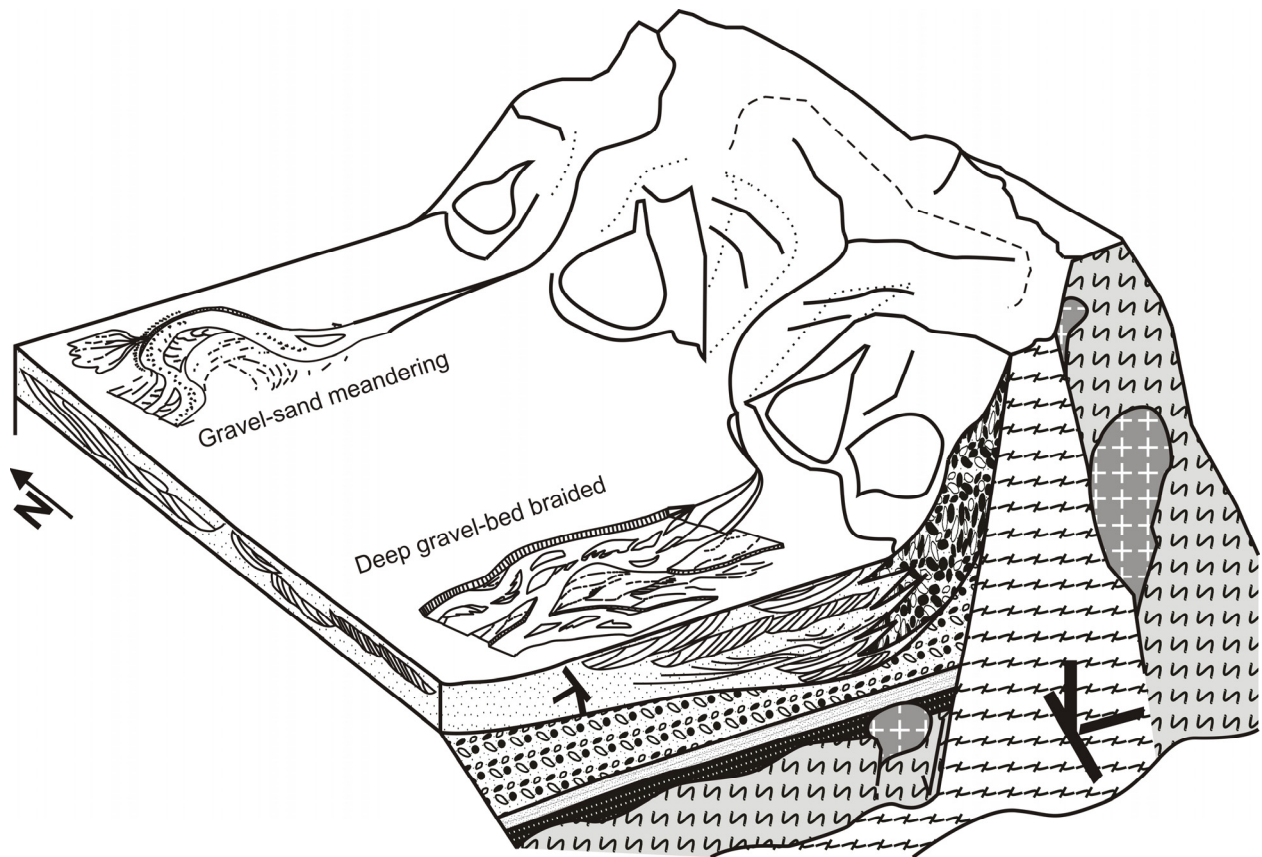


Fig. 7.17: Sketch for El Alamar Formation depositional environment, with its probable source rocks. Fluvial styles are oriented according the measured paleocurrents. Subsurface interpretations include the interpreted fluvial-architectural design, and the underlying units from the Precambrian– Paleozoic crystalline basement. Rock-type pattern fills are in Appendix.

Alternatively, when the tectonic mechanism relies only on lithospheric thinning the patterns of preexistent weak zones contribute for extension into an *amagmatic paradox* (e.g., Milanovsky, 1983; Milani and Davison, 1988; Magnavita *et al.*, 1994; Magnavita and de Silva, 1995; Olsen, 1997; Hopper and Buck, 1998).

In addition, the tectonic force needed for amagmatic extension of initially thick lithosphere may be up to an order of magnitude greater than the available (Kuszniir and Park, 1987; Hopper and Buck 1993; Buck, 2004). Particularly this incongruent basin genetic relationship in northeastern Mexico is determined by the lack of alkaline volcanism and the morphological complexity of the crystalline basement, its physical characteristics, distribution, and the preexisting fault array system. Therefore, the recorded rift is the southernmost expression of the asymmetric circum-Atlantic rifting; it is governed primarily by strike-slip systems, and with a no magmatic history (Ocampo-Díaz, 2011). If this late statement is correct then the strict rift lays in the Gulf of Mexico (Pindell *et al.*, 2002; Mickus *et al.*, 2009). The composition of sandstones reflects their native depositional system, its relationship to the structural style, and the processes dependant to the plate-tectonic setting.

The absence for an associated bimodal volcanism signature from pre- and syn-rift stages on El Alamar Formation for the Late Triassic enables to propose a rigid crystalline basement crust with characteristics of a dense crust. This configuration for northeastern Mexico enables that when thinning of the thermally dense lithosphere an initial uplift and source rocks exposure iniciates. The crust is covered by a sequence related to

recycling and cannibalism from basement rocks and sedimentary cover with fault array activation and rift extensional activity in an amagmatic zone.

7.7.2. Jurassic

7.7.2.1 Early–Middle Jurassic

During the Pliensbachian–Aalenian (~189.5–171.6 Ma) Mexico was configured by the exerted controls from a frontal subduction at the paleo-Pacific margin in North and South America, and by the separation between South America and Africa (Dickinson and Lawton, 2001; García-Díaz, 2004; Pindell and Kennan, 2009; Pindell *et al.*, 2009). The opening of the Gulf of Mexico remained restricted and contributes for the sedimentation of continental deposits in valleys subordinated by flanking horsts. The Yucatan block lay near the present coast of Tamaulipas (Godinez-Urban, 2009; Godinez-Urban *et al.*, 2011a).

The West Pangaeian arc, a convergent plate margin at the paleo-Pacific (Dickinson and Lawton, 2001), favored the emplacement of volcano–plutonic rocks in the buried petrotectonic sets (e.g., Sierra Madre and Maya Block). The plate margin convergence direction varied in its angle of incidence, with a low angle at the north (Sinaloa–Sonora–Arizona–California) and a higher angle at the center of the Mexican territory (Fig. 7.18).

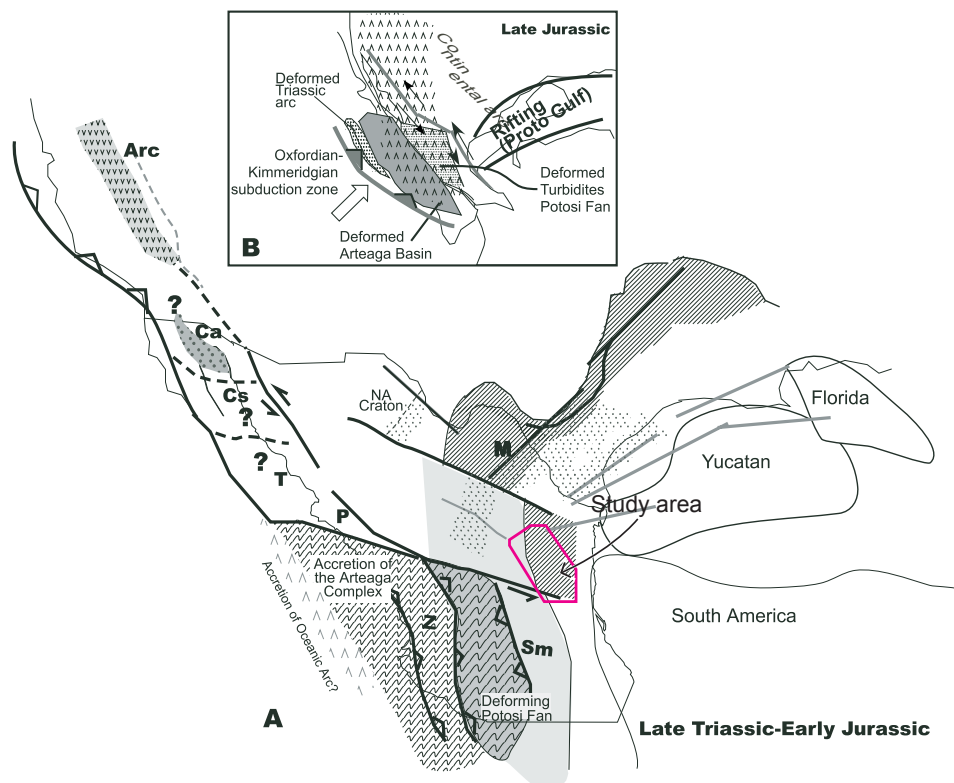


Fig. 7.18: (A) Tectonic reconstruction by Early Jurassic time. Rocks of Triassic submarine fan and Triassic ocean basin were accreted toward continental margin. (B) After collision of Arteaga basin, arc magmatism was widespread in Zihuatanejo, Central, and Sierra Madre terranes. Abbreviations of names for terranes after Centeno-García *et al.*, 2005.

The convergent forces of continental arcs in the central zone of Mexico influenced for nonmarine deposits, marginal marine, and volcanic successions [Nazas Arc–Chapolapa–Todos Santos; Fig. 7.19], with genetically related basins interpreted as fore arc, back arc, and intra arc (e.g., Busby, 1988a; Busby *et al.*, 1998; Bassett and Busby, 2005; Busby *et al.*, 2005; Barboza-Gudiño *et al.*, 2008; González-León *et al.*, 2009; Venegas-Rodríguez *et al.*, 2009; Rubio-Cisneros *et al.*, 2011; Rubio-Cisneros and Lawton, 2011, Godínez-Urban, 2009).

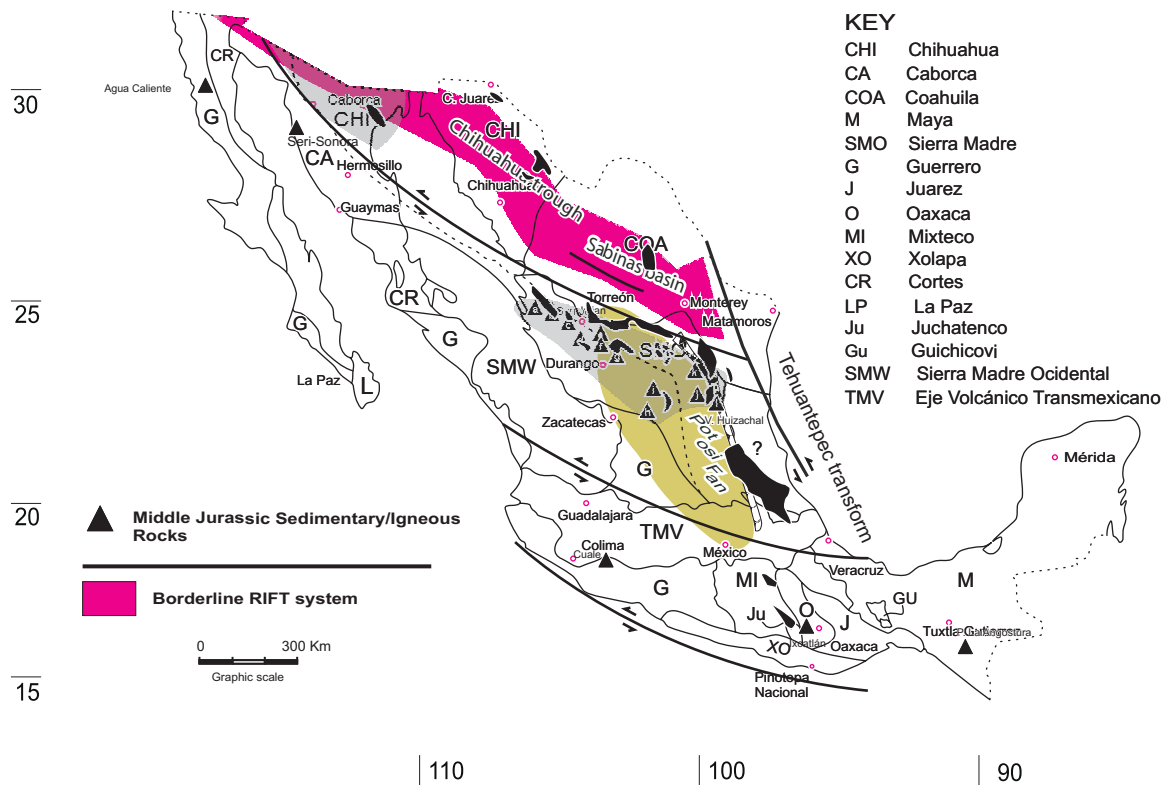


Fig. 7.19: Compiled geological elements interpreted for the Early–Middle Jurassic depositional environments, adapted from Campa and Coney (1983), Centeno-García (2005), Anderson *et al.* (2005), García-Díaz (2004), and Mickus *et al.* (2009). Notice the black polygons that represent Jurassic outcrops. Borderline RIFT system is now considered Border Rift System to avoid confusion with Cenozoic California Borderland province related to strike-slip faulting. Border Rift System is defined by siliciclastic.

The volcanic rock composition oscillated between intermediate and felsic, ranging from basaltic-andesitic lavas to intermediate compositional pyroclastic rocks, and rhyolitic-rhyodacitic domes ca. ~ 230 Ma to 189 ± 0.2 Ma (Fig. 7.20; Bartolini, 1998; Bartolini *et al.*, 2003; Fastovsky *et al.*, 2005; Barboza-Gudiño *et al.*, 2008; González-León *et al.*, 2009; Venegas-Rodríguez *et al.*, 2009; Chiapas: Castro-Mora *et al.*, 1975).

The volcanic successions from the Nazas–Chapolapa–Todos Santos arcs are characterized by complex pyroclastic flow deposits (lahars, ignimbrites and other types of tuffs) and volcanic debris flows (Mixon, 1963; Schermer and Busby, 1994; Fackler-Adams *et al.*, 1997; Godínez-Urban, 2009).

In northeastern Mexico the nature of the extensional basin-fill was related to subsidence rate in the valleys of the extensional depocenter. Volcanic activity had a mayor influence on sedimentation at an extensional setting.

The sedimentary scenario includes a transitional crust juxtaposed by a dynamic effect from the basin-forming mechanism of subduction. Sediments accumulated between the volcanic center and the basement barriers from the future Huizachal-Peregrina Anticlinorium, and deposited in an individual (half-?) graben separated by interbasinal ridges. La Boca Formation was deposited by dominant axial longitudinal drainage systems parallel to basement axis. The entry point of clastics into the Valle de Huizachal depocenter was from an axial flowing fluvial system. Valley incision controlled sediment routing systems to construct fluvial styles. Rivers incised into bedrock and alluvial sedimentary gravity flows with banks of sediments (Fig. 7.21). Rivers incised (avulsion) by sediment load plucking of blocks from the bed and cavitation (Hancock *et al.*, 1998).

The lower member of La Boca Formation is restricted to a mechanism of asthenospheric flow due to subduction of cold lithospheric slabs that change the temperature in the mantle. Thermal differentiation on a region floored by continental lithosphere previously extended may undergo extension within the arc system. [Back arc] extensional basins may form with extensional arc systems where the velocity of the roll back exceeds the oceanward velocity of the overriding plate (e.g., Allen and Allen, 1990; Busby *et al.*, 2002).

The upper member of La Boca formation tends to low sediment supply rates compared to the tectonic subsidence rate. This stratigraphic interval depends on the sediment accumulation over the duration of the eustatic loading or flexural mechanism. A plausible explanation for these processes is the presence of several unconformities underlying La Joya Formation at the Valle de Huizachal.

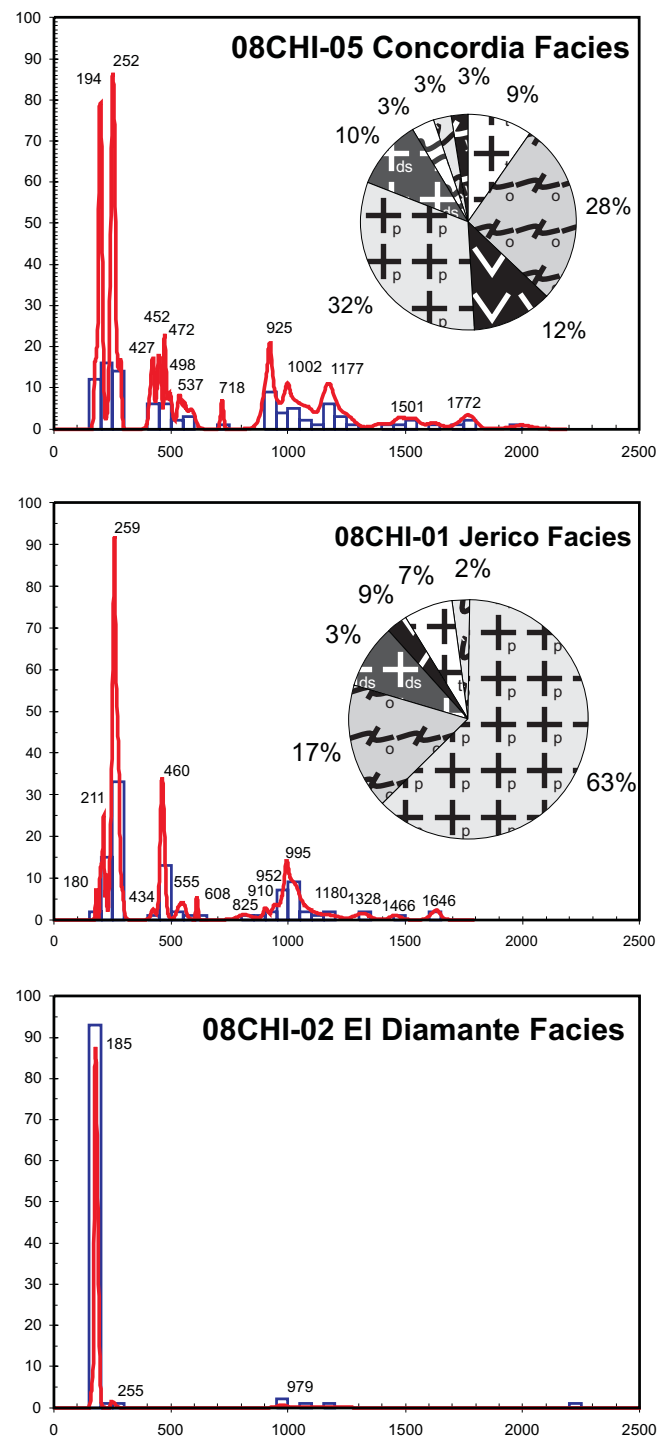


Fig. 7.20: U-Pb age probability plots and pie charts for the main group of detrital zircons in the Todos Santos Formation (Godínez-Urban, 2009; Godínez-Urban *et al.* 2011a and Lawton *et al.*, 2010). Pattern fills can be consulted at Fig. 7.15.

A plausible explanation for these processes is the presence of several unconformities underlying La Joya Formation at the Valle de Huizachal.

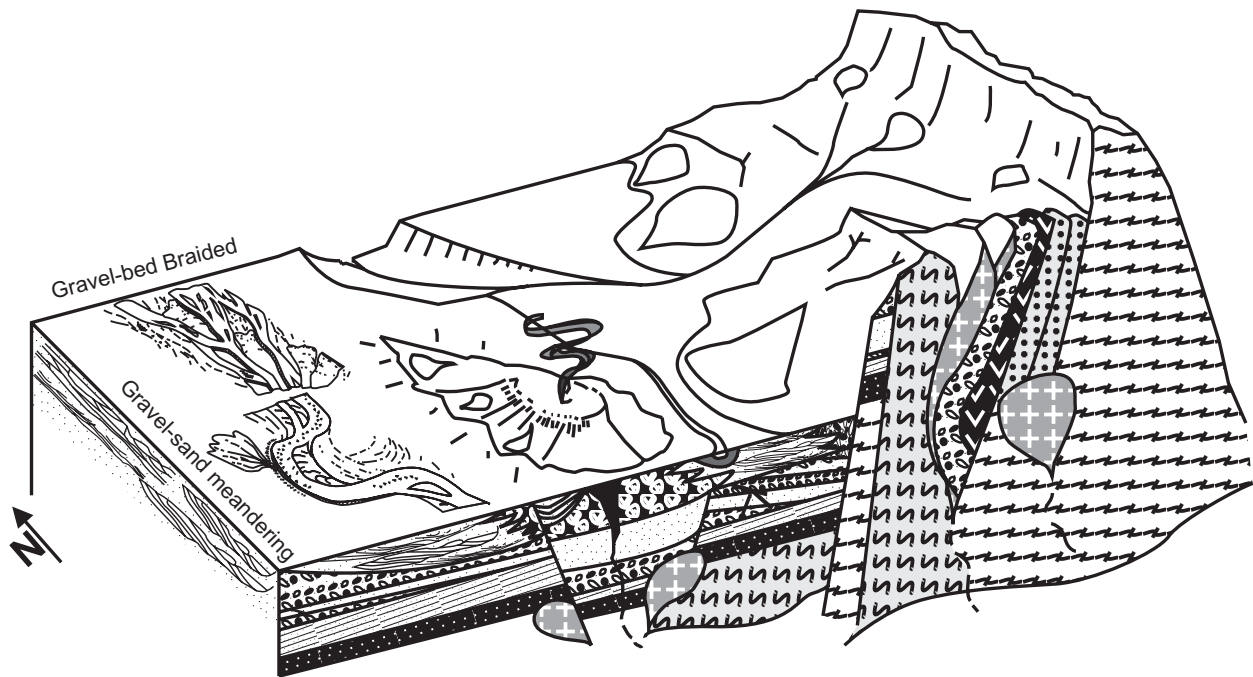


Fig. 7.21: Sketch for La Boca Formation depositional environment, with its probable source rocks. Fluvial styles are oriented according the measured paleocurrents. Subsurface interpretations include the interpreted fluvial-architectural design, and the subsequent underlying depositional sequences form El Alamar Formation, and the Paleozoic-Precambrian crystalline basement. Rock-type pattern fills are in caption for Fig. 7.17.

Subduction did not deform La Boca Formation and the rest of the Huizachal Group probably because the strike-slip or transtensional tectonics at the paleo-Pacific border extended into northeastern Mexico (Fig. 7.22; see Bassett and Busby, 2005) probably since the Late Triassic (Turner 2001; Alejandro-Torres, 2010). Obliquely convergent margins with strike-slip partitioning favor wrench-dominated transpression because the instantaneous strain is consistent with transcurrent movement, whereas finite strain records contractional deformation (e.g., Teysier and Markley, 1995).

La Boca stands for an abrupt compositional signature variation in source rocks, conditioned by the compositional and nature of a manifesting adjacent arc and pre-established rocks. Principal components suggest rejuvenation of

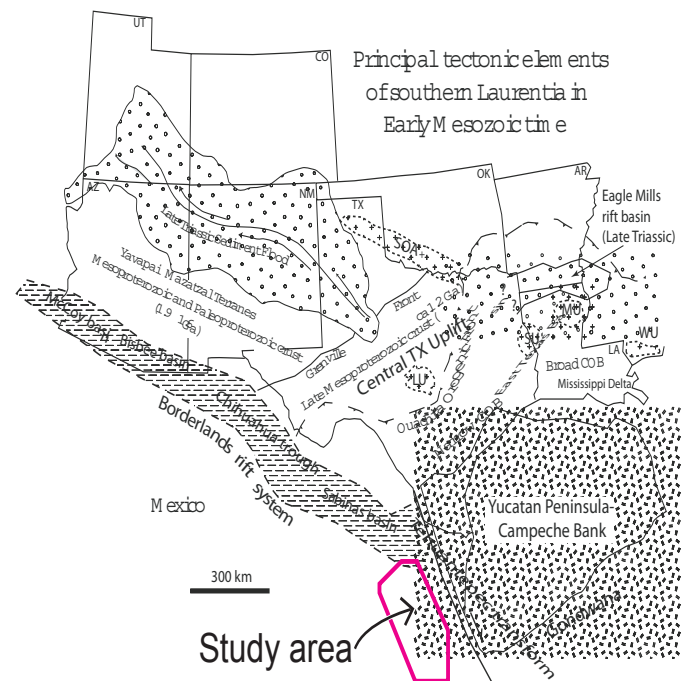


Fig. 7.22: Early Mesozoic tectonic map of southwest Laurentia (after Mickus *et al.*, 2009). Borderlands rift system is now considered Border Rift System to avoid confusion with Cenozoic California Borderland province related to strike-slip faulting. Border Rift System is defined by siliciclastic. Buried and partially exposed uplifts of interest: WU– Wiggins Uplift, LU– Llano Uplift. COB– Continent-ocean boundary.

Principal components suggest rejuvenation of

source areas related to the input of lithic fragments from volcanic and metamorphic composition, and feldspars (Fig. 7.14).

7.7.2.2 Middle Jurassic

Beginning in Middle Jurassic time, a shift in the subhorizontal subduction existed for massive coarse-grained red beds to generate from exhumation and erosion of the petroTECTONIC assemblages and their pre-Mesozoic sedimentary cover (e.g., La Joya and San Ricardo Formations). This lapse enhanced rejuvenation of basement faulting and source areas (e.g., Ocampo-Díaz and Rubio-Cisneros, *submitted*).

In addition, North–South America, and Africa developed a major fragmentation (Marton and Buffler, 1994; Marton, 1995; Pindell and Kennan, 2002; Bird, 2004; Bird *et al.*, 2005; Pindell *et al.*, 2006; Fillon, 2007; Pindell *et al.*, 2009). The mid-angle subduction that prevailed at the north of the Mexican territory generate continental arcs: Alisitos (Baja California, Sonora, Sinaloa, California, Arizona; Busby-Spera, 1988b; Shermer and Busby, 1994; Goldhammer, 1999; Critelli *et al.*, 2002; Busby, 2004; Basett and Busby, 2005, Busby *et al.*, 2005, Vega-Granillo *et al.*, 2008; González-León *et al.*, 2009).

At ~173 Ma the Cordilleran magmatic arc, the subducting plate, and volcanic trench experienced rollback into the west with evidences at Zacatecas, San Luís, Potosí, Sonora y California; although the arc migrated, the plate rolled back and the trench retreated (Fig. 7.23; Dickinson, 2004; Anderson *et al.*, 2005; Busby *et al.*, 2005; González-León, 2005; Wright and Wyld, 2007; Fastovsky *et al.*, 2005, Barboza-Guidiño *et al.*, 2008, Godínez-Urban, 2009; Rubio-Cisneros and Lawton, 2011; Ward, 1995; Rosaz, 1989).

The plate motion to the west contributes for a more advance stadium of breakup of Pangea with the separation of the Yucatan Block.

The influence of tectonic effects was intensified to the middle of Middle Jurassic with a major asthenospheric thermal event (Zacatecas, Durango), basement exhumation (Nuevo León, Tamaulipas), and volcanic emplacements an successions (Guerrero, Chihuahua, Sinaloa?, California; Damon *et al.*, 1981; Molina-Garza *et al.*, 1992; Morgan, 1983; May 1971).

The cooling of the Lower Jurassic volcanic successions and the sediment accumulation lead to a partial loading or flexural basin-forming mechanism. Thickening of the lithosphere by cooling causes subsidence and fault reactivation from previous extensional arrays. Dynamic effects of asthenospheric flow may also cause subsidence. The buoyancy effects of changes in temperature in the mantle with the uplift of the Early Jurassic continental arcs and basement blocks controlled the subsidence during Middle Jurassic.

However, subsidence may have also been related to isostatic consequences in changes in crustal and lithospheric thickness by extensional tectonics and sedimentary carapace erosion (e.g., Sholz and Contreras, 1998; Prosser, 1993; Ingersoll and Busby, 1995; Miall, 1999; Allen and Densmore, 2000; Bruijne and Andriessen, 2000; Gupta and Cowie, 2000; Einsele, 2000; Corner *et al.*, 2002; Menzies *et al.*, 2002; Hansen and Nielsen, 2003; Allen and Allen, 2005; Nittrouer *et al.*, 2007; Bradley, 2008; Hsiao *et al.*, 2010).

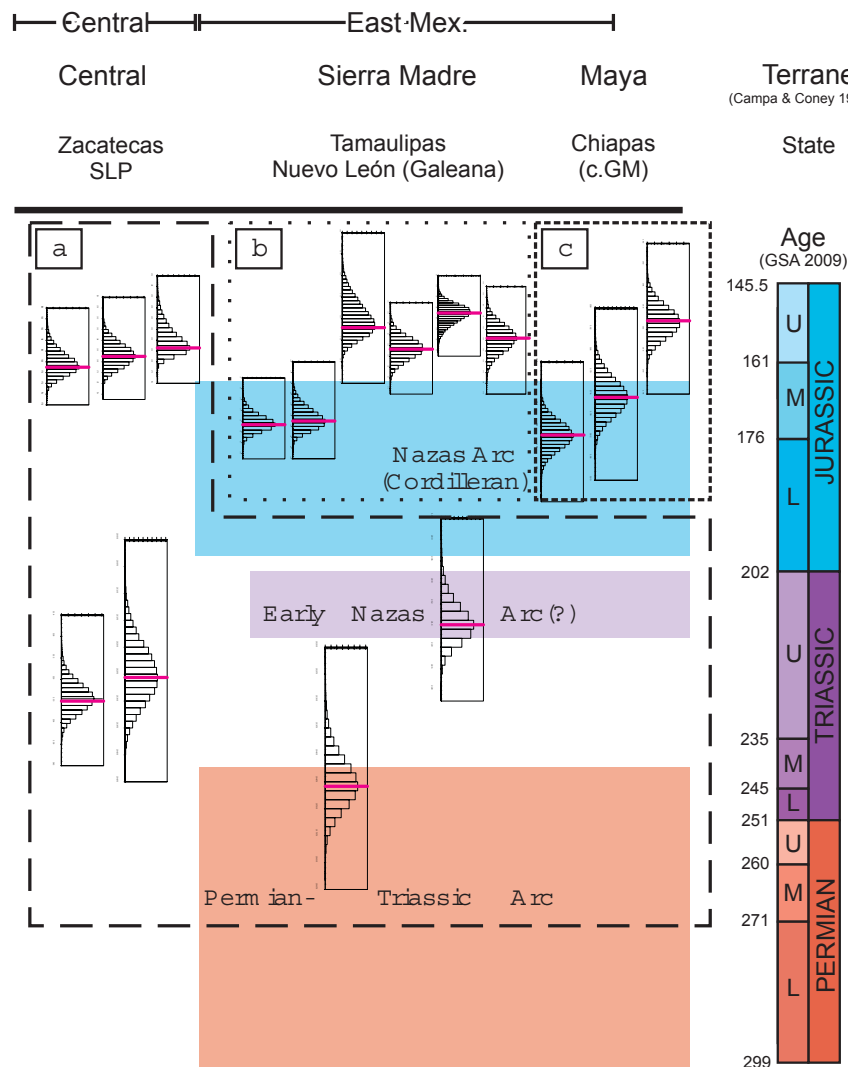


Fig. 7.23: Youngest U-Pb detrital zircon ages and tectonomagmatic events from for correlated red beds at different localities in México. Notice the volcanic age variability. Sketch adapted from Lawton *et al.*, 2010. Plotted data from: a– Barboza-Gudiño *et al.* (2010), b– Rubio-Cisneros and Lawton (2011); Lawton *et al.* (2010), and c– Godínez-Urban *et al.* (2011a); Lawton *et al.* (2010). SLP– San Luis Potosí; c.GM–circum Gulf of Mexico

Whichever mechanism was operating they juxtaposed tectonic scenarios of a roll back at the west (Pacific) and a spreading center at the east (Atlantic).

On the Early to Middle Jurassic there is a magmatic arc extensional rate activity developing a back arc basin-type, with source rocks generation or rejuvenation. The thinning of the compositionally low-density crust causes subsidence, and is represented by the different angular unconformities and the sedimentary recycling index (SeReIn) values recorded in the sequence. The latter should consider that the total initial and long-term effect of stretching typical continental lithosphere is regional subsidence (McKenzie, 1978).

This could have lead to the development of the Monterrey–Miquihuana Trough by the Late Jurassic–Early Cretaceous with the deposition of a thick sedimentary sequence of the La Casita Formation on a strike-slip basin-type (Rubio-Cisneros and Ocampo-Díaz, 2010).

La Joya formation records the initiation of a juvenile oceanic spreading center. The related extensional tectonics with faulting ends with the reactivation of older pre-existing normal faults from the deeply subsiding depocenters, which were walled off by major border faults. La Joya sediment supply was concentrated at accommodation of alluvial rivers with beds and banks of sediments caused by an isostatic shift.

The Middle Jurassic is characterized by a tectonic period of intermixing or transitional tectonic configurations that developed over crustal heterogeneities with old rigid basement and juvenile carapace. These conditions were set in motion since the Late Triassic. The La Joya Formation represents a lack on similarity of compositional signature to a specific basin-type (Rubio-Cisneros and Ocampo-Díaz, 2011a). The La Joya remarks a period with evident changes in rock associations in which the unstable components progressively disappear with a subsequent low-rate recycling from the preexisting formations, suggesting a moderately input form sedimentary sources but major contribution from metamorphic rocks (Fig. 7.14; Fig. 7.16; Fig. 7.24).

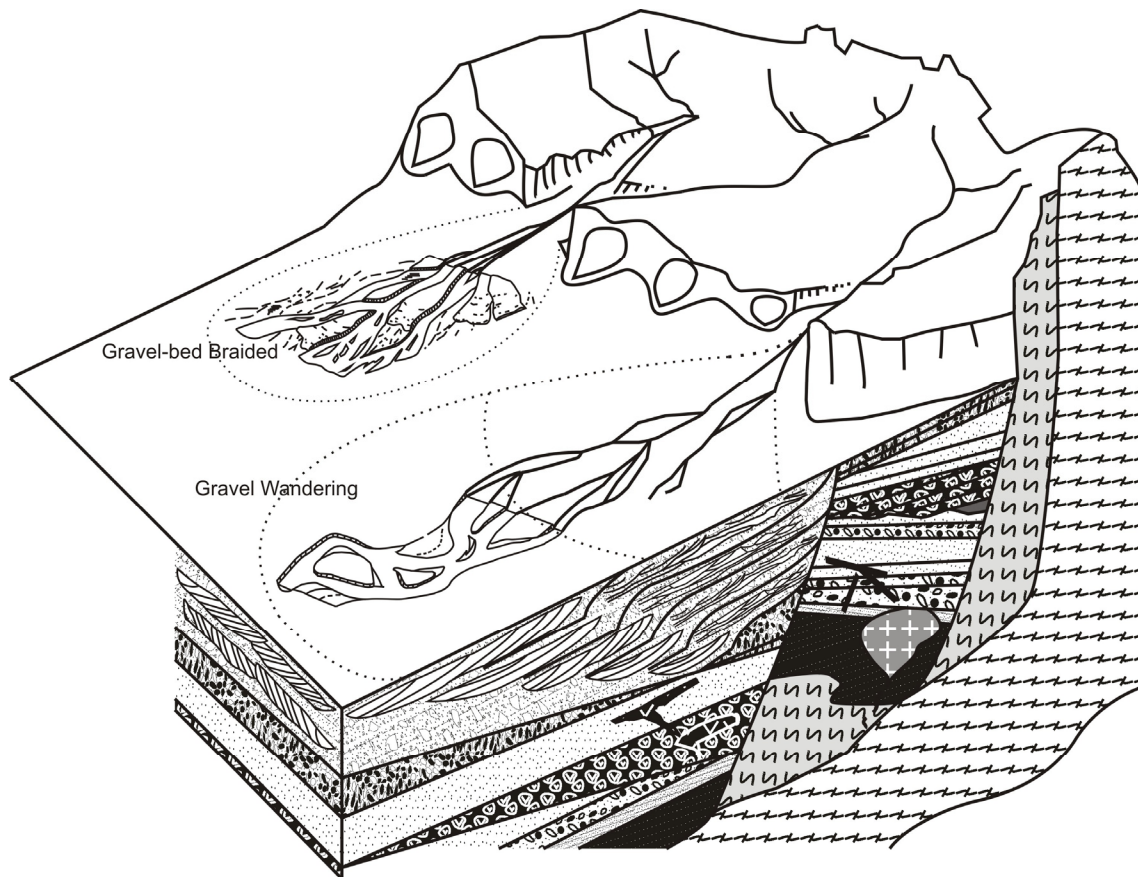


Fig. 7.24: Sketch for La Joya Formation alluvial fan with its fluvial style depositional environments and its most probable source rocks. Fluvial styles are oriented according the measured paleocurrents. Subsurface interpretations include the interpreted fluvial-architectural design, and the subsequent underlying depositional sequences form La Boca and El Alamar formations, and the Paleozoic-Precambrian crystalline basement. Rock-type pattern fills are in Fig. 7.17.

Hybrid or mixed-transition compositional basins are a product of hybrid tectonics settings and a sedimentary cyclic diversion. Basins are classified according to its tectonic setting at the time of deposition of a given stratigraphic interval. In addition, because the tectonic activity may change rapidly stratigraphic intervals may present different detrital mode values that reflect a hybrid compositional record. Hence, any type of (compositional) basin can evolve to any other basin-type whenever elements from both volcano-bounded and

fault-bounded types merge (e.g., rift to back arc). These are best represented by troughs with normal, reverse, or strike-slip faults along part or in all of their margins, but where most of the topography/bathymetry relief is defined by constructional volcanic ridges (Ingersoll and Busby, 1995).

La Joya Formation pinches out onto basement highs and is overlain by Oxfordian evaporate strata (Salvador, 1987). The uppermost La Joya Formation marks the onset of prolonged Late Jurassic marine transgression (Winkler and Buffler, 1988; Rueda-Gaxiola *et al.*, 1991; Goldhammer, 1999). Drifting at the east from the nuclear Mexico enhanced a major separation of Pangea. The sea floor spreading detached and translated Yucatan, activating normal faults in areas once occupied by the Yucatan Block and where newly formed sabkhas emerge (Salvador, 1987; Salvador, 1991; Marton and Buffler, 1994; MacRae, 1994; Marton, 1995; Alaníz-Álvarez *et al.*, 1996; Pindell *et al.*, 2006; Fillon, 2007; Pindell and Kennan, 2009). Nonmarine salt brines invaded the paleoborders from elevated tectonic elements that testify the interaction between terrigenous clastic depositional systems and evaporites (La Gloria and Olvido Formations). During the Oxfordian the Yucatan Block continues a displacement and rotation for the first related deposits of the Tethys Sea incursion.

The displacement of the Maya Block during the aperture of the Gulf of Mexico occurred along the Tehuantepec transform, also known as the Tamaulipas-Chiapas or Poza Rica (Pindell, 1985; Sánchez-Barreda, 1981; Ortega-Gutiérrez *et al.*, 1994; Dickinson and Lawton, 2001; Pindell *et al.*, 2006; Dickinson, 2009; Mickus *et al.*, 2009; Salvador, 1987; Bird and Burke, 2006). This structure favored the displacement and rotation of the Yucatan Block into the south with counterclockwise loci of $\sim 10^\circ$ (Fig. 7.25; Molina-Garza *et al.*, 1992; Dickinson and Lawton, 2001; Pindell and Kennan, 2002; Pindell and Kennan, 2009) and $\sim 45^\circ$ (Godínez-Urban, 2009; Godínez-Urban *et al.*, 2011).

The join between the Tehuantepec transform fault and Texas or the Volcanic Rift Margin marks the termination of the California–Coahuila Rift or the Border Rift (Marton and Buffler, 1994; Lawton and McMillan, 1999), which extends E-SE south from California to northeastern Tamaulipas (Marton and Buffler, 1994). These Rift segments contain the McCoy–Bisbee–Chihuahua–Sabinas basins with aulacogen characteristics. The borderland rift system meets on a regional doming, possibly due to a mantle plume or other cause of buoyant mantle, near the mouth of the Rio Grande at $\sim 120^\circ$ angles (Mickus *et al.*, 2009).

The temporally related tectonic systems with extensional, transform, and subduction characteristics in the Mexican territory may have generated major faulting segments for the geo-setting of the Late Jurassic (e.g., Mojave–Sonora Megashield Anderson and Silver, 1979; Iriondo *et al.*, 2005; Molina-Garza and Iriondo, 2005; Anderson and Mahoney, 2006). Faulting arrays developed strike-slip basin-types with basin-fills from Early–Middle Jurassic arc-related sequences, like the Monterrey Trough on the Late Jurassic–Early Cretaceous with the deposition of a thick sedimentary sequence from the La Casita Formation (Ocampo-Díaz, 2011).

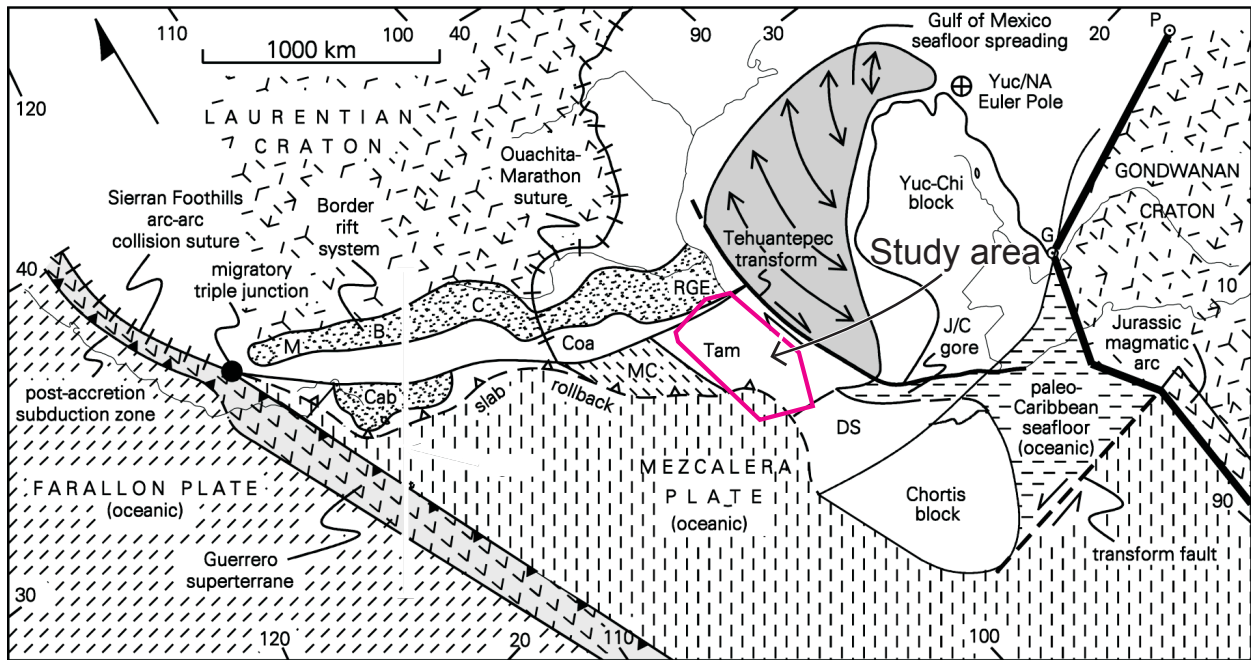


Fig. 7.25: Geotectonic reconstruction of Mexico from Middle Jurassic time (164 Ma, base of the Callovian) to the Jurassic-Cretaceous time boundary (144 Ma). Euler pole for Yucatán (Yuc) rotation (anticlockwise) with respect to North America (NA) after Marton and Buffler (1994). South of migratory triple junction, solid barbs are on overriding plate of Guerrero intraoceanic island-arc complex, and open barbs are on dormant continental-margin subduction zone (subducted slab rolling back to induce intra-arc rifting within continental margin). Abbreviations: B–Bisbee basin, C–Chihuahua trough, Cab–Caborca block, Coa–Coahuila block, DS–Del Sur block, G–Guajira Peninsula, J/C–Juarez/ Cuicateco terrane, M–McCoy basin, MC–Mesa Central subduction complex, P–Península de Paria, RGE–Rio Grande embayment, Tam–Tampico block, Yuc-Chi–Yucatán-Chiapas block. From Dickinson and Lawton, 2001).

8. CONCLUSIONS

This work focuses on the nature (qualitative and quantitative) of a systems approach in sedimentary geology phenomena, rather than a developmental approach.

Stratigraphy and Sedimentology

The depositional systems of northeastern Mexico for Upper Triassic to Middle Jurassic red beds are grouped by three main formations. El Alamar, La Boca, and La Joya formations make up the Huizachal Group, with depositional ages that oscilate from Middle–Upper Triassic to Lower–Middle Jurassic. The depositional environments, facies and age, which are linked to the process of sediment routing and specific basin-forming mechanisms, define the succession. Geological processes gave pace for the distribution and type of source area. The different driving mechanisms for tectonomagmatic events condition the activation for allogenic and autogenic factors that are printed in the sink.

Facies (lithofacies, facies associations) and architectural element analysis in the studied area indicate the evolution of continental depositional environments, consisting of gravel- and sand-dominated rivers with high and low sinuosity characteristics. The Huizachal Group records fluvial styles that oscillated from mix-energy to low- and high-energy systems. High- and mix load systems transported fluvial products from basement highs on the east (e.g., Huizachal-Peregrina Anticlinorium), with the formation of sedimentary gravity flows and gravel bed bars. Sediments were shed to the main areas from the southernmost escarpment of the Texas Uplift and the west footwall from what is now the Huizachal-Peregrina Anticlinorium.

Fluvial style was a complex response to a number of autocyclic and allocyclic controls. Allogenic factors produce effects over depositional styles, depositional systems, and basin settings. Autogenic factors incorporate variations in composition (facies) and geometry of sand bodies. Effects like shifts in sediment flow, accommodation, and supply depend on the magnitude and scale for each factor. Effects like amalgamation, aggradation, degradation and flooding were interpreted by surface architecture found on bounding surfaces. Low accommodation/supply processes stack fluvial elements one another into high subsidence rates. Meanwhile, high accommodation/supply processes control-flooding environments and conditioned sediment dispersion of low suspended load styles. The facies models use to explain the association of facies helps to elucidate the latter. Factors are best constrained by allostratigraphic techniques, with architectural element analysis and surfacetypes treated as approaches under the auspice of allostratigraphy.

Petrography

Compositional variations in the Huizachal Group resulted from petrogenetic randomization in nature and the heterogeneity of the sources. Comparative analyses of light and heavy minerals, and geochemistry that compositional characteristics for the Huizachal Group are defined by the litho-tectonic evolution of the

basement, volcanic successions, and the geology of fluvial styles of Upper Triassic to Middle Jurassic sedimentary cover.

The [multi-] stages of geologic evolution for the Huizachal Group are recorded in petrofacies from detrital modes of sand and on heavy mineral indices, which explain specific source rocks and tectonic setting. Petrofacies suggest detrital input from (1) low- to high-grade metamorphic rocks and recycled sedimentary detritus from preexisting units of schist and slates (metapelite [Lmp_{2,3-4}], metapsammite/metafelsite [Lmf_{2,3-4}], metabasite grains [Lmb₁₋₂]; and (2) volcanic and epiclastic rocks with felsic, basic, and plutonic/granitic sources (microlitic and felsitic textures, lathwork lithic fragments, phaneritic–equigranular, and tuffaceous textures).

Heavy mineral indices were chiefly provided by (i) low- to high-grade metamorphic source rocks (LgM, Gt, HgM), (ii) the subsequent input from amphiboles (Hb, &A), pyroxenes (CPX, OPX), olivine, and spinel (OS) were largely supplied by the rejuvenation of intermediate, mafic source rocks, and (iii) an enrichment in heavy mineral assemblages was derived from sedimentary and felsic igneous source rocks (ZTR).

The sediment genesis for the Huizachal Group developed over crustal heterogeneities from old rigid crystalline basement units and juvenile volcanic carapace. The results from petrofacies and heavy mineral indices support an interpretation for a genesis of an extensional basin by the uplifting of basement massifs that evolved from (1) an undissected rift (suture/orogen) within an *amagmatic paradox* lithospheric thinning, (2) to a subsequent extensional back arc, and (3) a final stage of tectonic reactivation with exhumation and unroofing of the underlying strata.

Sandstone composition from each formation represents the terminal print for source-to-sink sediment flux across each tectonic setting. The relationship between sediment composition and erosional evolution of source areas provides sufficient data to guide a better interpretation for depocenters and the type of source area rejuvenance by using the sedimentary recycling index.

Geochemistry

Whole-rock geochemistry of the Huizachal Group is controlled by the sediment classification from the mixture of detritus of high- to low-grade metamorphic, dominant intermediate–felsitic volcanic, and minor constituents from plutonic provenance, albeit in different proportions for sedimentary recycling, mineral fractionation, and weathering.

Two main geochemical groups, clastics and volcanics, eventually dominated the tectonic setting during the genesis of the Huizachal Group. The clustering of major elements gives a general interpretation for the mineral and chemical attribution from argillaceous minerals, phyllosilicates, feldspars (Al₂O₃–P₂O₅–K₂O), heavy mineral assemblages (TiO₂ and P₂O₅), and ferric fraction from epimatrix or indicator minerals of volcanic aggregates (Fe₂O₃, MgO, TiO₂, and Cr₂O₃).

Classification– Sandstones for the Huizachal Group are geochemically classified as lithic arenites, with slight variations to arkose, subarkose, and greywacke. Clastics reveal a litharenite to sublitharenite (SiO₂) classification and a profound heterogeneity of the sources; from the grouping of progressive alteration in

feldspars, clay minerals, and an input of the mica group ($\text{Al}_2\text{O}_3\text{--P}_2\text{O}_5\text{--K}_2\text{O}$). Clastics represent more mature sandstones than volcanics, richer in matrix and rutile content (TiO_2). Volcanics are classified under the nature of greywacke and arkose rocks (quartz: SiO_2 ; feldspars: K_2O), with an input from mafic minerals from epiclastic or acid rocks ($\text{Fe}_2\text{O}_3 + \text{MgO}$).

Source area composition— In correspondence with Bulk earth composition, both sets show similar patterns with enrichment from Large Ion Lithophile Elements (LILE: Rb, Cs, Ba, Sr), depletion of High fFeld Strength Elements (HFSE: Y, Zr, Nb, Hf, Th, U), and REE (La, Ce, Sm Yb). Nevertheless, samples for the clastics dataset are more enriched by LILE. Transition Trace Elements (TTE: Co, Ni, V, Sc) are derived mainly from phyllosilicates and other related minerals to volcanic and igneous sources (Al_2O_3 , Fe_2O_3 , MgO, TiO_2 , P_2O_5).

The occupied tectonic scenarios for the clastics and volcanics datasets (SiO_2 vs. the $\text{K}_2\text{O} / \text{Na}_2\text{O}$ ratio) are passive continental margin (i.e. to stable provenance areas), active continental margin, and arc setting.

The clastics sample set comes from intermediate and basic source rocks, but also indicates a more heterogeneous group apart from volcanics with metamorphic lithologies as phyllite for a source rock ($\text{SiO}_2 / \text{K}_2\text{O}$ of ~ 43 and ~ 520 for Ti/Nb; Th/Sc ratio). The volcanics dataset relies as a more homogeneous compositional set in a mixed zone meddling rhyolitic and basaltic compositions or differentiated sources ($\text{SiO}_2 / \text{K}_2\text{O} \sim 19$ and Ti/Nb ~ 446 ; Ti/Nb: 300–400).

Some samples may present a variable [confidence region] Ti /Nb ratio that reflects the main components from the available rock sources or principal components as a result of the strongly tectonized state of the related source-massifs, juxtaposed tectonic environments, and the great transport variability of the sedimentary environment. The volcanic localities show more differentiated Ti/Nb ratios indicating either different provenance areas (igneous and metamorphic) or compositional trends toward Upper Continental Crust.

The La–Th–Sc diagram for determining tectonic environments and a related source for provenance indicates active continental margins and passive margins for the volcanic set of samples. The clastics sample set display a mean compositional value for clays, silts, sands, and gravels from mixed sources of typical granitic gneiss and metabasic rock-types.

Weathering— CIA weathering index is capable of explaining the dissolution of a single mineral. The CIA mean compositional values for the clastics set fall within a value of ~ 60 and between ~ 39 for volcanics. Clastics data presents contracting Na^+ and Ca^{2+} modifications and change rock composition toward the A apex with even higher CIA values than the volcanic samples. The framework heterogeneity and a possibly distinct sorting history gave the clastics a higher proportion of clay minerals and consequently a higher CIA. Volcanic samples trend toward the A apex for samples approaching the A-K join with a weathering of an average granodiorite or upper continental crust resulting from the transformation of labile components made by volcanic rock fragments, feldspars, and plagioclase.

The MFW index supports the bulk geochemical response during weathering. The MFW values expressed for the volcanic sample set records a more felsitic–intermediate signature near the variance of igneous minerals with high F compositions or reference rocks samples of (1) rhyolite, (2) granite, and (2) dacite. Weathering

interpretations rely on evidence for processes affecting REE distributions during weathering of granitic rocks by the replacement of primary trace phosphatic minerals (e.g., monazite, allanite, apatite) by secondary LREE-enriched phosphates.

Samples from outcrops with volcanic affinity present REE concentrations controlled by mineral replacements, possibly hydrothermal, during liberation and encapsulated volcanic-related processes. Few of these samples show on the measured sections an upsection source area transition (volcanic < metamorphic).

Clastics present some rich igneous mineral samples with F–W trending join toward the W vertex, and represent a mineralogical weathering translation for the decomposition of plagioclases to kaolinite. But it also includes a transformation of muscovite to illite during weathering. This transformation is expressed with an increase in the W value, and a mineralogical translation along the M–W, probably attributed to the mineralogy from the underlying basement units (chlorite to biotite).

Radiogenic isotopes

U-Pb detrital-zircon ages from the Huizachal Group consist of four groups indicating a mixed provenance: (1) Precambrian grains (~1.3–1.0 Ga) derived from Oaxaquia (Novillo Gneiss); (2) early–middle Paleozoic grains (430–300 Ma) derived from peri-Gondwanan accreted rocks and peri-Gondwanan early-middle Paleozoic magmatic arc (Granjeno Schist, tonalite, and Asseradero Rhyolite); (3) Permian–Triassic grains (296–222 Ma) derived from volcanic and plutonic rocks (East Mexican Arc); and (4) Early–Middle Jurassic grains (199–164 Ma), locally derived from the Nazas arc. Groups 1–3 increase in abundance upsection as a result of unroofing of Jurassic volcanic and sedimentary carapace from uplifted basement.

Details of the provenance analysis of this work have been integrated with previous interpretations to achieve an explanatory function by linking field and lab observations into a coherent synthesis. Geological systems and their main discriminant compositional parameters with specific values have a consistent influence from basin-forming mechanics. The vertical succession of the Huizachal Group depends mainly on basement relief, extensional loci, volcanic juxtaposition, and the mode in which accumulation and supply migrate during the evolution of the depocenters.

8.1. Suggestions

Tacking the factors that control sediment composition is the most difficult petrologic problem in sedimentary geology, but aiming for its solution may succeed in making a contribution for a better understanding of how to quantify them. From a sedimentary geological outlook, to search for a tectonic solution shall include a holistically statistical conception as manage by a source-to-sink approach. Sedimentary geology can give an assertive feeling of truth for source-to-sink analysis by means of sedimentary provenance analyses unless accompanied by extensive empirical research to identify the correct auxiliary assumptions.

This work discarded some complements for the geology of deposits, because they remain unaligned to the principle purpose of this study. Nevertheless, their study represents advantages for a better basin analysis and

for provenance interpretations. One of these studies represents the facies analysis in volcanic depocenters by explaining and interpreting any of the possible types of pyroclastic deposits and their related source of expelling.

The set up for new problem solving issues in the Huizachal Group contribute for the geological record. The volcanic succession within the Huizachal Group still remains absent on interpretations for pyroclastic fragments, flows and deposits, bed or stratum, textures, and classification and nomenclature.

Rock weathering was partially precluded on this thesis, but other functionalities remain excluded. It can serve to unveil soil formation including those related to volcanic ash transformation. Pedofacies analysis may also serve to refine bounding surfaces interpretations and several other systematics for surface architecture.

Other implications like porosity loss can be obtained by measuring sedimentary parameters (α) to calculate subsidence and thermal histories. This method operates under the scope of Geohistory Analysis (*cf.*, Allen and Allen, 1990), which can be correlated with petrography of light minerals

Moreover, the author encourages the use of other isotopic methods to correlated previous contributions for a better systems approach in sedimentary geology. Ideally, cross-disciplinary approaches advocate benefits by collective research.

REFERENCES

- Abzalov, M.Z., 1998, Chrome-spinels in gabbro-wehrlite intrusions of the Pechenga area, Kola Peninsula, Russia: emphasis on alteration features: *Lithos*, v. 43, p. 109-134.
- Agrawal, S., 1999, Geochemical discrimination diagrams: A simple way of replacing eye-fitted field boundaries with probability based classifier surfaces: *Journal-Geological Society of India*, v. 54, p. 335-346.
- Agrawal, S., Guevara, M., and Verma, S.P., 2004, Discriminant analysis applied to establish major-element field boundaries for tectonic varieties of basic rocks: *International Geology Review*, v. 46, p. 575-594.
- Aitchison, J., 1986, *The statistical analysis of compositional data*: London, Chapman & Hall, 410 p.
- Aitchison, J., 1992, On criteria for measures of compositional difference: *Mathematical Geology*, v. 24, p. 365-379.
- Aitchison, J., and Greenacre, M., 2002, Biplots of compositional data: *Journal of the Royal Statistical Society. Series C (Applied Statistics)*, v. 51, p. 375-392.
- Aitken, J.F., and Flint, S.S., 1995, The application of high-resolution sequence stratigraphy to fluvial systems: a case study from the Upper Carboniferous Breathitt Group, eastern Kentucky, USA: *Sedimentology*, v. 42, p. 3-30.
- Alaniz-Alvarez, S.A., van der Heyden, P., Samaniego, A.F.N., and Ortega-Gutierrez, F., 1996, Radiometric and kinematic evidence for Middle Jurassic strike-slip faulting in southern Mexico related to the opening of the Gulf of Mexico: *Geology*, v. 24, p. 443-446.
- Alejandro-Torres, F., 2010, Análisis estructural de las rocas del Triásico en el distrito minero de Galeana, Nuevo León [Tesis de Licenciatura thesis]: Linares, Universidad Autónoma de Nuevo León, 130 p.
- Almazán-Vazquez, E., 1988, El Cámbrico-Ordovícico de Arivechi, en la región centro oriental del Estado de Sonora: *Universidad Nacional Autónoma de México, Instituto de Geología, Revista*, v. 8, p. 58-66.
- Alvarez, W., 2010, Contingency and continuity in earth history and big history Abstracts with Programs - Geological Society of America.
- Allen, J.R., and Allen, P., 2005, *Basin Analysis: Principles and applications*: Oxford, Blackwell Science Ltd, 549 p.
- Allen, J.R.L., 1968, *Current ripples*: North Holland, Amsterdam, Elsevier.
- Allen, J.R.L., 1971, Transverse erosional marks of mud and rock: their physical basis and geological significance: *Sedimentary Geology*, v. 5, p. 167-385.
- Allen, J.R.L., 1978, Studies in fluvial sedimentation: an exploratory quantitative model for the architecture of avulsion-controlled alluvial suites: *Sedimentary Geology*, v. 21, p. 129-147.
- Allen, J.R.L., 1982, *Sedimentary structures: Their character and physical basis*: Amsterdam, Elsevier.
- Allen, J.R.L., 1983a, Studies in fluvial sedimentation: Bars, bar-complexes and sandstone sheets (low-sinuosity braided streams) in the brownstones (L. Devonian), welsh borders: *Sedimentary Geology*, v. 33, p. 237-293.
- Allen, J.R.L., 1983b, River bedforms: progress and problems, in Collinson, J.D., and Lewin, J., eds., *Modern and ancient fluvial systems*, International Association of Sedimentologists, Special Publication 6, p. 19-33.
- Allen, J.R.L., 1983c, Gravel overpassing on humpback bars supplied with mixed sediment: examples from the Lower Old Red Sandstone, southern Britain: *Sedimentology*, v. 30, p. 285-294.
- Allen, J.R.L., 1984, Parallel lamination developed from upper-stage plane beds: A model based on the larger coherent structures of the turbulent boundary layer: *Sedimentary Geology*, v. 39, p. 227-242.
- Allen, P.A., and Allen, J.R., 1990, *Basin analysis: principles and applications*: London, Blackwell Scientific Publications.
- Allen, P.A., and Densmore, A.L., 2000, Sediment flux from an uplifting fault block: *Basin Research*, v. 12, p. 367-380.
- Amorosi, A., Colalongo, M.L., Dinelli, E., Lucchini, F., and Vaiani, S.C., 2007, Cyclic variations in sediment provenance from late Pleistocene deposits of the eastern Po Plain, Italy, in Arribas, J., Critelli, S., and Johnsson, M.J., eds., *Sedimentary Provenance and Petrogenesis: Perspectives from Petrography and Geochemistry*, Volume Special Paper 420: Tulsa, Geological Society of America p. 13-24.
- Amorosi, A., and Zuffa, G.G., 2011, Sand composition changes across key boundaries of siliciclastic and hybrid depositional sequences: *Sedimentary Geology*, v. 236, p. 153-163.
- Andel, T.H.v., 1959, Reflections on the interpretation of heavy mineral analyses: *Journal of Sedimentary Research*, v. 29, p. 153-163.
- Anderson, T.H., and Mahoney, J.B., 2006, Late Jurassic basins: The tracks of a continental-scale transform from the Gulf of Mexico to Alaska, in Haggart, J.W., Enkin, R.J., and Monger, J.W.H., eds., *Paleogeography of the North American Cordillera: Evidence For and Against Large-Scale Displacements*, Volume 46, Geological Association of Canada, Special Paper, p. 369-375.
- Anderson, T.H., Rodríguez-Castañeda, J.L., and Silver, L.T., 2005, Jurassic rocks in Sonora, Mexico: Relations to the Mojave-Sonora megashear and its inferred northwestward extension, in Anderson, T.H., Nourse, J.A., McKee, J.W., and Steiner, M.B., eds., *The*

- Mojave-Sonora megashear hypothesis: Development, assessment, and alternatives: Boulder, Geological Society of America, Special Paper 393, p. 51-95.
- Anderson, T.H., and Silver, L.T., 1979, The role of the Mojave-Sonora Megashear in the tectonic evolution of northern Mexico, in Anderson, T.H., and Roldán-Quintana, J., eds., *Geology of northern Sonora*: Hermosillo, Universidad nacional Autónoma de México, Instituto de Geología.
- Anfuso, G., Achab, M., Cultrone, G., and López-Aguayo, F., 1999, Utility of heavy minerals distribution and granulometric analyses in the study of coastal dynamics: application to the littoral between Sanlúcar de Barrameda and Rota (Cadiz, southwest Iberian Peninsula): *Boletín del Instituto Español de Oceanografía*, v. 15, p. 243-250.
- Aponte-Barrera, M., 1974, *Estratigrafía del Paleozoico (Cámbrico-Pensilvanico) del centro de Sonora*: Thesis, Instituto Politécnico Nacional, Escuela Superior de Ingeniería y Arquitectura, México, DF, p. 67.
- Arribas, J., Alonso, A., Mas, R., Tortosa, A., Rodas, M., Barrenechea, J.F., Alonso-Azcarate, J., and Artigas, R., 2003, Sandstone petrography of continental depositional sequences of an intraplate rift basin: western Cameros Basin (North Spain): *Journal of Sedimentary Research*, v. 73, p. 309-327.
- Arribas, J., Gómez-Gras, D., Rosell, J., and Tortosa, A., 1990, Estudio comparativo entre las areniscas paleozóicas y triásicas de la isla de menorca: evidencias de procesos de reciclado: *Revista de la Sociedad Geológica de España*, v. 3, p. 105-116.
- Arribas, M.E., and Arribas, J., 2007, Interpreting carbonate particles in modern continental sands: An example from fluvial sands (Iberian Range, Spain), in Arribas, J., Critelli, S., and Johnsson, M.J., eds., *Sedimentary Provenance and Petrogenesis: Perspectives from Petrography and Geochemistry*, Volume Special Paper 420: Tulsa, Geological Society of America p. 167-179.
- Arvizu, H.E., Iriondo, A., Izaguirre, A., Chávez-Cabello, G., Kamenov, G.D., Solís-Pichardo, G., Foster, D.A., and Lozano-Santa Cruz, R., 2009, Rocas graníticas pérmicas en la Sierra Pinta, NW de Sonora, México: Magmatismo de subducción asociado al inicio del margen continental activo del SW de Norteamérica: *Revista Mexicana de Ciencias Geológicas*, v. 26, p. 709-728.
- Aubert, D., Stille, P., and Probst, A., 2001, REE fractionation during granite weathering and removal by waters and suspended loads: Sr and Nd isotopic evidence: *Geochimica et Cosmochimica Acta*, v. 65, p. 387-406.
- Aubry, M.-P., 1995, From chronology to stratigraphy: interpreting the Lower and Middle Eocene stratigraphic record in the Atlantic Ocean, in Berggren, W.A., Kent, D.V., Aubry, M.-P., and Hardenbol, J., eds., *Geochronology, Time Scales, and Global Stratigraphic Correlation*: Tulsa, SEPM (Society for Sedimentary Geology), Special Publication 54, p. 213-274.
- Augustsson, C., 2003, *Provenance of Late Palaeozoic sediments in the southern Patagonian Andes: age estimates, sources, and depositional setting* [Doktorgrades der Naturwissenschaften thesis]: Münster, Germany, Westfälische Wilhelms-Universität, 94 p.
- Baaske, U.P., 2005, *Sequence stratigraphy, sedimentology and provenance of the Upper Cretaceous siliciclastic sediments of South Jordan* [Doktors der Naturwissenschaften thesis]: Stuttgart, Universität Stuttgart, 136 p.
- Bahlburg, H., 1998, The geochemistry and provenance of Ordovician turbidites in the Argentine Puna: *Geological Society of London, Special Publications*, v. 142, p. 127-142.
- Bahlburg, H., and Dobrzinski, N., 2011, A review of the Chemical Index of Alteration (CIA) and its application to the study of Neoproterozoic glacial deposits and climate transitions, in Arnaud, E., and Shields-Zhou, G., eds., *The Geological Record of Neoproterozoic Glaciations*: London, Geological Society of London, Memoirs 36, p. 81-92.
- Bailey, A.M., Roberts, H.H., and Blackson, J.H., 1998, Early diagenetic minerals and variables influencing their distributions in two long cores (. 40 M), Mississippi River Delta Plain: *Journal Of Sedimentary Research*, v. 68, p. 185-197.
- Ballance, P.F., 1980, Models of sediment distribution in non-marine and shallow marine environments in oblique-slip fault zones, in Ballance, P.F., and Reading, H.G., eds., *Sedimentation in Oblique-Slip Mobile Zones*, Volume 4, Blackwell Publishing Ltd., p. 229-236.
- Banfield, J.F., and Eggleton, R.A., 1989, Apatite replacement and rare earth mobilization, fractionation, and fixation during weathering: *Clays and Clay Minerals*, v. 37, p. 113-127.
- Barboza-Gudiño, J.R., 2008, Detrital zircon geochronology of Triassic Fluvial and submarine fan deposits from northeastern Mexico: stratigraphy, paleogeography, and tectonic implications: *Abstracts with Programs - Geological Society of America*, v. 40, p. 197.
- Barboza-Gudiño, J.R., 2009, El Alamar Formation; the only Triassic succession of the Huizachal Group in northeastern Mexico: *Abstracts with Programs - Geological Society of America*, v. 41, p. 29.
- Barboza-Gudiño, J.R., Orozco-Esquivel, M.T., Gómez-Anguiano, M., and Zavala-Monsiváis, A., 2008, The Early Mesozoic volcanic arc of western North America in northeastern Mexico: *Journal of South American Earth Sciences*, v. 25, p. 49-63.
- Barboza-Gudiño, J.R., Ramírez-Fernández, J.A., Torres-Sánchez, S.A., and Valencia, V., 2011, Geocronología de circones detríticos del Esquisto Granjeno en el noreste de México: implicaciones tectónicas, in Montalvo-Arrieta, J.C., Chávez-Cabello, G., and Velasco-Tápia, F., eds., *Avances y paradigmas de la tectónica y la historia geológica del Noreste de México*, Volume 2, *Boletín de la Sociedad Geológica de México*, p. 201-216.
- Barboza-Gudiño, J.R., Tristán-González, M., and Torres-Hernández, J.R., 1999, Tectonic settling of pre-Oxfordian units from central and northeastern Mexico: A review, in Bartolini, C., Wilson, J.L., and Lawton, T.F., eds., *Mesozoic Sedimentary and Tectonic History of North-Central Mexico*, Volume 340: Boulder, Colorado, Geological Society of America, Special Paper 340, p. 197-210.

- Barboza-Gudiño, J.R., Zavala-Monsiváis, A., Venegas-Rodríguez, G., and Barajas-Nigoche, L.D., 2010, Late Triassic stratigraphy and facies from northeastern Mexico: Tectonic setting and provenance: *Geosphere*, v. 6, p. 621-640.
- Barceló-Vidal, C., Pawlowsky, V., and Grunsky, E., 1996, Some aspects of transformations of compositional data and the identification of outliers: *Mathematical Geology*, v. 28, p. 501-518.
- Barth, A.P., Wooden, J.L., Coleman, D.S., and Fanning, C.M., 2000, Geochronology of the Proterozoic basement of southwesternmost North America, and the origin and evolution of the Mojave crustal province: *Tectonics*, v. 19, p. 616-629.
- Bartholomew, M.J., Evans, M.A., Rich, F.J., Brodie, B.M., and Heath, R.D., 2009, Rifting and drifting in south carolina: fracture History in Alleghanian granites and costal plain strata; Fieldtrip - Annual Meeting Carolina Geological Society, Volume Geography Contribution Series: Carolina, USA, Georgia Southern University Department of Geology, p. 51.
- Bartholomew, M.J., and Hatcher Jr, R.D., 2010, The Grenville orogenic cycle of southern Laurentia: Unraveling sutures, rifts, and shear zones as potential piercing points for Amazonia: *Journal of South American Earth Sciences*, v. 29, p. 4-20.
- Bartok, P., 1993, PreBreakup geology of the Gulf of Mexico-Caribbean_ Its relation to Triassic and Jurassic rift systems of the region: *Tectonics*, v. 12, p. 441-459.
- Bartolini, C., 1998, Stratigraphy, geochronology, geochemistry and tectonic setting of the Mesozoic Nazas Formation, north-central Mexico [dissertation thesis]: El Paso, The University of Texas.
- Bartolini, C., Lang, H., and Spell, T., 2003, Geochronology, geochemistry, and tectonic setting of the Mesozoic Nazas arc in north-central Mexico, and its continuation to north South America, in Bartolini, C., Buffler, R.T., and Blickwede, J.F., eds., *The Circum-Gulf of Mexico and the Caribbean: Hydrocarbon habitats, basin formation and plate tectonics*: Tulsa, American Association of Petroleum Geologists, Memoir 79, p. 427-461.
- Bartolini, C., Lang, H., and Stinnesbeck, W., 1999, Volcanic rock outcrops in Nuevo León, Tamaulipas and San Luis Potosí, Mexico: Remnants of the Permian-Early Triassic magmatic arc, in Bartolini, C., Wilson, J.L., and Lawton, T.F., eds., *Mesozoic Sedimentary and tectonic History of North-Central Mexico*: Boulder, Colorado, Geological Society of America, Special Paper 340, p. 388.
- Bassett, K.N., and Busby, C.J., 2005, Tectonic setting of the Glance Conglomerate along the Sawmill Canyon fault zone, southern Arizona: A sequence analysis of an intra-arc strike-slip basin, in Anderson, T.H., Nourse, J.A., McKee, J.W., and Steiner, M.B., eds., *The Mojave-Sonora megashear hypothesis: Development, assessment, and alternatives*: Boulder, Geological Society of America, Special Paper 393, p. 377-400.
- Basu, A., 1985, Influence of climate and relief on compositions of sands released at source area, in Zuffa, G.G., ed., *Provenance of Arenites*: Netherlands, Dordrecht D. Reidel Publishing Company, p. 1-18.
- Basu, A., Blanchard, D.P., and Brannon, J.C., 1982, Rare earth elements in the sedimentary cycle: a pilot study of the first leg: *Sedimentology*, v. 29, p. 737-742.
- Basu, A., Young, S.W., Suttner, L.J., James, W.C., and Mack, G.H., 1975, Re-evaluation of the use of undulatory extinction and polycrystallinity in detrital quartz for provenance interpretation: *Journal of Sedimentary Research*, v. 45, p. 873-882.
- Bates, R.L., and Jackson, J.A., 1987, *Glossary of Geology*: American Geological Institute: Alexandria, Virginia, v. 788.
- Bauluz, B., Mayayo, M.J., Fernandez-Nieto, C., and Gonzalez Lopez, J.M., 2000, Geochemistry of Precambrian and Paleozoic siliciclastic rocks from the Iberian Range (NE Spain): implications for source-area weathering, sorting, provenance, and tectonic setting: *Chemical Geology*, v. 168, p. 135-150.
- Belcher, R.C., 1979, Depositional environments, paleo- magnetism, and tectonic significance of Huizachal red beds (lower Mesozoic), northeastern Mexico, [Ph.D. thesis]: Austin, University of Texas, 276 p.
- Belousova, E.A., Griffin, W., O'Reilly, S., and Fisher, N., 2002, Igneous zircon: trace element composition as an indicator of source rock type: *Contributions to Mineralogy and Petrology*, v. 143, p. 602-622.
- Berner, R.A., 1969, Goethite stability and the origin of red beds: *Geochimica et Cosmochimica Acta*, v. 33, p. 267-273.
- Bertling, M., Braddy, S.J., Bromley, R.G., Demathieu, G.R., Genise, J., Mikulášek, R., Nielsen, J.K., Nielsen, K.S.S., Rindsberg, A.K., Schirf, M., and Uchman, A., 2006, Names for trace fossils: a uniform approach: *Lethaia*, v. 39, p. 265 - 286.
- Best, J.L., Ashworth, P.J., Bristow, C.S., and Roden, J., 2003, Three-dimensional sedimentary architecture of a large, mid-channel sand braid bar, Jamuna River, Bangladesh: *Journal of Sedimentary Research*, v. 73, p. 516-530.
- Best, J.L., and Brayshaw, A.C., 1985, Flow separation--a physical process for the concentration of heavy minerals within alluvial channels: *Journal of the Geological Society*, v. 142, p. 747-755.
- Bhatia, M.R., 1983, Plate tectonics and geochemical composition of sandstones: *The Journal of Geology*, v. 91, p. 611-627.
- Bhatia, M.R., 1985a, Plate tectonics and geochemical composition of sandstones: A reply: *The Journal of Geology*, v. 93, p. 85-87.
- Bhatia, M.R., 1985b, Rare earth element geochemistry of Australian Paleozoic graywackes and mudrocks: provenance and tectonic control: *Sedimentary Geology*, v. 45, p. 97-113.
- Bhatia, M.R., and Crook, K.A.W., 1986, Trace element characteristics of graywackes and tectonic setting discrimination of sedimentary basins: *Contributions to Mineralogy and Petrology*, v. 92, p. 181-193.

- Bickford, M.E., Soegaard, K., Nielsen, K.C., and McLelland, J.M., 2000, Geology and geochronology of Grenville-age rocks in the Van Horn and Franklin Mountains area, west Texas: Implications for the tectonic evolution of Laurentia during the Grenville: *Geological Society of America Bulletin*, v. 112, p. 1134-1148.
- Bird, D., 2001, Shear margins: Continent-ocean transform and fracture zone boundaries: *The Leading Edge*, v. 20, p. 150-159.
- Bird, D.E., 2004, Jurassic tectonics of the Gulf of Mexico and central Atlantic Ocean [Ph.D. thesis]: United States -- Texas, University of Houston, 161 p.
- Bird, D.E., and Burke, K., 2006, Pangea breakup: Mexico, Gulf of Mexico, and Central Atlantic Ocean: Expanded Abstracts of the Technical Program, v. Society of Exploration Geophysics 76th Annual International Meeting and Exposition, p. 1013-1016.
- Bird, D.E., Burke, K., Hall, S.A., and Casey, J.F., 2005, Gulf of Mexico tectonic history: Hotspot tracks, crustal boundaries, and early salt distribution: *American Association of Petroleum Geologists Bulletin*, v. 89, p. 311-328.
- Blatt, H., 1967a, Provenance determinations and recycling of sediments: *Journal of Sedimentary Research*, v. 37, p. 1031-1044.
- Blatt, H., 1967b, Original characteristics of clastic quartz grains: *Journal of Sedimentary Research*, v. 37, p. 401-424.
- Blatt, H., Middleton, G.V., and Murray, R., 1972, *Origin of sedimentary rock*: Englewood Cliffs, Prentice-Hall.
- Blinski, H., 2008, Weathering of sandstones studied from the composition of stream sediments of the Kupa River (Croatia): *Mineralogical Magazine*, v. 72, p. 23-26.
- Bluck, B.J., 1967, Deposition of some Upper Old Red Sandstone conglomerates in the Clyde area: A study in the significance of bedding: *Scottish Journal of Geology*, v. 3, p. 139-167.
- Bock, B., Hurowitz, J.A., McLennan, S.M., and Hanson, G.N., 2004, Scale and timing of Rare Earth Element redistribution in the Taconian foreland of New England: *Sedimentology*, v. 51, p. 885-897.
- Bock, B., McLennan, S.M., and Hanson, G.N., 1998, Geochemistry and provenance of the Middle Ordovician Austin Glen Member (Normanskill Formation) and the Taconian Orogeny in New England: *Sedimentology*, v. 45, p. 635-655.
- Boese, E., 1923a, Vestiges of an ancient continent in northeast Mexico: *American Journal of Science*, v. s5-6, p. 127-136.
- Boese, E., 1923b, Vestiges of an ancient continent in northeast Mexico: *American Journal of Science*, v. s5-6, p. 310-337.
- Bokman, J., 1952, Clastic quartz particles as indices of provenance: *Journal of Sedimentary Petrology*, v. 22, p. 17-24.
- Bond, G.C., Nickeson, P.A., and Kominz, M.A., 1984, Breakup of a supercontinent between 625 Ma and 555 Ma: new evidence and implications for continental histories: *Earth and Planetary Science Letters*, v. 70, p. 325-345.
- Boucot, A.J., Blodgett, R.B., and Stewart, J.H., 1997, European province Late Silurian brachiopods from the Ciudad Victoria area, Tamaulipas, northeastern Mexico, in Klapper, G., Murphy, M.A., and Talent, J.A., eds., *Paleozoic Sequence Stratigraphy, Biostratigraphy, and Biogeography: Studies in Honor of J. Granville ("Jess") Johnson*: Boulder, Geological Society of America, Special Papers 321, p. 273-293.
- Bouma, A.H., 1962, *Sedimentology of some flysch deposits: a graphic approach to facies interpretation*: Amsterdam, Elsevier.
- Bradley, D.C., 2008, Passive margins through earth history: *Earth-Science Reviews*, v. 91, p. 1-26.
- Bridge, J.S., 1984, Large-scale facies sequences in alluvial overbank environments: *Journal of Sedimentary Research*, v. 54, p. 583-588.
- Bridge, J.S., 1985, Paleochannel patterns inferred from alluvial deposits; a critical evaluation: *Journal of Sedimentary Research*, v. 55, p. 579-589.
- Bridge, J.S., 1993a, Description and interpretation of fluvial deposits: a critical perspective: *Sedimentology*, v. 40, p. 801-810.
- Bridge, J.S., 1993b, The interaction between channel geometry, water flow, sediment transport and deposition in braided rivers, in Best, J.L., and Bristow, C.S., eds., *Braided Rivers, Volume 75*: London, Geological Society of London, Special Publication 75, p. 13-71.
- Bridge, J.S., 1993c, A revised alluvial stratigraphy model, in Marzo, M., and Puigdefàbregas, C., eds., *Alluvial Sedimentation, International Association of Sedimentologists, Special Publication 17*, p. 319-336.
- Bridge, J.S., 2003, *Rivers and floodplains: forms, processes, and sedimentary record*: Oxford, Wiley-Blackwell.
- Bridge, J.S., 2006, Fluvial facies models: recent developments, in Posamentier, H.W., and Walker, R., eds., *Facies models revisited: Tulsa, SEPM (Society for Sedimentary Geology), Special Publication 84*, p. 85-170.
- Bridges, L.W., 1971, Paleozoic history of the southern Chihuahua tectonic belt: *The Geologic Framework of the Chihuahua Belt: Midland, Texas, West Texas Geological Society, Publication*, p. 71-59.
- Briggs, G., and Cline, L.M., 1967, Paleocurrents and source areas of late Paleozoic sediments of the Ouachita Mountains, southeastern Oklahoma: *Journal of Sedimentary Research*, v. 37, p. 985-1000.
- Bristow, C.S., 1987, Brahmaputra river: channel migration and deposition, in Ethridge, F.G., Flores, R.M., and Harvey, M.D., eds., *Recent Developments in Fluvial Sedimentology: Tulsa, SEPM (Society for Sedimentary Geology), Special Publication 39*, p. 63-74.
- Bristow, C.S., 1993, Sedimentology of the Rough Rock: a Carboniferous braided river sheet sandstone in northern England, in Best, J.L., and Bristow, C.S., eds., *Braided Rivers, Volume 75*: London, Geological Society of London, Special Publications 75, p. 291-304.

- Bromley, R., and Asgaard, U., 1979, Triassic freshwater ichnocoenoses from Carlsberg Fjord, East Greenland: *Palaeogeography, Palaeoclimatology, Palaeoecology*, v. 28, p. 39-80.
- Bromley, R.G., 1990, *Trace fossils: Biology and taphonomy*, Unwin Hyman: London, 280 p.
- Bromley, R.G., and Ekdale, A.A., 1986, Composite ichnofacies and tiering of burrows: *Geological Magazine*, v. 123, p. 59-65.
- Bruijine, C.H.d., and Andriessen, P.A.M., 2000, Interplay of intraplate tectonics and surface processes in the Sierra de Guadarrama (central Spain) assessed by apatite fission track analysis: *Phys. Chem. Earth (A)*, v. 25, p. 555-563.
- Brunner, P., 1975, Estudio estratigráfico del Devónico en el área de El Bísani, Caborca, Sonora: Instituto Mexicano del Petróleo, *Revista*, v. 7, p. 16-45.
- Buatois, L.A., and Mangano, M.G., 1993a, Ecospace utilization, paleoenvironmental trends, and the evolution of early nonmarine biotas: *Geology*, v. 21, p. 595-598.
- Buatois, L.A., and Mángano, M.G., 1993b, Trace fossils from a Carboniferous turbiditic lake: Implications for the recognition of additional nonmarine ichnofacies: *Ichnos: An International Journal of Plant & Animal*, v. 2, p. 237-258.
- Buatois, L.A., and Mángano, M.G., 1995, The paleoenvironmental and paleoecological significance of the lacustrine Mermia ichnofacies: An archetypical subaqueous nonmarine trace fossil assemblage: *Ichnos*, v. 4, p. 151-161.
- Buatois, L.A., and Mángano, M.G., 2002, Trace fossils from Carboniferous floodplain deposits in western Argentina: implications for ichnofacies models of continental environments: *Palaeogeography, Palaeoclimatology, Palaeoecology*, v. 183, p. 71-86.
- Buatois, L.A., Mángano, M.G., Genise, J.F., and Taylor, T.N., 1998, The ichnologic record of the continental invertebrate invasion; evolutionary trends in environmental expansion, ecospace utilization, and behavioral complexity: *Palaios*, v. 13, p. 217-240.
- Buatois, L.A., Mángano, M.G., Wu, X., and Zhang, G., 1996, Trace fossils from Jurassic lacustrine turbidites of the anyao formation (Central China) and their environmental and evolutionary significance: *Ichnos*, v. 4, p. 287-303.
- Buck, S.G., 1983, The Saaiplaas quartzite member: a braided system of gold- and uranium-bearing channel placers within the Proterozoic Witwatersrand Supergroup of South Africa, in Collison, J.D., and Lewis, J., eds., *Modern and ancient fluvial systems*, vol. 6, p. 549-562.
- Buck, W., 1991, Modes of continental lithospheric extension: *Journal of Geophysical Research*, v. 96, p. 20161-20178.
- Buck, W.R., 2004, Consequences of asthenospheric variability on continental rifting, in Karner, G.D., Taylor, B., Driscoll, N.W. and Kohlstedt, D.L., ed., *Rheology and deformation of the lithosphere at continental margins*. Margins, Theoretical and Experimental Earth Science. Columbia University Press, New York., p. 1-30.
- Buitrón-Sánchez, B.E., Gomez-Espinosa, C., Almazan-Vazquez, E., and Vachard, D., 2007, A late Atokan regional encrinite (early late Moscovian, Middle Pennsylvanian) in the Sierra Agua Verde, Sonora State, NW Mexico, in Álvaro, J.J., Aretz, M., Boulvain, F., Munnecke, A., Vachard, D., and Vennin, E., eds., *Palaeozoic Reefs and Bioaccumulations: Climatic and Evolutionary Controls*: London, Geological Society of America, Special Publications 275, p. 201-209.
- Burckhardt, C., 1930, Synthetique sur le Mesozoique mexicain: *Society of Paleontology Suisse Memoir*, v. 49-50, p. 1-280.
- Burckhardt, C., and Scalia, S., 1905, La fauna marine du Trias supérieru de Zacatecas, México: *Boletín del Instituto de Geología, Universidad Nacional Autónoma de México*, v. 21, p. 44.
- Busby-Spera, C.J., 1988a, Evolution of a Middle Jurassic back-arc basin, Cedros Island, Baja California: Evidence from a marine volcanoclastic apron: *Geological Society of America Bulletin*, v. 100, p. 218-233.
- Busby-Spera, C.J., 1988b, Spceulative tectonic model for the early Mesozoic are of the southwest Cordilleran United States: *Geology*, v. 16, p. 1121-1125.
- Busby, C., 2004, Continental growth at convergent margins facing large ocean basins: a case study from Mesozoic convergent-margin basins of Baja California, Mexico: *Tectonophysics*, v. 392, p. 241- 277.
- Busby, C., 2005, Possible distinguishing characteristics of very deepwater explosive and effusive silicic volcanism: *Geology*, v. 33, p. 845-848.
- Busby, C., Smith, D., Morris, W., and Fackler-Adams, B., 1998, Evolutionary model for convergent margins facing large ocean basins: Mesozoic Baja California, Mexico: *Geology*, v. 26, p. 227-230.
- Busby, C.J., Bassett, K.N., Steiner, M.B., and Riggs, N.R., 2005, Climatic and tectonic controls on Jurassic intra-arc basins related to northward drift of North America, in Anderson, T.H., Nourse, J.A., McKee, J.W., and Steiner, M.B., eds., *The Mojave-Sonora megashear hypotisis: Development, assessment, and alternatives*: Boulder, Geological Society of America, Special Paper 393, p. 359-376.
- Busby, C.J., Schermer, E.R., and Mattinson, J.M., 2002, Extensional arc setting and ages of Middle Jurassic eolianites, Cowhole Mountains (eastern Mojave Desert block, California), in Glazner, A.F., Walker, J.D., and Bartley, J.M., eds., *Geologic Evolution of the Mojave Desert and Southwestern Basin and Range*: Boulder, Geological Society of America, Memoir 195, p. 79-91.
- Byers, C.W., 1982, Geological significance of marine biogenic sedimentary structures, in McCall, P.L., and Tavesz, M.J.S., eds., *Animal sediment relations, Volume 221-256*: New York, Plenum, p. 221-256.

- Caja, M.A., 2004, Procedencia y diagénesis de los sedimentos del Jurásico Superior-Cretácico Inferior (Facies Weald) en la subcuencas occidentales de la Cuenca del Maestrazgo, Cordillera Ibérica Oriental [PhD thesis]: Madrid, Universidad Complutense de Madrid, 293 p.
- Caja, M.A., Marfil, R., Lago, M., Salas, R., and Ramseyer, K., 2007, Provenance discrimination of Lower Cretaceous synrift sandstones (eastern Iberian Chain, Spain): Constraints from detrital modes, heavy minerals, and geochemistry, in Arribas, J., Critelli, S., and Johnsson, M.J., eds., *Sedimentary Provenance and Petrogenesis: Perspectives from Petrography and Geochemistry*, Volume Special Paper 420: Tulsa, Geological Society of America p. 181-197.
- Cameron, K.L., López, R., Ortega-Gutiérrez, F., Solari, L.A., Keppie, D., and Schulze, C., 2004, U-Pb Geochronology and Pb isotope compositions of leached feldspars: constrains on the origin and evolution of grenvillian rocks from eastern and southern Mexico, in Tollo, R.P., Corriveau, L., McLelland, J., and Bartholomew, M.J., eds., *Proterozoic Tectonic Evolution of the Grenville Orogen in North America*: Geological Society of America, Memoir, 197: Boulder, Colorado, Geological Society of America, p. 755-769.
- Campa, U.M.F., 1981, Conjuntos estratotectónicos de la Sierra Madre del Sur, región comprendida entre los estados de Guerrero, Michoacán, México y Morelos: *Boletín de la Sociedad Geológica Mexicana*, v.?, p. 45-67.
- Campa, U.M.F., and Coney, P.J., 1983, Tectono-stratigraphic terranes and mineral resource distributions of Mexico: *Canadian Journal of Earth Sciences* v. 20, p. 1040-1051.
- Campbell, M., and Crocker, J., 1993, Geology west of the Canal de Las Ballenas, Baja California, Mexico, in Gastil, R.G., and Miller, H.G., eds., *The Pre-Batholithic Stratigraphy of Peninsular California*: Boulder, Geological Society of America, Special Paper 279, p. 61-76.
- Cant, D.J., and Walker, R.G., 1978, Fluvial processes and facies sequences in the sandy braided South Saskatchewan River, Canada: *Sedimentology*, v. 25, p. 625-648.
- Cantú-Chapa, A., 1969, Una nueva localidad del Triásico Superior marino en México:: *Instituto Mexicano del Petróleo Revista*, v. 1, p. 71-72.
- Caracciolo, L., and Critelli, S., 2010, Quantitative models in sediment generation: Book of abstracts - 1st WGSF Workshop, p. 84.
- Carpenter, D.L., 1997, Tectonic history of the metamorphic basement rocks of the Sierra del Carmen, Coahuila, Mexico: *Geological Society of America Bulletin*, v. 109, p. 1321-1332.
- Carrillo-Bravo, J., 1959, Notas sobre el Paleozoico de la región de Ciudad Victoria, Tamaulipas: *Boletín de la Asociación Mexicana de Geólogos Petroleros*, v. 11, p. 1-98.
- Carrillo-Bravo, J., 1961, Geología del Anticlinorio Huizachal-Peregrina al NW de Ciudad Victoria, Tamaulipas: *Boletín de la Asociación Mexicana de Geólogos del Petróleo*, v. 13 (1/2), p. 1-98.
- Carrillo-Martínez, M., 1971, Geología de la hoja San José de Gracia, Sinaloa (tesis profesional): México, D.F., Universidad Nacional Autónoma de México, p. 154.
- Carroll, D., 1953, Weatherability of zircon: *Journal Of Sedimentary Petrology*, v. 23, p. 106-116.
- Cas, R.A.F., and Wright, J.V., 1987, Volcanic successions, modern and ancient: A geological approach to processes, products, and successions, Allen & Unwin (London and Boston).
- Centeno-García, E., 2005, Review of Upper Paleozoic and Lower Mesozoic stratigraphy and depositional environments of central and west Mexico: Constraints on terrane analysis and paleogeography, in Anderson, T.H., Nourse, J.A., McKee, J.W., and Steiner, M.B., eds., *The Mojave-Sonora megashear hypothesis: Development, assessment, and alternatives*: Boulder, Colorado, Geological Society of America, Special Paper 393, p. 233-258.
- Centeno-García, E., and Silva-Romo, G., 1997, Petrogenesis and tectonic evolution of central Mexico during Triassic-Jurassic time: *Revista Mexicana de Ciencias Geológicas*, v. 14 (2), p. 244-260.
- Clark, J., 1962, Field interpretation of red beds: *Geological Association of America Bulletin*, v. 73, p. 423-428.
- Clark, J.M., and Hopson, J.A., 1985, Distinctive mammal-like reptile from Mexico and its bearing on the phylogeny of the Tritylodontidae: *Nature*, v. 315, p. 398-400.
- Clark, J.M., Montellano, M., Hopson, J.A., and Fastovsky, D.E., 1994, An Early or Middle Jurassic tetrapod assemblage for the La Boca Formation, northeastern Mexico, *The Shadows of the Dinosaurs: Early Mesozoic*: New York, Cambridge University, p. 295-302.
- Clark, J.M., Montellano, M., Hopson, J.A., and Hernandez, R.R., 1991, Mammals and other tetrapods from the Early Jurassic La Boca Formation, northeastern Mexico (abstract): *Journal of Vertebrate Paleontology*, v. 11, p. 23A.
- Clothingh, S., Sassi, W., Horvath, F., and Puigdefabregas, C., 1993, Basin analysis and dynamics of sedimentary basin evolution an introduction: *Sedimentary Geology*, v. 86, p. 14.
- Collinson, J.D., 1970, Bedforms of the Tana River, Norway: *Geografiska Annaler. Series A, Physical Geography*, v. 52, p. 31-56.
- Collinson, J.D., 1978, Vertical sequence and sandy body shape in alluvial sequences, in Miall, A.D., ed., *Fluvial sedimentology*, *Canadian Society of Petroleum Geologists, Memoir 5*, p. 577-586.
- Collinson, J.D., and Thompson, D.B., 1989, *Sedimentary Structures*: London, Unwin-Hyman, Ltd, 207 p.

- Condie, K.C., 1986, Geochemistry and tectonic setting of Early Proterozoic supracrustal rocks in the southwestern United States: *The Journal of Geology*, v. 94, p. 845-864.
- Condie, K.C., 1993, Chemical composition and evolution of the upper continental crust: Contrasting results from surface samples and shales: *Chemical Geology*, v. 104, p. 1-37.
- Condie, K.C., 2007, Accretionary orogens in space and time, in Hatcher Jr., R.D., Carlson, M.P., McBride, J.H., and Martínez Catalán, J.R., eds., *4-D Framework of Continental Crust*: Boulder, Geological Society of America, *Memoirs* 200, p. 145-158.
- Condie, K.C., Dengate, J., and Cullers, R.L., 1995, Behavior of rare earth elements in a paleoweathering profile on granodiorite in the Front Range, Colorado, USA: *Geochimica et Cosmochimica Acta*, v. 59, p. 279-294.
- Condie, K.C., Macke, J.E., and Reimer, T.O., 1970, Petrology and geochemistry of Early Precambrian Graywackes from the Fig Tree Group, South Africa: *Geological Society of America Bulletin*, v. 81, p. 2759-2776.
- Coney, P.J., Jones, D.L., and Monger, J.W.H., 1980, Cordilleran suspect terranes: *Nature*, v. 288, p. 329-333.
- Contreras, J., and Scholz, C.H., 2001, Evolution of stratigraphic sequences in multisegmented continental rift basins: Comparison of computer models with the basins of the East African Rift System: *American Association of Petroleum Geologists Bulletin*, v. 85, p. 1565-1581.
- Coombs, D.S., 1997, A note on the terrane concept, based on an introduction to the Terrane '97 conference, Christchurch, New Zealand, February, 1997: *American Journal of Science*, v. 297, p. 762-764.
- Cooper, G.A., and Arellano, A.R.V., 1946, Stratigraphy near Caborca, northwest Sonora, Mexico: *American Association of Petroleum Geologists Bulletin*, v. 30, p. 606-617.
- Corfu, F., Hanchar, J.M., Hoskin, P.W.O., and Kinny, P., 2003, Atlas of Zircon Textures: Reviews in Mineralogy and Geochemistry, v. 53, p. 469-500.
- Corner, B., Cartwright, J., and Swart, R., 2002, Volcanic passive margin of Namibia: A potential fields perspective, in Menzies, M.A., Klemperer, S.I., Ebinger, C.J., and Baker, J., eds., *Volcanic Rifted Margins*, Volume Special Paper 362: Boulder, Colorado, Geological Society of America, p. 203-220.
- Corona-Esquivel, R., 1981, Estratigrafía de la región comprendida entre Olinalá y Tecoyucan, noreste del estado de Guerrero: Universidad Nacional Autónoma de México, Instituto de Geología, *Boletín*, v. 58, p. 119.
- Cox, R., and Lowe, D.R., 1995, A conceptual review of regional-scale controls on the composition of clastic sediment and the evolution of continental blocks and their sedimentary cover: *Journal of Sedimentary Research*, v. 65, p. 1-12.
- Cox, R., Lowe, D.R., and Cullers, R.L., 1995, The influence of sediment recycling and basement composition on evolution of mudrock chemistry in the southwestern United States: *Geochimica et Cosmochimica Acta*, v. 59, p. 2919-2940.
- Crittelli, S., 1999, The interplay of lithospheric flexure and thrust accommodation in forming stratigraphic sequences in the southern Apennines foreland basin system. Italy: *Lincei Scienze Fische e Naturali, Rendiconti, Series IX*, v. 10, p. 257-326.
- Crittelli, S., and Ingersoll, R.V., 1994, Sandstone petrology and provenance of the Siwalik Group (northwestern Pakistan and western-southeastern Nepal): *Journal of Sedimentary Research*, v. 64, p. 815-823.
- Crittelli, S., and Le Pera, E., 1994, Detrital modes and provenance of Miocene sandstones and modern sands to the Southern Apennines thrust-top basins (Italy): *Journal of Sedimentary Research*, v. 64, p. 824-835.
- Crittelli, S., Marsaglia, K.M., and Busby, C.J., 2002, Tectonic history of a Jurassic backarc-basin sequence (the Gran Canon Formation, Cedros Island, Mexico), based on compositional modes of tuffaceous deposits: *Geological Society of America Bulletin*, v. 114, p. 515-527.
- Crittelli, S., Mongelli, G., Perri, F., Martín-Algarra, A., Martín-Martín, M., Perrone, V., Dominici, R., Sonnino, M., and Zaghoul, M.N., 2008, Compositional and geochemical signatures for the sedimentary evolution of the Middle Triassic-Lower Jurassic continental redbeds from Western-Central Mediterranean Alpine Chains: *The Journal of Geology*, v. 116, p. 375-386.
- Crittelli, S., and Reed, W.E., 1999, Provenance and stratigraphy of the Devonian (Old Red Sandstone) and Carboniferous sandstones of Spitsbergen, Svalbard: *Europea Journal Mineralogists.*, v. 11, p. 149-166.
- Cross, T.A., and Lessenger, M.A., 1998, Sediment volume partitioning: rationale for stratigraphic model evaluation and high-resolution stratigraphic correlation, in Gradstein, F.M., Sandvik, K.O., and Milton, N.J., eds., *Sequence Stratigraphy, Concepts and Applications*: Elsevier, Amsterdam, *NPF Spec. Publ.*, 8, p. 171-195.
- Cross, W., 1902, The development of systematic petrography in the nineteenth century: *The Journal of Geology*, v. 10, p. 451-499.
- Crowley, K.D., 1983, Large-scale bed configurations (macroforms), Platte River Basin, Colorado and Nebraska: Primary structures and formative processes: *Geological Society of America Bulletin*, v. 94, p. 117-133.
- Culotta, R.C., Latham, T., Sydow, M., Oliver, J., Brown, L., and Kaufman, S., 1992, Deep structure of the Texas Gulf passive margin and its Ouachita-Precambrian basement; results of the COCORP San Marcos Arch survey: *American Association of Petroleum Geologists Bulletin*, v. 76, p. 270-283.
- Cullers, R.L., 1994, The controls on the major and trace element variation of shales, siltstones, and sandstones of Pennsylvanian-Permian age from uplifted continental blocks in Colorado to platform sediment in Kansas, USA: *Geochimica et Cosmochimica Acta*, v. 58, p. 4955-4972.

- Chandler, C.E., 1957, A petrographic study of sedimentary rocks of Peregrina Canyon, State of Tamaulipas, Mexico [MSc thesis]: Louisiana, Louisiana State University, 87 p.
- Chayes, F., 1949, On ratio correlation in petrography: *The Journal of Geology*, v. 57, p. 239-254.
- Cheel, R.J., 1984, Sediment transport and deposition under upper flow regime plane bed conditions [PhD thesis]: Hamilton, McMaster University.
- Cheel, R.J., and Middleton, G.V., 1986, Horizontal laminae formed under upper flow regime plane bed conditions: *The Journal of Geology*, v. 94, p. 489-504.
- Christian, M.R., 2008, *Developments in Marine Geology*: Amsterdam, Elsevier, 3-22 p.
- Dalrymple, R.W., Boyd, R.O.N., Zaitlin, B.A., Schumm, S.A., and Ethridge, F.G., 1994, History of research, types and internal organisation of incised-valley systems: introduction to the volume origin, evolution and morphology of fluvial valleys, in Dalrymple, R.W., Boyd, R., and Zaitlin, B.A., eds., *Incised-Valley Systems*: Tulsa, SEPM (Society for Sedimentary Geology), Special Publication 51, p. 3-10.
- Dalziel, I.W.D., 1997, Neoproterozoic-Paleozoic geography and tectonics; review, hypothesis, environmental speculation: *Geological Society of America Bulletin*, v. 109, p. 16-42.
- Dalziel, I.W.D., Dalla Salda, L.H., and Gahagan, L.M., 1994, Paleozoic Laurentia-Gondwana interaction and the origin of the Appalachian-Andean mountain system: *Geological Society of America Bulletin*, v. 106, p. 243-252.
- Dalziel, I.W.D., Sharon, M., and Gahagan, L.M., 2000, Laurentia-Kalahari collision and the assembly of Rodinia: *The Journal of Geology*, v. 108, p. 499-513.
- Dallmeyer, R.D., Caen-Vachette, M., and Villeneuve, M., 1987, Emplacement age of post-tectonic granites in southern Guinea (West Africa) and the peninsular Florida subsurface: Implications for origins of southern Appalachian exotic terranes: *Geological Society of America Bulletin*, v. 99, p. 87-93.
- Damon, P.E., Shafiqullah, M., and Clark, K.F., 1981, Evolution de los arcos magmáticos en México y su relación con la metalogénesis: *Revista Instituto de Geología, UNAM*, v. 5, p. 223-238.
- Danhke, G.L., 1989, Investigación y comunicación, in Fernández-Collado, C., Danhke, G.L., and (comps.), eds., *La comunicación humana: ciencia social*: México, McGraw-Hill, p. 385-454.
- Dapples, E.C., 1972, Some concepts of cementation and lithification of sandstones: *American Association of Petroleum Geologists Bulletin*, v. 56, p. 3-25.
- Davies, S., Hampson, G., Flint, S., and Elliott, T., 1999, Continent-scale sequence stratigraphy of the Namurian, Upper Carboniferous and its applications to reservoir prediction, in Fleet, A.J., and Boldy, S.A.R., eds., *Petroleum Geology of Northwest Europe: Proceedings, 5th Conference*, Geological Society of London, p. 757-770.
- Davis, M.H., 2005, The tectonics of Tranquitas: A field study of rift through passive margin development and Laramide deformation in Triassic and Jurassic strata of the Sierra Madre Oriental, NE Mexico [MSc thesis]: Austin, University of Texas at Austin, 122 p.
- de Barros, C.E., Nardi, L.V.S., Dillenburg, S.R., Ayup, R., Jarvis, K., and Baitelli, R., 2010, Detrital minerals of modern beach sediments in Southern Brazil: A provenance study based on the chemistry of zircon: *Journal of Coastal Research*, v. 26, p. 80-93.
- de Cserna, Z., 1969, Tectonic framework of southern Mexico and its bearing on the problem of continental drift: *Boletín de la Sociedad Geológica Mexicana*, v. XXX, p. 159-168.
- de León-Gómez, H., 1988, Geologische Kartierung (1: 10.000) des Gebietes El Porvenir am Ostrand des Aramberri Uplifts. Sierra Madre Oriental. México [Diplomakartierung thesis]: Clausthal, der Technischen Universität Clausthal., 64 p.
- DeCelles, P.G., and Hertel, F., 1989, Petrology of fluvial sands from the Amazonian foreland basin, Peru and Bolivia: *Geological Society of America Bulletin*, v. 101, p. 1552-1562.
- Der Voo, R.V., 1988, Paleozoic paleogeography of North America, Gondwana, and intervening displaced terranes: Comparisons of paleomagnetism with paleoclimatology and biogeographical patterns: *Geological Society of America Bulletin*, v. 100, p. 311-324.
- Derkachev, A.N., Nikolaeva, N.A., Maria, A.M., and David, T.W., 2007, Chapter 17 Multivariate analysis of heavy mineral assemblages of sediments from the Marginal Seas of the Western Pacific, *Developments in Sedimentology, Volume 58*: Amsterdam, Elsevier, p. 439-464.
- Dewey, J., and Spall, H., 1975, Pre-Mesozoic plate tectonics: How far back in Earth history can the Wilson Cycle be extended?: *Geology*, v. 3, p. 422-424.
- Dewey, J.F., 1988, Lithospheric stress, deformation, and tectonic cycles: the disruption of Pangaea and the closure of Tethys, in Audley-Charles, M.G., and Hallam, A., eds., *Gondwana and Tethys*: London, Geological Society of London, Special Publications 37, p. 23-40.
- Dewey, J.F., 2007, The secular evolution of plate tectonics and the continental crust: An outline, in Hatcher Jr., R.D., Carlson, M.P., McBride, J.H., and Martínez Catalán, J.R., eds., *4-D Framework of Continental Crust*: Boulder, Geological Society of America, Memoirs 200, p. 1-7.
- Díaz, T., and Humphrey, J.D., 1953, Itinerario de la excursión al Cañón de la Peregrina, Tamaulipas: Primera Convención de la Asociación Mexicana de Geólogos Petroleros, v. Guidebook, p. 6.

- Diaz, T., and Navarro, A., 1964, Lithology and stratigraphic correlation of the upper Paleozoic in the region of Palomas, Chihuahua: *Geology of Mina Plomosas-Placer de Guadalupe area, Chihuahua, Mexico--field trip guide book: West Texas Geol. Soc. Pub.*, p. 64-50.
- Dickinson, W.R., 1970, Interpreting detrital modes of graywacke and arkose: *Journal of Sedimentary Research*, v. 40, p. 695-707.
- Dickinson, W.R., 1971a, Plate tectonics in geologic history: *Science*, v. 174, p. 107-113.
- Dickinson, W.R., 1971b, Plate tectonic models of geosynclines: *Earth and Planetary Science Letters*, v. 10, p. 165-174.
- Dickinson, W.R., 1974, Sedimentation within and beside ancient and modern magmatic arcs, in Dott, J., R. H., and Shaver, R.H., eds., *Modern and Ancient Geosynclinal Sedimentation: Tulsa, SEPM (Society for Sedimentary Geology), Special Publication 19*, p. 230-239.
- Dickinson, W.R., 1976, Sedimentary basins developed during evolution of Mesozoic-Cenozoic arc-trench system in western North America: *Canadian Journal of Earth Sciences*, v. 13, p. 1268-1287.
- Dickinson, W.R., 1980, Plate tectonics and key petrologic associations, in Strangway, D.W., ed., *The continental crust and its mineral deposits, Volume 20: Toronto, Canada, Geological Association of Canada, Special Paper* p. 341-60.
- Dickinson, W.R., 1981, Plate tectonics and the continental margin of California, in Ernst, W.G., ed., *The geotectonic development of California, Englewood Cliffs: New Jersey, Prentice-Hall Inc.*, p. 1-28.
- Dickinson, W.R., 1985, Interpreting provenance relations from detrital modes of sandstone, in Zuffa, G.G., ed., *Provenance of Arenites: Netherlands, Dordrecht D. Reidel Publishing Company*, p. 333-361.
- Dickinson, W.R., 1993, Basin geodynamics: *Basin Research*, v. 5, p. 195-196.
- Dickinson, W.R., 2004, Evolution of the North American Cordillera: *Annual Review of Earth and Planetary Sciences*, v. 32, p. 13-45.
- Dickinson, W.R., 2008, Impact of differential zircon fertility of granitoid basement rocks in North America on age populations of detrital zircons and implications for granite petrogenesis: *Earth and Planetary Science Letters*, v. 275, p. 80-92.
- Dickinson, W.R., 2009, The Gulf of Mexico and the southern margin of Laurentia: *Geology*, v. 37 (5), p. 479-480.
- Dickinson, W.R., Beard, L.S., Brakenridge, G.R., Erjavec, J.L., Ferguson, R.C., Inman, K.F., Knepp, R.A., Lindberg, F.A., and Ryberg, P.T., 1983, Provenance of North American Phanerozoic sandstones in relation to tectonic setting: *Geological Society of America Bulletin*, v. 94, p. 222-235.
- Dickinson, W.R., and Gehrels, G.E., 2008, Insights into the paleogeography of Laurentia derived from U-Pb ages of detrital zircons in Mesozoic strata of the Colorado Plateau: *Abstracts with Programs - Geological Society of America*, v. 40, p. 57.
- Dickinson, W.R., and Gehrels, G.E., 2008a, U-Pb Ages of detrital zircons in relation to paleogeography: Triassic paleodrainage networks and sediment dispersal across southwest Laurentia: *Journal of Sedimentary Research*, v. 78, p. 745-764.
- Dickinson, W.R., and Gehrels, G.E., 2009a, U-Pb ages of detrital zircons in Jurassic eolian and associated sandstones of the Colorado Plateau: Evidence for transcontinental dispersal and intraregional recycling of sediment: *Geological Society of America Bulletin*, v. 121, p. 408-433.
- Dickinson, W.R., and Gehrels, G.E., 2009b, Use of U-Pb ages of detrital zircons to infer maximum depositional ages of strata: A test against a Colorado Plateau Mesozoic database: *Earth and Planetary Science Letters*, v. 288, p. 115-125.
- Dickinson, W.R., and Gehrels, G.E., 2010, Insights into North American paleogeography and paleotectonics from U-Pb ages of detrital zircons in Mesozoic strata of the Colorado Plateau, USA: *International Journal of Earth Sciences*, v. 99, p. 1247-1265.
- Dickinson, W.R., Gehrels, G.E., and Stern, R.J., 2010, Late Triassic Texas uplift preceding Jurassic opening of the Gulf of Mexico: Evidence from U-Pb ages of detrital zircons: *Geosphere*, v. 6, p. 641-662.
- Dickinson, W.R., and Lawton, T.F., 2001, Carboniferous to Cretaceous assembly and fragmentation of Mexico: *Geological Society of America Bulletin*, v. 113, p. 1142-1160.
- Dickinson, W.R., Stewart, J.H., and Poole, F.G., 1974, Plate tectonics and sedimentation. Lower Paleozoic and uppermost Precambrian Cordilleran Migeocline, Great Basin, Western United States, in Dickinson, W.R., ed., *Tectonics and Sedimentation: Tulsa, SEPM (Society for Sedimentary Geology), Special Publication 22*, p. 1-27.
- Dickinson, W.R., and Sucek, C.A., 1979, Plate tectonics and sandstone compositions: *American Association of Petroleum Geologists Bulletin*, v. 63, p. 2164-2182.
- Dinelli, E., Lucchini, F., Mordenti, A., and Paganelli, L., 1999, Geochemistry of Oligocene-Miocene sandstones of the northern Apennines (Italy) and evolution of chemical features in relation to provenance changes: *Sedimentary Geology*, v. 127, p. 193-207.
- Dinis, P.A., and Soares, A.F., 2007, Stable and ultrastable heavy minerals of alluvial to nearshore marine sediments from Central Portugal: Facies related trends: *Sedimentary Geology*, v. 201, p. 1-20.
- Dorsey, G.E., 1926, The origin of the color of red beds: *The Journal of Geology*, v. 34, p. 131-143.
- Dowe, D.S., Nance, R.D., Keppie, J.D., Cameron, K.L., Ortega-Rivera, A., Ortega-Gutiérrez, F., and Lee, J.W.K., 2005, Deformational history of the Granjeno Schist, Ciudad Victoria, Mexico: Constraints on the closure of the Rheic Ocean?: *International Geology Reviews*, v. 47, p. 920-937.

- Drake, C.L., 1972, Future considerations concerning geodynamics: *American Association of Petroleum Geologists Bulletin*, v. 56, p. 260-268.
- Drake, N.A., Bryant, R.G., Millington, A.C., and Townshend, J.R.G., 1994, Playa sedimentology and geomorphology: mixture modelling applied to landsat thematic mapper data of Chott el Djerid, Tunisia, in Renaut, R.W., and Last, W.M., eds., *Sedimentology and Geochemistry of Modern and Ancient Saline Lakes*: Tulsa, SEPM (Society for Sedimentary Geology), Special Publication 50, p. 125-131.
- Duzgoren-Aydin, N.S., Aydin, A., and Malpas, J., 2002, Re-assessment of chemical weathering indices: case study on pyroclastic rocks of Hong Kong: *Engineering Geology*, v. 63, p. 99-119.
- Egozcue, J.J., Pawlowsky-Glahn, V., Mateu-Figueraz, G., and Barceló-Vidal, C., 2003, Isometric logratio transformations for compositional data analysis: *Mathematical Geology*, v. 35 (3), p. 279-300.
- Einsele, G., 2000, *Sedimentary basins, evolution, facies, and sediment budget*: Berlin, Springer-Verlag, 792 p.
- Einsele, G., and Seilacher, A., 1982, *Cyclic and event stratification*: Berlin, Springer-Verlag, p p.
- Emmett, T.F., 1996, The provenance of pre-Scandian continental flakes within the Caledonide Orogen of south-central Norway, in Brewer, T.S., ed., *Precambrian Crustal Evolution in the North Atlantic Region*: London, Geological Society of London, Special Publications 112, p. 359-366.
- Ernst, W.G., 2007, Speculations on evolution of the terrestrial lithosphere-asthenosphere system--Plumes and plates: *Gondwana Research*, v. 11, p. 38-49.
- Ethridge, F.G., Wood, L.J., and Schumm, S.A., 1998, Cyclic variables controlling fluvial sequence development: Problems and perspectives, in Shanley, K.W., and McCabe, P.J., eds., *Relative Role of Eustasy, Climate, and Tectonism in Continental Rocks*: Tulsa, SEPM (Society for Sedimentary Geology), Special Publication 59, p. 17-29.
- Fabuel-Perez, I., Redfern, J., and Hodgetts, D., 2009, Sedimentology of an intra-montane rift-controlled fluvial dominated succession: The Upper Triassic Oukaimeden Sandstone Formation, Central High Atlas, Morocco: *Sedimentary Geology*, v. 218, p. 103-140.
- Fackler-Adams, B.N., Busby, C.J., and Mattinson, J.M., 1997, Jurassic magmatism and sedimentation in the Palen Mountains, southeastern California: Implications for regional tectonic controls on the Mesozoic continental arc: *Geological Society of America Bulletin*, v. 109, p. 1464-1484.
- Farmer, J.D., 1990, A Rosetta stone for connectionism: *Physica D: Nonlinear Phenomena*, v. 42, p. 153-187.
- Fastovsky, D.E., Clark, J.M., Strater, N.H., Montellano, M., R, R.H., and Hopson, J.A., 1995, Depositional environments of a Middle Jurassic terrestrial vertebrate assemblage, Huizachal Canyon, Mexico: *Journal of Vertebrate Paleontology*, v. 15, p. 561-575.
- Fastovsky, D.E., Hermes, O.D., Strater, N.H., Bowring, S.A., Clark, J.M., Montellano, M., and Hernandez R, R., 2005, Pre-Late Jurassic, fossil-bearing volcanic and sedimentary red beds of Huizachal Canyon, Tamaulipas, Mexico, in Anderson, T.H., Nourse, J.A., McKee, J.W., and Steiner, M.B., eds., *The Mojave-Sonora megashear hypothesis: Development, assessment, and alternatives*: Boulder, Colorado, Geological Society of America, Special Paper 393, p. 401-426.
- Fedo, C.M., Nesbitt, H.W., and Young, G.M., 1995, Unraveling the effects of potassium metasomatism in sedimentary rocks and paleosols, with implications for paleoweathering conditions and provenance: *Geology*, v. 23, p. 921-924.
- Fehr, W.R., and Bonnard, E.G., 1930, Geological cross-section through the Sierra Madre Oriental from Mecapalapa to Cueva Ahumada, unpublished Geological Report, Volume 367, Mexican Eagle Oil Company.
- Feldman, M.L., 1987, Paleozoic framework of Gulf of Mexico, Medium: X; Size: Pages: 555 p.
- Felicka, E., 2000, Heavy minerals in the Carboniferous sediments of the Intra-Sudetic Basin as palaeogeographic indicators: *Geologia Sudetica*, v. 33, p. 49-65.
- Feng, R., and Kerrich, R., 1990, Geochemistry of fine-grained clastic sediments in the Archean Abitibi greenstone belt, Canada: Implications for provenance and tectonic setting: *Geochimica et Cosmochimica Acta*, v. 54, p. 1061-1081.
- Fielding, C.R., and Gibling, M.R., 2005, Distinguishing between channel and valley fills: definitions, diagnostic criteria and dimensional data, 8th Int. Conf. on Fluvial Sedimentology, Delft, August 7-12, 2005, p. 101 (Abstract volume).
- Filguera-Flores, M., 2010, Evaluación del uso de estructuras de paleocorrientes en secuencias deformadas: Formación Mezcala, Cretácico Superior, Norte del Estado de Guerrero [Tesis de Licenciatura thesis]: Taxco el Viejo, Universidad Autónoma de Guerrero, 90 p.
- Fillon, R.H., 2007, Mesozoic Gulf of Mexico basin evolution from a planetary perspective and petroleum system implications: *Petroleum Geoscience*, v. 13, p. 105-126.
- Fischer, K., 1989, Prozesse und Produkte lateritischer Verwitterung in oberkretazischen Sedimenten Oberägyptens und des Nordsudans: Berlin, Berliner Geowissenschaftliche Abhandlungen. Reihe A, Band 115, 123 p.
- Fischer, R., and Smith, G., 1991, Volcanism, tectonism, and sedimentation, in Fischer, R.V., and Smith, G.A., eds., *Sedimentation in volcanic settings*: Tulsa, SEPM (Society for Sedimentary Geology), Special Publication 45, p. 1-5.
- Fisher, R.V., 1983, Flow transformations in sediment gravity flows: *Geology*, v. 11, p. 273-274.

- Flawn, P.T., and Díaz-Gonzalez, T.E., 1959, Problems of Paleozoic tectonics in north-central and northeastern Mexico: *American Association of Petroleum Geologists Bulletin*, v. 43, p. 224-230.
- Flint, S.S., Aitken, J., and Hampson, G., 1995, Application of sequence stratigraphy to coal-bearing coastal plain successions: implications for the UK Coal measures, in Whateley, M.G., and Spears, D.A., eds., *European Coal Geology*: London, Geological Society of London, Special Publication 82, p. 1-16.
- Flores, R.M., and Shideler, G.L., 1982, Discriminant analyses of heavy minerals in beach and dune sediments of the Outer Banks barrier, North Carolina: *Geological Society of America Bulletin*, v. 93, p. 409-413.
- Floyd, P.A., Winchester, J.A., and Park, R.G., 1989, Geochemistry and tectonic setting of lewisian clastic metasediments from the Early Proterozoic Loch Maree Group of Gairloch, NW Scotland: *Precambrian Research*, v. 45, p. 203-214.
- Folk, R.L., 1976, Reddening of desert sands; Simpson Desert, N. T., Australia: *Journal of Sedimentary Research*, v. 46, p. 604-615.
- Force, E.R., 1980, The provenance of rutile: *Journal of Sedimentary Research*, v. 50, p. 485-488.
- Fralick, P., 2003, Geochemistry of clastic sedimentary rocks: ratio techniques, in Lentz, D.R., ed., *Geochemistry of sediments and sedimentary rocks: Evolutionary consideration to Mineral deposits-forming environments*, Volume 4: New Fouland, Canada, Geological Association of Canada, *GeoText* 4, p. 85-103.
- Fralick, P.W., and Kronberg, B.I., 1997, Geochemical discrimination of clastic sedimentary rock sources: *Sedimentary Geology*, v. 113, p. 111-124.
- Frey, R.W., Pemberton, S.G., and Fagerstrom, J.A., 1984, Morphological, ethnological, and environmental significance of the ichnogenes *Scoyenia* and *Ancorichnus*: *Journal of Paleontology*, v. 58, p. 511-528.
- Freydier, C., Lapierre, H., Briquet, L., Tardy, M., Coulon, C., and Martínez, J., 1997, Volcaniclastic sequences with continental affinities within the Late Jurassic–Early Cretaceous intraoceanic Arc terrane (western Mexico): *The Journal of Geology*, v. 105, p. 483-502.
- Friedman, G.M., 1962, On sorting, sorting coefficients, and the lognormality of the grain-size distribution of sandstones: *The Journal of Geology*, v. 70, p. 737-753.
- Friis, H., 1978, Heavy-mineral variability in miocene marine sediments in Denmark: a combined effect of weathering and reworking: *Sedimentary Geology*, v. 21, p. 169-188.
- Frostick, L.E., 1986, *Sedimentation in the African Rifts*: London, Geological Society of London, Special Publication 25, 373 p.
- Frostick, L.E., and Reid, I., 1987, Tectonic control of desert sediments in rift basins ancient and modern, in Frostick, L.E., and Reid, I., eds., *Desert Sediments: Ancient and Modern*: London, Geological Society of London, Special Publications 35, p. 53-68.
- Frostick, L.E., and Steel, R.J., 1993, *Tectonic controls and signatures in sedimentary successions*, Wiley Online Library.
- Fulford, M.M., and Busby, C.J., 1999, Tectonic controls on non-marine sedimentation in a Cretaceous fore-arc basin, Baja California, Mexico, in Frostick, L.E., and Steel, R., eds., *Tectonic Controls and Signatures in Sedimentary Successions*, Volume 20, Blackwell Publishing Ltd., p. 301-333.
- Galehouse, J.S., 1971, Point counting, in Carver, R.E., ed., *Procedures in Sedimentary Petrology*: New York, Wiley-Interscience, p. 385-407.
- García-Díaz, J.L., 2004, *Etude Géologique de la Sierra Madre del sur aux environs de Chilpancingo et D'Olinala, Gro: Une contribution à la connaissance de l'évolution géodynamique de la marge pacifique du Mexique depuis le Jurassique* [PhD thesis]: Chambéry, University de Savoie, 148 p.
- García-Obregón, R., 2007, *Cartografía geológica y petrología del vulcanismo mesozoico en el Valle de Huizachal, Tamaulipas* [Tesis de Licenciatura thesis]: Linares, Universidad Autónoma de Nuevo León, 137 p.
- Garrels, R.M., and Mackenzie, F.T., 1971, *Evolution of sedimentary rocks*: New York, Norton, 397 p.
- Garrison, J.R., 1978, Reinterpretation of isotopic age data from the Granjeno Schist, Ciudad Victoria, Tamaulipas: *Revista - Instituto de Geología*, v. 2, p. 87-89.
- Garzanti, E., 1991, Non-Carbonate intrabasinal grains in arenites: Their recognition, significance, and relationship to eustatic cycles and tectonic setting: *Journal of Sedimentary Petrology*, v. 61 (6), p. 959-975.
- Garzanti, E., and Andò, S., 2007, Chapter 29 Plate tectonics and heavy mineral Suites of modern sands, in Mange, M.A., and Wright, D.T., eds., *Developments in Sedimentology*, Volume Volume 58: Amsterdam, Elsevier, p. 741-763.
- Garzanti, E., Andò, S., Maria, A.M., and David, T.W., 2007a, Chapter 20 Heavy mineral concentration in modern sands: Implications for provenance interpretation, in Mange, M.A., and Wright, D.T., eds., *Developments in Sedimentology*, Volume Volume 58: Amsterdam, Elsevier, p. 517-545.
- Garzanti, E., Andò, S., and Vezzoli, G., 2006, The continental crust as a source of sand (Southern Alps Cross Section, Northern Italy): *The Journal of Geology*, v. 114, p. 533-554.
- Garzanti, E., Andò, S., and Vezzoli, G., 2008, Settling equivalence of detrital minerals and grain-size dependence of sediment composition: *Earth and Planetary Science Letters*, v. 273, p. 138-151.

- Garzanti, E., Ando, S., Vezzoli, G., and Dell'era, D., 2003, From rifted margins to foreland basins: Investigating provenance and sediment dispersal across Desert Arabia (Oman, U.A.E.): *Journal of Sedimentary Research*, v. 73, p. 572-588.
- Garzanti, E., Doglioni, C., Vezzoli, G., and Ando, S., 2007b, Orogenic belts and orogenic sediment provenance: *The Journal of Geology*, v. 115, p. 315-334.
- Garzanti, E., and Vezzoli, G., 2003, A classification of metamorphic grains in sands based on their composition and grade: *Journal of Sedimentary Research*, v. 73, p. 830-837.
- Garzanti, E., Vezzoli, G., Andò, S., and Castiglioni, G., 2001, Petrology of rifted-margin sand (Red Sea and Gulf of Aden, Yemen): *The Journal of Geology*, v. 109, p. 277-297.
- Gastil, R.G., and Miller, R.H., 1983, Prebatholithic terranes of southern and peninsular California, USA, and Mexico: Status report: Pre-Jurassic rocks in western North American suspect terranes: *Soc. Econ. Paleontologists and Mineralogists, Pacific Sec.*, p. 49-61.
- Gawthorpe, R.L., and Leeder, M.R., 2000, Tectono-sedimentary evolution of active extensional basins: *Basin Research*, v. 12, p. 195-218.
- Gazzi, P., 1966, Le arenarie del flysch sopracretaceo dell'Appennino modenese; Correlazioni con il flysch di Monghidoro: *Mineral et Petrographica Acta*, v. 12, p. 67-97.
- Gehrels, G.E., 2000, Introduction to detrital zircon studies of Paleozoic and Triassic strata in western Nevada and northern California, in Soreghan, M.J., and Gehrels, G.E., eds., *Paleozoic and Triassic Paleogeography and Tectonics of Western Nevada and Northern California*, Volume 347: Boulder, Colorado, Geological Society of America, Special Paper 347, p. 1-17.
- Gehrels, G.E., and Stewart, J.H., 1998, Detrital zircon U-Pb geochronology of Cambrian to Triassic miogeoclinal and eugeoclinal strata of Sonora, Mexico: *Journal of Geophysical Research*, v. 103, p. 2471-2487.
- Gehrels, G.E., Valencia, V.A., and Ruiz, J., 2008, Enhanced precision, accuracy, efficiency, and spatial resolution of U-Pb ages by laser ablation-multicollector-inductively coupled plasma-mass spectrometry: *Geochemistry, Geophysics, Geosystems*, v. 9.
- Genise, J.F., MaNgano, M.G., Buatois, L.A., Laza, J.H., and Verde, M., 2000, Insect trace fossil associations in paleosols: The *Coprinisphaera* Ichnofacies: *Palaios*, v. 15, p. 49-64.
- Germanoski, D., and Schumm, S.A., 1993, Changes in braided river morphology resulting from aggradation and degradation: *The Journal of Geology*, v. 101, p. 451-466.
- Gibling, M.R., 2006, Width and thickness of fluvial channel bodies and valley fills in the geological record: A literature compilation and classification: *Journal of Sedimentary Research*, v. 76, p. 731-770.
- Gill, J.B., Hiscott, R.N., and Vidal, P., 1994, Turbidite geochemistry and evolution of the Izu-Bonin arc and continents: *Lithos*, v. 33, p. 135-168.
- Girty, G.H., Hanson, A.D., Knaack, C., and Johnson, D., 1994, Provenance determined by REE, Th, and Sc analyses of metasedimentary rocks, Boyden Cave roof pendant, central Sierra Nevada, California: *Journal of Sedimentary Research*, v. 64, p. 68-73.
- Godínez-Urban, A., Lawton, T.F., Molina Garza, R.S., Iriondo, A., Weber, B., and López-Martínez, M., 2011a, Jurassic volcanic and sedimentary rocks of the La Silla and Todos Santos Formations, Chiapas: Record of Nazas arc magmatism and rift-basin formation prior to opening of the Gulf of Mexico: *Geosphere*, v. 7, p. 121-144.
- Godínez-Urban, A., Molina Garza, R.S., Geissman, J.W., and Wawrzyniec, T., 2011b, Paleomagnetism of the Todos Santos and La Silla Formations, Chiapas: Implications for the opening of the Gulf of Mexico: *Geosphere*, v. 7, p. 145-158.
- Godínez-Urban, D., 2009, Paleomagnetismo de la Formación Todos Santos, Chiapas, México [MSc thesis]: Juriquilla, Querretaro, Centro de Geociencias, Universidad Autónoma de México, 160 p.
- Goldhammer, R.K., 1999, Mesozoic sequence stratigraphy and paleogeographic evolution of northeast Mexico, in Bartolini, C., Wilson, J.L., and Lawton, T.F., eds., *Mesozoic Sedimentary and Tectonic History of North-Central Mexico*, Volume 340: Boulder, Colorado, Geological Society of America, Special Paper, 340, p. 1-58.
- Goldhammer, R.K., and Johnson, C.A., 2001, Middle Jurassic-Upper Cretaceous paleogeographic evolution and sequence-stratigraphic framework of the northwest Gulf of Mexico rim, in Bartolini, C., Buffler, R.T., and Cantú-Chapa, A., eds., *The Western Gulf of Mexico Basin: Tectonics, Sedimentary Basins, and Petroleum Systems*: Tulsa, The American Association of Petroleum Geologists, Memoir 75, p. 45-81.
- Goldring, R., 1993, Ichnofacies and facies interpretation: *Palaios*, v. 8, p. 403-405.
- Gómez-Luna, M.E., Cedillo-Pardo, E., Montero, B.C.y., Gallo-Padilla, I., and Martínez-Cortés, A., 1998, Un nuevo perfil del Ladiniano-Cárnico Inferior con fauna de amonoides en La Ballena, Zacatecas, México: *Revista Mexicana De Ciencias Geológicas*, v. 15, p. 38-45.
- González-Acebrón, L., Arribas, J., and Mas, R., 2007, Provenance of fluvial sandstones at the start of late Jurassic-Early Cretaceous rifting in the Cameros Basin (N. Spain): *Sedimentary Geology*, v. 202, p. 138-157.
- González-Álvarez, I., Agnieszka Kusiak, M., and Kerrich, R., 2006, A trace element and chemical Th-U total Pb dating study in the lower Belt-Purcell Supergroup, Western North America: Provenance and diagenetic implications: *Chemical Geology*, v. 230, p. 140-160.

- González-León, C.M., Stanley, G.D., Gehrels, G.E., and Centeno-García, E., 2005, New data on the lithostratigraphy, detrital zircon and Nd isotope provenance, and paleogeographic setting of the El Antimonio Group, Sonora, Mexico, in Anderson, T.H., Nourse, J.A., McKee, J.W., and Steiner, M.B., eds., *The Mojave-Sonora megashear hypothesis: Development, assessment, and alternatives*: Boulder, Colorado, Geological Society of America, Special Paper 393, p. 259-282.
- González-León, C.M., Valencia, V.A., Lawton, T.F., Amato, J.M., Gehrels, G.E., Leggett, W.J., Montijo-Contreras, O., and Fernández, M.A., 2009, The lower Mesozoic record of detrital zircon U-Pb geochronology of Sonora, México, and its paleogeographic implications: *Revista Mexicana De Ciencias Geológicas*, v. 26, p. 301-314.
- Grajales-Nishimura, J.M., 1988, Geology, geochronology, geochemistry, and tectonic implications of the Juchatengo green rock sequence. State of Oaxaca, southern México.: MSc Thesis, University of Arizona.
- Grajales-Nishimura, J.M., Centeno-García, E., Keppie, D., and Dostal, J., 1999, Geochemistry of Paleozoic basalts from the Juchatengo complex Mexico: tectonic implications: *Journal of South American Earth Sciences*, v. 12, p. 537-544.
- Grajales-Nishimura, N., Terrell, D.J., and Damon, P.E., 1992, Evidencias de la prolongación del arco magmático cordillerano del Triásico Tardío-Jurásico en Chihuahua, Durango y Coahuila: *Boletín de la Asociación Mexicana de Geólogos Petroleros*, v. 42, p. 1-18.
- Grauch, R.I., 1989, Rare earth elements in metamorphic rocks, in Lipin, B.R., and McKay, G.A., eds., *Geochemistry and Mineralogy of Rare Earth Elements*, Reviews in Mineralogy Volume 21, p. 147-167.
- Gray, G.G., Lawton, T.F., and Anonymous, 2008a, Evidence for basement type distribution from zircon U/Pb age spectra from Jurassic and Cretaceous sandstones, greater monterrey area, Mexico: *Abstracts with Programs - Geological Society of America*, v. 40, p. 199.
- Gray, G.G., Lawton, T.F., and Murphy, J.J., 2008b, Looking for the Mojave-Sonora megashear in northeastern Mexico, in Moore, G., ed., *Looking for the Mojave-Sonora megashear in northeastern Mexico*, Volume 14: Houston, Texas, 5–9 October 2008, Geological Society of America, Field Guide 14, p. 1-26.
- Gupta, S., and Cowie, P., 2000, Processes and controls in the stratigraphic development of extensional basins: *Basin Research*, v. 12, p. 185-194.
- Gursky, H.-J., and Ramirez-Ramirez, C., 1986, Notas preliminares sobre el descumbrimiento de volcanitas ácidas en El Cañón de Caballeros (Núcleo del anticlinorio Huizachal-Peregrina, Tamaulipas, México): *Actas de la Facultad de Ciencias de la Tierra, Universidad Autónoma de Nuevo León, Linares, México*, v. 1, p. 11-22.
- Gursky, H.J., 1996, Paleozoic stratigraphy of the Peregrina Canyon area, Sierra Madre Oriental: *Zentralblatt für Geologie und Paläontologie*, v. 1, p. 973-989.
- Gursky, H.J., and Michalzik, D., 1989, Lower Permian turbidites in the Northern Sierra Madre Oriental: *Zentralblatt für Geologie und Paläontologie, Geology Paleontology*, v. I (5/6), p. 821-838.
- Haenggi, W.T., and Muehlberger, W.R., 2005, Chihuahua trough—A Jurassic pull-apart basin, in Anderson, T.H., Nourse, J.A., McKee, J.W., and Steiner, M.B., eds., *The Mojave-Sonora megashear hypothesis: Development, assessment, and alternatives*: Boulder, Colorado, Geological Society of America Special Paper 393, p. 619-630.
- Hale-Erich, W.S., and Coleman, J.L., 1993, Ouachita-Appalachian juncture; a Paleozoic transpressional zone in the southeastern U.S.A: *American Association of Petroleum Geologists Bulletin*, v. 77, p. 552-568.
- Hampson, G.J., Davies, S.J., Elliott, T., Flint, S.S., and Stollhofen, H., 1999, Incised valley fill sandstone bodies in Upper Carboniferous fluvio-deltaic strata: recognition and reservoir characterization of Southern North Sea analogues, in Fleet, A.J., and Boldy, S.A.R., eds., *Petroleum Geology of Northwest Europe: Proceedings 5th Conference*, The Geological Society of London, p. 771–788.
- Hampson, G.J., Elliott, T., and Davies, S.J., 1997, The application of sequence stratigraphy to Upper Carboniferous fluvio-deltaic strata of the onshore UK and Ireland: implications for the southern North Sea: *Journal of the Geological Society*, v. 154, p. 719-733.
- Hancock, G.S., Anderson, R.S., and Whipple, K.X., 1998, Beyond power: Bedrock river incision process and form Rivers over rock, in Tinkler, K.J., and Wohl, E.E., eds., *Rivers over rock: fluvial processes in Bedrock channels*: Washington, American Geophysical Union, Geophysical Monograph 107, p. 35-60.
- Handschy, J.W., and Dyer, R., 1987, Polyphase deformation in Sierra del Cuervo, Chihuahua, Mexico: Evidence for ancestral Rocky Mountain tectonics in the Ouachita foreland of northern Mexico: *Geological Society of America Bulletin*, v. 99, p. 618-632.
- Handschy, J.W., Keller, G.R., and Smith, K.J., 1987, The Ouachita System in northern Mexico: *Tectonics*, v. 6, p. 323-330.
- Hansen, D.L., and Nielsen, S.B., 2003, Why rifts invert in compression: *Tectonophysics*, v. 373, p. 5-24.
- Hatcher, J., R.D., 1984, Southern and central Appalachian basement, in Bartholomew, M.J., ed., *The Grenville Event in the Appalachians and Related Topics*: Boulder, Geological Society of America, Special Paper 194, p. 149–153.
- Hatcher Jr., R.D., Bream, B.R., and Merschat, A.J., 2007, Tectonic map of the southern and central Appalachians: a tale of three orogens and a complete Wilson cycle, in Hatcher, R.D.J., Carlson, M.P., McBride, J.H., and Catalan, J.R.M., eds., *4-D Framework of Continental Crust*: Boulder, Geological Society of America, Memoir 200, p. 595–632.
- Hatcher, R.D., 2007, 4-D framework of continental crust: Boulder, Geological Society of America, Memoir 200, 641 p.
- Hay, D.C., and Dempster, T.J., 2009, Zircon alteration, formation and preservation in sandstones: *Sedimentology*, v. 56, p. 2175-2191.

- Heatherington, A.L., and Mueller, P.A., 1991, Geochemical evidence for Triassic rifting in southwestern Florida: *Tectonophysics*, v. 188, p. 291-302.
- Heier, K.S., 1973, Geochemistry of granulite facies rocks and problems of their origin: *Philosophical Transactions of the Royal Society of London. Series A, Mathematical and Physical Sciences*, v. 273, p. 429-442.
- Heim, A., 1940, The front ranges of the Sierra Madre Oriental, México, from Ciudad Victoria to Tamazunchale: *Eclogae Geologicae Helveticae*, v. 33, p. 313-352.
- Hein, F.J., and Walker, R.G., 1977, Bar evolution and development of stratification in the gravelly, braided, Kicking Horse River, British Columbia: *Canadian Journal of Earth Sciences*, v. 14, p. 562-570.
- Heinrich, E.W., 1956, *Microscopic petrography*: New York, McGraw-Hill, 296 p.
- Heller, P., Peterman, Z.E., O'Neil, J.R., and Shafiqullah, M., 1985, Isotopic provenance of sandstones from the Eocene Tyee Formation, Oregon Coast Range: *Geological Society of America Bulletin*, v. 96, p. 770-780.
- Heller, P.L., and Frost, C.D., 1988, Isotopic provenance of clastic deposits; application of geochemistry to sedimentary provenance studies, in Kleinspehn, K., and Paola, C., eds., *New Perspectives in Basin Analysis*: New York, Springer-Verlag, p. 27-42.
- Heller, P.L., Paola, C., Hwang, I-G., John, B., and Steel, R., 2001, Geomorphology and sequence stratigraphy due to slow and rapid base-level changes in an experimental subsiding basin (XES 96-1): *American Association of Petroleum Geologists Bulletin*, v. 85, p. 817-838.
- Hemming, S.R., and McLennan, S.M., 2001, Pb isotope compositions of modern deep sea turbidites: *Earth and Planetary Science Letters*, v. 184, p. 489-503.
- Henning, C.L., 1913, Die red beds: *Geologische Rundschau*, v. 4, p. 228-244.
- Henning, C.L., 1914, Die red beds: *Die Naturwissenschaften*, v. 2, p. 177-180.
- Henry, D.J., and Dutrow, B.L., 1992, Tourmaline in a low grade clastic metasedimentary rock: an example of the petrogenetic potential of tourmaline: *Contributions to Mineralogy and Petrology*, v. 112, p. 203-218.
- Hernández-Sampieri, R.H., Fernández-Collado, C.F., and Baptista-Lucio, P.B., 1998, *Metodología de la investigación*: Mexico, McGraw-Hill, p. 501.
- Herrmann, U.R., Nelson, B.K., and Ratschbacher, L., 1994, The origin of a terrane: U/Pb zircon geochronology and tectonic evolution of the Xolapa complex (southern Mexico): *Tectonics*, v. 13, p. 455-474.
- Herron, M.M., 1988, Geochemical classification of terrigenous sands and shales from core or log data: *Journal of Sedimentary Research*, v. 58, p. 820-829.
- Hibbard, J.P., Van Staal, C.R., and Rankin, D.W., 2007, A comparative analysis of pre-Silurian crustal building blocks of the northern and the southern Appalachian orogen: *American Journal of Science*, v. 307, p. 23-45.
- Hickey, R.L., Frey, F.A., Gerlach, D.C., and López-Escobar, L., 1986, Multiple sources for basaltic arc rocks from the Southern Volcanic Zone of the Andes (34°41'S): trace element and isotopic evidence for contributions from subducted oceanic crust, mantle, and continental crust: *Journal of Geophysical Research*, v. 91 (B6), p. 5963-5983.
- Hill, R.T., 1893, The Cretaceous formations of Mexico and their relations to North American geographic development: *American Journal of Science*, 3rd Ser., v. 45, p. 307-324.
- Hills, J.M., 1972, Late Paleozoic sedimentation in west Texas Permian basin: *American Association of Petroleum Geologists Bulletin*, v. 56, p. 2303-2322.
- Hiscott, R.N., 1978, Provenance of Ordovician deep-water sandstones, Tourelle Formation, Quebec, and implications for initiation of the Taconic orogeny: *Canadian Journal of Earth Science*, v. 15, p. 1579-1597.
- Hiscott, R.N., 1984, Ophiolitic source rocks for Taconic-age flysch: Trace-element evidence: *Geological Society of America Bulletin*, v. 95, p. 1261-1267.
- Hiscott, R.N., and Ghibaudo, G., 1981, Deep-sea fan deposits in the Macigno Formation (middle-upper Oligocene) of the Gordana Valley, Northern Apennines, Italy; discussion and reply: *Journal of Sedimentary Research*, v. 51, p. 1015-1026.
- Holbrook, J., 2001, Origin, genetic interrelationships, and stratigraphy over the continuum of fluvial channel-form bounding surfaces: an illustration from middle Cretaceous strata, southeastern Colorado: *Sedimentary Geology*, v. 144, p. 179-222.
- Hole, M.J., Trewin, N.H., and Still, J., 1992, Mobility of the high field strength, rare earth elements and yttrium during late diagenesis: *Journal of the Geological Society*, v. 149, p. 689-692.
- Homewood, P.W., Mauriaud, P., and Lafont, F., 2002, Best practices in sequence stratigraphy for explorationists and reservoir engineers: *Bull. Centre Rech. Elf Explor. Prod., Mem.*, 25. 81 pp.
- Hoppe, M., Barboza-Gudiño, J.R., and Schulz, H.M., 2002, Late Triassic submarine fan in northwestern San Luis Potosí, México - lithology, facies and diagenesis: *Neues Jahrbuch Geologie und Paläontologie*, v. 2002 (12), p. 705-724.
- Hopper, J.R., and Buck, W.R., 1993, The Initiation of rifting at constant tectonic force: Role of diffusion creep: *Journal of Geophysical Research*, v. 98, p. 16213-16221.

- Hopper, J.R., and Roger Buck, W., 1998, Styles of extensional decoupling: *Geology*, v. 26, p. 699-702.
- Horton, J.W., Drake, A.A., and Rankin, D.W., 1989, Tectonostratigraphic terranes and their Paleozoic boundaries in the central and southern Appalachians, in Dallmeyer, R.D., ed., *Terranes in the circum-Atlantic Paleozoic orogens*: Boulder, Geological Society of America, Special Paper 230, p. 213-245.
- Horton, J.W., Jr., Drake, A.A., Jr., Rankin, D.W., and Dallmeyer, R.D., 1994, Preliminary tectonostratigraphic terrane map of the central and southern Appalachians, IMAP: USGS Numbered Series, p. 1 map :col. :84 x 90 cm., on sheet 101 x 137 cm., on sheet 30 x 24 cm. +1 pamphlet (15 p. ; 28 cm.).
- Hoskin, P.W.O., and Schaltegger, U., 2003, The composition of zircon and igneous and metamorphic petrogranesis, in Hanchar, J.M., and Hoskin, P.W.O., eds., *Zircon, Volume 53*: Washington, Mineralogical Society of America y Geochemical Society. *Reviews in Mineralogy and Geochemistry* 53, p. 27-62.
- Hounslow, M.W., and Morton, A.C., 2004, Evaluation of sediment provenance using magnetic mineral inclusions in clastic silicates: comparison with heavy mineral analysis: *Sedimentary Geology*, v. 171, p. 13-36.
- Hovius, N., 1998, Controls on sediment supply by large rivers, in Shanley, K.W., and McCabe, P.J., eds., *Relative Role of Eustasy, Climate, and Tectonism in Continental Rocks*: Tulsa, SEPM (Society for Sedimentary Geology) Special Publication 59, p. 3-16.
- Hovius, N., and Leeder, M., 1998, Invited Editorial: Clastic sediment supply to basins: *Basin Research*, v. 10, p. 1-5.
- Hsiao, L.Y., Graham, S.A., and Tilander, N., 2010, Stratigraphy and sedimentation in a rift basin modified by synchronous strike-slip deformation: southern Xialiao basin, Bohai, offshore China: *Basin Research*, v. 22, p. 61-78.
- Hubert, J.F., 1962, A zircon-tourmaline-rutile maturity index and the interdependence of the composition of heavy mineral assemblages with the gross composition and texture of sandstones: *Journal of Sedimentary Research*, v. 32, p. 440-450.
- Hubert, J.F., and Forlenza, M.F., 1988, Sedimentology of braided-river deposits in Upper Triassic Wolfville redbeds, southern shore of Cobequid Bay, Nova Scotia, Canada, in Manspeizer, W., ed., *Triassic-Jurassic Rifting and the Opening of the Atlantic Ocean*: Amsterdam, Elsevier.
- Humphrey, W.E., 1956a, Notes on the Geology of northeast Mexico: *Corpus Christi Geological Society, Annual Meeting, Guidebook*, p. 55.
- Humphrey, W.E., 1956b, Tectonic framework of northeast Mexico: *Gulf Coast Association Geological Society Transactions*, v. VI, p. 25-35.
- Humphrey, W.E., and Díaz, T., 2003, Jurassic and Lower Cretaceous stratigraphy and tectonics of northeast Mexico, in Wilson, J.L., and Jordan, C., eds., *Report of investigations, Volume 267*: Austin, University of Texas, p. 151.
- Hunter, R.E., 1977, Terminology of cross-stratified sedimentary layers and climbing-ripple structures: *Journal of Sedimentary Research*, v. 47, p. 697-706.
- Imbrie, J., and Van Andel, T.H., 1964, Vector analysis of heavy-mineral data: *Geological Society of America Bulletin*, v. 75, p. 1131-1156.
- Imlay, R.W., 1936, Evolution of the Coahuila Peninsula, Mexico, part IV, geology of the western part of the Sierra de Parras: *Geological Society of America Bulletin*, v. 47, p. 1091-1152.
- Imlay, R.W., 1937, Lower Neocomian fossils from the Miquihuana region, Mexico: *Journal of Paleontology*, v. 11, p. 552-574.
- Imlay, R.W., 1943a, Evidence for Upper Jurassic landmass in eastern Mexico: *American Association of Petroleum Geologists Bulletin*, v. 27, p. 524-529.
- Imlay, R.W., 1943b, Jurassic formations of Gulf region [of North America including United States, Mexico, and Cuba]: *American Association of Petroleum Geologists Bulletin*, v. 27, p. 1407-1533.
- Imlay, R.W., 1943c, Upper Jurassic ammonites from the Placer de Guadalupe District, Chihuahua, Mexico: *Journal of Paleontology*, v. 17, p. 527-543.
- Imlay, R.W., Cepeda, E., Alvarez, M., and Diaz-Gonzalez, T.E., 1948, Stratigraphic relations of certain Jurassic formations in eastern Mexico: *American Association of Petroleum Geologists Bulletin*, v. 32, p. 1750-1761.
- Ingersoll, R.V., 1974, Surface textures of first cycle quartz sand grains: *Journal of Sedimentary Petrology*, v. 44, p. 151-157.
- Ingersoll, R.V., 1978, Petrofacies and petrologic evolution of the Late Cretaceous fore-arc basin, northern and central California: *The Journal of Geology*, v. 86, p. 335-352.
- Ingersoll, R.V., 1983, Petrofacies and provenance of Late Mesozoic forearc basin, Northern and Central California: *American Association of Petroleum Geologists Bulletin*, v. 67, p. 1125-1142.
- Ingersoll, R.V., 1990, Actualistic sandstone petrofacies: Discriminating modern and ancient source rocks: *Geology*, v. 18, p. 733-736.
- Ingersoll, R.V., and Busby, C.J., 1995, Tectonics of sedimentary basins, in Busby, C.J., and Ingersoll, R.V., eds., *Tectonics of Sedimentary Basins*: Cambridge, MA, Blackwell, p. 1 – 52.
- Ingersoll, R.V., and Eastmond, D.J., 2007, Composition of modern sand from the Sierra Nevada, California, U.S.A.: Implications for actualistic petrofacies of continental-margin magmatic arcs: *Journal of Sedimentary Research*, v. 77, p. 784-796.

- Ingersoll, R.V., Fullard, T.F., Ford, R.L., Grimm, J.P., Pickle, J.D., and Sares, S.W., 1984, The effect of grain size on detrital modes; a test of the Gazzi-Dickinson point-counting method: *Journal of Sedimentary Research*, v. 54, p. 103-116.
- Ingersoll, R.V., Kretchmer, A.G., and Valles, P.K., 1993, The effect of sampling scale on actualistic sandstone petrofacies: *Sedimentology*, v. 40, p. 937-953.
- Ingersoll, R.V., and Suczek, C.A., 1979, Petrology and provenance of Neogene sand from Nicobar and Bengal Fans, DSDP sites 211 and 218: *Journal of Sedimentary Petrology*, v. 49, p. 1217-1228.
- Inman, D.L., Ewing, G.C., and Corliss, J.B., 1966, Coastal sand dunes of Guerrero Negro, Baja California, Mexico: *Geological Society of America Bulletin*, v. 77, p. 787-802.
- Iriondo, A., Martínez-Torres, L.M., Kunk, M.J., Atkinson, W.W., Premo, W.R., and McIntosh, W.C., 2005, Northward Laramide thrusting in the Quitovac region, northwestern Sonora, Mexico: Implications for the juxtaposition of Paleoproterozoic basement blocks and the Mojave-Sonora megashear hypothesis, in Anderson, T.H., Nourse, J.A., McKee, J.W., and Steiner, M.B., eds., *The Mojave-Sonora megashear hypothesis: Development, assessment, and alternatives*: Boulder, Colorado, Geological Society of America, Special Paper 393, p. 631-669.
- James, K.H., 2009a, In situ origin of the Caribbean: discussion of data, in James, K.H., Lorente, M.A., and Pindell, J.L., eds., *The Origin and Evolution of the Caribbean Plate*: London, Geological Society of London, Special Publications 328, p. 77-125.
- James, K.H., 2009b, Evolution of Middle America and the in situ Caribbean Plate model, in James, K.H., Lorente, M.A., and Pindell, J.L., eds., *The Origin and Evolution of the Caribbean Plate*: London, Geological Society of London, Special Publications 328, p. 127-138.
- Jenchen, U., 2001, *Facies und geochemie in kontinentalen Trias-Becken im westlichen Argentinien und in Patagonien (300 - 500 S)* [PhD thesis]: Münster, Universität Münster, 441 p.
- Jenchen, U., 2007a, La Popa Basin, NE Mexico: an Analog for Near Salt Deformation and Hydrocarbon Trapping: Guide Book: Linares, Force- Field Trip to the La Popa Basin (October 24 - 28, 2007), p. 60.
- Jenchen, U., 2007b, Análisis sedimentológico, petrográfico y geoquímico de sedimentos clásticos en el Noreste de México: Reporte técnico anual (inédito), Proyecto CT 1377-06: Programa de Apoyo a la Investigación Científica y Tecnología (PAICyT), v. Universidad Autónoma de Nuevo León, p. 24
- Jenchen, U., and Rosenfeld, U., 1998, Fazies und Geochemie in pazifikwärtigen kontinentalen Trias-Becken des südlichen Südamerika (30°-50°S) [unpublished thesis]: Münster, DFG-Abschlussbericht, 141 p.
- Jenchen, U., and Rosenfeld, U., 2002, Continental Triassic in Argentina: response to tectonic activity: *Journal of South American Earth Sciences*, v. 15, p. 461-479.
- Jenchen, U., and Rosenfeld, U., 2007, Geochemical investigations as a tool to sedimentary analyses demonstrated in Argentinean continental Triassic sediments Methods and aspects: *Neues Jahrbuch für Geologie und Paläontologie - Abhandlungen*, v. 246, p. 37-61.
- Johnson, M.J., 1993, The system controlling the composition of clastic sediments, in Johnson, M.J., and Basu, A., eds., *Processes controlling the composition of clastic sediments*, Volume 284: Boulder, Colorado, Geological Society of America, Special Paper, 284, p. 1-19.
- Jones, N.M., McKee, J.W., Anderson, T.H., and Silver, L.T., 1995, Jurassic volcanic rocks in northeastern Mexico: A possible remnant of a cordilleran magmatic arc, in Jaques-Ayala, C., González-León, C.M., and Roldán Quintana, J., eds., *Studies on the Mesozoic of Sonora and adjacent areas*, Volume 301: Boulder, Colorado, Geological Society of America, Special Paper 301, p. 179-190.
- Jones, N.W., McKee, J.W., Marquez, D.B., Tovar, J., Long, L.E., and Laudon, T.S., 1984, The Mesozoic La Mula Island, Coahuila, México: *Geological Society of America Bulletin*, v. 95, p. 1226-1241.
- Joo, Y.J., Lee, Y.I., and Bai, Z., 2005, Provenance of the Qingshuijian Formation (Late Carboniferous), NE China: Implications for tectonic processes in the northern margin of the North China block: *Sedimentary Geology*, v. 177, p. 97-114.
- Karlstrom, K.E., Åhäll, K.-I., Harlan, S.S., Williams, M.L., McLelland, J., and Geissman, J.W., 2001, Long-lived (1.8-1.0 Ga) convergent orogen in southern Laurentia, its extensions to Australia and Baltica, and implications for refining Rodinia: *Precambrian Research*, v. 111, p. 5-30.
- Karner, G.D., Taylor, B., Driscoll, N.W., and Kohlstedt, D.L., 2004, *Rheology and deformation of the lithosphere at continental margins*: New York, Columbia University Press, 351 p.
- Kasanzu, C., Maboko, M.A.H., and Manya, S., 2008, Geochemistry of fine-grained clastic sedimentary rocks of the Neoproterozoic Ikorongo Group, NE Tanzania: Implications for provenance and source rock weathering: *Precambrian Research*, v. 164, p. 201-213.
- Katz, M.B., 1985, The tectonics of Precambrian craton--mobile belts: progressive deformation of polygonal miniplates: *Precambrian Research*, v. 27, p. 307-319.
- Keller, G.R., and Shurbet, D.H., 1975, Crustal structure of the Texas Gulf Coastal Plain: *Geological Society of America Bulletin*, v. 86, p. 807-810.
- Keppie, D., 2004, Terranes of Mexico revisited: A 1.3 Billion year odyssey: *Internacional Geology Review*, v. 46, p. 765-794.

- Keppie, J.D., and Dostal, J., 2007, Rift-related basalts in the 1.21.3Ga granulites of the northern Oaxacan Complex, southern Mexico: evidence for a rifted arc on the northwestern margin of Amazonia: *Proceedings of the Geologists' Association*, v. 118, p. 63-74.
- Keppie, J.D., Dostal, J., Cameron, K.L., Solari, L.A., Ortega-Gutiérrez, F., and Lopez, R., 2003, Geochronology and geochemistry of Grenvillian igneous suites in the northern Oaxacan Complex, southern Mexico: tectonic implications: *Precambrian Research*, v. 120, p. 365-389.
- Keppie, J.D., Dostal, J., Nance, R.D., Miller, B.V., Ortega-Rivera, A., and Lee, J.K.W., 2006, Circa 546 Ma plume-related dykes in the ~1 Ga Novillo Gneiss (east-central Mexico): Evidence for the initial separation of Avalonia: *Precambrian Research*, v. 147, p. 342-353.
- Keppie, J.D., Dostal, J., Ortega-Gutierrez, F., and Lopez, R., 2001, A Grenvillian arc on the margin of Amazonia: evidence from the southern Oaxacan Complex, southern Mexico: *Precambrian Research*, v. 112, p. 165-181.
- Keppie, J.D., and Ortega-Gutiérrez, F., 2010, 1.3-0.9 Ga Oaxaquia (Mexico): Remnant of an arc/backarc on the northern margin of Amazonia: *Journal of South American Earth Sciences*, v. 29, p. 21-27.
- King, R.E., 1934, The Permian of southwestern Coahuila, Mexico: *American Journal of Science*, v. s5-27, p. 98-112.
- Knighton, A.D., 1998, *Fluvial Forms and Processes, A New Perspective*: London, Arnold, 383 p.
- Knighton, A.D., 1999, Downstream variation in stream power: *Geomorphology*, v. 29, p. 293-306.
- Kocurek, G., and Dott, R.H., 1981, Distinctions and uses of stratification types in the interpretation of eolian sand: *Journal of Sedimentary Research*, v. 51, p. 579-595.
- Krabbendam, M., 2001, When the Wilson Cycle breaks down: how orogens can produce strong lithosphere and inhibit their future reworking, in Miller, J.A., Holdsworth, R.E., Buick, I.S., and Hand, M., eds., *Continental Reactivation and Reworking*: London, Geological Society of London, Special Publications 184, p. 57-75.
- Kramer, J.R., 1968, Mineral-water equilibria in silicate weathering, International Geological Congress, 23rd session, Section 6, 149-160.
- Krenn, E., Ustaszewski, K., and Finger, F., 2008, Detrital and newly formed metamorphic monazite in amphibolite-facies metapelites from the Motajica Massif, Bosnia: *Chemical Geology*, v. 254, p. 164-174.
- Krogh, T.E., Kamo, S.L., and Bohor, B.F., 1993, Fingerprinting the K/T impact site and determining the time of impact by UPb dating of single shocked zircons from distal ejecta: *Earth and Planetary Science Letters*, v. 119, p. 425-429.
- Krynine, P.D., 1949, The origin of red beds: *Academic Science Transactions*, N.Y., v. 11, p. 60-58.
- Kusznir, N.J., and Park, R.G., 1987, The extensional strength of the continental lithosphere: its dependence on geothermal gradient, and crustal composition and thickness, in Dewey, J.F., and Hancock, P.L., eds., *Continental Extensional Tectonics*, : London, Geological Society London, Special Publications 28, p. 35-52.
- Lambeck, A., Huston, D., Maidment, D., and Southgate, P., 2008, Sedimentary geochemistry, geochronology and sequence stratigraphy as tools to typecast stratigraphic units and constrain basin evolution in the gold mineralised Palaeoproterozoic Tanami Region, Northern Australia: *Precambrian Research*, v. 166, p. 185-203.
- Laubach, S.E., and Ward, M.E., 2006, Diagenesis in porosity evolution of opening-mode fractures, Middle Triassic to Lower Jurassic La Boca Formation, NE Mexico: *Tectonophysics*, v. 419, p. 75-97.
- Lawlor, P.J., Ortega-Gutiérrez, F., Cameron, K.L., Ochoa-Camarillo, H., Lopez, R., and Sampson, D.E., 1999, U-Pb geochronology, geochemistry, and provenance of the Grenvillian Huiznopala Gneiss of Eastern Mexico: *Precambrian Research*, v. 94, p. 73-99.
- Lawrence, R.L., Cox, R.n., Mapes, R.W., and Coleman, D.S., 2011, Hydrodynamic fractionation of zircon age populations: *Geological Society of America Bulletin*, v. 123, p. 295-305.
- Lawton, T.F., Barboza-Gudiño, J.R., González-León, C.M., Gary, G., Iriondo, A., Leggett, W.J., Peryam, T.C., and Rubio-Cisneros, I.I., 2010, Latest Triassic-Middle Jurassic age of Cordilleran-Nazas Arc in Mexico, indicated by U-PB Detrital Zircon and volcanic rock ages: *Abstracts with Programs - Geological Society of America*.
- Lawton, T.F., Bradford, I.A., Vega, F.J., Gehrels, G.E., and Amato, J.M., 2009, Provenance of Upper Cretaceous-Paleogene sandstones in the foreland basin system of the Sierra Madre Oriental, northeastern Mexico, and its bearing on fluvial dispersal systems of the Mexican Laramide Province: *Geological Society of America Bulletin*, v. 121, p. 820-836.
- Lawton, T.F., and McMillan, N.J., 1999, Arc abandonment as a cause for passive continental rifting: Comparison of the Jurassic Mexican Borderland rift and the Cenozoic Rio Grande rift: *Geology*, v. 27, p. 779-782.
- Lazzeri, J.J., 1979, *Stratigraphy and igneous petrology of the Middle Jurassic La Joya Formation. Miquihuana.. Aramberri-Mezquitla and Real deCatorce areas. México [MSc thesis]*: New Orleans, University of New Orleans, 109 p.
- Leeder, M., 1999, *Sedimentology and sedimentary basins*: Oxford, Blackwell Science Ltd.
- Leeder, M.R., 1983, On the interactions between turbulent flow, sediment transport and bedform mechanics in channelized flows, in Collinson, J.D., and Lewin, J., eds., *Modern and ancient fluvial systems*, International Association of Sedimentologists, Special Publication 6, p. 5-18.

- Leeder, M.R., 1993, Tectonic controls upon drainage basin development, river channel migration and alluvial architecture: implications for hydrocarbon reservoir development and characterization: Geological Society of London, Special Publications, v. 73, p. 7-22.
- Leeder, M.R., and Gawthorpe, R.L., 1987, Sedimentary models for extensional tilt-block/half-graben basins, in Coward, M.P., Dewey, J.F., and Hancock, P.L., eds., Continental Extensional Tectonics: London, Geological Society of London, Special Publications 28, p. 139-152.
- Leier-Engelhardt, P., 1993, Middle Paleozoic strata of the Sierra de Las Pintas, northeastern Baja California Norte, Mexico, in Gastil, G., and Miller, R.H., eds., The prebatholithic stratigraphy of peninsular California: Boulder, Geological Society of America, Special Paper 279, p. 23-42.
- Lentz, D.R., 2003, Geochemistry of sediments and sedimentary rocks: historical to research perspectives, in Lentz, D.R., ed., Geochemistry of sediments and sedimentary rocks: Evolutionary consideration to Mineral deposits-forming environments: New Fouland, Canada, Geological Association of Canada, GeoText 4, p. 1-6.
- Li, C., and Yang, S., 2010, Is chemical index of alteration (CIA) a reliable proxy for chemical weathering in global drainage basins?: American Journal of Science, v. 310, p. 111-127.
- Longoria, J.F., 1993, La tectonoestratigrafía: un ensayo de metodología para el análisis de terrenos con un ejemplo en México: Boletín de la Asociación Mexicana de Geólogos Petroleros, v. XLII, p. 31-47.
- Longoria, J.F., and Salvador, A., 1988, Late Triassic-Jurassic paleogeography and origin of Gulf of Mexico Basin; discussion and reply: American Association of Petroleum Geologists Bulletin, v. 72, p. 1411-1422.
- Lopez, R., Cameron, K.L., and Jones, N.W., 2001, Evidence for Paleoproterozoic, Grenvillian, and Pan-African age Gondwanan crust beneath northeastern Mexico: Precambrian Research, v. 107, p. 195-214.
- Lorenz, J.C., 1988, Triassic-Jurassic rift-basin sedimentology: New York, Van Nostrand Reinhold Company, 315 p.
- Loring, D.H., 1991, Normalization of heavy-metal data from estuarine and coastal sediments: ICES J. Mar. Sci., v. 48, p. 101-115.
- Lothinger, C.L., 1993, Alloctonous Ordovician strata of Rancho San Marcos, Baja California Norte, México, in Gastil, G., and Miller, R.H., eds., The prebatholithic stratigraphy of peninsular California: Boulder, Geological Society of America, Special Paper 279, p. 11-22.
- Loverlock, J., 2000, The ages of GAIA: a biography of our living Earth: Oxford, Oxford University Press.
- Lucas, S.G., and Estep, J.W., 1999, Permian, Triassic, and Jurassic stratigraphy, biostratigraphy, and sequence stratigraphy in the Sierra del Álamo Muerto, Sonora, México, in Bartolini, C., Wilson, J.L., and Lawton, T.F., eds., Mesozoic sedimentary and tectonic history of north-central Mexico: Boulder, Geological Society of America, Special Paper, 340, p. 161-170.
- Ludwig, K.R., 2005, Isoplot© version 3.0: http://www.bgc.org/isoplot_etc/software.html (accessed September 2006).
- Lunt, I.A., and Bridge, J.S., 2004, Evolution and deposits of a gravelly braid bar, Sagavanirktok River, Alaska: Sedimentology, v. 51, p. 415-432.
- Lunt, I.A., Bridge, J.S., and Tye, R.S., 2004, A quantitative, three-dimensional depositional model of gravelly braided rivers: Sedimentology, v. 51, p. 377-414.
- Lyatsky, H.V., Friedman, G.M., and Lyatsky, V.B., 1999, Principles of practical tectonic analysis of cratonic regions: with particular reference to western North America: Heidelberg, Springer-Verlag, 312 p.
- Mack, G.H., 1984, Exceptions to the relationship between plate tectonics and sandstone composition: Journal of Sedimentary Research, v. 54, p. 212-220.
- Mack, G.H., and Leeder, M.R., 1999, Climatic and tectonic controls on alluvial-fan and axial-fluvial sedimentation in the Plio-Pleistocene Palomas half graben, southern Rio Grande Rift: Journal of Sedimentary Research, v. 69, p. 635-652.
- MacRae, G., 1994, Mesozoic development of the Desoto Canyon Salt Basin in the framework of the early evolution of the Gulf of Mexico [PhD thesis]: United States -- Texas, Texas A&M University, 159 p.
- Magnavita, L.P., Davison, I., and Kuszniir, N.J., 1994, Rifting, erosion, and uplift history of the Recôncavo-Tucano-Jatobá Rift, northeast Brazil: Tectonics, v. 13, p. 367-388.
- Magnavita, L.P., and de Silva, H.T.F., 1995, Rift border system; the interplay between tectonics and sedimentation in the Reconcavo Basin, northeastern Brazil: American Association of Petroleum Geologists Bulletin, v. 79, p. 1590-1607.
- Mancini, E.A., and Markham Pucket, T., 2005, Jurassic and Cretaceous Transgressive-Regressive (T-R) Cycles, Northern Gulf of Mexico, USA: Stratigraphy, v. 2, p. 31-48.
- Mange, M.A., and Maurer, H.F.W., 1992, Heavy minerals in colour: London, Chapman & Hall, 147 p.
- Mange, M.A., Morton, A.C., Maria, A.M., and David, T.W., 2007, Chapter 13 Geochemistry of heavy minerals, Developments in Sedimentology, Volume Volume 58: Amsterdam, Elsevier, p. 345-391.
- Marfil, R., Hall, A., Garcia-Gil, S., and Stamatakis, M.G., 1998, Petrology and geochemistry of diagenetically altered tuffaceous rocks from the Middle Triassic of central Spain: Journal Of Sedimentary Research, v. 68, p. 391-403.

- Marsaglia, K.M., 1991, Provenance of sand and sandstone from a rifted continental arc Gulf of California, Mexico, in R., F., and A., S.G., eds., *Sedimentation in Volcanic Settings: Tulsa, SEPM (Society of Economic Paleontologists and Mineralogists), Special Publication 45*, p. 237-248.
- Marsaglia, K.M., DeVaughn, A.M., James, D.E., and Marden, M., 2010, Provenance of fluvial terrace sediments within the Waipaoa sedimentary system and their importance to New Zealand source-to-sink studies: *Marine Geology*, v. 270, p. 84-93.
- Marsaglia, K.M., and Ingersoll, R.V., 1992, Compositional trends in arc-related, deep-marine sand and sandstone: A reassessment of magmatic-arc provenance: *Geological Society of America Bulletin*, v. 104, p. 1637-1649.
- Marsaglia, K.M., and Tazaki, K., 1992, Diagenetic trends in ODP Leg 126 sandstones:, in Taylor, B., and Fujioka, K., eds., *Proceeding of the Ocean Drilling Program, Scientific results: College Station, TX (Ocean Drilling Program), 126*, p. 125-138.
- Marsaglia, K.M., Pavia, J.A., and Maloney, S.J., 2007, Petrology and provenance of Eocene-Albian sandstones and grainstones recovered during ODP Leg 210: implications for passive margin (rift-to-drift) sandstone provenance models, in Tucholke, B.E., Sibuet, J.-C., and Klaus, A., eds., *Proceedings, Ocean Drilling Program, Scientific Results, 210*, p. 1-47.
- Martin-Fernandez, J.A., and Thio-Henestrosa, S., 2006, Rounded zeros: some practical aspects for compositional data, in Buccianti, A., Mateu-Figueras, G., and Pawlowsky-Glahn, V., eds., *Compositional Data Analysis in the Geosciences: From Theory to Practice, Volume 264: London, Geological Society of London, Special Publications 264*, p. 191-201.
- Marion, G., and Buffler, R.T., 1994, Jurassic Reconstruction of the Gulf of Mexico Basin: *International Geology Reviews*, v. 36, p. 545-586.
- Marion, G.L., 1995, Jurassic evolution of the southeastern Gulf of Mexico [PhD thesis]: United States -- Texas, The University of Texas at Austin, 276 p.
- Maruyama, S., Santosh, M., and Zhao, D., 2007, Superplume, supercontinent, and post-perovskite: Mantle dynamics and anti-plate tectonics on the Core-Mantle Boundary: *Gondwana Research*, v. 11, p. 7-37.
- Marzoli, A., Renne, P.R., Piccirillo, E.M., Ernesto, M., Gellieni, G., and De Min, A., 1999, Extensive 200-million-year-old continental flood basalts of the Central Atlantic Magmatic Province: *Science*, v. 284, p. 616-618.
- Mastalerz, K., and Wojedowa, J., 1993, Alluvial-fan sedimentation along an active strike-slip fault: Plio-Pleistocene Pre-Kaczawa fan, SW Poland, in Marzo, M., and Puigdefábregas, C., eds., *Alluvial Sedimentation, Volume 17, Blackwell Ltd.*, p. 293-304.
- May, P.R., 1971, Pattern of Triassic-Jurassic Diabase Dikes around the North Atlantic in the Context of Predrift Position of the Continents: *Geological Society of America Bulletin*, v. 82, p. 1285-1292.
- McBride, E.F., 1963, A classification of common sandstones: *Journal of Sedimentary Research*, v. 33, p. 664-669.
- McBride, J.H., and Nelson, K.D., 1991, Deep seismic reflection constraints on Paleozoic crustal structure and definition of the Moho in the buried Southern Appalachian Orogen, *Continental Lithosphere: Deep Seismic Reflections, American Geophysical Union, Geodynamics 22*, p. 9-20.
- McCabe, P.J., and Jones, C.M., 1977, Formation of reactivation surfaces within superimposed deltas and bedforms: *Journal of Sedimentary Research*, v. 47, p. 707-715.
- McCaffrey, W.D., Kneller, B.C., and Peakall, J., 2001, Particulate gravity currents, *International Association of Sedimentologists, Special Publication Number 31: London, Blackwell Science Ltd*, p. 302.
- McCall, G.J.H., 2005, Gaia, in Selley, R.C., Cocks, L.R.M., and Plime, I.R., eds., *Encyclopedia of Geology, Volume II G-M: Amsterdam, Elsevier*, p. 1-6.
- McCann, T., 1991, Petrological and geochemical determination of provenance in the southern Welsh Basin, in Morton, A.C., Todd, S.P., and Houghton, P.D.W., eds., *Developments in Sedimentary Provenance Studies: London, Geological Society of London, Special Publications 57*, p. 215-230.
- McDaniel, D.K., Hemming, S.R., McLennan, S.M., and Hanson, G.N., 1994, Petrographic, geochemical, and isotopic constraints on the provenance of the early Proterozoic Chelmsford Formation, Sudbury Basin, Ontario: *Journal of Sedimentary Research*, v. 64, p. 362-372.
- McKee, E.D., 1966, Structures of dunes at white sands national monument, New Mexico (and a comparison with structures of dunes from other selected areas) 1: *Sedimentology*, v. 7, p. 3-69.
- McKee, E.D., 1979, A study of global sand seas, U.S. Geological Survey Professional Paper 1052.
- McKee, E.D., and Weir, G.W., 1953, Terminology for stratification and cross-stratification in sedimentary rocks: *Geological Society of America Bulletin*, v. 64, p. 381-390.
- McKee, J.W., Jones, N.W., and Anderson, A., 1997, Is "Nazas" a junior synonym of "Huizachal", and does it matter?: *Geological Society of America, Abstracts With Programs*, v. 29.
- McKee, J.W., Jones, N.W., and Anderson, T.H., 1988, Las Delicias basin: A record of late Paleozoic arc volcanism in northeastern Mexico: *Geology*, v. 16, p. 37-40.
- McKenzie, D., 1978, Some remarks on the development of sedimentary basins: *Earth and Planetary Science Letters*, v. 40, p. 25-32.

- McLennan, S.M., 1989, Rare earth elements in sedimentary rocks; influence of provenance and sedimentary processes: *Reviews in Mineralogy and Geochemistry*, v. 21, p. 169-200.
- McLennan, S.M., 2001, Relationships between the trace element composition of sedimentary rocks and upper continental crust: *Geochemistry, Geophysics, Geosystems*, v. 2.
- McLennan, S.M., Bock, B., Hemming, S.R., Hurowitz, J.A., Lev, S.M., and McDaniel, D.K., 2003, The roles of provenance and sedimentary processes in the geochemistry of sedimentary rocks, in Lentz, D.R., ed., *Geochemistry of sediments and sedimentary rocks: Evolutionary consideration to Mineral deposits-forming environments*, Volume 4: New Fouland, Canada, Geological Association of Canada, *GeoText* 4, p. 7-38.
- McLennan, S.M., Hemmings, S., McDaniel, D.K., and Hanson, G.N., 1993, *Geochemical approaches to sedimentation, provenance, and tectonics*: Boulder, Geological Society of America, Special Paper 284.
- McLennan, S.M., and Murray, R.W., 1999, Geochemistry of sediments, in Marshall, C.P., and Fairbridge, R.W., eds., *Encyclopedia of Geochemistry*: Dordrecht, Kluwer Academic Publishers, p. 282-292.
- McLennan, S.M., and Taylor, S.R., 1991, Sedimentary rocks and crustal evolution: Tectonic setting and secular trends: *The Journal of Geology*, v. 99, p. 1-21.
- McLennan, S.M., Taylor, S.R., and Eriksson, K.A., 1983, Geochemistry of Archean shales from the Pilbara Supergroup, Western Australia: *Geochimica et Cosmochimica Acta*, v. 47, p. 1211-1222.
- McLennan, S.M., Taylor, S.R., McCulloch, M.T., and Maynard, J.B., 1990, Geochemical and Nd-Sr isotopic composition of deep-sea turbidites: Crustal evolution and plate tectonic associations: *Geochimica et Cosmochimica Acta*, v. 54, p. 2015-2050.
- McLeod, A.E., Underhill, J.R., Davies, S.J., and Dawers, N.H., 2002, The influence of fault array evolution on synrift sedimentation patterns: Controls on deposition in the Strathspey-Brent-Statfjord Half Graben, Northern North Sea: *American Association of Petroleum Geologists Bulletin*, v. 86, p. 1061-1093.
- Meert, J.G., and Van Der Voo, R., 1997, The assembly of Gondwana 800-550 Ma: *Journal of Geodynamics*, v. 23, p. 223-235.
- Meiburg, P., Chapa-Guerrero, J.R., Grotehusmann, I., Kustusch, T., Lentzy, P., De León-Goómez, H., and Mansilla-Terán, M., 1987, El basamento precretácico de Aramberri, estructura clave para comprender el "decóllement" de la cubierta jurásica-cretácica de la Sierra Madre Oriental, México.: *Actas de la Facultad de Ciencias de la Tierra, Universidad Autónoma de Nuevo León, Linares, Mexico*, v. 2, p. 15-22.
- Menzies, M.A., Klemperer, S.L., Ebinger, C.J., and Baker, J., 2002, Characteristics of volcanic rifted margins, in Menzies, M.A., Klemperer, S.L., Ebinger, C.J., and Baker, J., eds., *Volcanic Rifted Margins*, Volume Special Paper 362: Boulder, Colorado, Geological Society of America, p. 1-14.
- Miall, A.D., 1973, Markov chain analysis applied to an ancient alluvial plain succession: *Sedimentology*, v. 20, p. 347-364.
- Miall, A.D., 1977, A review of the braided-river depositional environment: *Earth-Science Reviews*, v. 13, p. 1-62.
- Miall, A.D., 1978, *Fluvial sedimentology*, Canadian Society of Petroleum Geologists, Memoir 5.
- Miall, A.D., 1984, Variations in fluvial style in the lower Cenozoic synorogenic sediments of the Canadian Arctic Islands: *Sedimentary Geology*, v. 38, p. 499-523.
- Miall, A.D., 1985, Architectural-element analysis: A new method of facies analysis applied to fluvial deposits: *Earth-Science Reviews*, v. 22, p. 261-308.
- Miall, A.D., 1986, Effects of Caledonian tectonism in Arctic Canada: *Geology*, v. 14, p. 904-907.
- Miall, A.D., 1988, Reservoir heterogeneities in fluvial sandstones; lessons from outcrop studies: *American Association of Petroleum Geologists Bulletin*, v. 72, p. 682-697.
- Miall, A.D., 1991, Sedimentology of a sequence boundary within the nonmarine Torrvio Member, Gallup Sandstone (Cretaceous), San Juan Basin, New Mexico., in Miall, A.D., and Tyle, N., eds., *The three-dimensional facies architecture of terrigenous clastic sediments, and its implications for hydrocarbon discovery and recovery*: Tulsa, SEPM (Society of Economic Paleontologists and Mineralogists), *Conc. Sedimentol. Paleontol.* 3, p. 224-232.
- Miall, A.D., 1993, The architecture of fluvial-deltaic sequences in the Upper Mesaverde Group (Upper Cretaceous), Book Cliffs, Utah, in Best, J.L., and Bristow, C.S., eds., *Braided Rivers*: London, Geological Society of London, Special Publication 75, p. 305-332.
- Miall, A.D., 1994, Reconstructing fluvial macroform architecture from two-dimensional outcrops; examples from the Castlegate Sandstone, Book Cliffs, Utah: *Journal of Sedimentary Research*, v. 64, p. 146-158.
- Miall, A.D., 1995, Whither stratigraphy?: *Sedimentary Geology*, v. 100, p. 5-20.
- Miall, A.D., 1996, *The geology of fluvial deposits: sedimentary facies, basin analysis, and petroleum geology*: Heidelberg, Springer-Verlag.
- Miall, A.D., 1999, *Principles of sedimentary basin analysis* Berlin, Springer-Verlag.
- Miall, A.D., 2000, *Fluvial sedimentology VI*, in Smith, N.D., and Rogers, J., eds., *Sedimentary Geology*, International Association of Sedimentologists Special Publication 28, p. 241-243.
- Miall, A.D., 2005, Testing for eustatic sea-level control in the Precambrian sedimentary record: *Sedimentary Geology*, v. 176, p. 9-16.

- Mickus, K., Stern, R.J., Keller, G.R., and Anthony, E.Y., 2009, Potential field evidence for a volcanic rifted margin along the Texas Gulf Coast: *Geology*, v. 37 (5), p. 387–390.
- Michalzik, D., 1986, Procedencia y parámetros ambientales de los lechos rojos Huizachal, en el área de Galeana, Nuevo León, México: *Actas de la Facultad de Ciencias de la Tierra, Universidad Autónoma de Nuevo León, Linares, Mexico*, v. 2, p. 15-22.
- Michalzik, D., 1988, Trias bis tiefste Unter-Kreide der nordöstlichen Sierra Madre Oriental, Mexico: Fazielle Entwicklung eines passiven Kontinentalrandes [PhD thesis]: Darmstadt, Technischen Hochschule Darmstadt, 247 p.
- Michalzik, D., 1991, Facies sequence of Triassic-Jurassic red beds in the Sierra Madre Oriental (NE Mexico) and its relation to the early opening of the Gulf of Mexico: *Sedimentary Geology*, v. 71, p. 243-259.
- Michalzik, D., and Shumann, D., 1994, Lithofacies relations and palaeoecology of a Late Jurassic to Early Cretaceous fan delta to shelf depositional system in the Sierra Madre Oriental of North-East Mexico: *Sedimentology*, v. 41, p. 463-477.
- Middleton, G.V., 1960, Chemical composition of sandstones: *Geological Society of America Bulletin*, v. 71, p. 1011-1026.
- Middleton, G.V., 1965, Antidune cross-bedding in a large flume: *Journal of Sedimentary Research*, v. 35, p. 922-927.
- Middleton, G.V., 1966a, Experiments on density and turbidity currents. 1: Motion of the head: *Canadian Journal of Earth Sciences*, v. 4, p. 475-505.
- Middleton, G.V., 1966b, Experiments on density and turbidity currents. 2: Uniform flow of density currents: *Canadian Journal of Earth Sciences*, v. 3, p. 627-637.
- Middleton, G.V., 1973, Johannes Walther's law of the correlation of facies: *Bulletin of the Geological Society of America*, v. 84, p. 979-988.
- Middleton, G.V., 1977, Introduction - progress in hydraulic interpretation of sedimentary structures, in Middleton, G.V., ed., *Sedimentary processes: hydraulic interpretation of primary sedimentary structures*: Tulsa, SEPM (Society of Economic Paleontologists and Mineralogists) Reprinted Series 3, p. 1-15.
- Milani, E.J., and Davison, I., 1988, Basement control and transfer tectonics in the Recôncavo-Tucano-Jatobá rift, Northeast Brazil: *Tectonophysics*, v. 154, p. 41-50, 53-70.
- Milanovsky, E.E., 1983, Major stages of rifting evolution in the earth's history: *Tectonophysics*, v. 94, p. 599-607.
- Miller, B.V., Dostal, J., Keppie, J.D., Nance, R.D., Ortega-Rivera, A., and Lee, J.K.W., 2007, Ordovician calc-alkaline granitoids in the Acatlán Complex, southern Mexico: Geochemical and geochronologic data and implications for the tectonics of the Gondwanan margin of the Rheic Ocean, in Linnemann, R., Ulf, Nance, D., Kraft, P., and Zulauf, G., eds., *Geological Society of America, Special Papers 423*, p. 465-475.
- Mixon, R.B., 1963, The Jurassic formations of the Ciudad Victoria region Tamaulipas Mex: Louisiana, Louisiana State University, 70 p.
- Mixon, R.B., Murray, G.E., and Díaz, T., 1959, Age and correlation of Huizachal Group (Mesozoic), state of Tamaulipas, Mexico: *American Association of Petroleum Geologists Bulletin*, v. 43, p. 757-771.
- Molina-Garza, R.S., and Iriondo, A., 2005, La megacizalla Mojave-Sonora: La hipótesis, la controversia y el estado actual del conocimiento: *Boletín de la Sociedad Geológica Mexicana*, v. 57 (1), p. 1-26.
- Molina-Garza, R.S., Van Der Voo, R.O.B., and Urrutia-Fucugauchi, J., 1992, Paleomagnetism of the Chiapas Massif, southern Mexico: Evidence for rotation of the Maya Block and implications for the opening of the Gulf of Mexico: *Geological Society of America Bulletin*, v. 104, p. 1156-1168.
- Molina Garza, R.S., and Geissman, J.W., 1996, Timing of deformation and accretion of the Antimonio terrane, Sonora, from paleomagnetic data: *Geology*, v. 24, p. 1131-1134.
- Molinaroli, E., Blom, M., and Basu, A., 1991, Methods of provenance determination tested with discriminant function analysis: *Journal of Sedimentary Research*, v. 61, p. 900-908.
- Moral Cardona, J.P., Gutiérrez Mas, J.M., Sánchez Bellón, A., Domínguez-Bella, S., and Martínez López, J., 2005, Surface textures of heavy-mineral grains: a new contribution to provenance studies: *Sedimentary Geology*, v. 174, p. 223-235.
- Morgan, W.J., 1983, Hotspot tracks and the early rifting of the Atlantic: *Tectonophysics*, v. 94, p. 123-139.
- Morris, J.A., 2006, Mesoproterozoic geology of northeastern Llano Uplift, southwest Council Creek quadrangle, Burnet County, central Texas [MSc thesis]: United States -- Texas, Stephen F. Austin State University, 392 p.
- Morton, A.C., and Hallsworth, C., 1994, Identifying provenance-specific features of detrital heavy mineral assemblages in sandstones: *Sedimentary Geology*, v. 90, p. 241-256.
- Morton, A.C., Hallsworth, C., Maria, A.M., and David, T.W., 2007, Chapter 7 Stability of detrital heavy minerals during burial diagenesis, *Developments in Sedimentology, Volume Volume 58*: Amsterdam, Elsevier, p. 215-245.
- Morton, A.C., and Hallsworth, C.R., 1999, Processes controlling the composition of heavy mineral assemblages in sandstones: *Sedimentary Geology*, v. 124, p. 3-29.
- Morton, A.C., Humphreys, B., Dharmayanti, D.A., and Sundoro, 1994, Palaeogeographic implications of the heavy mineral distribution in Miocene sandstones of the North Sumatra Basin: *Journal of Southeast Asian Earth Sciences*, v. 10, p. 177-190.

- Morton, A.C., and Johnsson, M.J., 1993, Factors influencing the composition of detrital heavy mineral suites in Holocene sands of the Apure River drainage basin, Venezuela, in Johnsson, M.J., and Basu, A., eds., Processes controlling the composition of clastic sediments: Boulder, Geological Society of America, Special Paper 284, p. 171-185.
- Mosher, S., 1998, Tectonic evolution of the southern Laurentian Grenville orogenic belt: Geological Society of America Bulletin, v. 110, p. 1357-1375.
- Mueller, P.A., Heatherington, A.L., Wooden, J.L., Shuster, R.D., Nutman, A.P., and Williams, I.S., 1994, Precambrian zircons from the Florida basement: A Gondwanan connection: *Geology*, v. 22, p. 119-122.
- Muir, J.M., 1936, Geology of the Tampico region. México: American Association of Petroleum Geologists Bulletin, p. 280.
- Mulchay, R.B., and Velasco, J.R., 1954, Sedimentary rocks at Cananea: Sonora, Mexico, and tentative correlation with the sections at Bisbee and the Swisshelm Mountains, Arizona: *Mining Engineering*, v. 6, p. 628-632.
- Mullan, H.S., 1978, Evolution of part of the Nevadan orogen in northwestern Mexico: *Bulletin of the Geological Society of America*, v. 89, p. 1175.
- Murillo-Muñeton, G., 1994, Petrologic and geochronologic study of Grenville-age granulites and post-granulite plutons from the La Mixtequita area, state of Oaxaca in southern Mexico, and their tectonic significance [M.F.A. thesis]: California, University of Southern California, 163 p.
- Murillo-Muñeton, G., and Anderson, J.L., 1994, A New Grenville-age granulite terrane in southern Mexico: Geological Society of America Annual Meeting, Seattle, Abstracts with Programs, p. A48.
- Murphy, J.B., Keppie, J.D., Dostal, J., and R.D., N., 1999, Neoproterozoic-early Paleozoic evolution of Avalonia, in Ramos, V.A., and Keppie, J.D., eds., *Laurentia-Gondwana Connections Before Pangea*: Boulder, Geological Society of America, Special Paper 336, p. 253-266.
- Murphy, J.B., Cousens, B.L., Braid, J.A., Strachan, R.A., Dostal, J., Keppie, J.D., and Nance, R.D., 2010, Highly depleted oceanic lithosphere in the Rheic Ocean: Implications for Paleozoic plate reconstructions: *Lithos*, v. In Press, Corrected Proof.
- Murphy, J.B., and Nance, R.D., 1991, Supercontinent model for the contrasting character of Late Proterozoic orogenic belts: *Geology*, v. 19, p. 469-472.
- Murphy, J.B., and Nance, R.D., 2005, Do Supercontinents Turn Inside-in or Inside-out?: *International Geology Review*, v. 47, p. 591-619.
- Nance, R.D., Fernández-Suarez, J., Keppie, J.D., Storey, C., and Jeffries, T.E., 2007, Provenance of the Granjeno Schist, Ciudad Victoria, Mexico: Detrital zircon U-Pb age constraints and implication for the Paleozoic paleogeography of the Rheic Ocean, in Linnemann, U., Nance, R.D., Kraft, P., and Zulauf, G., eds., *The evolution of the Rheic Ocean: From Avalonian-Cadomian active margin to Alleghenian-Variscan collision*: Boulder, Colorado, Geological Society of America, Special Paper 423, p. 453-464.
- Nance, R.D., Gutierrez-Alonso, G., Keppie, J.D., Linnemann, U., Murphy, J.B., Quesada, C., Strachan, R.A., and Woodcock, N.H., 2010, Evolution of the Rheic Ocean: *Gondwana Research*, v. 17, p. 194-222.
- Nance, R.D., Keppie, J.D., Miller, B.V., Murphy, J.B., and Dostal, J., 2009, Palaeozoic palaeogeography of Mexico: constraints from detrital zircon age data, in Grocott, J., McCaffrey, K.J.W., and Taylor, G., eds., *Vertical Coupling and Decoupling in the Lithosphere*: London, Geological Society of London, Special Publications 327, p. 239-269.
- Nance, R.D., Murphy, J.B., Strachan, R.A., Keppie, J.D., Gutierrez-Alonso, G., Fernandez-Suarez, J., Quesada, C., Linnemann, U., D'Lemos, R., and Pisarevsky, S.A., 2008, Neoproterozoic-early Palaeozoic tectonostratigraphy and palaeogeography of the peri-Gondwanan terranes: Amazonian v. West African connections, in Ennih, N., and Liégeois, J.P., eds., *Geological Society of London, Special Publications 297*, p. 345-383.
- Nathan, S., 1976, Geochemistry of the Greenland Group (early Ordovician), New Zealand: *New Zealand Journal of Geology and Geophysics*, v. 19, p. 683-706.
- Nesbitt, H.W., 1979, Mobility and fractionation of rare earth elements during weathering of a granodiorite: *Nature*, v. 279, p. 206-210.
- Nesbitt, H.W., 2003, Petrogenesis of siliciclastic and sedimentary rocks, in Lentz, D.R., ed., *Geochemistry of sediments and sedimentary rocks: Evolutionary consideration to Mineral deposits-forming environments, Volume 4*: New Foulard, Canada, Geological Association of Canada, *GeoText 4*, p. 39-51.
- Nesbitt, H.W., Fedo, C.M., and Young, G.M., 1997, Quartz and feldspar stability, steady and non-steady-state weathering, and petrogenesis of siliciclastic sands and muds: *The Journal of Geology*, v. 105, p. 173-191.
- Nesbitt, H.W., and Young, G.M., 1982, Early Proterozoic climates and plate motions inferred from major element chemistry of lutites: *Nature*, v. 299, p. 715-717.
- Nesbitt, H.W., and Young, G.M., 1984, Prediction of some weathering trends of plutonic and volcanic rocks based on thermodynamic and kinetic considerations: *Geochimica et Cosmochimica Acta*, v. 48, p. 1523-1534.
- Nesbitt, H.W., and Young, G.M., 1996, Petrogenesis of sediments in the absence of chemical weathering: effects of abrasion and sorting on bulk composition and mineralogy: *Sedimentology*, v. 43, p. 341-358.
- Nesbitt, H.W., Young, G.M., McLennan, S.M., and Keays, R.R., 1996, Effects of chemical weathering and sorting on the petrogenesis of siliciclastic sediments, with implications for provenance studies: *The Journal of Geology*, v. 104, p. 525-542.

- Nicholas, R.L., and Rozendal, R.A., 1975, Subsurface positive elements within Ouachita Foldbelt in Texas and their relation to paleozoic cratonic margin: *American Association of Petroleum Geologists Bulletin*, v. 59, p. 193-216.
- Nieto-Samaniego, A.F., Alaniz-Alvarez, S.A., and Camprubí, A., 2005, La Mesa Central de México: estratigrafía, estructura y evolución tectónica cenozoica: *Boletín de la Sociedad Geológica Mexicana*, v. Volumen Conmemorativo del Centenario, Temas selectos de Geología Mexicana, LVII, p. 285-318.
- Nittrouer, C.A., Austin, J.A., Field, M.E., Kravitz, J.H., Syvitski, J.P.M., and Wiberg, P., 2007, Continental margin sedimentation: From sediment transport to sequence stratigraphy, Volume Special Publication 37, International Association of Sedimentologists, Special Publication 37, Blackwell Publishin Ltd.
- Ocampo-Díaz, Y.Z.E., 2011, Implicaciones tectono-sedimentarias de las intercalaciones clásticas en el límite Jurásico-Cretácico del noreste de México (Fosa de Monterrey y Cuenca de Sabinas) [PhD thesis]: Linares, Universidad Autónoma de Nuevo León, 316 p.
- Ocampo-Díaz, Y.Z.E., and Jenchen, U., submitted, Provenance and tectonic setting of the Galeana Sandstone Member, NE Mexico: Petrographical and geochemical evidences: *Geosphere*, v. XXX, p. XXX.
- Ocampo-Díaz, Y.Z.E., Jenchen, U., and Guerrero-Suastegui, M., 2008, Facies y sistemas de depósito del Miembro Arenoso Galeana (Formación Taraises, Cretácico Inferior, NE de México): *Revista Mexicana de Ciencias Geológicas*, v. 25, p. 438-464.
- Ocampo-Díaz, Y.Z.E., and Rubio-Cisneros, I.I., Submitted, Análisis composicional y evidencias de reciclamiento sedimentario asociado a las discordancias del Noreste de México, un ejemplo del Triásico Tardío-Cretácico Temprano: *Boletín de la Sociedad Geológica Mexicana*, v. XXX, p. XXX-XXX.
- Ochoa, M., Arribas, M.E., Arribas, J., and Mas, R., 2007, Significance of geochemical signatures on provenance in intracratonic rift basins: Examples from the Iberian plate, in Arribas, J., Critelli, S., and Johnsson, M.J., eds., *Sedimentary Provenance and Petrogenesis: Perspectives from Petrography and Geochemistry*, Volume Special Paper 420: Tulsa, Geological Society of America p. 199-219.
- Ohta, T., and Arai, H., 2007, Statistical empirical index of chemical weathering in igneous rocks: A new tool for evaluating the degree of weathering: *Chemical Geology*, v. 240, p. 280-297.
- Okada, H., 1966, Non-greywacke "turbidite" sandstones in the Welsh Geosyncline: *Sedimentology*, v. 21, p. 1-232.
- Olsen, P.E., 1997, Stratigraphic record of the Early Mesozoic breakup of Pangea in the Laurasia-Gondwana rift system: *Annual Review of Earth and Planetary Sciences*, v. 25, p. 337-401.
- Orozco, M.T., 1991, Geotermobarometría de granulitas precámbricas del basamento de la Sierra Madre Oriental: *Conveccion sobre la Evolucion Geologica de Mexico Memoria*, p. 138-140.
- Ortega-Gutierrez, F., 1981, Metamorphic belts of southern Mexico and their tectonic significance: *Geofísica Internacional*, v. 20, p. 177-202.
- Ortega-Gutierrez, F., 1993, Tectonostratigraphic analysis and significance of the Paleozoic Acatlán Complex of southern México, in Ortega-Gutiérrez, F., *et al.*, eds., ed., First circum-Pacific and circum-Atlantic terrane conference, Guanajuato, México: México, D.F., Universidad Nacional Autónoma de México, Instituto de Geología, p. 54-60.
- Ortega-Gutiérrez, F., Ruiz, J., and Centeno-García, E., 1995, Oaxaquia, a Proterozoic microcontinent accreted to North America during the late Paleozoic: *Geology*, v. 23 (12), p. 1127-1130.
- Ortega-Gutiérrez, F., Sedlock, R.L., and Speed, R.C., 1994, Phanerozoic tectonic evolution of Mexico, in Speed, R.C., ed., *Phanerozoic evolution of North American continent-ocean transitions*: Boulder, Colorado, Geological Society of America, *Continent-Ocean Transect Volume*, p. 265-306.
- Ortega-Obregon, C., Keppie, J.D., Solari, L.A., Ortega-Gutierrez, F., Dostal, J., Lopez, R., Ortega-Rivera, A., and Lee, J.W.K., 2003, Geochronology and geochemistry of the ~917 Ma, calc-alkaline Etna Granitoid Pluton (Oaxaca, Southern Mexico): Evidence of Post-Grenvillian subduction along the northern margin of Amazonia: *International Geology Review*, v. 45, p. 596-610.
- Ortega-Gutiérrez, F., 1978, El Gneiss Novillo y rocas metamórficas asociadas en los Cañones de Novillo y Peregrina, área de Ciudad Victoria, Tamulipas: *Revista del Instituto de Geología, Univerisdad Nacional Autónoma de México*, v. 2, p. 19-30.
- Ostroumov, V., Rachold, V., Vasiliev, A., and Sorokovikov, V., 2005, An application of a Markov-chain model of shore erosion for describing the dynamics of sediment flux: *Geo-Marine Letters*, v. 25, p. 196-203.
- Owen, G., 2003, Load structures: gravity-driven sediment mobilization in the shallow subsurface, in Van Rensbergen, P., Hilhs, R.R., Maltman, A.J., and Morley, C.K., eds., *Subsurface Sediment Mobilization*, Volume Special Publications 216: London, Geological Society, London, p. 21-34.
- Padilla y Sanchez, R.J., 1982, Geologic evolution of the Sierra Madre Oriental between Linares, Concepcion del Oro, Saltillo, and Monterrey, Mexico [PhD thesis]: United States -- Texas, The University of Texas at Austin, 274 p.
- Pantoja-Alor, J., 1970, Rocas sedimentarias paleozoicas de la región centro-septentrional de Oaxaca: *Sociedad Geológica Mexicana. Libro Guía de la Excursión México-Oaxaca (1970)*, p. 67-84.
- Paola, C., Wiele, S.M., and Reinhart, M.A., 1989, Upper-regime parallel lamination as the result of turbulent sediment transport and low-amplitude bed forms: *Sedimentology*, v. 36, p. 47-59.

- Parsons, I., Thompson, P., Lee, M.R., and Cayzer, N., 2005, Alkali feldspar microtextures as provenance indicators in siliciclastic rocks and their role in feldspar dissolution during transport and diagenesis: *Journal of Sedimentary Research*, v. 75, p. 921-942.
- Patterson, W.D., 1978, *Geology of Permian rock near Asención northern Chihuahua, Mexico* [MSc thesis]: EL Paso, EL Paso University, 70 p.
- Pawlowsky-Glahn, V., and Olea, R.A., 2004, *Geostatistical analysis of compositional data*: Oxford, Oxford University Press.
- Pe-Piper, G., and Dolansky, L.M., 2005, Early diagenetic origin of Al phosphate-sulfate minerals (woodhouseite and crandallite series) in terrestrial sandstones, Nova Scotia, Canada: *American Mineralogist*, v. 90, p. 1434-1441.
- Pemberton, S.G., 1992, *Applications of ichnology to petroleum exploration*: Tulsa, SEPM (Society of Sedimentary Geology), Core Workshop 17.
- Pemberton, S.G., Spila, S., Pulham, A.J., Sauders, T., MacEachern, J.A., and Sinclair, I.K., 2001, *Ichnology and sedimentology of shallow to marginal marine systems: Ben Nevis & Avalon Reservoirs, Jeanne d'Arc Basin, Geological Association of Canada, Short Course Notes Volume 15*.
- Peterson, J.A., 2009, *Geochemical provenance of clastic sedimentary rocks in the Western Cordillera: Utah, Colorado, Wyoming, and Oregon* [MSc thesis]: Logan, Utah State University, 108 p.
- Pettijohn, F.J., 1931, Petrography of the beach sands of Southern Lake Michigan: *The Journal of Geology*, v. 39, p. 432-455.
- Pettijohn, F.J., 1963, *Chemical composition of sandstones, excluding carbonate and volcanic sands: representative analyses*: U.S. Geological Survey Professional Paper 400-S, 19 pp.
- Pettijohn, F.J., 1975, *Sedimentary rocks*: New York, Harper & Brothers, Second Edition p.
- Pettijohn, F.J., Potter, P.E., and Siever, R., 1972, *Sand and Sandstone*: New York, Springer-Verlag, 553 p.
- Pettijohn, F.J., Potter, P.E., and Siever, R., 1987, *Sand and Sandstone*: Berlin, Springer-Verlag, 833 p.
- Pindell, J., and Kennan, L., 2002, *Mexico and Gulf of Mexico*: London, Exploration Framework Atlas Series: Volume 4: Tectonics Analysis.
- Pindell, J.K., L.; Stanek, K. P.; Maresch, W. V.; Draper, G, 2006, Foundations of Gulf of Mexico and Caribbean evolution: eight controversies resolved: *Geologica Acta*, v. 4, p. 303.
- Pindell, J.L., 1985, Alleghenian reconstruction and subsequent evolution of the Gulf of Mexico, Bahamas, And Proto-Caribbean: *Tectonics*, v. 4 (1), p. 1-39.
- Pindell, J.L., and Barrett, S.F., 1990, Geological evolution of the Varibbean region: a plate tectonic perspective, in Dengo, G., and Case, J.E., eds., *The Geology of North America: The Caribbean Region, Volume H*: Boulder, Geological Society of America, p. 405-432.
- Pindell, J.L., and Dewey, J.F., 1982, Permo-Triassic reconstruction of western Pangea and the evolution of the Gulf of Mexico/Caribbean region: *Tectonics*, v. 1, p. 179-211.
- Pindell, J.L., and Kennan, L., 2009, Tectonic evolution of the Gulf of Mexico, Caribbean and northern South America in the mantle reference frame: an update, in James, K.H., Lorente, M.A., and Pindell, J.L., eds., *The Origin and Evolution of the Caribbean Plate, Volume 328*: London, Geological Society of London, Special Publications 328, p. 1-55.
- Pindell, J.L., Kennan, L., Rosenfeld, J., and Granath, J., 2002, Análisis paleogeográfico Mesozoico-Cenozoico y dinámica de cuencas en el Golfo de México profundo y márgenes: la relación entre evolución tectonosedimentaria y sistemas petroleros, *Tectonic Analysis Inc., Pemex Exploración y Producción*, 328 p.
- Pindell, J.L., Kennan, L., Wright, D., and Erikson, J., 2009, Clastic domains of sandstones in central/eastern Venezuela, Trinidad, and Barbados: heavy mineral and tectonic constraints on provenance and palaeogeography, in James, K.H., Lorente, M.A., and Pindell, J.L., eds., *The Origin and Evolution of the Caribbean Plate, Volume 328*: London, Geological Society of London, Special Publications 328, p. 743-797.
- Pisarevsky, S.A., Wingate, M.T.D., Powell, C.M., Johnson, S., and Evans, D.A.D., 2003, Models of Rodinia assembly and fragmentation: *Geological Society of London, Special Publications 206*, p. 35-55.
- Plank, T., and Langmuir, C.H., 1998, The chemical composition of subducting sediment and its consequences for the crust and mantle: *Chemical Geology*, v. 145, p. 325-394.
- Plint, A.G., 1983, Sandy fluvial point-bar sediments from the Middle Eocene of Dorset, England, in Collison, J.D., and Lewin, J., eds., *Modern and ancient fluvial systems*, 6, 355-368.
- Poole, F.G., and Madrid, R.J., 1988, Comparison of allochthonous Paleozoic eugeoclinal rocks in the Sonoran, Marathon, and Antler orogens: *Geological Society of America Annual Meeting, Seattle, Abstracts with Programs*, v. 20, p. 267.
- Poole, F.G., Repetski, J.E., Harris, A.G., Ross, R.J., Jr., Ketner, K.B., Amaya-Martinez, R., and Morales-Ramirez, J.M., 1995, Ordovician carbonateshelf rocks of Sonora, Mexico, in Cooper, J.D., Droser, M.L., and Finney, S.C., eds., *Ordovician Odyssey: Short Papers for the Seventh International Symposium on the Ordovician System*: Fullerton, Calif., Pacific Section Society for Sedimentary Geology (SEPM), book no. 77, p. 267-275.
- Potter, P.E., and Pettijohn, F.J., 1977, *Paleocurrents and basin analysis*: New York, Springer-Verlag.

- Price, J.R., and Velbel, M.A., 2000, Weathering of the Eaton Sandstone (Pennsylvanian), Grand Ledge, Michigan: Geochemical mass-balance and implications for reservoir properties beneath unconformities: *Journal Of Sedimentary Research*, v. 70, p. 1118–1128.
- Price, J.R., and Velbel, M.A., 2003, Chemical weathering indices applied to weathering profiles developed on heterogeneous felsic metamorphic parent rocks: *Chemical Geology*, v. 202, p. 397-416.
- Price, R.C., Gray, C.M., Wilson, R.E., Frey, F.A., and Taylor, S.R., 1991, The effects of weathering on rare-earth element, Y and Ba abundances in Tertiary basalts from southeastern Australia: *Chemical Geology*, v. 93, p. 245-265.
- Prosser, S., 1993, Rift-related linked depositional system and their seismic expression, in Williams, G.D., and Dobb, A., eds., *Tectonics and Seismic Sequence Stratigraphy*: London, Geological Society of London, Special Publication 71, p. 35-66.
- Prothero, D.R., 1990, *Interpreting the stratigraphic record*: New York, W.H. Freeman and Company, 555 p.
- Puigdefàbregas, C., 1993, Controls on fluvial sequence architecture, Brisbane 5th International Conference on Fluvial Sedimentology Proceedings p K42 K48.
- Pupin, J.P., 1980, Zircon and granite petrology: *Contributions to Mineralogy and Petrology*, v. 73, p. 207-220.
- Rahmani, R.A., 1973, Grain surface etching features of some heavy minerals: *Journal of Sedimentary Research*, v. 43, p. 882-888.
- Ramirez-Ramirez, C., 1978, Reinterpretación tectónica del Esquisto Granjeno de Ciudad Victoria, Tamaulipas: Universidad Nacional Autónoma de México, Instituto de Geología, Revista, v. 2, p. 31-36.
- Ramírez-Ramírez, C., 1992, Pre-Mesozoic geology of Huizachal-Peregrina Anticlinorium, Ciudad Victoria, Tamaulipas, and adjacent parts of eastern Mexico [PhD thesis]: Austin, University of Texas at Austin, 450 p.
- Ramos-Ledezma, A., 2007, Análisis microfascial del intervalo Jurásico-Cretácico Inferior en un corte del flanco sur del Valle de Huizachal, Tamaulipas, México [MSc thesis]: Linares, Universidad Autónoma de Nuevo León, 113 p.
- Reese, J.F., Mosher, S., Connelly, J., and Roback, R., 2000, Mesoproterozoic chronostratigraphy of the southeastern Llano uplift, central Texas: *Geological Society of America Bulletin*, v. 112, p. 278-291.
- Reineck, H.E., and Singh, I.B., 1980, *Depositional sedimentary environment*: New York, Springer-Verlag.
- Restrepo-Pace, P.A., 1992, Petrotectonic characterization of the Central Andean Terrane, Colombia: *Journal of South American Earth Sciences*, v. 5, p. 97-116.
- Retallack, G.J., 2001, *Soils of the past; An Introduction to Paleopedology*: Oxford, Blackwell, 404 p.
- Reyment, R., and Savazzi, E., 1999, *Aspects of multivariate statistical analysis in geology*: Amsterdam, Elsevier, 285 p.
- Reynaud, J.-Y., Dalrymple, R.W., Vennin, E., Parize, O., Besson, D., and Rubin, J.-L., 2006, Topographic controls on production and deposition of tidal cool-water carbonates, Uze' S Basin, Se France: *Journal Of Sedimentary Research*, v. 76, p. 117–130.
- Rhee, C., 2006, Conceptual problems and recent progress in fluvial sequence stratigraphy: *Geosciences Journal*, v. 10, p. 433-443.
- Ricci-Lucchi, F., 1985, Influence of transport processes and basin geometry on sand composition, in Zuffa, G.G., ed., *Provenance of Arenites*: Netherlands, Dordrecht D. Reidel Publishing Company, p. 309-332.
- Richards, H.G., 1963, Stratigraphy of earliest Mesozoic sediments in southeastern Mexico and western Guatemala: *American Association of Petroleum Geologists*, v. 47, p. 1861-1870.
- Rino, S., Kon, Y., Sato, W., Maruyama, S., Santosh, M., and Zhao, D., 2008, The Grenvillian and Pan-African orogens: World's largest orogenies through geologic time, and their implications on the origin of superplume: *Gondwana Research*, v. 14, p. 51-72.
- Robb, G.L., 1947, Red bed coloration: *Journal of Sedimentary Research*, v. 19, p. 99-103.
- Robert, C.M., 2008, Chapter Seven Aulacogens, in Christian, M.R., ed., *Developments in Marine Geology, Volume Volume 3*: Amsterdam, Elsevier, p. 239-248.
- Robison, R.A., and Pantoja-Alor, J., 1968, Tremadocian trilobites from the Nochixtlán in region, Oaxaca, Mexico: *Journal of Paleontology*, v. 42, p. 767-800.
- Roddaz, M., Viers, J., Brusset, S., Baby, P., Boucayrand, C., and Hérail, G., 2006, Controls on weathering and provenance in the Amazonian foreland basin: Insights from major and trace element geochemistry of Neogene Amazonian sediments: *Chemical Geology*, v. 226, p. 31-65.
- Rogers, J.J.W., 1996, A history of continents in the past three billion years: *The Journal of Geology*, v. 104, p. 91-107.
- Rollinson, H.R., 1993, *Using geochemical data: evaluation, presentation, interpretation*: London, Essex (Longman), 352 p.
- Ronov, A.B., and Yaroshevskiy, A.A., 1969, Chemical composition of the Earth crust, *The Earth's Crust and Upper Mantle* AGU, Mono, 13, 37.
- Rosaz, T., 1989, Les passages des Cordillères Nord-Américaines aux Sierras Madres Mexicaines le long du Texas Lineament Géologie du SW du Nouveau-Mexique (USA): *Bulletin des Centre de Recherches Exploration-Production Elf-Aquitaine*, v. 13 (2), p. 247-275.

- Roser, B.P., and Korsch, R.J., 1986, Plate tectonics and geochemical composition of sandstones: A discussion: *The Journal of Geology*, v. 93, p. 81-84.
- Roser, B.P., and Korsch, R.J., 1988, Provenance signatures of sandstone-mudstone suites determined using discriminant function analysis of major-element data: *Chemical Geology*, v. 67, p. 119-139.
- Roser, B.P., and Nathan, S., 1997, An evaluation of elemental mobility during metamorphism of a turbidite sequence (Greenland Group, New Zealand): *Geological Magazine*, v. 134, p. 219-234.
- Ross, C.A., and Ross, J.R.P., 1985, Late Paleozoic depositional sequences are synchronous and worldwide: *Geology*, v. 13, p. 194-197.
- Rowley, D.B., and Pindell, J.L., 1989, End Paleozoic-Early Mesozoic western Pangean reconstruction and its implications for the distribution of Precambrian and Paleozoic rocks around Meso-America: *Precambrian Research*, v. 42, p. 411-444.
- Rubatto, D., 2002, Zircon trace element geochemistry: partitioning with garnet and the link between U-Pb ages and metamorphism: *Chemical Geology*, v. 184, p. 123-138.
- Rubatto, D., and Gebauer, D., 2000, Use cathodoluminescence for U-Pb zircon dating by ion microprobe: some examples from the western Alps, in Pagel, M., Barbin, V., Blanc, P., and Ohnenstetter, D., eds., *Cathodoluminescence in Geosciences*: Berlin, Springer-Verlag, p. 373-400.
- Rubin, D.M., and Hunter, R.E., 1983, Reconstructing bedform assemblages from compound cross-bedding (geometry-reconstruction), in Brookfield, M.E., and Ahlbrandt, T.S., eds., *Eolian sediments and processes*, U.S. Geological Survey, p. 407-427.
- Rubio-Cisneros, I.I., 2008a, Análisis geoquímico y petrográfico de areniscas de las Formaciones Huizachal y La Joya (Triásico Superior - Jurásico Inferior), NE de México [Tesis de Licenciatura thesis]: Linares, Universidad Autónoma de Nuevo León, 121 p.
- Rubio-Cisneros, I.I., 2008b, Geochemistry and petrography of sandstones from the Huizachal and La Joya formations (Upper Triassic - Lower Jurassic), NE of Mexico: *Abstracts with Programs - Geological Society of America*, v. 40, p. 481.
- Rubio-Cisneros, I.I., and Lawton, T.F., 2010, Provenance interpretations combining petrography and Zircon U-Pb ages of sandstones in continental red beds at Valle de Huizachal, Tamaulipas, NE Mexico: Record of Early-Middle Jurassic Arc volcanism and transition to crustal extension: *Abstracts with Programs - Geological Society of America*.
- Rubio-Cisneros, I.I., and Lawton, T.F., 2011, Detrital zircon U-Pb ages of sandstones in continental red beds at Valle de Huizachal, Tamaulipas, NE Mexico: Record of Early-Middle Jurassic arc volcanism and transition to crustal extension: *Geosphere*, v. 7, p. 1-12.
- Rubio-Cisneros, I.I., and Ocampo-Díaz, Y.Z.E., 2010, Compositional analysis and sedimentary recycling evidences associated to unconformities in the northeastern Mexico, a Late Triassic-Early Cretaceous example: *Abstracts with Programs - Geological Society of America*, v. 42, p. 70.
- Rubio-Cisneros, I.I., Ramírez-Fernández, J.A., and García-Obregón, R., 2011, Análisis preliminar de procedencia de rocas clásticas jurásicas del Valle de Huizachal, Sierra Madre Oriental: Influencia del vulcanismo sinsedimentario y el basamento cristalino, in Montalvo-Arrieta, J.C., Chávez-Cabello, G., and Velasco-Tapia, F., eds., *Avances y paradigmas de la tectónica y la historia geológica del Noreste de México*, Volume 63, *Boletín de la Sociedad Geológica de México*, p. 137-156.
- Rueda-Gaxiola, J., 1993, El método palinoestratigráfico (Palinología Sensu lato) aplicado a la exploración petrolera: *Acta Mexicana de Ciencias y Tecnología*, v. XI, p. 23-33.
- Rueda-Gaxiola, J., Dueñas, M.A., Rodríguez, J.L., M., M., and Uribe, G., 1993a, Los Anticlinorios de Huizachal-Peregrina y de Huayacocotla: Dos partes de la fosa de Huayacocotla-El Alamar: *Boletín de la Asociación Mexicana de Geólogos Petroleros*, v. 43, p. 1-29.
- Rueda-Gaxiola, J., López-Ocampo, E., Dueñas, M.A., Rodríguez, J.L., Minero, M., and Uribe, G., 1993b, Los anticlinorios de Huizachal-Peregrina y de Huayacocotla: Dos partes de la fosa de Huayacocotla-El Alamar. II. El Alogrupo Los San Pedros: *Boletín de la Asociación Mexicana de Geólogos Petroleros*, v. 43, p. 1-33.
- Rueda-Gaxiola, J., López-Ocampo, E., Dueñas, M.A., Rodríguez, J.L., and Torres-Rivero, A., 1999, Palynostratigraphical method: Basis for defining stratigraphy and age of the Los San Pedros allogroup, Huizachal-Peregrina Anticlinorium, Mexico, in Bartolini, C., Wilson, J.L., and Lawton, T.F., eds., *Mesozoic Sedimentary and tectonic history of north-central Mexico*: Boulder, Colorado, Geological Society of America, Special Paper 340, p. 229-269.
- Rueda-Gaxiola, J., Minero, M., and Uribe, G., 1991, Las condiciones de depósito, tectónicas, climáticas y diagenéticas del Alogrupo La Boca (Anticlinorio de Huizachal-Peregrina) a partir del análisis de Difracción y Fluorescencia de Rayos X: *Actas de la Facultad de Ciencias de la Tierra, Universidad Autónoma de Nuevo León, Linares, México*, v. 6, p. 207-209.
- Ryer, T.A., 1994, Interplay of tectonics eustasy and sedimentation in the formation of Mid Cretaceous clastic wedges Central and Northern Rocky Mountain regions, in Dolson, J.C., Hendricks, M.L., and Wescott, W.A., eds., *Unconformity Related Hydrocarbon Exploration and Exploitation in Sedimentary Sequences Denver Rocky Mountain Association of Geologists* p 35.
- Sadowski, G.R., and Bettencourt, J.S., 1996, Mesoproterozoic tectonic correlations between eastern Laurentia and the western border of the Amazon Craton: *Precambrian Research*, v. 76, p. 213-227.
- Salvador, A., 1987, Late Triassic-Jurassic paleogeography and origin of Gulf of Mexico basin: *American Association of Petroleum Geologists Bulletin*, v. 71, p. 419-451.
- Salvador, A., 1991, The Gulf of Mexico basin, Volume J: Boulder, Colorado, Geological Society of America, *Geology of North America*, p. 568.

- Samson, S., Hibbard, J., and Wortman, G., 1995, Nd isotopic evidence for juvenile crust in the Carolina terrane, southern Appalachians: *Contributions to Mineralogy and Petrology*, v. 121, p. 171-184.
- Sánchez-Barreda, L.A., 1981, Geologic evolution of the Continental Margin of the Gulf of Tehuantepec in southwestern Mexico [PhD thesis]: United States -- Texas, The University of Texas at Austin, 269 p.
- Santosh, M., Maruyama, S., and Yamamoto, S., 2009, The making and breaking of supercontinents: Some speculations based on superplumes, super downwelling and the role of tectosphere: *Gondwana Research*, v. 15, p. 324-341.
- Sauderson, H.C., and Lockett, F.P.J., 1983, Flume experiments on bedforms and structures at the dune-plane bed transition, in Collinson, J.D., and Lewin, J., eds., *Modern and ancient fluvial systems*, International Association of Sedimentologists, Special Publication 6, p. 49-58.
- Schedl, A., and Wiltschko, D.V., 1984, Sedimentological effects of a moving terrain: *The Journal of Geology*, v. 92, p. 273-287.
- Scherer, H.H., Ernst, W.G., and Wooden, J.L., 2010, Regional detrital zircon provenance of exotic metasandstone blocks, Eastern Hayfork Terrane, Western Paleozoic and Triassic Belt, Klamath Mountains, California: *The Journal of Geology*, v. 118, p. 641-653.
- Schermer, E.R., and Busby, C., 1994, Jurassic magmatism in the central Mojave Desert: Implications for arc paleogeography and preservation of continental volcanic sequences: *Geological Society of America Bulletin*, v. 106, p. 767-790.
- Schermer, E.R., Howell, D.G., and Jones, D.L., 1984, The origin of allochthonous terranes: Perspectives on the growth and shaping of continents: *Annual Review of Earth and Planetary Sciences*, v. 12, p. 107-131.
- Schlager, W., 1991, Depositional bias and environmental change--important factors in sequence stratigraphy: *Sedimentary Geology*, v. 70, p. 109-130.
- Schlager, W., 1993, Accommodation and supply--a dual control on stratigraphic sequences: *Sedimentary Geology*, v. 86, p. 111-136.
- Schmidt-Effing, R., 1980, The Huayacocotla Sulacogen in Mexico (Lower Jurassic) and the origin of the gulf of Mexico. , in I Pilger, R.H., ed., *The origin of the gulf of Mexico and the early opening of central North Atlantic Ocean*, Volume 1, p. 1-405.
- Schmidt, P.W., and Embleton, B.J.J., 1976, Palaeomagnetic results from sediments of the Perth Basin, Western Australia, and their bearing on the timing of regional lateritisation: *Palaeogeography, Palaeoclimatology, Palaeoecology*, v. 19, p. 257-273.
- Schneider, E.D., and Sagan, D., 2005, *La Termodinámica de la Vida*: Espana, TusQuets, 438 p.
- Scholz, C.H., and Contreras, J.C., 1998, Mechanics of continental rift architecture: *Geology*, v. 26, p. 967-970.
- Scholl, D.W., Vallier, T.L., and Stevenson, A.J., 1986, Terrane accretion, production, and continental growth: A perspective based on the origin and tectonic fate of the Aleutian-Bering Sea region: *Geology*, v. 14, p. 43-47.
- Scholl, D.W., and von Huene, R., 2007, Crustal recycling at modern subduction zones applied to the past--issues of growth and preservation of continental basement crust, mantle geochemistry, and supercontinent reconstruction: *Boulder, Geological Society of America, Memoirs 200*, p. 9-32.
- Schrödinger, E., 1985, *Ciencia y Humanismo*: Espana, TusQuets, 83 p.
- Schumm, S.A., 1977, *The fluvial system*: New York, Wiley, 338 p.
- Schumm, S.A., 1981, Evolution and response of the fluvial system, sedimentologic implications, in Ethridge, F.G., and Flores, R.M., eds., *Recent and ancient nonmarine depositional environments: models for exploration*: Tulsa, SEPM (Society of Economic Paleontologists and Mineralogists), Special Publication 31, p. 19-29.
- Schumm, S.A., 1991, *To interpret the Earth ten ways to be wrong*: New York Cambridge University Press, 133 p.
- Schumm, S.A., Dumont, J.F., and Holbrook, J.M., 2000, *Active tectonics and alluvial rivers*: New York, Cambridge University Press, 276 p.
- Schumm, S.A., Mosley, M.P., and Weaver, W.E., 1987, *Experimental fluvial geomorphology*: New York, Wiley.
- Schwarzacher, W., 1975, *Sedimentation models and quantitative stratigraphy*: Amsterdam, Elsevier.
- Sedlock, R.L., Ortega-Guitierrez, F., and Speed, R.C., 1993, Tectonostratigraphic terranes and tectonic evolution of Mexico: *Boulder, Geological Society of America, Special Paper 278*, 152 p.
- Seilacher, A., 1954, Ökologie der triassischen Muschel *Lima lineata* (Schloth) und ihrer Epöken: *Neues Jahrb. Geol. Paleäontol., Monatsh.*, p. 163-183.
- Seilacher, A., 1963, Lebensspuren und Salinitätsfazies: *Fortschr. Geol. Rheinl. Westfalens*, v. 10, p. 81-94.
- Seilacher, A., 1964, Biogenic sedimentary structures, in Imbrie, J., and Newell, N., eds., *Approaches to Paleocology*: New York, Wiley, p. 296-316.
- Seilacher, A., 1967, Bathymetry of trace fossils: *Marine Geology*, v. 5, p. 413-428.
- Shan, G., Luo, T.-C., Zhang, B.-R., Zhang, H.-F., Han, Y.-w., Zhao, Z.-D., and Hu, Y.-K., 1998, Chemical composition of the continental crust as revealed by studies in East China: *Geochimica et Cosmochimica Acta*, v. 62, p. 1959-1975.

- Shanley, K.W., and McCabe, P.J., 1993, Alluvial architecture in a sequence stratigraphy framework: a case history from the Upper Cretaceous of southern Utah, USA, in Flint, S.S., and Bryant, I.D., eds., *The geological modelling of hydrocarbon reservoirs and outcrop analogues*, International Association of Sedimentologists, Special Publication 15, p. 21-56.
- Shanley, K.W., and McCabe, P.J., 1994, Perspectives on the sequence stratigraphy of continental strata: *American Association of Petroleum Geologists Bulletin*, v. 78, p. 544-568.
- Shanmugam, G., 1988, Origin, recognition and importance of erosional unconformities in sedimentary basins, in Kleinspehn, C.P., and Paola, C., eds., *New perspectives in basin analysis*: New York, Springer-Verlag, p. 83-109.
- Shepard, W., 1986, *North American aulacogens*, Medium: X; Size: Pages: 1056 p.
- Shukla, U.K., Singh, I.B., Srivastava, P., and Singh, D.S., 1999, Paleocurrent patterns in braid-bar and point-bar deposits; examples from the Ganga River, India: *Journal of Sedimentary Research*, v. 69, p. 992-1002.
- Shurbet, D.H., and Cebull, S.E., 1987, Tectonic interpretation of the westernmost part of the Ouachita-Marathon (Hercynian) orogenic belt, west Texas-Mexico: *Geology*, v. 15, p. 458-461.
- Silva-Pineda, A., 1970, *Plantas del Pensilvánico de la región de Tehuacán, Puebla*: Universidad Nacional Autónoma de México, Instituto de Geología, Paleontología Mexicana, v. 29, p. 47.
- Silva-Pineda, A., and Buitrón-Sánchez, B.E., 1999, Mesozoic redbed floras in east-central Mexico and their stratigraphic relationships with marine beds, in Bartolini, C., Wilson, J.L., and Lawton, T.F., eds., *Mesozoic sedimentary and tectonic history of north-central Mexico*: Boulder, Geological Society of America, Special Paper, 340, p. 161-170.
- Silva-Romo, G., Arellano-Gil, J., Mendoza-Rosales, C., and Nieto-Obregón, J., 2000, A submarine fan in the Mesa Central, Mexico: *Journal of South American Earth Sciences*, v. 13, p. 429-442.
- Simons, D.B., Richardson, E.V., and Nordin, C.F., 1965, Sedimentary structures generated by flow in alluvial channels, in Middleton, G.V., ed., *Primary Sedimentary Structures and Their Hydrodynamic Interpretation*: Tulsa, SEPM (Society for Sedimentary Geology), Special Publication 12, p. 34-52.
- Sinclair, H.D., 1997, Tectonostratigraphic model for underfilled peripheral foreland basins: An Alpine perspective: *Geological Society of America Bulletin*, v. 109, p. 324-346.
- Sloss, L.L., 1988, Forty years of sequence stratigraphy: *Geological Society of America Bulletin*, v. 100, p. 1661-1665.
- Sloss, L.L., 1991, The tectonic factor in sea level change: A countervailing view: *Journal of Geophysical Research*, v. 96, p. 6609-6617.
- Smith, A.G., and Livermore, R.A., 1991, Pangea in Permian to Jurassic time: *Tectonophysics*, v. 187, p. 135-179.
- Smith, D.G., 1973, Aggradation of the Alexandra-North Saskatchewan River, Banff Park, Alberta, in Morisawa, ed., *Fluvial geomorphology*. Proceedings of the 4th annual geomorphology symposium, publications in geomorphology: SUNY-Binghamton, New York, p. 201-219.
- Smith, D.G., 1983, Anastomosed fluvial deposits: modern examples from Western Canada, in Collison, J.D., and Lewis, J., eds., *Modern and ancient fluvial systems* 6, p. 155-168.
- Smith, D.G., 1986, Anastomosing river deposits, sedimentation rates and basin subsidence, Magdalena River, northwestern Colombia, South America: *Sedimentary Geology*, v. 46, p. 177-196.
- Smith, D.L., 1982, Review of the tectonic history of the Florida basement: *Tectonophysics*, v. 88, p. 1-22.
- Smith, N.D., 1970, The braided stream depositional environment: Comparison of the Platte River with some Silurian clastic rocks, North-Central Appalachians: *Geological Society of America Bulletin*, v. 81, p. 2993-3014.
- Smith, N.D., 1972, Some sedimentological aspects of planar cross-stratification in a sandy braided river: *Journal of Sedimentary Research*, v. 42, p. 624-634.
- Smith, S.A., 1990, The sedimentology and accretionary styles of an ancient gravel-bed stream: the Budleigh Salterton Pebble Beds (Lower Triassic), southwest England: *Sedimentary Geology*, v. 67, p. 199-219.
- Smoot, J.P., and Olsen, P.E., 1985, Massive mudstones in basin analysis and paleoclimatic interpretation of the Newark Supergroup, in Robinson, G.R., and Froelich, A.J., eds., *Proceedings of the second U.S. Geological Survey workshop on the early Mesozoic basins of the eastern United States*, Volume 946, U.S. Geological Survey Circular 946, p. 29-33.
- Smosna, R., Bruner, K.R., and Burns, A., 1999, Numerical analysis of sandstone composition, provenance, and paleogeography: *Journal of Sedimentary Research*, v. 69, p. 1063-1070.
- Sneh, A., 1983, Desert stream sequences in the Sinai Peninsula: *Journal of Sedimentary Research*, v. 53, p. 1271-1279.
- Soegaard, K., 1990, Fan-delta and braid-delta systems in Pennsylvanian Sandia Formation, Taos Trough, northern New Mexico: Depositional and tectonic implications: *Geological Society of America Bulletin*, v. 102, p. 1325-1343.
- Solari, L.A., Keppie, J.D., Ortega-Gutiérrez, F., Cameron, K.L., Lopez, R., and Hames, W.E., 2003, 990 and 1100 Ma Grenvillian tectonothermal events in the northern Oaxacan Complex, southern Mexico: roots of an orogen: *Tectonophysics*, v. 365, p. 257-282.
- Solari, L.A., Ortega-Gutiérrez, F., Elías-Herrera, M., Gómez-Tuena, A., and Schaaf, P., 2010, Refining the age of magmatism in the Altos Cuchumatanes, western Guatemala, by LA-ICPMS, and tectonic implications: *International Geology Review*, v. 52, p. 977-998.

- Sour-Tovar, F., Alvarez, F., and Martinez Chacon, M.L., 2005, Lower Mississippian (Osagean) spire-bearing brachiopods from Canon de la Peregrina, north of Ciudad Victoria, Tamaulipas, Northeastern Mexico: *Journal of Paleontology*, v. 79, p. 469-485.
- Speed, R.C., 1979, Collided Paleozoic Microplate in the Western United States: *The Journal of Geology*, v. 87, p. 279-292.
- Stattegger, K., 1987, Heavy minerals and provenance of sands; modeling of lithological end members from river sands of northern Austria and from sandstones of the Austroalpine Gosau Formation (Late Cretaceous): *Journal of Sedimentary Research*, v. 57, p. 301-310.
- Stear, W.M., 1985, Comparison of the beadform distribution and dynamics of modern and ancient sandy ephemeral flood deposits in the Southwestern Karoo region, South Africa: *Sedimentary Geology*, v. 45, p. 209-230.
- Steel, R.J., 1974, New red sandstone floodplain and piedmont sedimentation in the Hebridean province, Scotland: *Journal of Sedimentary Research*, v. 44, p. 336-357.
- Steel, R.J., and Thompson, D.B., 1983, Structures and textures in Triassic braided stream conglomerates ('Bunter' Pebble Beds) in the Sherwood Sandstone Group, North Staffordshire, England: *Sedimentology*, v. 30, p. 341-367.
- Stewart, J.H., 1988, Latest Proterozoic and Paleozoic southern margin of North America and the accretion of Mexico: *Geology*, v. 16, p. 186-189.
- Stewart, J.H., Amaya-Martinez, R., Stamm, R., Wardlaw, B., Stanley, G.D., and Stevens, C.H., 1997, Stratigraphy and regional significance of Mississippian to Jurassic rocks in Sierra Santa Teresa, Sonora, Mexico: *Revista Mexicana De Ciencias Geologicas*, v. 14, p. 115-135.
- Stewart, J.H., Blodgett, R.B., Boucot, A.J., and Carter, J.L., 1993, Middle Paleozoic exotic terrane near Ciudad Victoria, Northeastern Mexico, and the southern margin of Paleozoic North America: *Proceedings of the First Circum-Pacific and Circum-Atlantic terrane Conference: Universidad Nacional Autónoma de México, Instituto de Geología*, p. 147-149.
- Stewart, J.H., Blodgett, R.B., Boucot, A.J., Carter, J.L., and López, R., 1999, Exotic Paleozoic strata of Gondwana provenance near Ciudad Victoria, Tamaulipas, México, in Ramos, V.A., and Keppie, D., eds., *Laurentia-Gondwana connections before Pangea: Boulder, Colorado, Geological Society of America, Special Paper 336*, p. 227-252.
- Stewart, J.H., Poole, F.G., and Geological, S., 2002, *Inventory of Neoproterozoic and Paleozoic strata in Sonora, Mexico, US Dept. of the Interior, US Geological Survey*.
- Stewart, J.H., Poole, F.G., Ketner, K.B., Madrid, R.J., Roldán-Quintana, J., and Amaya-Martinez, R., 1990, Tectonics and stratigraphy of the Paleozoic and Triassic southern margin of North America, Sonora, Mexico, in Gehrels, G.E., and Spencer, J.E., eds., *Geologic excursions through the Sonoran Desert Region, Arizona and Sonora: Arizona Geological Survey Special Paper 7*, p. 183-202.
- Stock, J.M., and Lee, J., 1994, Do microplates in subduction zones leave a geological record?: *Tectonics*, v. 13, p. 1472-1487.
- Storey, B.C., and Meneilly, A.W., 1985, Petrogenesis of metamorphic rocks within a subduction-accretion terrane, Signy Island, South Orkney Islands: *Journal of Metamorphic Geology*, v. 3, p. 21-42.
- Stow, D.A.V., 1979, Distinguishing between fine-grained turbidites and contourites on the Nova Scotian deep water margin: *Sedimentology*, v. 26, p. 371-387.
- Stow, D.A.V., 2006, *Sedimentary rocks in the field, A color guide: San Diego, Academic Press*.
- Straub, K.M., Paola, C., Mohrig, D., Wolinsky, M.A., and George, T., 2009, Compensational stacking of channelized sedimentary deposits: *Journal of Sedimentary Research*, v. 79, p. 673-688.
- Strong, N., and Paola, C., 2006, Fluvial landscapes and stratigraphy in a flume: *The Sedimentary Record*, v. 4, p. 4-7.
- Suttner, L.J., Basu, A., and Mack, G.H., 1981, Climate and the origin of quartz arenites: *Journal of Sedimentary Research*, v. 51, p. 1235-1246.
- Swan, A.R.H., and Sandilands, M.H., 1995, *Introduction to geological data analysis: London, Wiley-Blackwell*, 496 p.
- Tardy, M., Blanchet, R., and Zimmermann, M., 1989, Les linéaments du Texas et Caltam entre Cordillères Américaines et Sierras Madre Mexicanes: *Nature, Origine et Évolution structurale: Bulletin des Centre de Recherches Exploration-Production Elf-Aquitaine*, v. 13 (2), p. 219-227.
- Taylor, S.R., and McLennan, S.M., 1981, The composition and evolution of the continental crust: Rare Earth Element evidence from sedimentary rocks: *Philosophical Transactions of the Royal Society of London. Series A, Mathematical and Physical Sciences*, v. A301, p. 381-399.
- Taylor, S.R., and McLennan, S.M., 1985, *The continental crust: its composition and evolution: Oxford, Blackwell* 312 p.
- Taylor, S.R., and McLennan, S.M., 1995, The geochemical evolution of the continental crust: *Reviews of Geophysics*, v. 33, p. 241-265.
- Taylor, S.R., and McLennan, S.M., 2009, *Planetary crust: Their composition, origin and evolution: New York, Cambridge University Press*, 378 p.
- Teyssier, C., Tikoff, B., and Markley, M., 1995, Oblique plate motion and continental tectonics: *Geology*, v. 23, p. 447-450.
- Todd, S.P., 1996, Process deduction from fluvial sedimentary structures, in Carling, P.A., and Dawson, M.R., eds., *Fluvial Dynamics and Stratigraphy: Chichester, Wiley*, p. 299-350.

- Tohver, E., Teixeira, W., van der Pluijm, B., Geraldès, M.C., Bettencourt, J.S., and Rizzotto, G., 2006, Restored transect across the exhumed Grenville orogen of Laurentia and Amazonia, with implications for crustal architecture: *Geology*, v. 34, p. 669-672.
- Torres-Sánchez, S.A., Ramírez-Fernández, J.A., and Barboza-Gudiño, J.R., 2010, Petrologic comparison between Paleozoic basement from two different localities in northeastern Mexico: Caballeros Canyon, Tamaulipas and Aramberri Uplift, Nuevo Leon: Abstracts with Programs - Geological Society of America.
- Torres-Vargas, R., Ruiz, J., Murillo-Muneton, G., and Grajales-Nishimura, J.M., 1993, The Paleozoic magmatism in Mexico: evidences for the shift from circum-Atlantic to circum-Pacific tectonism: Proceedings of the 1st Circum-Pacific and Circum-Atlantic Terrane Conference, Instituto de Geología, Universidad Nacional Autónoma de México, p. 154-155.
- Torres, R., Ruiz, J., Patchett, P.J., and Grajales-Nishimura, J.M., 1999, Permo-Triassic continental arc in eastern Mexico: Tectonic implications for reconstructions of southern North America, in Bartolini, C., Wilson, J.L., and Lawton, T.F., eds., *Mesozoic Sedimentary and Tectonic History of North-Central Mexico*: Boulder, Colorado, Geological Society of America, Special Paper, 340, p. 191-196.
- Tortosa, A., Palomares, M., and Arribas, J., 1991, Quartz grain types in Holocene deposits from the Spanish Central System: some problems in provenance analysis, in Morton, A.C., Todd, S.P., and Houghton, P., eds., *Developments in Sedimentary Provenance Studies*, Volume 57: London, Geological Society, Special Publication 57, p. 47-54.
- Totten, M.W., Hanan, M.A., and Weaver, B.L., 2000, Beyond whole-rock geochemistry of shales: The importance of assessing mineralogic controls for revealing tectonic discriminants of multiple sediment sources for the Ouachita Mountain flysch deposits: *Geological Society of America Bulletin*, v. 112, p. 1012-1022.
- Toulkeridis, T., Clauer, N., Kröner, A., Reimer, T., and Todt, W., 1999, Characterization, provenance, and tectonic setting of Fig Tree greywackes from the Archaean Barberton Greenstone Belt, South Africa: *Sedimentary Geology*, v. 124, p. 113-129.
- Tribovillard, N., Lyons, T.W., Riboulleau, A., and Bout-Roumazeilles, V., 2008, A possible capture of molybdenum during early diagenesis of dysoxic sediments: *Bulletin de la Société Géologique de France*, v. 179, p. 3-12.
- Tröger, W.E., and Bambauer, H.U., 1967, *Optische Bestimmung der gesteinsbildenden Minerale: Teil 2, Textband*, Schweizerbart.
- Trudgill, B., and Underhill, J.R., 2002, Introduction to the structure and stratigraphy of rift systems: *American Association of Petroleum Geologists Bulletin*, v. 86, p. 931-933.
- Tull, J.F., Barineau, C.I., Mueller, P.A., and Wooden, J.L., 2007, Volcanic arc emplacement onto the southernmost Appalachian Laurentian shelf: Characteristics and constraints: *Geological Society of America Bulletin*, v. 119, p. 261-274.
- Tunbridge, I.P., 1981, Sandy high-energy flood sedimentation--Some criteria for recognition, with an example from the Devonian of S.W. England: *Sedimentary Geology*, v. 28, p. 79-95.
- Türk, G., 1982, Markov Chain analysis: *Mathematical Geology*, v. 14, p. 539-542.
- Turner, J.R., 2001, Evidence for strike-slip faulting in the Smackover formation of northeast Texas and south Arkansas and its geological implications, Volume 51, *Gulf Coast Association of Geological Societies Transactions*.
- Turner, P., 1980a, *Developments in Sedimentology*, Volume Volume 29: Amsterdam, Elsevier, p. iii-iii.
- Turner, P., 1980b, Chapter 1 The Geological framework of continental red beds, *Developments in Sedimentology*, Volume Volume 29: Amsterdam, Elsevier, p. 1-68.
- Turner, S., and Rushmer, T., 2009, Similarities between mantle-derived A-type granites and voluminous rhyolites in continental flood basalt provinces: *Earth and Environmental Science Transactions of the Royal Society of Edinburgh*, v. 100, p. 51-60.
- Unrug, R., 1997, Rodinia to Gondwana: The geodynamic map of Gondwana supercontinent assembly: *GSA Today*, v. 7, p. 1-6.
- Vachard, D., Flores de Dios, A., and Buitrón, B., 2004, Guadalupian and Lopingian (Middle and Late Permian) deposits from Mexico and Guatemala, a review with new data: *Geobios*, v. 37, p. 99-115.
- Vachard, D., Fourcade, E., Romero, J.E., Méndez, J., Cosillo, A., Alonzo, M., Requena, J., Azema, J., and Cros, P., 1997, Foraminifères *et algues* du Permien du Guatemala: *Geobios*, v. 30, p. 745-784.
- Valloni, R., 1985, Reading provenance from modern marine sands, in Zuffa, G.G., ed., *Provenance of Arenites*: Netherlands, Dordrecht D. Reidel Publishing Company, p. 309-332.
- Van Houten, F.B., 1973, Origin of red beds a review-1961-1972: *Annual Review of Earth and Planetary Sciences*, v. 1, p. 39-61.
- van Millot, G., 1970, *Geology of clays*: New York, Springer-Verlag, 429 p.
- Van Wagoner, J.C., Mitchum, R.M., Campion, K.M., and Rahmanian, V.D., 1990, Siliciclastic sequence stratigraphy in well logs, cores, and outcrops, *American Association of Petroleum Geologists, Methods of Exploration Series 7*, 55 p.
- Van Wagoner, J.C., Posamentier, H.W., Mitchum, R.M., Vail, P.R., Sarg, J.F., Loutit, T.S., Hardenbol, J., and Jervey, M.T., 1988, An overview of the fundamentals of sequence stratigraphy and key definitions quantitative geological modeling of siliciclastic rock sequences and their seismic expression, in Wilgus, C.K., Hastings, B.S., Posamentier, H., Wagoner, J.V., Ross, C.A., and Kendall, C.G.S.C., eds., *Sea-Level Changes*: Tulsa, SEPM (Society for Sedimentary Geology), Special Publication 42, p. 39-45.

- Vaughan, A.P.M., Leat, P.T., and Pankhurst, R.J., 2005, Terrane Processes at the Margins of Gondwana, in Vaughan, A.P.M., Leat, P.T., and Pankhurst, R.J., eds., *Terrane Processes at the Margins of Gondwana*: London, Geological Society of London, Special Publications 246, p. 439.
- Vaughn Barrie, J., 1981, Hydrodynamic factors controlling the distribution of heavy minerals (Bristol Channel): *Estuarine, Coastal and Shelf Science*, v. 12, p. 609-619.
- Vavra, G., 1990, On the kinematics of zircon growth and its petrogenetic significance: a cathodoluminescence study: *Contributions to Mineralogy and Petrology*, v. 106, p. 90-99.
- Veevers, J.J., 2005, Edge tectonics (trench rollback, terrane export) of Gondwanaland-Pangea synchronized by supercontinental heat: *Gondwana Research*, v. 8, p. 449-456.
- Vega-Granillo, R., Salgado-Souto, S., Herrera-Urbina, S., Valencia, V., Ruiz, J., Meza-Figueroa, D., and Talavera-Mendoza, O., 2008, U-Pb detrital zircon data of the Rio Fuerte Formation (NW Mexico): Its peri-Gondwanan provenance and exotic nature in relation to southwestern North America: *Journal of South American Earth Sciences*, v. 26, p. 343-354.
- Veizer, J., 1973, Sedimentation in Geologic History: Recycling vs. Evolution or Recycling with Evolution: *Contributions to Mineralogy and Petrology*, v. 38, p. 261-278.
- Venegas-Rodríguez, G., Barboza-Gudiño, J.R., and López-Doncel, R.A., 2009, Geocronología de circones detríticos en capas del Jurásico Inferior de las áreas de la Sierra de Catorce y El Alamito en el estado de San Luis Potosí: *Revista Mexicana De Ciencias Geológicas*, v. 26, p. 466-481.
- Verdecchia, S.O., and Baldo, E.G., 2010, Geoquímica y procedencia de los metasedimentos ordovícicos del complejo metamórfico La Cébila, provincia de La Rioja, Argentina: *Revista Mexicana De Ciencias Geológicas*, v. 27 (1), p. 97-111.
- Villaseñor-Martínez, A.B., Martínez-Cortés, A.M., and Contreras y Montero, B., 1987, Bioestratigrafía del Paleozoico Superior de San Salvador Pantlanoaya, Puebla, México: *Revista de la Sociedad Mexicana de Paleontología*, v. 1, p. 396-417.
- Visher, G.S., 1965, Fluvial processes as interpreted from ancient and recent fluvial deposits, in Middleton, G.V., ed., *Primary Sedimentary Structures and Their Hydrodynamic Interpretation*: Tulsa, SEPM (Society for Sedimentary Geology), Special Publication 12, p. 116-132.
- Vistelius, A.B., 1949, On the question of the mechanism of the formation of strata: *Akad. Nauk S.S.S.R.*, v. 65, p. 191-194.
- Viswanathan, K., 1981, The crystal structure of a Mg-rich carpholite: *American Mineralogist*, v. 66, p. 1080-1085.
- Viveros, M., 1965, Geología del área Cabullona-Caloso, Municipio de Agua Prieta, Sonora: México, D.F., Universidad Nacional Autónoma de México, Facultad de Ingeniería, tesis profesional, p. 80 (inérita).
- von Eynatten, H., 2004, Statistical modelling of compositional trends in sediments: *Sedimentary Geology*, v. 171, p. 79-89.
- von Huene, R., and Scholl, D.W., 1991, Observations at convergent margins concerning sediment subduction, subduction erosion, and the growth of continental crust: *Reviews of Geophysics*, v. 29, p. 279-316.
- Walker, J.D., 1988, Permian and Triassic rocks of the Mojave Desert and their implications for timing and mechanisms of continental truncation: *Tectonics*, v. 7, p. 685-709.
- Walker, J.D., and Geissman, J.W., 2009, 2009 GSA Geologic Time Scale: : *GSA Today*, v. 19, p. 60.
- Walker, N., 1992, Middle Proterozoic geologic evolution of Llano uplift, Texas: Evidence from U-Pb zircon geochronometry: *Geological Society of America Bulletin*, v. 104, p. 494-504.
- Walker, T.R., 1967, Formation of red beds in modern and ancient deserts: *Geological Society of America Bulletin*, v. 78, p. 353-368.
- Walker, T.R., Waugh, B., and Grone, A.J., 1978, Diagenesis in first-cycle desert alluvium of Cenozoic age, southwestern United States and northwestern Mexico: *Geological Society of America Bulletin*, v. 89, p. 19-32.
- Walsh, S.L., 2001, Notes on geochronologic and chronostratigraphic units: *Geological Society of America Bulletin*, v. 113, p. 704-713.
- Wandres, A.M., Bradshaw, J.D., Weaver, S., Maas, R., Ireland, T., and Eby, N., 2004, Provenance of the sedimentary Rakaia subterranean, Torlesse Terrane, South Island, New Zealand: the use of igneous clast compositions to define the source: *Sedimentary Geology*, v. 168, p. 193-226.
- Ward, P.L., 1995, Subduction cycles under western North America during the Mesozoic and Cenozoic eras, in Miller, D.M., and Busby, C., eds., *Jurassic, Magmatism and Tectonics of the North American Cordillera*, Volume 299: Boulder, Colorado, Geological Society of America, Special Publication 299, p. 1-45.
- Wardlaw, B.R., Furnish, W.M., and Nestell, M.K., 1979, Geology and paleontology of the Permian beds near Las Delicias, Coahuila, Mexico: *Geological Society of America Bulletin*, v. 90, p. 111-116.
- Watson, H.J., 1958, Geology of Novillo Canyon. Tamaulipas [MSc thesis]: Louisiana, Louisiana State University, 56 p.
- Weber, B., Cameron, K.L., Osorio, M., and Schaaf, P., 2005, A Late Permian tectonothermal event in Grenville crust of the Southern Maya Terrane: U-Pb zircon ages from the Chiapas Massif, Southeastern Mexico: *International Geology Review*, v. 47, p. 509 - 529.
- Weber, B., Gruner, B., Hecht, L., Molina-Garza, R., and Köhler, H., 2002, El descubrimiento de basamento metasedimentario en el Macizo de Chiapas: La "Unidad la Sepultura": *GEOS*, v. 22, p. 2-11.

- Weber, B., and Hecht, L., 2003, Petrology and geochemistry of metigneous rocks from a Grenvillian basement fragment in the Maya block: the Guichicovi complex, Oaxaca, southern Mexico: *Precambrian Research*, v. 124, p. 41-67.
- Weber, B., and Köhler, 1999, Sm-Nd, Rb-Sr and U-Pb geochronology of a Grenville Terrane in Southern Mexico: Origin and geologic history of the Guichicovi Complex: *Precambrian Research*, v. 96, p. 245-262.
- Weber, B., Schaaf, P., Valencia, V.A., Iriondo, A., and Ortega-Gutiérrez, F., 2006, Provenance ages of late Paleozoic sandstones (Santa Rosa Formation) from the Maya block, SE Mexico. Implications on the tectonic evolution of western Pangea: *Revista Mexicana de Ciencias Geológicas*, v. 23, p. 262-276.
- Weber, J.N., and Middleton, G.V., 1961a, Geochemistry of the turbidites of the Normanskill and Charny formations-I: Effect of turbidity currents on the chemical differentiation of turbidites: *Geochimica et Cosmochimica Acta*, v. 22, p. 200-243.
- Weber, J.N., and Middleton, G.V., 1961b, Geochemistry of the turbidites of the Normanskill and Charny formations-II: Distribution of trace elements: *Geochimica et Cosmochimica Acta*, v. 22, p. 244-288.
- Weber, M.B.I., Cardona, A., Paniagua, F., Cordani, U., Sepulveda, L., and Wilson, R., 2009, The Cabo de la Vela Mafic-Ultramafic Complex, Northeastern Colombian Caribbean region: a record of multistage evolution of a Late Cretaceous intra-oceanic arc, in James, K.H., Lorente, M.A., and Pindell, J.L., eds., *The Origin and Evolution of the Caribbean Plate*, Volume 328: London, Geological Society of London, Special Publications 328, p. 549-568.
- Weber, R., 1997, How old is the Triassic flora of Sonora and Tamaulipas and news on Leonardian floras in Puebla and Hidalgo, México: *Revista Mexicana De Ciencias Geologicas*, v. 14, p. 225-243.
- Weber, R., and Ceballos-Ferriz, S.R.S., 1994, Perfil actual y perspectivas de la Paleobotánica en México: *Boletín de la Sociedad Botánica de México*, v. 55, p. 141-148.
- Wedepohl, K., 1991, Chemical composition and fractionation of the continental crust: *Geologische Rundschau*, v. 80, p. 207-223.
- Weltje, G.J., 2002, Quantitative analysis of detrital modes: statistically rigorous confidence regions in ternary diagrams and their use in sedimentary petrology: *Earth-Science Reviews*, v. 57, p. 211-253.
- Weltje, G.J., 2006, Ternary sandstone composition and provenance: an evaluation of the 'Dickinson model', in Buccianti, A., Mateu-Figueras, G., and Pawlowsky-Glahn, V., eds., *Compositional Data Analysis in the Geosciences: From Theory to Practice*, Volume 264: London, Geological Society of London, Special Publications, 264, p. 79-99.
- Wheeler, H.E., 1964, Baselevel, lithosphere surface, and time-stratigraphy: *Geological Society of America Bulletin*, v. 75, p. 599-610.
- White, A.F., and Brantley, S.L., 2003, The effect of time on the weathering of silicate minerals: why do weathering rates differ in the laboratory and field?: *Chemical Geology*, v. 202, p. 479-506.
- White, G.W., 1980, Permian-Triassic continental reconstruction of the Gulf of Mexico-Caribbean area: *Nature*, v. 283, p. 823-826.
- Widdowson, M., 1997, The geomorphological and geological importance of palaeosurfaces, in Widdowson, M., ed., *Palaeosurfaces: Recognition, Reconstruction and Palaeoenvironmental Interpretation*: London, Geological Society of London, Special Publications 120, p. 1-12.
- Wilson, J.L., 1990, Basement structural controls on Mesozoic carbonate facies in Northeastern Mexico-a review: *Actas de la Facultad de Ciencias de la Tierra, Universidad Autónoma de Nuevo León, Linares, México*, v. 4, p. 5-45.
- Wilson, M., 2007, *Igneous Petrogenesis*: Dordrecht, Springer-Verlag, 466 p.
- Wilson, R.C.L., Whitmarsh, R.B., Taylor, B., and Froitheim, N., 2001, Non-volcanic rifting of continental margins: A comparison of evidence from land and sea: London, Geological Society of London, Special Publications, 187, 577 p.
- Willan, R.C.R., and Hunter, M.A., 2005, Basin evolution during the transition from continental rifting to subduction: Evidence from the lithofacies and modal petrology of the Jurassic Latady Group, Antarctic Peninsula: *Journal of South American Earth Sciences*, v. 20, p. 171-191.
- Winkler, C.D., and Buffler, R.T., 1988, Paleogeographic evolution of early deep water Gulf of Mexico and margins, Jurassic to Middle Cretaceous (Comanchean): *American Association of Petroleum Geologists Bulletin*, v. 72, p. 318-346.
- Withers, A.C., Essene, E.J., and Zhang, Y., 2003, Rutile/TiO₂ phase equilibria: *Contributions to Mineralogy and Petrology*, v. 145, p. 199-204.
- Witte, W.K., and Kent, D.V., 1991, Tectonic implications of a Remanetization Event in the Newark Basin: *Journal of Geophysical Research*, v. 96, p. 19569-19582.
- Womack, W.R., and Schumm, S.A., 1977, Terraces of Douglas Creek, northwestern Colorado: An example of episodic erosion: *Geology*, v. 5, p. 72-76.
- Woods, R.D., and Addington, J.W., 1973, Pre-Jurassic geologic framework northern Gulf basin: *Trans. Gulf Coast Assoc. Geol. Soc.*, v. 23, p. 92-108.
- Wright, F.E., 1912, Microscopical petrography from the quantitative viewpoint: *The Journal of Geology*, v. 20, p. 481-501.
- Wright, J.E., and Wyld, S.J., 2007, Alternative tectonic model for Late Jurassic through Early Cretaceous evolution of the Great Valley Group, California, in Cloos, M., Carlson, W.D., Gilbert, M.C., Liou, J.G., and Sorensen, S.S., eds., *Convergent Margin Terranes and Associated Regions: A Tribute to W.G. Ernst*: Boulder, Geological Society of America, Special Paper 419, p. 1-15.

- Wright, P.V., and Marriott, S.B., 1993, The sequence stratigraphy of fluvial depositional systems: the role of floodplain sediment storage: *Sedimentary Geology*, v. 86, p. 203-210.
- Young, G.M., and Nesbitt, H.W., 1998, Processes controlling the distribution of Ti and Al in weathering profiles, siliciclastic sediments and sedimentary rocks: *Journal of Sedimentary Research*, v. 68, p. 448-455.
- Yuen, D.A., Maruyama, S., Karato, S.-i., Windley, B.F., Monnereau, M., Hansen, U., Kameyama, M., and Matyska, C., 2007, *Superplumes: Beyond plate tectonics*: Heidelberg, Springer-Verlag, 569 p.
- Zaghloul, M.N., Critelli, S., Perri, F., Mongelli, G., Perrone, V., Sonnino, M., Tucker, M., Aiello, M., and Ventimiglia, C., 2010, Depositional systems, composition and geochemistry of Triassic rifted-continental margin redbeds of the Internal Rif Chain, Morocco: *Sedimentology*, v. 57, p. 312–350.
- Zeibig, G., 1991, Elementkorrelationen in klastischen Sedimenten und ihre Ursachen: *Zbl. Geol. Paläont, Teil I*, v. 1990 (8), p. 1155-1174.
- Zimmermann, U., 1999, *Sedimentpetrographische, geochemische und isotopengeochemische Methoden zur Bestimmung der Beziehung von Provenienz und Ablagerungsraum an aktiven Kontinentalrändern: Das ordovizische Back-Arc-Becken in der Süd-Puna, Hochland im Nordwesten Argentiniens*. [PhD thesis]: Heidelberg, University of Heidelberg, 282 p.
- Zuffa, G.G., 1980, Hybrid arenites; their composition and classification: *Journal of Sedimentary Research*, v. 50, p. 21-29.
- Zuffa, G.G., 1985, Optical analyses of arenites: influence of methodology on compositional results, in Zuffa, G.G., ed., *Provenance of Arenites*: Netherlands, Dordrecht D. Reidel Publishing Company, p. 165-189.
- Zuffa, G.G., Cibir, U., and Di Giulio, A., 1995, Arenite petrography in sequence stratigraphy: *The Journal of Geology*, p. 451-459.
- Zuffa, G.G., and Critelli, S., 2010, Sourceland controls and dispersal pathways reflected in clastic sediment composition, *Book of abstracts - 1st WGSG Workshop, Università della Calabria*, p. 1.
- Zuffa, G.G., Gaudio, W., and Rovito, S., 1980, Detrital mode evolution of the rifted continental-margin Longobucco Sequence (Jurassic), Calabrian Arc, Italy, in Caracciolo, L., and Critelli, S., eds., *Book of abstracts - 1st WGSG Workshop, Volume 50*, p. 51-61.

APPENDIX FOR CHAPTER 2: Transition frequency matrix markov chain

1) Lomas de San Paulo Tranquilas
SW from Cerro de la Nieve

Facies	St	Fm	Se	Gmm	Fl	Sh	P	Sp	Sm	Sp
St	0.90410959	0.07671233	0	0.00273973	0.00821918	0.00273973	0.00273973	0.00273973	0.00273973	0
Fm	0.22115385	0.74038462	0.03846154	0	0	0	0	0	0	0
Se	0.03703704	0.03703704	0.88888889	0	0.03703704	0	0	0	0	0
Gmm	0.02777778	0	0.97222222	0	0	0	0	0	0	0
Fl	0.03571429	0	0	0.89285714	0.03571429	0	0	0.03571429	0	0
Sh	0	0	0	0.04545455	0.90909091	0.04545455	0	0	0	0
P	0.15384615	0	0	0	0	0.76923077	0.07692308	0	0	0
Sp	0.03703704	0	0	0	0	0	0.95555556	0.04444444	0	0.96296296

2) Cañón Alamar

Facies	Sh	St	Fm	Gcm	Gh	P	Fl	Sp	Se	Af	Sl	Gp	Sm	Gmg	Gt
Sh	0.73333333	0.13333333	0.03333333	0	0	0	0.06666667	0	0.03333333	0	0	0	0	0	0
St	0.02173913	0.70652174	0.19565217	0	0.01086957	0.0326087	0	0	0.0326087	0	0	0	0	0	0
Fm	0.00826446	0.0661157	0.83471074	0.0661157	0	0	0	0	0.00826446	0.00826446	0	0	0	0	0.00826446
Gcm	0.02702703	0.08108108	0	0.75675676	0.08108108	0	0	0.02702703	0	0	0	0	0	0	0.02702703
Gh	0.21428571	0	0	0	0.71428571	0	0	0	0	0	0	0.07142857	0	0	0
P	0	0	0	0	0.69230769	0.15384615	0	0	0	0	0	0.07692308	0	0.07692308	0
Fl	0	0.03571429	0.03571429	0.07142857	0	0.07142857	0.78571429	0.75	0	0	0	0	0	0	0
Sp	0	0.25	0	0	0	0	0	0	0.5	0	0.25	0	0	0	0
Se	0	0.25	0	0	0	0	0	0	0	0.5	0.25	0	0	0	0
Af	0	0.11111111	0	0	0	0	0	0	0	0.88888889	0	0	0	0	0
Sl	0	0.11111111	0	0	0	0	0	0	0	0.88888889	0	0	0	0	0
Gp	0	0.33333333	0	0.08333333	0	0	0	0	0.83333333	0.83333333	0	0	0	0	0
Sm	0	0.33333333	0	0	0	0	0	0	0	0	0	0.83333333	0	0	0
Gmg	0	0	0	0.14285714	0	0	0	0	0	0	0	0	0.66666667	0	0
Gt	0	0	0	0.14285714	0	0	0	0	0	0	0	0	0.14285714	0.85714286	0.71428571

3) Aramberri

Ab Uplift s. west flank

Facies	Fm	Af	Fl	Gcm	Cb	Sh	St
Fm	0.79136691	0.10071942	0	0.00719424	0.02158273	0.04316547	0.03597122
Af	0.17073717	0.65853659	0.14634146	0.02439024	0	0	0
Fl	0.5	0	0.41666667	0.08333333	0	0	0
Gcm	0.04651163	0	0	0.93023256	0.02325581	0	0
Cb	0.33333333	0	0	0	0.55555556	0.11111111	0
Sh	0.54545455	0	0	0	0	0.45454545	0
St	0.38461538	0	0	0	0	0	0.61538462

4) Cañón el Olmo

Facies	Fm	St	Af	Gmm	Fl	Se	Sr	Gmg	Gp	Sh	Gci	Gh	Sm	Cb
Fm	0.9245283	0.04402516	0	0.01257862	0.00628931	0.00628931	0	0	0	0	0	0.00628931	0	0
St	0.0620155	0.85271318	0.00775194	0.02325581	0.00775194	0	0.03100775	0.00775194	0.00775194	0	0	0	0	0
Af	0.05263158	0.05263158	0.84210526	0	0.05263158	0	0	0	0	0	0	0	0	0
Gmm	0	0.16666667	0	0.79166667	0	0	0	0	0.04166667	0	0	0	0	0
Fl	0	0	0.33333333	0	0.66666667	0	0	0	0	0	0	0	0	0
Se	0	0.05	0	0	0	0.9	0.05	0	0	0	0	0	0	0
Sr	0.05882353	0.11764706	0	0	0	0	0.76470588	0	0	0.05882353	0	0	0	0
Gmg	0	0.33333333	0	0	0	0	0	0.66666667	0	0	0	0	0	0
Gp	0	0.08333333	0	0	0	0	0.08333333	0	0.83333333	0	0	0	0	0
Sh	0.05555556	0	0.05555556	0	0	0	0	0.05555556	0	0.72222222	0	0	0.05555556	0.05555556
Gci	0	0	0	0	0	0	0	0	0	0	0.83333333	0.16666667	0	0
Gh	0	0	0	0	0	0	0	0	0	0.07692308	0.07692308	0.84615385	0	0
Sm	0	0	0	0	0	0	0	0	0	0.16666667	0	0	0.83333333	0

5) Cañón La Boca

*not available

6) Cañón Caballeros

Facies	Gmg	St	Fm	Gmm	Fl	Gt	Se-Ss	Sh	Gh	Gci	P	Gcm
Gmg	0.92	0.02	0.04	0.02	0	0	0	0	0	0	0	0
St	0	0.69230769	0.23076923	0.01923077	0	0	0.05769231	0	0	0	0	0
Fm	0.01090909	0.04363636	0.91636364	0.00363636	0.00363636	0.00727273	0	0	0.00727273	0	0.00363636	0.00363636
Gmm	0	0.01315789	0.03947368	0.94736842	0	0	0	0	0	0	0	0
Fl	0	0	0.02439024	0	0.91463415	0	0.01219512	0.04878049	0	0	0	0
Gt	0	0	0	0	0.03225806	0.93548387	0	0.03225806	0	0	0	0
Se-Ss	0	0.03333333	0.06666667	0	0.03333333	0	0.83333333	0.03333333	0	0	0	0
Sh	0.03846154	0	0.03846154	0	0	0	0	0.92307692	0	0	0	0
Gh	0	0	0	0	0	0.07692308	0	0	0.84615385	0.07692308	0	0
Gci	0.11111111	0	0	0	0	0	0	0	0	0.88888889	0	0
P	0	0.16666667	0	0	0	0.07407407	0	0	0	0	0.83333333	0
Gcm	0	0	0	0	0	0	0	0	0	0	0	0.92592593

7) Cañón Huizachal-Peregrina

*not available

8) Cañón Novillo

Facies	Sh	St	Fm	Gt	Se	Gmg	Gmm	Gcm	Gh	P
Sh	0.88461638	0.11538462	0	0	0	0	0	0	0	0
St	0.05882353	0.85294118	0.02941176	0	0	0	0.02941176	0.02941176	0	0
Fm	0	0	0.75	0	0.25	0	0	0	0	0
Gt	0	0	0	0.88888889	0	0	0	0	0.11111111	0
Se	0	0	0	0	0.83333333	0.16666667	0	0	0	0
Gmg	0	0.07692308	0	0	0	0.80769231	0.03846154	0.03846154	0	0.03846154
Gmm	0	0.25	0	0	0	0.71875	0.03125	0.03125	0	0
Gcm	0	0	0	0.05263158	0	0.10526316	0	0.84210526	0	0
Gh	0	0	0	0	0	0.04166667	0	0	0.95833333	0
P	0	0	0	0	0.25	0	0	0	0	0.75

9) Valle de Huizachal

a) Volcanic core, La Boca lower member

Facies	Fm	FI	St	SI	Sh	Ss	Gh	Gcm	Gmm
Fm	0.7107438	0.0661157	0.09090909	0.00826446	0.07438017	0.02479339	0	0.00826446	0.01652893
FI	0.16666667	0.70833333	0	0	0.08333333	0.04166667	0	0	0
St	0.25714286	0	0.02857143	0	0.68571429	0	0.02857143	0	0
SI	0.33333333	0	0	0.66666667	0	0	0	0	0
Sh	0.15068493	0.05479452	0	0	0.79452055	0	0	0	0
Ss	0.27777778	0.05555556	0	0	0	0.66666667	0	0	0
Gh	0	0.11111111	0	0	0.11111111	0	0.77777778	0	0
Gcm	0.08333333	0	0	0	0	0.08333333	0	0.83333333	0
Gmm	0	0.16666667	0	0	0	0	0	0.16666667	0.66666667

9) Valle de Huizachal

b) Quarry east from volcanic core, La Boca upper member

Facies	Gcm	Gmm	Gh	Se	Ss	Sp	Sh	SI	St	Sr	Fm	FI	Af	Cb
Gcm	0.88888889	0	0	0.05555556	0	0	0	0	0	0	0	0.05555556	0	0
Gmm	0.08333333	0.91666667	0	0	0	0	0	0	0	0	0	0	0	0
Gh	0	0.33333333	0.66666667	0	0	0	0	0	0	0	0	0	0	0
Se	0	0	0	0.71428571	0.07142857	0.14285714	0	0	0	0.07142857	0	0	0	0
Ss	0.03448276	0	0	0.03448276	0.75862069	0.06896552	0	0	0.10344828	0	0	0	0	0
Sp	0	0	0	0.07692308	0.07692308	0.61538462	0	0	0.07692308	0.15384615	0	0	0	0
Sh	0	0	0	0.05	0.05	0	0.55	0	0.05	0.05	0.15	0.1	0	0
SI	0	0	0	0	0	0	0	0.66666667	0.33333333	0	0	0	0	0
St	0	0	0.01315789	0.01315789	0.02631579	0.06896552	0.01315789	0	0.69736842	0.09210526	0.14473684	0	0	0
Sr	0	0	0	0.03448276	0.03448276	0.06896552	0.03448276	0.03448276	0.03448276	0.68965517	0.10344828	0	0	0
Fm	0	0	0	0	0.02325581	0	0	0	0.18604651	0.04651163	0.65116279	0	0.02325581	0.06976744
FI	0	0	0	0	0.2	0	0	0	0.2	0	0	0.6	0	0
Af	0	0	0	0	0	0	0	0	0	0	0.33333333	0	0.66666667	0
Cb	0	0	0	0	0	0	0	0	0	0	0.33333333	0	0	0.66666667

9) Valle de Huizachal

c) La Joya, madout forsets

Facies	Gcm	Gt	Sh	SI	St	Fm	P	Af	Cb
Gcm	0.88888889	0	0	0	0	0	0.11111111	0	0
Gt	0.08333333	0.91666667	0	0	0	0	0	0	0
Sh	0.33333333	0	0.66666667	0	0	0	0	0	0
SI	0	0.125	0	0.66666667	0.875	0	0	0	0
St	0	0	0	0.16666667	0	0.66666667	0	0.16666667	0
Fm	0	0	0	0	0	0	0.66666667	0	0.33333333
P	0	0	0	0	0	0	0	0.66666667	0
Af	0	0	0	0	0.33333333	0	0	0	0.66666667
Cb	0	0	0	0	0	0.33333333	0	0	0.66666667

10) Miquihuana

Northwestern flank

Facies	Sh	FI	Fm	P	Cb	St	Sp
Sh	0.7804878	0.02439024	0.19512195	0	0	0	0
FI	0.28571429	0.71428571	0	0	0	0	0
Fm	0.00873362	0.0074556	0.97525473	0.00436681	0.00727802	0.0014556	0.0014556
P	0.05555556	0	0.11111111	0.83333333	0	0	0
Cb	0	0	0.66666667	0	0.33333333	0	0
St	0	0	0.5	0	0	0.5	0
Sp	0	0	1	0	0	0	0

APPENDIX FOR CHAPTER 3: DETRITAL MODES

Sample	Formation	Q	Qm	Qmr	Qmo	Qp	Qp2-3	Qp3-3	F	Plg	K	Lt	Lm	Lm?	Lmc	Lmc1	Lmc2	Lmf	Lmf1	Lmf2	Lmf3	Lmf4	Lmp	Lmp1	Lmp2	Lmp3	Lmp4	
VH 3101A	La Boca low. m.	205	90	53	37	115	64	51	90	81	9	99	10					10	8	1	1							
VH 3101B	La Boca low. m.	182	96	42	54	86	53	33	88	86	2	122	14					13	9	4								
VH 3102B	La Boca low. m.	79	51	22	29	28	11	17	171	171		143	1					1	1									
VH 3103	La Boca low. m.	77	41	19	22	36	13	23	129	120	9	182	1					4	3									
VH 3104	La Boca low. m.	189	152	87	65	37	12	25	98	80	18	204	10					4	3									
VH 2101	La Boca upp. m.	394	282	118	164	112	36	76	9	3	85	25						11	5	3	3		14	9	4	1		
VH 2102	La Boca upp. m.	296	170	78	92	126	28	98	12	10	2	182	70					9	7	1	1	1	58	48	8	2		
VH 2103	La Boca upp. m.	308	213	91	122	95	24	71	12	11	1	167	45	2				6	4	1	1	1	22	16	4	1	1	
VH 2103A	La Boca upp. m.	191	138	72	66	53	5	48	86	65	21	222	25					5	1	3	1		19	15	1	3		
VH 2104	La Boca upp. m.	237	187	92	95	50	19	31	69	57	12	186	32					11	8	3	1		15	11	3	1		
VH 2105	La Boca upp. m.	134	62	40	22	72	18	54	118	80	38	260	14					8	6	8			6	6				
VH 2106	La Boca upp. m.	214	151	71	80	63	17	46	78	66	12	190	23					8	6	1	1		10	7	3			
VH 2107	La Boca upp. m.	318	166	88	78	152	18	134	4	2	2	156	56					28	8	18	2		12	6	2	4		
VH 2108	La Boca upp. m.	276	224	127	97	52	17	35	78	65	13	118	34					5	5				21	21				
VH 2201	La Boca upp. m.	388	285	138	147	103	39	64	14	13	1	93	32					21	18	1	2		6	6				
VH 2202	La Boca upp. m.	213	154	83	71	59	23	36	76	68	8	222	29					12	12				8	7				
VH 2203	La Boca upp. m.	312	222	108	114	90	18	72	36	26	10	136	40					12	12				20	14	4	2		
VH 2204	La Boca upp. m.	250	194	118	76	56	36	20	34	32	2	199	68					10		10			46	38	8			
VH 2205	La Boca upp. m.	280	220	110	110	60	20	40	6	4	2	167	60					16	16				48	30	6	12		
VH 2206	La Boca upp. m.	274	178	90	88	96	20	76	8	4	4	195	30					16	16				12	10	2			
VH 2207	La Boca upp. m.	289	194	74	120	95	14	81	10	7	3	136	61					23	16	6	1		34	25	3	6		
VH 3108	La Boca upp. m.	252	159	102	57	93	24	69	9	8	1	105	17					12	3	5	2	2	4	2	2	2	8	
VH 3109	La Boca upp. m.	288	184	98	86	104	34	70	18	12	6	151	56					10	6	2	2		36	22	6	8		
VH 0110C	La Joya	246	160	74	86	86	34	52	23	14	7	125	17					14	7	6	1	2	2	2	2	2	1	
VH 0111	La Joya	257	172	97	75	85	31	54	40	30	10	68	17					13	4	6	2	1	3	2	1			
VH-Gü 1	La Boca upp. m.	253	174	89	85	79	41	38	21	16	5	159	32					19	11	5	3		10	8	2	2	2	
VH-Gü 8	La Boca upp. m.	312	241	133	108	71	20	51	11	11	163	42					14	6	4	4		21	15	2				
VH-Gü 9	La Boca upp. m.	300	216	95	121	84	22	62	14	13	1	185	41					3					2	36	31	4	1	
VH-Gü 10	La Boca upp. m.	315	227	118	109	88	25	63	11	10	1	162	58					21	8	12			1	27	20	2	5	
VH-Gü 11	La Boca upp. m.	282	185	107	78	97	38	59	18	16	2	192	88					20	10	9	1		55	43	7	5		
VH-Gü 13	La Boca upp. m.	167	121	57	64	46	19	27	15	10	5	152	25					1	1				21	18	3			
VH-Gü 14	La Boca upp. m.	333	202	94	108	131	40	91	11	10	1	152	63					14	8	6			42	38	4			
VH-Gü 16	La Boca upp. m.	325	203	75	128	122	28	94	11	8	3	132	51					22	16	3	1		17	15	1	1		
VH-Gü 18	La Boca upp. m.	299	205	79	126	94	25	69	21	14	7	180	70					17	9	8	1		42	38	2	2		
VH-Gü 19	La Boca upp. m.	277	181	44	137	96	17	79	16	16		216	51					16	12	3	1		27	17	10			
VH-Gü 21	La Joya	341	182	53	129	159	34	125	12	8	4	146	33					23	11	7	5		9	7	2	2	4	
VH-Gü 23	La Joya	334	208	62	146	126	36	90	10	8	2	158	46					22	8	10	4		16	6	6	4		
VH-Gü 24	La Joya	316	184	56	128	132	46	86	20	18	2	157	44					26	10	10	6		14	10	4			
LSPT RCII 07	El Alamar low. m.	329	258	179	79	71	16	55	31	31	126	48						21	20	1			21	14	7			
LSPT RCII 08	El Alamar low. m.	335	249	143	106	86	32	54	19	19	132	45						18	16	1	1		24	18	2	4		
LSPT RCII 14	El Alamar low. m.	292	199	117	82	93	17	76	14	14	173	87						29	14	14	1		41	17	10	8	6	
LSPT RCII 15	El Alamar low. m.	303	237	156	81	66	17	49	31	26	5	141	82					13	6	7			53	23	19	6	5	
LSPT RCII 16	El Alamar low. m.	277	208	113	95	69	26	43	37	35	2	172	78					17	4	9	4		41	15	16	5	5	
LSPT RCII M2	Mina la Huiche L.110	374	277	105	172	97	30	83	21	21	87	22	7					15	15				12	9	2	1		
LSPT RCII M3	Mina la Huiche L.165	382	269	76	193	113	30	67	18	18	93	45						11	11				7	5	1	1		
LSPT RCII M4	Mina la Huiche L.200	370	315	156	159	55	22	33	18	18		93	45					18	15	3			20	13	3	4		
LSPT(C) La Nieve) 3	El Alamar upp. m.	312	254	143	111	58	21	37	36	35	1	161	89					27	13	11			52	13	29	4	6	
LSPT(C) La Nieve) 4	El Alamar upp. m.	319	247	131	116	72	25	47	31	31	152	79						26	14	10	2		38	17	11	6	4	
LSPT RCII 21	La Joya	299	240	134	106	59	25	34	16	16	175	53						17	14	3			30	24	1	5		
LSPT(C) La Nieve) 1	La Joya	328	287	184	103	41	27	14	40	39	1	97	39					12	5	6	1		16	3	13			
LSPT(C) La Nieve) 2	La Joya	304	270	159	111	34	23	11	14	14	175	88						24	9	15			48	4	33	6	5	

Light mineral content (table 2)

Sample	Formation	Lmb	Lmb1	Lmb2	Lmb3	Lmb4	Lv	Lvmi	Lvf	Lvl	Lv Tobaceous	Lvp	Lv?	Qz Glass	Lsp	Lch	Lp	Lsv	Lsc	Lsm	Ch	HM?	Zr	Mica?	Bio	Mus
VH3101A	La Boca low. m.						73	45	26	2		1			4	3	8				2	2				
VH3101B	La Boca low. m.	1	1				80	22	49	5	4				11	5	11				1	1	1			7
VH3102B	La Boca low. m.						99	58	36	4	1	1			1	1	40				1	3				4
VH3103	La Boca low. m.						154	136	18							1	25				6	6				2
VH3104	La Boca low. m.	6	4	2			153	113	14	11	6	1		9	40						3	3	1			1
VH2101	La Boca upp. m.						42	21	16	1	4				17						1	3	1			7
VH2102	La Boca upp. m.	3	3				73	46	20	2	4		1		38						1	1	1			1
VH2103	La Boca upp. m.	15	8	1	6		63	29	18	1	14			1	58						3	2				4
VH2103A	La Boca upp. m.	1	1				136	68	52	9	6	1		1	60							1				3
VH2104	La Boca upp. m.	6	6				116	86	22	4	3	1		1	37						3					1
VH2105	La Boca upp. m.						148	102	20	18	2	22	2	4	54			22			6	6				2
VH2106	La Boca upp. m.	5	2	2	1		120	86	20	3	2	3	8	1	41						10	3				2
VH2107	La Boca upp. m.	16	12	2	2		58	54	4	4	2	2		36	2					2	2					2
VH2108	La Boca upp. m.	7	7				55	30	23		1	1		25	1						7	3	1			7
VH2201	La Boca upp. m.	4	2	1	1		44	22	17		4	1		15	1					1	2	1				1
VH2202	La Boca upp. m.	5	3	1	1		117	91	16	5	4	18	1		39						7					1
VH2203	La Boca upp. m.	8	8				64	56	6	6	2	2		24	4						4					2
VH2204	La Boca upp. m.	10	6	4	4		88	70	10	2	6	1		42	10						4					14
VH2205	La Boca upp. m.	12	2	2	8		82	68	10		4	1		24	2						10	4				4
VH2206	La Boca upp. m.	2	2				138	98	20		20	1		24	2											10
VH2207	La Boca upp. m.	4	1	1	2		73	47	13	3	10	1		13							2	3				2
VH3108	La Boca upp. m.	1	1				65	60	5		5	5		13							25	8				6
VH3109	La Boca upp. m.	6	2	2	2		94	68	16	2	8	1		13							20	4				2
VH0110C	La Joya						71	36	22	13		12		13							21	13				3
VH0111	La Joya	1	1	1			31	26	5		1			17							2					2
VH-Gü 1	La Boca upp. m.	3	2	1			59	23	25	11				66							29	3				12
VH-Gü 8	La Boca upp. m.	6	2	1	3		84	37	35	4	8	6		23	1						5	2				5
VH-Gü 9	La Boca upp. m.	2	2				85	29	19	11	26	10		36	3						7	1				3
VH-Gü 10	La Boca upp. m.	9	7	2			62	28	27		6	3	1	29	7						2	1				2
VH-Gü 11	La Boca upp. m.	13	3	9	1		80	45	11	2	21	5	1	13	1						6	3	1			2
VH-Gü 13	La Boca upp. m.	3	3				69	46	1	8	14	23		12	1						6	3	1			2
VH-Gü 14	La Boca upp. m.	7	1	2	4		65	32	16	10	7	4		14	2						3	3				1
VH-Gü 16	La Boca upp. m.	12	4	5	3		72	50	7	5	10	1		14	4						8					1
VH-Gü 18	La Boca upp. m.	7	2		5		72	43	19	7	3	5		28							1	1				1
VH-Gü 19	La Boca upp. m.	5	3	1	1		79	54	11	8	6	15		54	1						1	1				2
VH-Gü 21	La Joya	1	1				64	35	9	11	9	5		39							4					
VH-Gü 23	La Joya	6	2		4		64	32	16	8	8	4		40							4					2
VH-Gü 24	La Joya	4	4				64	32	14	12	6	1		47							2	4				4
LSPTRCII 07	El Alamar low. m.	6	6				37	16	7		14	5		36								4				14
LSPTRCII 08	El Alamar low. m.	3	2	1			33	11		1	21	4		50								1	2			13
LSPTRCII 14	El Alamar low. m.	17	13	4			62	33	26	3	10	10		14								3	2			18
LSPTRCII 15	El Alamar low. m.	16	5	8	3		41	29	3		9	8		10							1	8	7			3
LSPTRCII 16	El Alamar low. m.	20	10	10			48	31	3	2	12	12		34							9					17
LSPTRCII M2	Mina la Huiche L. 110	3	2	1			37	17			16	4		4								5	1			6
LSPTRCII M3	Mina la Huiche L. 165	4	3	1			45	19			26	3		17								4	1			11
LSPTRCII M4	Mina la Huiche L. 200	7	5	1	1		27	14			13	2		19								1	5			6
LSPT(C La Nieve) 3	El Alamar upp. m.	10	2	7			43	38			5	15		14								1				1
LSPT(C La Nieve) 4	El Alamar upp. m.	15	6	4	5		53	33	11	6	3	9		11								1	2			8
LSPT(C La Nieve) 1	La Joya	6	5		1		19	10			9	4		98							9	2	4			11
LSPT(C La Nieve) 2	La Joya	16	9	7	1		64	30	1	1	32	9		14							2	2				4

Light mineral content (table 4)

Sample	Formation	Q	Qm	Qmr	Qmo	Qp	Qp2-3	Qp>3	F	Plg	K	Lt	Lm	Lm?	Lmc	Lmc1	Lmc2	Lmf	Lmf1	Lmf2	Lmf3	Lmf4	Lmp	Lmp1	Lmp2	Lmp3	Lmp4
CC1112.01	La Boca	408	124	38	86	284	24	260	2	2		68	18					2	2				16	16			
CC1112.02	La Boca	494	210	68	142	284	64	220	11	10	1	80	8					2	2				6	6			
CC1112.03	La Boca	374	272	194	78	102	50	52	32	30	2	85	1					4	2	2			1	1			
CC1112.04	La Boca	350	266	120	146	84	52	32	40	34	6	93	32	8				4	2				18	4	13	1	
CC1112.05	La Boca	410	330	113	217	80	35	45	26	25	1	56	4					1	1				3	3			
CC2801	La Joya	405	289	102	187	116	48	68	11	11	20	64	23					10	10				9	6	1	1	1
CC2802	La Joya	348	276	57	219	72	21	51	22	20	2	107	39					18	16	2			13	10	1	1	1
COI06.10	La Boca	380	273	98	175	107	31	76	1	1	1	137	62					7	7				53	23	30		
COI06.09	La Boca	371	338	168	170	33	24	9	2	1	1	80	40					1	1				37	30	5	2	
COI06.08	La Boca	202	143	121	22	59	35	24	3	3	3	76	18	1				1	1				14	9	4	1	
COI06.07	La Boca	385	243	117	126	142	37	105	5	3	2	94	33	2				8	6	2			17	10	6	1	
COI06.06	La Boca	405	266	104	162	139	38	101	1	1	1	73	34					11	5	5	1		19	13	5	1	
COI06.05	La Boca	354	210	86	124	144	39	105	2	3	3	132	51					17	6	8			19	13	6		
COI06.04	La Boca	430	370	130	240	60	45	15	2	1	1	52	37	2			2	4	1			3	9	2	6	1	
COI0101A	La Joya	360	300	67	233	60	20	40	29	29		109	32					13	12				11	3	5	2	1
COI0102	La Joya	365	289	26	263	76	23	53	21	21		104	25					14	13	1			6	1	3	1	1
CN290809.01	La Joya	279	155	56	99	124	14	110	10	3	7	173	43					18	13	5			2	2			
CN290809.02	La Joya	264	160	82	78	104	36	68	4	4	4	175	45	4				14	14				14	14	14		
CN290809.03	La Joya	387	273	61	212	114	25	89	9	3	6	97	30					19	10	8		1	7	4	3		
CN290809.04	La Joya	344	215	83	132	129	29	100	6	5	1	143	40					29	8	16	1	4	10	6	3		1
CN290809.05	La Joya	383	226	95	131	157	33	124	8	6	2	94	16					12	8	4			3	1	1		1
CN290809.06	La Joya	278	216	85	131	62	14	48	23	18	5	183	47	1				6	6				31	22	9		
CN290809.07	La Joya	336	278	138	140	58	22	36	38	34	4	96	34					4	4				26	17	8	1	
CN290809.15	La Joya	270	158	60	98	112	16	96	28	12	16	110	10										10	4	6		
CHP190909.06	La Boca	308	166	56	110	142	22	120	16	13	3	161	57					31	29	2			20	20			
CHP190909.07	La Boca	316	209	91	118	107	34	73	8	6	2	136	51					16	16				31	31			
CHP190909.09	La Boca	352	244	63	181	108	26	82	16	13	3	104	53					20	15	5			28	23	4	1	
CHP190909.10	La Boca	384	269	82	187	115	28	87	14	12	2	94	31					19	10	9			9	3	5	1	
CHP190909.11	La Boca	370	236	40	196	134	44	90	4	4		180	66					14	14				48	16	28	4	
CHP190909.12	La Boca	467	263	42	221	204	21	183	6	6	3	33	6										3	3			
CHP190909.13	La Boca	388	328	158	170	60	58	2	64	58	6	58	20										20	18	2		
CHP190909.14	La Joya	312	243	135	108	69	23	46	32	28	4	124	65					26	24	2			21	18	3		
CHP190909.15	La Joya	344	241	83	158	103	44	59	13	11	2	133	30					13	8	3	2		11	6	3	2	
CHP190909.16	La Joya	385	238	92	146	147	31	116	24	13	11	75	17					12	12				4	1	3		
CHP190909.17	La Joya	363	252	109	143	111	39	72	18	18		101	20					5	3	2			10	6	3	1	
Ab1111.06a	La Boca	318	279	124	155	39	26	13	36	34	2	121	32					8	3	5			20	18	2		
Ab1111.07a	La Boca	290	253	97	156	37	28	9	30	27	3	163	20					1	1				13	11	2		
Ab1111.08a	La Boca	390	362	204	158	28	26	2	36	34	2	32	4					2	2				2	2			
Ab1111.09a	La Boca	382	304	124	180	78	44	34	11	11		104	21					6	4	2			12	12			
Ab1111.10b	La Boca	394	355	182	173	39	31	8	42	42		59	13					3	3				10	10			
Ab1111.11b	La Boca	325	292	144	148	33	29	4	85	82	3	80	15					4	4				11	4	7		
Ab1111.12b	La Boca	330	269	180	89	61	35	26	64	63	1	87	12					4	3	1			4	1	3		
Ab1111.13b	La Boca	368	337	179	158	31	21	10	74	66	8	80	8					4	4				8	6	2		
Ab1111.14b	La Boca	303	256	168	88	47	34	13	85	84	1	130	7					4	4				6	1	5		
Ab1111.15b	La Boca	239	237	135	102	2	1	1	68	64	4	147	19										6	1			
Ab1111.16b	La Boca	348	321	136	185	27	25	2	72	70	2	75	18										13	13			

Light mineral content (table 5)

Sample	Formation	Lmb	Lmb1	Lmb2	Lmb3	Lmb4	Lv	Lvmi	Lvf	Lvl	LvTobaceous	Lvp	Lv?	Qz Glass	Lsp	Leh	Lp	Lsv	Lsc	Lsm	Ch	HM?	Zr	Mica?	Bio	Mus	
CC 1112 01	La Boca	2	2				30	26	4	4		4			12			4		4							
CC 1112 02	La Boca						24	24		10		4			34			4							4		
CC 1112 03	La Boca						30	28	2	12		4			36	2		4				2			10	2	
CC 1112 04	La Boca	2	2				32	16	12	2	2	1			28			4						10	2		
CC 1112 05	La Boca	4	2	2			41	40	1	1		1			10			4					1	6	1	1	
CC 2801	La Joya	8	7	1			27	9	4	4	14	1			13			6				4	13	1	2		
CC 2802	La Joya						45	33	1	2	9	1			22			2				2	21	1			
COI 06 10	La Boca	2	1	1			39	33	1	2	3	10			24			2				1	7				
COI 06 09	La Boca	3	1	2			35	32	3	1	1	4			4			2				9	8	11	2	1	
COI 06 08	La Boca	2	2				46	43	1	2	2	2			8			2				4	3	11	3	3	
COI 06 07	La Boca	6			6		41	28	9	4	4	3			14			3				9	2	1	3	2	
COI 06 06	La Boca	4	1	1			19	10	8	1	1	1			18			1				5	7	1	2	1	
COI 06 05	La Boca	15	2	2	11		42	23	9	10	10	13			19	1		6				6	2		2	4	
COI 06 04	La Boca	22	3	6	13		3	2	1	1	7	12			11			2				6	7	1	1	5	
COI 0101A	La Joya	8	6	1	1		53	14	31	1	7	12			12			3				1	7	1	1	2	
COI 0102	La Joya	5	2	2	1		48	14	20	6	7	7			30			1				1	8				
CN 290809 01	La Joya	23	22	1			115	32	61	11	11				15			1				1	1	1	3		
CN 290809 02	La Joya	10	6	4			104	34	56	10	4				22	2		2				1	1	2		3	
CN 290809 03	La Joya	4	2	2			60	33	24	1	1	1		1	6			1				1	1	1	1	1	
CN 290809 04	La Joya	1	1				85	56	11	5	3			10	18							4	2	1	1	1	
CN 290809 05	La Joya	1	1	1			65	43	8	5	7			2	13			3				5	3	1		1	
CN 290809 06	La Joya	9	3	1			82	65	5	7	5	16			33			5				4	5	5		4	
CN 290809 07	La Joya	4					44	40	2	2	2	2			14			2				8	16				
CN 290809 15	La Joya						54	26	22	6		32			14								2	2		2	
CHP 190909 06	La Boca	6	2	3	1		52	18	14	3	17	1			50			1				4	1	1	9	1	
CHP 190909 07	La Boca	4	1	2	1		46	24	7	4	5	3			36			1				1	5	5	10	10	
CHP 190909 09	La Boca	5	2	3			30	27	2	2	1	5			16			3				3	5	1	10	1	
CHP 190909 10	La Boca	3	1	1	1		49	33	6	2	8	1			13			1				1	2	1	3	2	
CHP 190909 11	La Boca	4		2	2		34	16	6		12	2			78			3				2	2	6		6	
CHP 190909 12	La Boca						9	9		6		6			9								3	3		3	
CHP 190909 13	La Boca						12	10		10		10			2								6	4	6	6	6
CHP 190909 14	La Joya	18	9	7	2		42	34	1	2	7	2			15			1				2	4	17	1	1	
CHP 190909 15	La Joya	6	3	1	2		52	50	1	1		7			42	1		1				4	4	3	3	3	
CHP 190909 16	La Joya	1	1	1			33	12	12	3	6	2			23			3				1	1	9	9	1	
CHP 190909 17	La Joya	5		2	3		39	36		1	2	6			33			3				6	2	3	1	1	
Ab 1111 06a	La Boca	4	2	2			60	42	12	4	2	11			17			1				1	1	6	9	4	
Ab 1111 07a	La Boca	6		4	2		95	25	27	20	22	28			1			6				1	1	7	7	1	
Ab 1111 08a	La Boca						12	8	4		16											4	4	4	10	2	
Ab 1111 09a	La Boca	3		3			57	27	28	2	11				11			4				1	1	5	5	1	
Ab 1111 10b	La Boca						27	5	21	1		9			7			3				2	2	4	1	1	
Ab 1111 11b	La Boca						35	21	12	1	1	7			20			3				2	1	5	5	1	
Ab 1111 12b	La Boca	4		3	1		64	24	36	3	1	3			8			2				2	1	1	1	1	
Ab 1111 13b	La Boca						30	14	16		32				8			2				2	2	2	12		
Ab 1111 14b	La Boca	3	2	1			65	30	27	5	3	24			12			22				1	1	1	5	5	
Ab 1111 15b	La Boca	13	1	12			57	20	32	5		34			17			20				1	1	3			
Ab 1111 16b	La Boca	5	5				34	24	6	4		9			9			5					1	1	3	3	

Light mineral content (table 6)

Sample	Formation	Matrix	Matrix ?	Micrit	Sparit	Illite/Smectita	Matrix-Fe	Epi-Mx	Pseudo-Mx	Cement	Fe-Ox	Opaques	Sericite	Chlorite	Accessory(SiO2)	TOTAL
CC 1112 01	La Boca	12						12					100			590
CC 1112 02	La Boca	10	4	4	2								196			795
CC 1112 03	La Boca	222		148	64			10					26			755
CC 1112 04	La Boca	74		18				37		56	14		14			597
CC 1112 05	La Boca	42			5								18			562
CC 2801	La Joya	34	1	2	31							1				540
CC 2802	La Joya	29	17	1	11											532
COI 06 10	La Boca	19						19					2	1		549
COI 06 09	La Boca	23						23			1	1	5	5		536
COI 06 08	La Boca	10						10		2			9	1		328
COI 06 07	La Boca	9						9			1	1	2	3		524
COI 06 06	La Boca	15	1					14					3	3		517
COI 06 05	La Boca	1						1					9	3		523
COI 06 04	La Boca	19		1				12		6						533
COI 0101A	La Joya	11	6		4			1		1						522
COI 0102	La Joya	16	12		4						1					517
CN 290809 01	La Joya	9	9					4			7			1		487
CN 290809 02	La Joya	21	3					4		14		2		2		470
CN 290809 03	La Joya	5	5								7			1		512
CN 290809 04	La Joya	9	6	3							3					516
CN 290809 05	La Joya	9	9								3			3		517
CN 290809 06	La Joya	78		74				4						7		592
CN 290809 07	La Joya	1						1			47	5		5		568
CN 290809 15	La Joya	30						16		14				4		442
CHP 190909 06	La Boca	12	7	5												515
CHP 190909 07	La Boca	49	1	2	46									1		541
CHP 190909 09	La Boca	19		19							1	1		4		525
CHP 190909 10	La Boca	28		17	11									2		532
CHP 190909 11	La Boca	4	4								10					578
CHP 190909 12	La Boca	237						237								746
CHP 190909 13	La Boca	39		39									1			671
CHP 190909 14	La Joya	22	5		17			6			2	2	35	2		521
CHP 190909 15	La Joya	12		6	3						2	2		1		557
CHP 190909 16	La Joya	19		16							7			1		524
CHP 190909 17	La Joya	17		4	13								22	3	1	545
Ab 1111 06a	La Boca	102			71			31					62	7		667
Ab 1111 07a	La Boca	117		1	89			22		5			32	5	2	658
Ab 1111 08a	La Boca	114			114								28	20		652
Ab 1111 09a	La Boca	41			26			15					24	2		571
Ab 1111 10b	La Boca	50			50								2			558
Ab 1111 11b	La Boca	43			38			5					3		1	548
Ab 1111 12b	La Boca	70		1	69								10			569
Ab 1111 13b	La Boca									10						550
Ab 1111 14b	La Boca	7		4				3								526
Ab 1111 15b	La Boca	40			32	3		5					13			514
Ab 1111 16b	La Boca	25			19			6					6	1		532

Light mineral content (table 7)

Sample	Formation	Q	Qm	Qmr	Qmo	Qp	Qp2-3	Qp>3	F	Plg	K	Lt	Lm	Lm?	Lmc	Lmc1	Lmc2	Lmf	Lmf1	Lmf2	Lmf3	Lmf4	Lmp	Lmp1	Lmp2	Lmp3	Lmp4	
CA2001 09	El Alamar	363	272	105	167	91	30	61				128	40					4	4				32	30	2			
CA2001 10	El Alamar	353	267	73	194	86	17	69	7		7	140	33					3	3				31	25	6			
CA2001 08	El Alamar	398	290	134	156	108	16	92	10		10	89	18					3	3				14	11	2		1	
CA2001 07	El Alamar	372	308	115	193	64	13	51	15		15	109	24					3	1	2			19	17	2			
CA2001 07b	El Alamar	384	285	82	203	99	22	77	13		13	102	24					3	2	1			20	19	1			
CA2001 DK	El Alamar	394	246	77	169	148	30	118	31		30	1	67	18				4	4				12	12				
CA2001 06	El Alamar	406	295	76	219	111	29	82	15		14	83	24					8	4	4			16	14	2			
CA2001 06b	El Alamar	338	272	54	218	66	27	39	24		24	130	47					13	1	11	1		25	20	4		1	
CA2001 05	El Alamar	402	253	72	181	149	24	125	23		20	3	80	7				4	2	2			3	3				
CA2001 05b	El Alamar	386	303	120	183	83	23	60	28		26	2	77	8				15	1	8	6		8	2			6	
CA2001 04	El Alamar	365	266	45	221	99	34	65	24		23	1	86	35				2	2				13	11	2			
CA2001 03	El Alamar	363	275	108	167	88	36	52	25		25	103	18					2	2				16	15	1			
CA2001 02	El Alamar	367	290	72	218	77	23	54	32		31	1	86	38				17	6	4	7		19	16	3			
CA2001 01	El Alamar	416	278	72	206	138	32	106	12		12	69	14					6	6				8	6	2			
CB 13 01	El Alamar upp. m.	351	303	96	207	48	27	21	12		10	2	133	36		2		9	9				18	16	1		1	
CB 13 02	El Alamar upp. m.	218	185	73	112	33	32	1	20		18	2	46	7				1	1									
CB 13 03	El Alamar low. m.	476	372	136	236	104	50	54	44		40	4	140	41				1	1				36	33	3			
CB 13 06	Boca	184	152	75	77	32	23	9	24		22	2	45	23				1	1				22	21	1			
CB 13 07	Boca	352	257	127	130	95	82	13	62		58	4	63	27				3	3				23	21	1		1	
CB 13 09	Boca	734	632	282	350	102	96	6	70		66	4	180	64				6	6	3	3		57	51	6			
CB 13 11	La Joya	417	238	116	122	179	85	94	4		2	2	52	13				6	6				7	6	1			
CB 13 12	La Joya	374	232	82	150	142	75	67	6		5	1	110	29				7	5	2			21	18	3			
Mi 20 06	La Joya?	304	272	58	214	32	32		36		34	2	128	54				6	4	2			42	14	28			
Mi 20 05	La Boca												208															
Mi 20 04	La Boca	277	256	80	176	21	20	1	52		44	8	120	36									36	32	4			
Mi 20 03	La Boca	338	298	136	162	40	32	8	48		36	12	76	14									14	14				
Mi 20 02	La Boca																											
Mi 20 01	La Boca	432	366	166	200	66	44	22	34		24	10	121	29				2	2				24	18	6			
Mi 20 10b	La Boca	289	267	104	163	22	19	3	76		70	6	117	12		2							10	10				
Mi 20 09b	La Boca	342	286	78	208	56	48	8	62		56	6	102	22									22	18	4			
Mi 20 02b	La Boca	249	215	87	128	34	24	10	78		70	8	213	10				4	2	2			6	6				
Mi 20 01b	La Boca	299	259	72	187	40	24	16	47		41	6	113	14									9	3	6			
Mi 20 08	La Boca	228	211	79	132	17	11	6	86		78	8	179	2				2	2									
Mi 20 07	La Boca	370	332	66	266	38	32	6	36		30	6	119	25		3		2	2				20	20				

Light mineral content (table 8)

Sample	Formation	Lmb	Lmb 1	Lmb 2	Lmb 3	Lmb 4	Lv	Lvmi	Lvf	Lvl	Lv Tobaccoous	Lvp	Lv ?	Qz Glass	Lsp	Lch	Lp	Lsv	Lsc	Lsm	Ch	HM ?	Zr	Mica ?	Bio	Mus
CA2001 09	El Alamar	4		3	1		38	33	2			3	11		39							1	2		4	
CA2001 10	El Alamar	2		2			37	28	5			4	7		59		2		2		1			1	3	
CA2001 08	El Alamar	1			1		36	26	5			5	5		30										1	
CA2001 07	El Alamar	2			2		54	53				1	10		19			2					3	1	3	
CA2001 07b	El Alamar	1			1		30	26	1			3	7		40		1				1				1	
CA2001 DK	El Alamar	2		1	1		15	14	1				5		29						2		2	1		
CA2001 06	El Alamar						28	27	1				9		21			1								
CA2001 06b	El Alamar	9	5		3		35	28	7				2		45						2	2	2	5		
CA2001 05	El Alamar						31	27	1	3			12		23		3				1				1	
CA2001 05b	El Alamar						32	30				2	7		28			2					1	4	4	
CA2001 04	El Alamar	7		1	6		23	22	1				1		27			4			1		13	3	1	
CA2001 03	El Alamar						23	22	1	1			1		61						1				5	
CA2001 02	El Alamar	2			2		10	9	1				1		37						4		1	2	9	
CA2001 01	El Alamar						18	16		2			1		34					2		6			1	
CB13 01	El Alamar upp. m.	4			4		56	32	23			1	21		20						1		3		1	
CB13 02	El Alamar upp. m.	6			6		35	29				6	4								1		6	6	4	
CB13 03	El Alamar low. m.	4	1	2	1		58	30	19	2		7	24		17						2	13		1	3	
CB13 06	Boca						3	1				2	11		8						1		3	2	3	
CB13 07	Boca	1			1		17	13	4				12		7								7	1	2	
CB13 09	Boca	1	1				54	41	13				23		39							17		11	3	
CB13 11	La Joya						15	2	8	1		4	1		23						2		4		2	
CB13 12	La Joya	1			1		15	4	9	1		1	32		34										1	
Mi20 06	La Joya?	6	2	2	2		50	20	22			2	16		6							2	6		6	
Mi20 05	La Boca						176			160		16	8		8			16								
Mi20 04	La Boca						48	32	14			2	4		28			4					8	2	6	
Mi20 03	La Boca						42	22	16			4	20									16			2	
Mi20 02	La Boca																									
Mi20 01	La Boca	3	3				66	6	30	2		26	24		2		2					12	2	6	2	
Mi20 10b	La Boca						50	10	24	2		7	24		7			1			2		11	4	5	
Mi20 09b	La Boca						60	10	32			8	14		10								14	6	8	
Mi20 ?02b	La Boca						166	8	132	2		22	1		2								4		2	
Mi20 ?01b	La Boca	3	1		2		86	9	62	4		9	1		2			1				7	7	4	2	
Mi20 08	La Boca						89	35	41	7		6	41		37			10					7	2	3	
Mi20 07	La Boca						66	12	34			8	18		12							8	2		4	

Light mineral content (table 9)

Sample	Formation	Matrix	Matrix ?	Micrit	Sparit	Illite/Smectita	Matrix-Fe	Epi-Mx	Pseudo-Mx	Cement	Fe-Ox	Opaques	Sericite	Chlorite	Accessory(SiO2)	TOTAL
CA 2001 09	Ei Alamar	14						14					7	1		523
CA 2001 10	Ei Alamar	15						15						1		522
CA 2001 08	Ei Alamar	10			1			9					3	3		514
CA 2001 07	Ei Alamar	13		1				12						4		524
CA 2001 07b	Ei Alamar	13						13								514
CA 2001 DK	Ei Alamar	6						6			1			3		511
CA 2001 06	Ei Alamar	9						8	1							513
CA 2001 06b	Ei Alamar	26		26				5						2		535
CA 2001 05	Ei Alamar	5						59			1			4		514
CA 2001 05b	Ei Alamar	88		3	26			7		12		3		5		603
CA 2001 04	Ei Alamar	42		35				7					9	1		525
CA 2001 03	Ei Alamar	35		34	1			7						1		555
CA 2001 02	Ei Alamar	35		30	28			12					4	1		541
CA 2001 01	Ei Alamar	70						12								583
CB 13 01	Ei Alamar upp. m.	63						63								568
CB 13 02	Ei Alamar upp. m.	114		10				104		10		1		9		447
CB 13 03	Ei Alamar low. m.	28						28					10	1		731
CB 13 06	Boca	131		97				34				1		4		408
CB 13 07	Boca	35						35						5		546
CB 13 09	Boca	229		183				46				3		1		1276
CB 13 11	La Joya	4						4		48		1		1		542
CB 13 12	La Joya	34		15				19		40		2				573
Mi 20 06	La Joya?	13		13						25		2		4		534
Mi 20 05	La Boca	324						324								532
Mi 20 04	La Boca	98		62	20			16					26	2		601
Mi 20 03	La Boca	4		4						126		8		4		646
Mi 20 02	La Boca															
Mi 20 01	La Boca	112		80	22			10		104				2		841
Mi 20 10b	La Boca	85		44	30			11			2		12			620
Mi 20 09b	La Boca	23		21	2					144		2				723
Mi 20 ?02b	La Boca	10		10												566
Mi 20 ?01b	La Boca	6						6						7		506
Mi 20 08	La Boca	66		41	17			8					20			600
Mi 20 07	La Boca	32		30	2					124		2		2		709

Abbreviations for heavy minerals indices at Table 3.3. low. m. – Lower Member. upp. m. – Upper Member. Mx–Matrix. ?–undifferentiated. Component. Samples Gü– remake point-counting from Ramos-Ledezma, 2007

APPENDIX FOR CHAPTER 4: HEAVY MINERAL INDICES

Heavy mineral content (table 1)

Sample	RCII 08	RCII 14	RCII 15	RCII 16	LSPT...03	LSPT...04
Formation/ unit Rock-type	El Alamar low. m. ss	El Alamar low. m. ss	El Alamar low. m. ss	El Alamar low. m. ss	El Alamar upp. m. ss	El Alamar upp. m. ss
ZTR Σ	10	3	13	8	17	13
Zircon Σ	8		4	3	7	2
Euhedral	1				4	1
Subhedral	1		1	3	1	1
Subhedral purple						
Anhedral	4		3			
Elongated					1	
Round colorless	2				1	
Round purple						
Rutile	2	3	6	2	9	10
Tourmaline			3	3	1	1
T & Σ	9	5	8	1	2	7
Sphene (Titanita)	2		1		2	1
Anatase						
Brookite	2	5	3	1		2
Apatite	5		3			2
Monazite						
Baryte			1			2
LgM Σ	28	71	37	25	29	43
Epidote		1	2			
Zoisite	2	3	3	2	7	2
Clinozoisite		3				
Axinite						
Allanite						
Chloritoid	8	2	18	9	10	12
Chlorite	1	3	1	6	6	11
Chlorite-(Mg ²⁺)						
Serpentinite			4	2	4	4
Prehnite	17	58	9	5	2	14
Pumellyte		1		1		
Talc						
Garnet Σ	1			1		1
HgM Σ	2				2	1
Staurolite	2				1	
Andalusite						1
Kyanite						
Sillimanite					1	
Hb Σ				1		
Green Hb						
Brown Hb				1		
Hb (?)						
&A Σ					1	
Amphibol (?)					1	
Actinolite						
Tremolite						
tPx Σ	10	2		2		5
Pyroxene						
Clinopyroxene						
Orthopyroxene						
Hypersthene	1					
Diopside						
Enstatita						
Diallage						
Auguite-Aegirine	9	2		2		5
OS Σ			7			4
Olivine						
Spinel			7			4
others HM Σ	4	2	12	12	7	7
Xenotime						
Topaz						
Mica(?)	4	2	12	12	7	7
Muscovite	3	2	6	6	7	2
Biotite	1		6	6		5
Shard						
Σ Opaque	23	4	6	3	55	15
Σ Crystalline	64	83	77	50	58	81
Σ Crystalline+Opaque	87	87	83	53	113	96

Heavy mineral content (table 2)

Sample	VH 3101 A	VH 3103	VH 3104	VH 3106	VH 3108	VH 3109	
Formation/ unit Rock-type	La Boca low. m. ss	La Boca low. m. ss	La Boca low. m. ss	La Boca upp. m. ss	La Boca upp. m. ss	La Boca upp. m. ss	
ZTR Σ		1				13	
Zircon Σ		1					
Euhedral		1					
Subhedral							
Subhedral purple							
Anhedral							
Elongated							
Round colorless							
Round purple							
Rutile						10	
Tourmaline						3	
T & Σ				1	16	8	
Sphene (Titanita)						1	
Anatase							
Broockite					15		
Apatite				1	1	7	
Monazite							
Baryte							
LgM Σ		2	3	24	20	11	28
Epidote						1	
Zoisite					1		
Clinzoisite							1
Axinite							
Allanite					2		
Chloritoid	2				2	3	
Chlorite			1	1		5	15
Chlorite-(Mg ⁺)				2			7
Serpentinite			2	2			1
Prehnite				17	10	1	2
Pumellyte				2		1	
Talc							2
Garnet Σ					2	2	
HgM Σ						1	
Staurolite						1	
Andalusite							
Kyanite							
Sillimanite							
Hb Σ		1	2		6		1
Green Hb					2		
Brown Hb			2				
Hb (?)		1			4		1
&A Σ		2	3		3		2
Amphibol (?)		2	3		3		
Actinolite							
Tremolite							2
tPx Σ		3	4	2	4	4	1
Pyroxene						1	
Clinopyroxene		1	2		1	1	
Ortoproxene			2		1		
Hypersthene		1			1		
Diopside		1					
Enstatita							
Diallage							
Auguite-Aegirine				2	1	2	1
OS Σ		3			2	2	
Olivine		3			2	1	
Spinel						1	
others HM Σ			1	3	6	1	1
Xenotime						1	
Topaz							
Mica(?)			1	3	6		1
Muscovite				1	4		1
Biotite			1	2	2		
Shard							
Σ Opaque		25	80	69	66	20	61
Σ Crystalline		12	13	30	59	42	33
Σ Crystalline+Opaque		37	93	99	125	62	94

Heavy mineral content (table 3)

Sample	VH 0110	VH 0111	RCII 21	RCII 22	LSPT...-01	LSPT...-02	CN...-07	CHP...-14
Formation/ unit Rock-type	La Joya ss	La Joya ss	La Joya ss	La Joya ss	La Joya ss	La Joya ss	La Joya ss	La Joya ss
ZTR Σ	11	9	16	13	7	2		
Zircon Σ	6	6	8	1	1			
Euhedral	1							
Subhedral	4	1	4	1				
Subhedral purple		2						
Anhedral	1	2	4					
Elongated								
Round colorless		1			1			
Round purple								
Rutile	2		7	9	6			
Tourmaline	3	3	1	3		2		
T & Σ	7	8	16	4	6	6		
Sphene (Titanita)	7		2	1	2			
Anatase			4					
Brookite		6	3				1	
Apatite		1	4	1	1			
Monazite		1						
Baryte			3	2	3	5		
LgM Σ	29	20	33	42	13	12		3
Epidote	6							
Zoisite		4	5	5	2	2		
Clinozoisite								
Axinite								
Allanite								
Chloritoid	6	4	8	29				3
Chlorite	3	1	4	6	3	3		
Chlorite-(Mg ⁺)								
Serpentinite	3	1	1	1		3		
Prehnite	11	10	14	1	8	4		
Pumellyte			1					
Talc								
Garnet Σ	4	2	3		2	1		1
HgM Σ	7	6	2	2	9	1		1
Staurolite	5			2				
Andalusite		4			6			1
Kyanite	2	2			3	1		
Sillimanite			2					
Hb Σ	2	1	3					
Green Hb								
Brown Hb	2	1						
Hb (?)			3					
&A Σ								1
Amphibol (?)								1
Actinolite								
Tremolite								
tPx Σ	2	4	14		1			6
Pyroxene								
Clinopyroxene	1							5
Ortopyroxene					1			
Hypersthene	1	1						1
Diopside								
Enstatita		1						
Diallage								
Auguite-Aegirine		2	14					
OS Σ			2					3
Olivine								3
Spinel			2					
Others HM Σ	8	14	7	10		6		4
Xenotime		1				1		
Topaz						2		
Mica(?)	8	13	7	10		3		4
Muscovite	7	6	3	9		2		4
Biotite	1	7	4	1		1		
Shard								
Σ Opaque	14	7	40	13	29	23		53
Σ Crystalline	70	64	96	71	38	28		19
Σ Crystalline+Opaque	84	71	136	84	67	51		72

Heavy mineral content (table 4)

Sample	CC 2803	CN...-10	CN...-11	CN...-12	CN...-13	CN...-14	CHP...-02	CHP...-03
Formation/ unit	GS	NG	NG	NG	NG/GS	GS	Paleo. sed.	Paleo. sed.
Rock-type	Schist	Ba Gn W	Ba Gn B	Dike at NG	Tonalite	Schist	ss	ss
ZTR Σ	1	12		3		4	1	13
Zircon Σ	1	1		1		4	1	7
Euhedral	1					4	1	
Subhedral				1				5
Subhedral purple								
Anhedral								1
Elongated								
Round colorless								
Round purple		1						1
Rutile		11						5
Tourmaline				2				1
T & Σ	3	44	6	8		1	3	3
Sphene (Titanita)		42	1					3
Anatase								
Broockite	3	2		8			3	
Apatite			1			1		
Monazite			4					
Baryte								
LgM Σ	19	27	2	12	14	23	133	45
Epidote								
Zoisite							16	1
Clinozoisite				2				
Axinite								1
Allanite								
Chloritoid	9	21	1		3	5	11	5
Chlorite	5	5			3	6	7	2
Chlorite (Mg ⁺)					5		2	
Serpentinite	2		1				3	1
Prehnite	1	1				3	4	33
Pumellyte	1					2	1	2
Talc	1			2				2
Garnet Σ	2	40	91	3				2
HgM Σ			3		1	3		2
Staurolite			3					
Andalusite								2
Kyanite								
Sillimanite					1	3		
Hb Σ			1	40	41	21		
Green Hb					17			
Brown Hb			1		24			
Hb (?)				40		21		
& A Σ				8	7	18		
Amphibol (?)				5	6	15		
Actinolite				3		1		
Tremolite					1	2		
tPx Σ	1	1	2	20	14	10		1
Pyroxene				5				
Clinopyroxene				5	6			
Orthopyroxene	1				3	6		
Hypersthene				2	5	1		1
Diopside								
Enstatita								
Diallage						2		
Auguite-Aegirine		1	2	8		1		
OS Σ	3	1	2	2	1		2	3
Olivine					1			
Spinel	3	1	2	2			2	3
others HM Σ	5	3	6	2	20	6	2	2
Xenotime	1	1	2		1			
Topaz	1	2			2			
Mica(?)	3		4	2	17	6	2	2
Muscovite	1		4		14	6	2	2
Biotite	2			2	3			
Shard				1				
Σ Opaque	20		6		4	4	34	194
Σ Crystalline	34	128	113	98	98	86	141	71
Σ Crystalline+Opaque	54	128	119	98	102	90	175	265

Abbreviations for heavy minerals indices at Table 4.1. low. m.= Lower Member. upp. m.= Upper Member.

ss= sandstone. NG= Novillo Gneis. GS= Granjeno Schist. Paleo. sed.= Paleozoic sedimentary.

Ba Gn W= Banded Augen Gneis white band. Ba Gn B= Banded Augen Gneis black band.

Σ= sum. ?= undifferentiated. HM= heavy minerals.stalline+Opaque

Basic statistics for all heavy mineral indices considered in this work after Garzanti and Andò, 2007

a) Crystalline basement units (NG - Novilb Gneiss, Dk - Dikes at NG, GS - Granjeno Schist, To - Tonalite)								
	Valid N	Mean	Confidence -95.000%	Confidence +95.000%	Geometric Mean	Median	Variance	Std.Dev.
ZTR	6	1.3873	0.214	2.5600	0.5409	1.7003	1.2	1.1175
T&	6	2.2647	0.537	3.9924	1.2223	2.4022	2.7	1.6462
LgM	6	3.7080	2.078	5.3379	3.3820	3.6570	2.4	1.5531
Gt	6	2.6450	-0.272	5.5621	0.7628	1.9963	7.7	2.7797
HgM	6	0.7680	-0.109	1.6450	0.2383	0.5516	0.7	0.8357
Hb	6	2.6543	-0.042	5.3505	0.7515	2.6132	6.6	2.5691
&A	6	1.5288	-0.267	3.3244	0.3387	1.2584	2.9	1.7110
tPx	6	2.3841	1.113	3.6549	2.1032	2.3737	1.5	1.2109
OS	6	1.2595	0.346	2.1728	0.7691	1.2081	0.8	0.8703
others HM	6	2.4827	1.438	3.5277	2.3191	2.3156	1.0	0.9957

b) Unmetamorphosed Paleozoic strata								
	Valid N	Mean	Confidence -95.000%	Confidence +95.000%	Geometric Mean	Median	Variance	Std.Dev.
ZTR	2	4.4849	-30.17	39.140	3.5603	4.4849	14.88	3.8571
T&	2	3.3236	-2.92	9.569	3.2870	3.3236	0.48	0.6951
LgM	2	13.5328	-1.28	28.342	13.4825	13.5328	2.72	1.6483
Gt	2	1.6371	-18.21	21.484	0.4904	1.6371	4.88	2.2090
HgM	2	1.6371	-18.21	21.484	0.4904	1.6371	4.88	2.2090
Hb	2	0.0752	-	-	0.0752	0.0752	0.00	0.0000
&A	2	0.0752	-	-	0.0752	0.0752	0.00	0.0000
tPx	2	1.2213	-13.34	15.785	0.4219	1.2213	2.63	1.6209
OS	2	3.0949	-6.06	12.245	3.0100	3.0949	1.04	1.0184
others HM	2	2.7870	-2.45	8.024	2.7563	2.7870	0.34	0.5829

c) El Estemar								
	Valid N	Mean	Confidence -95.000%	Confidence +95.000%	Geometric Mean	Median	Variance	Std.Dev.
ZTR	6	6.4199	4.4644	8.3754	6.1696	6.8902	3.47	1.8634
T&	6	4.5024	3.0226	5.9823	4.3216	4.1808	1.99	1.4101
LgM	6	11.2291	9.2459	13.2123	11.0964	11.2627	3.57	1.8898
Gt	6	1.2006	-0.1527	2.5539	0.4165	0.8608	1.66	1.2895
HgM	6	1.4731	-0.2806	3.2268	0.4556	0.8608	2.79	1.6711
Hb	6	0.5281	-0.6436	1.6998	0.1322	0.0765	1.25	1.1165
&A	6	0.4989	-0.5977	1.5955	0.1308	0.0765	1.09	1.0450
tPx	6	2.8590	0.1810	5.5370	1.0740	3.1766	6.51	2.5518
OS	6	1.4547	-0.9248	3.8341	0.2870	0.0765	5.14	2.2674
others HM	6	5.4520	3.3832	7.5208	5.1474	5.3659	3.89	1.9714

d) La Boca

	Valid N	Mean	Confidence -95.000%	Confidence +95.000%	Geometric Mean	Median	Variance	Std.Dev.
<i>ilr-ZTR</i>	6	2.3301	-1.5506	6.2109	0.3259	0.0726	13.67	3.6979
<i>ilr-T&</i>	6	3.1464	-0.7796	7.0725	0.6483	1.6974	14.00	3.7411
<i>ilr-LgM</i>	6	9.7280	6.6485	12.8076	9.3801	8.6147	8.61	2.9345
<i>ilr-Gt</i>	6	1.2526	-0.6740	3.1792	0.2667	0.0726	3.37	1.8358
<i>ilr-HgM</i>	6	0.5389	-0.6598	1.7376	0.1339	0.0726	1.30	1.1423
<i>ilr-Hb</i>	6	3.3543	0.4662	6.2424	1.1934	4.0667	7.57	2.7520
<i>ilr-&A</i>	6	3.8040	0.4332	7.1748	1.2922	4.1490	10.32	3.2120
<i>ilr-tPx</i>	6	5.6886	3.4057	7.9716	5.3548	4.8816	4.73	2.1754
<i>ilr-OS</i>	6	2.5688	-0.7560	5.8936	0.5836	1.7095	10.04	3.1682
<i>ilr-others HM</i>	6	3.6089	1.4676	5.7503	2.1230	3.9822	4.16	2.0405

e) La Joya

	Valid N	Mean	Confidence -95.000%	Confidence +95.000%	Geometric Mean	Median	Variance	Std.Dev.
<i>ilr-ZTR</i>	7	3.4672	1.9932	4.9412	2.1154	4.1558	2.54	1.5937
<i>ilr-T&</i>	7	3.2955	1.8326	4.7585	2.0124	3.7627	2.50	1.5819
<i>ilr-LgM</i>	7	5.9397	5.0317	6.8477	5.8645	5.8384	0.96	0.9818
<i>ilr-Gt</i>	7	2.0284	1.1845	2.8722	1.3380	2.1838	0.83	0.9125
<i>ilr-HgM</i>	7	2.8812	1.8430	3.9194	2.7131	2.5843	1.26	1.1226
<i>ilr-Hb</i>	7	0.8219	-0.0860	1.7297	0.2243	0.0463	0.96	0.9816
<i>ilr-&A</i>	7	0.4089	-0.4783	1.2961	0.0822	0.0463	0.92	0.9593
<i>ilr-tPx</i>	7	2.1371	0.5847	3.6894	0.8706	1.9821	2.82	1.6785
<i>ilr-OS</i>	7	0.8748	-0.5866	2.3363	0.1476	0.0463	2.50	1.5802
<i>ilr-others HM</i>	7	3.5539	1.9901	5.1176	2.1506	3.9628	2.86	1.6909

Statistical canonical discriminant function
values for heavy minerals indices.

	Function 1	Function 2
<i>ilr-ZTR</i>	1.10360	0.18737
<i>ilr-T&</i>	0.34874	-0.22644
<i>ilr-LgM</i>	3.37830	0.02390
<i>ilr-Gt</i>	1.80254	-0.66758
<i>ilr-HgM</i>	1.73857	-0.70874
<i>ilr-Hb</i>	0.05602	-1.22326
<i>ilr-&A</i>	2.06597	0.20774
<i>ilr-tPx</i>	0.14466	0.74217
<i>ilr-OS</i>	1.60973	-0.26912
<i>ilr-others HM</i>	1.38489	-0.15022
Chi-Sqr.	95.88308	54.46105
Cum. Prop.	0.70050	0.84534

APPENDIX FOR CHAPTER 5: GEOCHEMICAL ANALYSES

Sample	Formation	Rock-type	SiO ₂	Al ₂ O ₃	Fe ₂ O ₃	MgO	CaO _{tot}	CaO(Carb)	CaO*	CO ₂	Na ₂ O	K ₂ O	MnO	TiO ₂	P ₂ O ₅	Cr ₂ O ₃	LoI
RCII-1	El Alamar low. m.	ss	65.73	10.52	8.61	2.41	4.24	4.33	2.470104514	3.4	0.51	1.21	0.15	0.8	0.14	0.006	5.6
RCII-2	El Alamar low. m.	dike/sill	41.93	17.43	10.01	2.32	9.29	9.06	5.354205818	7.11	4.56	2.02	0.17	1.12	0.18	0.004	10.9
RCII-3	El Alamar low. m.	dike/sill	52.61	18.42	6.45	1.12	5.41	5.03	3.14672184	3.95	7.2	1.44	0.12	0.76	0.24	0.002	6.2
RCII-4	El Alamar low. m.	dike/sill	59.72	19.12	4.72	0.96	1.6	1.25	0.976618956	0.98	8.85	0.75	0.04	0.99	0.21	0.002	3
RCII-7	El Alamar low. m.	ss	74.93	9.95	7.38	1.34	0.29	0.85	0.229572446	0.04	0.92	1.38	0.02	0.81	0.12	0.008	2.8
RCII-8	El Alamar low. m.	ss	72.44	7.85	3.5	1.09	6.02	0.85	3.625801734	0.67	0.62	1.61	0.04	0.52	0.09	0.004	6.1
RCII-9	El Alamar low. m.	ss	76.81	9.64	3.72	0.66	1.66	1.47	1.009657704	1.15	1.43	1.68	0.05	0.78	0.08	0.006	3.5
RCII-10	El Alamar low. m.	ss	70.42	14.1	6.34	0.81	0.21	0.01	0.184766845	0.01	0.8	1.63	0.02	0.89	0.04	0.009	4.7
RCII-11	El Alamar low. m.	ss	73.31	11.51	7.13	0.99	0.16	0.05	0.154162449	0.04	0.46	1.32	0.04	0.88	0.03	0.006	4.1
RCII-12	El Alamar low. m.	ss	71.38	12.87	7.08	1.08	0.18	0.05	0.165854308	0.04	0.65	1.44	0.04	0.87	0.04	0.008	4.3
RCII-13	El Alamar low. m.	ss	66.5	15.75	7.17	1.12	0.16	0.05	0.153457949	0.04	0.85	1.83	0.05	0.79	0.06	0.008	5.7
RCII-14	El Alamar low. m.	ss	64.92	11.56	15.98	2.33	0.11	0.06	0.123065552	0.05	0.12	0.44	0.1	0.44	0.07	0.005	3.9
RCII-15	El Alamar low. m.	ss	70.24	11.16	6.37	1.67	1.37	1.15	0.841953829	0.9	1.3	1.36	0.06	2.59	0.22	0.011	3.3
RCII-RE 15	El Alamar low. m.	ss	69.86	11.29	6.55	1.7	1.4	1.12	0.8602907	0.88	1.3	1.38	0.06	2.52	0.23	0.012	3.5
RCII-16	El Alamar upp. m.	ss	79.32	9.66	3.42	0.82	0.72	0.66	0.471045334	0.52	1.74	1.35	0.04	0.67	0.06	0.005	2.2
RCII-17	El Alamar upp. m.	ss	74.75	10.62	6.61	1.32	0.25	0.04	0.206059895	0.03	0.77	1.49	0.02	0.92	0.12	0.006	3.1
RCII-18	El Alamar upp. m.	ss	81.32	10.44	6.96	1.48	0.31	0.05	0.240559804	0.04	0.64	1.34	0.03	0.67	0.16	0.005	3.6
RCII-19	El Alamar upp. m.	ss	84.16	8.29	3.46	0.52	0.28	0.05	0.224313601	0.04	1.52	1.23	0.02	1.4	0.09	0.005	2
RCII-20	El Alamar upp. m.	ss	81.7	8.48	3.18	0.5	0.31	0.06	0.242567306	0.05	1.69	1.15	0.01	0.31	0.06	0.002	2.5
RCII-21	El Alamar upp. m.	dike/sill	80.15	9.04	2.77	0.48	0.97	0.76	0.616932652	0.6	1.35	1.7	0.03	0.45	0.08	0.003	3
RCII-22	La Joya	ss	72.6	5.45	3.1	1.2	8.31	0.18	5.009706967	0.14	0.48	0.86	0.02	0.47	0.08	0.002	7.3
RCII-23	La Joya	ss	54.74	17.69	7.92	2.71	4.08	4.09	2.37928814	3.21	5.73	1.07	0.11	0.7	0.22	0.001	5
RCII-24	La Joya	ss	83.85	7.81	2.5	0.44	0.24	0.04	0.201740384	0.03	1.75	1.1	0.01	0.39	0.05	0.003	1.9
RCII-M1	Mina la Huiche L.1	ss	81.83	5.2	1.92	0.38	3.95	3.96	2.308695476	3.11	0.76	1.05	0.08	0.36	0.07	0.003	3.8
RCII-M2	Mina la Huiche L.110	ss	76.97	10.25	4.99	1.37	0.48	0.36	0.336105026	0.28	1.16	1.86	0.03	0.41	0.06	0.004	2.3
RCII-M3	Mina la Huiche L.165	ss	86.3	6.65	1.75	0.39	0.65	0.6	0.431240911	0.47	1.27	1.06	0.03	0.22	0.05	0.002	1.5
RCII-RE M3	Mina la Huiche L.166	ss	86.46	6.61	1.87	0.38	0.64	0.6	0.425277565	0.47	1.26	1.06	0.05	0.23	0.05	0.003	1.4
RCII-M4	Mina la Huiche L.200	ss	78.94	8.97	1.32	0.61	2.48	3.35	1.448444362	2.63	0.68	2.29	0.11	0.68	0.07	0.005	3.8
RCII-M5	Mina la Huiche L.225	dike/sill	51.57	16.75	8.27	1.89	6.63	7.12	3.818118581	5.59	1.68	2.93	0.22	0.82	0.25	0.005	8.7
Canon El Alamar																	
CA 200201	El Alamar	ss	74.32	7.46	3.22	1.1	5.13		2.977923323	4.1	0.94	1.27	0.11	0.59	0.1	0.008	5.7
CA 200202	El Alamar	ss	76.35	10.32	4.24	1.89	0.37		0.274105716	0.14	2.09	0.87	0.04	0.82	0.11	0.011	2.8
CA 200203	El Alamar	ss	68.59	10.83	4.86	1.86	4.04		2.35982809	3.15	1.82	1.39	0.12	0.74	0.12	0.012	5.5
CA 200204	El Alamar	ss	79.14	8.7	3.51	1.57	0.28		0.222351767	0.07	1.64	0.76	0.04	1.54	0.13	0.02	2.4
CA 200205	El Alamar	ss	89.21	5.31	1.38	0.72	0.1		0.118488373	0.03	1.43	0.45	0.03	0.2	0.04	0.003	1.1
CA 200206	El Alamar	ss	85.89	7.16	1.48	1.08	0.15		0.148645936	0.02	1.91	0.49	0.02	0.23	0.04	0.003	1.5
CA 200207	El Alamar	ss	80.21	8.44	3.46	1.99	0.34		0.256473346	0.16	1.21	0.85	0.06	0.73	0.07	0.004	2.6
CA 2502 DK	El Alamar	ss	82.56	7.87	2.37	1.21	0.19		0.171113153	0.04	1.48	0.89	0.09	0.68	0.07	0.007	2.1
CA 250205B	El Alamar	ss	75.74	9.04	3.3	1.73	2.77		1.639550795	2.09	1.64	0.89	0.07	0.8	0.08	0.01	3.8
CA 250206B	El Alamar	ss	78.01	9.04	3.61	1.51	1.43		0.875462244	1.07	1.25	1.13	0.07	0.64	0.07	0.004	3.1
CA 250207B	El Alamar	ss	82.67	7.33	3.26	1.11	0.23		0.194966537	0.04	0.93	1.01	0.05	0.76	0.07	0.002	2.5
CA 250208B	El Alamar	ss	85.11	6.38	3.3	1.19	0.14		0.14319384	0.005	0.93	0.69	0.04	0.23	0.04	0.005	1.9
CA 250209B	El Alamar	ss	77.29	8.97	4.88	2.31	0.98		0.619616501	0.71	0.06	1.46	0.07	0.4	0.06	0.003	3.4
CA 250210B	El Alamar	ss	84.23	6.96	2.92	1.21	0.17		0.160849044	0.05	0.72	1.02	0.04	0.26	0.05	0.005	2.4
Canon El Alamar																	
COL 0101	La Boca	ss	82.55	6.4	5.12	2.04	0.08		0.106455681	0.04	0.05	0.35	0.04	0.51	0.03	0.009	3.4
COL 0102	La Boca	ss	77.1	9.99	2.21	1.01	2.14		1.294110982	1.23	1.49	2.26	0.04	0.26	0.04	0.005	3.4
COL 0103	La Boca	ss	54.56	16.91	8.71	5.55	6.7		4.027688933	0.79	1.63	0.58	0.12	0.69	0.07	0.005	4.3
COL 0603	La Boca	ss	84.76	6.63	3.28	0.53	0.17		0.160019796	0.05	0.32	0.68	0.01	0.8	0.02	0.005	2.8
COL 0604	La Boca	ss	82.83	6.2	5.43	0.58	0.14		0.14268259	0.02	0.21	0.44	0.02	1.51	0.04	0.005	2.5
COL 0605	La Boca	ss	71.8	10.47	5.42	3.49	1.46		0.891178449	1.12	0.07	0.61	0.09	1.68	0.09	0.029	4.6
COL 0606	La Boca	ss	84.41	8.59	1.36	0.67	0.18		0.165407475	0.06	0.45	1.27	0.01	0.52	0.03	0.009	2.5
COL 0607	La Boca	ss	85.59	7.86	1.55	0.62	0.13		0.136578411	0.03	0.24	1.53	0.04	0.48	0.04	0.009	1.9
COL 0608	La Joya	ss	73.45	8.63	5.71	2.21	2.33		1.331832757	3.42	0.13	1.33	0.22	0.38	0.08	0.004	5.4
COL 0610	La Joya	ss	80.92	9.06	3.25	1.14	0.61		0.408258359	0.41	0.15	1.77	0.07	0.43	0.1	0.003	2.4

Sample	Formation	Rock-type	Be	Sc	V	Co	Ni	Zn	As	Cd	Ga	Rb	Sr	Y	Zr	Nb	Mo	Sn	Sb	Bi	Ag	Au	Hg	Ba	
<i>Lomas de San Paulo Tranquitas</i>																									
RCII - 1	El Alamar low. m.	ss	10	79	29	33	100	13	42	52	33	327	10.1	676											
RCII - 2	El Alamar low. m.	dike/sill	43	403	29	11	38	20	63	104	26	76	3.5	742											
RCII - 3	El Alamar low. m.	dike/sill	18	191	12	6	23	19	40	114	30	118	5.5	513											
RCII - 4	El Alamar low. m.	dike/sill	18	241	23	15	12	17	20	94	19	95	4.4	476											
RCII - 7	El Alamar low. m.	ss	9	78	20	38	48	11	45	37	17	323	9.8	654											
RCII - 8	El Alamar low. m.	ss	7	56	7	13	42	9	53	80	16	186	6.2	524											
RCII - 9	El Alamar low. m.	ss	8	65	11	15	31	10	48	75	21	264	8.4	396											
RCII - 10	El Alamar low. m.	ss	14	105	5	20	70	16	59	63	35	272	11.7	664											
RCII - 11	El Alamar low. m.	ss	11	82	25	25	136	47	25	387	12.2	387	12.2	664											
RCII - 12	El Alamar low. m.	ss	13	87	7	26	130	14	51	55	25	323	11.6	649											
RCII - 13	El Alamar low. m.	ss	16	114	9	33	136	17	66	61	27	205	11.1	737											
RCII - 14	El Alamar low. m.	ss	9	69	19	37	258	14	16	15	16	102	5.7	627											
RCII - 15	El Alamar low. m.	ss	16	144	12	21	51	12	41	38	35	1317	23.6	253											
RCII - RE 15	El Alamar low. m.	ss	16	140	13	19	53	12	43	40	42	1363	24.1	401											
RCII - 16	El Alamar upp. m.	ss	9	61	7	14	29	9	39	30	18	153	6.2	393											
RCII - 17	El Alamar upp. m.	ss	9	70	16	21	52	11	43	24	13	286	9.7	453											
RCII - 18	El Alamar upp. m.	ss	10	68	22	32	55	11	44	28	16	260	8.5	568											
RCII - 19	El Alamar upp. m.	ss	8	66	6	10	24	9	33	53	26	420	14	709											
RCII - 20	El Alamar upp. m.	ss	6	43	4	12	26	8	32	57	19	72	3.4	306											
RCII - 21	El Alamar upp. m.	dike/sill	6	53	5	14	20	10	46	64	29	124	5.1	362											
RCII - 22	La Joya	ss	4	40	9	13	44	6	29	88	9	228	5.5	533											
RCII - 23	La Joya	ss	15	167	19	3	48	18	26	385	23	116	5.9	321											
RCII - 24	La Joya	ss	5	49	5	11	16	9	33	63	12	105	5.5	357											
RCII - M1	Mina la Huiche L.1	ss	5	41	2	5	13	5	31	424	12	124	3.8	3763											
RCII - M2	Mina la Huiche L.110	ss	8	66	10	20	27	14	56	264	10	109	5.2	1135											
RCII - M3	Mina la Huiche L.165	ss	4	35	8	9	15	8	31	26	12	81	3.1	253											
RCII - RE M3	Mina la Huiche L.166	ss	4	33	7	9	16	7	31	26	11	83	3	253											
RCII - M4	Mina la Huiche L.200	ss	7	63	8	3	6	10	77	28	16	279	7.5	391											
RCII - M5	Mina la Huiche L.225	dike/sill	18	225	24	19	57	19	81	142	23	104	4.6	1017											
<i>Canon EL Alamar</i>																									
CA 200201	El Alamar	ss	1	8	91	9.9	22.6	40	1.6	0.1	10.4	51.8	44.3	23	209.5	8.4	0.2	1	0.4	0.1	0.1	0.1	0.1	0.1	399
CA 200202	El Alamar	ss	1	10	134	14	21.1	33	1.3	0.1	13.9	38.1	61.3	20.7	390	11.2	0.2	1	0.3	0.1	0.1	0.1	0.5	0.02	257
CA 200203	El Alamar	ss	2	12	122	17.2	30.9	43	2.4	0.1	14.5	57.2	66.1	30.3	261.4	10.3	0.1	2	0.5	0.1	0.1	0.5	0.04	397	
CA 200204	El Alamar	ss	1	11	141	12.9	22.4	49	0.5	0.1	10.9	30.9	45.4	46.6	134.6	17.6	0.05	2	0.1	0.1	0.1	0.5	0.03	227	
CA 200205	El Alamar	ss	1	2	118	4.3	9.4	27	0.9	0.1	6.3	15.9	40.9	4.9	122.3	2.7	0.1	1	0.2	0.2	0.2	0.5	0.02	130	
CA 200206	El Alamar	ss	1	3	47	6.3	10.9	20	0.5	0.1	7.8	18.5	50.7	6.3	102.9	2.8	0.2	1	0.1	0.1	0.1	0.5	0.01	127	
CA 200207	El Alamar	ss	1	8	78	8.8	11.8	62	3.5	0.1	9.5	29.7	36.7	16.8	249.5	7.1	0.1	1	0.1	0.1	0.1	0.5	0.01	212	
CA 2502 DK	El Alamar	ss	1	6	774	11.4	23.6	47	1.7	0.1	8	32	45.2	14.5	167.9	6.8	0.1	1	0.1	0.1	2.6	1.8	0.09	303	
CA 250205B	El Alamar	ss	1	8	96	10.7	24.5	41	0.7	0.1	10.6	35.1	59.1	19.6	368	9.4	0.05	1	0.1	0.1	0.1	0.5	0.02	237	
CA 250206B	El Alamar	ss	1	9	73	8.2	15.2	59	4.9	0.1	10.2	39.1	47.4	17.4	221	7.2	0.05	1	0.1	0.1	0.1	0.5	0.01	265	
CA 250207B	El Alamar	ss	1	6	76	7.1	11.4	156	4.9	0.4	7.6	32.9	20.4	32.6	220.8	6.2	0.05	1	0.1	0.1	0.1	0.5	0.04	365	
CA 250208B	El Alamar	ss	1	4	33	6.1	12.7	40	3.2	0.1	6.8	22.3	20.6	7.3	72.5	2.7	0.2	1	0.1	0.1	0.1	0.7	0.01	267	
CA 250209B	El Alamar	ss	1	8	74	12.2	16.1	72	0.6	0.1	9.8	53.5	14.5	13.6	118.5	4.9	0.05	1	0.1	0.1	0.1	0.5	0.01	480	
CA 250210B	El Alamar	ss	1	5	40	6.5	10.9	38	1.8	0.1	7.4	33.4	22.5	12.5	65.4	2.7	0.3	1	0.1	0.1	0.1	0.5	0.03	320	
<i>Canon El Olmo</i>																									
COL 0101	La Boca	ss	1	10	87	33.7	31.9	74	0.5	0.1	8.1	13.5	9.1	4.9	52.2	5.2	0.2	1	0.1	0.1	0.1	1.3	0.05	147	
COL 0102	La Boca	ss	1	5	30	4	3.9	28	2.5	0.1	10	63.3	27.1	12.3	97.7	6.5	0.2	1	0.1	0.1	0.1	1.5	0.04	263	
COL 0103	La Boca	ss	1	33	193	24.2	8.4	59	1.1	0.1	16.6	13.6	245.1	13.6	51.5	2.4	0.2	1	0.1	0.1	0.1	2	0.04	213	
COL 0603	La Boca	ss	1	5	52	13.7	19	18	0.5	0.1	8	17.3	29.6	6	171	8.8	0.05	1	0.1	0.1	0.1	0.5	0.02	141	
COL 0604	La Boca	ss	1	6	79	31.4	59.9	29	0.7	0.1	9.1	11.4	37.2	16.2	222.4	18.7	0.1	1	0.1	0.1	0.1	0.5	0.01	113	
COL 0605	La Boca	ss	1	16	192	22.3	30.4	37	0.5	0.1	12	27.1	17.5	21.4	343.4	16	0.2	1	0.1	0.1	0.1	1.3	0.04	336	
COL 0606	La Boca	ss	2	7	68	4.3	22.2	23	3.3	0.1	9.6	51.8	26.8	14.6	121.3	7.4	0.05	2	0.1	0.1	0.1	1.1	0.01	314	
COL 0607	La Boca	ss	1	6	60	3.7	18.4	20	6.4	0.1	8.2	52.3	13.8	13.3	117.3	5.9	0.2	2	0.1	0.1	0.1	1.3	0.01	280	
COL 0608	La Joya	ss	1	6	49	8.3	26.9	58	5.5	0.1	10.6	60.4	22.9	24.1	207.1	8.3	0.1	3	0.1	0.1	0.1	1.3	0.01	268	
COL 0610	La Joya	ss	1	5	48	8.8	14	54	4.1	0.2	10.2	68.8	19.2	15.4	180.2	10.7	0.1	2	0.1	0.2	0.1	0.5	0.04	410	

Geochemical content (Table 3)

Sample	Formation	Hf	W	Ta	Ti	Se	Pb	Th	U	Cs	Cu	La	Ce	Pr	Nd	Sm	Eu	Gd	Tb	Dy	Ho	Er	Tm	Yb	Lu
RCH1-1	El Alamar low. m.	9.1	0.7	0.7	0.7	0.07	7.5	1.6	2.1	2.1	36.9	87.3	10.48	38.4	7.6	1.64	5.91	1.05	5.86	1.2	3.64	0.51	3.59	0.5	
RCH1-2	El Alamar low. m.	2.6	0.2	0.2	0.2	4	6.9	2	1.2	1.2	22.1	46.9	6.21	24.6	5.76	2.3	5.56	0.9	4.17	0.87	2.29	0.39	2.02	0.34	
RCH1-3	El Alamar low. m.	3.7	0.3	0.3	0.3	2	9.2	2.8	0.6	0.6	31.2	60.4	7.96	31.1	6.24	1.88	5.83	0.96	5	0.96	2.65	0.45	2.31	0.39	
RCH1-4	El Alamar low. m.	3	0.3	0.3	0.3	2	9.2	2.3	0.6	0.6	9.7	19.6	3.23	14.1	3.85	1.39	4.54	0.77	3.7	0.69	1.95	0.36	1.88	0.31	
RCH1-7	El Alamar low. m.	9	0.8	0.8	0.8	1	6.9	2	3.4	3.4	15.7	33.9	4.04	15.5	3.6	0.96	3.52	0.54	3.33	0.65	1.9	0.32	1.89	0.28	
RCH1-8	El Alamar low. m.	5.1	0.05	0.5	0.5	1	4.9	1.3	3	3	18.3	37.9	4.07	14.6	3.2	0.84	2.84	0.48	2.58	0.56	1.67	0.24	1.62	0.22	
RCH1-9	El Alamar low. m.	7.5	0.6	0.6	0.6	7	5.5	1.4	2.6	2.6	27.6	60.7	6.9	25.1	5.1	1.07	4.2	0.7	3.82	0.74	2.16	0.32	1.96	0.29	
RCH1-10	El Alamar low. m.	7.2	1.1	1.1	1.1	6	8	2.4	6.2	6.2	31.4	68.2	7.69	27	4.9	1.19	5.01	0.99	5.83	1.19	3.68	0.5	3.37	0.49	
RCH1-11	El Alamar low. m.	11	1	1	1	31	9	3.1	4.9	4.9	27.5	57.5	6.32	21.4	4.2	1.1	3.6	0.73	4.23	0.88	2.97	0.48	2.77	0.45	
RCH1-12	El Alamar low. m.	9.3	0.8	0.8	0.8	27	8.5	2.9	4.7	4.7	26.2	54.5	6.16	21.7	4.3	1.06	3.8	0.69	4.01	0.9	2.69	0.4	2.56	0.43	
RCH1-13	El Alamar low. m.	6.2	0.9	0.9	0.9	16	10.4	2.7	5.3	5.3	29.8	64.4	7.13	26.3	4.9	1.07	3.95	0.73	4.53	0.9	2.85	0.46	2.68	0.41	
RCH1-14	El Alamar low. m.	3.1	0.4	0.4	0.4	2	5	1.4	1.7	1.7	19.3	42.5	4.59	16.7	3.3	0.71	2.84	0.5	2.64	0.57	1.83	0.23	1.65	0.25	
RCH1-15	El Alamar low. m.	36.1	1.8	1.8	1.8	1	20	4.5	3	3	64.1	74.9	28.9	7.5	1.8	7.44	1.09	6.65	1.3	4	0.61	4.4	0.7	4.4	
RCH1-RE 15	El Alamar low. m.	37.4	1.7	1.7	1.7	1	20.6	4.4	3.3	3.3	25.8	64	7.48	30.1	7.5	1.8	7.12	1.13	6.99	1.43	4.75	0.7	4.57	0.76	
RCH1-16	El Alamar upp. m.	4.3	0.5	0.5	0.5	0.07	4.2	1	2.1	2.1	11.2	24.9	2.89	11	3.2	0.96	3.48	0.57	2.96	0.6	1.72	0.25	1.63	0.26	
RCH1-17	El Alamar upp. m.	7.8	0.9	0.9	0.9	0.07	7.5	1.5	3.4	3.4	13	28.8	3.33	14.6	3.4	0.85	3.13	0.42	2.55	0.48	1.54	0.22	1.57	0.26	
RCH1-18	El Alamar upp. m.	7.2	0.6	0.6	0.6	0.07	6.3	1.7	3.4	3.4	14.9	32.1	3.67	14.2	3.5	0.9	3.35	0.53	3.12	0.61	1.93	0.3	1.75	0.29	
RCH1-19	El Alamar upp. m.	11.1	0.9	0.9	0.9	2	7.9	1.4	1.3	1.3	31.5	71.7	8.01	31.6	3.8	1.48	5.49	0.85	4.77	0.96	2.86	0.39	2.38	0.37	
RCH1-20	El Alamar upp. m.	2	0.2	0.2	0.2	11	3.3	1	2.8	2.8	18.5	40.1	4.66	17.7	3.8	1.05	3.39	0.55	3.17	0.63	1.95	0.25	1.54	0.25	
RCH1-21	El Alamar upp. m.	3.8	0.4	0.4	0.4	3	4.3	1	1.4	1.4	22.7	50.1	5.69	23	5.1	1.49	5.32	0.86	4.55	0.92	2.81	0.41	2.61	0.42	
RCH1-22	La Joya	6.4	0.5	0.5	0.5	0.07	5.6	1.4	1.4	1.4	10	21.4	2.34	9.5	2.3	0.47	1.67	0.25	1.68	0.34	1.12	0.18	0.98	0.16	
RCH1-23	La Joya	3.7	0.4	0.4	0.4	0.07	10	2.9	1.1	1.1	33.1	66.5	7.24	29.7	5.7	1.61	4.06	0.7	4.25	0.75	2.55	0.35	1.98	0.31	
RCH1-24	La Joya	2.9	0.4	0.4	0.4	1	3.7	1	1.5	1.5	16.9	36.8	4.4	18.4	4.4	1.08	3.33	0.47	2.41	0.4	1.28	0.2	1.21	0.2	
RCH1-M1	Mina la Huiche L.1	3.8	0.3	0.3	0.3	2	3	1	2	2	8.7	19	2.54	10.2	2.56	0.74	2.65	0.44	2.12	0.43	1.19	0.19	1.1	0.18	
RCH1-M2	Mina la Huiche L.110	3.1	0.3	0.3	0.3	0.07	4.7	1.1	4.1	4.1	16.7	38.7	4.79	18.3	3.48	0.79	2.67	0.4	1.89	0.36	0.97	0.19	1.09	0.19	
RCH1-M3	Mina la Huiche L.165	2.6	0.2	0.2	0.2	1	3.6	0.8	1.8	1.8	20	44.2	5.26	19.5	3.52	0.79	2.41	0.43	2.12	0.41	1.11	0.18	1.06	0.17	
RCH1-RE M3	Mina la Huiche L.166	2.6	0.2	0.2	0.2	1	2.6	0.8	1.9	1.9	19.8	44.1	5.25	19.4	3.58	0.81	2.5	0.42	2.09	0.4	1.06	0.18	1	0.17	
RCH1-M4	Mina la Huiche L.200	7.8	0.5	0.5	0.5	5	5.9	1.6	5.5	5.5	25.4	55.9	6.76	24.9	4.63	1.09	3.65	0.58	2.77	0.57	1.54	0.27	1.48	0.24	
RCH1-M5	Mina la Huiche L.225	3.2	0.3	0.3	0.3	6	10.4	3.3	6.4	6.4	26.4	57.5	7.37	28.9	6.31	2.04	5.49	0.83	3.96	0.74	2.07	0.34	1.89	0.31	
<i>Canon El Alamar</i>																									
CA 200201	El Alamar	6.1	1	0.5	0.1	0.5	3.6	5.7	1.6	3.4	51.5	18.7	38.4	4.88	20.2	3.97	0.95	3.98	0.67	3.89	0.75	2.2	0.34	2.11	0.34
CA 200202	El Alamar	10.1	1	0.7	0.1	0.5	3.8	7.3	1.7	3.3	6.8	18.7	39.3	4.96	21	3.82	0.91	3.63	0.6	3.67	0.74	2.01	0.33	2.01	0.33
CA 200203	El Alamar	7.2	1	0.7	0.1	0.5	6.7	6.7	1.7	4	6.6	22.7	47.3	6.73	28.6	5.74	1.37	5.85	0.92	5.17	1.01	2.95	0.45	2.86	0.46
CA 200204	El Alamar	35.4	1	1.1	0.1	0.5	1.8	10.9	2.7	2.7	6.6	21.6	49.1	6.1	25.4	4.96	1.28	6.24	1.2	7.45	1.49	4.41	0.63	4.12	0.7
CA 200205	El Alamar	3.4	1	0.2	0.1	0.5	1.7	2.1	0.5	1	112.9	4.6	9.8	1.19	5.2	0.94	0.26	0.9	0.15	0.79	0.16	0.53	0.1	0.64	0.1
CA 200206	El Alamar	3.1	1	0.2	0.1	0.5	0.5	2.5	0.4	1.4	2.3	7.4	15.4	1.96	8.5	1.32	0.42	1.26	0.18	1.03	0.24	0.6	0.1	0.63	0.1
CA 200207	El Alamar	7.2	1	0.6	0.1	0.5	1.7	6.2	1.4	2.3	19.3	16.4	35.8	4.18	16.6	2.98	0.71	2.89	0.48	2.66	0.57	1.61	0.25	1.48	0.24
CA 2502 DK	El Alamar	4.9	1	0.4	0.1	0.5	1.4	3.2	9	2.8	211.8	13.5	30.8	3.88	15.9	3.21	0.62	3.14	0.51	2.8	0.55	1.63	0.23	1.49	0.23
CA 250205B	El Alamar	9.6	1	0.5	0.1	0.5	1.9	4.9	1.2	3.1	5	14.1	32.7	3.84	16.5	3.07	0.85	3.21	0.52	3.21	0.66	1.97	0.28	1.94	0.3
CA 250206B	El Alamar	6.2	1	0.5	0.1	0.5	8.9	7	2.7	3.5	146.2	16.3	37	4.48	18.8	3.45	0.87	3.33	0.53	2.99	0.59	1.7	0.27	1.62	0.26
CA 250207B	El Alamar	6.2	1	0.4	0.1	0.5	25.5	6.2	1.6	1.7	5.4	21.5	46.7	5.49	21.2	4.09	1.17	4.85	0.9	5.52	1.12	3.04	0.4	2.3	0.34
CA 250208B	El Alamar	2	1	0.2	0.1	0.5	2.3	3.1	1.8	1.7	2.9	11.4	25.7	2.95	11.8	2	0.45	1.57	0.24	1.26	0.24	0.72	0.12	0.78	0.12
CA 250209B	El Alamar	3.3	1	0.3	0.1	0.5	0.7	4.9	1.2	4.7	2.4	17.1	35.3	4.13	15.9	2.8	0.59	2.54	0.39	2.3	0.45	1.45	0.19	1.35	0.22
CA 250210B	El Alamar	2.2	1	0.2	0.1	0.5	3.2	3.3	1.1	2.4	3.7	14.1	32.1	3.74	15.3	2.78	0.67	2.64	0.42	2.46	0.43	1.25	0.19	1.1	
<i>Canon El Olmo</i>																									
COL 0101	La Boca	1.9	1	0.3	0.1	0.5	0.5	2.7	0.4	0.7	1.4	7.6	16.9	1.98	7.8	1.37	0.28	1.07	0.16	0.76	0.18	0.57	0.09	0.64	0.1
COL 0102	La Boca	3.3	1	0.5	0.1	0.5	2	9.9	1.7	5.5	0.6	11.1	24.2	2.82	10.8	2.13	0.48	1.98	0.35	1.94	0.42	1.32	0.23	1.52	0.24
COL 0103	La Boca	1.4	1	0.2	0.1	0.5	0.9	2.3	1.1	0.9	89.7	7.6	18.7	2.22	9.4	2.14	0.74	2.34	0.41	2.4	0.51	1.53	0.23	1.56	0.23
COL 0603	La Boca	5.1	1	0.4	0.1	0.5	1.6	4.1	0.6	1.1	0.5	16.8	38.2	4.25	15.8	2.45	0.58	1.66	0.23	1.19	0.23	0.69	0.11	0.77	0.11
COL 0604	La Boca	6.7	1	0.9	0.1	0.5	11.7	1.5	0.9	1.4	40.9	89.4	9.35	31.3	4.2	0.82	3.62	0.57	3.11	0.66	2.1	0.32	2.08	0.32	
COL 0605	La Boca	9.3	1	0.9																					

Geochemical content (Table 4)

Sample	Formation	Rock-type	SiO ₂	Al ₂ O ₃	Fe ₂ O ₃	MgO	CaO _{total}	CaO(Carb)	CaO*	CO ₂	Na ₂ O	K ₂ O	MnO	TiO ₂	P ₂ O ₅	Cr ₂ O ₃	LoI
Carron La Boca (Carron Los San Pedro)																	
CB 1301	El Alamar upp. m.	ss	81.27	8.06	3.7	1.1	0.08		0.10575118	0.04	0.55	1.32	0.02	0.59	0.06	0.005	3.2
CB 1302	El Alamar upp. m.	ss	67.78	17.09	3.38	1.24	1.02		0.640121884	0.76	0.55	4.68	0.03	0.72	0.13	0.005	3.2
CB 1303	El Alamar low. m.	ss	79.09	7.67	5.49	2	0.09		0.111585693	0.03	0.77	0.72	0.05	1.36	0.08	0.01	2.5
CB 1304	El Alamar low. m.	ss	62.27	16.64	7.99	3.57	0.59		0.39683883	0.34	0.2	3.34	0.08	0.79	0.18	0.009	4.1
CB 1305	La Boca	volcanic	64.21	17.06	5.63	2.03	1.24		0.765862166	0.92	0.78	3.84	0.05	0.84	0.13	0.01	4
CB 1306	Boca	ss	68.73	15.02	5.43	1.7	0.33		0.249759831	0.12	1.43	3.09	0.04	0.84	0.16	0.009	3.1
CB 1307	Boca	ss	67.82	15.22	5.99	1.78	0.31		0.240665804	0.03	1.46	3.18	0.04	0.84	0.17	0.009	3
Carron La Boca (Los San Pedro)																	
CB 1309	Boca	ss	75.93	11.76	3.71	1.51	0.34		0.256215678	0.14	1.6	1.94	0.04	0.69	0.11	0.005	2.2
CB 1310	Boca	ss	76.88	11.47	3.12	1.68	0.21		0.183017011	0.02	1.85	1.72	0.05	0.61	0.1	0.005	2.2
CB 1311	La Joya	ss	83.28	9.8	2.85	0.07	0.01		0.066140008	0.005	0.18	0.48	0.005	0.68	0.02	0.009	2.6
CB 1312	La Joya	ss	78.37	10.57	5.95	0.38	0.01		0.065905175	0.005	0.27	0.61	0.005	0.91	0.03	0.013	2.8
CB 2081	La Joya	ss	69.97	6.02	1.46	0.65	12.03		6.916126168	9.32	0.82	1.1	0.09	0.13	0.04	0.005	7.7
CB 2082	La Joya	ss	77.65	9.86	2.13	0.86	2.94		1.731301183	2.4	1.5	2.28	0.05	0.25	0.04	0.005	2.4
CB 2083	La Joya	ss	71.17	12.41	5.72	1.97	0.75		0.487609536	0.49	2.39	1.8	0.13	0.92	0.16	0.008	2.4
Carron Caballeros																	
CC 2801	La Joya	ss	68.31	5.77	1.35	0.62	11.44		6.564523586	9.32	0.78	1.05	0.09	0.16	0.03	0.002	10.4
CC 2802	La Joya	ss	76.61	9.59	2.01	0.84	2.86		1.690305079	2.21	1.49	2.24	0.05	0.23	0.03	0.002	4
CC 2803	GS	sch	71.14	12.3	5.68	1.99	0.73		0.470229513	0.65	2.36	1.81	0.13	0.94	0.16	0.009	2.6
Carron Huizachal-Petregrinal																	
CHP 190909 01	GS	sch	80.63	8.04	0.88	0.6	2.41		1.442063665	1.62	2.11	2.81	0.02	0.21	0.03	0.003	2.2
CHP 190909 02	Paleozoic sed.	ss	71.41	14.44	4.72	0.75	0.06		0.094547737	0.005	0.17	3.52	0.01	0.77	0.08	0.011	4
CHP 190903	Paleozoic sed.	ss	72.08	13.35	6.03	0.48	0.03		0.076892533	0.005	0.17	2.52	0.005	0.54	0.07	0.007	4.6
CHP 190909 04	Paleozoic sed.	ss	59.45	11.88	4.83	1.74	8.48		4.886133952	6.74	2.46	0.91	0.11	0.48	0.08	0.004	9.5
CHP 190909 05	Paleozoic sed.	ss	35.92	8.84	9.38	7.83	14.26		7.964355626	17.52	1.07	0.42	0.2	0.42	0.13	0.003	21.4
CHP 190909 06	La Boca	ss	77.69	9.68	4.87	1.04	0.27		0.216986922	0.08	0.59	2.13	0.02	0.49	0.09	0.008	3.1
CHP 190909 07	La Boca	ss	68.79	10.57	5	1.47	4.26		2.495005701	3.04	0.55	2.6	0.02	0.66	0.11	0.001	5.8
Carron Huizachal-Petregrinal																	
CHP 190909 09	La Boca	ss	70.28	11.8	4.71	1.84	1.62		0.986675151	1.09	0.4	3.99	0.04	0.72	0.13	0.012	4.4
CHP 190909 10	La Boca	ss	73.88	8.14	2.83	1.28	4.41		2.579366228	3.21	0.91	2.59	0.04	0.5	0.08	0.008	5.2
CHP 190909 11	La Boca	ss	85.51	5.53	4.5	1	0.07		0.101685251	0.005	0.05	0.91	0.02	0.15	0.03	0.005	2.2
CHP 190909 12	La Boca	ss	81.79	9.47	2.09	0.96	0.36		0.268846871	0.14	0.48	1.53	0.02	0.41	0.08	0.003	2.8
CHP 190909 13	La Boca	ss	71.56	9.92	2.92	0.8	4.8		2.800924062	3.54	1.27	1.95	0.08	0.43	0.07	0.005	6.1
CHP 190909 14	La Joya	ss	67.73	11.57	3.85	1.73	3.44		2.023264985	2.52	0.72	4.9	0.04	0.64	0.13	0.01	5.1
CHP 190909 15	La Joya	ss	68.79	9.83	3.26	1.55	5.01		2.916012499	3.81	0.62	4.24	0.05	0.57	0.11	0.008	5.9
CHP 190909 16	La Joya	ss	75.04	7.13	2.32	1.96	4.6		2.677567144	3.66	0.53	2.12	0.05	0.38	0.07	0.007	5.5
Carron Novillo																	
CN 290109 01	La Joya	ss	81.19	6.52	1.97	0.79	2.28		1.361555833	1.68	0.91	2.41	0.16	0.38	0.07	0.009	3.2
CN 290809 02	La Joya	ss	77.3	9.61	3.08	2.58	0.24		0.199543716	0.06	0.68	2.97	0.03	0.47	0.1	0.009	2.8
CN 290809 03	La Joya	ss	78.64	9.59	2.76	1.53	0.18		0.165126973	0.02	0.73	3.8	0.02	0.49	0.1	0.008	2.1
CN 290809 04	La Joya	ss	75.65	9.92	4.37	1.71	0.21		0.183528261	0.005	0.78	3.66	0.02	0.78	0.1	0.013	2.7
CN 290809 05	La Joya	ss	78.54	9.16	3.52	1.35	0.21		0.182570178	0.04	0.66	3.69	0.05	0.54	0.09	0.01	2.2
CN 290809 06	La Joya	ss	76.15	10.28	3.86	1.4	0.19		0.171090319	0.02	0.66	4.45	0.02	0.66	0.1	0.013	2.2
CN 290809 07	La Joya	ss	63.79	9.83	2.72	1.31	8.18		4.736757224	5.86	0.51	4.36	0.08	0.36	0.1	0.006	8.7
CN 290809 08	NG	Gn Agn	59.17	15.41	9.98	0.69	3.06		1.843229638	0.94	2.92	4.95	0.11	1.28	0.44	0.005	2.1
CN 290809 09	NG	Gn Gef	64.85	17.31	4.51	1.18	1.42		0.869415733	1.1	0.07	4.39	0.02	0.9	0.03	0.011	4.6
CN 290809 10	NG	Gn Bn	49.9	15.6	12.9	2.67	6.17		3.67061576	1.58	3.67	1.58	0.15	2.84	0.67	0.005	3.6
CN 290809 11	NG	Gn Bk	45.76	16.66	14.04	6.57	6.22		3.662481026	3.1	2.37	0.59	0.23	0.49	0.08	0.024	6.6
CN 290809 12	NG	Gn Ba Dk	51.49	13.09	11.87	8	6.11		3.68708916	0.04	2.34	1.92	0.15	1.69	0.68	0.058	2.3
CN 290809 13	NG/GS	Tona	50.98	13.14	12.21	8.11	6.15		3.712563544	0.02	2.57	1.38	0.16	1.84	0.64	0.063	2.4
CN 290809 14	GS	Sch	50.07	14.37	11.69	5.48	7.2		4.334253041	0.02	3.22	1.62	0.15	2.79	0.83	0.024	2.1
CN 290809 15	La Joya	ss	73.29	11.36	4.38	1.91	0.26		0.21264049	0.005	0.79	4.29	0.02	0.68	0.13	0.011	2.8

Geochemical content (table 5)

Sample	Formation	Rock-type	Be	Sc	V	Co	Ni	Zn	As	Cd	Ga	Rb	Sr	Y	Zr	Nb	Mo	Sn	Sb	Bi	Ag	Au	Hg	Ba
Canon La Boca (Canon Los San Pedro)																								
CB 1301	El Alamar upp. m.	ss	2	7	145	3.3	30	97	10.4	0.3	9.2	46	23.4	14.8	183.4	6	0.05	1	0.1	0.1	0.1	2.7	0.01	261
CB 1302	El Alamar upp. m.	ss	1	16	101	8.5	9.2	35	0.6	0.1	19.5	170.3	21.5	34.1	305.1	13.7	0.05	2	0.1	0.1	0.1	0.5	0.01	1000
CB 1303	El Alamar low. m.	ss	1	12	176	2.7	9	160	20.1	1	9.5	23.8	27.5	20.1	412.2	9.7	0.5	1	0.8	0.1	0.7	4.6	1.14	127
CB 1304	El Alamar low. m.	ss	3	17	124	15.8	34.1	95	7	0.1	20.9	138.5	32.2	35.8	183.3	18.9	0.05	4	0.1	0.1	0.1	0.5	0.03	667
CB 1305	La Boca	volcanic	3	17	120	11.1	33.6	86	5.9	0.1	21.4	164.9	49.9	29	204.2	19.6	0.05	4	0.6	0.2	0.1	1.5	0.03	748
CB 1306	Boca	ss	3	14	89	13	27.2	73	4.7	0.1	19.4	145.3	69.2	32.8	312.1	18.8	0.2	4	0.4	0.3	0.1	0.5	0.01	630
CB 1307	Boca	ss	3	14	93	14.2	26.5	72	4.1	0.1	18.8	139	75	35.2	314.7	19.8	0.1	4	0.4	0.3	0.1	0.9	0.01	645
Canon La Boca (Los San Pedro)																								
CB 1309	Boca	ss	2	10	63	9	16.4	47	3.4	0.1	14.2	91.8	66.6	28.2	336.3	15.4	0.1	3	0.2	0.2	0.1	0.5	0.01	388
CB 1310	Boca	ss	3	8	67	9.6	20	80	0.9	0.1	13.4	81.9	69.4	22.1	294.3	13.7	0.1	3	0.1	0.1	0.2	0.8	0.01	331
CB 1311	La Joya	ss	1	10	83	1	2.4	1	0.5	0.1	10.1	18.7	18.5	9	147.3	6.5	0.1	1	0.3	0.1	0.1	0.5	0.02	166
CB 1312	La Joya	ss	1	13	102	10	9.9	4	0.5	0.1	11.4	25	29	12.8	144.3	8.5	0.05	1	0.2	0.1	0.1	1.2	0.02	226
CB 2081	La Joya	ss	1	5	27	2.7	1.1	7	2.2	0.2	5.4	25.7	37.4	8.1	42.9	0.8	0.05	1	0.1	0.1	0.1	1.7	0.01	183
CB 2082	La Joya	ss	2	5	30	3	2.4	17	3.5	0.1	9.9	64.8	32.8	11.2	118.7	6.4	0.05	1	0.2	0.1	0.1	0.5	0.08	264
CB 2083	La Joya	ss	2	13	93	13.1	26.1	76	5.1	0.1	16.4	69.8	64.2	29.8	280	14.9	0.2	2	0.3	0.1	0.1	1.8	0.02	287
Canon Caballeros																								
La Joya		ss	1	4	24	2.5	20	9	2.3	0.2	5.7	24.5	34.3	8.3	29.8	1.1	0.1	1	0.1	0.1	0.1	0.5	0.1	176
La Joya		ss	1	4	31	2.9	20	20	4	0.1	9.6	61.7	32.4	8.8	110.9	6	0.05	1	0.2	0.1	0.1	0.7	0.06	255
GS		sch	1	13	90	12.6	33	83	5.7	0.1	16.1	65.2	62	29.8	289.3	14.2	0.2	3	0.4	0.1	0.1	0.8	0.02	290
Canon Huizachal-Peregrina																								
CHP 190909 01	GS	sch	1	1	20	2.6	3	7	0.5	0.1	9.5	71.4	115.3	6.2	194.5	1.9	0.2	1	0.1	0.1	0.1	0.5	0.01	588
CHP 190909 02	Paleozoic sed.	ss	2	11	76	12.3	24.7	65	0.5	0.1	16.4	109.1	19.3	20.6	208.4	12.4	0.3	2	0.1	0.1	0.1	0.5	0.07	525
CHP 190909 03	Paleozoic sed.	ss	2	7	59	13.6	67.3	48	3.9	0.1	13.4	70	19.4	16.9	198.8	7.2	0.4	1	0.1	0.1	0.1	0.5	0.1	378
CHP 190909 04	Paleozoic sed.	ss	1	11	69	7.3	9.2	59	7.2	0.1	11	25.7	134.9	15	105.8	3	0.4	1	0.7	0.1	0.1	0.5	0.06	278
CHP 190909 05	Paleozoic sed.	ss	1	13	84	10.8	12.6	48	12	0.1	9.8	11.1	101.1	27.7	37.4	1.3	0.3	1	1.2	0.1	0.3	0.5	0.1	93
CHP 190909 06	La Boca	ss	1	7	58	6.4	19.7	22	0.5	0.1	9.7	46.1	15.1	10.4	128.4	5.8	0.1	1	0.2	0.1	0.1	0.5	0.08	618
CHP 190909 07	La Boca	ss	1	9	70	7.1	26.1	24	0.6	0.1	10.8	57.5	42.3	17.1	166.1	7.4	0.1	1	0.3	0.1	0.1	0.5	0.03	1019
Canon Huizachal-Peregrina																								
CHP 190909 09	La Boca	ss	2	11	82	8.7	21.3	25	0.7	0.1	13.5	89.8	28.4	23.2	260.8	8.8	0.1	2	0.8	0.1	0.1	0.5	0.05	266
CHP 190909 10	La Boca	ss	1	6	49	5.4	12.7	20	0.7	0.1	8.3	48.6	81	15.1	145.2	5.1	0.05	1	0.2	0.1	0.1	0.5	0.04	1023
CHP 190909 11	La Boca	ss	1	9	72	14.5	30.9	90	0.9	0.1	6.5	29.5	14	9.2	52.2	1.7	0.2	1	0.8	0.1	0.1	1.5	0.88	632
CHP 190909 12	La Boca	ss	1	9	76	6.4	5.1	19	0.7	0.1	9.8	47.4	27.6	15.7	107.5	4.5	0.05	1	0.6	0.1	0.1	0.5	0.73	326
CHP 190909 13	La Boca	ss	2	7	40	4.1	8.8	17	6.8	0.1	10.8	65.7	68.9	21.9	179	8.6	0.2	1	2.4	0.1	0.1	0.5	0.25	849
CHP 190909 14	La Joya	ss	1	9	73	7.3	14.7	29	1.4	0.1	13.1	82.1	56.9	18.1	226.1	8.8	0.1	2	0.4	0.1	0.1	0.5	0.01	411
CHP 190909 15	La Joya	ss	1	8	65	7.7	15	28	1.2	0.2	10.4	61.9	53.1	16	171.4	5.8	0.1	1	0.1	0.1	0.1	0.1	0.02	339
CHP 190909 16	La Joya	ss	1	7	54	5.5	24	50	0.9	0.1	8.4	46.9	55	12	97.9	4	0.3	1	0.1	0.1	0.1	0.1	0.02	1716
Canon Nevado																								
CN 290109 01	La Joya	ss	1	5	39	52.8	20	42	12.2	0.2	6.2	42	32.6	18.8	407.2	5.7	3	1	0.3	0.1	0.3	1.6	0.57	326
CN 290809 02	La Joya	ss	1	8	65	7	26.9	110	0.9	0.1	10.2	44.9	25.7	8.1	108.3	4.8	0.05	1	0.1	0.1	0.1	0.5	0.02	707
CN 290809 03	La Joya	ss	1	8	56	4.8	15.9	48	0.5	0.1	10.1	59.3	20.6	9.6	145.6	5.3	0.05	1	0.1	0.1	0.1	0.5	0.01	315
CN 290809 04	La Joya	ss	1	9	77	6.6	24.5	58	1.4	0.1	10.1	60	21.9	9.8	226.3	7.2	0.1	1	0.3	0.1	0.1	0.5	0.02	219
CN 290809 05	La Joya	ss	1	8	70	5.6	28.4	45	1.5	0.1	10.1	56.4	19.9	8.9	155.3	5.3	0.2	1	0.3	0.1	0.1	0.5	0.03	261
CN 290809 06	La Joya	ss	1	8	67	6	18.8	38	1.3	0.1	10.5	70.4	26.6	12.5	277.8	7.4	0.1	1	0.4	0.1	0.1	0.5	0.01	304
CN 290809 07	La Joya	ss	1	7	48	4.9	15.9	24	1.9	0.1	9.6	70.6	68.3	18.2	89.6	4.1	0.2	1	0.3	0.1	0.1	0.5	0.01	269
CN 290809 08	NG	Gn Agn	2	20	27	8.1	4.1	40	3	0.1	26.4	83.4	191.5	75.7	1435.1	36	0.9	1	0.6	0.1	0.1	0.5	0.01	1473
CN 290809 09	NG	Gn Gf	1	20	123	5.3	16.4	47	6.2	0.1	23.3	114.8	19	22.6	210.5	14.3	0.6	1	0.2	0.1	0.1	3.6	0.01	672
CN 290809 10	NG	Gn Bn	2	18	152	28.8	11.4	93	3.1	0.1	21.2	27.9	482.4	36	270.2	26.7	1.5	2	0.5	0.1	0.1	0.5	0.03	816
CN 290809 11	NG	Gn Bk	1	51	324	43.1	17.6	121	9.8	0.1	16.3	16.9	203.3	18	54.6	1.1	0.1	1	0.1	0.1	0.1	0.5	0.04	192
CN 290809 12	NG	Gn Bn Dk	2	21	136	34.2	42.1	109	0.7	0.1	18.2	38.3	397.5	27.5	192.3	10.4	0.1	1	0.1	0.1	0.1	0.5	0.04	576
CN 290809 13	NG/GS	Tona	2	21	147	34.3	39.8	103	0.7	0.1	19	27.8	410.5	30	218.6	11.5	0.2	1	0.1	0.1	0.1	0.5	0.03	479
CN 290809 14	GS	Sch	2	22	195	38.4	32.2	71	2.3	0.1	20.5	25.1	764.6	36.2	292.4	14.3	0.5	1	0.2	0.1	0.1	0.5	0.02	846
CN 290809 15	La Joya	ss	1	11	88	7.4	26.3	58	1.7	0.1	12.3	76.1	26.9	15.6	316.3	8.6	0.2	1	0.3	0.1	0.1	0.5	0.02	282

Geochron: Izalco (table 6)

Sample	Formation	Hf	W	Ta	Tl	Se	Pb	Th	U	Cs	Cu	La	Ce	Pr	Nd	Sm	Eu	Gd	Tb	Dy	Ho	Er	Tm	Yb	Lu
Canon-La Boca (Canon Los San Pedro)																									
CB 1301	El Alamar upp. m.	5.1	1	0.4	0.1	0.5	2.2	6.3	2.4	2.8	98.4	14	29.9	3.8	17.1	3.1	0.68	2.78	0.46	2.6	0.51	1.45	0.24	1.58	0.23
CB 1302	El Alamar upp. m.	9.2	2.1	1.1	0.1	0.5	0.8	13.7	3.3	4.6	0.4	31	67.5	7.83	30.5	5.64	1.4	5.4	0.92	5.41	1.13	3.59	0.54	3.48	0.58
CB 1303	El Alamar upp. m.	11.5	1.7	0.7	0.1	0.5	558.1	12.7	4.3	1.5	45.4	25	55.6	6.26	26	4.36	0.84	4.06	0.62	3.47	0.7	2.07	0.33	2.13	0.35
CB 1304	El Alamar low. m.	5	2.9	1.4	0.1	0.5	0.4	16.1	3	6.5	3.1	45.2	96.8	10.86	42	7.47	1.75	6.96	1.11	6.38	1.23	3.62	0.54	3.38	0.48
CB 1305	La Boca	6.1	2.2	1.4	0.1	0.5	7.9	15.6	2.6	10.5	57.8	34.6	74.3	38.6	32	5.82	1.09	5.23	0.86	4.81	1.03	3.02	0.45	3.07	0.52
CB 1306	Boca	9.5	2.4	1.5	0.1	0.5	11.1	16.5	2.9	8.7	1.3	44.4	91	10.14	38.2	6.88	1.32	6.06	1.01	5.56	1.15	3.22	0.51	3.31	0.55
CB 1307	Boca	9.5	2.7	1.5	0.1	0.5	9.6	15.5	2.9	8.1	1.4	44.5	96.2	10.91	41.6	7.48	1.4	6.53	1.08	5.98	1.2	3.69	0.56	3.68	0.55
Canon-La Boca (Los San Pedro)																									
CB 1309	Boca	10.2	1.8	1.1	0.1	0.5	8.6	12.3	2.7	5.9	3.4	34.1	72.9	8.18	32.3	5.62	1.04	4.94	0.81	4.53	0.93	2.84	0.44	2.87	0.45
CB 1310	Boca	9.3	2	1.1	0.1	0.5	1.6	12.2	2.6	4.8	165.9	32.7	72.5	8.4	33.7	5.79	1	4.51	0.72	3.97	0.77	2.31	0.36	2.43	0.37
CB 1311	La Boca	4.4	0.5	0.3	0.1	0.5	1.4	4.6	1	0.7	2.2	13.6	33.2	3.44	13.4	2.6	0.62	2.21	0.33	1.75	0.33	1.04	0.14	0.94	0.15
CB 1312	La Boca	4.6	0.8	0.6	0.1	0.5	1.8	5.3	1	1.3	1.6	20.8	46.1	5.83	21.3	3.99	0.95	3.01	0.47	2.43	0.48	1.34	0.22	1.34	0.21
CB 2081	La Boca	1.6	0.5	0.1	0.1	0.5	1.6	0.9	0.4	2.8	0.1	3.6	5.7	1.05	4.5	1.23	0.36	1.29	0.21	1.11	0.26	0.78	0.13	0.84	0.14
CB 2082	La Boca	3.5	1.1	0.6	0.1	0.5	2.1	7.2	1.4	5.8	0.4	11.7	24.5	2.86	10.3	2.02	0.49	1.78	0.31	1.84	0.39	1.19	0.19	1.46	0.23
CB 2083	La Boca	8	1.3	1.1	0.1	0.5	3.3	10.9	2.4	2.2	13.2	30.9	73.5	8.16	31.6	6.22	1.29	5.73	0.93	5.19	1.06	3.27	0.48	3.06	0.49
Canon Caballeros																									
CC 2801	La Boca	0.9	0.5	0.1	0.1	0.5	1.9	0.8	0.4	2.9	0.4	3.5	5.6	1	4.4	1.19	0.36	1.24	0.21	1.15	0.28	0.78	0.13	0.83	0.15
CC 2802	La Boca	3.1	1	0.5	0.1	0.5	2.5	6	1.2	5.6	0.8	10.2	20.9	2.51	9.8	1.82	0.42	1.52	0.25	1.39	0.3	0.9	0.16	1.08	0.19
CC 2803	GS	8.6	1.2	0.9	0.1	0.5	3.7	9.6	2.4	2.4	1.5	28.9	65.7	7.72	30.5	5.94	1.25	5.4	0.9	5.14	1.04	3.01	0.47	3.07	0.47
Canon Huizachal-Fenergrina																									
CHP 190909 01	GS	6.2	0.5	0.1	0.1	0.5	2.6	1.6	0.4	0.2	6.3	8.7	17.6	17.6	2.21	10.1	2.09	0.98	0.23	1.09	0.18	0.5	0.09	0.54	0.08
CHP 190909 02	Paleozoic sed.	5.8	0.9	0.9	0.1	0.5	1.3	7	1.8	3.5	15.2	25.8	54.9	6.68	26.9	5.09	1.02	4.17	0.65	3.6	0.73	2.24	0.35	2.29	0.34
CHP 190909 03	Paleozoic sed.	5.9	0.5	0.4	0.1	0.5	3.2	3.7	1.6	1.6	21.3	20.7	45.7	5.44	22.2	3.86	0.78	3.06	0.53	3.05	0.61	1.68	0.26	1.65	0.26
CHP 190909 04	Paleozoic sed.	3.3	0.6	0.2	0.1	0.5	5.7	2.4	0.7	1.7	7.9	9.3	18	2.29	9.6	2.33	0.65	2.86	0.45	2.45	0.52	1.54	0.24	1.66	0.26
CHP 190909 05	Paleozoic sed.	0.9	0.5	0.1	0.1	0.5	13.9	1.1	0.7	1.5	7.5	6.4	12.4	1.79	8.8	2.82	1.05	4.17	0.7	4.15	0.8	2.24	0.31	1.93	0.29
CHP 190909 06	La Boca	3.7	1.2	0.4	0.1	0.5	0.7	4.3	1.1	3.9	0.1	8	16.6	2.16	9.6	1.89	0.45	1.85	0.33	1.95	0.38	1.19	0.19	1.14	0.17
CHP 190909 07	La Boca	4.2	1.1	0.5	0.1	0.5	1.4	5.1	1.3	6	0.1	11.3	23.9	3.51	14.9	3.39	0.84	3.15	0.53	2.96	0.58	1.57	0.24	1.64	0.25
Canon Huizachal-Fenergrina																									
CHP 190909 09	La Boca	7.1	1.3	0.6	0.1	0.5	2.9	6.4	2.2	5.4	0.1	24.5	45.3	5.79	23.8	4.36	1.03	4.3	0.71	4.05	0.78	2.38	0.33	2.11	0.33
CHP 190909 10	La Boca	3.9	0.5	0.4	0.1	0.5	1.1	4	1	2.5	0.1	15.3	27.3	3.76	14.8	2.85	0.74	2.55	0.44	2.45	0.5	1.32	0.19	1.32	0.18
CHP 190909 11	La Boca	1.7	0.5	0.1	0.1	0.5	1.3	2.6	1.2	1.6	0.8	6.2	11.6	1.61	6.2	1.48	0.34	1.5	0.26	1.53	0.33	0.93	0.14	0.96	0.14
CHP 190909 12	La Boca	3.2	0.8	0.4	0.1	0.5	1.1	3.1	1.4	5.8	0.2	11.7	24.9	3.08	12.9	2.51	0.53	2.3	0.43	2.54	0.53	1.55	0.24	1.57	0.23
CHP 190909 13	La Boca	4.8	1.1	0.7	0.1	0.5	5.2	7	1.6	4.2	0.5	15.9	32.9	4.05	16.4	3.41	0.74	3.52	0.62	3.6	0.7	2.17	0.34	2.23	0.33
CHP 190909 14	La Boca	6.1	0.6	0.7	0.1	0.5	5.8	7.5	2.3	6.4	0.1	22.4	45.3	5.52	22	3.95	0.83	3.35	0.55	3.35	0.66	2	0.31	1.99	0.29
CHP 190909 15	La Boca	4.3	0.6	0.4	0.1	0.5	3.2	4.7	1.4	3.1	1	15.3	32.3	3.99	15.9	3.16	0.78	2.9	0.49	2.58	0.53	1.52	0.23	1.56	0.24
CHP 190909 16	La Boca	2.7	0.6	0.3	0.1	0.5	0.8	3.4	1.1	5.5	231.2	12.7	26.4	3.24	12.4	2.5	0.73	2.41	0.4	2.24	0.43	1.22	0.2	1.27	0.2
Canon Novillo																									
CN 290109 01	La Boca	10.4	1	0.5	0.4	0.5	19.9	4.5	2.3	1.6	419.9	14.3	35.4	4.16	18.8	4.36	1.07	4.17	0.69	3.87	0.7	2.02	0.28	1.87	0.28
CN 290809 02	La Boca	2.8	0.9	0.4	0.1	0.5	0.8	4.1	1.1	2.7	45.7	10	21.2	2.48	9.3	1.64	0.4	1.54	0.25	1.61	0.31	0.92	0.17	1.11	0.16
CN 290809 03	La Boca	3.7	0.6	0.5	0.1	0.5	0.8	3.8	1.2	2.8	0.2	10.6	2.2	2.75	10.9	2.37	0.51	1.9	0.31	1.81	0.34	1.06	0.16	1.09	0.17
CN 290809 04	La Boca	6.5	1.1	0.5	0.1	0.5	2.4	5.6	1.5	3	0.5	13.6	28.8	3.5	13.6	2.69	0.57	2.21	0.34	2.03	0.39	1.1	0.18	1.18	0.19
CN 290809 05	La Boca	4.3	0.9	0.5	0.1	0.5	2.5	4	1.4	2	2.5	8.7	18.7	2.32	8.9	2.07	0.44	1.69	0.29	1.75	0.33	1.02	0.17	1.15	0.16
CN 290809 06	La Boca	7.3	0.9	0.6	0.1	0.5	2.8	5.9	1.7	4	0.1	12.5	25.5	3.1	13.6	2.49	0.56	2.19	0.39	2.34	0.51	1.55	0.25	1.65	0.25
CN 290809 07	La Boca	2.6	0.5	0.6	0.1	0.5	2.1	3.7	1.1	4.4	0.5	12.9	29.7	4.33	19.1	4.77	1.31	4.36	0.72	3.85	0.68	1.9	0.25	1.6	0.24
CN 290809 08	NG	35	0.5	2	0.1	0.5	1.4	1.1	1.1	0.5	0.9	44.2	107.3	15.21	74.2	17.03	4.04	17.5	2.79	15.89	2.99	8.5	1.26	8.16	1.24
CN 290809 09	NG	6.5	1.3	0.7	0.1	0.5	1	2.5	0.6	0.6	58.5	27.3	49.7	5.28	19.8	4	9.07	2.54	8.65	1.36	4.26	0.87	2.61	0.42	2.73
CN 290809 10	NG	7.7	0.5	1.8	0.1	0.5	2.3	0.6	0.5	0.5	15.3	30.3	71.9	9.33	41.2	9.07	2.54	8.65	1.36	7.39	1.39	3.8	0.55	3.4	0.49
CN 290809 11	NG	1.7	0.5	0.1	0.1	0.5	2.5	0.9	0.4	0.6	1.7	8.3	19.1	2.52	11	3.11	1.03	3.3	0.56	2.98	0.61	1.64	0.25	1.71	0.24
CN 290809 12	NG	5.1	0.5	0.6	0.1	0.																			

Sample	Formation	Rock-type	SiO ₂	Al ₂ O ₃	Fe ₂ O ₃	MgO	CaO _{total}	CaO(Carb)	CaO*	CO ₂	Na ₂ O	K ₂ O	MnO	TiO ₂	P ₂ O ₅	Cr ₂ O ₃	Lol	
Geochemical content (table 7)																		
Arambeeri																		
Ab 1111 01	Pre Ox?	ss	43.04	5.76	1.09	0.57	25.17		14.39817802	19.7	1.15	2.52	0.17	0.21	0.04	0.004	20.2	
Ab 1111 02	Pre Ox?	ss	56.66	8.07	2.95	1.07	13.77		7.902812567	10.78	1.33	2.58	0.12	0.67	0.09	0.009	12.6	
Ab 1111 03	Pre Ox?	ss	68.25	10.87	3.8	1.36	4.13		2.423980868	2.87	1.52	3.36	0.06	0.42	0.08	0.01	6	
Ab 1111 04	Pre Ox?	ss	67.39	11.6	4.35	1.77	3.49		2.057982213	2.39	1.78	4	0.06	0.45	0.11	0.011	4.8	
Ab 1111 05	Pre Ox?	ss	51.6	7.77	2.22	1.07	17.63		10.12878717	13.02	1.33	2.37	0.15	0.42	0.07	0.008	15.3	
Ab 1111 06a	La Boca	tuff	61.68	15.7	5.45	3.83	0.82		0.541433788	0.17	0.85	6.49	0.05	0.54	0.11	0.013	4.3	
Ab 1111 07a	La Boca	tuff	64.42	9.4	2.86	1.86	7.78		4.495731551	5.94	1.6	3.26	0.14	0.45	0.09	0.008	7.8	
Ab 1111 08a	La Boca	ss	46.32	6.69	1.79	1	21.37		12.22444948	16.97	1.12	2.46	0.29	0.33	0.07	0.005	18.4	
Ab 1111 09a	La Boca	ss	64.03	7.23	1.44	0.73	11.66		6.70591936	9	1.13	3.18	0.14	0.26	0.06	0.005	10	
Ab 1111 10b	La Boca	ss	70.59	10.76	1.76	0.36	4.16		2.433690909	3.11	2.15	5.03	0.13	0.3	0.08	0.004	4.6	
Ab 1111 11b	La Boca	ss	72.1	11.54	2.61	0.74	1.78		1.084732188	1.04	2.27	4.68	0.06	0.35	0.09	0.004	3.7	
Ab 1111 12b	La Boca	ss	62.4	8.72	1.07	0.47	11.27		6.482104527	8.75	1.97	3.38	0.19	0.22	0.05	0.002	10.1	
Ab 1111 13b	La Boca	ss	68.78	9.93	1.64	0.39	5.47		3.207860577	3.33	1.92	4.45	0.1	0.24	0.06	0.002	6.9	
Ab 1111 14b	La Boca	ss	75.81	11.45	1.95	0.81	0.41		0.3025416	0.04	2.37	4.7	0.02	0.26	0.06	0.005	2.1	
Ab 1111 15b	La Boca	ss	72.13	10.98	2.88	0.89	2.21		1.326053408	1.49	2.87	3.84	0.04	0.35	0.08	0.005	3.6	
Ab 1111 16b	La Boca	ss	71.18	11.51	2.17	0.86	2.64		1.570782959	1.84	2.47	4.56	0.04	0.26	0.07	0.004	4.1	
Miguiruarra																		
Mi 20 06	La Joya?	ss	70.1	11.49	3.59	2.26	6.28		1.577725606	1.42	2.28	2.91	0.06	0.75	0.13	0.009	3.6	
Mi 20 05	La Boca	ss	60.06	12.91	4.2	2.25	2.63		3.644340957	4.62	3.28	2.79	0.09	0.81	0.17	0.011	7	
Mi 20 04	La Boca	ss	65.67	10.72	3.96	2.29	5.04		2.951497029	3.28	2.03	2.86	0.07	0.89	0.13	0.011	6	
Mi 20 03	La Boca	ss	69.1	9.94	3.67	2.01	4		2.353357198	2.64	1.61	3.05	0.07	1.04	0.12	0.013	5.2	
Mi 20 02	La Boca	ss	62.72	10.31	4.51	1.45	7.28		4.209129743	5.58	0.89	4.17	0.06	0.72	0.12	0.007	7.6	
Mi 20 01	La Boca	ss	70.97	11.56	4.12	1.92	2.27		1.372588477	1.14	3.94	1.52	0.06	0.76	0.13	0.01	2.6	
Mi 20 10b	La Boca	ss	67.7	10.92	4.2	1.5	4.93		2.886241055	3.27	4.06	1.2	0.09	0.81	0.13	0.01	4.3	
Mi 20 09b	La Boca	ss	54.48	13.9	2.66	0.76	10.92		6.285505743	8.36	6.55	0.75	0.13	0.38	0.1	0.004	9.3	
Mi 20 202b	La Boca	ss	63.98	11.25	3.91	1.01	5.86		3.410967751	4.16	1.02	6.49	0.07	0.76	0.11	0.007	5.3	
Mi 20 201b	La Boca	ss	65.86	12.19	4.06	1.39	4.86		2.845860966	3.23	4.65	1.16	0.08	0.7	0.13	0.008	4.8	
Mi 20 08	La Boca	ss	55.27	8.18	2.41	0.98	14.66		8.411502207	11.42	1.77	1.96	0.14	0.38	0.1	0.005	13.5	
Valle de Huizachal																		
VH 0110	La Joya	ss	74.88	6	1.53	0.65	7.08		4.108654315	5.07	0.24	2.81	0.08	0.36	0.06	0.005	6.2	
VH 0111	La Joya	ss	68.82	8.82	2.74	1.24	6.79		3.938186278	4.97	0.46	3.94	0.07	0.5	0.1	0.007	6.4	
VH 2101	La Boca upp. m.	ss	70.03	11.24	5.47	3.45	1.23		0.778432645	0.39	3.47	1.35	0.12	0.73	0.11	0.007	2.7	
VH 3101	La Boca low. m.	ss	62.08	13.61	4.21	1.54	5.67		3.308464838	3.85	4.02	2.5	0.08	0.57	0.1	0.009	5.5	
VH 3102	La Boca low. m.	ss	60.57	12.89	5.58	3.27	5.47		3.198271579	3.57	2.89	2.15	0.1	0.77	0.12	0.01	6	
VH 3103	La Boca low. m.	ss	73.26	11.5	4.33	2.26	0.78		0.516686738	0.21	1.29	2.81	0.05	0.55	0.09	0.008	2.9	
VH 3104	La Boca low. m.	ss	62.45	13.45	2.34	2.79	4.61		2.697307313	3.18	0.07	4.72	0.05	0.82	0.18	0.015	8.3	
VH 3105	La Boca upp. m.	tuff	57.9	11.48	4.6	1.91	8.56		4.946723879	6.3	0.09	4.07	0.08	0.91	0.17	0.021	10.1	
VH 3106	La Boca upp. m.	ss	58.21	12.04	4.13	2.28	7.85		4.539262304	5.86	0.16	4.64	0.08	0.6	0.13	0.013	9.7	
VH 3107	La Boca upp. m.	ss	79.99	8.09	1.9	1.64	1.36		0.843368151	0.78	0.04	2.58	0.02	0.36	0.08	0.007	3.9	
VH 3108	La Boca upp. m.	ss	67.12	10.28	3.82	1.49	5.11		2.973343293	3.85	0.17	4.13	0.05	0.69	0.15	0.012	6.9	

Geochemical content (Table 8)



























Sample	Formation	Rock-type	Be	Sc	V	Co	Ni	Zn	As	Cd	Ga	Rb	Sr	Y	Zr	Nb	Mo	Sn	Sb	Bi	Ag	Au	Hg	Ba
Ab1111 01	Pre Oxf?	ss	1	4	24	5.8	13.3	16	10.1	0.1	5	54.8	157.9	11.1	57.6	3	0.3	1	0.5	0.1	0.5	0.5	0.02	497
Ab1111 02	Pre Oxf?	ss	1	7	57	3.7	13.3	29	2.1	0.1	7.9	75.1	97.1	21	167.2	7.5	0.2	2	0.4	0.1	0.1	1.9	0.03	422
Ab1111 03	Pre Oxf?	ss	1	8	58	6.2	25.9	46	2.4	0.1	10.8	96.5	54	13.8	113.9	5.9	0.1	2	0.4	0.2	0.1	1.2	0.02	1000
Ab1111 04	Pre Oxf?	ss	1	9	62	6.7	30.3	54	1.9	0.1	11.8	108.3	57.7	15.6	124.7	5.9	0.1	2	0.8	0.2	0.1	0.5	0.01	831
Ab1111 05	Pre Oxf?	ss	1	6	47	3.2	12.1	38	1.7	0.1	7.5	70.4	120.2	18.4	119.3	4.9	0.2	1	0.2	0.1	0.1	1.5	0.02	333
Ab1111 06a	La Boca	tuff	3	11	73	11.2	37.3	108	6.5	0.1	18	164.1	37.5	25.1	178.2	11.1	0.1	3	1.1	0.2	0.1	0.9	0.06	538
Ab1111 07a	La Boca	tuff	1	7	48	6.9	20.6	88	4.8	0.1	8.5	71.2	122.9	26.1	140.3	6.4	0.2	2	0.8	0.1	0.1	0.7	0.02	1745
Ab1111 08a	La Boca	ss	1	5	35	6.7	14.8	25	9.3	0.2	7.2	56.7	142.6	17.1	124.9	4.2	0.1	1	0.3	0.1	0.4	0.8	0.08	646
Ab1111 09a	La Boca	ss	1	4	28	5	13.2	19	3.3	0.1	6.8	67.6	94.1	10.6	66.4	3	0.05	1	0.2	0.1	0.1	0.5	0.05	1016
Ab1111 10b	La Boca	ss	1	6	24	2	7.8	19	3	0.1	7.4	85.2	52	11.4	96.7	3.9	0.8	1	0.4	0.1	0.1	0.5	0.01	582
Ab1111 11b	La Boca	ss	1	5	28	3.6	12	36	3.9	0.1	9.4	86.8	61.9	13	139.5	4.2	0.4	1	0.5	0.1	0.1	0.5	0.01	627
Ab1111 12b	La Boca	ss	1	4	15	1.7	4.1	9	2.8	0.1	6.5	70.4	86	19	82.8	2.1	1	1	0.3	0.1	0.1	0.5	0.02	772
Ab1111 13b	La Boca	ss	1	4	21	1.9	6.1	16	2.9	0.1	6.9	81.2	60.4	14.4	114.9	2.7	0.7	1	0.4	0.1	0.1	0.5	0.01	589
Ab1111 14b	La Boca	ss	1	4	29	3.5	10.2	18	1.8	0.1	8.9	111.1	62.4	5.5	102.4	2.9	0.3	1	0.4	0.1	0.1	0.5	0.01	798
Ab1111 15b	La Boca	ss	1	6	34	4.5	12.5	22	3	0.1	10	83.1	68.3	10.7	125.8	4.1	0.3	1	0.6	0.1	0.1	0.5	0.01	609
Ab1111 16b	La Boca	ss	1	6	40	4.1	13.3	22	2	0.1	10	97.1	75.4	9.9	117	3.4	0.2	2	0.2	0.1	0.1	1.8	0.01	1039
Miquthuana																								
Mi20 06	La Joya?	ss	2	11	84	10.2	32	46	1.8	0.1	12.8	70.1	89.5	27.5	342.6	11.9	0.2	2	0.1	0.1	0.1	0.5	0.01	268
Mi20 05	La Boca	ss	1	12	154	9.7	19.1	40	2.4	0.1	12.6	58.3	110.5	26.9	315.8	11.6	0.2	3	0.1	0.1	0.1	0.5	0.01	286
Mi20 04	La Boca	ss	1	12	92	10.1	24	40	2.9	0.1	11.2	54.7	102.6	25.4	423.1	12.5	0.1	2	0.1	0.1	0.1	0.5	0.01	1752
Mi20 03	La Boca	ss	1	12	110	9.5	27	37	3	0.1	10.6	58.7	69.5	29.1	577.2	13.1	0.1	2	0.1	0.1	0.1	0.7	0.01	271
Mi20 02	La Boca	ss	1	11	74	7.5	28	20	1.1	0.1	12.1	76.8	75.3	24.2	280.4	10.9	0.2	2	0.1	0.1	0.1	1.1	0.01	304
Mi20 01	La Boca	ss	2	11	90	9.5	24	52	2.1	0.1	13.1	48.3	101.3	30.5	418	12.4	0.2	2	0.1	0.1	0.1	0.5	0.01	184
Mi20 10b	La Boca	ss	1	11	86	7.6	25	36	2.5	0.1	10.8	38.8	113.1	31.4	448.7	12.6	0.2	2	0.1	0.1	0.1	1.7	0.01	184
Mi20 09b	La Boca	ss	1	6	42	3.4	8.3	14	3.5	0.1	8.3	21.1	185.8	22.3	176	7.1	0.1	2	0.1	0.1	0.1	0.5	0.01	91
Mi20 202b	La Boca	ss	2	9	75	5	8.4	16	1.9	0.1	9.8	74.2	84.1	29.9	484.9	11.7	0.2	2	0.1	0.1	0.1	0.5	0.01	575
Mi20 201b	La Boca	ss	1	10	74	6.6	13.5	32	4.6	0.1	10.1	36.2	137.1	27.7	327.5	11.2	0.2	2	0.2	0.1	0.1	0.5	0.01	144
Mi20 08	La Boca	ss	1	6	75	38.3	15.4	40	12.4	0.1	6.3	29.9	495.7	12.6	135.4	5	4	1	0.4	0.1	0.4	1.3	0.14	3883
VH 0110	La Joya	ss	1	7	74	14.4	7.8	10	27.3	0.1	5.8	41.3	50.6	10.6	385.1	4.8	4.2	1	1.4	0.1	0.8	0.5	0.2	389
VH 0111	La Boca	ss	1	7	80	5.4	11.9	18	1.1	0.1	9.6	65.1	38.6	16.3	209.5	6.2	0.1	1	0.5	0.1	0.1	1.3	0.01	593
VH 3101	La Boca upp. m.	ss	1	15	183	23.2	19.7	128	2	0.1	11.1	35.7	73.9	29.7	126.2	7.1	0.3	1	0.2	0.1	0.1	0.5	0.03	315
VH 3102	La Boca low. m.	ss	1	12	119	7.8	12.8	34	3.2	0.1	11.3	69.1	124.5	29.6	216.1	11.2	0.4	2	0.3	0.2	0.1	0.5	0.01	450
VH 3103	La Boca low. m.	ss	1	13	114	15.8	22.3	98	3.1	0.1	14	60.4	105.6	28.6	178.3	10.7	0.3	2	0.2	0.1	0.1	1.6	0.01	342
VH 3104	La Boca low. m.	ss	2	11	68	13.3	18.5	59	2.8	0.1	14.3	86.3	48.8	31.5	185.2	11.2	0.2	2	0.2	0.2	0.1	0.8	0.02	591
VH 3105	La Boca upp. m.	tuff	2	13	222	12.3	31.9	69	6.5	0.1	14.7	90.7	31.1	20.9	227.8	11.5	0.05	2	0.1	0.1	0.1	1.7	0.14	582
VH 3106	La Boca upp. m.	ss	1	12	99	9.4	22.2	42	5.3	0.2	11.8	69.7	46.4	23.6	351.4	9.2	0.1	1	0.4	0.1	0.1	0.5	0.05	503
VH 3107	La Boca upp. m.	ss	1	11	92	10.9	25	40	3.1	0.1	13.3	79.1	57.5	23.6	164.1	6.9	0.05	1	0.3	0.1	0.1	0.5	0.02	910
VH 3108	La Boca upp. m.	ss	1	5	60	3.9	14	149	3.6	0.4	8.2	36.4	13.4	7.9	98.1	3.6	0.05	1	0.1	0.1	0.1	0.5	0.06	281
VH 3109	La Boca upp. m.	ss	1	9	84	6.1	18.2	32	1.4	0.1	10.2	62.3	34.2	19.5	332.2	8.9	0.2	1	0.3	0.1	0.1	0.5	0.02	561

Geochemical content (Table 9)

Sample	Formation	Hf	W	Ta	Ti	Se	Pb	Th	U	Cs	Cu	La	Ce	Pr	Nd	Sm	Eu	Gd	Tb	Dy	Ho	Er	Tm	Yb	Lu	
Arambeiri																										
Ab 1111 01	Pre Oxf?	1.7	0.5	0.2	0.1	0.5	0.1	10.9	3.9	1	2.1	4.7	10.4	22.7	2.65	10.2	2	0.53	2.06	0.33	1.74	0.36	1.01	0.16	0.96	
Ab 1111 02	Pre Oxf?	4.7	1.2	0.6	0.1	0.5	2.3	7.6	1.6	3.5	1	12	31.6	4.2	16.4	4	1.04	3.77	0.66	3.69	0.72	2.04	0.3	1.77	0.27	
Ab 1111 03	Pre Oxf?	3.5	1.1	0.6	0.1	0.5	1.1	6.5	1.5	6.5	0.5	12.9	28.7	3.33	13.1	2.73	0.68	2.51	0.44	2.41	0.5	1.45	0.24	1.5	0.22	
Ab 1111 04	Pre Oxf?	3.7	0.9	0.6	0.1	0.5	2.4	7.7	1.6	5.2	0.9	14.5	30.4	3.89	16.7	3.35	0.84	2.96	0.48	2.69	0.56	1.67	0.25	1.7	0.26	
Ab 1111 05	Pre Oxf?	3.3	1.1	0.4	0.1	0.5	9.8	5.4	1.4	3.9	2	12.7	35.2	4.27	17.1	3.78	0.99	3.47	0.61	3.28	0.61	1.7	0.25	1.54	0.23	
Ab 1111 06a	La Boca	5.5	1.1	0.9	0.1	0.5	4.9	11.7	3.6	15.1	0.8	17.5	41.6	5.42	22.6	4.56	0.81	3.86	0.71	4.22	0.92	2.66	0.4	2.55	0.37	
Ab 1111 07a	La Boca	3.9	0.9	0.4	0.1	0.5	3.9	6.9	1.9	4.4	0.6	30.1	60.6	6.8	25.8	5.53	1.16	5.16	0.83	4.4	0.81	2.17	0.31	1.99	0.29	
Ab 1111 08a	La Boca	3.6	0.7	0.3	0.1	0.5	6.8	3.41	0.9	2.1	111.6	12.8	29.5	3.9	16.4	3.41	0.77	3.26	0.56	3.02	0.6	1.64	0.24	1.49	0.22	
Ab 1111 09a	La Boca	2.2	0.7	0.4	0.1	0.5	4.1	4.2	1	2.4	28	10.9	24.8	2.93	11.6	2.21	0.57	2	0.34	1.86	0.37	1.09	0.16	1.02	0.14	
Ab 1111 10b	La Boca	2.8	0.9	0.2	0.2	0.5	1.5	6	1	2.2	0.7	8.1	17.3	2.21	8.9	1.87	0.38	1.88	0.32	1.79	0.36	1.11	0.18	1.16	0.17	
Ab 1111 11b	La Boca	3.7	0.9	0.3	0.1	0.5	2.2	6.8	1.3	2	0.6	12.6	34.4	3.33	12.9	2.83	0.66	2.58	0.4	2.31	0.44	1.24	0.19	1.17	0.19	
Ab 1111 12b	La Boca	2	0.5	0.2	0.1	0.5	1.3	6.1	0.8	2.2	0.8	18.6	44.2	4.67	17.9	3.43	0.73	3.07	0.49	2.66	0.54	1.62	0.25	1.65	0.24	
Ab 1111 13b	La Boca	3.2	0.6	0.3	0.1	0.5	1.5	5.9	1	2.3	0.3	14.7	28.5	3.23	12.6	2.57	0.57	2.46	0.4	2.27	0.45	1.31	0.18	1.23	0.18	
Ab 1111 14b	La Boca	2.9	0.7	0.2	0.1	0.5	1.3	6.9	1.1	3.5	1	6.6	14.1	1.62	6.1	1.17	0.28	1.01	0.16	0.89	0.2	0.67	0.1	0.69	0.11	
Ab 1111 15b	La Boca	3.6	0.9	0.3	0.1	0.5	2.6	7.8	1.6	3.6	0.6	11.8	18.4	2.44	8.6	1.85	0.34	1.64	0.31	1.73	0.37	1.12	0.16	1.1	0.18	
Ab 1111 16b	La Boca	3.3	0.7	0.2	0.1	0.5	1	6.5	1.8	3.7	0.6	9.6	22.6	2.77	10.7	1.98	0.4	1.79	0.28	1.59	0.33	1.11	0.18	1.25	0.19	
M. Iquihuana																										
Mi 20 06	La Joya?	9.2	1	0.7	0.1	0.5	5.4	9.4	2.7	4.1	39.8	29.7	65.2	7.47	29	5.5	1.13	5.21	0.86	5.06	1.02	2.86	0.42	2.85	0.43	
Mi 20 05	La Boca	8.2	1.1	0.8	0.1	0.5	8.6	10.6	2.8	3.9	27.5	20.7	41	5.29	21.9	4.63	0.8	4.39	0.72	4.19	0.9	2.79	0.41	2.88	0.44	
Mi 20 04	La Boca	11.6	0.8	0.9	0.1	0.5	6.6	10.5	2.8	2.4	9.6	25.2	54.3	6.79	27.3	5.14	1.01	4.63	0.77	4.34	0.88	2.78	0.43	2.73	0.45	
Mi 20 03	La Boca	14.9	1.2	0.9	0.1	0.5	6.9	11.4	3.3	3	19.5	28.2	58.8	7.24	29.4	5.83	1.22	5.43	0.89	4.87	1.03	3.21	0.48	3.25	0.48	
Mi 20 02	La Boca																									
Mi 20 01	La Boca	7.4	0.9	0.7	0.1	0.5	6.1	7.9	1.9	6.2	169.4	24.7	56.5	6.78	28.3	5.48	1.09	4.82	0.79	4.44	0.87	2.49	0.38	2.48	0.37	
Mi 20 10b	La Boca	10.6	0.9	0.9	0.1	0.5	9.9	10.2	3.4	2.2	3.5	30.3	63.6	7.64	30.5	6.13	1.17	5.45	0.94	5.14	1.04	3.24	0.48	3.26	0.48	
Mi 20 09b	La Boca	11.3	0.9	0.9	0.1	0.5	9.2	11.4	3	1.6	4.3	34.2	71.8	8.33	32.3	5.94	1.13	5.38	0.91	5.23	1.08	3.4	0.49	3.31	0.51	
Mi 20 702b	La Boca	4.7	0.6	0.7	0.1	0.5	7.4	8.6	1.8	0.8	2	25.2	43.9	6.28	24.9	4.38	0.74	3.83	0.62	3.54	0.72	2.3	0.33	2.36	0.35	
Mi 20 701b	La Boca	12.4	0.7	1.1	0.1	0.5	5.9	10.9	2.6	3.1	11.6	42.3	90	10.28	39.9	7.38	1.52	6.27	0.98	5.23	1	2.91	0.43	2.8	0.43	
Mi 20 08	La Boca	8.5	0.9	0.8	0.1	0.5	10.1	9.4	2.6	1.7	4.6	29.2	62.4	7.56	30.9	5.99	1.19	5.4	0.85	4.5	0.93	2.81	0.41	2.74	0.4	
Valle de Huizachal																										
VH 0110	La Joya	3.7	0.7	0.3	0.1	0.5	3.64	3.6	1.7	1.4	544.4	10.9	25.1	2.96	12.2	2.54	0.56	2.25	0.38	2.1	0.43	1.3	0.2	1.14	0.17	
VH 0111	La Joya	10.3	0.9	0.3	0.1	0.5	12.3	4.7	1.9	1.4	565.1	7.2	16.7	2.22	9.3	1.81	0.45	1.84	0.31	1.84	0.36	1.15	0.18	1.26	0.21	
VH 2101	La Boca upp. m.	6.1	0.7	0.5	0.1	0.5	2.7	5.1	1.5	3.9	2.4	14.3	34.3	4.49	19.2	3.65	0.92	3	0.52	2.72	0.55	1.47	0.25	1.63	0.24	
VH 3101	La Boca low. m.	3.2	1.3	0.5	0.1	0.5	10	4.2	1.8	1.3	2.7	35.2	56.1	8.29	34.5	6.09	1.52	6.22	0.93	4.87	0.91	2.4	0.34	2.06	0.3	
VH 3102	La Boca low. m.	6.3	1.2	0.8	0.1	0.5	17	8.6	2.5	3.1	1.5	38.8	76.4	9.44	37.1	6.36	1.25	5.82	0.91	4.81	0.98	2.86	0.45	2.92	0.45	
VH 3103	La Boca low. m.	4.9	0.9	0.8	0.1	0.5	14.3	6.7	2	3.2	6.4	21.4	39.8	5.49	23.2	4.91	1.15	4.79	0.83	4.99	1.04	2.89	0.45	2.75	0.43	
VH 3104	La Boca low. m.	5.5	1.2	0.9	0.1	0.5	14.3	7.9	3	4.5	0.6	34.6	67.9	7.99	30.9	6.39	0.98	6	1.08	5.98	1.2	3.25	0.49	3.06	0.44	
VH 3105	La Boca upp. m.	6.3	2.2	0.9	0.1	0.5	0.7	7.8	2.4	6.1	0.2	49.5	98.4	10.34	36.5	5.06	1	4.04	0.61	3.27	0.74	2.12	0.35	2.26	0.36	
VH 3106	La Boca upp. m.	9.5	1.1	0.7	0.1	0.5	6.1	6.1	1.7	3.6	1.7	24.6	49.4	6.71	26.7	5.05	1.09	4.65	0.74	3.93	0.79	2.19	0.34	2.08	0.32	
VH 3107	La Boca upp. m.	4.6	0.7	0.5	0.1	0.5	6.6	5.3	1.5	4.5	0.1	18.6	41	5.37	22.4	4.79	1.21	4.5	0.73	3.84	0.77	2.13	0.3	1.87	0.27	
VH 3108	La Boca upp. m.	2.8	0.6	0.2	0.2	0.5	14.4	3	0.8	2.2	134.7	8.2	15	2.02	8.7	1.57	0.32	1.4	0.23	1.39	0.28	0.83	0.12	0.88	0.13	
	La Boca upp. m.	9	0.8	0.6	0.1	0.5	4.8	6.9	2.2	3.1	1.9	20.8	38.8	5.28	22.5	4.11	0.93	3.6	0.58	3.46	0.7	2.02	0.32	2.12	0.34	

low. m. - lower member; upp. m. - upper member; Mina la Huiche L. - level within Mina la Huiche; NG- Novillo Gneiss; GS- Granjeno schist; Gn Agr- Novillo Augén Gneiss; GnBr- Novillo Gefalteter Gneiss; GnBk- Novillo black Banded Gneiss; GnBaDk- Dike intruding the Novillo Gneiss; Toma- Tomalite; Sch- Schist; ss- sandstone;

APPENDIX FOR PATTERN FILLS

	Gneis
	Grenville Gneis
	Oaxaquia Gneis
	Basement boulder
	Schist
	Collisional zone
	Rheic event
	Lithosphere
	Crust
	Gabbro
	Granite
	Plutonic rocks
	Plutonic rocks
	Devonian-Silurian Plutonic rocks
	Permian Plutonic rocks
	Triassic Plutonic rocks
	Plutonic-Volcanic rocks
	Volcanic rocks
	Volcanic Aramberri
	Volcanic rocks at Valle de Huizachal La Boca lower member
	Volcanic rocks at Valle de Huizachal La Boca upper member
	Basalts
	Rhyolite
	Epiclastic
	Terrigenous sediments
	Passive margin